DESIGN OF ROADSIDE BARRIER SYSTEMS

PLACED ON MECHANICALLY STABILIZED EARTH (MSE) RETAINING WALLS

A Dissertation

by

KANG MI KIM

Submitted to the Office of Graduate Studies of
Texas A&M University
in partial fulfillment of the requirements for the degree of

DOCTOR OF PHILOSOPHY

May 2009

Major Subject: Civil Engineering

DESIGN OF ROADSIDE BARRIER SYSTEMS

PLACED ON MECHANICALLY STABILIZED EARTH (MSE) RETAINING WALLS

A Dissertation

by

KANG MI KIM

Submitted to the Office of Graduate Studies of
Texas A&M University
in partial fulfillment of the requirements for the degree of

DOCTOR OF PHILOSOPHY

Approved by:

Co-Chairs of Committee,	Jean-Louis Briaud
	Paolo Gardoni
Committee Members,	Jose Roesset
	J.N. Reddy
	Roger P. Bligh
Head of Department,	David Rosowsky

May 2009

Major Subject: Civil Engineering

ABSTRACT

Design of Roadside Barrier Systems Placed on Mechanically Stabilized Earth (MSE) Retaining Walls. (May 2009)

Kang Mi Kim, B.S., Chonnam National University; M.S., Yonsei University, Korea

Co-Chairs of Advisory Committee: Dr. Jean-Louis Briaud
Dr. Paolo Gardoni

Millions of square feet of mechanically stabilized earth retaining wall are constructed annually in the United States. When used in highway fill applications in conjunction with bridges, these MSE walls are typically constructed with a roadside barrier system supported on the edge of the wall. This barrier system generally consists of a traffic barrier or bridge rail placed on a continuous footing or structural slab. The footing is intended to reduce the influence of barrier impact loads on the retaining wall system by distributing the load over a wide area and to provide stability for the barrier against sliding or overturning. The proper design of the roadside barrier, the structural slab, and the MSE wall system requires a good understanding of relevant failure modes, how barrier impact loads are transferred into the wall system, and the magnitude and distribution of these loads.

In this study, a procedure is developed that provides guidance for designing: 1. the barrier-moment slab, 2. the wall reinforcement, and 3. the wall panels. These design guidelines are developed in terms of AASHTO LRFD procedures. The research approach consisted of engineering analyses, finite element analyses, static load tests, full-scale dynamic impact tests, and a full-scale vehicle crash test. It was concluded that a 44.5 kN (10 kips) equivalent static load is appropriate for the stability design of the barrier-moment slab system. This will result in much more economical design than systems developed using the 240 kN (54 kips) load that some user agencies are using. Design loads for the wall reinforcement and wall panels are also presented.

DEDICATION

To my husband, Jun Kyung Park and my son, Minho with love

ACKNOWLEDGEMENTS

I would like to express my deepest gratitude to my advisor, Dr. Briaud, and my committee member, Dr. Bligh for excellent guidance, support, invaluable wisdom, and encouragement throughout the course of this research. The completion of this dissertation would not have been possible without their support. I also extend my gratitude to Dr. Gardoni, Dr. Roesset, and Dr. Reddy for being my co-advisor and committee members. This dissertation has been improved by their comments and fruitful discussions.

I would like to extend my sincere appreciation to Dr. Abu-Odeh for his help and discussion throughout my study and research. Thanks also go to my friends and colleagues and the department faculty and staff for making my time at Texas A&M University a great experience. I would like to especially thank the gang at Riverside Campus. Without all these people, this achievement would not be possible.

Finally, I would especially like to thank my mother, sisters, and brother for their encouragement and to my husband and my son for their consistent patience and love.

TABLE OF CONTENTS

Page

TABLE OF CONTENTS (CONTINUED)

Page

TABLE OF CONTENTS (CONTINUED)

Page

TABLE OF CONTENTS (CONTINUED)

Page

LIST OF FIGURES

Page

LIST OF FIGURES (CONTINUED)

Page

LIST OF FIGURES (CONTINUED)

Page

LIST OF FIGURES (CONTINUED)

Page

LIST OF FIGURES (CONTINUED)

Page

LIST OF FIGURES (CONTINUED)

Page

LIST OF FIGURES (CONTINUED)

Page

LIST OF FIGURES (CONTINUED)

Page

LIST OF FIGURES (CONTINUED)

Page

LIST OF FIGURES (CONTINUED)

Page

LIST OF TABLES

Page

LIST OF TABLES (CONTINUED)

Page

1 INTRODUCTION

1.1. Problem Statement

Millions of square feet of mechanically stabilized earth (MSE) retaining wall are constructed annually in the United States. When used in highway fill applications in conjunction with bridges, these MSE walls are typically constructed with a roadside barrier system supported on the edge of the wall. This barrier system generally consists of a traffic barrier or bridge rail placed on a continuous footing or structural slab. The footing is intended to reduce the influence of barrier impact loads on the retaining wall system by distributing the load over a wide area. The proper design of the roadside barrier, the structural slab, and the MSE wall system requires a good understanding of relevant failure modes, how barrier impact loads are transferred through the structural slab into the wall system, and the magnitude and distribution of these loads.

Current design procedures and standard details for placement of roadside barriers on retaining walls vary widely among state highway agencies. Most current designs are believed by engineers to be overly conservative. This is in part due to an inadequate understanding of how barrier impact loads are transferred and distributed to the slab and wall system. There is a need to develop standardized procedures for use by state highway agencies in designing economical roadside barrier systems placed on MSE retaining walls.

1.2. Objective and Research Approach

The objective of this study is to develop, in a format suitable for adoption by American Association of State Highway and Transportation Officials (AASHTO), procedures for designing roadside barrier systems placed on mechanically stabilized earth retaining structures. The following tasks were conducted to accomplish this objective of study:

This dissertation follows the style of *Journal of Transportation Research Record.*

Task 1. Review State of Practice

In this task, the state of practice for the barrier design, the MSE wall design, and the barrier system placed on MSE wall design is summarized in terms of AASHTO LRFD*(1)*. In addition, the survey is conducted to determine existing methodologies and details used in designing roadside barrier systems placed on MSE retaining walls.

Task 2. Conduct Barrier Stability Study

This task is discussing only the barrier design not the MSE wall design. The barriers need to be designed to satisfy three criterions during impact: 1. the barrier must not be broken (cracking of the concrete for example), 2. the barrier must not be overturned, and 3. the barrier must not slide away. This task addresses criterions 2 and 3 by discussing current practice including the evolution over the years of the impact loads considered in design, the magnitude of the equivalent static load that can be resisted by such a barrier, and then the magnitude of the dynamic load. Both analytical and experimental approaches are used to better understand the behavior of the barrier-moment slab system in the static and dynamic analyses.

Task 3. Conduct Reinforcement Pullout Test

The reinforcement pullout tests are conducted to evaluate the influence of rate effect on the pullout capacity of the reinforcement.

Task 4. Conduct 5-ft MSE Wall and Barrier Study with Bogie Impact

The capacity of the MSE wall and barrier is calculated by AASHTO LRFD to use the comparison with the results of the full scale tests. The finite element analysis using appropriate and representative barrier system on top of the MSE wall configuration is conducted. Based on the preliminary simulation, the full scale bogie test plan will be developed. The objectives of the full scale test with bogie include quantification of the

movement of the barrier-coping-moment slab system and measurement of the force distributions in the reinforcement strips due to a design impact load.

Task 5. Develop Preliminary Design Guidelines

The preliminary design guidelines of the barrier-moment slab system and the MSE wall reinforcement using the results of full scale bogie tests.

Task 6. Conduct 10-ft MSE Wall and Barrier Study with Vehicle Impact

The justification and the details of a full scale vehicle crash testing plan are developed for validating the preliminary procedures. The testing plan shall include a detailed description of the instrumentation to be used in the barrier, the load transfer system, and the MSE wall retaining wall system.

Task 7. Validate Design Procedure

The preliminary design procedures are validated by execution the full scale vehicular test for roadside barrier systems placed on MSE retaining walls. The design procedures are modified if necessary.

1.3. Organization of Dissertation

This dissertation is organized into seven sections. The first two sections (Sections 1 and 2) review the general problems of the design the barrier system place on MSE wall, as an introduction and motivation to the research investigations of this study. The third section contains the analysis of the barrier stability study to explain the behavior of the barrier under the static loading and dynamic impact load. Section 4 reports the reinforcement pullout test to evaluate the rate effect on the pullout capacity of the reinforcement. In Section 5, a numerical simulation and full scale MSE wall tests due to the bogie impact are conducted to develop the guideline for the design of the barrier atop MSE wall. Section 6 reports the results of a numerical simulation and another full scale test with the vehicular impact to validate the

preliminary design guidelines. In Section 7, the design procedures for the barrier system and MSE wall is developed. The justification of the procedures is presented in this section. The final section (Section 8) contains overall conclusions.

2 STATE OF THE PRACTICE

2.1 Design of MSE Wall

MSE walls are made of alternating layers of soil (fill) and reinforcement (Figure 2.1) (*2*). The fill must satisfy specifications (PI limits, percent passing #200 limits) and are generally sandy or rocky fills. The reinforcement is tied to panels erected vertically at the front of the wall. The reinforcement can be made of steel strips, bar mats, or geosynthetics. Each layer between reinforcement is compacted to the required compaction level. (Figure 2.2).

The idea of an MSE wall is to create a reinforced earth mass that is equivalent to a gravity wall. As such, the basic design consists of two parts: external stability design and internal stability design.

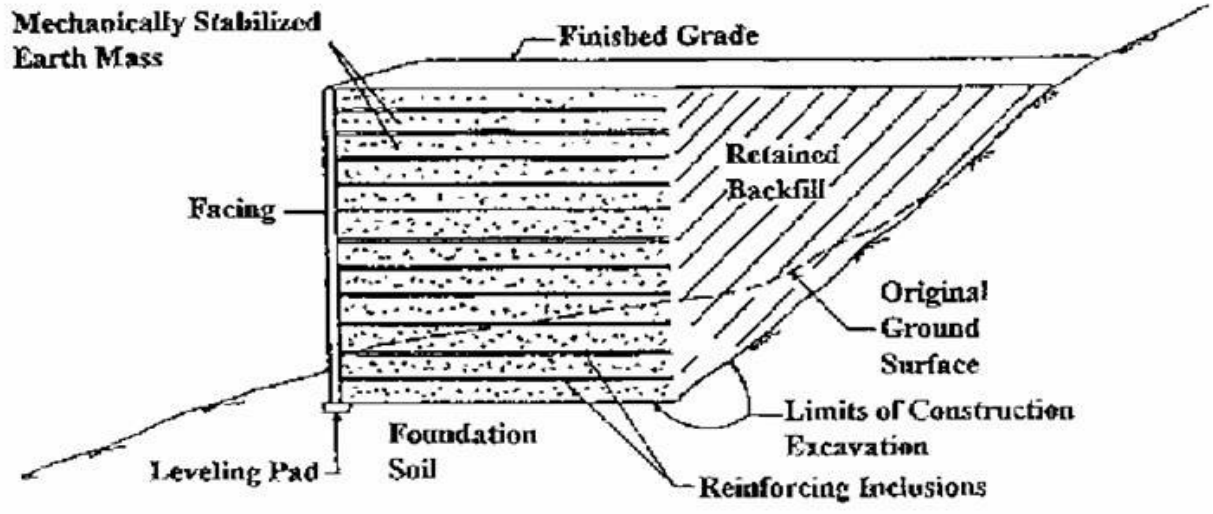

Figure 2.1 Principal elements of MSE wall (*2*)

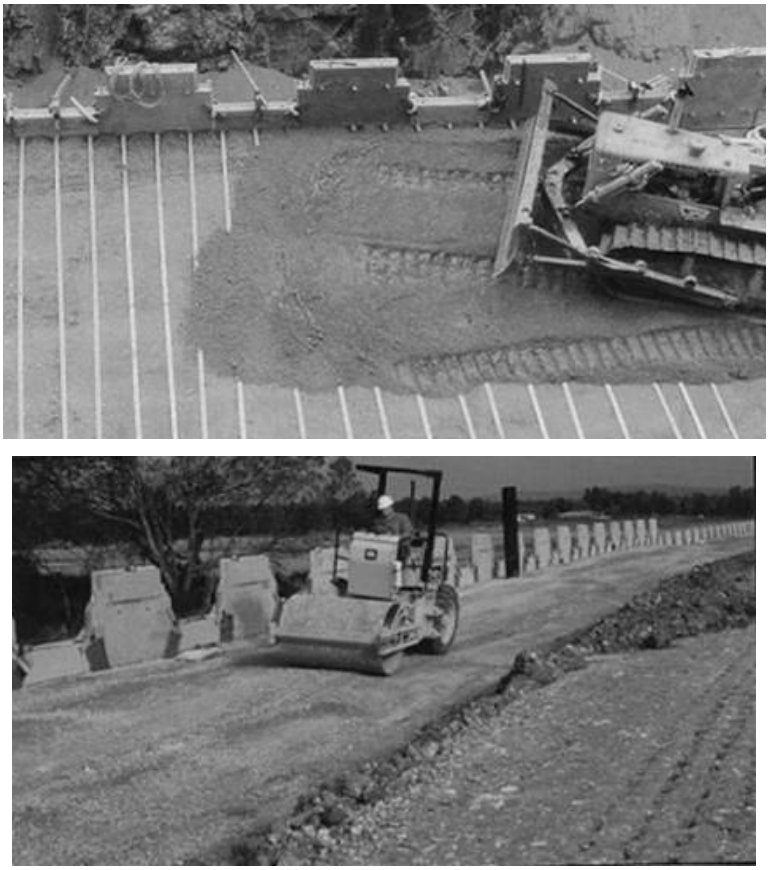

Figure 2.2 Construction of MSE wall (*2*)

2.1.1 External Stability

The external stability ensures that the wall is safe against sliding, overturning, bearing capacity failure, and slope stability failure (see Figure 2.3).

- Sliding design consists of ensuring that the active force developing behind the wall does not represent an unreasonable risk of overcoming the friction resistance at the base of the wall.
- Overturning design consists of ensuring that the moment created by the active force around the bottom of the front of the wall does not represent an unreasonable risk of overcoming the resisting moment due to the weight of the wall mass.
- Bearing capacity design consists of ensuring that the pressure due to the wall mass does not represent an unreasonable risk of overcoming the ultimate bearing capacity of the soil.

- Slope stability design consists of ensuring that the overall wall configuration does not represent an unreasonable risk of failing by general deep seated rotation.

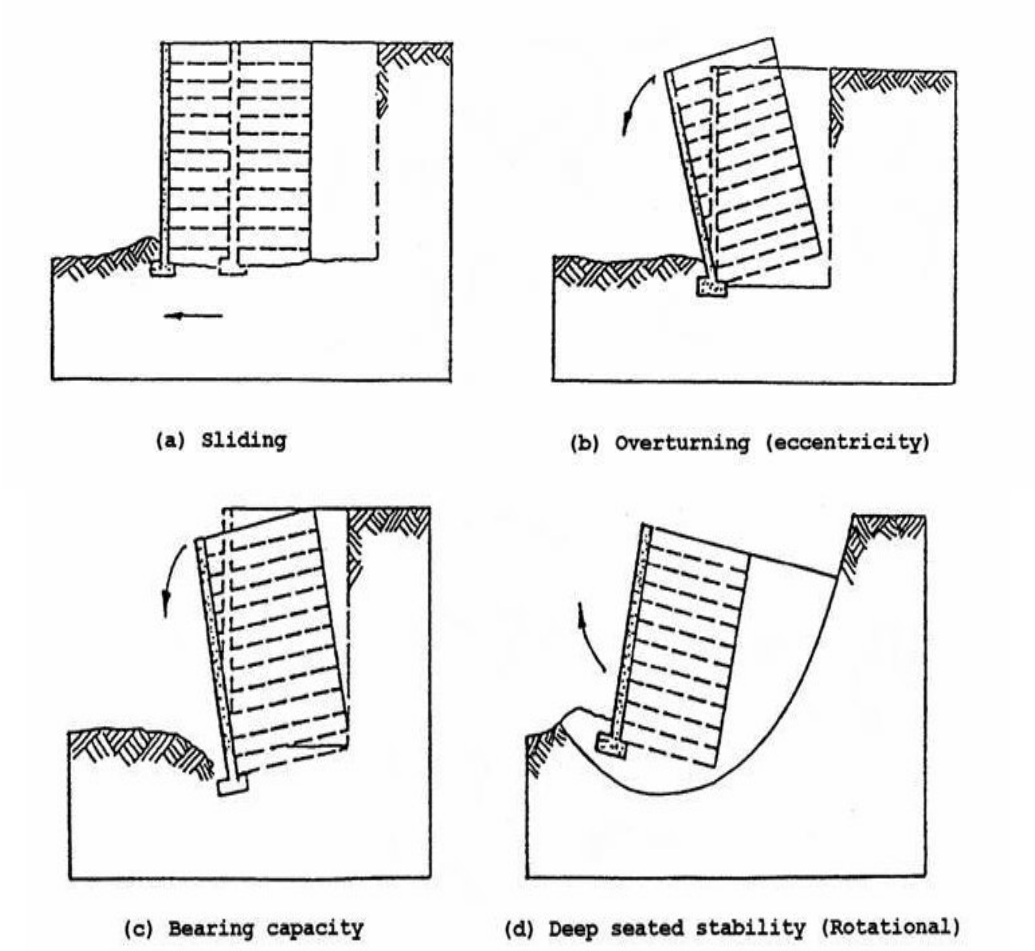

Figure 2.3 External stability considerations (*2*)

2.1.2 Internal Stability

The internal stability ensures that the wall mass is a coherent solid block with tensile resistance. This design addresses the issues of the load on the reinforcement, the required length of the reinforcement, and the stress in the reinforcement (see Figure 2.4).

- The load on the reinforcement is obtained by using a semi-empirical equation developed from experience. This equation expresses that the reinforcement must

safely resist the pressure on the panel that would develop in the soil if the reinforcement was not there.

- The length of the reinforcement is equal to the sum of the length required to safely resist in friction the load calculated in the previous step plus the length in the failing zone behind the wall. This length is usually calculated by a prescriptive approach, L = 0.7H.
- The stress in the reinforcement is the load divided by the reinforcement area after discounting the corrosion thickness and other factors if appropriate. This stress is checked to ensure that it is safely below the yield stress of the material used.

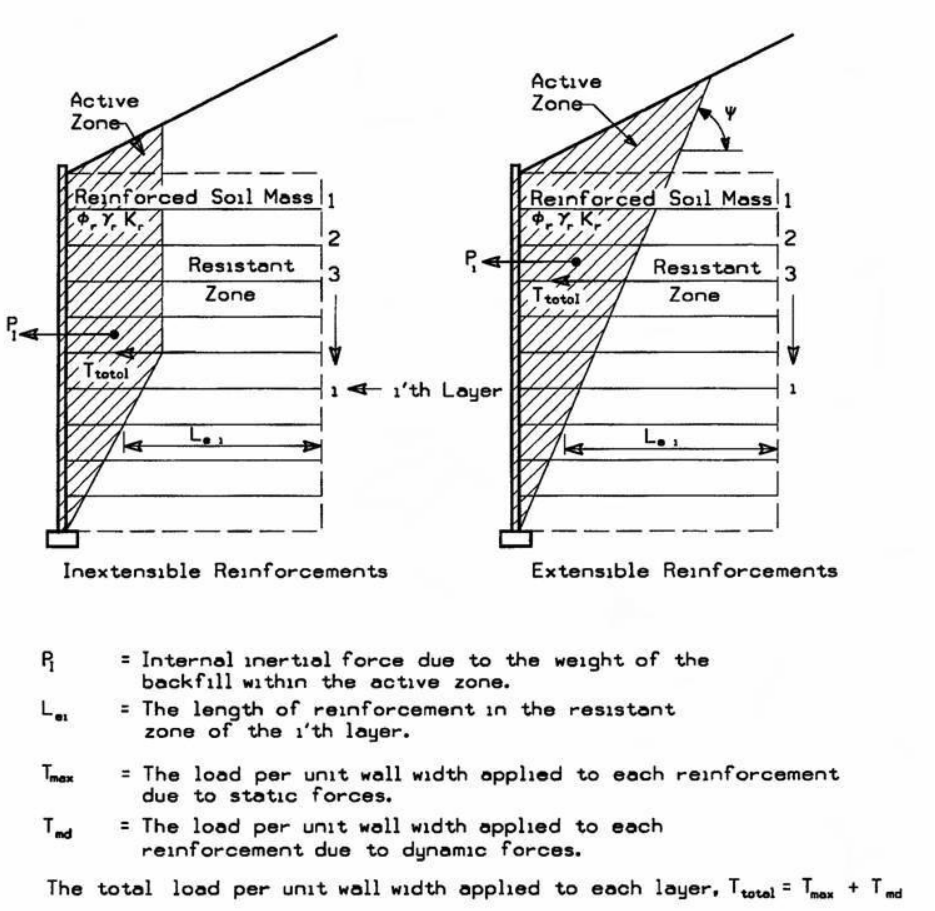

Figure 2.4 Internal stability considerations (*1*)

In AASHTO LRFD (*1*), to satisfy the internal stability, the static resistance (*P*) to pullout of the reinforcement should be at least equal to the static load (*T*) due to the earth pressure.

The static resistance (*P*) of the wall reinforcement in friction of one strip against soil is calculated using the following equation:

$$P = 2b \times L \times \sigma_v \times F^* \tag{2-1}$$

where b: Width of strip

L: Length of the strip

$\sigma_v = \gamma \times h$, *h*: Height of the strip from the roadside

F^*: Pullout friction factor as shown in Figure 2.5

To obtain the static load (*T*) expected per strip due to the soil the following equation in AASHTO LRFD is used.

$$T = A_t \times \sigma_h \tag{2-2}$$

where A_t: Tributary area of one strip

σ_h: Horizontal stress due to the soil, $\sigma_h = K_r \times \sigma_v$

Example applications of the AASHTO LRFD MSE wall design procedures are presented in Appendix A.

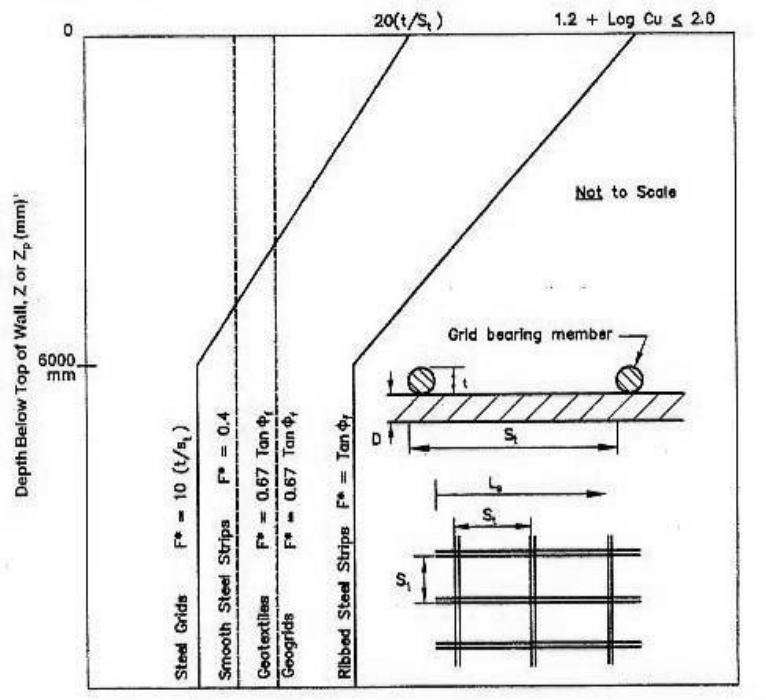

Figure 2.5 Default values for the pullout friction factor, F^* (AASHTO LRFD Figure 11.10.6.3.2-1) (*1*)

2.2 Design of Barrier

This section includes background regarding roadside barrier crash testing criteria, a history of the design loads, and design practice of roadside barriers.

2.2.1 Background of Barrier Crash Testing Guidelines

Guidelines for testing roadside appurtenances originated in 1962 with a one-page document – Highway Research Circular 482 *(3)* entitled "Proposed Full-Scale Testing Procedures for Guardrails." This document included four specifications on test article installation, one test vehicle, six test conditions, and three evaluation criteria. NCHRP Report 153 *(4)*, published in 1974, provided the first complete test matrix, which is entitled "Recommended Procedures for Vehicle Crash Testing of Highway Appurtenances." Parameters to be measured were specified along with methods and limiting values, and limited guidance on reporting formats

was included. These procedures gained wide acceptance following their publication, but it was recognized at that time that periodic updating would be needed.

In 1978, Transportation Research Circular 191 *(5)* "Recommended Procedures for Vehicle Crash Testing of Highway Appurtenances" was published to provide limited interim changes to NCHRP 153. An extensive revision and update was made in 1981 with the publication of NCHRP Report 230 *(6)* "Recommended Procedures for the Safety Performance Evaluation of Highway Appurtenances". This document specified different service levels for evaluating longitudinal barriers whose test matrices included vehicles ranging from small passenger cars to intercity buses.

NCHRP Report 350 *(7),* "Recommended Procedures for the Safety Performance Evaluation of Highway Features," which was published in 1993, provides current guidance on testing and evaluating roadside safety features. This 132-page document represented a comprehensive update to crash test and evaluation procedures. It incorporated significant changes and additions to procedures for safety performance evaluation, and updates reflecting the changing character of the highway network and the vehicles using it.

NCHRP Report 350 selected a 2,000 kg (4,409 lb) pickup truck as the design test vehicle to reflect the fact that over one half of new passenger vehicles sales in U.S. were in the "light truck" category. This change was made recognizing the differences in wheel bases, bumper heights, body stiffness and structure, front overhang, and other vehicular design factors associated with light trucks. NCHRP Report 350 further defines other supplemental test vehicles including an 8,000 kg (17,637 lb) single-unit cargo truck and 36,000 kg (79,366 lb) tractor-trailer vehicles to provide the basis for optional testing to meet higher performance levels.

Six test levels are defined for longitudinal barriers (e.g., bridge rails, median barriers, guardrails) that place an increasing level of demand on the structural capacity of a barrier system. The basic test level is Test Level 3 (TL-3). The structural adequacy test for this test level consists of a 2,000 kg (4,409 lb) pickup truck impacting a barrier at 100 km/h (62 mph) and 25 degrees. At a minimum, all barriers on high-speed roadways on the National Highway System (NHS) are required to meet TL-3 requirements. Many state transportation departments require that their bridge railings meet TL-4, which requires accommodation of an 8,000 kg (17,637 lb) single unit truck impacting a barrier at 80 km/h (50 mph) and 15 degrees. Higher

containment barriers are sometimes used when conditions such as a high percentage of truck traffic warrant. Such barriers are necessarily taller, stronger, and more expensive to construct.

Since publication of NCHRP Report 350*,* changes have occurred in vehicle fleet characteristics and testing technology. NCHRP Project 22-14(2) *(8)*, "Improvement of Procedures for the Safety-Performance Evaluation of Roadside Features," was initiated to take the next step in the continued advancement and evolution of roadside safety testing and evaluation. The results of this research effort culminated in the new document "Manual for Assessing Safety Hardware (MASH)" *(9)* that will be published by the AASHTO and will supersede NCHRP Report 350. Changes in the new guidelines include new design test vehicles, revised test matrices, and revised impact conditions. The weight and body style of the pickup truck changed from a 2,000 kg (4,409 lb), ¾-ton, standard cab pickup to a 2,270 kg (5,000 lb), ½-ton, 4-door pickup. For TL-4, the weight of the single unit truck increased from 8,000 kg (17,637 lb) to 10,000 kg (22,000 lb) and the speed increased from 80.47 km/h (50mph) to 90.12 km/h (56 mph). Although still a draft, many user agencies have already begun applying the MASH criteria in their crash test programs.

2.2.2 Background of Barrier Design Loads

Historically, the design of bridge rails has followed guidance contained in the AASHTO Standard Specifications. Prior to 1965, the AASHTO Standard Specifications required very simply that "Substantial railings along each side of the bridge shall be provided for the protection of traffic." It was specified that the top members of bridge railings be designed to simultaneously resist a lateral horizontal force of 2.19 kN/m (150 lb/ft) and a vertical force of 1.46 kN/m (100 lb/ft) applied at the top of the railing. The design load on lower rail members varied inversely with curb height, ranging from 7.3 kN/m (500 lb/ft) for no curb to 4.4 kN/m (300 lb/ft) for curb heights of 22.9 cm (9 in.) or greater. It was further specified that the railing have a minimum height of 68.6 cm (27 in.) and a maximum height of 106.7 cm (42 in.) above the roadway surface.

These loads are only a fraction of what is used today. Based on a poor accident history, accentuated by increased exposure due to dramatically increasing travel volumes, the engineering community came to realize that these criteria were inadequate. There was a

recognized need (and in the words of some and "urgent necessity") for a railing specification that established loading requirements more in line with the weights and increased speeds of vehicles of that day.

In 1962, the U.S. Department of Commerce, Bureau of Public Roads (BPR), now the FHWA, developed proposed revisions to the specifications for bridge railings. It was proposed that bridge railings and parapets be designed for a transverse load of 133.4 kN (30 kips) using plastic design procedures. This load was distributed among the horizontal railing members. A figure with 10 different railing types/configurations was provided to assist with distribution of the load. The difficulty of defining a static load that would be equivalent in effect to a vehicle impact on a railing was recognized. As part of the rationale for selecting the load of 133.4 kN (30 kips), reference was made to designs that met the proposed specification and which experience indicated would be adequate to resist the usual anticipated forces of impact.

Based on information received from a retired Texas Department of Transportation (TxDOT) bridge engineer involved in review of this proposal, many AASHTO members were unfamiliar with plastic design procedures and there was "great objection" to using it. Ultimately, after considerable discussion, comment, and revision, the AASHTO Committee on Bridges and Structures approved a revision to the railing specification in 1964.

The revised railing specifications were subsequently published in 1965 in the 9th edition of the AASHTO Standard Specifications for Highway Bridges *(10).* It required that rails and parapets be designed for a transverse load of 44.5 kN (10 kips) divided among the various rail members using an elastic analysis. The force was applied as a concentrated load at mid-span of a rail panel with the height and distribution of the load based on rail type and geometry as provided in an accompanying figure. Posts were designed for the transverse loading applied to each rail element plus a longitudinal load of ½ the transverse load. The transverse force on concrete parapet walls was distributed over a longitudinal length of 1.52 m (5 ft). Guidance on the effective length of slab resisting post loadings was provided for rail designs with and without a parapet. The height of the railing was required to be no less than 68.6 cm (27 in.). It was noted that railing configurations successfully crash tested were exempt from the design provisions.

The rationale for changing the 133.4 kN (30 kips) force proposed by the BPR to the 44.5 kN (10 kips) force ultimately adopted by AASHTO is not fully known. However, it can be shown that a 44.5 kN (10 kips) load with the rail resistance defined by elastic analysis is roughly equivalent to a 133.4 kN (30 kips) load with the rail resistance defined by plastic analysis following the BPR procedure. Such an equivalency may have been established to permit more familiar design procedures to be followed. The provisions in the 17th edition of the AASHTO Standard Specifications for Highway Bridges (2002) *(11)* are essentially the same as the revised specification adopted in 1965.

These requirements are intended to produce bridge rails that will function adequately for passenger cars for a reasonable range of impact conditions. The reserve load capacity of the rail, beyond its elastic strength offers some degree of protection for more severe impact conditions or for heavier vehicles. Several catastrophic accidents involving large vehicles increased awareness of design requirements for bridge rails and the need to extend protection beyond passenger cars.

In the first of two such studies, an instrumented concrete wall (shown in Figure 2.6) was designed to, for the first time, measure the magnitude and location of vehicle impact forces *(12)*. The wall consisted of four 3.05 m (10 ft) long panels laterally supported by four load cells. Each of the 106.7 cm (42 in.) tall × 61 cm (24 in.) thick panels was also instrumented with an accelerometer to account for inertia effects. Surfaces in contact with the supporting foundation and adjacent panels were Teflon coated to minimize friction. In this first study, eight full-scale crash tests were conducted using various sizes of passenger cars and buses. In the second such study *(13)*, a new wall with a height of 2.29 m (90 in.) was constructed using similar design details, and crash tests with a variety of trucks (up to and including a 36,300 kg (80,000 lb) tractor with tank-type trailer) were conducted. Speeds in these tests ranged from 80.5 km/h (50 mph) to 69.6 km/h (60 mph) and the impact angles ranged from 15 degrees to 25 degrees.

The data from the instrumented wall tests were analyzed to determine the resultant magnitudes, locations, and distributions of the contact forces. Maximum forces were obtained by averaging the data over 0.05 second (sec) intervals to reduce the effect of force "spikes" in the data that were believed to have little consequence to the required structural integrity of the bridge railings due to their short duration. Two forces were determined for each test – one

associated with the initial impact of the front corner of the vehicle, and one associated with the second impact or "backslap" as the rear of the vehicle rotates (yaws) into the rail as it is redirected. An example is shown in Figure 2.7.

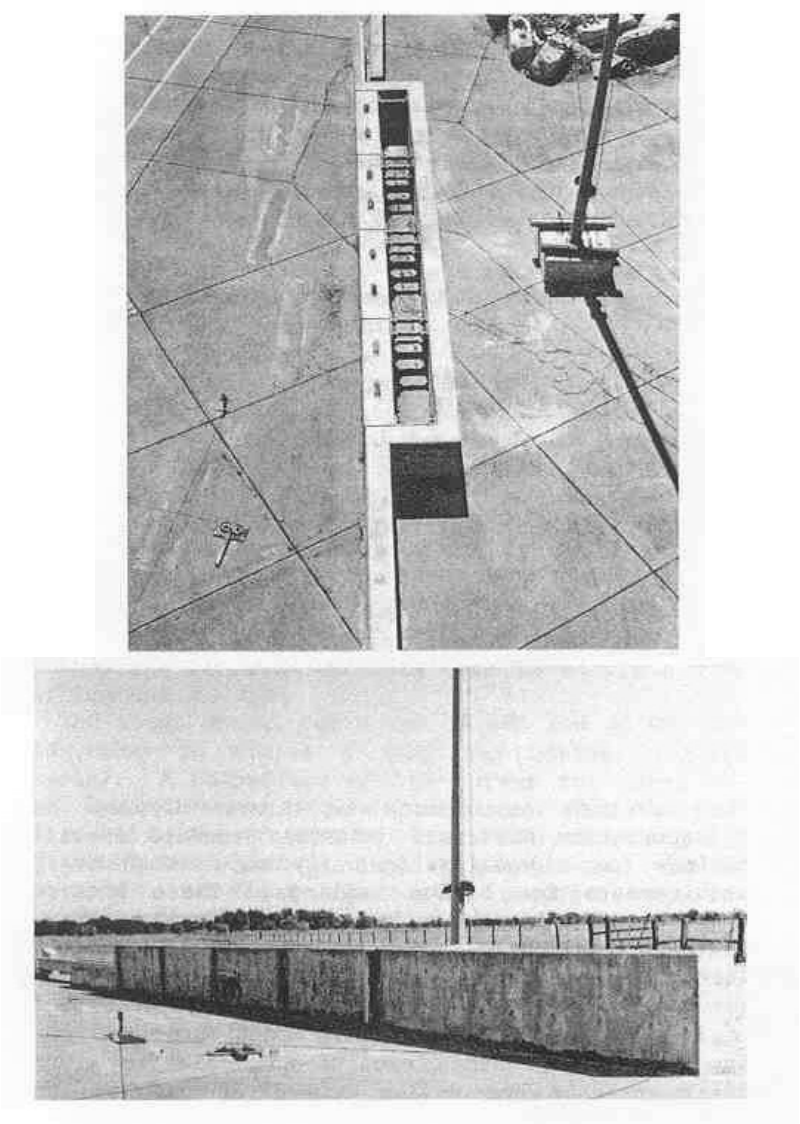

Figure 2.6 Instrumented wall *(12)*

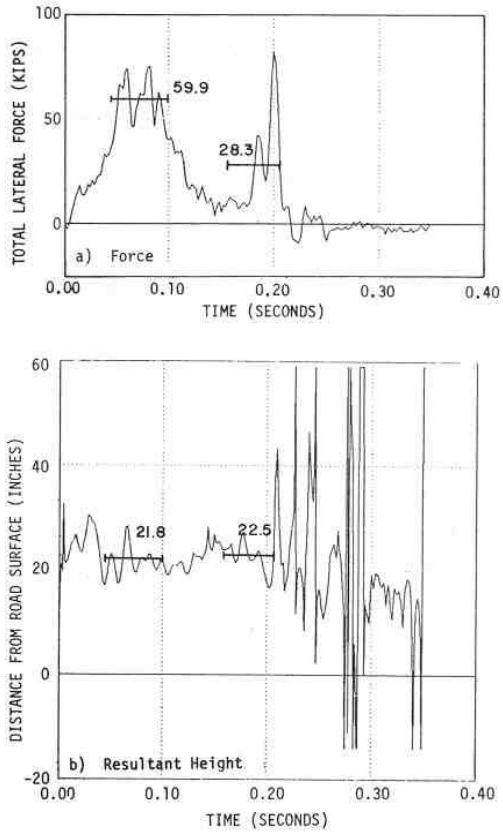

Figure 2.7 Magnitude and location of average resultant force *(12)*
(4,740-lb vehicle, 60 mph, 24 deg.)

The pressure of these resultant forces was assumed to be distributed as half a sine wave in both the horizontal and vertical directions (see Figure 2.8). The length of the contact area was measured from high-speed film. An example of the longitudinal distribution obtained in this manner is shown in Figure 2.9. It should be noted that the force measurements were obtained from a nearly rigid barrier and, therefore, are considered to represent the upper bound of forces that would be expected on an actual bridge railing. Any deformation of the bridge rail during impact will tend to reduce the magnitude of the impact forces below those obtained on the "nearly rigid" instrumented concrete wall.

Data from the instrumented wall studies was used to derive barrier design loads for various impact conditions included in the AASHTO Guide Specification for Bridge Rails *(14)* and subsequently, the AASHTO LRFD Bridge Design Specifications: Chapter 13 – Railings *(1)*.

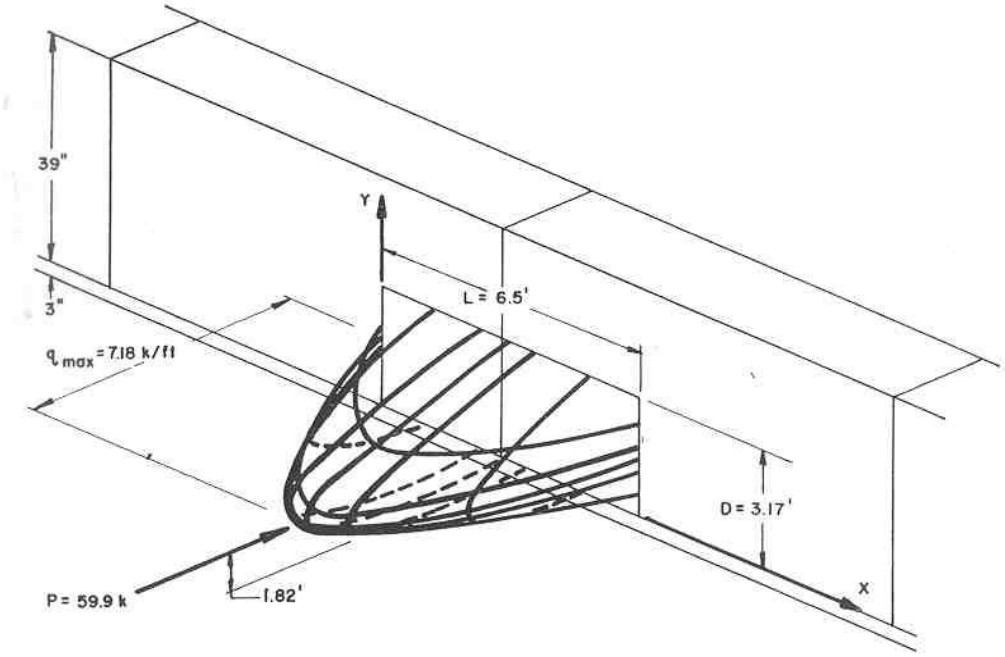

Figure 2.8 Distribution of contact pressure *(12)*

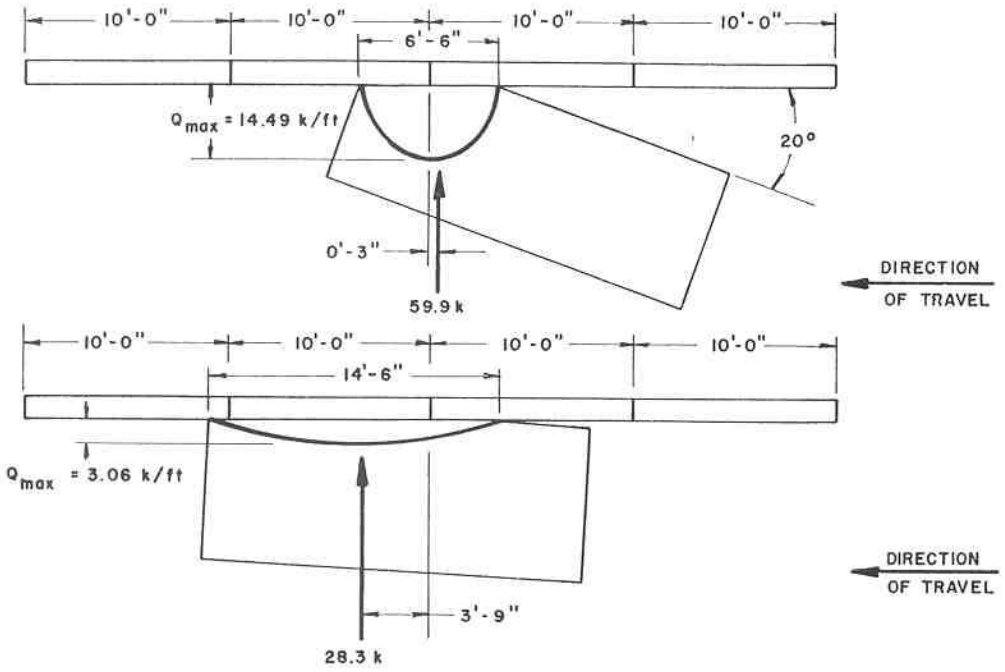

Figure 2.9 Longitudinal distribution for initial and final impacts *(12)*
(4,740 lb vehicle, 60 mph, 24 deg.)

2.2.3 Barrier Design Practice

As previously mentioned, the AASHTO Standard Specifications for Highway Bridges *(1)* specifies an elastic, allowable stress analysis methodology for designing bridge rails using a static load of 4,536 kg (10,000 lb) distributed among the various rail elements. These requirements have existing since their adoption in the 9th edition of the AASHTO Standard Specifications for Highway Bridge *(10)* in 1965.

It can be observed that measured dynamic impact forces obtained from full-scale vehicle crash tests into an instrumented concrete wall are significantly higher than static loads used in the design of bridge rails for passenger cars. Yet, this does not necessarily mean that railings designed for a static load of 4,536 kg (10,000 lb) following the AASHTO Standard Specifications for Highway Bridges are inadequate. This is because a railing system will generally have an ultimate strength well above that indicated by allowable stress design procedures. However, the amount of reserve capacity will vary depending on materials and design details, and is not predicted when allowable stress design methods are used. Ultimate strength design procedures provide a more accurate indication of the actual strength of a rail.

In 1984, Buth et al. *(15)* recommended that bridge rails be designed based on ultimate strength procedures using yield strength of the material with a factor of safety equal to 1.0. The capacity determined in this manner is compared to the dynamic impact loads determined from data measured in the instrumented wall testing programs. Such a design procedure is intended to produce yielding, but not ultimate failure/fracture when a design impact collision occurs. This premise should hold true provided the materials and structural elements have sufficient ductility and ultimate strength substantially greater than yield strength.

Such analyses are based on bending moments induced in the structure and the formation of plastic hinges at points of high bending moment. Thus, the failure mechanism of the rail must be known or assumed. The failure mechanism and the number of posts involved in the mechanism are dependent on how the load applied by the vehicle is distributed to the system. Investigation of several different failure mechanisms for a given rail system is typically required to determine the controlling mechanism (i.e., the mechanism that develops at the lowest load). One-span, two-span, and three-pan failure mechanisms are idealized in

Figure 2.10. The validity of an ultimate strength failure mechanism requires the structure to be able to deform enough to actually develop the failure mechanism.

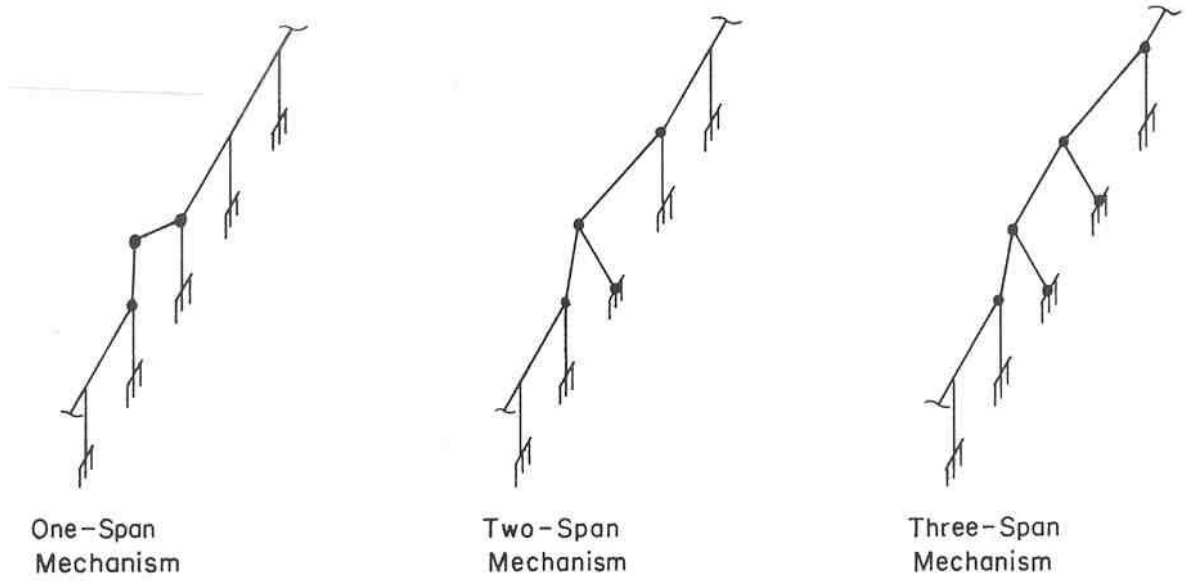

Figure 2.10 Idealized span based failure mechanisms *(15)*

Ultimate strength design procedures were widely used by roadside safety researchers in the 1980s to develop bridge rails capable of containing buses and trucks. In most cases, the impact performance of the rails was verified through full-scale crash testing. In 1989, these procedures were incorporated into the AASHTO Guide Specification for Bridge Rails. This specification prescribed three performance levels for bridge rails and warrants for their use. The test matrices associated with these performance levels included tests with trucks which, up to this time, had not been given consideration in testing documents such as NCHRP Report 230.

Impact conditions associated with Performance Level 1 (PL-1) included a 2,500 kg (5,400 lb) pickup truck impacting at a speed of 72.4 km/h (45 mph) and an angle of 20 degrees. For PL-2, the speed of the pickup truck test was increased to 96.5 km/h (60 mph) and a test with an 8,165 kg (18,000 lb) single unit truck impacting the barrier at a speed of 80.5 km/h (50 mph) and an angle of 15 degrees was added to the test matrix. The highest performance level, PL-3, incorporates a test with a 22,680 kg (50,000 lb) van-type tractor trailer impacting the barrier at a speed of 80.5 km/h (50 mph) and an angle of 15 degrees. The

design impact loads prescribed for each performance level were determined based on data measured in the previously described instrumented wall crash tests *(12) (13).*

In 1993, NCHRP Report 350 was published. This report contains six test levels for longitudinal barriers. Test levels 1 through 3 relate to passenger vehicles and vary by impact speed. Test levels 4 through 6 retain consideration of passenger cars, but also incorporate consideration of trucks. The impact conditions of TL-4 in NCHRP Report 350 are similar to those associated with PL-2 in the 1989 AASHTO Guide Specification for Bridge Rails. TL-4 is the test level used by most states to qualify the impact performance of their bridge rails - a fact that may be a hold over from prior use of the 1989 AASHTO Guide Specification for Bridge Rails.

Ultimate strength design procedures were subsequently adopted in the 1st edition of the AASHTO LRFD Bridge Design Specifications published in 1996 *(16)*. Rather than perpetuate two sets of impact performance criteria, the test levels of NCHRP Report 350 were adopted over the performance levels of the 1989 AASHTO Guide Specification.

Chapter 13 "Railings" of the AASHTO LRFD Bridge Design Specifications applies to the design of railings for bridges. Yield line theory considers the plastic strength of all the railing system components with consideration given to barrier geometry, material strengths, applied loading, and strength of the supporting bridge structure. Steel rail systems, concrete rail systems or a combination rail comprised of a steel rail on a concrete parapet can be evaluated using these design procedures. Based on the yield line theory, the limiting ultimate capacity of the railing system is calculated. This ultimate capacity is then compared to design forces derived from vehicular loads measured in actual crash testing.

Typically, capacities of the railing system are calculated at both mid-span of the railing system and at a joint or end of the rail system. The controlling yield line failure mechanism for a vertical concrete parapet loaded at mid-span is shown in Figure 2.11. The failure mechanism for loading at a joint or end is theoretically similar, but involves only a single "hinge" as shown in the illustration presented in Figure 2.12. For safety-shaped barriers, such as the New Jersey (N.J.) and F-shape barriers, the hinges or failure planes are often isolated in the upper, narrower portion of the barrier as shown in Figure 2.13. *(17)*

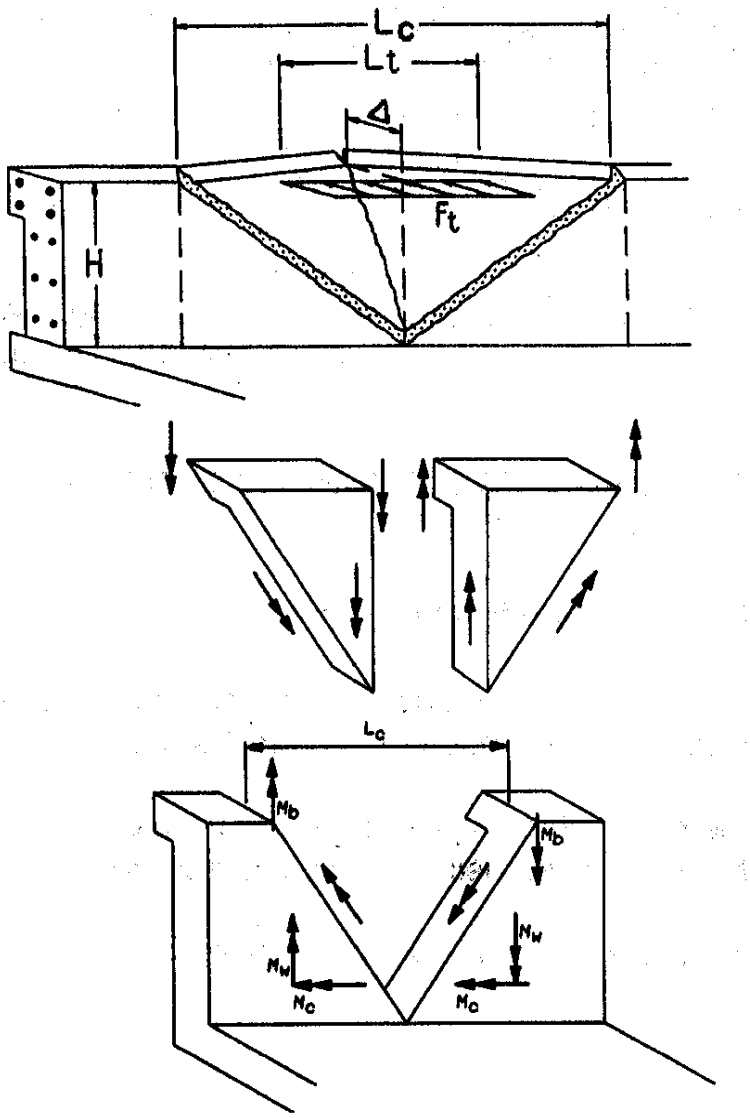

Figure 2.11 Idealized mid-span failure mechanism (*1*)

Post-and-beam types of bridge parapets are fabricated from concrete, structural steel or aluminum components, or a combination of these materials. Failure mechanisms in post-and-beam parapets can occur in several different modes. As the name implies, the impact loads must be transferred to the deck through discrete posts rather than through a continuous rail section. This can result in higher concentrations of load that can result in severe localized damage to the deck or slab if not properly designed.

The calculated ultimate strength or capacity of the rail is then compared to applicable design forces to assess its structural adequacy. The prescribed impact loads for different test

levels are presented in Table A13.2-1, Chapter 13 of the AASHTO LRFD Bridge Design Specifications. The loads are considered to be short duration, one-time loads. The barrier is sized such that it will have an ultimate strength, based on a yield line analysis that is equal to or greater than the specified load with no "factor of safety."

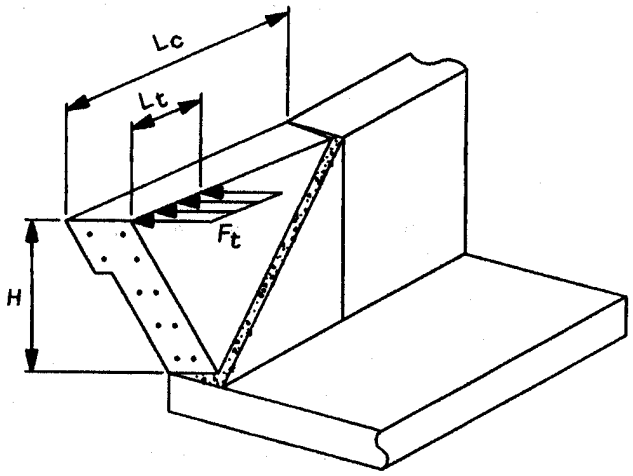

Figure 2.12 Failure mechanism at barrier joint or end *(1) (17)*

Figure 2.13 Typical failure pattern for safety-shaped barriers *(17)*

2.3 Design of the Barrier On Top of the MSE Wall

AASHTO Allowable Stress Design (ASD) and LRFD *(1)* use the same basic procedure to design a barrier on top of a MSE wall even though the impact specification was increased from 44.5 kN (10 kips) to 240 kN (54 kips) for the design of the traffic barrier. This section summarizes the current AASHTO LRFD design procedure for barriers mounted on the edge of MSE walls, compares the AASHTO ASD and LRFD procedures, and describes previous test results.

2.3.1 Design of MSE Wall for Barrier Impact

In AASHTO LRFD the following equation is used to calculate the load T expected in each strip due to the soil weight and the impact load:

$$T = A_t \times \left(\sigma_h + \Delta\sigma_{h,\max}\right) \tag{2-3}$$

where A_t is the panel tributary area of one strip, σ_h is horizontal stress due to the soil weight ($\sigma_h = K_r \times \sigma_v$), K_r is the horizontal earth pressure coefficient given by 1.7 K_a, $\Delta\sigma_{h,\max} = 2P_{h1}/l_1$ is the horizontal stress due to the impact load P_{h1} on the barrier, and l_1 is the depth of influence of the impact load down the wall face as shown in Figure 2.14.

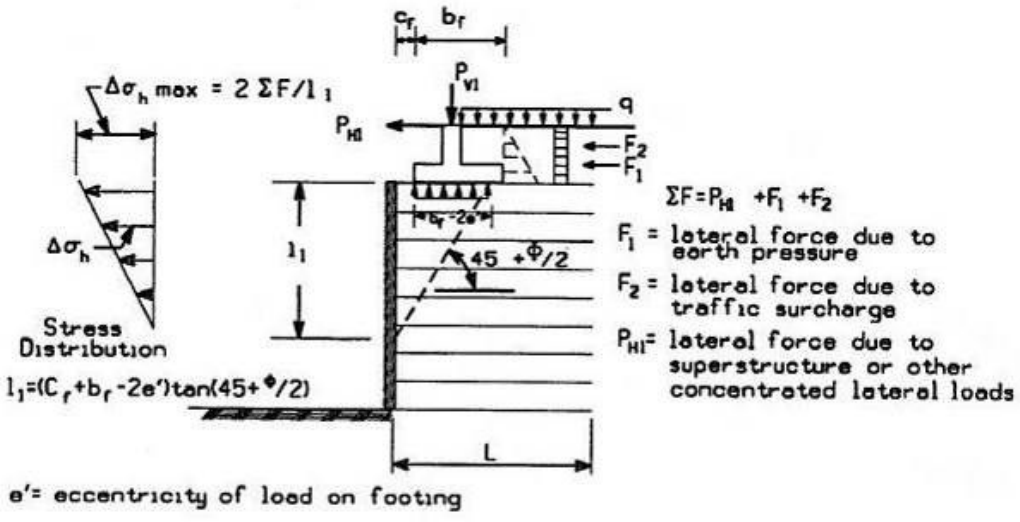

Figure 2.14 Distribution of stress from concentrated horizontal loads (AASHTO LRFD Figure 3.11.6.3-2 a) (*1*)

2.3.2 Comparison between ASD and LRFD

AASHTO is in the process of changing from ASD to LRFD. The 2002 AASHTO ASD makes use of a 44.5 kN (10 kips) load for the design of the traffic barrier and for the impact load that is distributed into the MSE wall below (in the form of added load for the reinforcement). The 2004 AASHTO LRFD specifies a 240 kN (54 kips) design load (corresponding to TL-3 and TL-4) for the traffic barrier and a 44.5 kN (10 kips) load for the design of the MSE wall. Therefore, there has been a significant increase in the design load for the barrier.

The 240 kN (54 kips) load level comes from measurements made on an instrumented barrier during impact, and therefore, is a dynamic load. The increase from 44.5 kN (10 kips) to 240 kN (54 kips) for the structural design of the barrier does not increase the size of the barrier significantly because the 44.5 kN (10 kips) load is used with an elastic design analysis while the 240 kN (54 kips) load is used with an ultimate strength analysis.

However when it comes to the moment slab design, the change from 44.5 kN (10 kips) static to 240 kN (54 kips) dynamic requires a proportional increase in the width of the moment slab if the 240 kN (54 kips) is used as a static load in the stability analysis of the barrier system. Indeed one would calculate a 1.37 m (4.5 ft) wide moment slab with AASHTO ASD and a 1.37 m (4.5 ft) x 54/10 = 7.4 m (24.3 ft) wide moment slab with AASHTO LRFD. This arises from the fact that 54 kips is taken as a static load when in fact it is a dynamic load. From experience, a 7.4 m (24.3 ft) wide moment slab would be unreasonably conservative. The objective is to find out how to take into consideration the 240 kN (54 kips) for overturning and sliding of the barrier.

The design of the barrier against overturning consists of applying the load to the barrier at the prescribed height and then using moment equilibrium to find out how wide the moment slab has to be while satisfying a factor of safety against overturning equal to 2. This factor of safety of 2 is consistent with the requirement for overturning of an MSE wall but is not explicitly written in the AASHTO ASD for overturning of barriers..

The design of the barrier against sliding consists of applying the load to the barrier and then using horizontal equilibrium to find out how wide the moment slab has to be while satisfying a factor of safety of 1.5. This factor of safety of 1.5 is consistent with the

requirement for sliding of an MSE wall but is not explicitly written in the AASHTO ASD for sliding of barriers.

In LRFD, the recommendations are not as detailed. The load factor γ is taken as 1.0 for the load combination of Service I and the resistance factor for sliding as 0.8 for cast-in-place concrete on soil. There are no recommendations for the resistance factor against overturning.

2.3.3 Previous Crash Test of Barrier on Edge of MSE Wall

In 1982, Terre Armee Internationale (TAI), which is closely related to the Reinforced Earth Company (RECO) in the U.S., performed a crash test of a barrier on top of an MSE wall (*18*). The test vehicle was a 12,020 kg (26,500 lb) bus which impacted the barrier at a speed of 19.7 km/h (44 mph) and an angle of 20 degrees, and. The impact severity was estimated to be 30% larger than the AASHTO PL-2 (*19*) loading condition.

The barrier was a N.J. shape barrier approximately 81.3 cm (32 in.) high as shown in Figure 2.15. The barrier reinforcement was minimal, consisting of two longitudinal No. 4 bars. The precast barrier units were 1.52 m (5 ft) long and tied to the moment slab through rebars. The moment slab was cast in place with a joint every 9.15 m (30 ft). The width of the moment slab was 1.25 m (4.1 ft), and its thickness was 25.4 cm (10 in.). The 25.4 cm (10 in.) of cover over the moment slab consisted of compacted soil and a layer of bituminous mix.

The MSE wall was 3.05 m (10 ft) high with two rows of 1.52 m (5 ft) tall panels. The reinforcement strips were 5 m (16.4 ft) long and the layers of strips were located at depths of 38 cm (15 in.) and 1.14 m (45 in.) below the bottom of the moment slab (best guess) and were 76.2 cm (2.5 ft) apart in the horizontal direction (best guess). A horizontal gap of 1.9 cm (¾ in.) was purposely left between the coping and the traffic face of the wall panels to avoid lateral contact with the wall panel during impact. Figure 2.16 shows the cracking on the front and back side of barrier after the crash test.

The test was considered successful. The bus was redirected and stayed upright. The barrier was damaged but the wall and the moment slab were not damaged. The upper part of the barrier was broken over a length of 2.2 m (7.2 ft) and a height of 50.8 cm (20 in.). The top panel of the wall moved 5 mm (0.19 in.) dynamically during the event and had 1.5 mm (0.06

in.) of residual movement after the impact. The bottom panel did not move. No wall damage occurred. The maximum deceleration on the front and rear axles of the bus was 8g (moving average) and 14g, respectively. The maximum dynamic force recorded on the most loaded strip was 28.91 kN (6.5 kips).

Figure 2.15 Precast barrier and coping with cast-in-place slab (*18*)

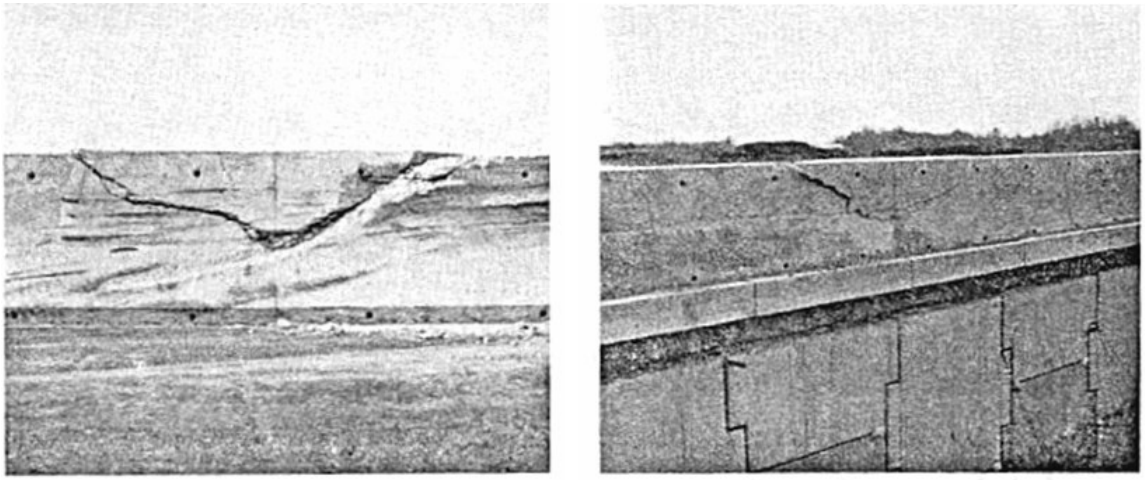

Figure 2.16 Barrier damage after RECO crash test (*18*)

The minimum reinforcement density for MSE walls gives a resistance of 42.3 kN/m (2.9 kips/ft) of wall at the top layer of strips. Pulling the strips out of the wall would require movement of the moment slab unit. For a joint spacing of the moment slab equal to 6.1 m (20 ft), the maximum load that the strips can resist at impact is 6.1 m (20 ft) × 42.3 kN/m (2.9 kips/ft) = 258 kN (58 kips) (static). The 1982 TAI test leads to a load of 28.91 kN (6.5 kips) × 6.1 m (20 ft) / 0.76 m (2.5 ft) = 231.3 kN (52 kips) (dynamic) if all strips within the 6.1 m (20 ft) section of barrier and moment slab were stressed at the maximum observed value. 258 kN (58 kips) (static resistance) is much higher than the 44.48 kN (10 kips) (static) required by AASHTO. Therefore, RECO concluded that the minimum reinforcement density is adequate to resist the impact load.

2.4 Survey of State DOTs

A comprehensive survey of the Nation's state transportation departments was conducted to obtain information regarding the design, construction, and performance of barriers mounted on top of MSE walls. Major categories of the survey included: MSE Walls, Barriers, Barrier Connection to Wall/Pavement, Design, and Performance. A total of 18 states responded to the survey: Alaska Department of Transportation (DOT) & PF, Arizona DOT, Arkansas Highway & DOT, Connecticut DOT, Georgia DOT, Hawaii DOT, Illinois DOT, Kansas DOT, Maryland State Highway Admin., Minnesota DOT, Mississippi DOT, Nevada DOT, NYS DOT Structures, Texas DOT, South Carolina DOT, Utah DOT, Washington State DOT, and WisDOT. The blank survey instrument is shown in Appendix B.

The data reduction of these responses is provided in two manners: 1) a weighted average based on the percent usage indicated by each state that provides an indication of national usage of different alternatives within a given category (herein referred to as *Weighted Percentage of Usage from Responding States*), and 2) an indication of the number of states indicating usage in a certain category (herein referred to as *Number of States Responding Positive Usage*). For example, in the MSE wall section of the survey, the respondents were not only asked if they use a certain type of wall reinforcement in their state, but also what percentage of each type of reinforcement is used. The percent usage (e.g., 45% steel strips, 45% bar mats, 10% geosynthetics) is used to compute a weighted average for all respondents

and is presumably indicative of average usage across the country. Additionally, the number (and corresponding percentage) of states indicating use of a given type of reinforcement is reported. Note that in the above example, the respondent indicated use of all three types of wall reinforcement and, therefore, positive usage would be indicated for each. When appropriate, the data has been presented in the form of pie charts for easier visualization of the responses. The survey question associated with each chart is provided for reference purposes. Certain data is presented in tables and/or in a written format.

2.4.1 MSE Walls

The survey section on *Mechanically Stabilized Earth Walls* includes questions regarding the percentage of the type of reinforcement, the type of facing panels, and type of barrier connections used in MSE walls in the responding state. Figure 2.17 through Figure 2.19 present the results for this survey section in the *Weighted Percentage of Usage from Responding States* format. Figure 2.17 indicates that approximately 57% of the MSE walls constructed within the responding states utilize steel strips as the means of reinforcement. This is followed by steel bar mats (24%) and geosynthetic grids (18%).

As shown in Figure 2.18, 80.7% of MSE wall construction incorporates concrete panels, while 19% are comprised of modular blocks. Entries made by responding states in the 'other' category for facing panel types noted use of wire-face walls, cast in-place concrete walls, Gabion/exposed rock, and two-stage walls. In regard to the type of panel-to-panel connections utilized in MSE walls, Figure 2.19 indicates the majority (55%) use dowels, followed by tongue-and-groove (16%), and ship-lap (12%) connections. In the 'other' category for facing panel connection type, states noted use of cast-in-place clips, friction or mesa, block lip, modular blocks, and RECO-lap. It should be noted that Georgia indicated 100% usage for both dowels and ship lap, and dowels were used in the analyses presented herein.

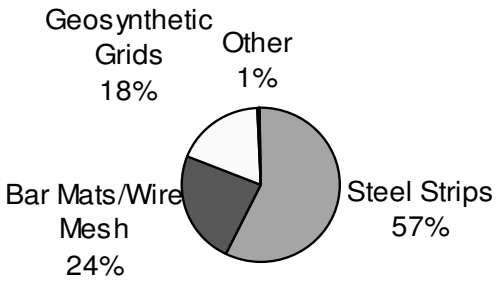

Figure 2.17 Type of reinforcement in MSE walls (Question 1)

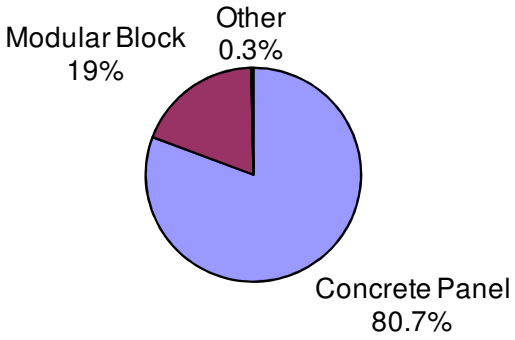

Figure 2.18 Type of facing panels in MSE walls (Question 2)

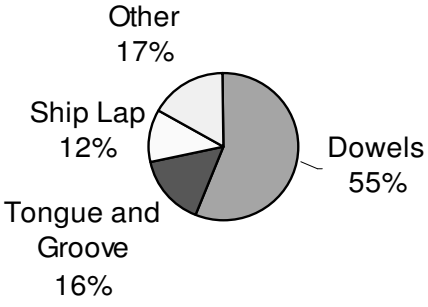

Figure 2.19 Type of facing panel connection (Question 3)

2.4.2 Barriers

The survey section for *Barriers* included questions regarding the percentage of the category of barrier used on MSE walls, types of guardrail and bridge rail used, and whether the barrier is precast or cast in-place. The survey also asked for the minimum segment length permissible for the precast barrier option. Figure 2.20 through Figure 2.24 present the survey results of eighteen responses for category of barriers, six responses for the type of guardrail, and eighteen responses for type of bridge rail question. Unless otherwise noted, the results are reported in the *Weighted Percentage of Usage from Responding States* format.

As shown in Figure 2.20 (which is presented in the *Number of States Responding Positive Usage* format), 13 of the eighteen states responding to the survey (72%) use only bridge rails atop MSE walls, while 5 states (28%) indicated use of both guardrail and bridge rail. There were no states that only used guardrail on MSE walls. When weighted averages of use are computed (see Figure 2.21), the results indicate that 90% of the MSE walls constructed with barriers on top utilize some type of bridge rail connected to a moment slab or pavement, while only 10% of such installations use guardrail mounted on soil-embedded posts.

Figure 2.22 shows the type of guardrail used by the six states indicating use of guardrail on MSE walls in Question 4 of the survey. Strong post W-beam is used 56% of the time, followed by box beam (18%), weak post W-beam (16%), and thrie beam (10%). The median offset from the edge of the MSE wall reported for post-mounted guardrail was 3 ft.

As mentioned earlier, all states responding to the survey indicated use of some percentage of bridge rail atop MSE walls. As indicated by the weighted averages shown in Figure 2.23, the vast majority (91%) of such installations incorporate some form of concrete safety shape barrier (e.g., N.J., F-shape). This is followed by vertical concrete parapets (6%) and concrete parapets combined with a steel railing (2%).

Figure 2.24 provides information regarding precast versus cast-in-place construction practices followed by the responding states. 76% of barrier construction on MSE walls uses cast-in-place coping and barrier. Precast coping and barrier segments are used 16% of the time, while use of a precast coping with cast-in-place barrier is limited to 8%. The median

minimum segment length for the six states indicating use of precast barrier segments was 4.57 m (15 ft).

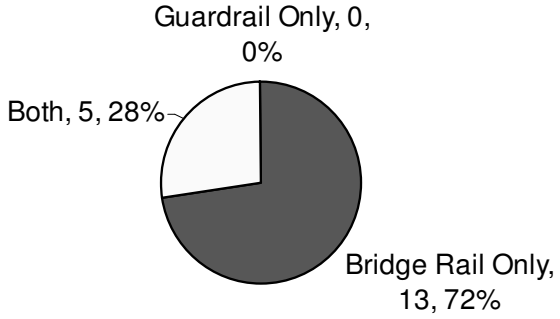

Figure 2.20 Percentage of states using different barrier categories (Question 4)

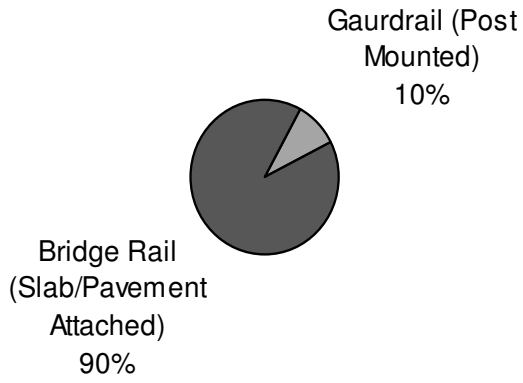

Figure 2.21 Category of barriers (Question 4)

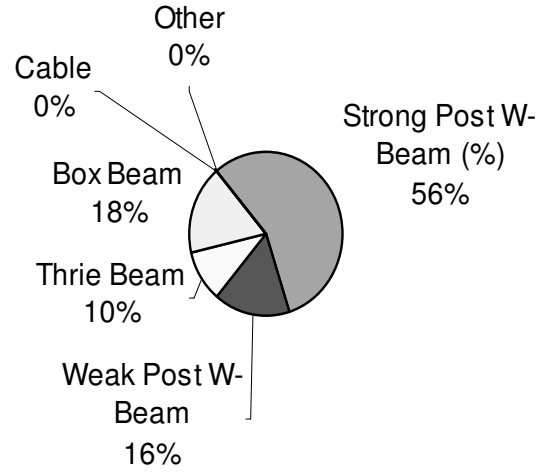

Figure 2.22 Type of guardrail (Question 5)

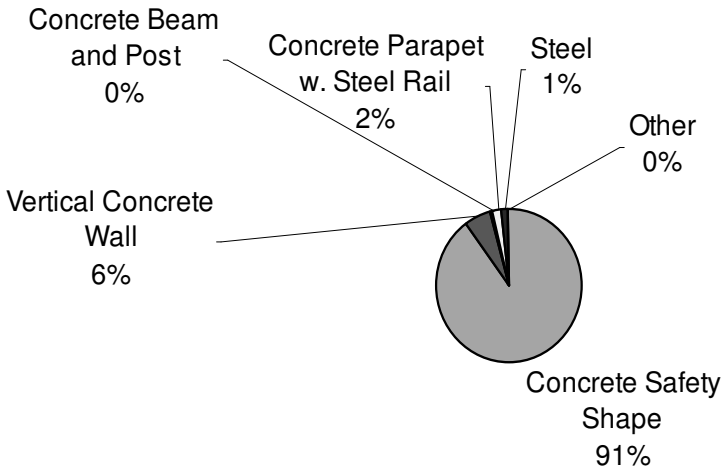

Figure 2.23 Type of bridge rail (Question 6)

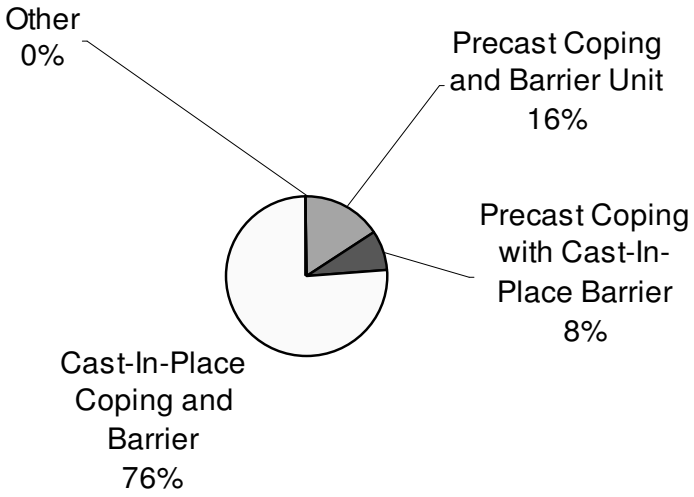

Figure 2.24 Precast barrier vs. cast-in-place barrier (Question 7)

2.4.3 Barrier Connection to Wall/Pavement

The survey section dealing with the *Barrier Connection to Wall/Pavement* included questions regarding the percentage of the different types of pavement used on top of MSE walls, the offset of post-mounted guardrails from the edge of the wall, and a series of questions specific to asphalt-concrete pavement (ACP) and reinforced-concrete pavement (RCP) applications. As shown in Figure 2.25 (which is presented in the *Number of States Responding Positive Usage* format), 11 of 17 states responding to this question (64%) use both RCP and ACP on MSE walls. Four states (24%) indicated use of only RCP, while

another 2 states (12%) use only ACP on MSE walls. When weighted averages of use are computed (see Figure 2.26), the results indicate a nearly 50-50 split between asphalt and reinforced-concrete pavement applications in regard to MSE wall construction.

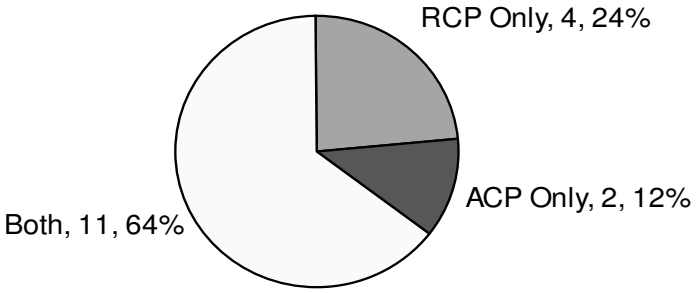

Figure 2.25 Use of different pavement types on MSE walls (Question 9)

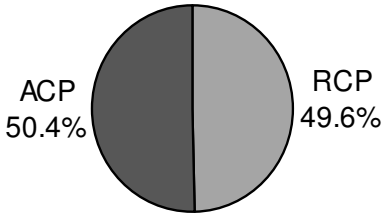

Figure 2.26 Pavement type (Question 9)

For slab attached bridge rails, the *Barrier Connection to Wall/Pavement* section of the survey is divided into asphalt concrete pavement and reinforced concrete pavement applications. Due to the nature of these questions, the results are reported using the *Number of States Responding Positive Usage* format. The survey responses related to the use of ACP on MSE walls with barriers are presented in Figure 2.27 through Figure 2.30. Supporting information for some of these questions and figures is presented in Table 2.1.

With reference to Table 2.1 (Question 11), the median thickness of the moment slab for MSE wall applications with ACP is 34.3 cm (13.5 in.). The median length of the moment slab used by the responding states is 6.5 ft (Table 2.1, Question 12). Figure 2.27 (which is based on survey Question 13) indicates that 50% of the responding states use continuous

barrier slabs and 50% use jointed barrier slabs. Those states indicating use of jointed slabs were asked a follow-up question regarding joint spacing. The median response, shown in Table 2.1 (Question 14), was 6.1 m (20 ft). The mean, standard deviation, median, and number of responses are reported for all such questions in which length or distance was requested. It should be noted that if the state responded in Metric units, the value was converted to English units, and when ranges were reported, an average value was used when computing the descriptive statistics mentioned above.

As shown in Figure 2.28, 67% of responding states report they offset their barriers from the face of the MSE wall and 33% install the barrier flush with the MSE wall. As shown in Table 2.1 (Question 16), the median barrier offset for those states that practice offsetting the barrier from the face of the MSE wall is only 13.97 cm (5.5 in.).

Figure 2.29 indicates that 92% of responding states recess the top wall panel into the bottom of the coping. This practice is followed to provide support for precast coping and barrier sections prior to their connection to cast-in-place slabs and as an aesthetic treatment to cover the "steps" in the panels along the top edge of the wall. The median distance that the top wall panel is recessed into the coping is 21.59 cm (8.5 in.). (see Table 2.1, Question 18). Additionally, 85% of states responded that lateral and vertical movement of the barrier system is isolated from the wall panels (see Figure 2.30).

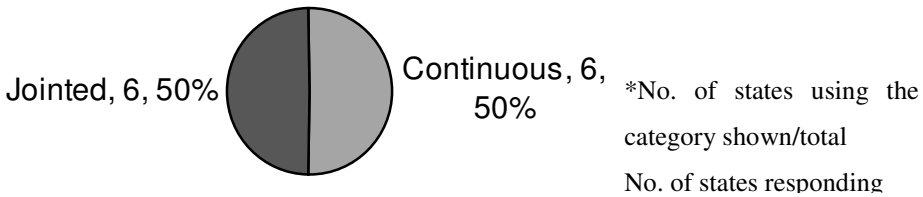

Figure 2.27 Continuous or jointed barrier slab/footing (ACP, Question 13)

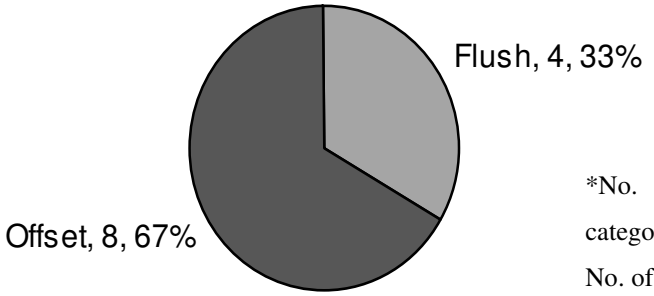

*No. of states using the category shown/total No. of states responding

Figure 2.28 Barrier flush or offset from face of wall (ACP, Question 13)

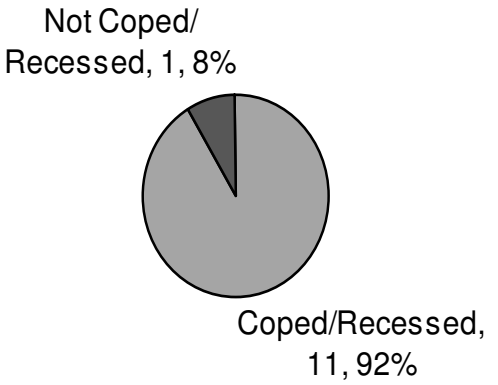

*No. of states using the category shown/total No. of states responding

Figure 2.29 Wall panel coped/recessed (ACP, Question 17)

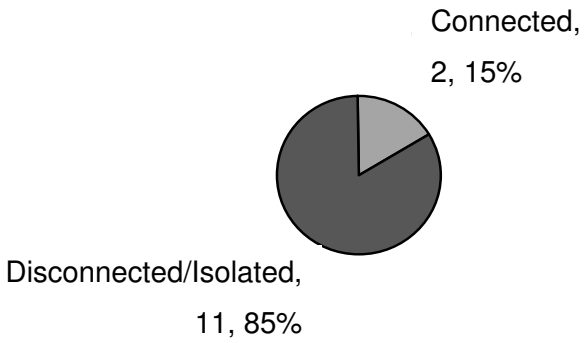

*No. of states using the category shown/total No. of states responding

Figure 2.30 Lateral and vertical barrier movement connected or disconnected/isolated from wall panel (ACP, Question 19)

Table 2.1 Survey Responses Related to MSE Walls with ACP

Survey Question No,	Description	Mean	Standard Deviation	Median	No. of Responses
(11)	Thickness of Barrier/Slab Footing (in)	15.0	4.2	13.5	12
(12)	Width of Slab/Footing (ft)	6.6	1.8	6.5	11
(14)	Joint spacing (ft)	32.9	28.0	20.0	6
(16)	Barrier offset from face of wall (in)	7.4	9.3	5.5	8
(18)	Wall panel recess distance into bottom of coping (in)	8.4	2.4	8.5	9

Although the percentages are slightly different, the responses obtained for MSE wall applications with RCP show the same trends as the MSE wall applications in which ACP is used. The survey responses related to the use of RCP on MSE walls with barriers are presented in Figure 2.31 through Figure 2.35. Additional information for RCP applications is presented in Table 2.2.

Table 2.2 shows that the median barrier slab thickness (Question 20) and width (Question 21) are 30.48 cm (12 in.) and 2.01 m (6.6 ft), respectively. Figure 2.31 shows that 57% of the MSE walls constructed with RCP incorporate continuous barrier slabs and 43% use jointed barrier slabs. The median joint spacing for those states indicating use of jointed slabs was 6.1 m (20 ft) (see Table 2.2, Question 23).

As shown in Figure 2.32, 60% of responding states report they offset their barriers from the face of the MSE wall, while the remaining 40% install the barrier flush with the MSE wall. The median barrier offset for those states that offset their barriers from the face of the MSE wall is 13.97 cm (5.5 in.). (see Table 2.2, Question 25).

The practice of recessing the top wall panels into the bottom of the wall coping is followed by 80% of the responding states (see Figure 2.33). The median distance that the top wall panel is recessed into the coping is 17.78 cm (7 in.) (see Table 2.2, Question 27). As

shown in Figure 2.34, 83% of states responded that lateral and vertical movement of the barrier system is isolated from the wall panels, while the remaining 17% indicated that the wall panels and barrier system are connected to one another.

A question specific to RCP applications (Question 29) is whether the barrier slab is integrally poured with the concrete pavement or doweled to it. Figure 2.35 shows that 55% of responding states use dowels to connect the barrier slab to the pavement, and 45% follow the practice of integrally casting the slab and pavement.

Table 2.2 Survey Responses Related to MSE Walls with RCP

Survey Question No,	Description	Mean	Standard Deviation	Median	Number of Responses
(20)	Thickness of Barrier/Slab Footing (in)	13.9	4.6	12.0	15
(21)	Width of Slab/Footing (ft)	6.7	1.2	6.6	12
(23)	Joint spacing (ft)	18.8	3.8	20.0	5
(25)	Barrier offset from face of wall (in)	4.9	3.6	5.5	8
(27)	Wall panel recess distance into bottom of coping (in)	6.9	3.8	7.0	11

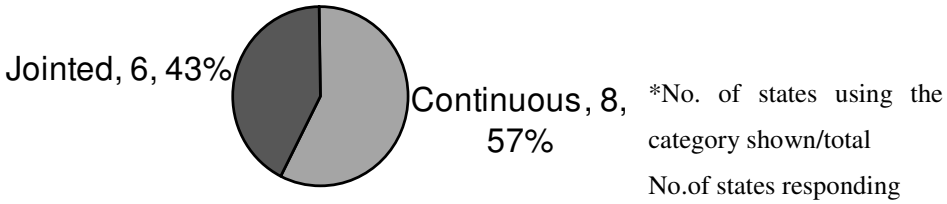

Figure 2.31 Continuous or jointed barrier/slab footing (RCP, Question 22)

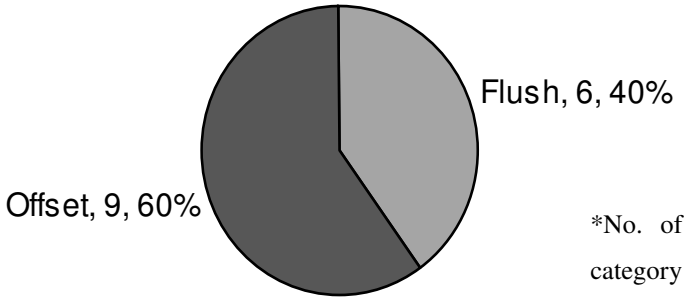

Figure 2.32 Flush or offset barrier from face of wall (RCP, Question 24)

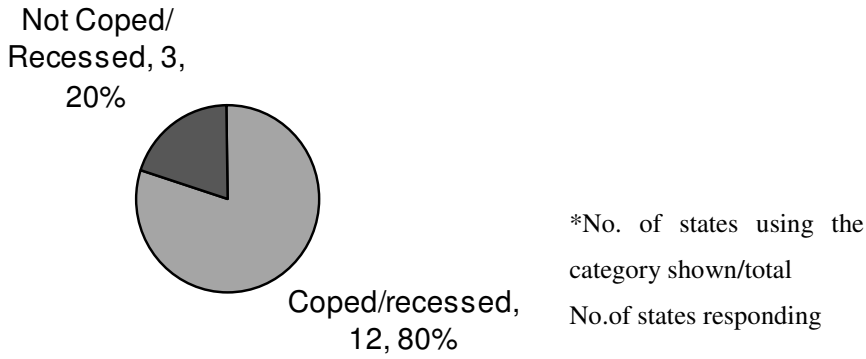

Figure 2.33 Wall panel coped/recessed (RCP, Question 26)

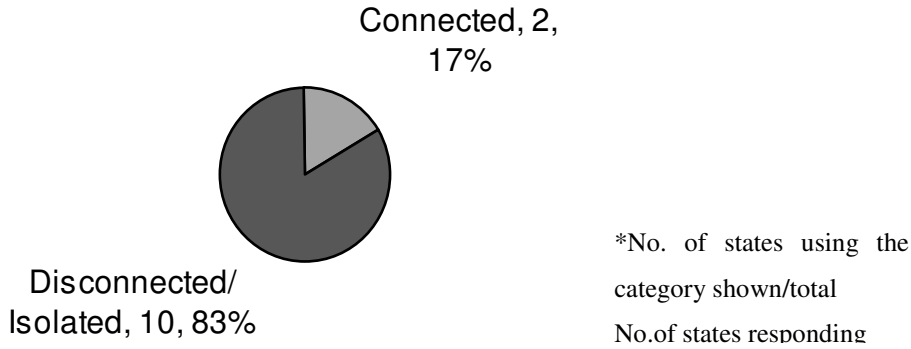

Figure 2.34 Lateral and vertical barrier movement connected or disconnected/isolated from wall panel (RCP, Question 28)

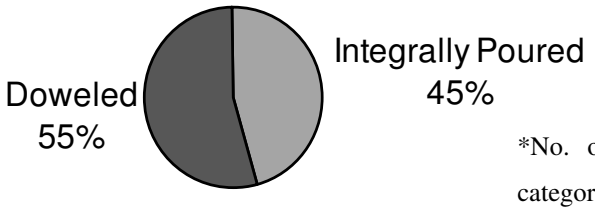

*No. of states using the category shown/total No.of states responding

Figure 2.35 Integrally poured or doweled into pavement (RCP, Question 29)

2.4.4 Design

For the *Design* section of the survey, only a few of the responses can be presented in graphical format. The questions referring to NCHRP Report 350 Test Level (Question 31), adherence to the AASHTO LRFD Bridge Design Specifications (*1*), Chapter 13 'Railings,' for bridge railing design (Question 32), and whether design procedures include calculation of bending moment in the pavement slab due to impact load on barrier (Question 38) are presented below in the *Number of States Responding Positive Usage* format. Question 30 regarding the magnitude of the barrier impact load transferred to the top of the MSE wall was not included in this summary due to the high variation in the numerical value of the responses. The varying responses may have been due to confusion regarding the intent of the question.

As shown in Figure 2.36, 76% of responding states use TL-4 barriers in conjunction with MSE wall applications. TL-3 and TL-5 barriers are both used by 12% of responding states. Figure 2.37 indicates that 58% of responding states use Chapter 13 "Railings" of the AASHTO *LRFD Bridge Specification* for bridge rail design, and 42% do not. It should be noted that compliance with the AASHTO LRFD Bridge Design Specifications is not required if a railing is successfully crash tested. The median impact load and impact location reported by the states specifying they do not follow AASHTO LRFD for bridge rail design are 44.48 kN (10 kips) and 83.82 cm (2.75 ft), respectively (see Table 2.3). Only 41% of responding states reported that they calculate the bending moment in the barrier slab due to vehicular impact load (see Figure 2.38).

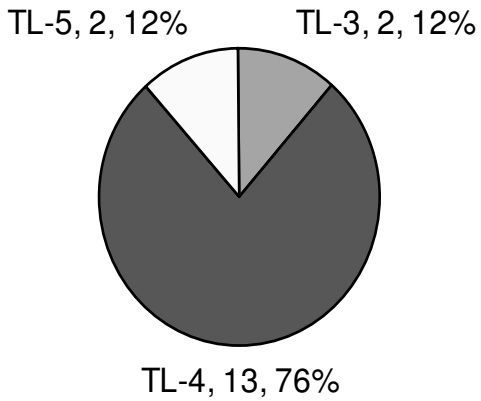

Figure 2.36 NHCRP Report 350 test level

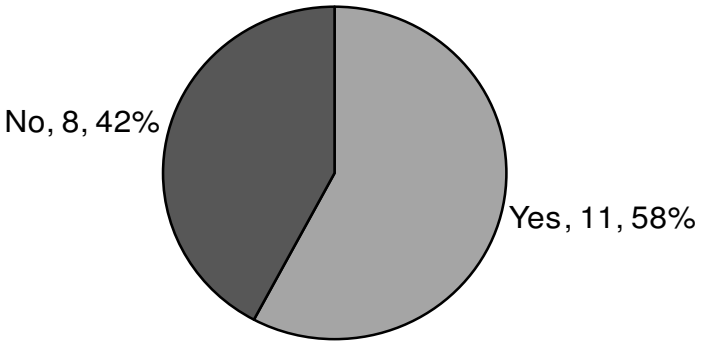

Figure 2.37 Use of *AASHTO LRFD Bridge Specification* for rail design (Question 32)

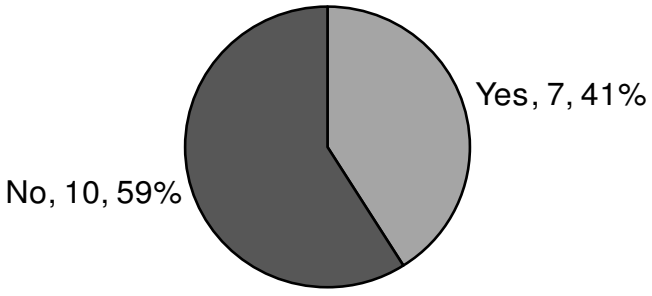

Figure 2.38 Calculation of bending moment in pavement slab due to barrier impact load (Question 38)

Table 2.3 Barrier Design Load and Location

Survey Question No.	Description	Mean	Standard Deviation	Median	No.of Responses
(33)	Magnitude of Barrier Design? (kips)	8.4	3.6	10	5
(34)	Height of the Applied Design Load? (ft)	2.8	0.2	2.75	5

2.4.5 Performance

The last section of the survey, *Performance*, included questions inquiring about the in-service performance and failure history of MSE walls and barriers on top of MSE walls. The survey responses for these questions are presented in Figure 2.39 and Figure 2.40 in the *Number of States Responding Positive Usage* format based on a total of eighteen responses.

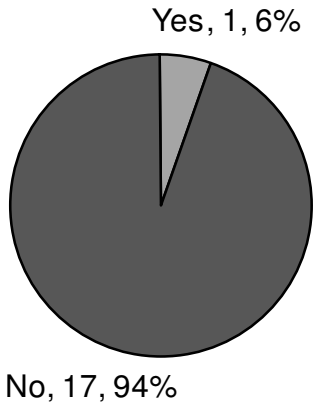

Figure 2.39 Failures of MSE walls or barriers atop MSE walls due to vehicular impact (Question 39)

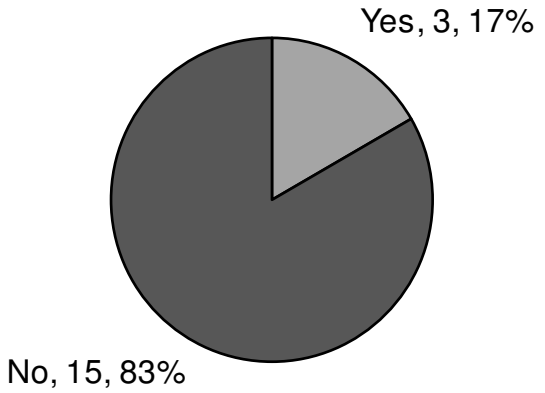

Figure 2.40 Other performance issues associated with MSE walls or barriers atop MSE walls (Question 40)

The only participating agency reporting failure of an MSE wall or barrier atop an MSE wall during vehicular impact was Georgia. Georgia DOT reported that "a semi-tractor trailer knocked off a section of barrier that was lacking strap anchorages." Minnesota, New York, and Washington reported various performance issues and/or design questions associated with MSE walls or barriers atop MSE walls. Minnesota DOT reported they have seen some connection details between the barrier and the slab that are not adequate.

3 BARRIER STABILITY STUDY

Pavements are often built on top of MSE walls. The most common scenario is the case of an MSE wall supporting the access embankment for an overpass. Because cars and trucks travel on top of the MSE wall, traffic barriers are required. In the case of a concrete pavement, these barriers are rigidly tied to the pavement to provide the resistance needed when an impact load is generated by an errant car or truck. In the case of an asphalt pavement, that resistance is not available and the barrier must resist the impact load on its own. In this case a barrier-moment slab system is used (Figure 3.1 and Figure 3.2) and the resistance is generated by the inertia force required to lift the moment slab.

This section discusses only the barrier and moment slab design, not the MSE wall design. A barrier built on top of an MSE wall needs to be designed to satisfy three criteria during impact: 1. the barrier must have sufficient strength to contain the impacting vehicle, 2. the barrier must not overturn, and 3. the barrier must not slide away. This section addresses criterion 2 and 3 by defining the magnitude of the static and dynamic loads that can be resisted by a barrier attached to a moment slab. Both analytical and experimental approaches are used to better understand the behavior of the barrier-moment slab system.

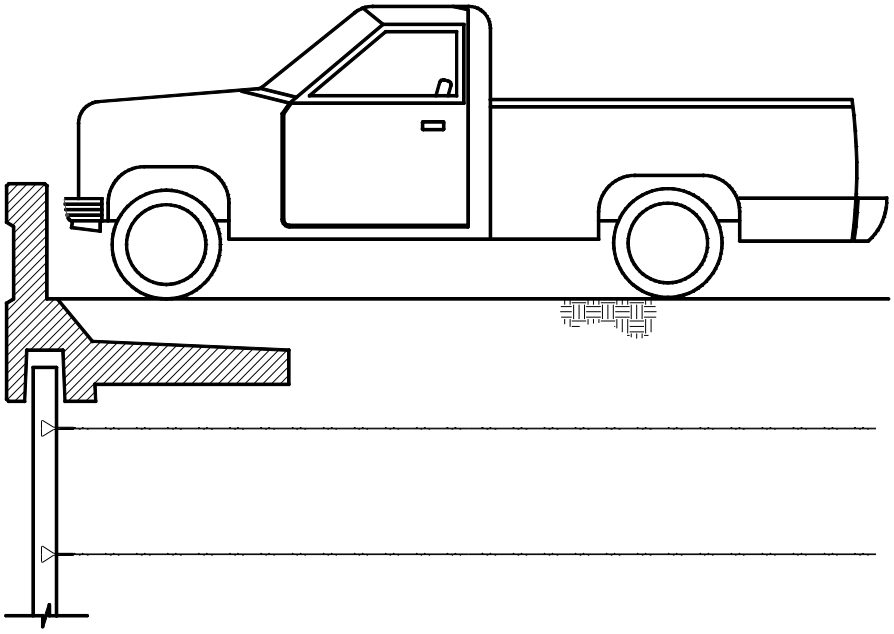

Figure 3.1 MSE retaining wall with a barrier

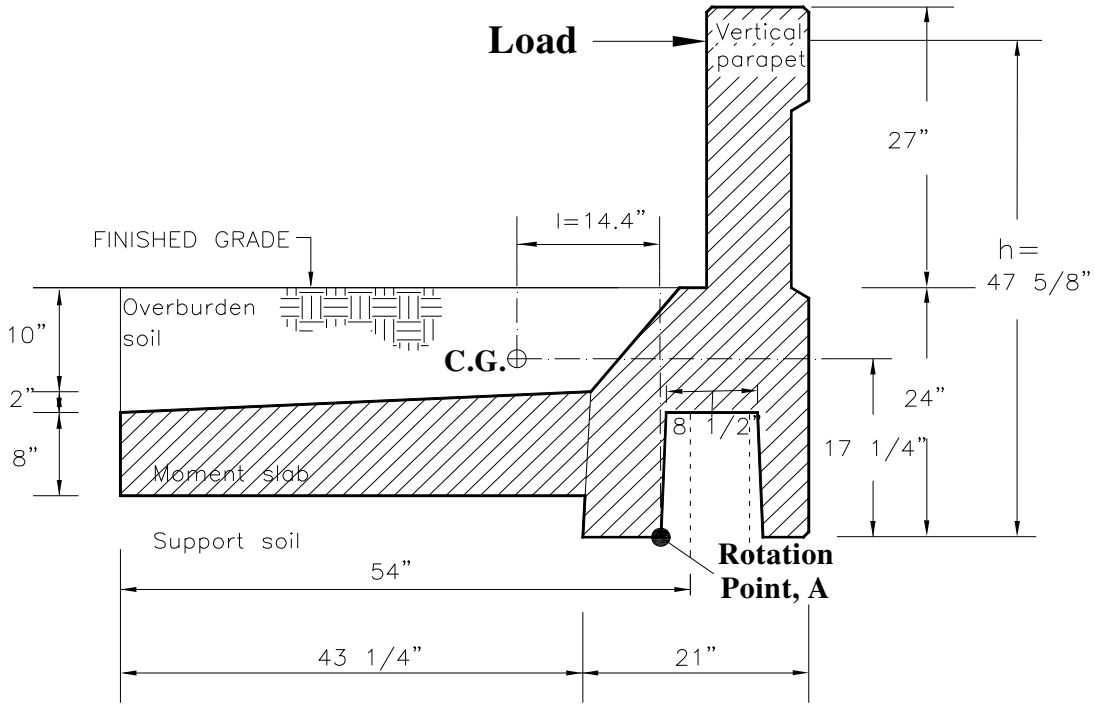

Figure 3.2 Details of the vertical barrier system

3.1 Description of Barrier

The barrier used in the stability study was a TxDOT T201 barrier with a height of 68.6 cm (27 in.) above grade and designed for TL-3 use. Figure 3.2 shows the dimensions of the vertical barrier and coping system as designed by RECO. The strength capacity of this vertical barrier is 325.34 kN (73.14 kips) calculated by ultimate strength analysis. The primary components of the barrier moment-slab system include a precast vertical barrier and coping section and a cast in-place moment slab. The precast vertical barrier is 241 mm (9 ½ in.) thick at the top. The cast in-place concrete moment slab is 1.37 m (4.5 ft) wide measured from the back of the panel to the end of the moment slab. In the field, the moment slab is typically 6.1 m (20 ft) to 9.15 m (30 ft) long between joints. In this study, a smaller 3.05 m (10 ft) long moment slab and barrier section was used so that the desired movement could be imparted to the barrier without structural failure. The precast barrier unit was connected to the cast in place moment slab by 12 No. 6 bars. The reinforcing bars in the moment slab consist of 12 transverse No. 6 bars and 5 longitudinal No. 4 bars.

The center of gravity (CG) of the barrier system including the precast barrier, cast in-place moment slab, and the soil above the moment slab is located as shown on Figure 3.2. The rotation point used for the overturning analysis is at the toe of the coping as shown in Figure 3.2. A concrete pad was placed under the inside leg of the coping so that the point of rotation would be well defined. The outside leg of the coping was unsupported. The moment arm, `l`, is from the CG of the barrier to the rotation point. The point of load application is located near the top of the barrier. The moment arm, `h`, is from the point of application of the load to the point of rotation A.

The moment slab was cast in place on a well graded road base material with a significant amount of fines and particles as large as 50 mm (2 in.). This material was heavily compacted by a hydraulic plate tamper attached to the back of a back-hoe. The dry density and water content of the soil in place were 18.6 kN/m^3 (118.3 pcf) and 7.17 %, respectively.

3.2 Static Analyses and Static Test

The purpose of the static analyses and static test is to explain the behavior of the barrier under static loading and to determine the maximum static force that can be resisted by a barrier in a sliding failure mode and in an overturning failure mode.

3.2.1 Static Analytical Solution

The static analysis for sliding and overturning is conducted using equilibrium equations. The static force F_s required to generate sliding is:

$$F_s = W \tan\phi \quad (3\text{-}1)$$

where W is the weight of the barrier, moment slab, and soil system (69.6 kN or 15.7 kips), $\tan\phi$ is the moment slab - soil friction coefficient, and ϕ is frictional angle of the soil. It is assumed that the moment slab - soil interface is rough enough that the failure plane is in the soil.

The equation for overturning equates the resisting moment and the moment causing overturning due to the applied force. The static force F_o required to generate overturning of the barrier-moment slab assembly is:

$$F_o = W\, l / h \quad (3\text{-}2)$$

where l is the moment arm of the weight of the system (0.369 m or 1.3 ft), and h is the moment arm of the force applied to the system (1.21 m or 3.97 ft) (Figure 3.2). It is assumed that the vertical barrier, moment slab, and overburden soil act as one system for the overturning analysis.

The required static forces F_s and F_o are shown on Figure 3.3 as a function of the length of the barrier – moment slab system. For the 3.05 m (10 ft) length barrier system, the required static force is 46.96 kN (10.6 kips) for sliding and 21.8 kN (4.9 kips) for overturning. Therefore, overturning controls the stability of the barrier.

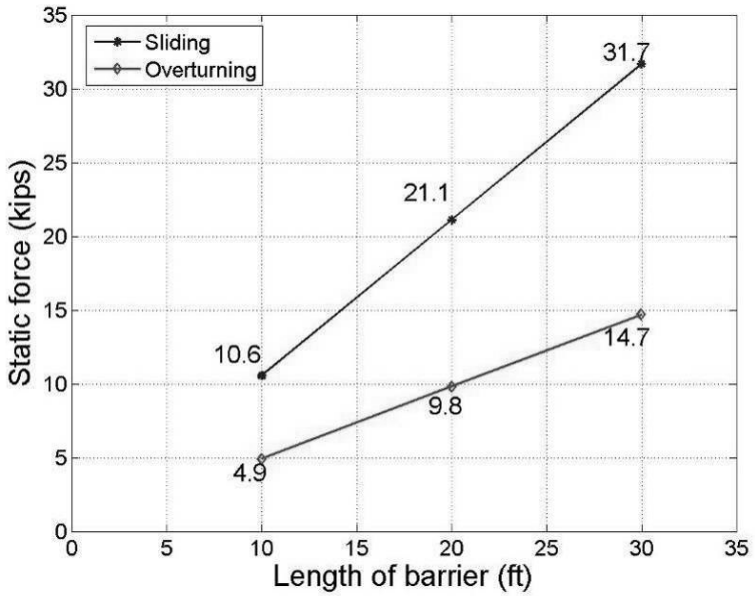

Figure 3.3 Required static force to induce sliding or overturning

3.2.2 Quasi-Static Finite Element Analysis

In order to further study of the static response of the barrier-moment slab system, a finite element model of the 3.05 m (10 ft) long barrier-moment slab system was developed (Figure 3.4) for use in LS-DYNA. LS-DYNA *(20)* is a general-purpose, nonlinear, explicit finite element code used to analyze the nonlinear dynamic response of three-dimensional structures. The code was originally developed by John Hallquist at Lawrence Livermore National Laboratory, and has since been enhanced by Livermore Software Technology Corporation (LSTC). Over the past 10 years, LS-DYNA has been extensively used in the performance evaluation of roadside safety hardware.

The vertical barrier, the moment slab, and the support pad at the bottom of the coping were represented by solid elements and defined as elastic materials (designated as MAT type 1 in LS-DYNA) with concrete material properties shown in Table 3.1. The soil was also represented by solid elements and defined as an elastic-plastic material (designated as MAT type 25 in LS-DYNA) with the properties shown in Table 3.1. Details of soil material model are presented in Section 5. The barrier stability model had a total of 34,274 solid elements.

The interface between the soil and barrier was modeled using contacts to capture the interface force generated between the concrete structure and the soil. A wood block was used as a means of providing distribution of the applied controlled quasi-static loading definition. The size of the wood block corresponded to the block used in the static load test. The model was initialized to account for gravitational loading on the soil mass before the application of the static load.

The barrier system failed by overturning, not by sliding. The result of the simulation is presented in Figure 3.5 as a load-displacement curve. The maximum load in the simulation is 35 kN (7.9 kips) while the static hand calculations gives 21.8 kN (4.9 kips). The difference is the soil resistance at the edges of the moment slab, which is accounted for in the simulation but not in the hand calculations.

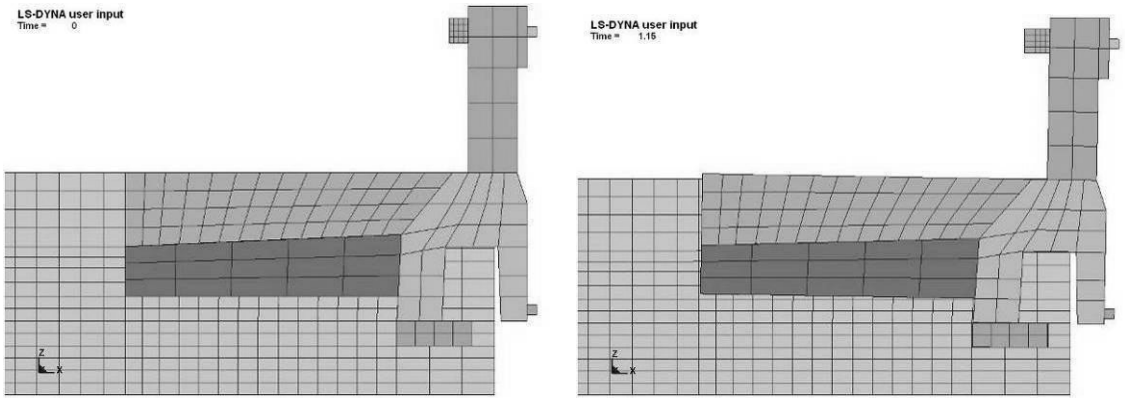

(a) **(b)**

Figure 3.4 Quasi-static finite element model (a) at rest and (b) end of the time

Table 3.1 Material Properties of Vertical Barrier, Moment Slab, and Soil

Material	Model	E (psi)	ν	ρ (lb/in^3)
Concrete	Vertical barrier, moment slab, and concrete pad	3.62E+6	0.17	0.084
Soil	Overburden soil, and support soil	0.00288	0.35	0.076

E is the young's modulus, ν is Poisson's ratio, and ρ is the mass density.

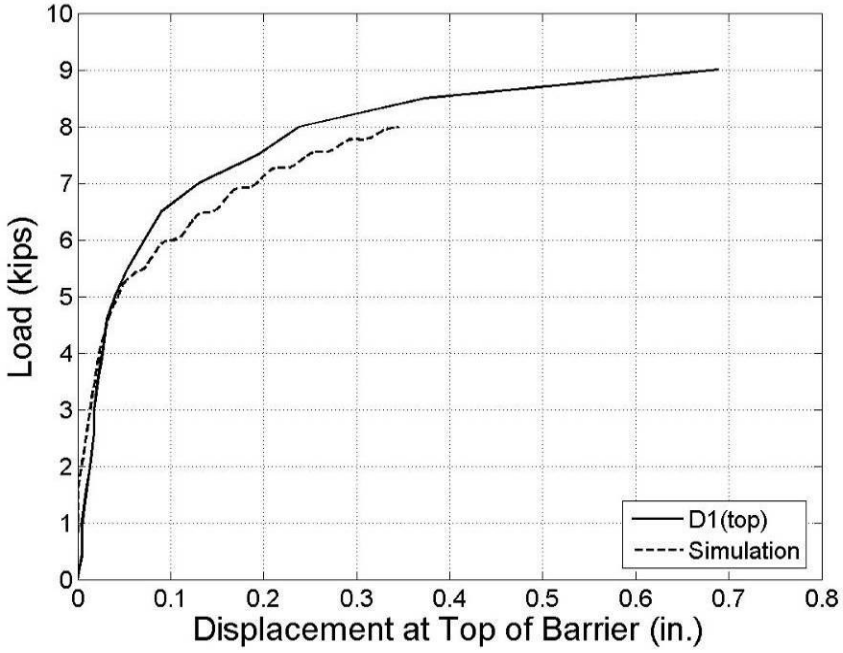

Figure 3.5 Comparison of static test and finite element static model

3.2.3 Full-Scale Static Test on Barrier

The purpose of the static load test was to verify the magnitude of force on the barrier required to initiate movement of the barrier-moment slab system. The setup for the static load test of the barrier system is illustrated in Figure 3.6 and Figure 3.7. A reaction post was anchored to an existing concrete apron. The load was applied to the top edge of the vertical concrete

barrier by means of a hydraulic cylinder. The load was distributed over a longitudinal barrier length of 1 m (3 ft) through the use of a steel spreader beam with a wood block applied to its face. An in-line load cell was used to measure the applied load. The load was applied in steps of 2.5 kN (500 lb), with each step lasting about 5 minutes. Displacement of the barrier, coping, and moment slab was recorded at the end of each load step using two dial gauges and an LVTD displacement sensor (D1). The LVTD was positioned behind and along the centerline of the barrier near its top edge. A dial gauge was placed along the same centerline near the bottom edge of the coping (D2). These two displacement measurement devices were secured to a steel frame. When the lateral load applied to the top of the barrier reached 36 kN (8 kips), the soil began to crack along the edges of the moment slab. The load test was stopped at a load of 40 kN (9 kips).

The force-displacement curves generated from the test data are shown in Figure 3.8. The load-deflection response of the barrier-moment slab system was linear up to a load of 22.3 kN (5 kips). This load corresponds quite well with the load capacity of this 3 m (10 ft) barrier system based on the static equilibrium analysis shown previously (Figure 3.3). Figure 3.8 indicates that the barrier had moved 1 mm (0.04 in.) at a load of 22.3 kN (5 kips). Upon further loading beyond 22.3 kN (5 kips), the displacement of the barrier increased in a more rapid, nonlinear manner. As shown in Figure 3.8, the final horizontal displacement at the top of the barrier (D1) was 18 mm (0.69 in.), while the displacement at the bottom of the coping (D2) was only 3 mm (0.114 in.). This indicates that the barrier-moment slab system experienced mostly a rotation failure with some sliding. At the time the load test was stopped, the shear strength of the soil had been exceeded and the load-deflection curve was nearly asymptotic.

Figure 3.5 shows the load test results compared to the numerical simulation. This comparison indicates that the static resistance is made of two components: the component due to the weight of the moment slab and overburden soil, and the component due to the friction between the moment slab-overburden soil and the surrounding soil. Back-calculations indicate that the average shear strength of the concrete soil interface at that shallow depth was 6.3 kPa or 126 psf. The results confirm that overturning is the likely mode of failure since sliding develops more resistance. This comparison also gives credibility to the numerical simulation.

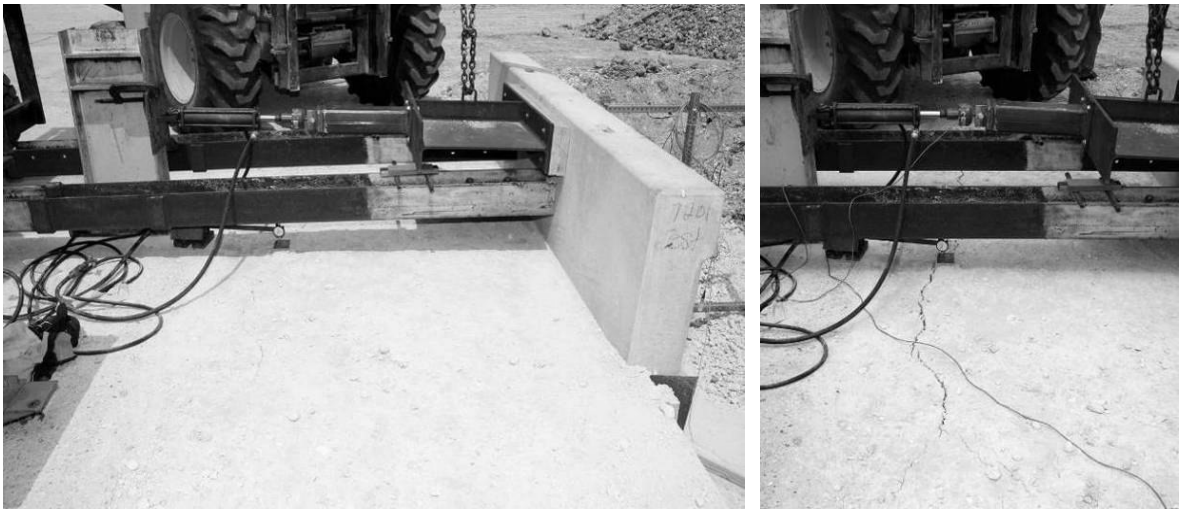

(a) **(b)**

Figure 3.6 Static test (a) beginning of test (b) end of test (note crack)

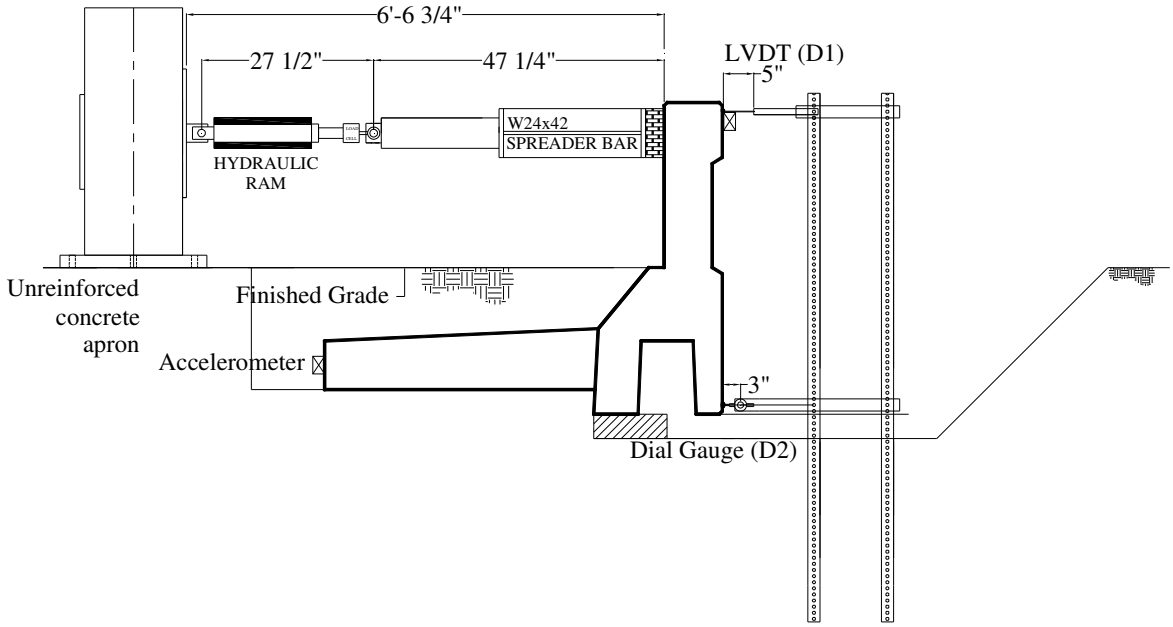

Figure 3.7 Static test installation

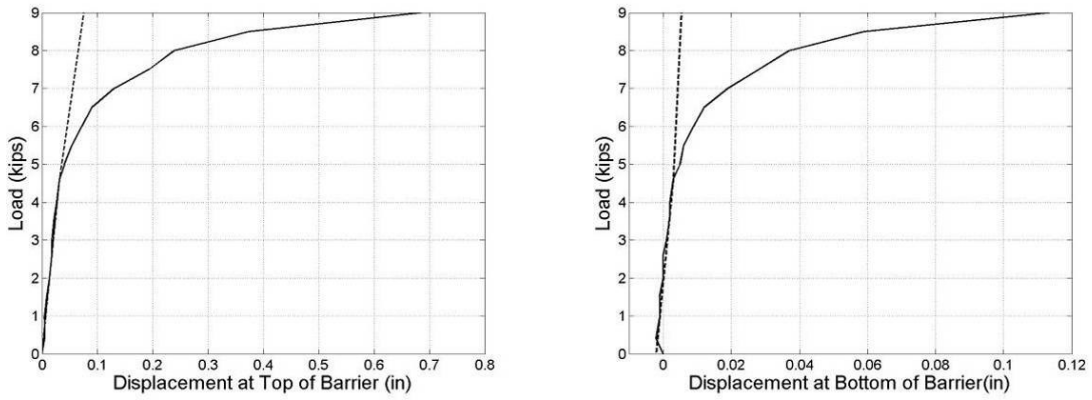

(a) **(b)**

Figure 3.8 Results of static test of (a) D1 and (b) D2

3.3 Dynamic Analyses and Dynamic Test

The purpose of these dynamic analyses is to explain theoretically the behavior of the barrier during impact and the results of the full-scale impact test. The purpose of the full-scale impact test is to verify the theoretical results and collect data at full-scale.

3.3.1 Full-Scale Dynamic Test (Bogie Test) on Barrier

Upon completion of the static load test, the soil on and around the moment slab was recompacted for a dynamic bogie impact. Two accelerometers were mounted to the barrier system to help analyze its dynamic behavior: one behind and along the centerline of the barrier at the height of impact oriented to measure longitudinal acceleration, and one on the end of the moment slab oriented to measure vertical acceleration. Additionally, the bogie vehicle was instrumented with an accelerometer.

In the first test, the 2,268 kg (5,000 lb) bogie vehicle (Figure 3.9(a)) impacted the center of the vertical barrier head-on at a speed of approximately 20.9 km/h (13 mph). The barrier system after impact is shown in Figure 3.9(b). The targets affixed to the end of the vertical barrier section were used as reference points to determine angular and translational displacement of the barrier from high-speed video. From the film analysis, the maximum

dynamic displacement of the barrier was 20 cm (4.9 in.) at the top and 69 mm (2.7 in.) at the ground level (Figure 3.10(a)). The maximum dynamic rotation angle of the barrier-coping section was 4.8 degrees. In addition to the rotation, the barrier also experienced approximately 25 mm (1 in.) of sliding. After the bogie impact, the barrier rebounded slightly and came to rest with a permanent displacement of 61 mm (2.4 in.) at the top and 36 mm (1.4 in.) at the ground level, with a rotation angle of 3.5 degrees.

Data obtained from the bogie-mounted accelerometer were analyzed and the results are presented in Figure 3.11. The acceleration history was treated using a 50 millisecond (msec) moving average (which is typically the duration selected for design) and then an SAE 60 Hz filter (which is used to reduce the noise in the data). As shown in Figure 3.11(b), the maximum acceleration was -8.5 g. Based on this acceleration and the mass of the bogie, the maximum impact force was calculated to be 189 kN (42.5 kips) (Figure 3.11(a)). The velocity-time and horizontal displacement-time histories of the bogie are shown in Figure 3.11(c) and (d), respectively. The maximum acceleration of the barrier, as measured by the accelerometer at the top of the barrier, was 2.8 g in the impact direction (Figure 3.12(a)). The velocity-time history of the barrier, as calculated by integration of the acceleration data, is shown in Figure 3.12(b). Figure 3.12(c) presents the horizontal displacement-time history of the barrier as determined by double integration of the acceleration data and through analysis of high-speed film.

The maximum acceleration of the moment slab, as measured by the accelerometer on the end of the moment slab (Figure 3.13), was 2.2 g in the vertical direction (Figure 3.13(a)). The velocity-time history and vertical displacement-time history of the end of the moment slab, as calculated by integration of the acceleration data, is shown in Figure 3.13(b) and (c), respectively. The maximum vertical displacement of the moment slab at its free edge was computed to be 9.14 cm (3.6 in.).

After recompacting the soil on and around the moment slab, second full-scale impact test was performed at a higher velocity 28.97 km/h (18 mph). From the film analysis, the maximum dynamic displacement of the barrier was 19.84 cm (7.81 in.) at the top of the barrier and 10.4 cm (4.09 in.) at the groundline. The maximum dynamic rotation angle of the barrier-coping section was 7.84 degrees. The displacement at the bottom of the coping was computed to be less than 7.6 mm (0.3 in.) (Figure 3.10(b)). This indicates that sliding did not

occur and provides further support that overturn rather than sliding is the critical failure mode for such a system. Using the acceleration and mass of the bogie impact vehicle, the maximum impact force was calculated to be 240.65 kN (54.1 kips) (Figure 3.14).

The maximum 50-msec average acceleration of the barrier, as measured by the accelerometer at the top of the barrier, was 2.5 g in the direction of impact (see Figure 3.15(a)). The displacement-time history obtained from double integration of the acceleration history looked suspect and was thought to be in error. Therefore, high-speed film was used to determine the displacement-time history of the barrier shown in Figure 3.15(b).

The maximum acceleration of the moment slab, as measured by the accelerometer on the end of the moment slab (Figure 3.16), was 3.9 g in the vertical direction. The acceleration data was lost at some time during the test, therefore, the maximum displacement of moment slab could not be determined.

Figure 3.17 shows the comparison of the load-displacement curves for the static test and the dynamic tests. As can be seen, the ratio between peak dynamic force and the peak static force is 4.5 for the 20.9 km/h (13 mph) impact test and 5.4 for the 28.97 km/h (18 mph) impact test.

(a) **(b)**

Figure 3.9 Bogie test (a) before with bogie and (b) after test

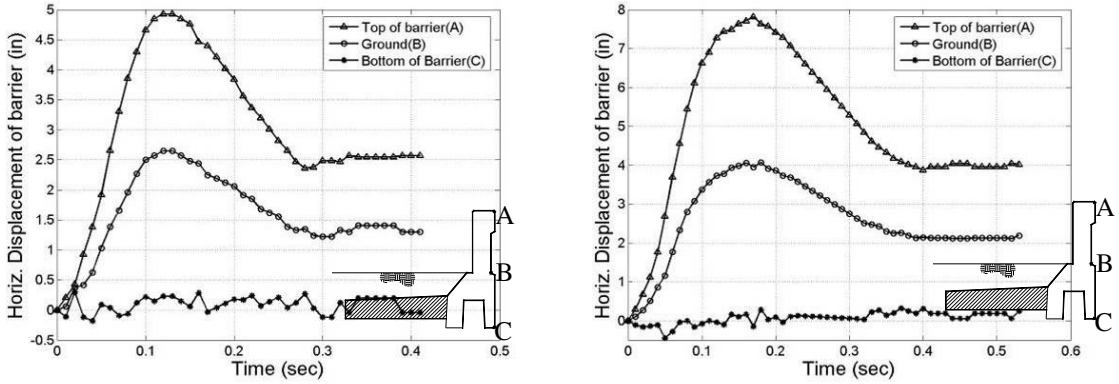

(a) **(b)**

Figure 3.10 Horizontal displacement of barrier measured from the film of the (a) 13 mph and (b) 18 mph impact test

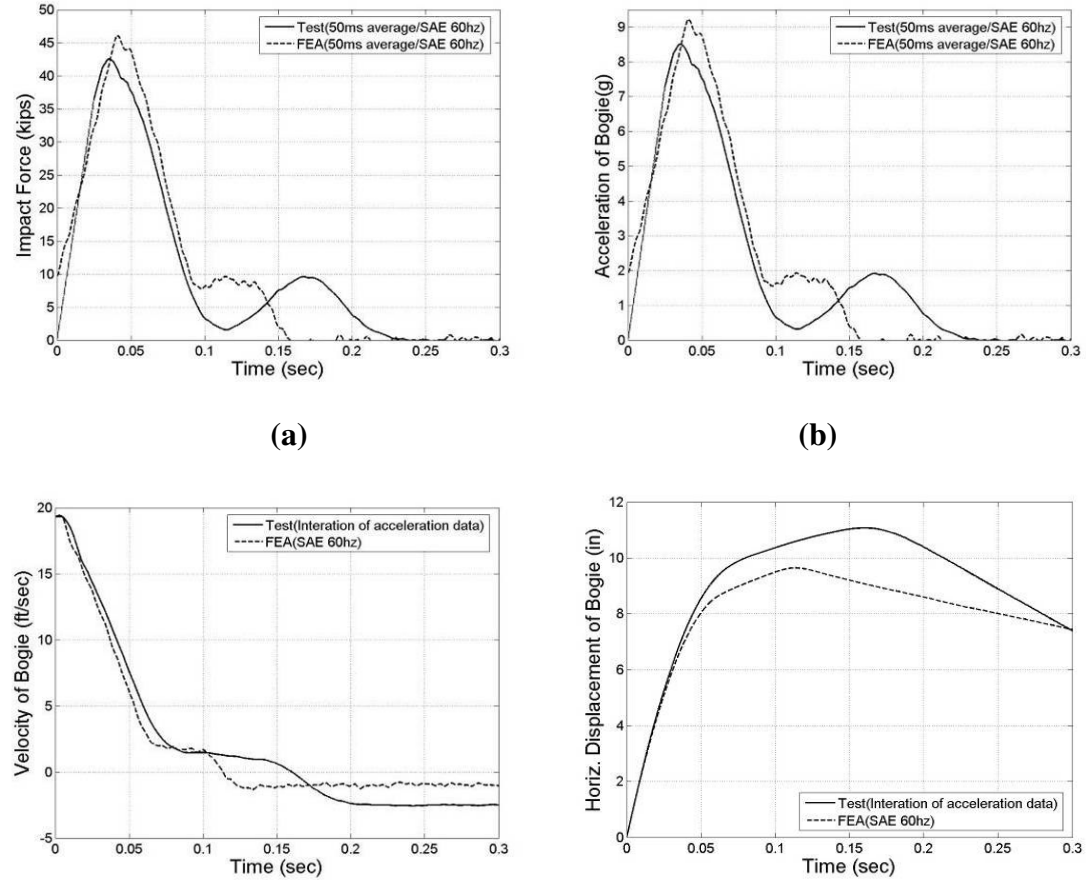

(a) **(b)**

(c) **(d)**

Figure 3.11 (a) Force, (b) acceleration, (c) velocity and (d) displacement of bogie of 13 mph dynamic test

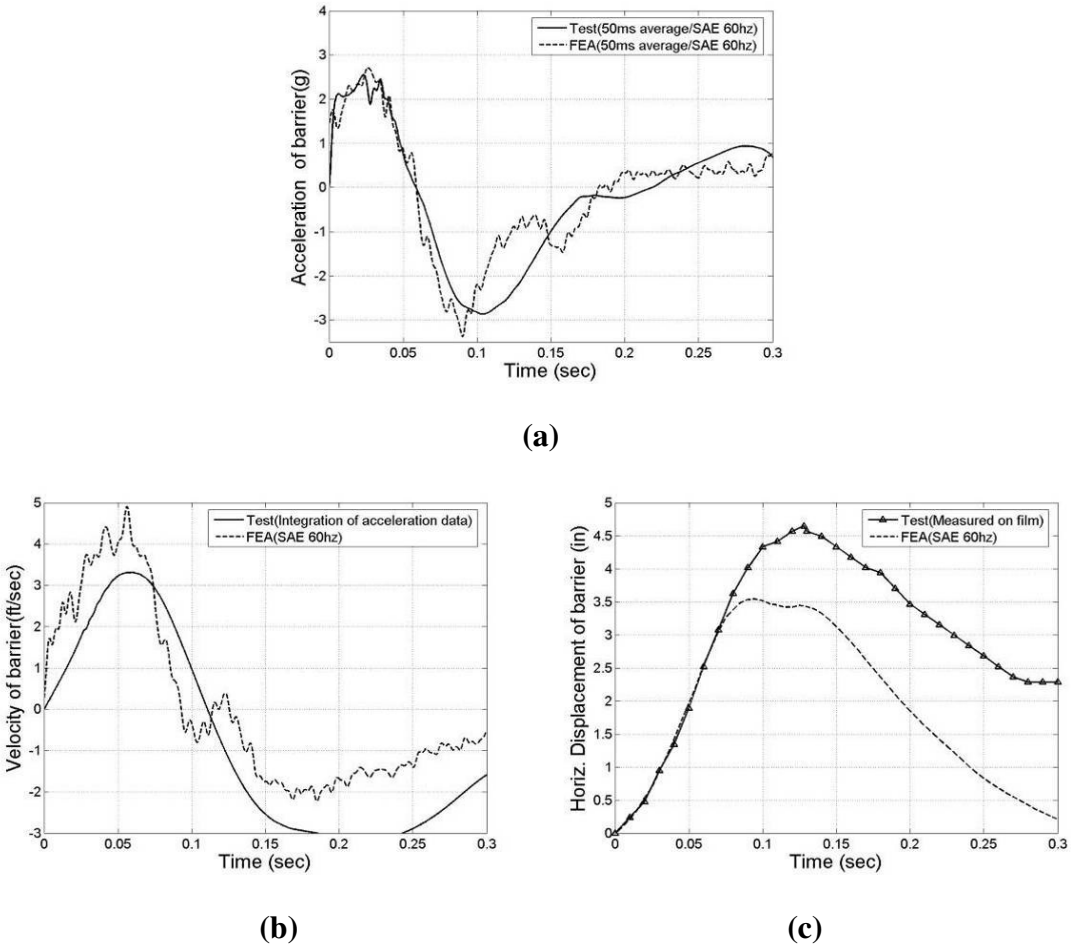

Figure 3.12 (a) Acceleration, (b) velocity, and (c) displacement of barrier of 13 mph dynamic test

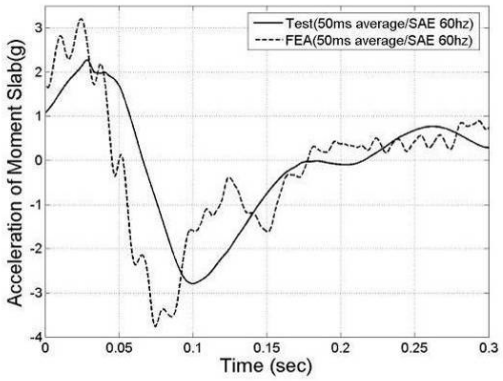

(a)

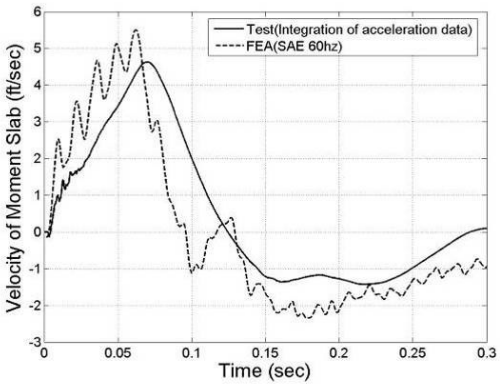

(b)

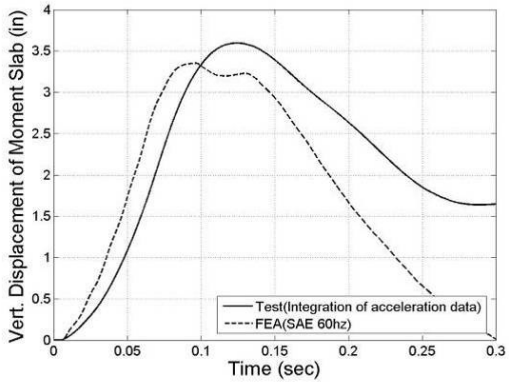

(c)

Figure 3.13 (a) Acceleration, (b) velocity, and (c) displacement of moment slab of 13 mph dynamic test

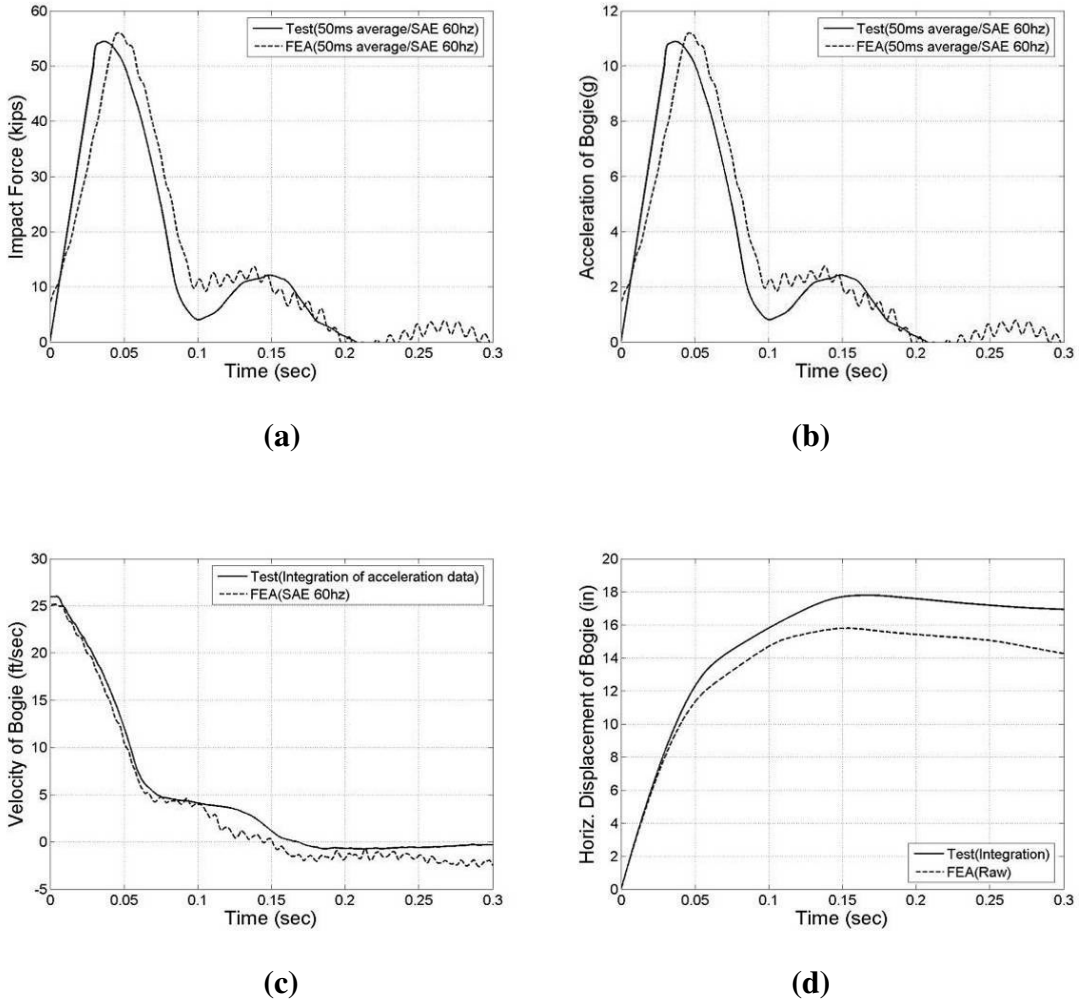

Figure 3.14 (a) Force, (b) acceleration, (c) velocity and (d) displacement of bogie of 18 mph dynamic test

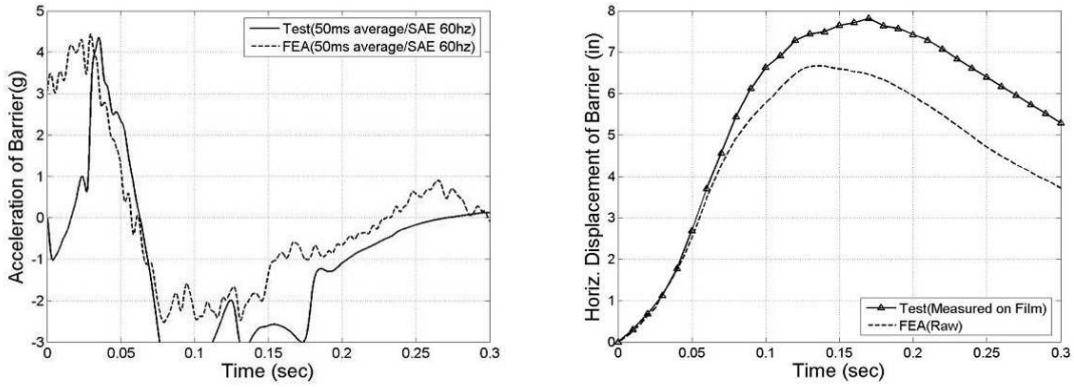

(a) **(b)**

Figure 3.15 (a) Acceleration and (b) displacement of barrier of 18 mph dynamic test

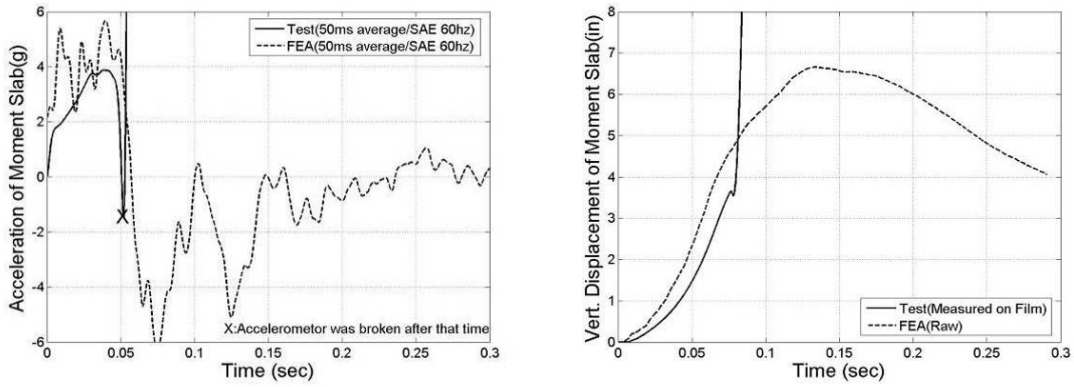

(a) **(b)**

Figure 3.16 (a) Acceleration and (b) displacement of moment slab of 18 mph dynamic test

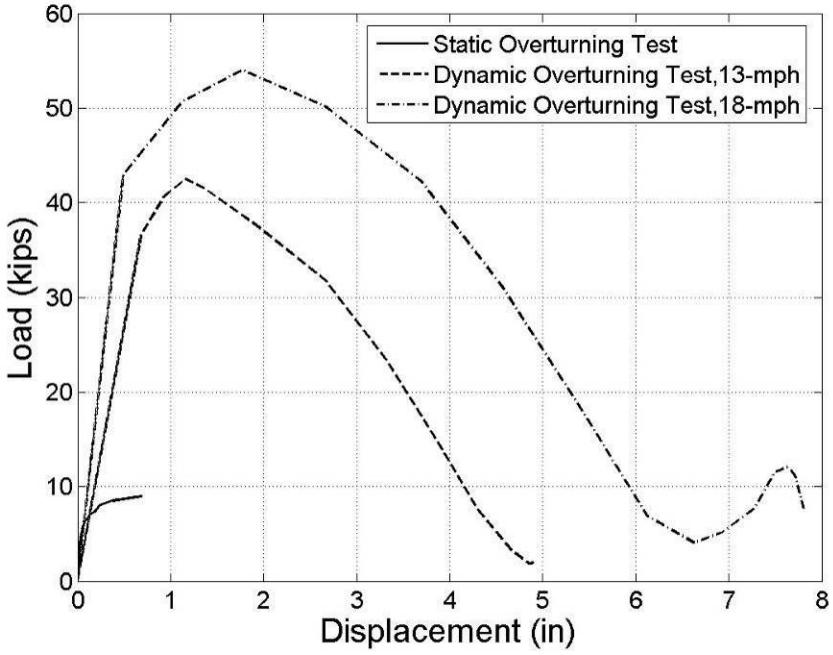

Figure 3.17 Comparison of static and dynamic overturning tests

3.3.2 Dynamic Analytical Simple Solution

1) Sliding

The fundamental equation of motion is:

$$\sum F_x = m\vec{a} \tag{3-3}$$

where ΣF_x is the sum of the external forces applied to the mass "*m*" and "*a*" is the acceleration of the mass. In the horizontal direction, the external forces consist of the impact force at the top of the barrier, F_{impact}, and the friction force $F_{friction}$ at the bottom of the barrier.

$$F_{impact} - F_{friction} = m\vec{a} \tag{3-4}$$

The impact force is obtained from the product of the mass of the bogie times the acceleration of the bogie (Figure 3.11(a)). The trace of this force as a function of time was simplified to a triangular shape as shown in Figure 3.18(a). The friction force is equal to the coefficient of friction tan ϕ, where ϕ is the friction angle of the soil, multiplied by the total weight W of the barrier. The weight of the barrier system as shown in Figure 3.2 is 69.6 kN

(15.65 kips). The friction angle of the soil was taken as 35 degrees. The mass of the barrier system is 7,096 kg (486 slug or 15,640 lb mass). Knowing the impact force, the friction force, and the mass of the barrier system, the acceleration of the barrier can be found using Eq. (3-4). The result is shown in Figure 3.18(b). The velocity history as a function of time was obtained by integration of the acceleration-time history curve (Figure 3.18(c)). Similarly, the displacement history as a function of time was obtained by double integration of the acceleration-time history curve (Figure 3.18(d)).

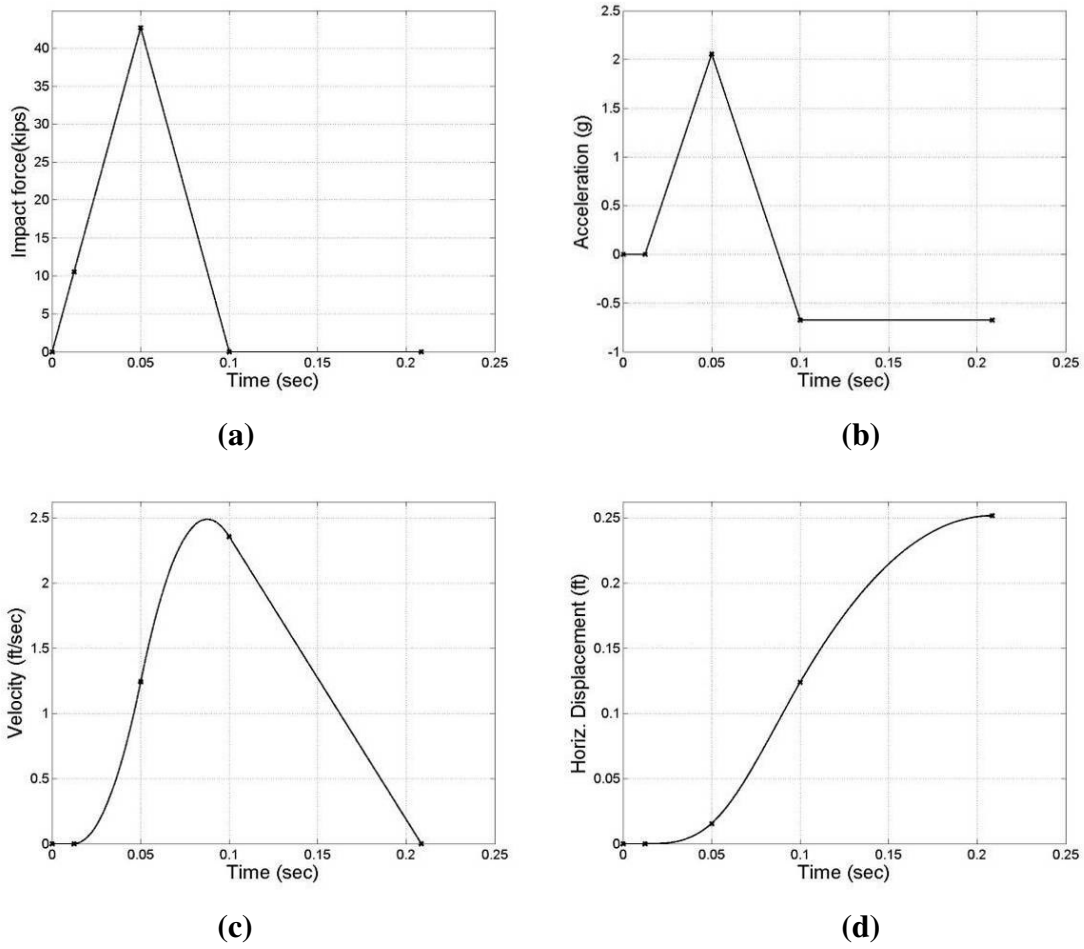

Figure 3.18 Analytical solution for sliding; (a) force, (b) acceleration, (c) velocity, and (d) displacement

2) Overturning

The fundamental equation for the rotation of the barrier *(21)* is:

$$\sum M_A = I_A \alpha \tag{3-5}$$

where ΣM_A is the sum of the external moments around point A applied to the barrier which has a mass moment of inertia I_A around the point of rotation and an angular acceleration α. The external moments are the moment due to the impact force and the moment due to the weight of the barrier (Figure 3.2) which gives:

$$(F_{impact} \times h) - (W \times l) = I_A \alpha \tag{3-6}$$

As mentioned before, the impact force (Figure 3.18(a)) and the weight of the barrier are known. The moment arms *h* and *l* are known (Figure 3.2) and assumed to be constant in a first analysis. The mass moment of inertia around the center of gravity can be expressed as $I_{CG} = \frac{1}{12} \sum m_i (x_i^2 + y_i^2)$ where the m_i values are the mass components of the barrier and the x_i and y_i values are the distances in the x and y directions from the individual centers of gravity of the mass components m_i and the CG of the entire barrier. To obtain the mass moment of inertia I_A with respect to an axis going through A different from the CG, one can use $I_A = I_{CG} + m(\overline{x}^2 + \overline{y}^2)$, where the term $\overline{x}^2 + \overline{y}^2$ represents the square of the distance from the rotation point A to the CG. The mass moment of inertia I_A was found to be 4691 kg-m^2 (3460 slug ft^2). Knowing the impact force, the weight, the moment arms and the mass moment of inertia, one can obtain the angular acceleration α by using Eq. (3-6). The linear acceleration at the point of impact is obtained by (Figure 3.19(b)):

$$\vec{a}_{(t)} = \alpha_{(t)} \times h \tag{3-7}$$

Then the velocity history as a function of time at the same point (Figure 3.19(c)) was obtained by integration of the acceleration-time history curve. Similarly, the displacement history as a function of time was obtained by double integration of the acceleration-time history curve (Figure 3.19(d)).

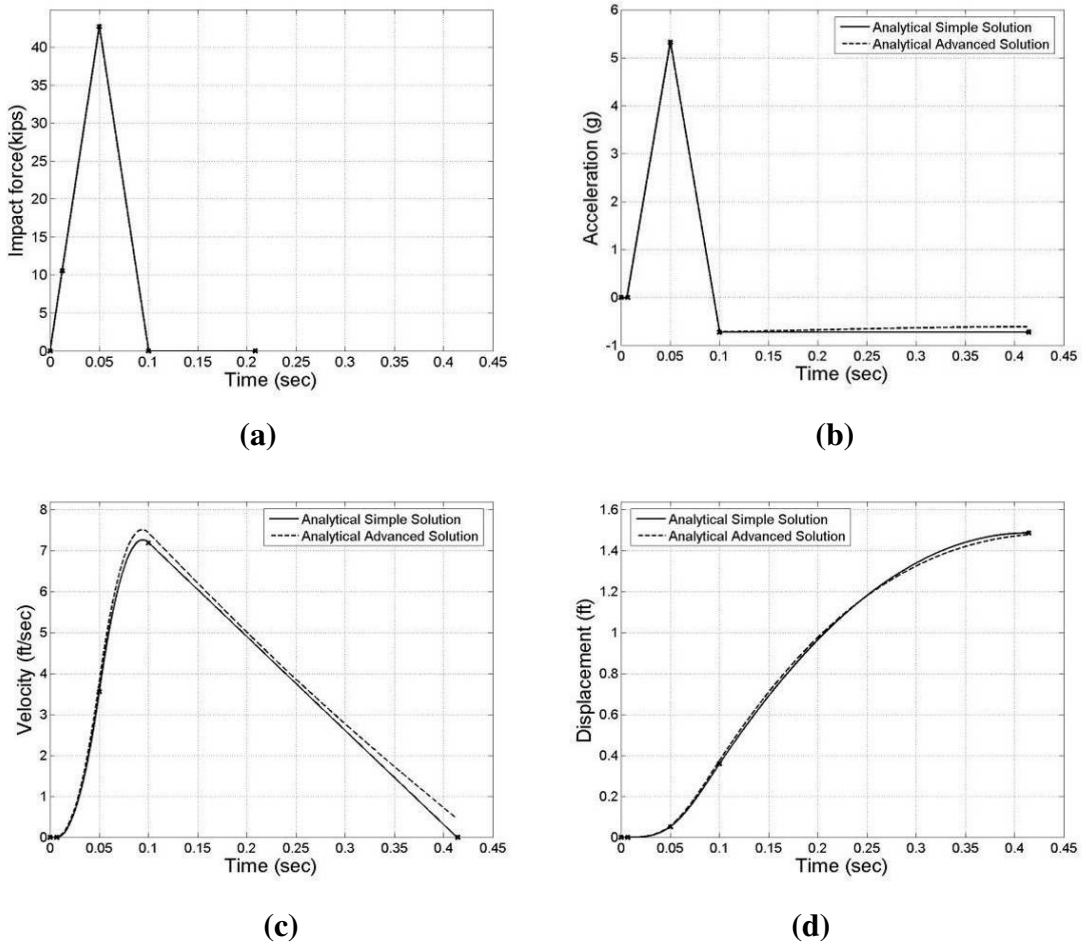

Figure 3.19 Comparison of analytical simple solution and advanced solution for overturning; (a) impact force, (b) acceleration, (c) velocity, and (d) displacement

3) Dynamic Analytical Advanced Solution

This solution addresses only the overturning case because it is the controlling case. Indeed the sliding requires a higher impact force to occur as shown in the previous static and dynamic analytical solutions. When the barrier rotates around A, the moment arms *h* and *l* are not constant as assumed in the first analysis. They can be expressed as:

$$h_{(t)} = h_0 \cos(\theta_{(t)}) \tag{3-8}$$

$$l_{(t)} = l_0 \cos(\theta_{(t)}) \tag{3-9}$$

where t is the time elapsed after impact and $\theta_{(t)}$ is the rotation angle. The moment arms vary as shown in Figure 3.20(a) and (b). Since the moment arms vary with time it is necessary to calculate the acceleration, velocity, and displacement in time steps. The results are shown on Figure 3.19. Also shown on Figure 3.19 are the results obtained when assuming that the moment arms do not vary in time. As can be seen there is not much difference in the results.

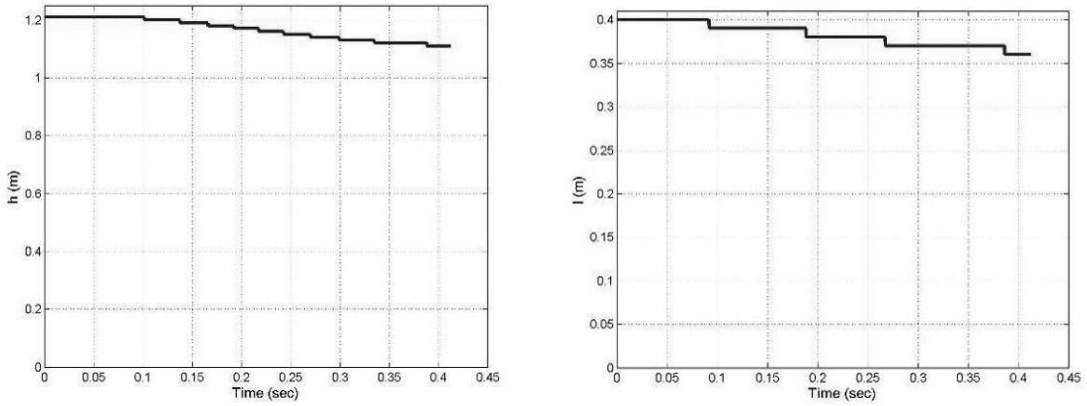

(a) **(b)**

Figure 3.20 Variations of (a) *h* and (b) *l*

3.3.3 Dynamic Finite Element Analysis

A finite element analysis using LS-DYNA was performed to simulate the dynamic impact behavior of the 3.05 m (10 ft) long vertical barrier-moment slab system. The results were used to further investigate the overturning behavior of the system when subjected to a dynamic impact load and to calibrate the model to improve the accuracy of subsequent predictive simulations used to design additional impact experiments. The system geometry and material properties used for the model were the same as those used in the quasi-static model. A 2,268 kg (5,000 lb) bogie was used to impact the barrier at a speed of 20.9 km/h (13 mph). Additionally, two accelerometers were incorporated into the finite element model to obtain accelerations of the barrier and moment slab for a comparison with the accelerations measured in the bogie tests (Section 3.3.1). The model was initialized to account for

gravitational loading on the soil mass before the dynamic bogie impact. Figure 3.21 shows images from the 20.9 km/h (13 mph) dynamic bogie impact simulation.

The deceleration of the bogie during impact as calculated by the finite element analysis is compared to the measured deceleration of the bogie in Figure 3.11(b). The comparison is reasonably good. The acceleration of the top of the barrier during the impact as calculated by the finite element analysis is compared to the measured acceleration at the top of the barrier in Figure 3.12(a). The comparison is also reasonably good. The horizontal displacement at the top of the barrier is compared to the measured displacement of the barrier obtained by high-speed film analysis in Figure 3.12(c). The curves deviate from one another at approximately 0.07 sec. The reason is that in the test, the soil fills the gap behind the moment slab and prevents the slab from returning to its initial position. This phenomemon is not captured in the finite element analysis. The acceleration of the end of the moment slab during the impact as calculated by the finite element analysis is compared to the measured acceleration of the moment slab in Figure 3.13(a). The comparison is also reasonably good.

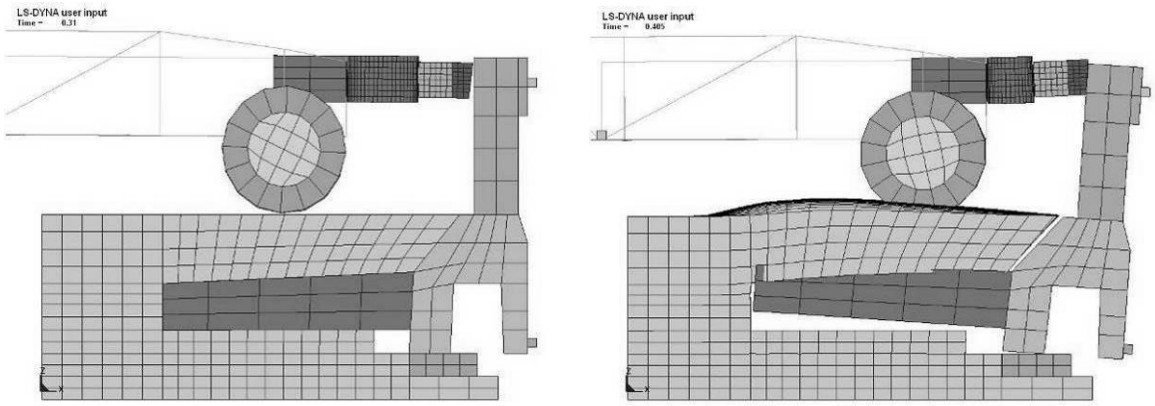

(a) **(b)**

Figure 3.21 Finite element model for overturning at (a) at rest and (b) at impact

3.4 Conclusions

The following conclusions are based on and limited to the content of this section:

1. The design impact loads for traffic barriers have evolved over the last 50 years. There are two primary values in case: 44.5 kN (10 kips) and 240 kN (54 kips). The 44.5 kN (10 kips) is an equivalent static load typically used in conjunction with an elastic analysis while the 54 kips is a dynamic load and is used in conjunction with an ultimate strength analysis. It is not proper to use the 240 kN (54 kips) as an equivalent static load when designing a moment slab as the results are excessively conservative.
2. Current practice uses an ASD approach. The LRFD approach is not complete yet.
3. A set of static and dynamic analytical calculations representing increasing levels of complexity are developed. One static load test and two impact tests were performed on a full-scale barrier. Comparison between the analytical results and the results of three full-scale barrier tests show good agreement.
4. Overturning occurs before sliding and therefore controls the design. This was shown analytically and confirmed by the full-scale static and dynamic test results.
5. There is a significant ratio between the static load and the dynamic load that the barrier can resist. For the 3.05 m (10 ft) barrier tested, the ultimate static load was 40.5 kN (9.1 kips). For the same barrier the maximum dynamic load in a 13 mph impact test was 189 kN (42.5 kips) for a dynamic to static ratio of 4.7. The maximum dynamic load in an 18 mph impact test was 240 kN (54 kips) for a dynamic to static ratio of 5.9. This is due to the inertial resistance of the system.
6. These ratios use a static load and a dynamic load which do not correspond to the same amount of displacement. If a tolerable displacement of 25 mm (1 in.) is targeted, then the static load is still 40.5 kN (9.1 kips) but the dynamic load drops to 170 kN (38.2 kips) for the 13 mph impact test (dynamic to static ratio of 4.2) and to 210 kN (47.2 kips) for the 18 mph impact test (dynamic to static ratio of 5.2).
7. Since the static load resisted by the dead weight alone of the 3.05 m (10 ft) long barrier is 22.8 kN (5.1 kips), for a barrier to resist an equivalent static design load of 44.5 kN (10 kips) with a factor of safety of 1.5, it needs to be at least 9.15 m (30 ft) long.

4 REINFORCEMENT PULLOUT TESTS

A series of pullout tests were performed to evaluate the influence of rate effect on the pullout capacity of the reinforcement. Ten tests were conducted, 7 on steel reinforcement strips and 3 on steel bar mats. The group that ran the pullout tests was GeoTesting Express in Atlanta.

4.1 Rate of Loading

Three testing times to failure were used: 0.05 sec, 5 sec, and 3600 sec. This covered 5 log cycles of time to failure.

4.2 Saturation

The question arose whether or not a fully saturated condition should be considered. The argument is that, according to theory, a saturated condition will lead to a decrease in resistance when the soil behavior goes from drained behavior to undrained behavior as the rate of loading is increased. The reason is that the pore pressures are higher in undrained conditions compared to drained conditions and, as a result, the effective stress is lower. Since the effective stress controls the strength, then undrained behavior leads to lower resistances than drained behavior. This was verified on pullout tests performed by Antonio Bobet *(22)* where the capacity dropped by about 30%. His study was requested by the Indiana DOT because some overpasses are in flood areas and the bottom of the wall may be submerged at times. After discussions with Antonio Bobet at Purdue, Pete Anderson at RECO, and Mark McClelland at TxDOT, it seems that

1. the saturated condition is rare and
2. when it happens it usually affects only the bottom of the wall, not the top where the strips loaded by the impact on the barrier are located.

Nevertheless, it is prudent to test that condition to cover all cases. Therefore the soil was tested under two moisture conditions: 1. at its optimum moisture content after proper compaction and 2. by saturating the soil after testing it in the unsaturated condition.

4.3 Fines

Highway jobs have strict tolerances on the gradation of the soil used as backfill. Commercial jobs are much less stringent and allow for a much higher percent fines. The tests were limited to a soil which satisfies the DOTs common guidelines. There are typically two types of soils used behind MSE walls: well graded sand or crushed rock (No.57 stones). The soil tested had the following characteristics:

1. Well graded sand
2. Less than 15% passing sieve No. 200
3. Less than 60% passing sieve No.40
4. Largest particle smaller than 7.62 cm (3 in.)

The grain size distribution of the sand used is given in Figure 4.1. A compaction test was also performed and is shown in Figure 4.2.

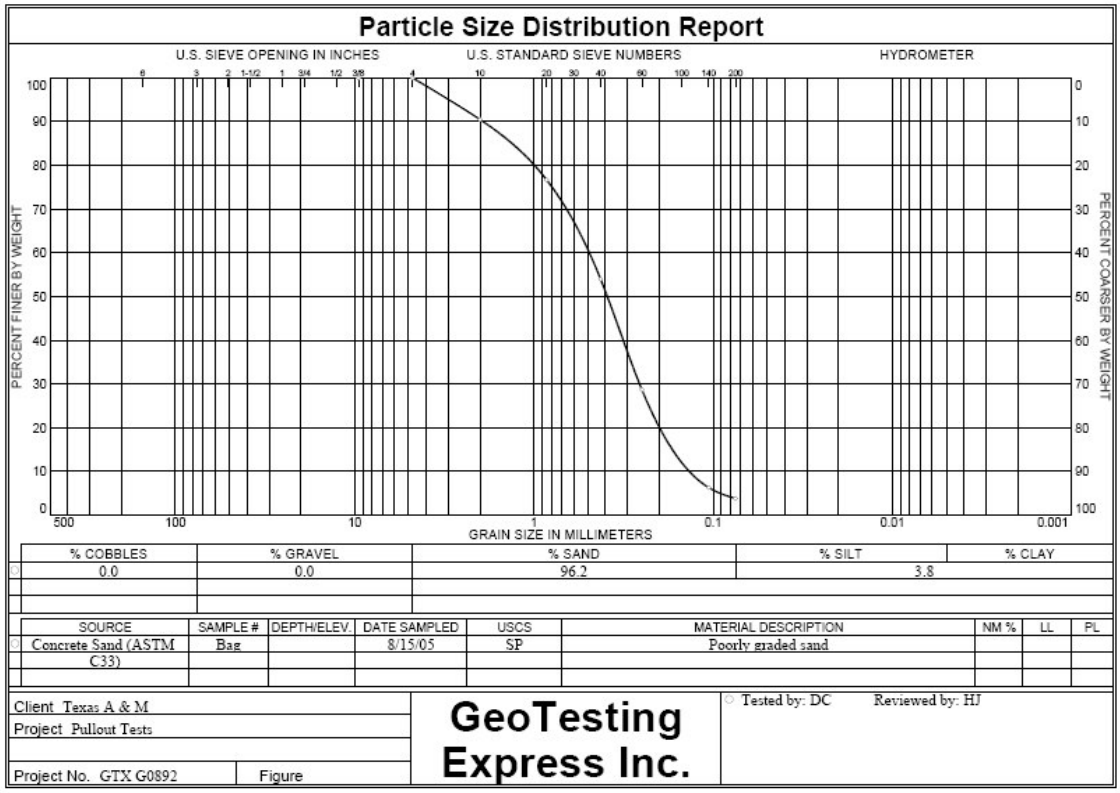

Figure 4.1 Grain size distribution of the sand used in the pullout experiments

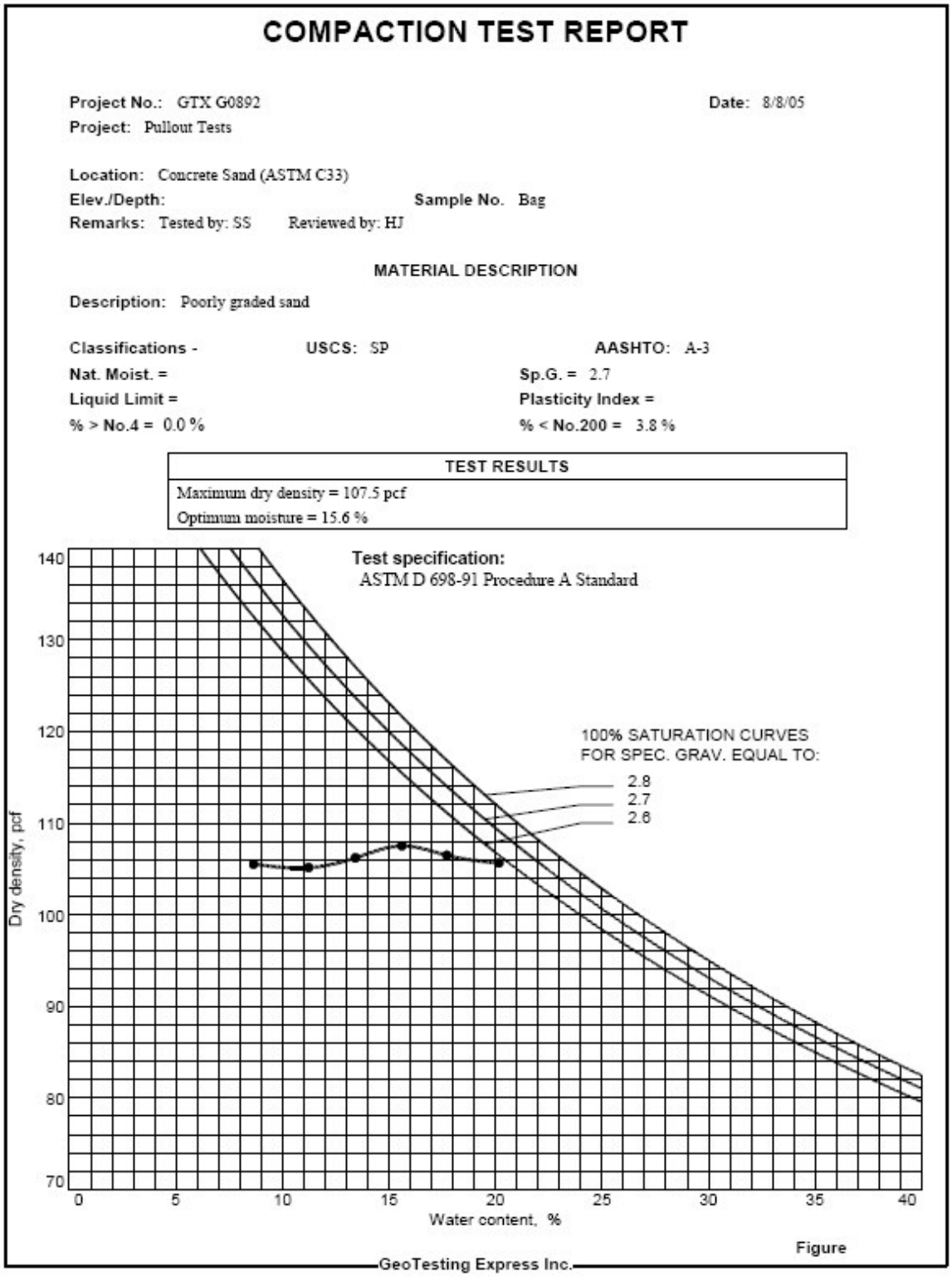

Figure 4.2 Compaction curve for the sand tested

4.4 Reinforcement

Geosynthetics represent a minor component of highway wall reinforcement according to the survey. Therefore, the tests focused on inextensible reinforcement.

Two types of reinforcing materials were used in the tests. One type was reinforcing strips provided by RECO. The other type was bar mats provided by Foster Geotechnical, now merged with RECO. The dimensions of the reinforcing strips and bar mats are included in Table 4.1. Concrete sand was used in the tests as the backfill material. The concrete sand was purchased from a retailed store and meets ASTM C33 requirements. A compaction and a gradation test were performed on the concrete sand. The gradation test results indicate the concrete sand meets the usual gradation requirements (Less than 15% passing sieve No. 200, less than 60% passing sieve No.40, and largest particle smaller than 3 inches).

Table 4.1 Dimension of the Reinforcing Strip and Bar Mat

	Length (in.)	Width (in.)	Thickness (in.)
Strip	60	2	0.2
Bat Mat	57.5	24.5	0.4

4.5 Number of Tests

A total of 10 pullout tests were performed as outlined below.

- Tests: two sets of 3 tests on the unsaturated backfill and one set of 4 tests on the saturated backfill.
- Time to failure: 0.05 sec, 5 sec, and 3600 sec, for each of the two sets on the unsaturated backfill ($3 \times 2 = 6$ tests) and 0.05 sec, 2 for 5 sec, and 3600 sec, for the set on the saturated backfill ($4 \times 1 = 4$ tests)
- Soil: well graded sand as described above; same soil for all 10 tests.
- Reinforcement: 7 tests on the steel reinforcement strips, 3 tests on the steel bar mats, length of reinforcement = 1.13 m (3.7 ft).

- Saturation: optimum water content and maximum dry density for 6 tests (3 on strips and 3 on bar mats); saturated condition for 4 tests (on strips).
- Box: 70.1 cm × 38.1 cm × 1.31 m (2.3 ft × 1.25 ft × 4.3 ft).

Table 4.2 summarizes the conditions for each test.

Table 4.2 Pullout Test Matrix

Test no.	Reinforcement	Target Time to Failure (sec)	Soil Condition
1	Single Strip	0.05	95% MDD @ OM
2	Single Strip	5	95% MDD @ OM
3	Single Strip	3600	95% MDD @ OM
4	Single Strip	0.05	95% MDD Saturated
5	Single Strip	5	95% MDD Saturated
6	Single Strip	5	95% MDD Saturated
7	Single Strip	3600	95% MDD Saturated
8	Bar Mat	0.05	95% MDD @ OM
9	Bar Mat	5	95% MDD @ OM
10	Bar Mat	3600	95% MDD @ OM

MDD = Maximum Dry Density; OM = Optimum Moisture

4.6 Procedure (Soil Installation, Rate of Loading, Testing)

A pullout test box was used in the tests. The box has approximate dimensions of 70.1 cm × 38.1 cm × 1.31 m (2.3 ft × 1.25 ft × 4.3 ft). Photos and sketches of the box are shown in Figure 4.3. Sand was first compacted near optimum moisture content to approximately 95% of the maximum dry density to a height 16.51 cm (6.5 in.) from the bottom of the box, and then the reinforcing strip or bar mat was placed. An additional 21.6 cm (8.5 in.) of sand was then placed and compacted to the top of the box. A steel plate was placed on the top of the sand. Dead weights were then placed on top of the steel plate to simulate three feet of soil overburden. A hydraulic loading system was attached to the front of the strip or bar mat to provide loading for slow and medium speed tests. A pneumatic loading system was used for high-speed tests. Figure 4.3 and Figure 4.4 show the box setup and the loading systems for the strips and bar mat, respectively. Two LVDTs were mounted to the box to monitor the deflection during the tests. A ruler was also attached to the piston to measure the deflection after the LVDTs reached their limit of 3.81 cm (1.5 in.). A load cell was attached to the piston to measure the load during the tests. The LVDTs and load cell were connected to a computer data acquisition system to acquire the data during the tests.

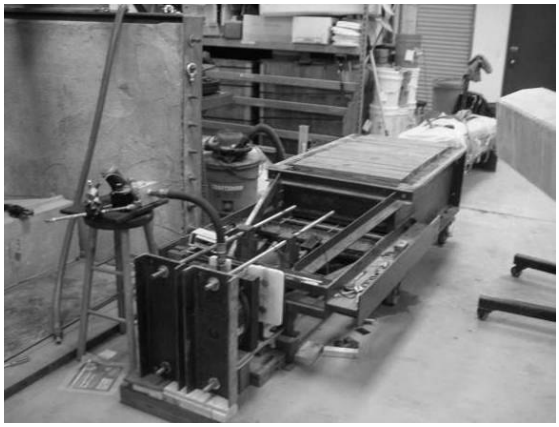

a) Pullout Box Set-up

(b) Surcharge to simulate depth

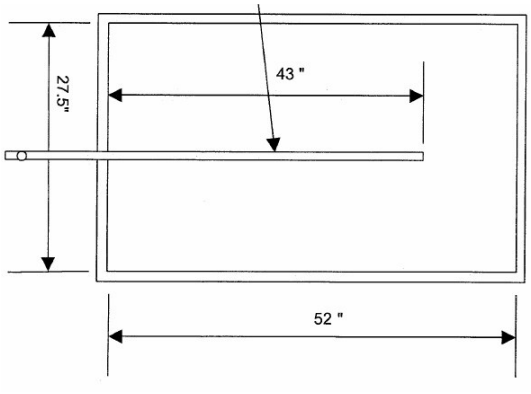

(c) Box dimensions and location of strip

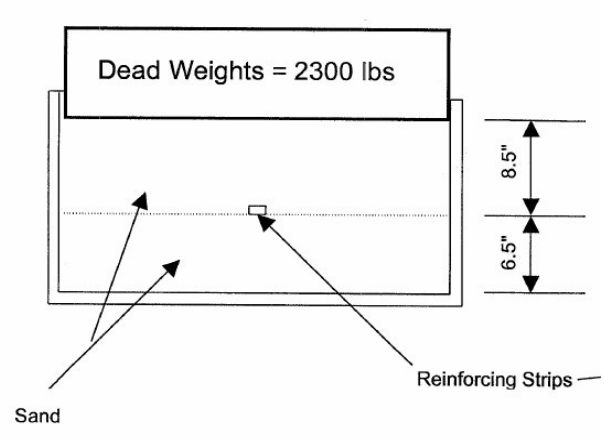

(d) Box dimensions and dead weight

(e) Placing the strip on the sand

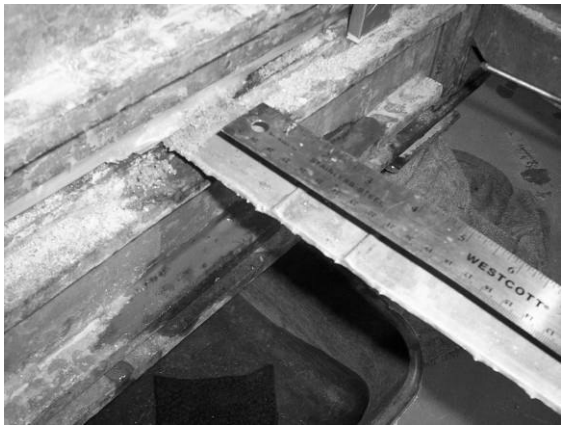

(f) Strip coming out of the front of the box

Figure 4.3 Test set-up with steel strip

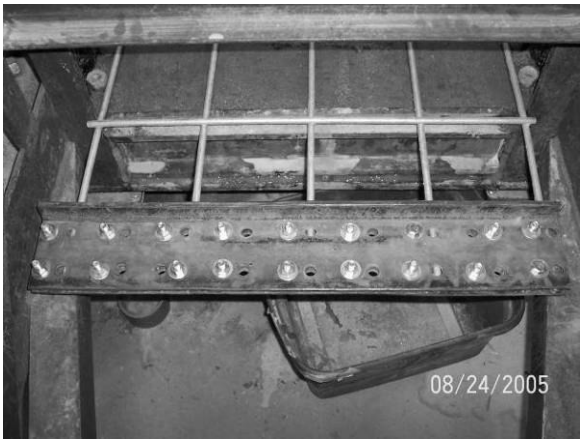

(a) Grabbing the bar mat

(b) Placing the bar mat on the sand

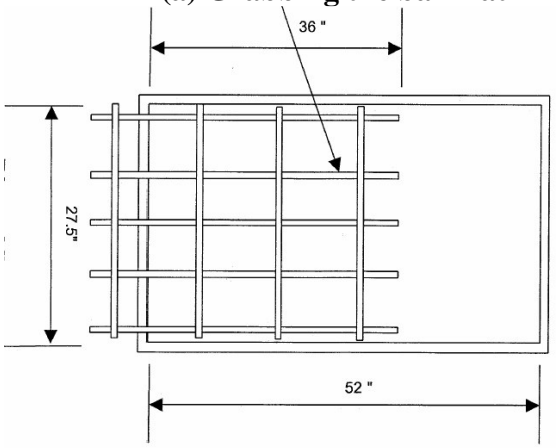

(c) Bar mat and box dimensions

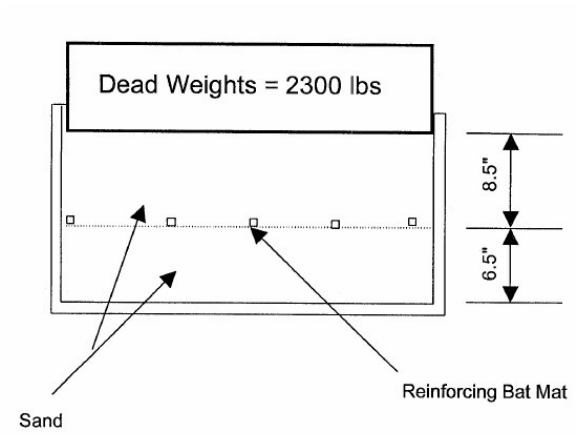

(d) Dead weight on bar mat

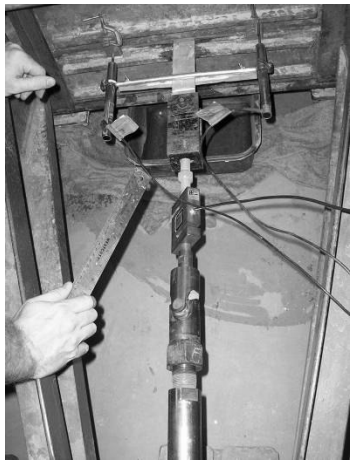

(e) Grabbing and loading the strip

Figure 4.4 Test set-up with bar mat

4.7 Results and Conclusion

The soil was compacted in layers up to the location of the reinforcement. A standard size steel strip and a standard size bar mat were installed and the compaction process was completed. A surcharge was placed on top of the sand to simulate a total of 0.91 m (3 ft) of soil cover on the reinforcement. Then the reinforcement was pulled to failure.

A load displacement curve was obtained for each test. The results are shown in Figure 4.5 to Figure 4.7 and Table 4.3. Figure 4.5 shows a summary of the test results at failure. The rate effect is shown for all tests on Figure 4.8. The data indicates that there is no particular trend in the effect of the rate of loading. Indeed the pullout resistance at the fastest rate is often larger or equal to the resistance at slower rates. Therefore, these tests are an indication that there is no reason to take into account the rate effect on the pullout capacity of the reinforcement.

The back-calculated F* values for the steel strips ranged from 1.7 to 3.87 and averaged 3.0. This is well within the range of values obtained in the literature (Figure 4.9) *(23)*.

The present AASHTO recommendations for calculating the resistance of MSE wall reinforcement to static loading lead to a predicted reinforcement resistance smaller or equal to the actual reinforcement resistance under impact loading (safe condition). On the basis of these few tests, it is suggested that the current AASHTO recommendations be used-as-is to calculate the resistance of the reinforcement to impact loads.

Tie Back Strip, Unsaturated, 0.00097 in/s

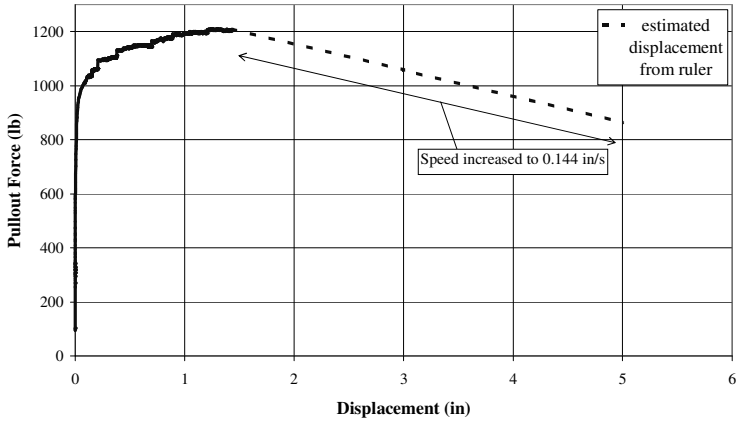

Tie Back Strip, Unsaturated, 0.12 in/s

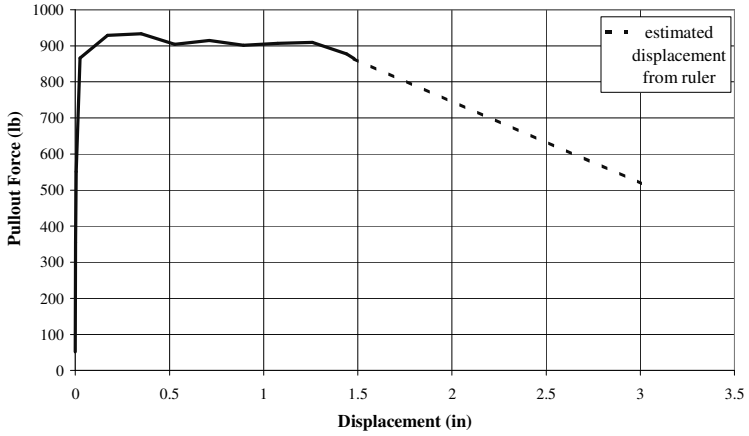

Tie Back Strip, Unsaturated, 3.84 in/s

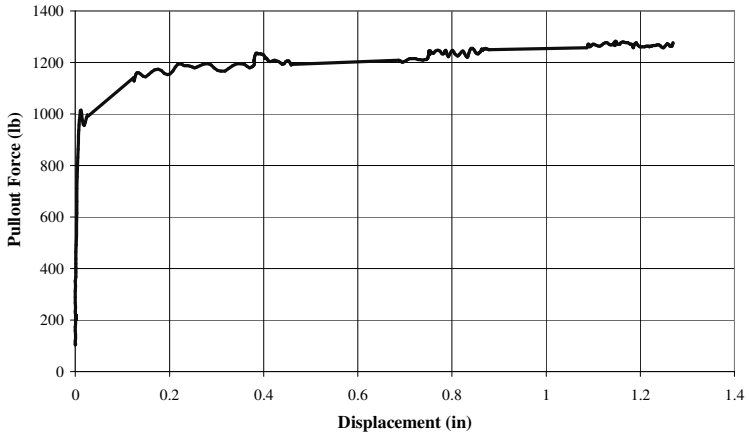

Figure 4.5 Load displacement curve obtained (tie back strip, unsaturated)

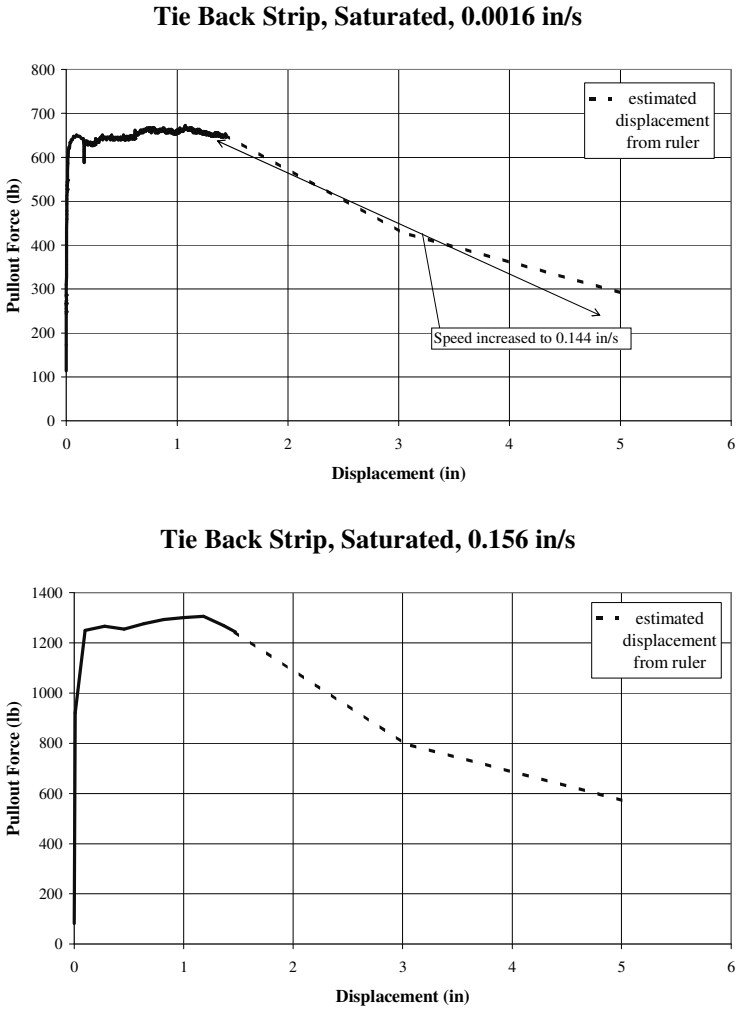

Figure 4.6 Load displacement curve obtained (tie back strip, saturated)

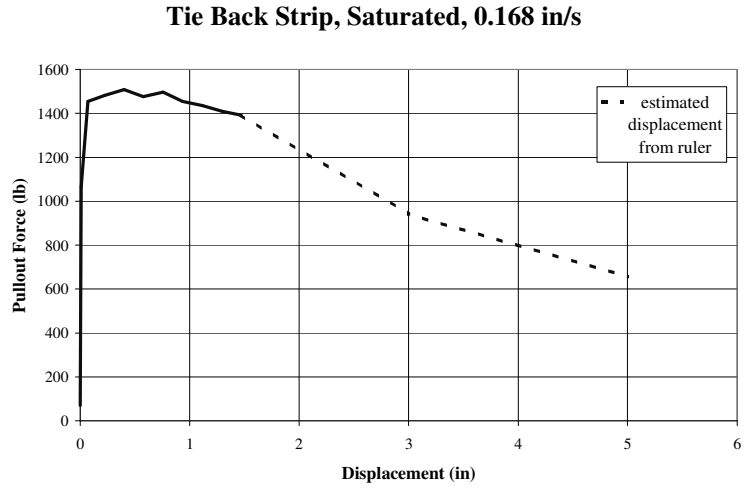

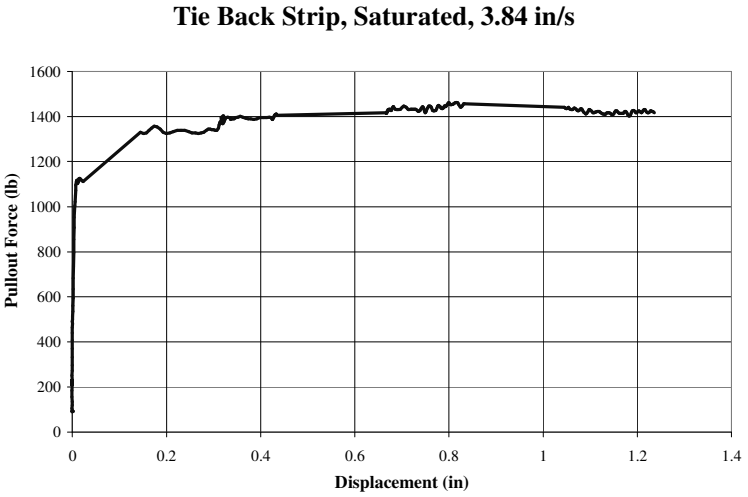

Figure 4.6 Load displacement curve obtained (tie back strip, saturated) (Continued)

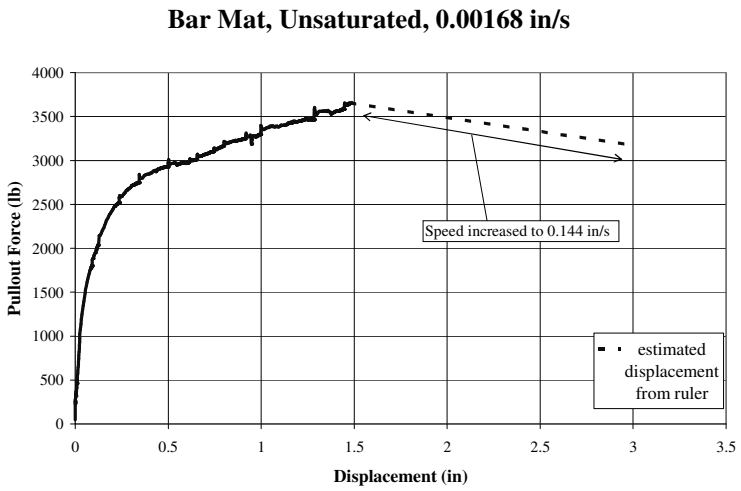

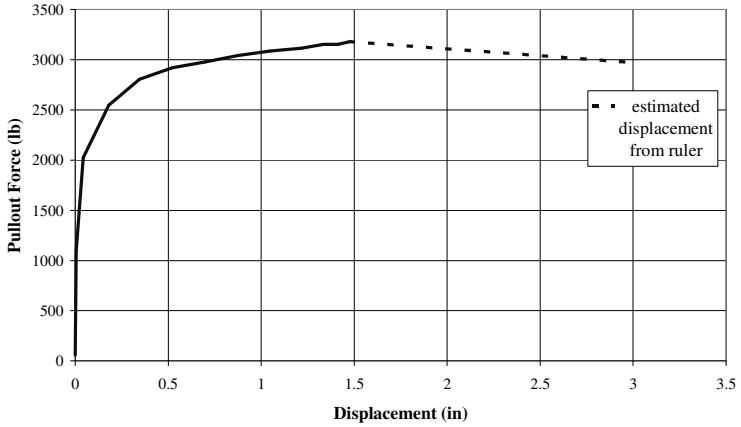

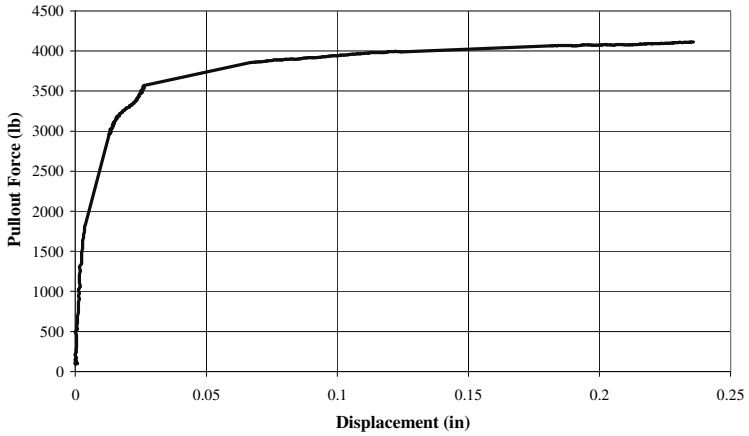

Figure 4.7 Load displacement curve obtained (bar mat)

Table 4.3 Pullout Test Results

a) Tie Back Strip[1], Unsaturated

Test Condition	Pullout Speed (in/s)	Dry Density of Sand (pcf)	Normal Load (lbs)	Specimen Width (ft)	Length of Imbedment (ft)	Pullout Force (lbf)	Elapsed Time at Peak (s)	Displacement at Peak (in)	Pullout Resistance[2] (lbf/ft)
Unsaturated	0.00097	101.5	2946	0.17	3.7	1212 (1163)	1287 (862)	1.24 (0.75)	7269 (6841)
Unsaturated	0.12	101.5	2946	0.17	3.7	933	5	0.35	5602
Unsaturated	3.84	101.5	2946	0.17	3.7	1141	0.05	0.12	6848

Notes: 1. Tie Back Strip Dimension: L=60 in., W=2 in., Thickness=0.2 in., Thickness at rib=0.3 in., length of imbedment=3.7ft
2. Pullout resistance = Pullout Force (lbf) / width of tie back strip (ft)
For samples whose peak value occurred after 0.75 in., values in ( ) represent values at 0.75 in. displacement

b) Tie Back Strip[1], Saturated

Test Condition	Pullout Speed (in/s)	Dry Density of Sand (pcf)	Normal Load (lbs)	Specimen Width (ft)	Length of Imbedment (ft)	Pullout Force (lbf)	Elapsed Time at Peak (s)	Displacement at Peak (in)	Pullout Resistance[2] (lbf/ft)
Saturated	0.0016	101.5	2946	0.17	3.7	650	66	0.09	3903
Saturated	0.156	101.5	2946	0.17	3.7	1306 (1286)	8 (6)	1.18 (0.75)	7835 (7720)
Saturated	0.168	101.5	2946	0.17	3.7	1508	4	0.40	9049
Saturated	3.48	101.5	2946	0.17	3.7	1357	0.06	0.17	8143

Notes: 1. Tie Back Strip Dimension: L=60 in., W=2 in., Thickness=0.2 in., Thickness at rib=0.3 in., length of imbedment=3.7ft
2. Pullout resistance = Pullout Force (lbf) / width of tie back strip (ft)
For samples whose peak value occurred after 0.75 in., values in ( ) represent values at 0.75 in. displacement

Table 4.3 Pullout Test Results (Continued)

c) Bar Mat[1]

Test Condition	Pullout Speed (in/s)	Dry Density of Sand (pcf)	Normal Load (lbs)	Specimen Width (ft)	Length of Imbedment (ft)	Pullout Force (lbf)	Elapsed Time at Peak (s)	Displacement at Peak (in)	Pullout Resistance[2] (lbf/ft)
Unsaturated	0.00168	101.5	2946	2	3	3655 (3129)	1811 (799)	>1.5 (0.75)	1837 (1565)
Unsaturated	0.144	101.5	2946	2	3	3180 (2996)	12 (6)	1.48 (0.75)	1590 (1499)
Unsaturated	1.08	101.5	2946	2	3	3900	0.17	0.09	1950

Notes: 1. Bar Mat Dimension: L=57.5 in., W=24.5 in., Bar Thickness=0.4 in., Joint Thickness=0.7 in., length of imbedment=3ft, 5 bars parallel to direction of force, 4 cross-bars (3 imbedded)

2. Pullout resistance = (Pullout Force (lbf) * number of bars per unit width (2.5 bars/ft)) / number of bars parallel to direction of force (5)

For samples whose peak value occurred after 0.75 in., values in ( ) represent values at 0.75 in. displacement

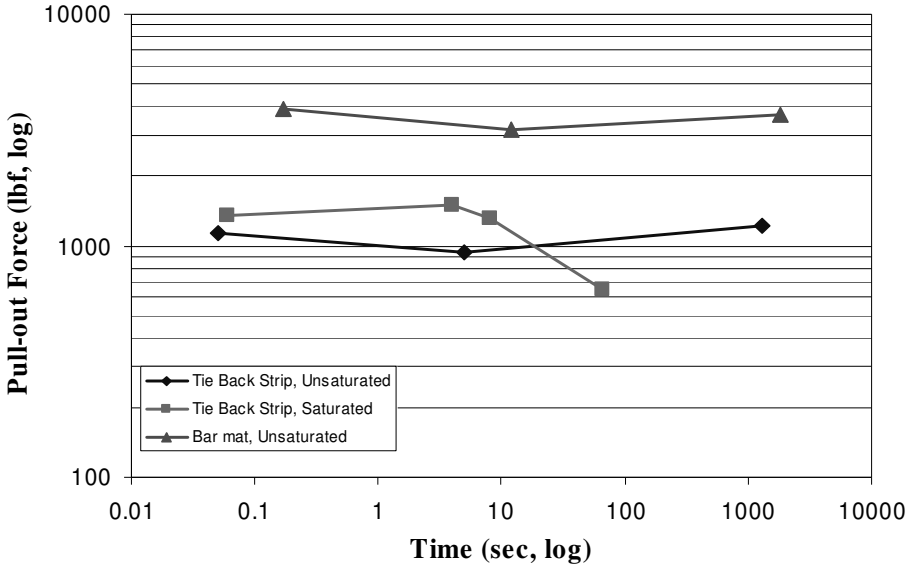

Figure 4.8 Pullout load at failure versus time to failure for all tests

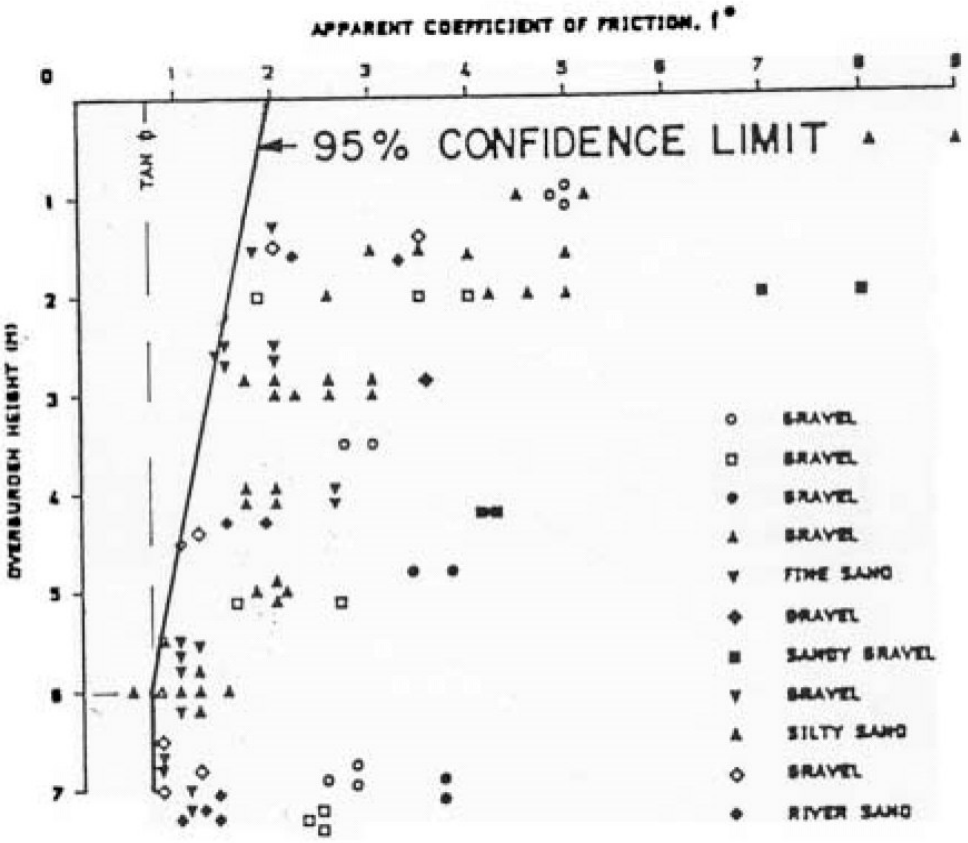

Figure 4.9 Values of apparent coefficient of friction (F*) from pullout tests *(23)*

5 5 FT HIGH MSE WALL AND BARRIER STUDY

The objectives of the bogie tests include quantification of the movement of the barrier, coping, and moment slab system and measurement of the force distributions in the reinforcement strips due to a design impact load. In order to help plan the bogie test wall and finite element models were developed and impact simulations using the bogie impactor were performed using LS-DYNA. The results of bogie tests were used to develop the design guidelines for scenarios that include a traffic barrier mounted on the edge of an MSE wall.

5.1 5 Ft High MSE Wall and Barrier Study Description

Half of the test wall was constructed using 2.43 m (8 ft) long reinforcement while the other half was constructed with 4.88 m (16 ft) long reinforcement strips. The 2.43 m (8 ft) long reinforcement strip represents the minimum length allowed in current practice and, therefore, constitutes the critical case for assessing wall displacement during a barrier impact. Such lengths are commonly used in short height wall segments such as at the beginning or ending of an elevated overpass structure. At the minimum 2.43 m (8 ft) length, current design procedures typically require a density of six reinforcement strips per wall panel (three in each of two different horizontal layers of reinforcement). The other half of the wall was constructed using 4.88 m (16 ft) long reinforcement strips. This length of reinforcement is a practical maximum length used in many MSE wall installations as wall height increases. The increased length increases the pullout resistance of the reinforcement. Therefore, a wall section with 4.88 m (16 ft) strips will constitute the critical case for assessing the magnitude and distribution of impact loads in the reinforcement.

A summary of the bogie impact test plan is shown in Table 5.1. Two different barrier types were used in the test program: a N.J. safety shape (Test 1), and a vertical barrier (Tests 2, 3, and 4). Bogie test 1 (N.J. shape) and test 4 (vertical barrier) were conducted over the portion of the wall with 4.88 m (16 ft) steel strip reinforcement. Bogie test 2 and test 3 involved impacts into vertical concrete barriers placed over wall segments with 2.43 m (8 ft) steel strip and bar mat reinforcement, respectively.

Table 5.1 Bogie Test Plan

Test Sequence	Barrier Type	Moment slab width	Barrier length	Reinforcement Type	Reinforcement Length
Test 1	New Jersey	4.5 ft	10 ft	Steel strips	16 ft
Test 2	Vertical wall	4.5 ft	10 ft	Bar mats	8 ft
Test 3	Vertical wall	4.5 ft	10 ft	Steel strips	8 ft
Test 4	Vertical wall	4.5 ft	10 ft	Steel strips	16 ft

The bogie test installation was planned on the premise that multiple impacts could be conducted on barrier segments connected to the same moment slab. This was planned with the understanding that if excessive motion of the barrier-moment slab system occurs during the first test associated with a given moment slab, the ability to conduct subsequent impact tests of other barrier sections connected to the same moment slab could be compromised. Further, if the motion results in contact with a wall panel, the integrity of the wall may be compromised. Thus, the impact speed of the bogie had to be carefully selected to achieve the desired result of identifying the failure mechanism of the barrier-moment slab system without imparting an unnecessarily high degree of damage to the underlying wall.

5.1.1 Calculation of MSE Wall Capacity

AASHTO LFRD *(1)* was used to estimate the forces expected on the reinforcement strips due to both gravity and impact loads for the 1.52 m (5 ft) high MSE wall. This information ultimately was compared to forces estimated through simulation and measured in the bogie tests as new design procedures were developed.

In the 2.43 m (8 ft) long strip case, resistances were calculated to be 6.58 kN (1.48 kips) (F*=1.789) at the upper most layer and 11.52 kN (2.59 kips) (F*=1.584) at the second layer. A density of 3 strips per layer per panel was used. The load per strip due to gravity was calculated to be 2.49 kN (0.56 kips) at the upper most layer and 4.89 kN (1.1 kips) at the second layer. In this analysis, the traffic surcharge was not considered. The load per strip due to the impact was calculated to be 1.82 kN (0.41 kips) at the upper most layer and 1.25 kN

(0.28 kips) at the second layer. Therefore, the total load per strip was 4.31 kN (0.97 kips) at the uppermost layer and 6.14 kN (1.38 kips) at the second layer. The ratios between the load and resistance are 1.53 at the uppermost layer and 1.88 at the second layer. A summary of resistance and load per strip is presented in Table 5.2**.**

In the 4.88 m (16 ft) long strip case, resistances were calculated to be 13.21 kN (2.97 kips) (F*=1.789) at the upper most layer and 23.09 kN (5.19 kips) (F*=1.584) at the second layer. A density of 2 strips per layer per panel was used. The load per strip due to gravity was calculated to be 3.69 kN (0.83 kips) at the upper most layer and 7.07 kN (1.59 kips) at the second layer. In this analysis, the traffic surcharge was not considered. The load per strip due to the impact was calculated to be 2.76 kN (0.62 kips) at the upper most layer and 1.87 kN (0.42 kips) at the second layer. Therefore, the total load per strip was 6.45 kN (1.45 kips) at the upper most layer and 8.94 kN (2.01 kips) at the second layer. The ratios between the load and resistance are 2.05 at the uppermost layer and 2.58 at the second layer. A summary of resistance and load per strip is presented in Table 5.3. For both cases, the total load was higher than the resistance at the upper most layer. The detailed calculations for designing the MSE test wall are provided in Appendix A.

Table 5.2 Resistance and Force in case of MSE Wall with 8 ft Long Strip

	(1) $\mathbf{T_{Static}}$ Static Load (kips)	**(2)** $\mathbf{T_{Dynamic}}$ Dynamic Load (kips)	**(3)=(1)+(2)** $\mathbf{T_{Total}}$ Total Load (kips)	**R** Resistance (kips)	**Factor of Safety**
Top Layer	0.56	0.41	0.97	1.48 (F*=1.79)	1.53
Second Layer	1.1	0.28	1.38	2.59 (F*=1.58)	1.88

Table 5.3 Resistance and Force in case of MSE Wall with 16 ft Long Strip

	(1) $\mathbf{T_{Static}}$ Static Load (kips)	**(2)** $\mathbf{T_{Dynamic}}$ Dynamic Load (kips)	**(3)=(1)+(2)** $\mathbf{T_{Total}}$ Total Load (kips)	**R** Resistance (kips)	**Factor of Safety**
Top Layer	0.83	0.62	1.45	2.97 (F*=1.79)	2.05
Second Layer	1.59	0.42	2.01	5.19 (F*=1.58)	2.58

5.1.2 Calculation of Barrier Capacity

It is important to be able to quantify the ultimate strength of the barrier sections used in the bogie test matrix to aid in analyses of the barrier-moment slab systems. For example, knowing the ultimate strength of the vertical wall section permitted the overturning test to be planned at an impact speed that will cause substantial movement (i.e., rotation) of the barrier- moment slab system without causing failure of the barrier. Also, the bogie impact speed for the planned bogie tests of the different barriers sections atop a 1.52 m (5 ft) tall MSE wall was selected such that the generated impact force would exceed the capacity of the barrier. In this way, the failure mode of the precast barrier unit can be identified and the maximum impact load will be applied to the supporting MSE wall and its reinforcement. For these reasons, the strength of the selected N.J. safety shape and vertical wall barrier sections was computed.

In regard to the analysis of the strength of a barrier, most references containing concrete barrier design information have used the yield line analysis approach (AASHTO LRFD A13.3.1). Yield line theory considers the plastic strength of all the railing system components with consideration given to barrier geometry, material strengths, applied loading, and strength of the supporting bridge structure. Steel rail systems, concrete rail systems or a combination rail comprised of a steel rail on a concrete barrier can be evaluated using these design procedures. Based on yield line theory, the limiting ultimate capacity of the railing systems used in the test program was calculated. It should be noted that this procedure

assumes that the underlying support structure for the barrier section (e.g., deck, foundation, etc.) has sufficient strength to develop the base moment capacity of the barrier such that the failure occurs in the barrier rather than the support structure. Although this may not necessarily be the case for the precast barrier-coping sections, the yield line analysis approach was used to establish what would be considered a maximum barrier capacity. This ultimate capacity was then compared to design forces derived from simulations to determine appropriate impact speeds for the bogie vehicle tests.

The ultimate load capacities calculated following the assumed yield line failure mechanism were 515.06 kN (115.79 kips) for the 81.28 cm (32 in.) tall N.J. barrier. This is much higher than the load capacity observed in previous dynamic bogie testing. The moment capacity of the "toe" of the safety-shape is large and, thus, typically restricts failure to the upper wall portion of the barrier. The ultimate load capacity of the upper wall portion of the N.J. barrier was calculated to be 329.26 kN (74.02 kips). The length of the failure mechanism calculated for the N.J. barrier section analyzed was 2.23 m (7.3 ft).

The ultimate load capacity calculated following the assumed yield line failure mechanism was 325.34 kN (73.14 kips) for the 68.58 cm (27 in.) tall vertical wall barrier. Note that the height of load application assumed for calculation of the ultimate barrier load capacities was the top of the barrier. The length of the failure mechanism calculated for the vertical wall barrier section analyzed was 1.65 m (5.4 ft). This indicates that, provided the coping has sufficient capacity to develop the ultimate strength of the barrier, the 3.05 m (10 ft) section length selected for evaluation in the bogie tests should be sufficient for developing the primary failure mechanism for each barrier type.

5.2 Finite Element Analysis

The complex nonlinear interactions that occur during an impact event are difficult to capture through conventional analytical means. Therefore, an explicit nonlinear finite element methodology was used to evaluate the dynamic impact performance of the representative barrier-moment slab - MSE wall configurations considered in the test plan.

5.2.1 Modeling Methodology

The methodology followed to model the barrier on top of the MSE wall, and then simulate bogie impacts consisted of the following steps:

1. Construct finite element model of the barrier and MSE wall.
2. Initialize the model of MSE wall and barrier to account for gravitational loading.
3. Simulate the bogie impact against the barrier.
4. Compare results with test data and calibrate the MSE wall and barrier finite element model if needed.
5. Identify any further investigation needed.

   The details of the finite element analysis are presented in the following sections.

1) Geometry and Meshing

The finite element representation of the MSE wall planned for use in the bogie test program consists of the following major components:

1- Precast concrete barrier-coping sections,
2- Cast-in-place moment slab,
3- Steel reinforcement in the barrier, moment slab, and wall panels,
4- MSE wall including the backfill soil, concrete wall panels, level-up concrete, pedestal, and wall reinforcement, and
5- Accelerometers on the barrier and moment slab.

The total length of the MSE wall model was 9.14 m (30 ft), which represented the length of one moment slab section. Three 3.05 m (10 ft) long barrier-coping sections were

attached to the 9.14 m (30 ft) long moment slab. Both full and half-panels were used to construct the wall (see Figure 5.1).

The concrete barrier and moment slab were modeled using solid elements, as were various components of the MSE wall including the soil, wall panels, leveling pad, and pedestal. Three-dimensional beam elements with six degrees at each end were used to model the steel rebar inside the barriers, moment slab, and wall panels. The steel strip reinforcement for the MSE wall was modeled using shell elements with 4 mm (0.16 in.) thickness and 50.8 mm (2 in.) width.

The elements of impact barrier located in the middle of the system were meshed using an element characteristic size of about 50 mm (2 in.) to capture the barrier deformation and damage due to the impact with more accuracy. The two other barriers were meshed more coarsely to reduce computational cost of the simulations since these barriers do not interact with the bogie. The soil was modeled as three components: the reinforced backfill, the overburden soil and the side soil for modeling continuity at the edges of the moment slab as shown in Figure 5.1 and Figure 5.2. The soil elements located beneath the barrier and moment slab were meshed relatively fine using an element characteristic size ranging from 50 mm (2 in.) to 101.6 mm (4 in.) to improve the robustness of the contact between the coping and top edge of the soil and better capture the load transfer from the barrier to the soil during the impact. The overburden soil and side boundary soil are rather coarsely meshed, while a finer mesh is used for the reinforced backfill to capture gravity and impact loads distributed into the soil through the MSE wall and the barrier with more accuracy.

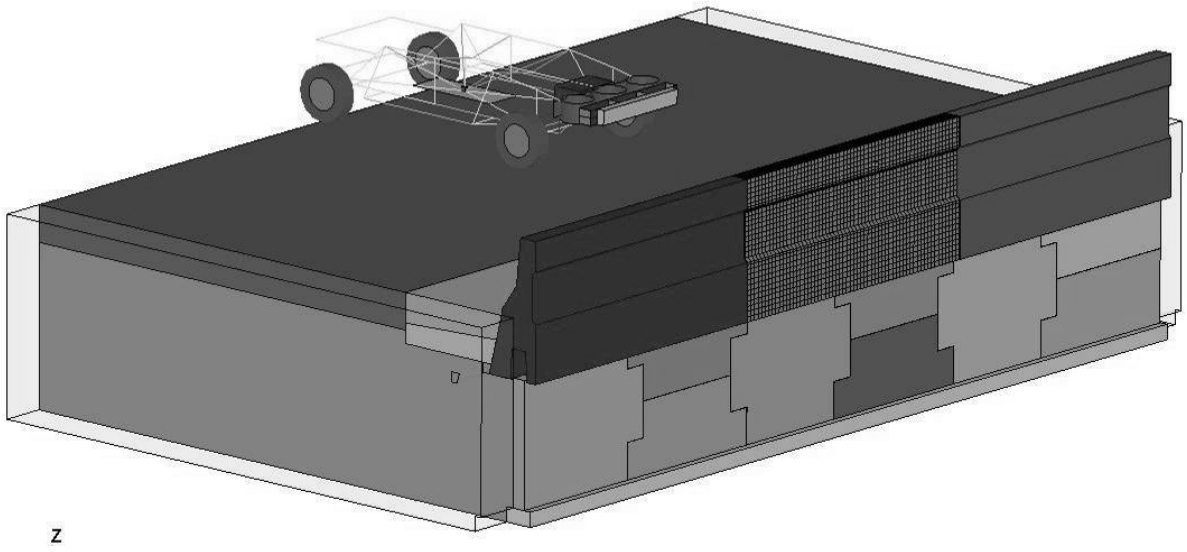

Figure 5.1 3D view of a MSE wall and barriers model with a bogie

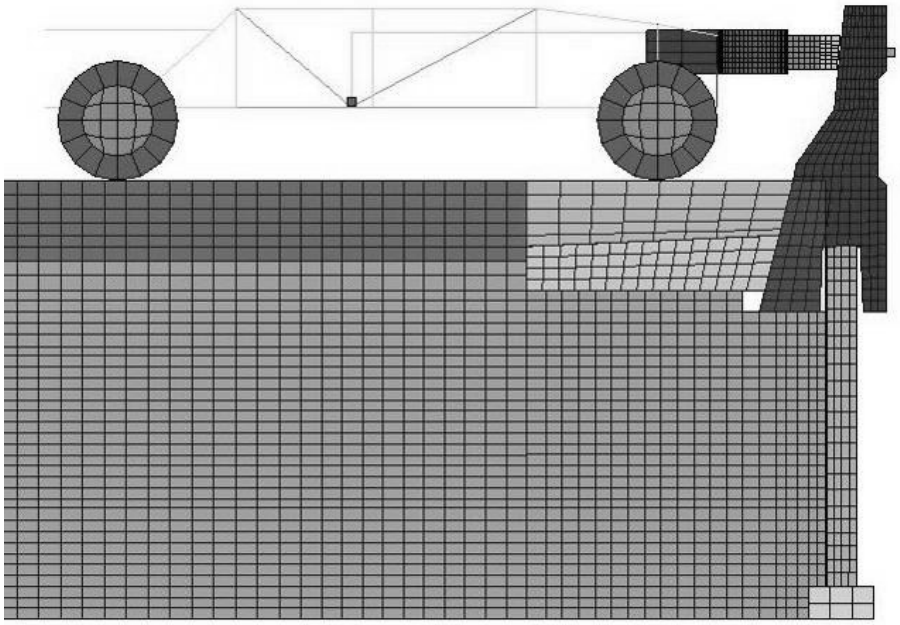

Figure 5.2 Side view of a MSE wall and barriers with a bogie

2) Contact

Although LS-DYNA features some of the most advanced contact algorithms available, capturing interaction between solid and beam or shell elements is rather complex. The requirement of matching nodes to merge the reinforcing steel inside the concrete continuum would dictate the creation of elements with poor aspect ratios and the creation of unnecessarily small element sizes, which has a significant effect on time step control *(24)*. To mitigate this problem, a different connection scheme was utilized between the barrier and the steel reinforcement that permits a more regular, uniform mesh of the concrete to be used throughout the barrier.

The steel reinforcements are coupled (rather than merged) to the surrounding concrete continuum to prevent the creation of poor quality elements. This was achieved using the *CONSTRAINED_LAGRANGE_ IN_SOLID feature in LS-DYNA. The use of this coupling permits the concrete mesh to be constructed without consideration of the location of steel reinforcement. The steel reinforcement is treated as a slave material that is coupled with a master material comprised of the moment slab and barrier concrete. The slave parts (i.e., steel reinforcing bars) can be placed anywhere inside the master continuum part without any special mesh accommodation. The soil and its reinforcement were methodologically modeled in a manner similar to the steel reinforcement in concrete to capture salient responses of the MSE wall. Reinforcing steel in the barriers sections and moment slab and steel reinforcement strips in the soil are shown in Figure 5.3 and Figure 5.4.

Another coupling mechanism, *CONTACT_TIED_SHELL_EDGE_TO_SURFACE was defined to account for the connection beween the panel and steel reinforcement.

The interface between the soil and concrete was modeled using contacts and/or constraints to capture interface (i.e., contact) forces generated between the concrete structure and the MSE wall. The contact friction was based on the estimated soil internal friction angle. Using a soil friction angle ϕ, of 35 degrees, the contact friction was calculated to be 0.7 (tan ϕ).

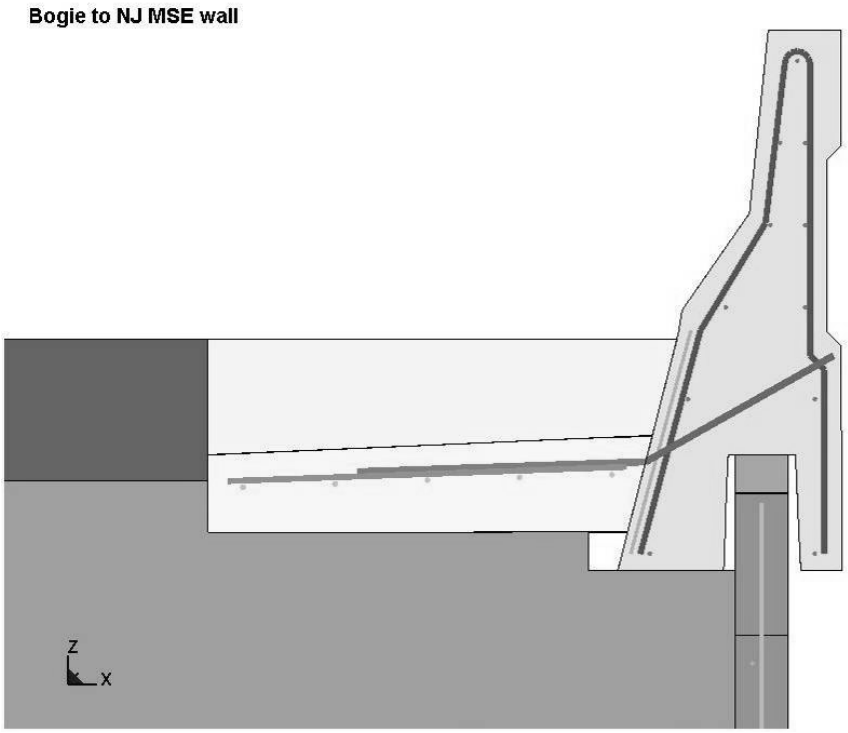

Figure 5.3 Rebars detail in N.J. barrier and moment slab

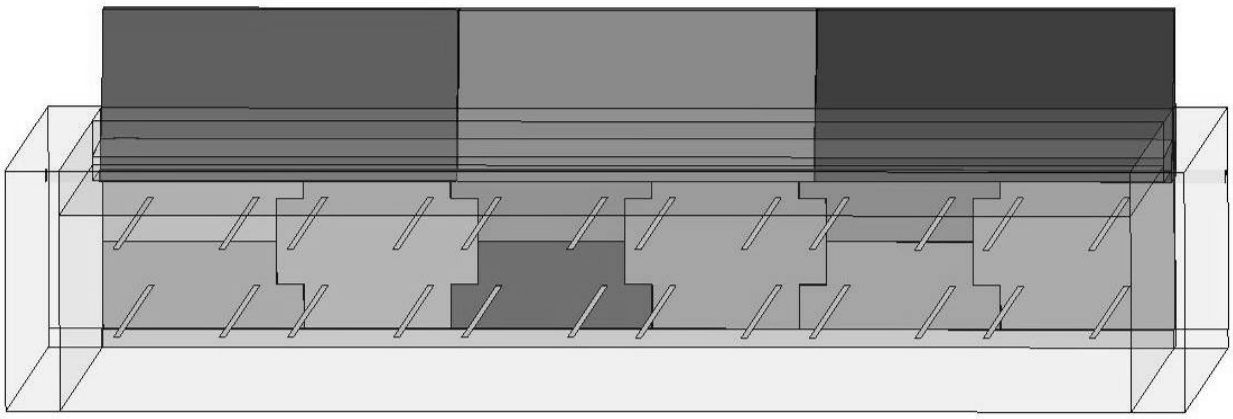

Figure 5.4 Interface between soil and strip shell element

3) Material Models and Model Parameters

Concrete and Steel Material

There are several material options to be considered for modeling the concrete structures in LS-DYNA. These material options range from the very simple elastic material to a nonlinear damage material model. The elastic material option can be useful in modeling areas that will not be subjected to significant stress in order to reduce computational costs of the simulation. If this approach is used, appropriate checks must be made to ensure the tensile stress in the concrete does not exceed its failure threshold *(24)*.

The outside barrier sections were modeled using elastic material (MAT type 1) as shown in Table 5.4. However, the middle barrier that was subjected to direct impact was modeled using a non-linear response concrete material model definition. In LS-DYNA 971, it is designated as material MAT type 159 developed by APTEK *(24)*. This is a more sophisticated but computationally expensive method to explicitly model concrete. In this model, a brittle material like concrete will lose (at a given rate) its ability to carry load when a specified damage/failure threshold is reached. This is very useful because it provides a more accurate representation of the failure mechanism of the concrete components, and better prediction of the impact load transfer. The parameters of MAT type 159 can be assigned using two additional concrete properties, the unconfined compressive strength of concrete f'_c and the maximum aggregate size, which was taken as 25.4 mm (1 in.).

The moment slab, the wall panels, the pedestal, and the level-up concrete were modeled using an elastic material model definition (MAT type 1). All steel rebars and steel strips were modeled using a piecewise linear plasticity material model (MAT type 24) that is representative of the actual stress-strain relationship of the material using the properties shown in Table 5.5. Steel rebar exhibits rate effects, and yields in a ductile manner until it breaks at an ultimate strain greater than approximately 20 percent. Before yield, the material is assumed to be linearly elastic. After yielding, the steel can undergo plastic deformation and strain hardening.

Table 5.4 Material Properties of Concrete Model

	E (psi)	ν	ρ (lb/in^3)	f'_c (psi)
Elastic Concrete (MAT type 1)	3.62E+6	0.17	0.084	-
Damage Concrete (MAT type 159)	-	-	0.084	4,000

* E is the young's modulus, ν is Poisson's ratio, ρ is the mass density, and f'_c is the compressive strength.

Table 5.5 Material Properties of Steel Model

	E (psi)	ν	ρ (lb/in^3)	Yield Stress (psi)
Steel (MAT type 24)	30.46E+6	0.29	0.28	60,000

* E is the young's modulus, ν is Poisson's ratio, and ρ is the mass density.

Soil Material

The soil was modeled using the two-invariant geological cap material model (MAT type 25) *(20)*. The advantage of the cap model over other models such as the Drucker-Prager formulation is the ability to model plastic compaction. In these models all purely volumetric response is elastic until the stress point hits the cap surface. Therefore, plastic volumetric strain (compaction) is generated at a rate controlled by the hardening law. Thus, in addition to controlling the amount of dilatency, the introduction of the cap surface adds another experimentally observed response characteristic of geological materials into the model *(25) (26)*.

The cap model is defined in terms of the first stress invariant $I_1 = trace(\sigma) = \sigma_{11} + \sigma_{22} + \sigma_{33}$ and the second deviatoric stress invariant $J_2 = 1/2 S_{ij} S_{ij} = 1/2(s_{11}^2 + s_{22}^2 + s_{33}^2)$, where σ is the stress tensor and $S_{ij} = \sigma_1 - \sigma_3$ is the deviatoric stress tensor. The yield surface of the cap model consists of three regions (Figure 5.5): a failure envelope $f_1(\sigma)$, an elliptical

cap $f_2(\sigma,\kappa)$, and a tension cutoff region $f_3(\sigma)$, where κ is the hardening parameter. The functional forms of the three surfaces are:

1. Failure envelope region: $f_1(\sigma)=\sqrt{J_{2D}}-F_e(I_1)=0$, for $T \le I_1 < L(\kappa)$ (5-1)

2. Cap region: $f_2(\sigma,\kappa)=\sqrt{J_{2D}}-F_c\left(I_1,\kappa\right)=0$, for $L(\kappa) \le I_1 < X(\kappa)$ (5-2)

3. Tension cutoff region: $f_3(\sigma)=T-I_1=0$, for $I_1=T$ (5-3)

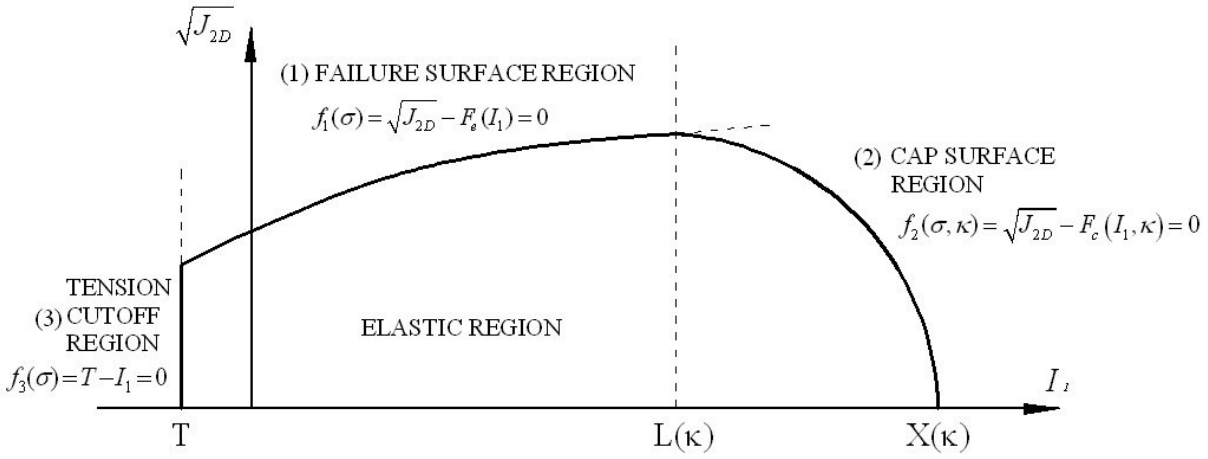

Figure 5.5 Yield surface of the cap model *(20)*

In the elastic region, $F_e(I_1)$ can be expressed as;

$$F_e(I_1)=\alpha-\gamma e^{-\beta I_1}+\theta I_1 \tag{5-4}$$

where the yield surface was determined by the parameters α, θ, γ, α and β which are usually evaluated by fitting a curve through failure data taken from a set of triaxial compression tests.

In Eq. (5-2), $F_c\left(I_1,\kappa\right)$ can be expressed as;

$$F_c\left(I_1,\kappa\right)=\frac{1}{R}\sqrt{\left[X(\kappa)-L(\kappa)\right]^2-\left[I_1-L(\kappa)\right]^2} \tag{5-5}$$

$$X(\kappa)=\kappa+RF_e(\kappa) \tag{5-6}$$

$$L(\kappa)=\begin{cases}\kappa & if\ \kappa>0\\ 0 & if\ \kappa\le 0\end{cases} \tag{5-7}$$

where $X(\kappa)$ is the intersection of the cap surface with the I_1 axis and the hardening parameter κ is related to the plastic volume change ε_v^p through the hardening law

$$\varepsilon_v^p = W\left\{1-\exp\left[-D(X(\kappa)-X_0\right]\right\} \tag{5-8}$$

where the values of parameters W and D are found from hydro static compression test data. The value of R is the ratio of major to minor axes of the quarter ellipse defining the cap surface. The parameters used in the numerical simulation are shown in Table 5.6.

To understand the failure behavior of the cap soil material, the various soil properties were collected as given in Table 5.6. Two different soil properties, McCormick Ranch Sand *(27)* and elasto-platic soil parameters given in NCHRP Report 556 *(28)* were compared to verify the cap property used in this study. The cap models for each case were plotted as shown in Figure 5.6. In the failure envelope $f_1(\sigma)$ and tension cutoff region $f_3(\sigma)$, the three soils show good agreement, but in the elliptical cap $f_2(\sigma,\kappa)$, the soil material used in simulation shows a larger cap surface area than the other soils due to the large R.

Table 5.6 Comparison of Cap Soil Properties

		Simulation	**McCormick Ranch Sand**	**NCHRP 556**
Elasticity	K (MPa)	22.219	459.676	52.19
	G (MPa)	7.407	275.792	24.087
Plasticity	α (MPa)	4.154	0.00186	0.01
	β (MPa^{-1})	0.0647	0.09718	0
	γ (MPa)	4.055	0.00117	0
	θ (radian)	0	0.02	0.2925
Hardening Law	W	0.08266	0.064	0.023
	D (MPa^{-1})	0.239	0.00725	0.87
	R	28	2.5	4
	X_0 (MPa)	-2.819	1.20658	0.01593
Tension Cut	T (MPa)	0	-2.06843	0

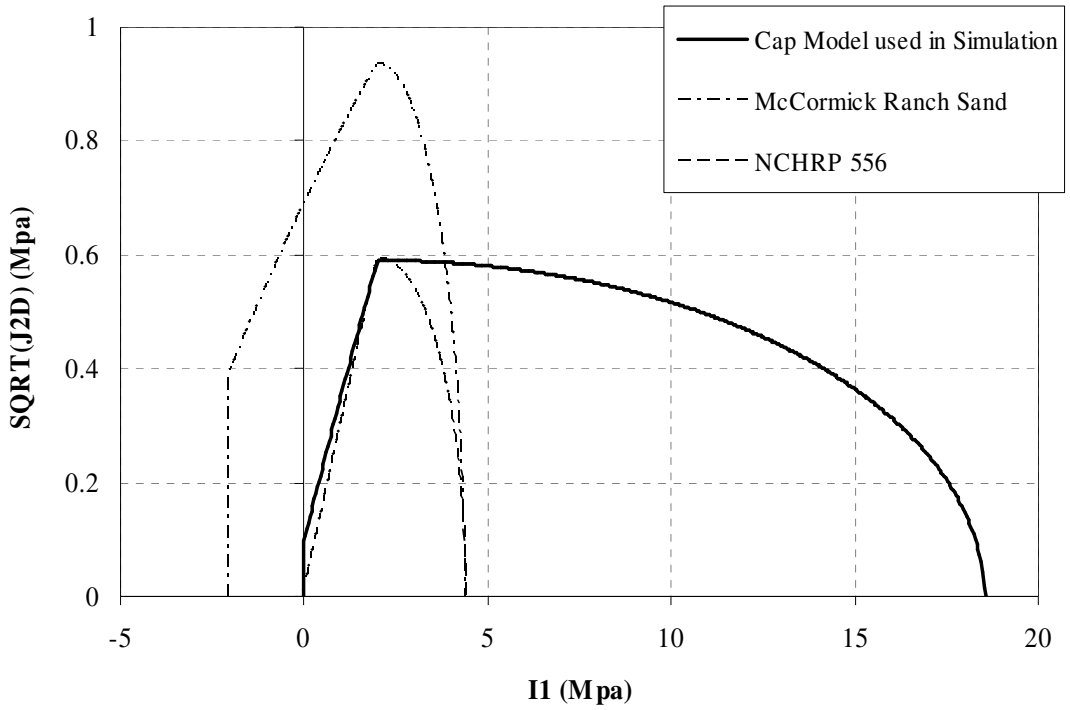

Figure 5.6 Comparison of cap models

4) Bogie Vehicle

The TTI test bogie is a 2,268 kg (5,000 lb) vehicle configured with three 304.8 mm (12 in.) diameter crushable steel cylinders on its nose assembly as shown in Figure 5.7. A spreader beam is attached across the three cylinders as shown in Figure 5.8. A wood block is attached to the face of the spreader beam to help dampen high frequency noise during an impact. The bogie has an accelerometer installed at its CG.

The finite element model of the bogie consisted of a simple representation of the vehicle chasses with a more detailed representation of the crushable nose assembly. Similar to the test bogie, an accelerometer was placed at the CG of bogie model. The finite element model of the bogie consists of 3,935 elements and 4,645 nodes.

(a) 5,000 lb TTI test bogie

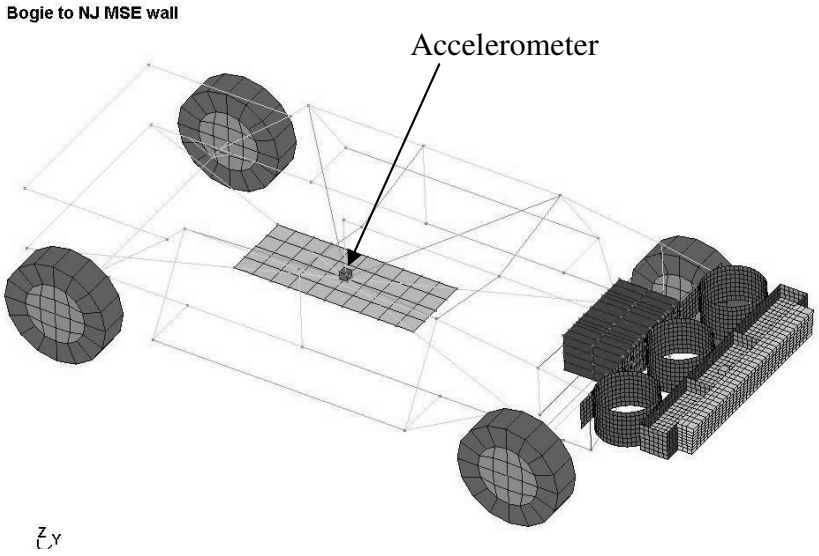

(b) 5,000 lb bogie model

Figure 5.7 5,000 lb bogie model

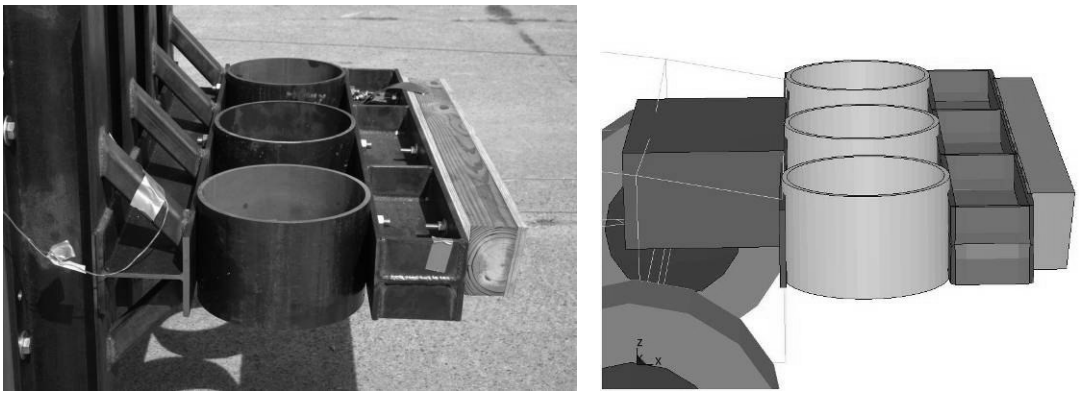

Figure 5.8 Detailed crushable cylinders of test bogie and numerical simulation

5) Initialization of the Model for Gravitational Loading

The MSE wall and barrier model was initialized to account for gravitational loading on the soil mass. Gravity loading effects soil pressure on the wall panels and the build up of initial stresses in the steel strips. This step had to be done prior to vehicular impact on the barrier. It was achieved by gradually ramping up gravity on the system while imposing a diminishing mass damping on the soil mass to prevent oscillatory forces from developing. The gravity loading and damping on the soil are shown in Figure 5.9.

The weight of the system was measured and used as a convergence criterion for the steady state solution for the MSE wall model with 4.88 m (16 ft) strips as shown in Figure 5.10. For example, the total mass of the finite element model with the N.J. barrier on top of the MSE wall with 4.88 m (16 ft) long strips is 277,549 kg (19,018 slug or 611,890 lb mass). The weight of the system is calculated to be 2,721.6 kN (611.85 kips) using the mass of the finite element model and the acceleration of gravity. Therfore, after accounting for gravitationad load, the weight of model system should converge to the calculated system weight. The weight of the finite element model was 2,717.7 kN (610.96 kips) at the end of initialization step. A reasonable agreement shows that the weight of the finite element model approached the calculated weight of the model system as shown in Figure 5.10.

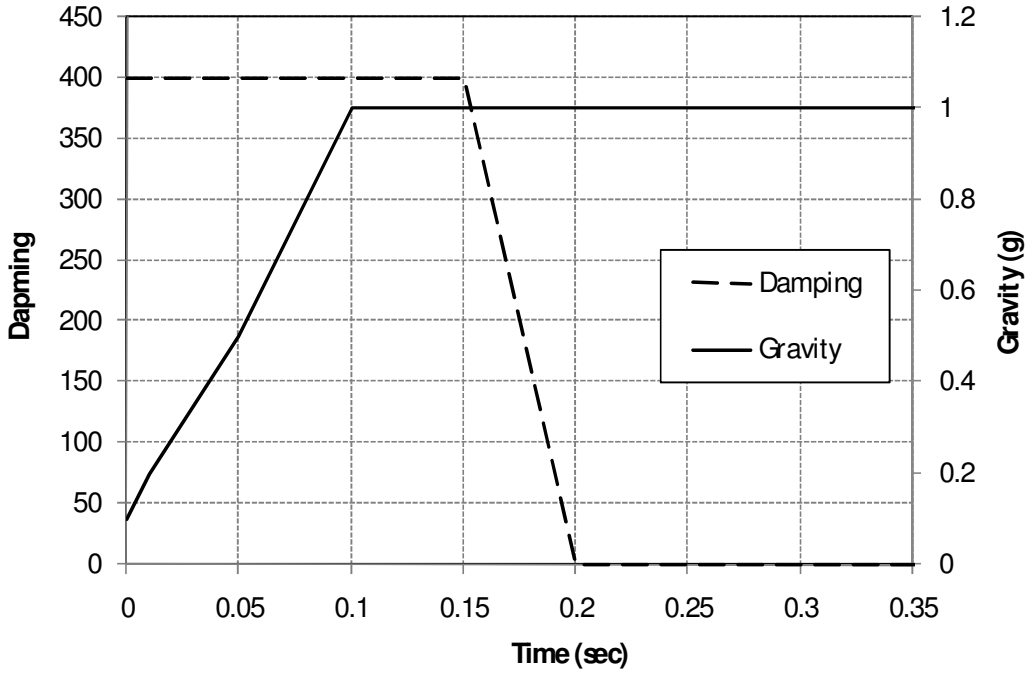

Figure 5.9 Gravity and damping of the MSE wall in steady state condition

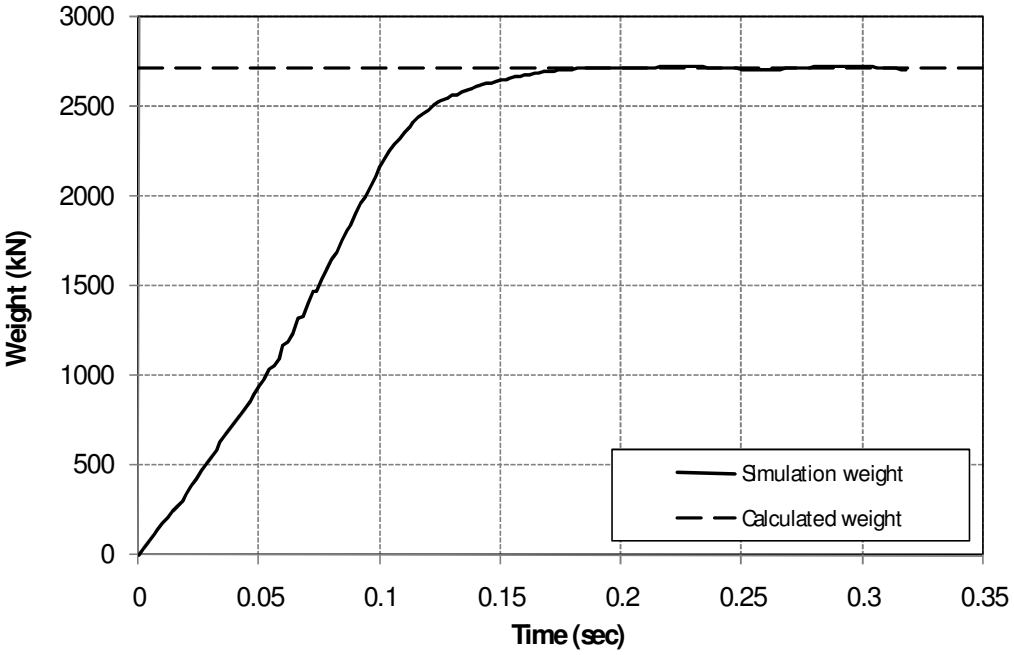

Figure 5.10 System weight of the MSE wall model

5.2.2 Finite Element Model Iteration: Boundary Condition

Initially, the overburden soil on the moment slab was defined to be continuous across the front traffic edge of the moment slab. Along the sides of the moment slab, the soil was discontinuous and only constrained in the longitudinal direction (y-direction in Figure 5.11) to retain it in place and properly account for mass and inertial effects.

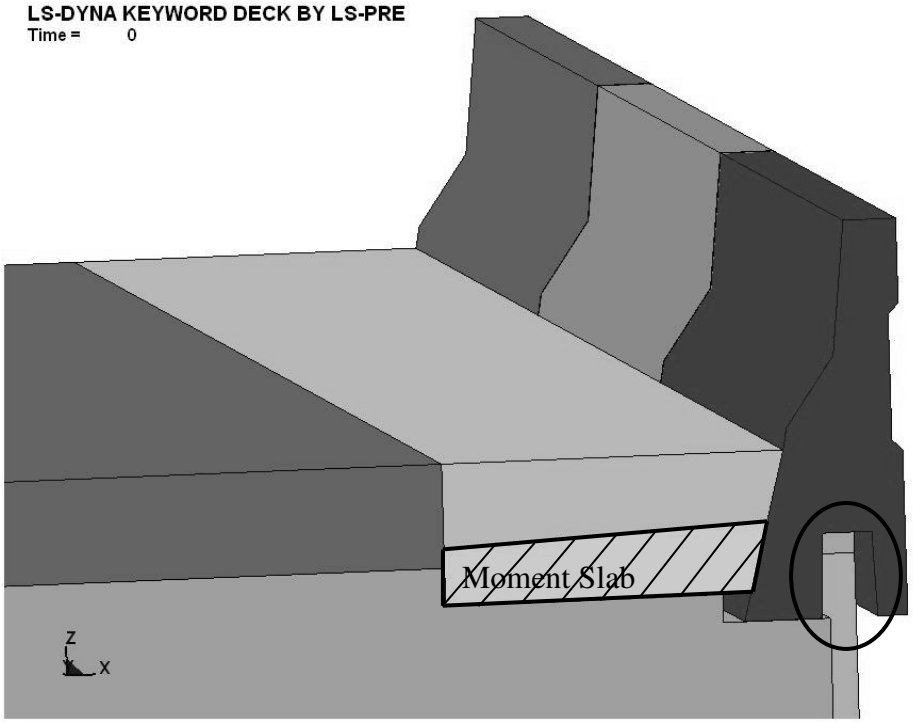

Figure 5.11 Side view of finite element model

Thus, the first attempted model did not account for any friction or shear strength that might exist along the sides of the moment slab (Figure 5.12(a)). The displacement of the barrier-moment slab system using this condition was greater than expected based on field experience with these systems. Additionally, the forces estimated in the strips were well above those computed based on current AASHTO LRFD design practice. The lateral displacement at the bottom edge of the coping was predicted to be of sufficient magnitude to contact and apply substantial force to the recessed wall panel (see the circle in Figure 5.11). This contact will undoubtedly increase the forces in the wall reinforcement, and has the potential to fracture the wall panel and/or result in sufficient movement of the panel to cause

pullout of the reinforcing strips. It was theorized that some of this “excessive movement” in the barrier-moment slab system might be attributed to the model’s neglect of friction along the sides of the overburden soil and moment slab. The sensitivity of the dynamic behavior of the system to the boundary conditions along its sides was investigated through additional simulations.

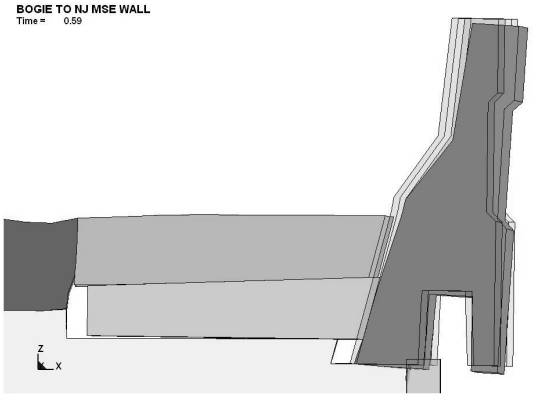

(a) No friction boundary condition

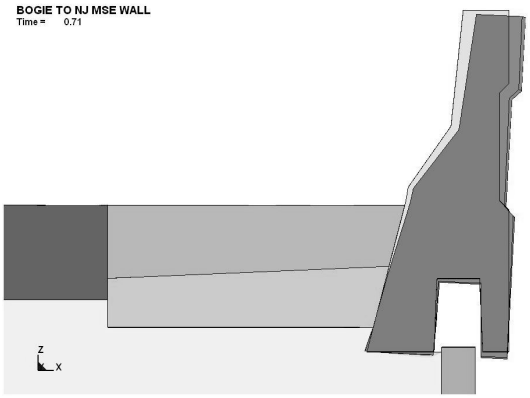

(b) Friction wall condition

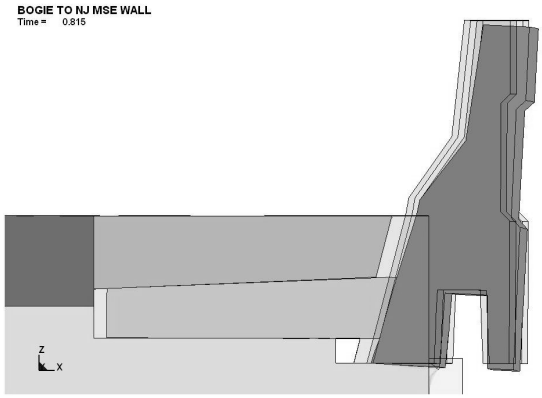

(c) Side soil condition

Figure 5.12 Comparison of simulation with different boundary condition

In practice, the boundary conditions for a barrier-moment slab system can vary from installation to installation. In some systems, adjacent moment slabs are doweled together - a practice that greatly enhances the shear resistance at the edge of the moment slab. If dowel bars are not used, the moment slab sections act independently of one another but there will

still be some shear capacity at the interface due to frictional contact. In both cases, the shear strength of the overburden soil and overlying pavement surface that is continuous across the moment slab interface will increase the overall resistance of the system to impact load.

The second attempted model was constructed the wall with the frictional contact on each side of the the barrier-coping-moment slab system and soil as shown in Figure 5.12 (b). The static and dynamic coefficients of friction were defined based on angles of internal friction of 35 degrees and 31 degrees, respectively.

As indicated by the results of these simulations as shown in row 1 and 2 of Table 5.7, friction at the ends of the moment slab and overburden soil can have a pronounced effect on the displacement and rotation of the barrier-moment slab system under impact load. The two simulations are thought to bracket the barrier movement likely to be observed in the bogie tests.

Table 5.7 Comparison of Displacements for Bogie Test Models

	Middle barrier at top (in.)	**Middle barrier at bottom (in.)**	**Strip at front at impact location (in.)**	**Strip at end at impact location (in.)**
No Side Friction	7.35 in.	4.25 in.	0.16 in. (4.0 mm)	0.13 in. (3.7 mm)
Side Wall	4.99 in.	0.03 in.	0.07 in. (2.0 mm)	0.065 in. (1.7 mm)
Continuous Soil	6.69 in.	3.3 in.	0.15 in. (4.0 mm)	0.128 in. (3.3 mm)

Given the range of movement observed at the bottom of the coping in the previous simulations, an additional simulation effort was undertaken in an attempt to more precisely define the soil and moment slab boundary conditions as shown in Figure 5.12 (c). The overburden soil was extended across the edges of the moment slab, and a soil continuum was modeled adjacent to the ends of the moment slab (replacing the previously modeled side wall).

The shear strength of the overburden soil was captured through the soil material model rather than through a defined frictional contact. The interface between the moment slab and adjacent soil were defined through definition of material contacts with friction coefficients assigned based on the angle of internal friction of the soil. Additionally, the row of elements directly beneath the moment slab and adjacent to the bottom edge of the coping were removed from the soil mesh (see the circle in Figure 5.12 (c)). Based on analyses of the previous simulations, it was theorized that these elements may be providing artificially high resistance to rotation of the barrier-moment slab system.

A comparison of displacements for the barrier-coping section obtained from the different simulations is shown in Table 5.7. The greatest movement was obtained for the model without side friction. The lowest displacements at the top and bottom of the barrier-coping section were obtained from the model in which the ends of the overburden soil and moment slab were in frictional contact with side walls. The model with continuous overburden soil across the ends of the moment slab fell between the other two. The fact that the simulation with continuous overburden soil is closer to the results of the model without side friction than the model with frictional side walls is at least partially due to the removal of a row of elements below the moment slab adjacent to the bottom edge of the coping.

Table 5.7 also shows a comparison of the displacement of the reinforcement strip directly under the point of impact, which is the one that experiences the highest impact load. The displacements at the end of the strip range from1.7 mm (0.065 in.) to 3.3 mm (0.13 in.). It should be noted that these displacements are due to transfer of the barrier impact load into the MSE wall (through the backfill soil) and do not include any movement that may arise due to direct contact between the coping and wall panels. While it is arguable which of the simulations most closely resembles reality, they collectively raised concern regarding the possibility of strip pullout. Movement of the strip along its entire length would limit the magnitude of the impact force. In other words, the maximum force due to impact that can be measured in the strips is limited by their pullout resistance. If pullout occurs, the maximum forces imparted to the reinforcement strips due to a barrier impact will be reduced.

Without further test data to validate the soil model and boundary conditions, it was unknown which of the modeling methodologies most closely resembles the actual system. Data derived from the bogie tests was later used to calibrate and validate the finite element

model so that additional simulations can be conducted with more confidence to support the development of new design guidelines and predict the performance of the barrier-moment slab system under a full-scale vehicular impact.

5.2.3 Simulated Impact into Barrier Placed on MSE Wall with 8 Ft Long Strip

The simulated bogie vehicle impacted the middle vertical barrier section at a speed of 32.67 km/h (20.3 mph). The point of impact was slightly offset from the centerline of the middle barrier section to align with one of the reinforcement strips (strip D1). To enable comparison of forces and displacements, selected strip locations were assigned an alphanumeric designator that describes its horizontal position relative to the bogie impact point and its vertical reinforcement layer. The location designator used is based on a density of 3 strips per layer per panel. For example, strip "D1" is positioned beneath the impact point in the first (i.e., upper) layer of reinforcement as shown in Figure 5.13.

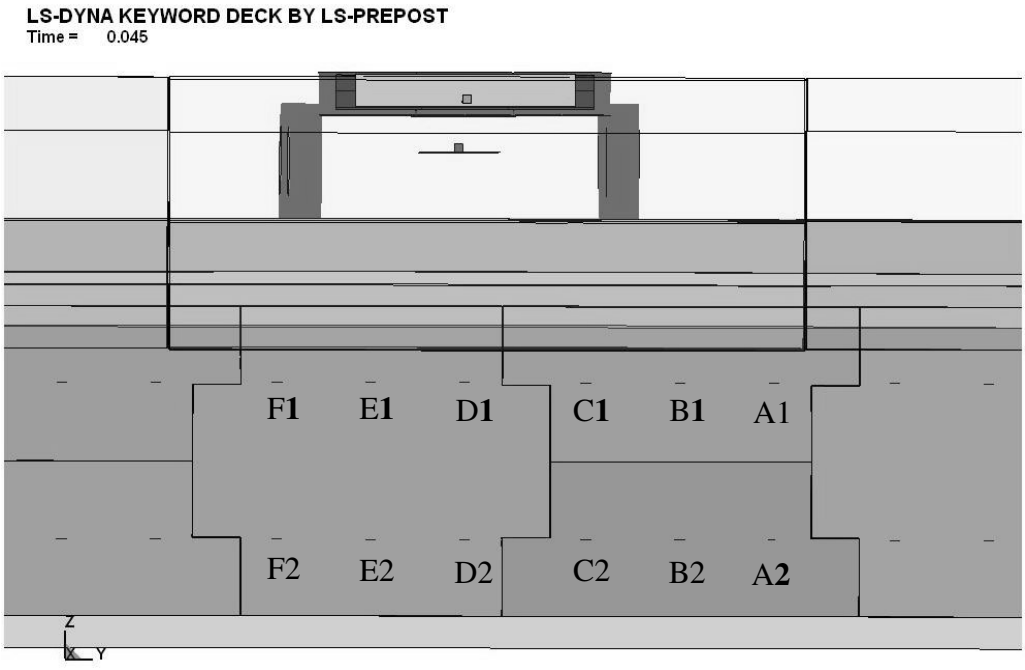

Figure 5.13 Strip location indicator

Sequential images from the simulation are shown in Figure 5.14. The maximum displacement at the top of the middle barrier was occurred at 0.07 sec. The maximum 50-msec average impact load was 346.38 kN (77.87 kips) at 0.04 sec as shown in Figure 5.15. The maximum dynamic displacement was 9.9 cm (3.9 in.) at the top of the barrier and 4.45 cm (1.75 in.) at the bottom of the coping. The permanent displacement was 5.4 cm (2.1 in.) at the top of the barrier and 3.3 cm (1.29 in.) at the bottom of the coping. The maximum dynamic displacement of the panel was 4.3 mm (0.17 in.) at the upper reinforcement layer and 1 mm (0.04 in.) at the second layer. The permanent displacement of the panel was 2.3 mm (0.09 in.) at the upper layer and 0.4 mm (0.02 in.) at the second layer (see Figure 5.16).

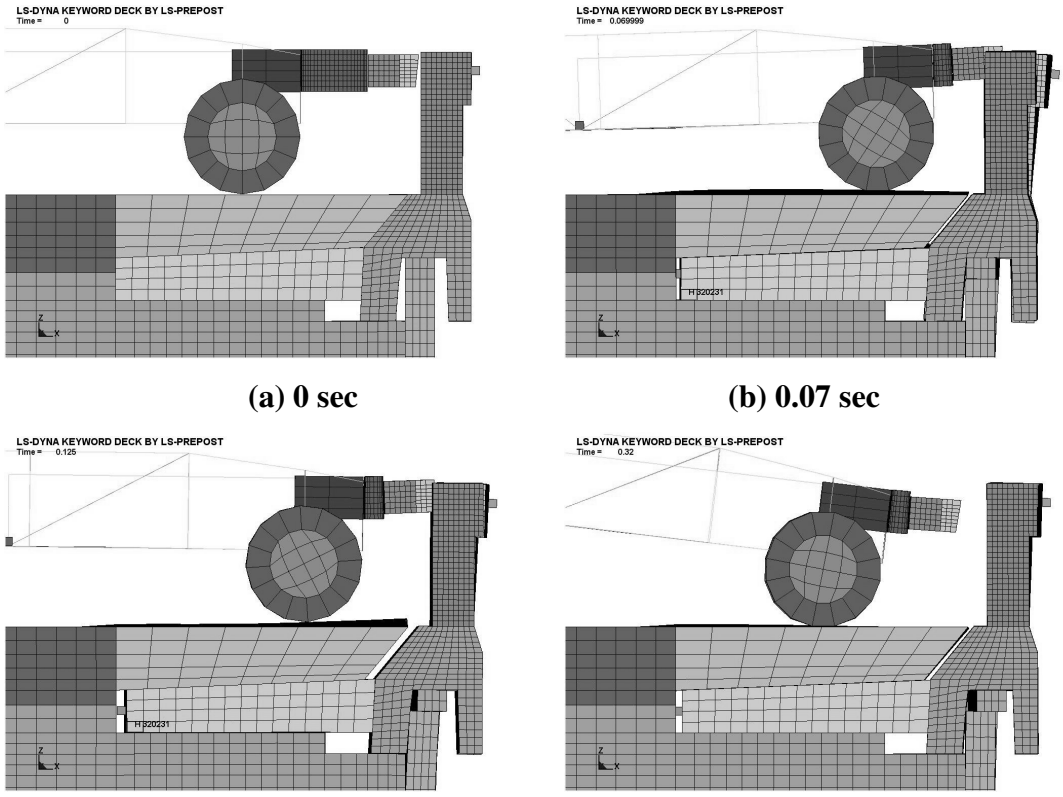

(a) 0 sec **(b) 0.07 sec**

(a) 0.125 sec **(b) 0.32 sec (final)**

Figure 5.14 Sequence image of model during impact

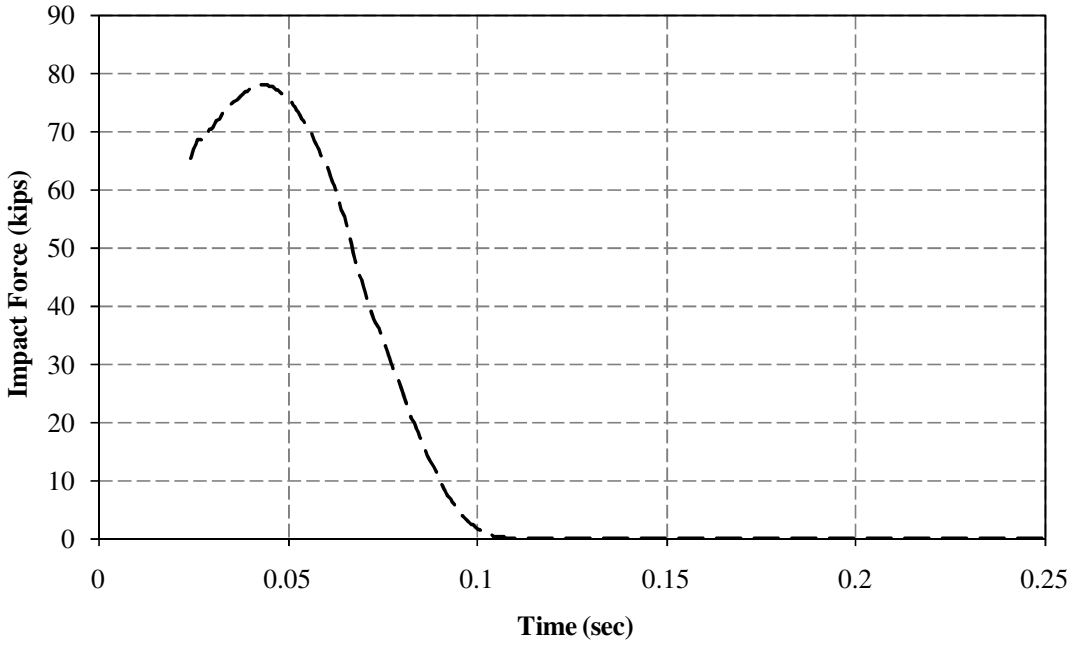

Figure 5.15 Impact load

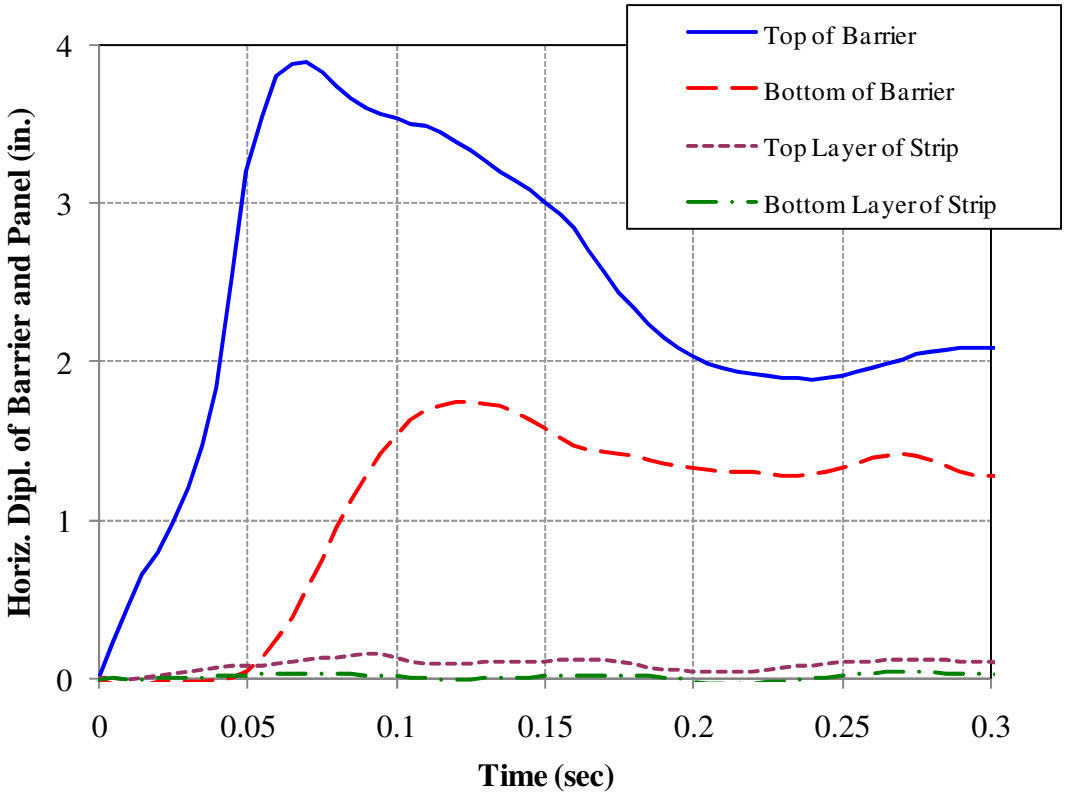

Figure 5.16 Displacement of barrier and panel

As shown in Figure 5.17, the damage profile that develops in the simulated barrier is similar to that observed in previous tests of N.J. profile barriers. It occurs above the toe of the barrier and has a parabolic shape. However, due to the short (3.05 m or 10 ft)) length of the precast barrier section that was modeled, much of the damage eventually radiates out to the free ends of the section.

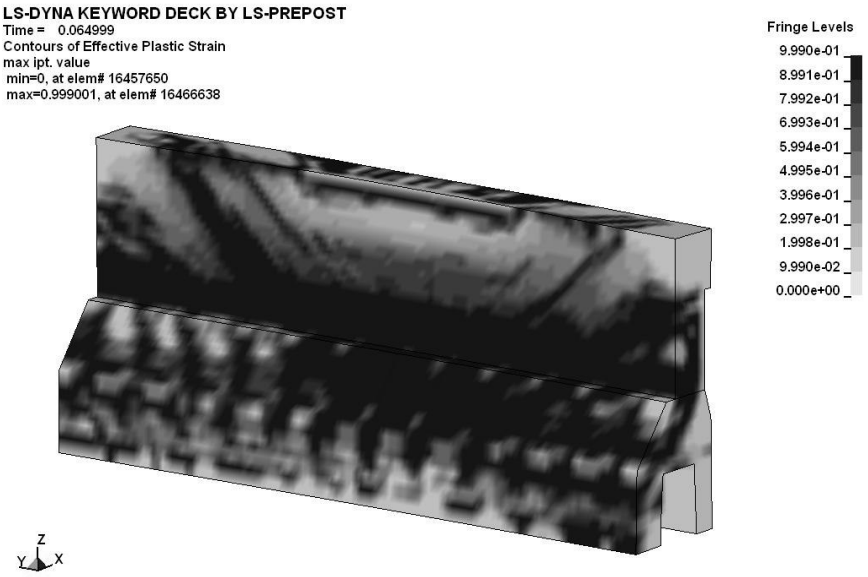

(a)

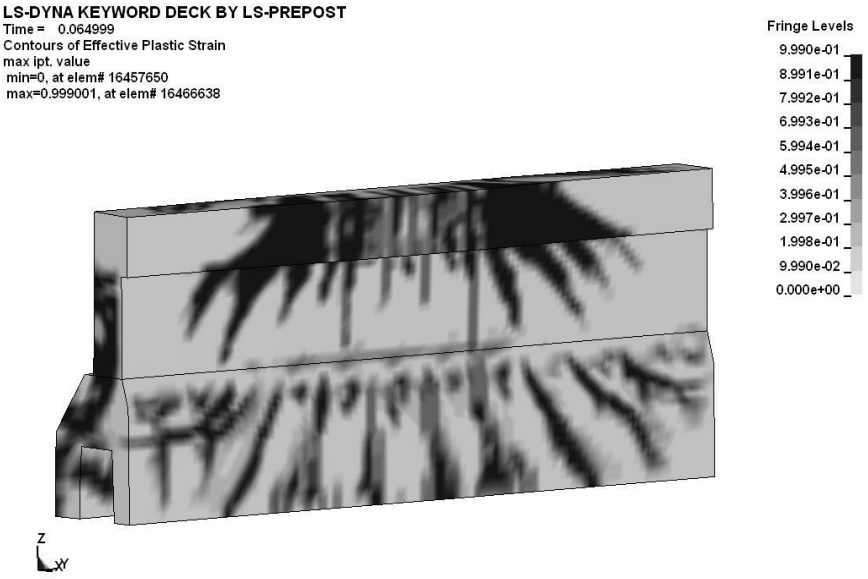

(b)

Figure 5.17 Concrete damage profile on (a) frontside and (b) backside of the barrier.

The strip load in the numerical simulation consists of the initialized static load and the dynamic impact load. Figure 5.18 shows the raw data of the total load in selected reinforcement strips. The maximum instantaneous load for strip "D1" was 21.31 kN (4.79 kips). The total maximum 50-msec tensile load for strip "D1" was 15.44 kN (3.47 kips) at a distance of 17.8 cm (7 in.) from the face of the panel which corresponds to the planned location of strain gages in the test installation (Figure 5.19).

The distributions of maximum load along the reinforcement strips at the uppermost reinforcement layer (D1) are presented in Figure 5.20. As expected, the maximum load in a given strip occurs near its attachment to the wall panel and the load decreases along its length. The loads in the strips attached to the wall panel below the point of impact in the middle of the barrier section have similar distributions. Table 5.8 shows the absolute maximum load in the strips at the location 17.8 cm (7 in.) from the wall end of the reinforcement.

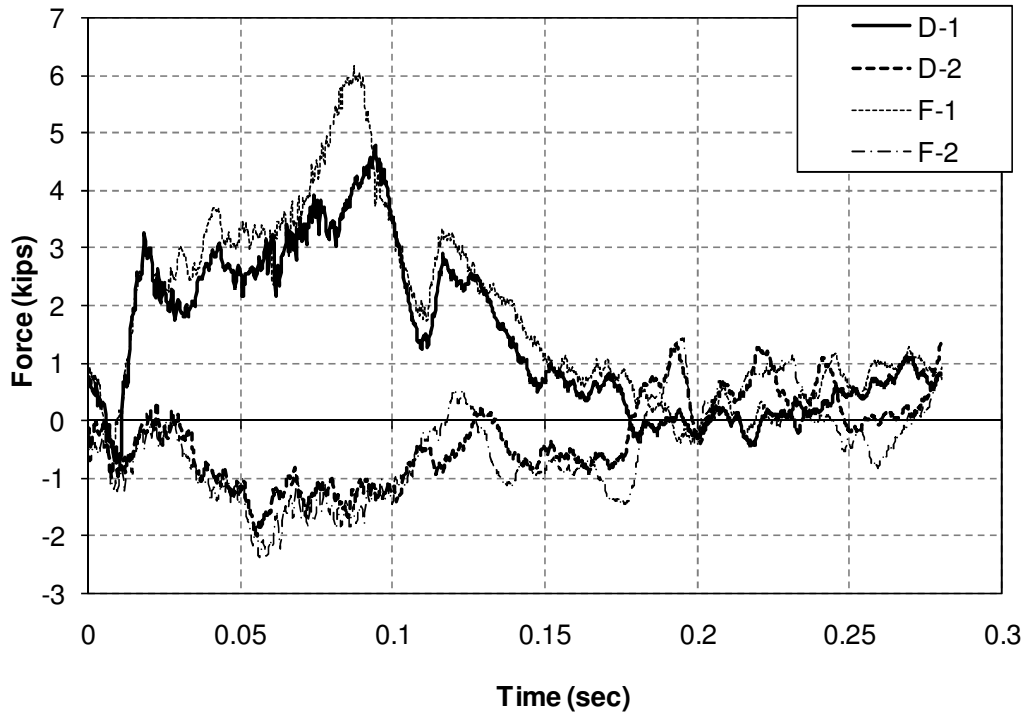

Figure 5.18 Raw data of load on the strip.

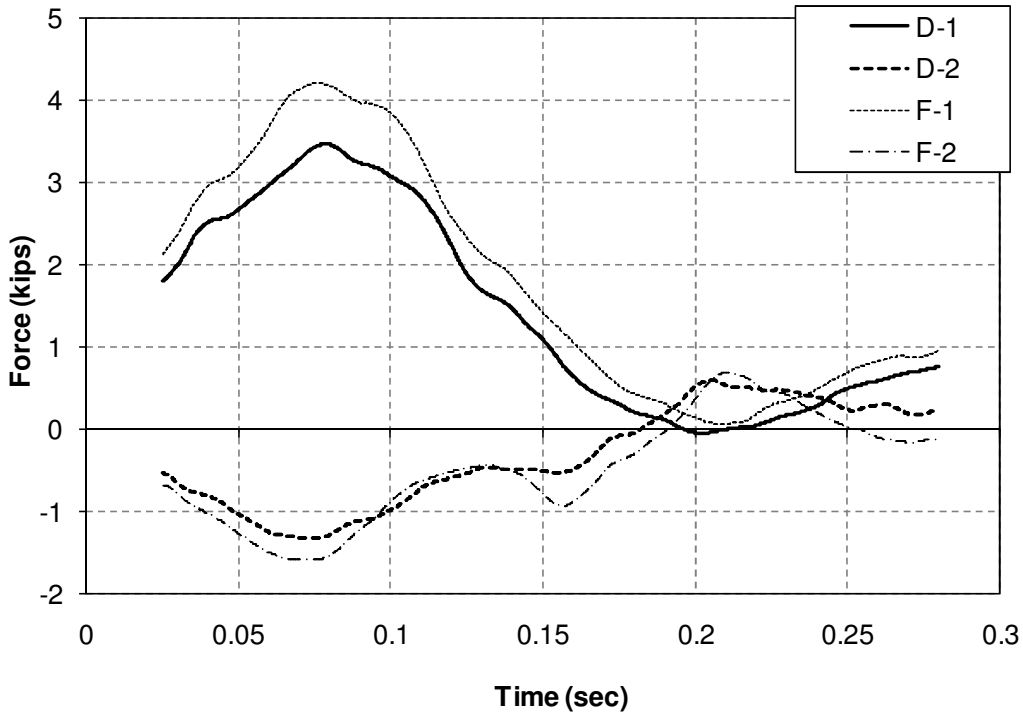

Figure 5.19 50 msec average load on the strip.

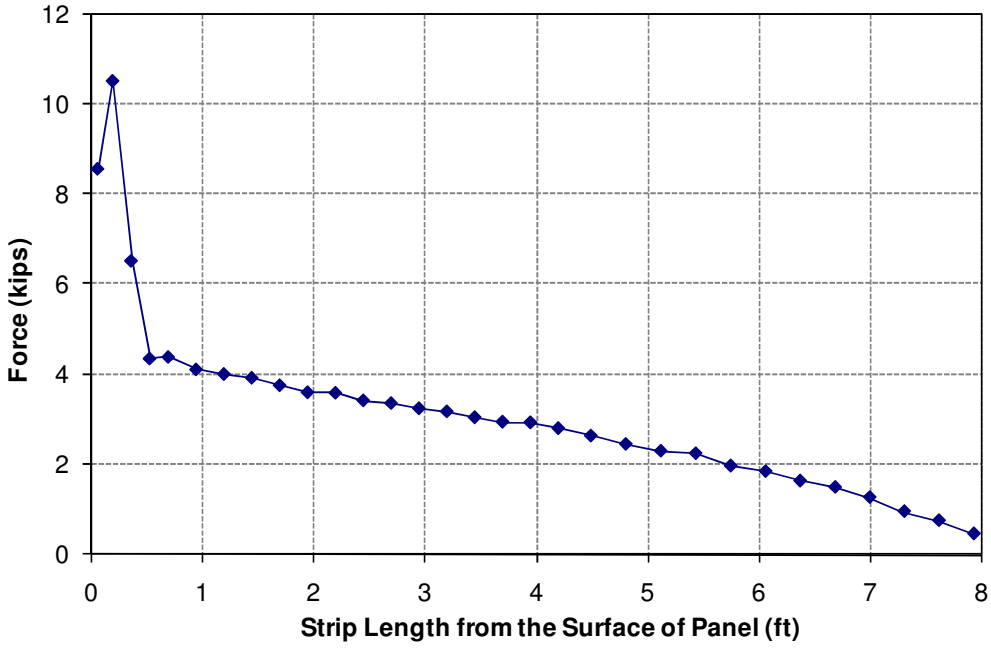

Figure 5.20 Distribution of load on the strip at 0.087 sec (D1)

Table 5.8 Load in Strips at 7 in Location from the Face of the Wall Panel

Location on Strip	D1	D2	F1	F2
Total max. Load (kips)	4.79	1.36	6.17	1.45
Total 50 msec average load (kips)	3.47	0.6	4.2	0.68

The strain on the wall panel surface was evaluated to check the resistance of the panel to barrier impact loads. Figure 5.21 shows the strains predicted in the numerical simulation at strip "D1". The maximum compressive strain was 0.0047 at 0.095 sec.

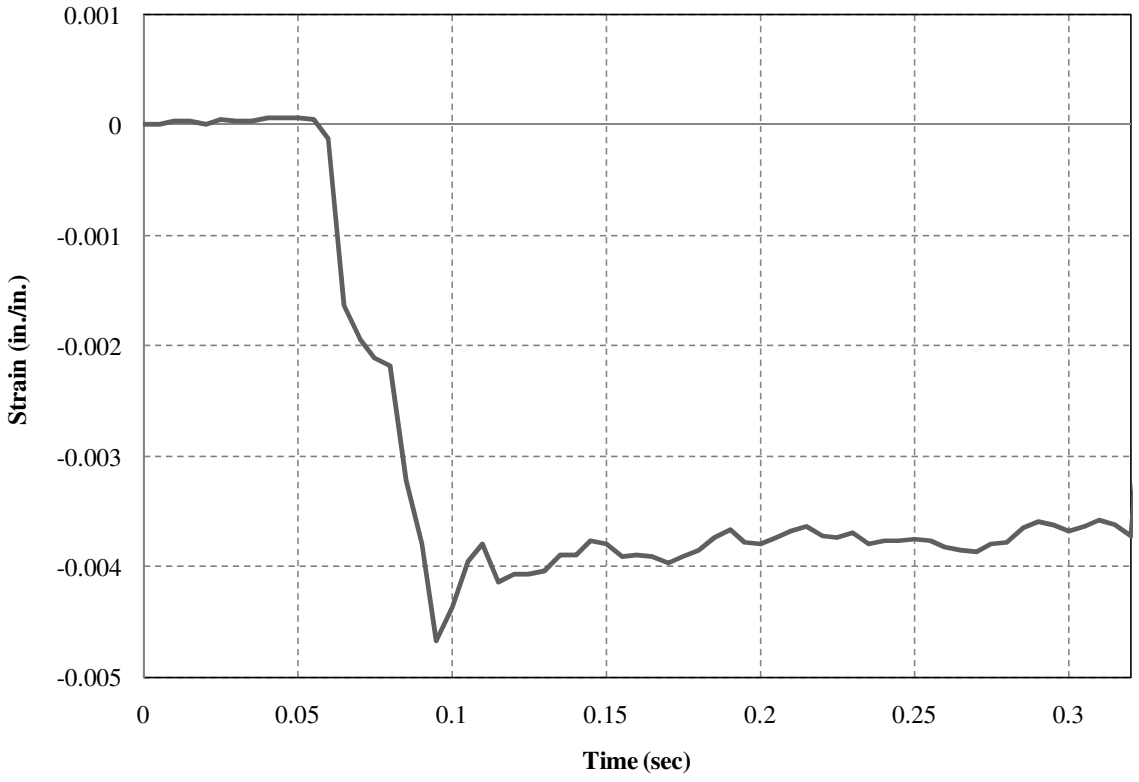

Figure 5.21 Panel strain at strip "D1" in MSE wall with 8 ft long strips

The maximum bending moment M_i, per unit length of wall at the top level of reinforcement can be calculated by a simple model as shown in Figure 5.22. The moment M_i, is generated from the horizontal shear load H on top of the panel times the moment arm *l* and the vertical load V which is transferred from the barrier to the panel during the impact times the moment arm (*t/2*) where *t* is the thickness of the panel. Because the simulation corresponded to a peak dynamic force of 346.38 kN (77.87 kips) when the design calls for 240 kN (54 kips), the results of the numerical simulation were decreased by the ratio of 240 kN / 346.38 kN (54 kips / 77.87 kip)

The distribution of shear load, vertical load, and bending moment along the panel at the time of peak force during the impact is shown in Figure 5.23, Figure 5.24, and Figure 5.25, respectively. In this case, the forces due to the rebars in the panel were neglected. The predicted shear load was 2.62 kN (0.59 kips) at the top of the panel during the impact due to the friction between the leveling pad and the panel. The vertical load transferred by the barrier was 9.61 kN (2.16 kips).

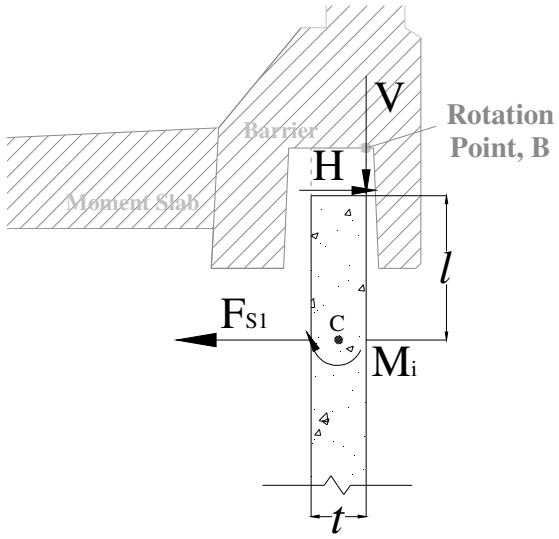

Figure 5.22 Free body diagram on the panel (rotation point B)

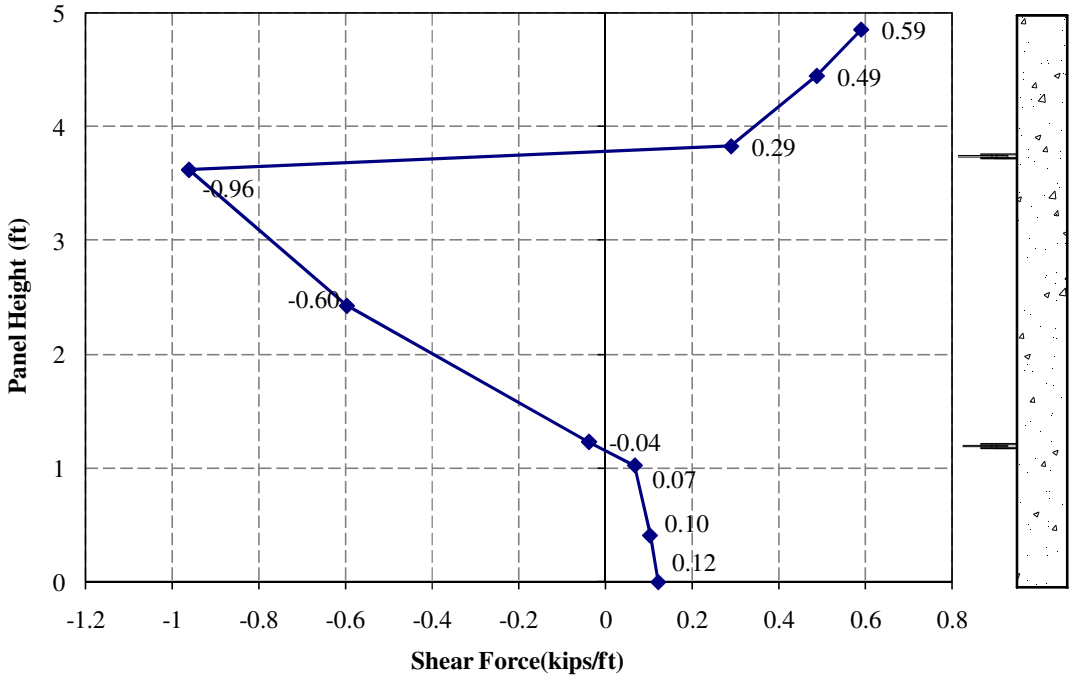

Figure 5.23 Shear load on the panel

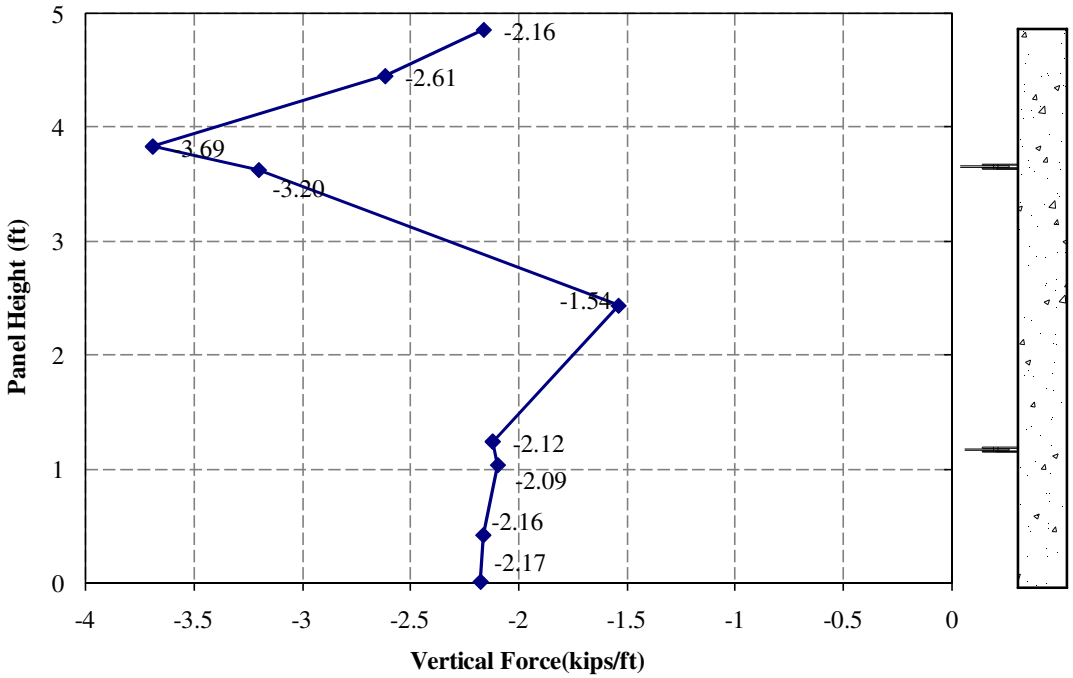

Figure 5.24 Vertical load on the panel

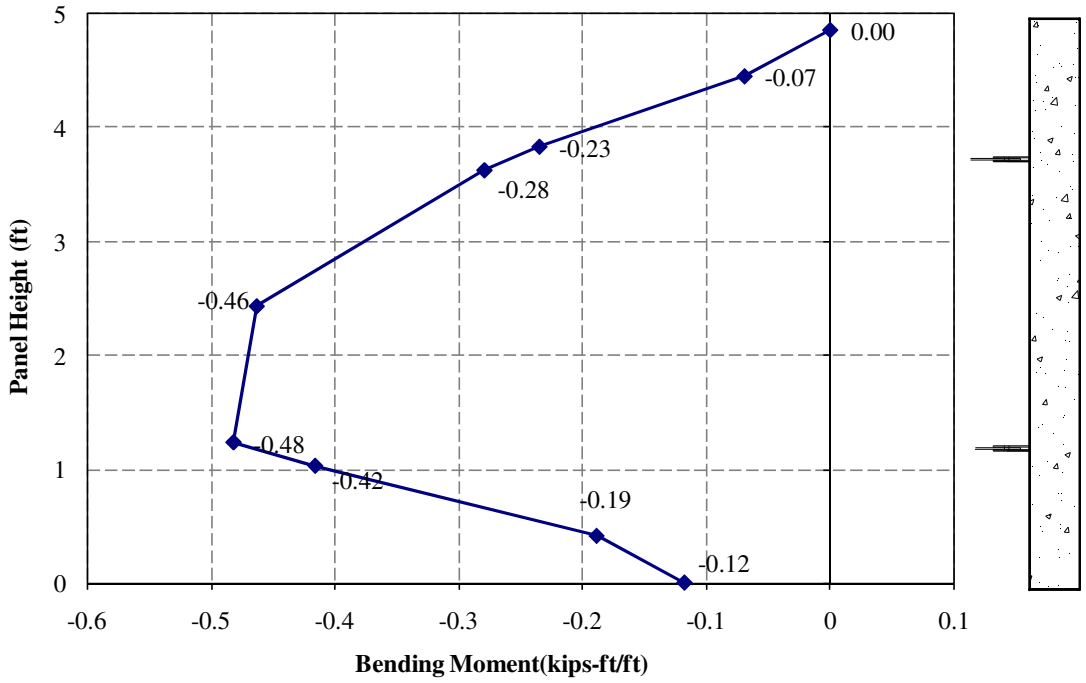

Figure 5.25 Bending moment on the panel

5.2.4 Simulated Impact into Barrier Placed on MSE Wall with 16 Ft Long Strip

The simulated bogie vehicle impacted the middle N.J. barrier section at a speed of 32.19 km/h (20 mph). The point of impact was slightly offset from the centerline of the middle barrier section to align with one of the reinforcement strips (strip D1). To enable comparison of forces and displacements, the same alphanumeric designators shown in Figure 5.13 were used

Sequential images from the simulation are shown in Figure 5.26. The maximum displacement at the top of the middle barrier was occurred at 0.07 sec. The maximum 50-msec average impact load was 359.06 kN (80.72 kips) at 0.038 sec (Figure 5.27). The maximum dynamic displacement was 10.87 cm (4.28 in.) at the top of the barrier and 3.33 cm (1.31 in.) at the bottom of the coping. The permanent displacement was 4.11 cm (1.62 in.) at the top of the barrier and 1.96 cm (0.77 in.) at the bottom of the coping. The maximum dynamic displacement of the panel was 5.6 mm (0.22 in.) at the upper reinforcement layer and 2.5 mm (0.1 in.) at the second layer. The permanent displacement of the panel was 1.5 mm (0.06 in.) at the upper layer and 0.8 mm (0.03 in.) at the second layer (see Figure 5.28). The damage profile that developed in the barrier is shown in Figure 5.29.

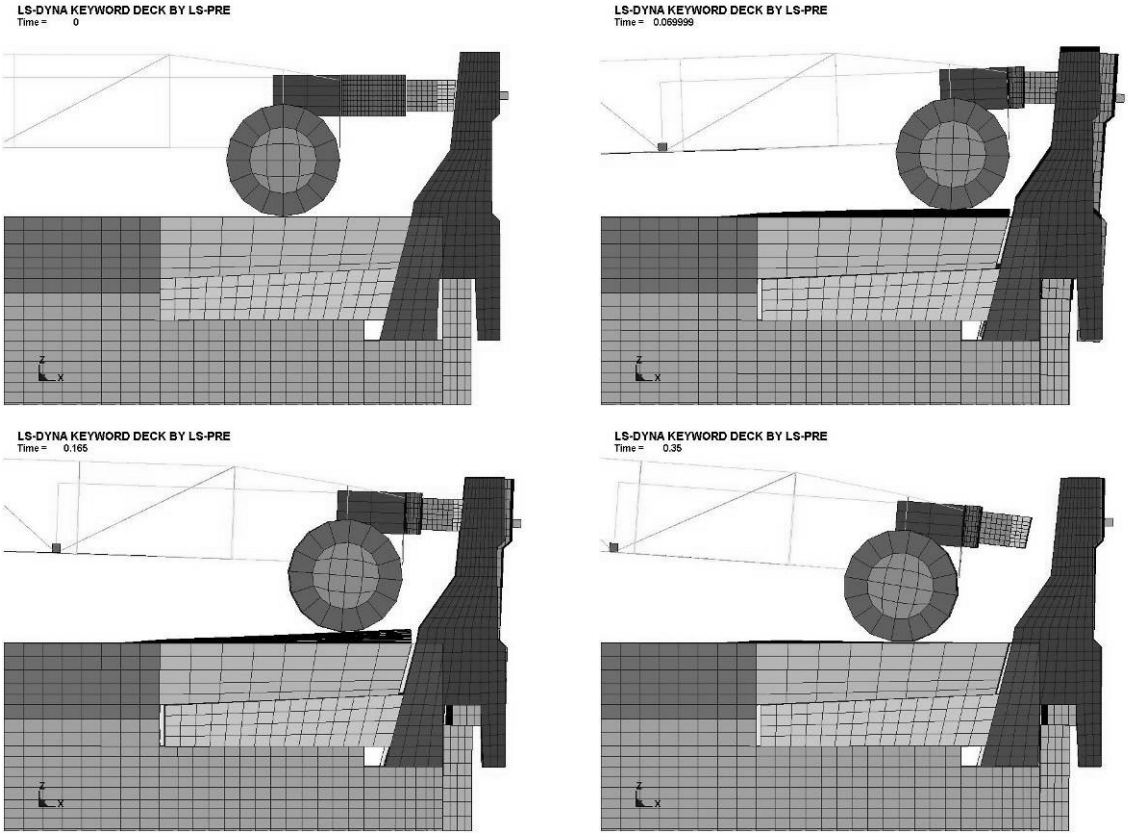

Figure 5.26 Sequence image of model during impact

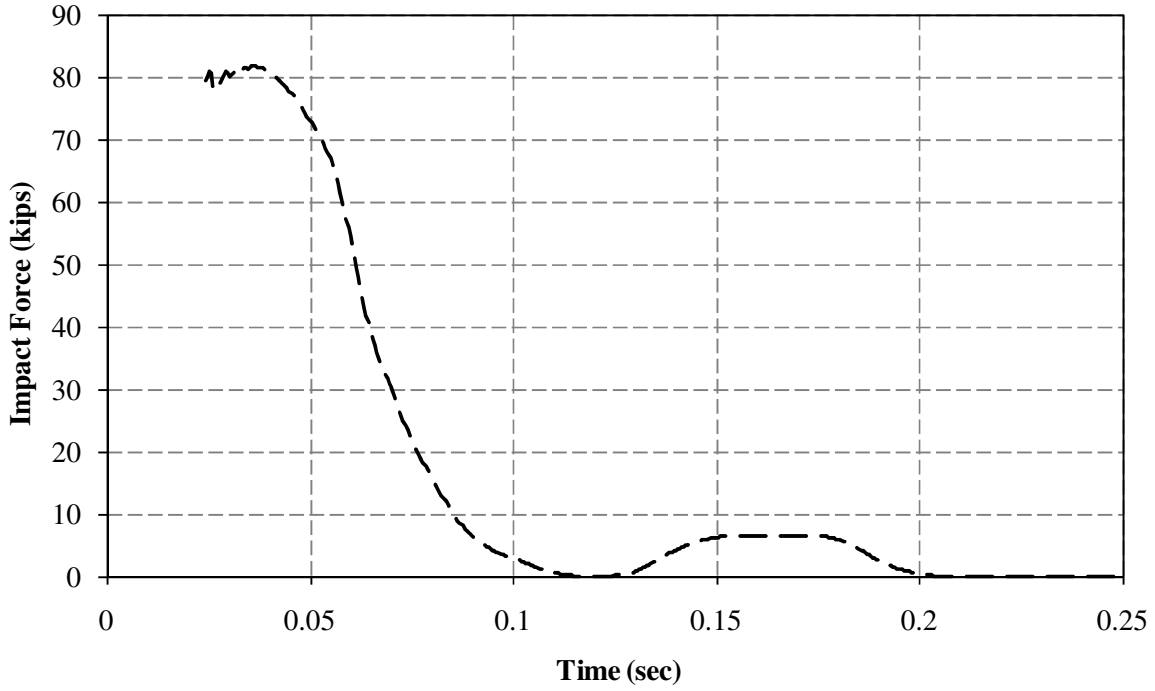

Figure 5.27 Impact load

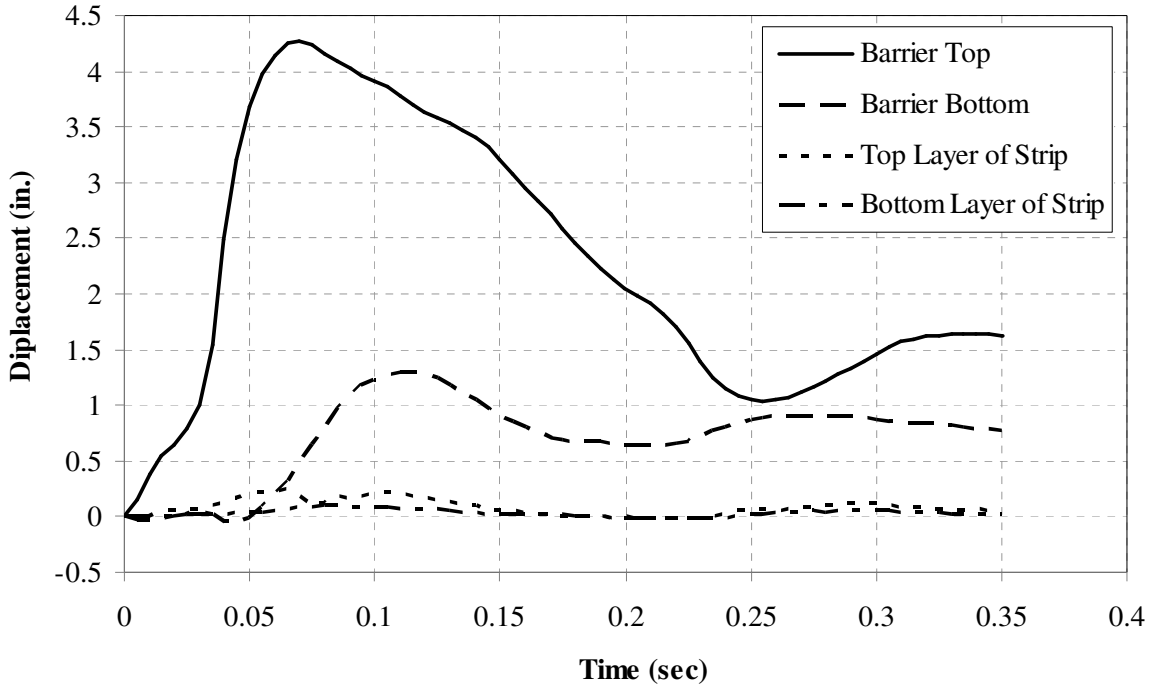

Figure 5.28 Displacement of barrier and panel

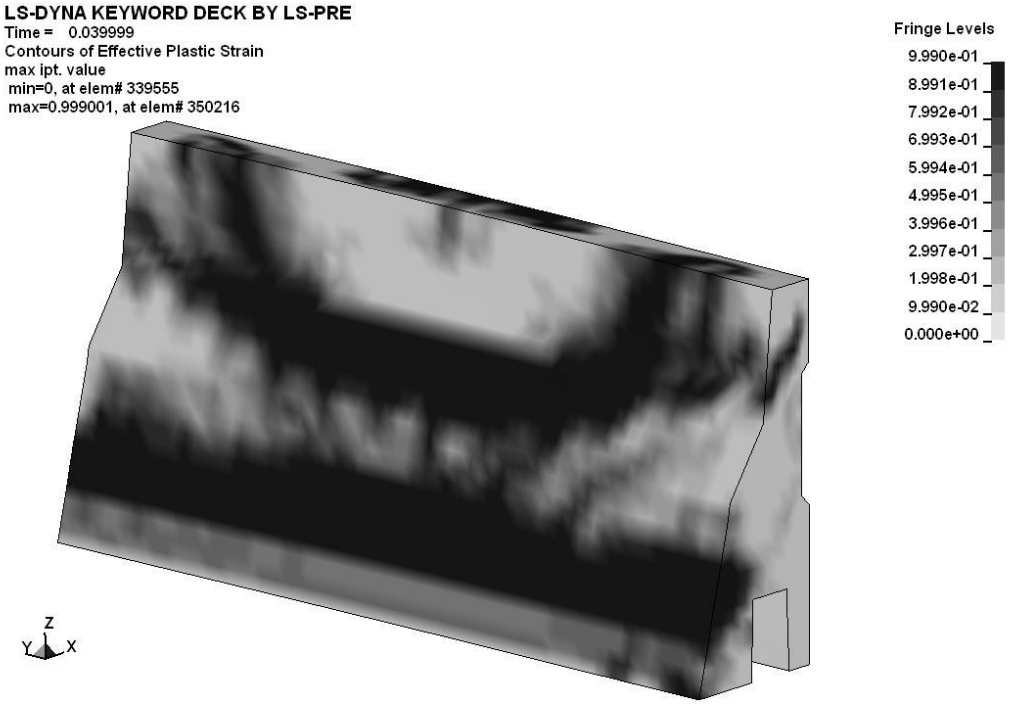

(a)

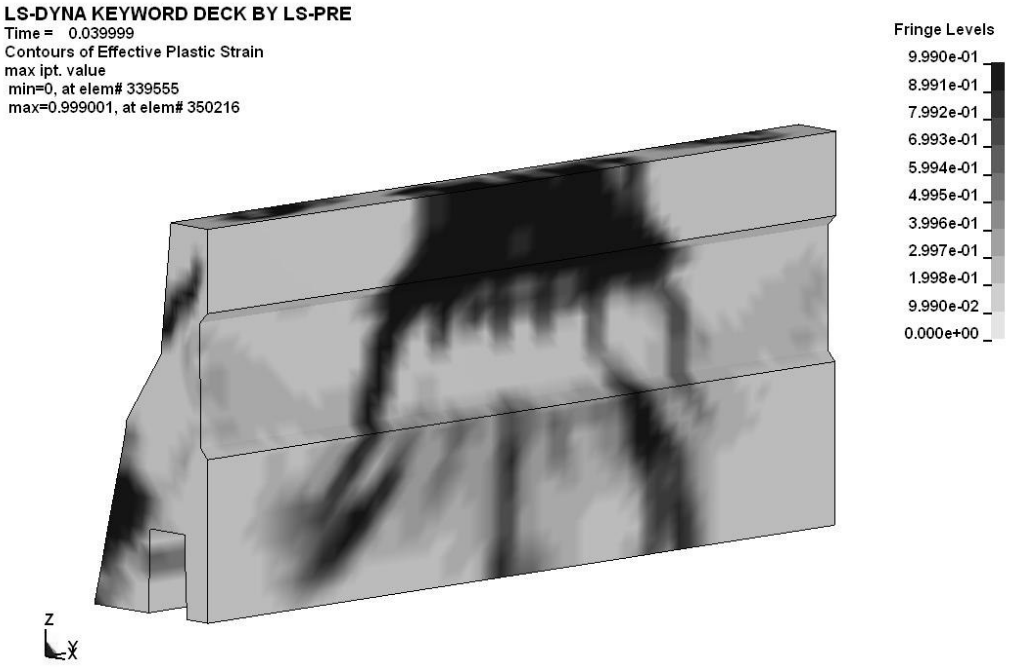

(b)

Figure 5.29 Concrete damage profile on (a) frontside and (b) backside of the barrier

Figure 5.30 shows the raw data of the total load in selected reinforcement strips. The maximum instantaneous load for strip "D1" was 39.86 kN (8.96 kips) at a distance of 17.8 cm (7 in.) from the face of the panel which corresponds to the planned location of strain gages in the test installation. The total maximum 50-msec tensile load in the wall reinforcement was 28.96 kN (6.51 kips) (Figure 5.31).

The distribution of maximum load along strip "D1" is presented in Figure 5.32. As expected, the maximum load occurs near its attachment to the wall panel and the load decreases along its length. The loads in the strips attached to the wall panel below the point of impact in the middle of the barrier section have similar distributions. Table 5.9 shows the summary of the load for the strips at a distance of 17.8 cm (7 in.) from the wall end of the reinforcement.

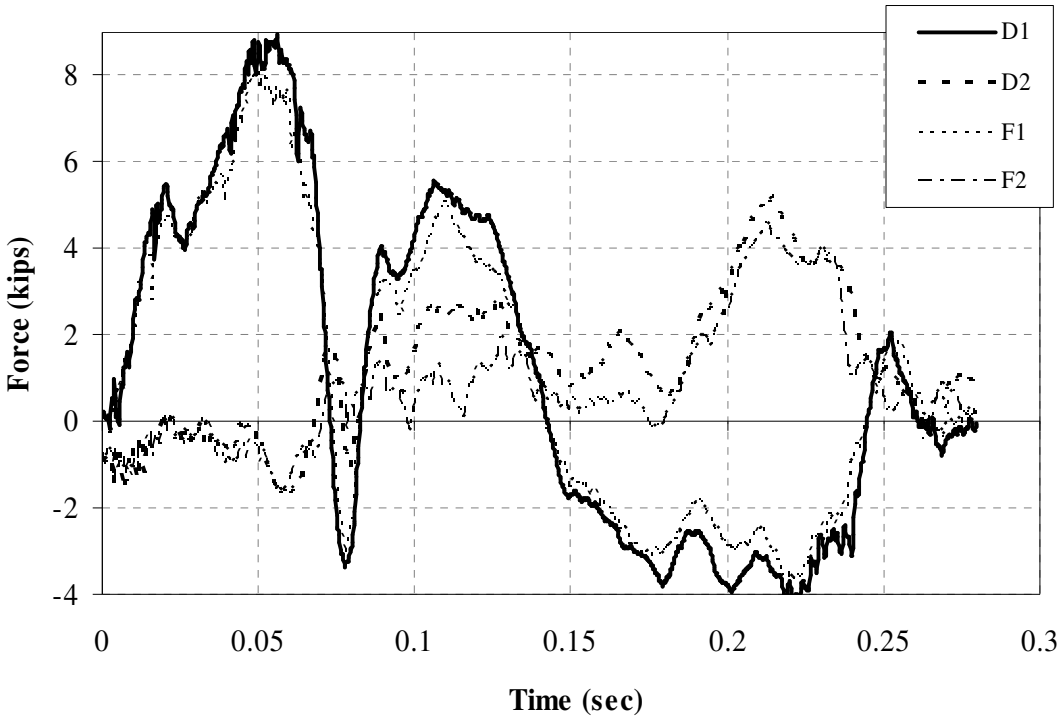

Figure 5.30 Raw data of load on the strip

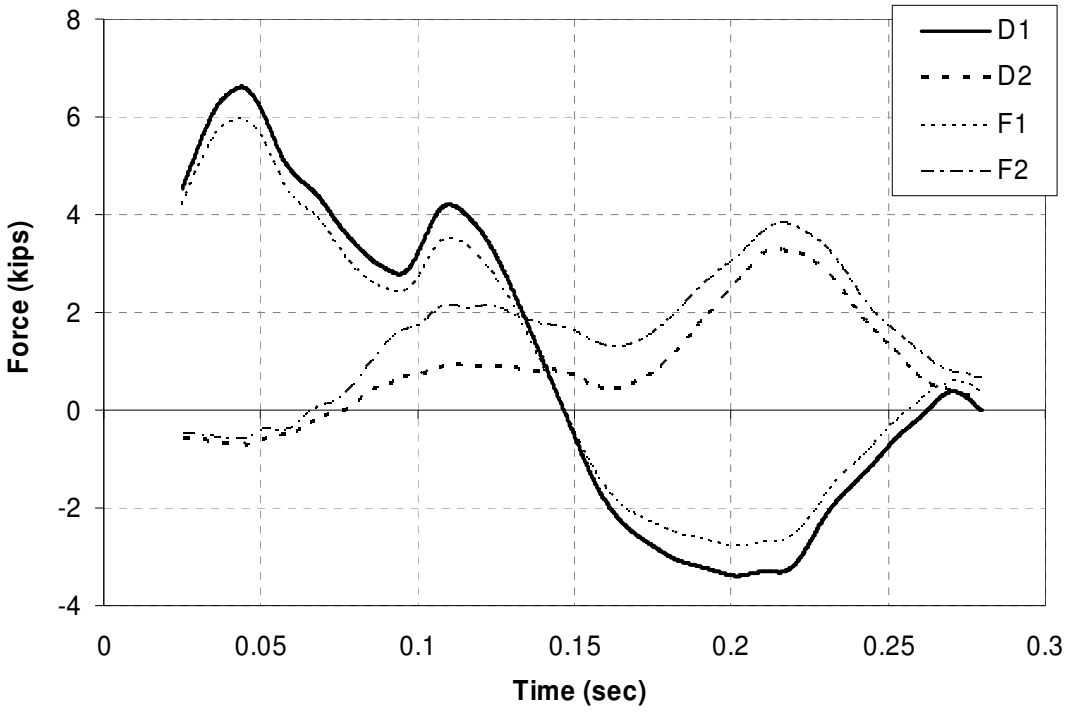

Figure 5.31 50 msec average load on the strip

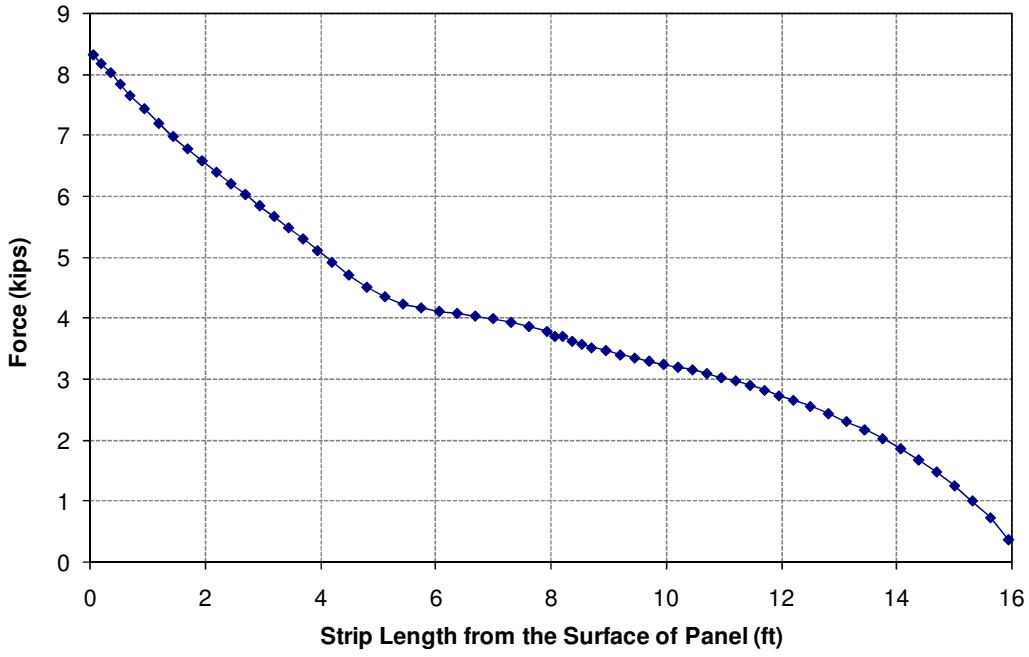

Figure 5.32 Distribution of load on the strip along the strip length. (D1)

Table 5.9 Load in Strips at 7 in Location from the Face of the Wall Panel

Location on Strip	D1	D2	F1	F2
Total max. Load (kips)	8.96	4.59	8.35	5.22
Total 50 msec average load (kips)	6.51	3.31	5.95	3.83

As in the previous simulation, the strain in the wall panel was evaluated to determine its ability to resist barrier impact loads. The results are shown in Figure 5.33. The maximum compressive strain was 0.0021 at 0.045 sec.

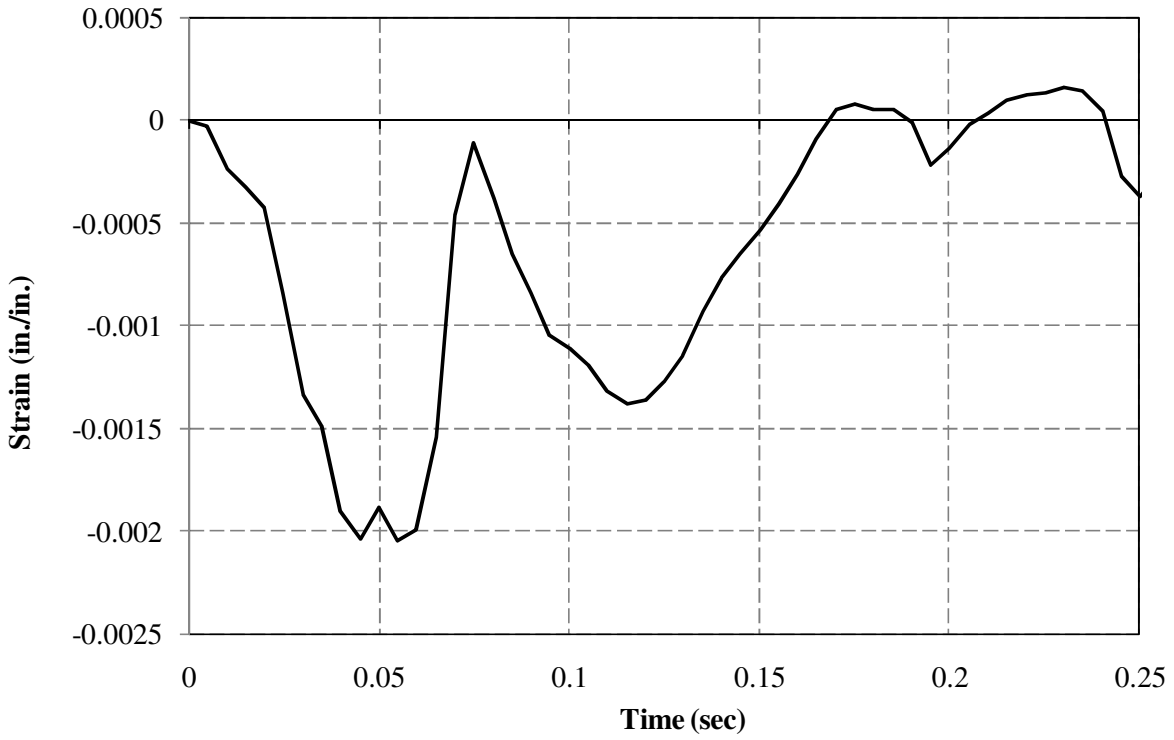

Figure 5.33 Panel strain at strip "D1" in MSE wall with 16 ft long strip

The maximum bending moment M_i, per unit length of wall at the location of top level of reinforcement can be calculated by the simple model shown previously in Figure 5.22. The moment M_i, is generated from the horizontal shear load H on top of the panel times the

moment arm *l* and the vertical load V which is transferred from the barrier to the panel during the impact times the moment arm (*t/2*) where *t* is the thickness of the panel. Because the simulation corresponded to a peak dynamic force of 359.06 kN (80.72 kips) when the design calls for 240 kN (54 kips), the results of the numerical simulation were decreased by the ratio of 240 kN / 359.06 kN (54 kips / 80.72 kip).

The distribution of the shear load, vertical load, and bending moment along the panel at the time of peak force during the impact is shown in Figure 5.34, Figure 5.35, and Figure 5.36, respectively. The predicted shear load was 6.98 kN (1.57 kips) at the top of the panel during the impact due to the friction between the leveling pad and the panel. The vertical load transferred by the barrier was 76.2 kN (17.13 kips). Using the shear and vertical loads, the bending moment was calculated to be 18.15 kN m/m (4.15 kips ft/ft) which is higher than the calculated strength of the panel by ACI specifications *(29)* (12.9 kN or 2.9 kips) (details of the calculations are presented in Section 7.4.3).

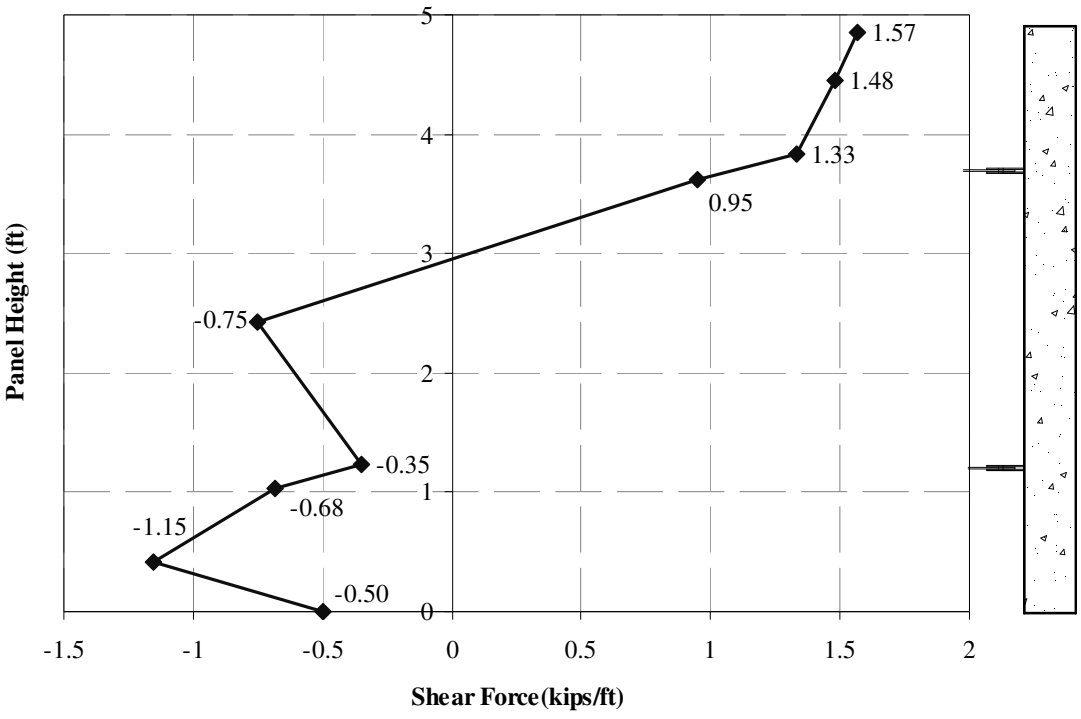

Figure 5.34 Shear load on the panel.

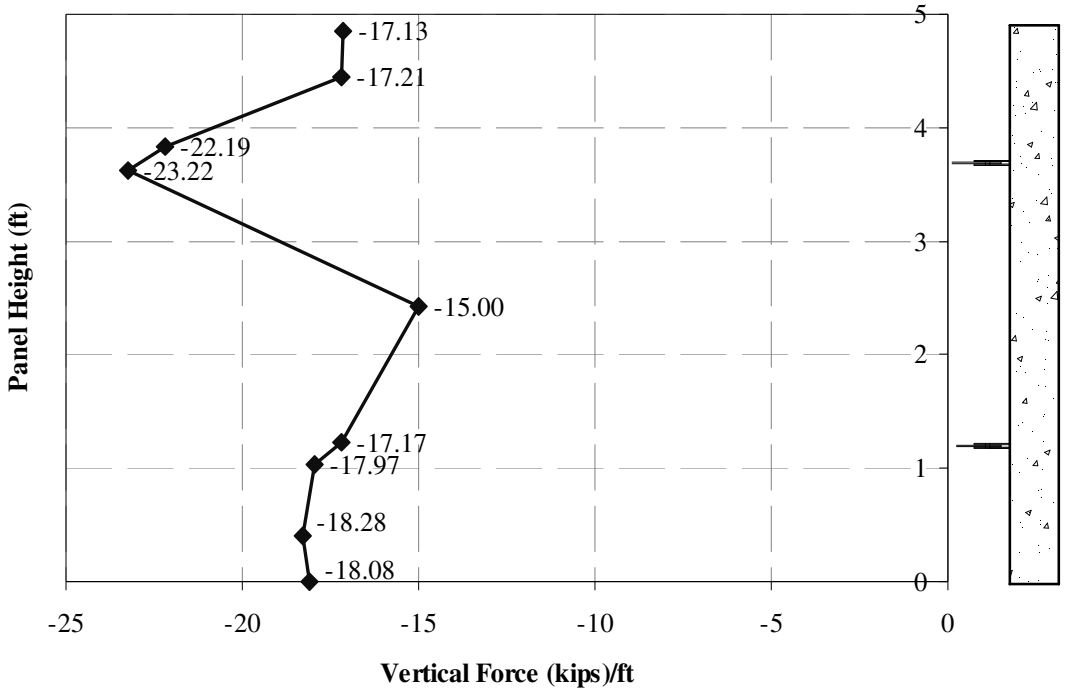

Figure 5.35 Vertical load on the panel.

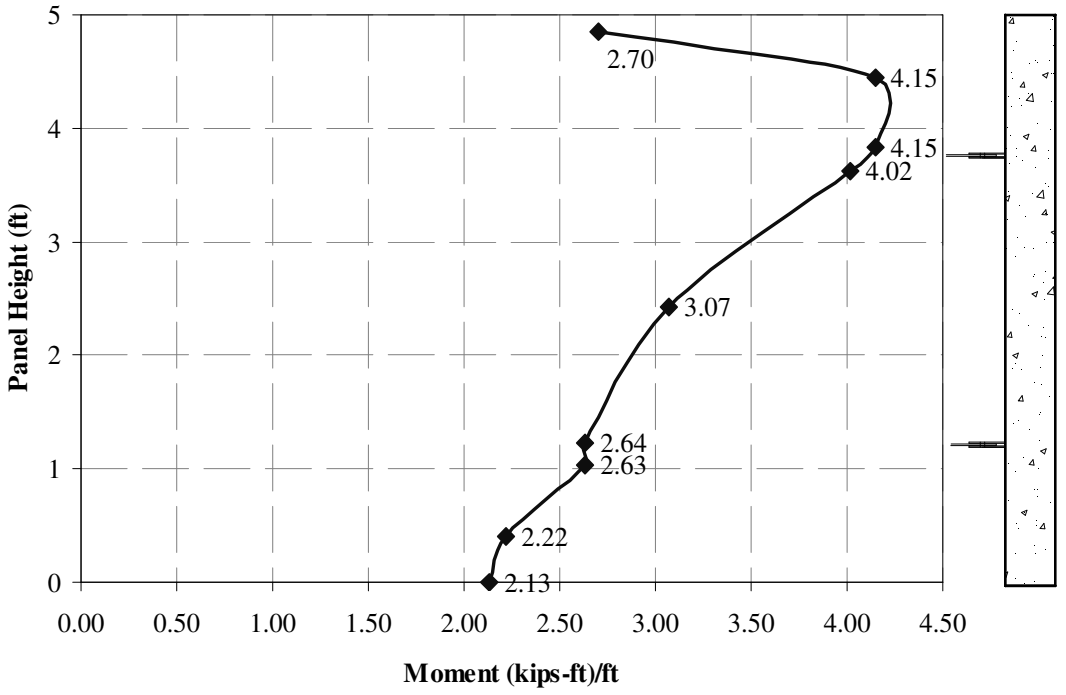

Figure 5.36 Bending moment on the panel.

5.3 Bogie Test

5.3.1 5 Ft High MSE Wall Construction and Test Installation

An elevation of the bogie test wall is shown in Figure 5.37. The total length of bogie test was approximately 18.29 m (60 ft). The MSE wall on which the six precast barrier and coping sections were placed was approximately 1.52 m (5 ft) tall and comprised of full and half-panel sections that were approximately 1.52 m (5 ft) wide. The wall panels were placed on a 30.48 cm (1 ft) wide x 15.24 cm (6 in.) thick concrete leveling pad. The MSE wall had two layers of reinforcement at depths of 26.21 cm (0.86 ft) and 1.01 m (3.32 ft) below the bottom of the moment slab. The vertical distance between the two reinforcement layers was 74.98 cm (2.46 ft). Half of the wall was constructed with 2.43 m (8 ft) reinforcement with a density of 3 strips per layer per panel and the other half with 4.88 m (16 ft) reinforcement with a density of 2 strips per layer per panel.

The wall panels were recessed inside the coping sections a distance of 20.32 cm (8 in.). The precast barrier-coping sections rested on a 10.16 cm (4 in.) thick leveling course of concrete placed on top of the wall panels. The moment slab connecting the precast barrier-coping sections was cast-in-place in two 9.14 m (30 ft) lengths. The two 1.37 m (4.5 ft) wide, 9.14 m (30 ft) long moment slabs were connected to one another using two No. 9 shear dowels.

The backfill for the wall was crushed rock that met the specifications for TxDOT Type A backfill *(30)*. The estimated friction angle for the crushed rock was 35 degrees and the unit weight was 20 kN/m^3 (0.125 kcf). The backfill was compacted in 0.15 m (6 in.) layers with 10 passes of a 1,320 kg (2,905 lb), 89 cm (35 in.) wide drum roller. Also, the surface layer of soil was recompacted after each test. A grain size analysis was performed for the backfill material to determine the relative proportions of different grain sizes as shown in Figure 5.38. The particle diameters corresponding to 10% fines, D10, and 60% fines, D60, were 0.075 mm and 6.8 mm, respectively. The coefficient of uniformity, Cu (= D60/D10) was determined to be 90.67, therefore, the friction factor, F* at ground level was determined to be 2.0 in accordance with AASHTO LRFD (see Figure 2.5).

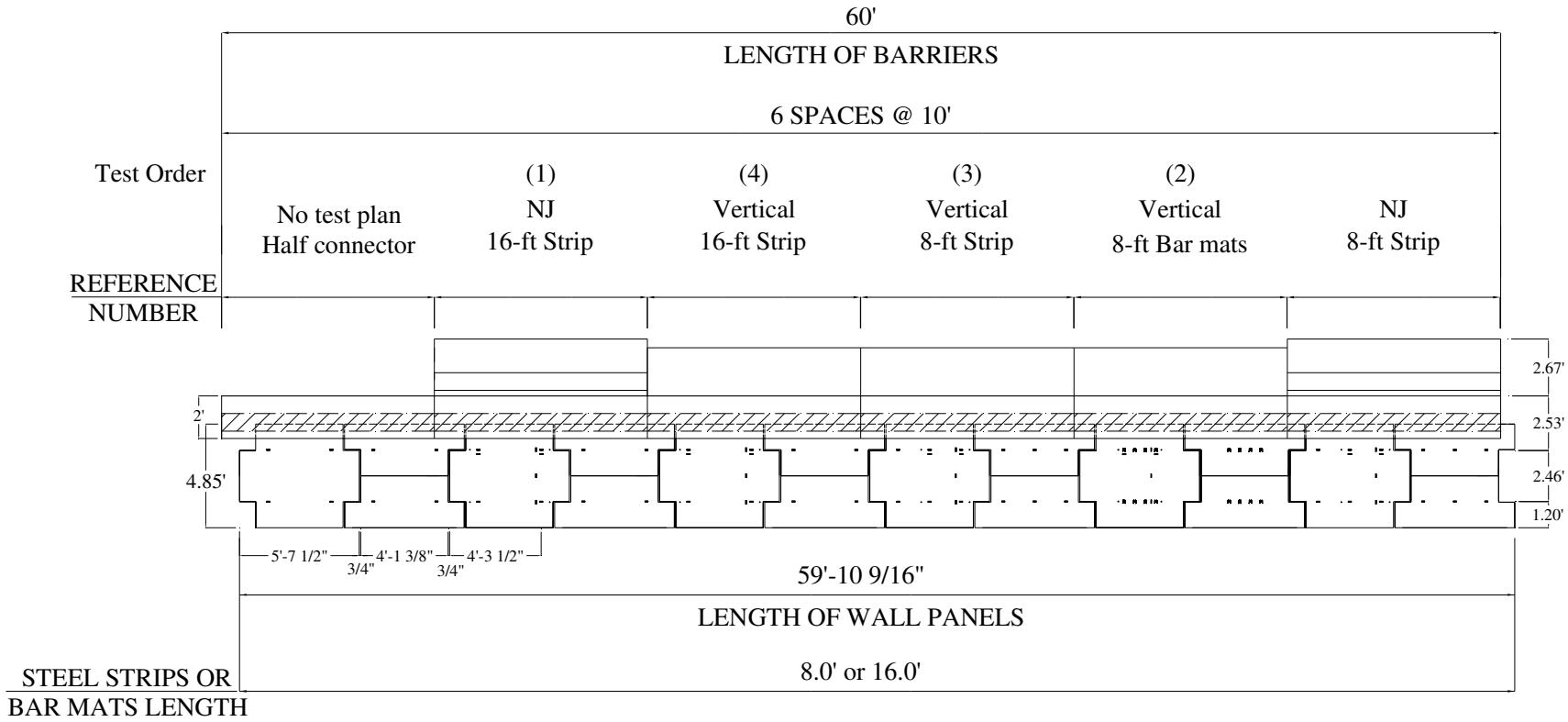

Figure 5.37 Overall elevation of installation for bogie tests

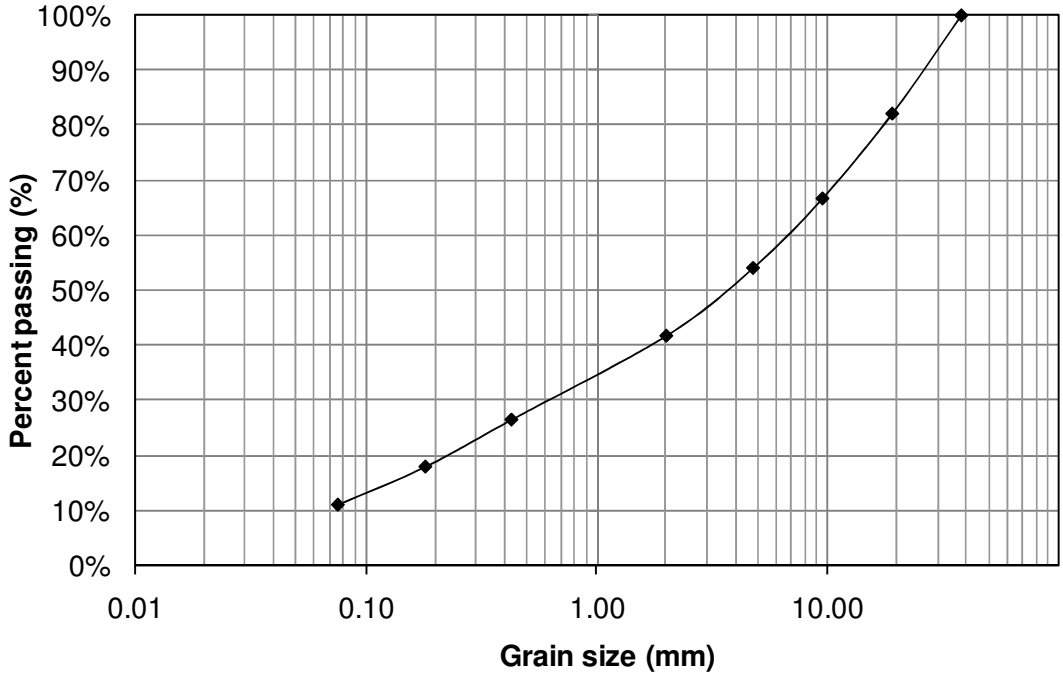

Figure 5.38 Particle size distribution curve of the backfill for bogie tests

Selected reinforcement in the MSE wall was instrumented with strain gages to capture the tensile forces transmitted into the reinforcement during the dynamic bogie vehicle impacts. A total of 8 strain gages were used for each reference test. The placement of these strain gages was selected to measure the maximum tensile load in each layer of reinforcement as well as give an indication of the distribution of forces in the lateral, longitudinal, and vertical directions. Five strain gages were used on the upper reinforcement layer, and three strain gages were placed on the lower reinforcement layer. Two strain gages were used on both layers of reinforcement adjacent to the wall panel at the point of impact to provide some redundancy at the location expected to experience maximum tensile loading.

A contact switch was placed on the top edge of the traffic face (inside face) of the concrete leveling pad cast on top of the wall panels inside the recess of the coping. The switch indicates the time (referenced from impact) at which the barrier slides and/or rotates sufficiently for the coping to contact the wall panel/level up concrete.

The full-height wall panel below the point of impact on the barrier was instrumented with five concrete strain gages to capture normal strains in the panel induced from impact loads transmitted into the MSE wall and generated from direct contact of the barrier-coping

section with the top of the wall panel. Two strain gages were placed in a horizontal position along the length of the panel just below the anchorages for the upper layer of reinforcement (region of maximum negative moment) that are below and immediately adjacent to the point of impact. These are the anchorage locations associated with the instrumented reinforcement. Three strain gages were placed in a vertical position along the height of the panel. A strain gage was placed adjacent to the anchorage locations for the upper and lower layer of reinforcement at the point of impact, and one strain gage was placed in the center of the panel between the two layers of reinforcement (region of maximum positive moment).

An accelerometer was mounted behind each barrier section at the height of impact to help analyze its dynamic response. An accelerometer also was placed on the end of each of the two 9.14 m (30 ft) long moment slabs at their midpoints to measure any acceleration or motion imparted to the moment slab during impact. Additionally, the bogie vehicle was instrumented with an accelerometer at its CG.

Angular and translational displacements and/or rotation of the barrier and wall panels were determined from high-speed video operating at 1000 frames/sec. Displacement gages were placed at the top and bottom of the precast barrier-coping section and at the upper and lower strip locations on the wall panel to assist with the displacement analysis.

String lines were placed behind the barrier and wall to measure their permanent deflection after impact. The four corner points on the barrier-coping sections and five points on each wall panel were measured. The distance from the string lines to the barrier and panel reference points were measured after each test.

A 2,268 kg (5,000 lb) bogie vehicle impacted each bogie test section at a speed of approximately 35.41 km/h (22 mph) for the N.J. barrier and 32.19 km/h (20 mph) for the vertical concrete barriers. Prior numerical simulation results indicated that these velocities would provide sufficient energy to fail the barrier-coping section. By loading each barrier-coping section beyond its ultimate strength, the maximum impact loading transferred into the MSE wall would be measured.

The test sequence was selected such that the first two tests involved impacting the barrier segments in the middle of each moment slab. The other two tests were conducted on similar vertical concrete barriers located on the end of each moment slab with different strip length and density.

The precast barrier-coping sections, concrete wall panels, and steel strip wall reinforcement were provided by RECO at no cost to the project. RECO also provided supervision of the construction of the wall. The bar mat reinforcement that was used in one of the reference tests was provided by Foster Geotechnical at no cost to the project. Detailed drawings of the reference bogie test installation and construction procedure are presented in Appendix C and Appendix D, respectively.

5.3.2 Bogie Test 1: New Jersey Barrier with 16 Ft Strips

The 2,268 kg (5,000 lb) bogie vehicle, shown in Figure 5.39, impacted the reference point of the N.J. profile barrier head-on at a speed of 35.08 km/h (21.8 mph). The reference impact point was 10.16 cm (4 in.) from the top of the barrier and 1.27 cm (0.5 in.) from the middle of the barrier to correspond to the location of the reinforcement in the underlying wall.

1) Data from Accelerometers

The accelerations at the top of the barrier and end of the moment slab exceeded the range set for the accelerometers at these locations. Therefore, a portion of the signal representing the peak acceleration of the barrier and moment slab was truncated as shown in Figure 5.40(b) and Figure 5.40(c). Consequently, the maximum 50-msec average acceleration provides lower values than expected. To prevent the reoccurrence of this problem, the range of accelerometer was increased for subsequent tests.

Data obtained from the bogie-mounted accelerometer were analyzed and the results are presented in Figure 5.41. As shown in Figure 5.41(b), the maximum 50-msec average acceleration was -14.45 g. Based on this acceleration and the mass of the bogie, the maximum 50-msec average impact force was calculated to be 326.5 kN (73.4 kips) (see Figure 5.41(a)). The velocity-time and horizontal displacement-time histories of the bogie are shown in Figure 5.41(c) and (d), respectively. These time histories were calculated through integration of the acceleration data.

The maximum 50-msec average acceleration of the barrier, as measured by the accelerometer at the top of the barrier, was 7.35 g in the direction of impact (see Figure

5.42(a)). The velocity-time history of the barrier, as calculated by integration of the raw acceleration data, is shown in Figure 5.42(b). The displacement-time history obtained from integration of the velocity history was known to have some inherent error due to the truncation of data from the barrier accelerometer. Figure 5.42(c) presents displacement-time history from both double integration of acceleration data and from analysis of the high-speed film which is considered to be more accurate.

The maximum 50-msec average acceleration of the moment slab is shown in Figure 5.43(a). The velocity-time and vertical displacement-time histories of the moment slab are shown in Figure 5.43(b) and (c), respectively. The velocity-time history and displacement-time histories were calculated by integration of the acceleration data.

Targets affixed to the displacement bars attached to the top and bottom of the barrier-coping section (see Figure 5.44 and Figure 5.45) were used as reference points to determine angular and translational displacement of the barrier from analysis of high-speed video. From the film analysis, the maximum dynamic displacement of the barrier was 15.6 cm (6.14 in.) at the top of the barrier and 2.85 cm (1.12 in.) at the bottom of the coping. The permanent displacement of the barrier was 7.62 cm (3 in.) at the top of the barrier and 1.4 cm (0.55 in.) at the bottom of the coping.

Two additional targets affixed to the displacement bars attached to the wall panel at locations corresponding to the upper and lower layers of wall reinforcement were used to determine angular and translational displacement of the panel from analysis of high-speed video. From the film analysis, the maximum dynamic displacement of the panel was 1.6 cm (0.63 in.) at the upper reinforcement layer of the panel. The permanent displacement of the panel was 6.1 mm (0.24 in.) at the upper reinforcement layer. No movement was measured at the bottom reinforcement layer of the panel. The corresponding displacement-time histories for the barrier-coping section and wall panel are shown in Figure 5.46. Figure 5.47 shows the force-displacement curve for the top of the barrier.

Figure 5.39 Bogie test 1: N.J. barrier with 16 ft long strip

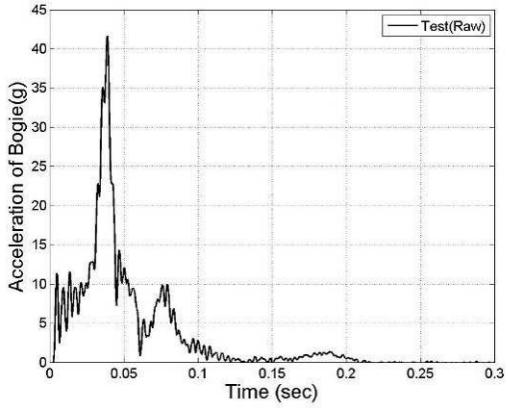

(a) Bogie

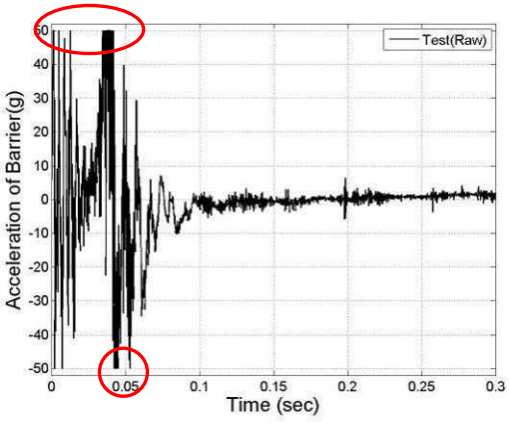

(b) Barrier

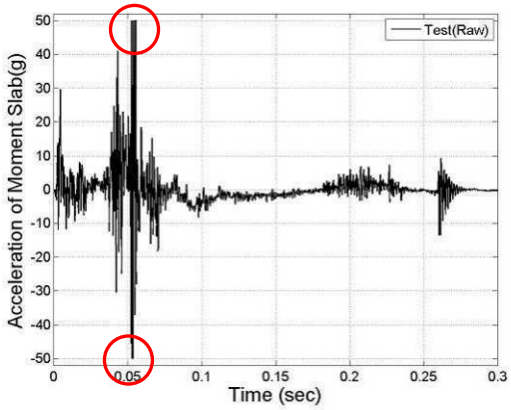

(c) Moment slab

Figure 5.40 Raw acceleration of bogie, barrier, and moment slab (Test 1)

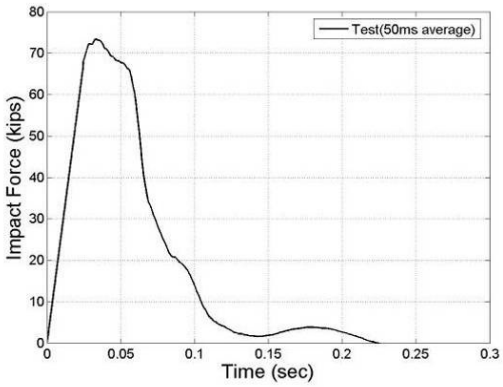

(a) Impact Force

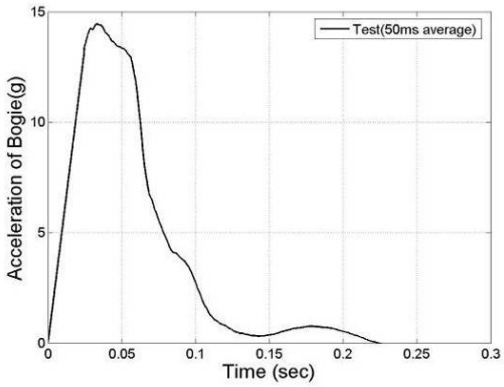

(b) Acceleration

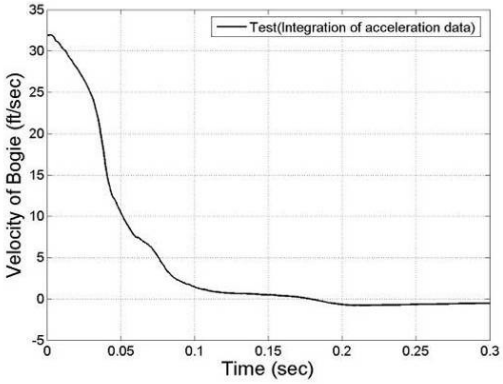

(c) Velocity

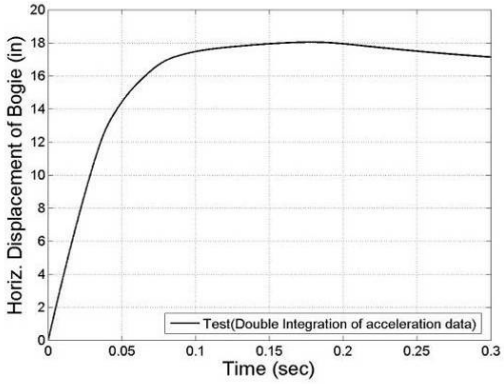

(d) Displacement

Figure 5.41 Force, acceleration, velocity, and displacement of bogie (Test 1)

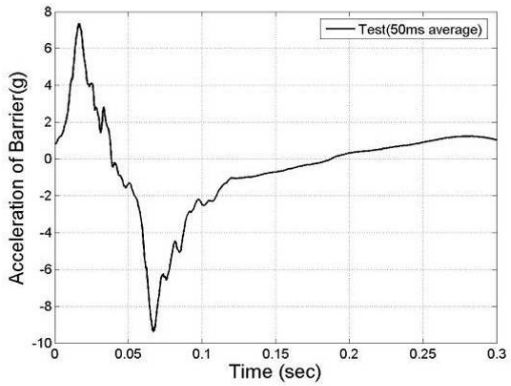

(a) Acceleration

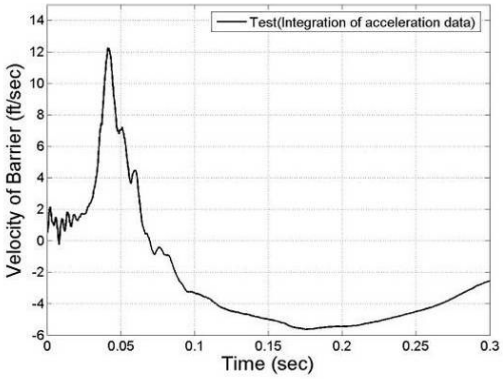

(b) Velocity

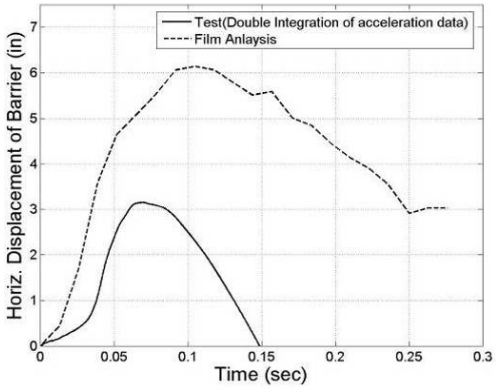

(d) Displacement

Figure 5.42 Acceleration, velocity, and displacement of barrier (Test 1)

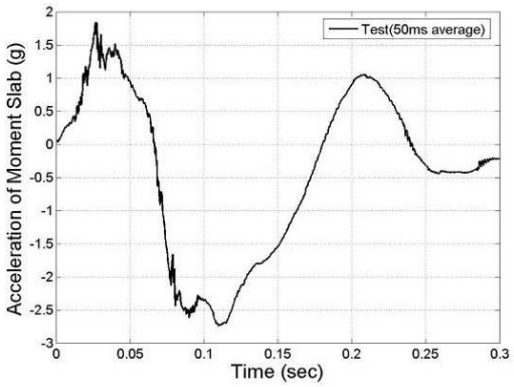

(a) Acceleration

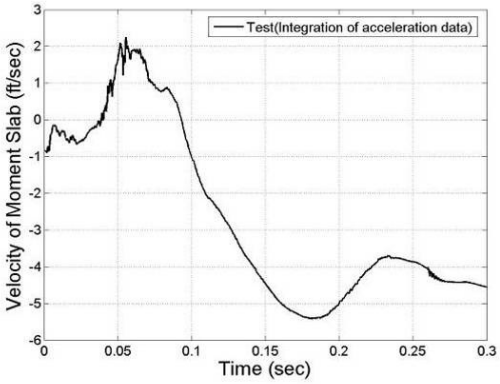

(b) Velocity

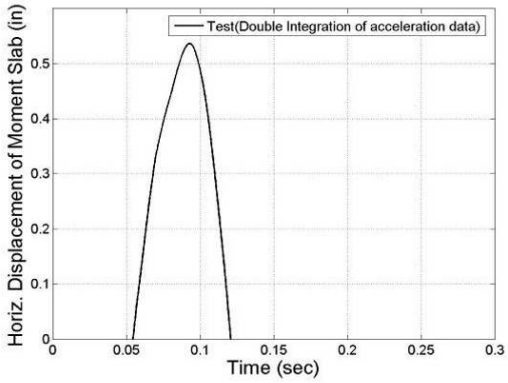

(d) Displacement

Figure 5.43 Acceleration, velocity, and displacement of moment slab (Test 1)

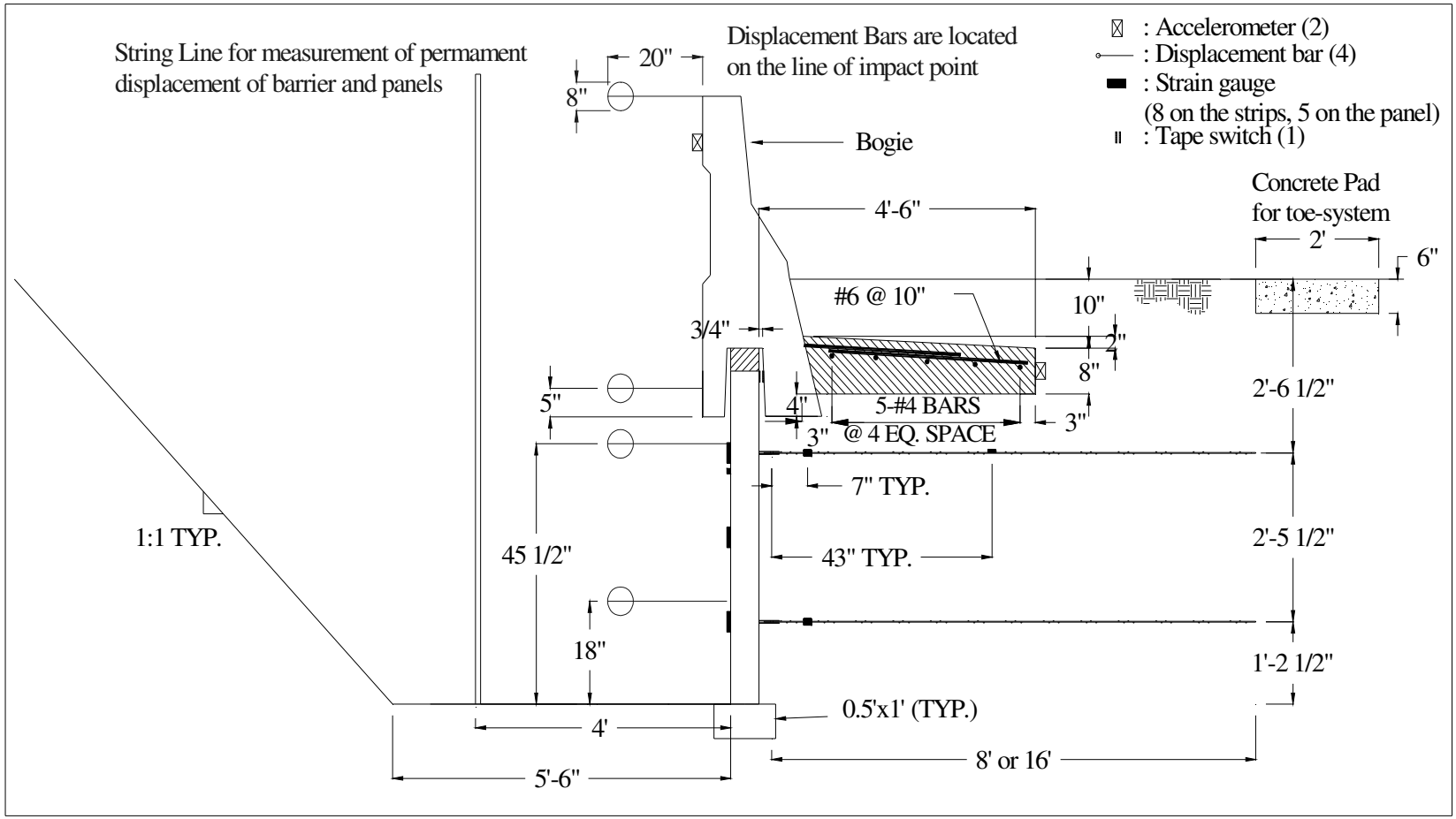

Figure 5.44 Side view of installation (Test 1)

Figure 5.45 Location of displacement bars affixed on the barrier and panels (Test 1)

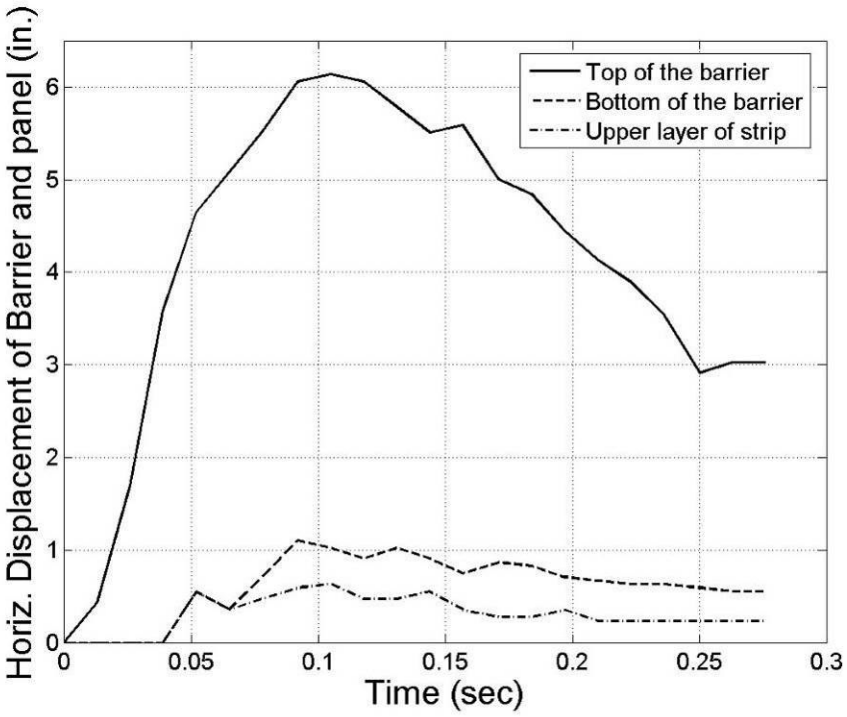

Figure 5.46 Horizontal displacement of barrier and panel measured from film (Test 1)

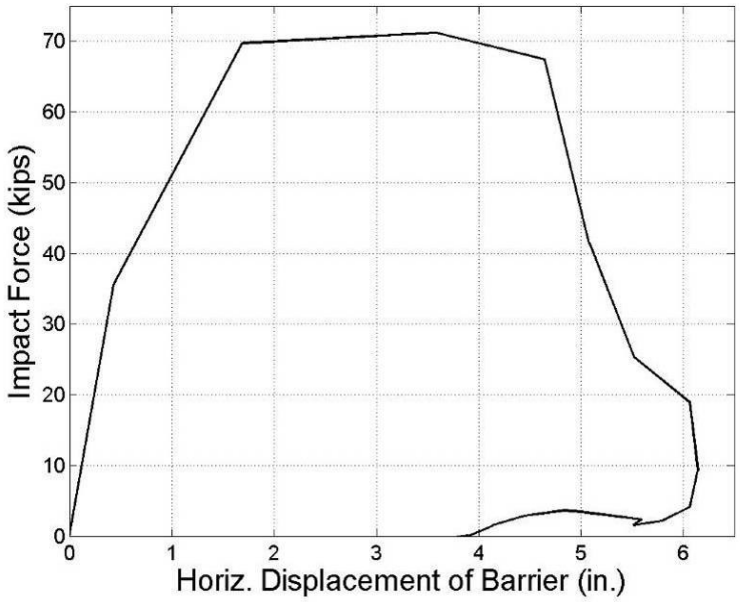

Figure 5.47 Force-displacement of the top of the barrier (Test 1)

2) Load in the Reinforcement Strips

As mentioned in a previous section, the wall reinforcement was instrumented with a total of 8 strain gages as shown in Figure 5.48 to capture the tensile forces transmitted into the reinforcement during the dynamic bogie vehicle impacts. To enable comparison of loads on the reinforcement strips, the strain gage locations were assigned a unique numeric designator. The first number indicates the location of the strain gage, and the second number indicates the reinforcement layer. For example, with reference to Figure 5.48, gage location "1-1" is positioned away from the wall on a strip beneath the impact point in the first (upper) layer of reinforcement.

Note that two strain gages were used at locations 2-1 and 2-2 adjacent to the wall panel at the point of impact to provide some measurement redundancy at the location expected to experience maximum tensile loading. One gage was placed on top of the reinforcement and one gage was placed on the bottom of the reinforcement. Measurements obtained from the strain gages during testing indicated that the reinforcement experienced some bending in addition to tensile loading. The strain gages on the top and bottom of the reinforcement enabled the bending to be canceled out and the average tensile force in the

reinforcement to be calculated. Due to the presence of bending, the average tensile loads obtained at gage locations 2-1 and 2-2 were given more credibility in the analysis of the test data and guideline development than the other locations. Note that these locations correspond to the point of impact and thus are expected to be the location of maximum loading in the reinforcement. These expectations were generally confirmed by the numerical simulations.

Raw data obtained from the strain gages on the strips were analyzed and the results are presented in Figure 5.49. The 50-msec average of the raw data was analyzed to obtain design loads for the strips, and the results are presented in Figure 5.50. The ultimate load obtained for the New Jersey barrier was 326.5 kN (73.4 kips), which exceeds the barrier design load of 240 kN (54 kips) prescribed by AASHTO LRFD. To obtain the load on the strips when the barrier impact force equaled the 240 kN (54 kips) design force, the data from the bogie accelerometer (Figure 5.41(a)) was used to find the time at which the design force was reached (0.0198 sec). This time, as well as the time of maximum load (0.0331 sec) is shown on Figure 5.49 and Figure 5.50. A complicating factor in the analysis is that the loads in the strips continued to increase after the maximum impact force in the barrier was reached. In other words, the time at which the maximum impact load occurred does not correspond to the time at which the maximum load in the strip occurred.

A contact switch placed on the top edge of the level-up concrete on top of the wall panels inside the recess of the coping indicated that the coping contacted the wall panel from 0.0784 sec to 0.1186 sec which, as shown in Figure 5.50, corresponds to a period of time after maximum impact load. Thus, the barrier-coping section continued in motion under its own momentum as the impact loads were decreasing. This motion likely contributes to the increase in loads in the strips beyond the time of maximum impact load.

It is assumed that an impact of lesser severity will follow a similar pattern of behavior. For example, if an impact produces a maximum force of 240 kN (54 kips), one would expect the loads in the strips to increase beyond the values corresponding to the time of maximum impact load. Thus, it is not necessarily appropriate to use the strip load corresponding to the time at which the 240 kN (54 kips) design load was reached in the bogie impact tests as the design strip load. Assuming the increase in strip load is proportional to the barrier impact load, the design strip loads corresponding to a design impact load of 240 kN (54 kips) can be estimated as follows:

$$\text{Estimated Strip Load} = \frac{54}{73.4} \times \text{Maximum Strip Load} \qquad (5\text{-}9)$$

Table 5.10 presents a summary of the strip loads from the first bogie impact test including the maximum force, maximum 50-msec average force, and an estimate of the maximum 50-msec average force for a 240 kN (54 kips) design impact. Note that only gage locations 2-1 and 2-2 had two strain gages that could be used to account for bending.

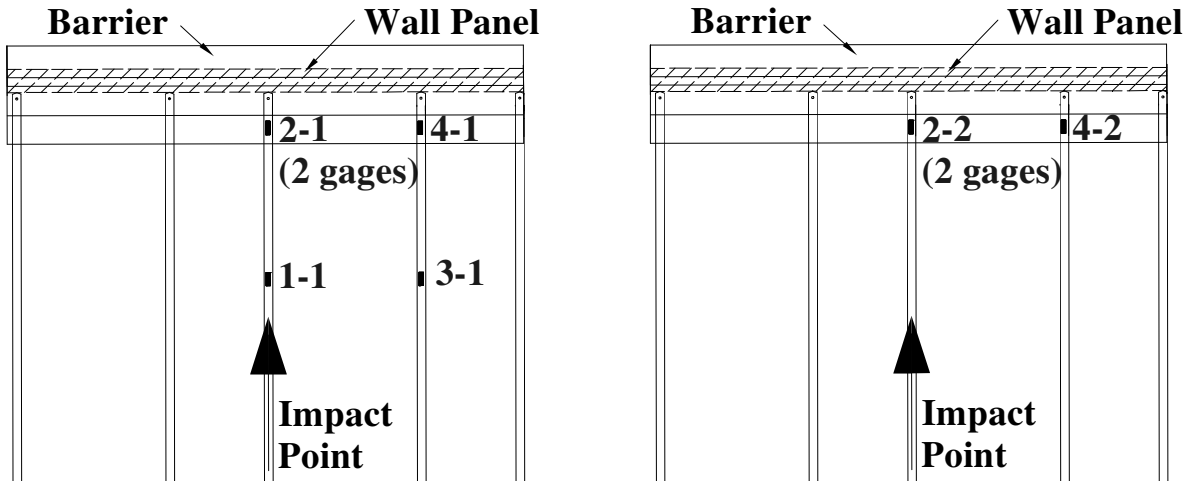

(a) Upper layer **(b) Bottom layer**

Figure 5.48 Location of strain gages and labeling (Test 1)

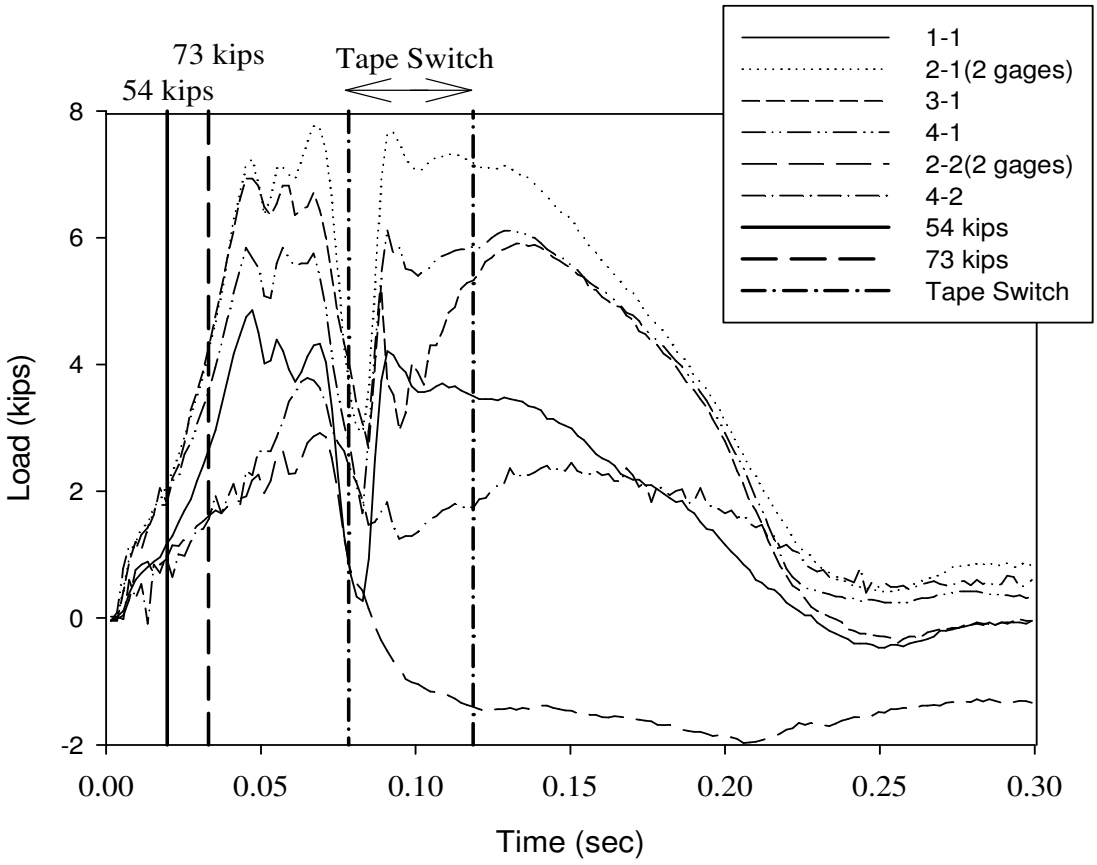

Figure 5.49 Strip load of raw data on the strips (Test 1)

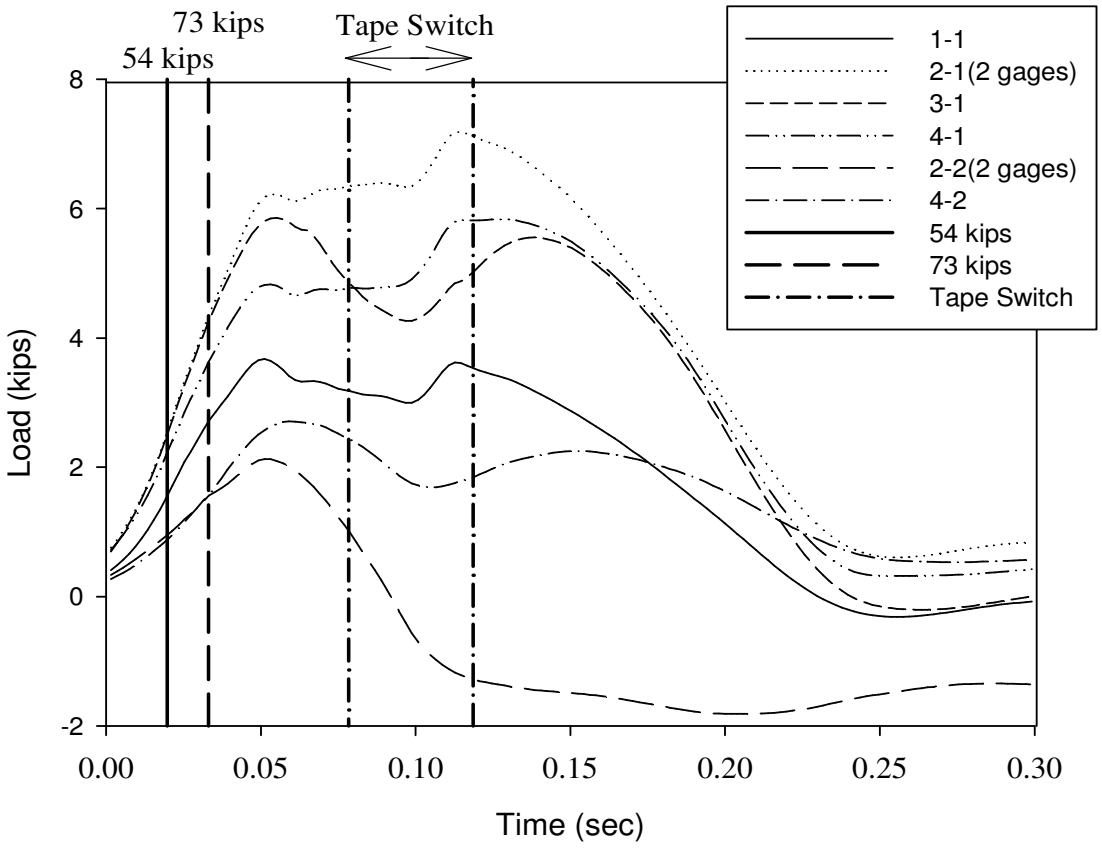

Figure 5.50 Strip load of 50 msec average on the strips (Test 1)

Table 5.10 Load on the Wall Reinforcement (Test 1)

	Upper layer (kips)				Bottom layer (kips)	
	Impact point, Behind (1-1)	Impact point, Front (2-1)	Next to impact point, Behind (3-1)	Next to impact point, Front (4-1)	Impact point, Front (2-2)	Next to impact point, Front (4-2)
Maximum Load from Raw Data (t = 0.0685 sec)	4.19	7.56	6.19	5.20	2.84	3.56
Maximum 50 msec avg. Load (t = 0.1139 sec)	3.62	7.19* (7.95-T 6.43-B)	4.87	5.82	-1.2* (-0.48-T -1.92-B)	1.78
Estimated Design Load	2.66	5.29	3.58	4.28	-0.88	1.31

* Average of top and bottom loads

3) Permanent Deflection of Barrier and Panels

The string lines located 1.22 m (4 ft) from the face of the wall panels were used to measure the permanent deflection of barriers and panels at different elevations after bogie vehicle impact. After bogie vehicle impact of the New Jersey barrier section, the permanent deflection was measured to be 83 mm (3.27 in.) and 70 mm (2.87 in.) at the top corners of the barrier and 20 mm (0.79 ins) and 13 mm (0.51 in.) at the bottom corners of the coping as shown in Figure 5.51. The permanent deflection obtained from the film analysis of the motion of the targets affixed to the barrier-coping section was 7.62 cm (3 in.) at top of the barrier and 1.4 cm (0.55 in.) at the bottom of the coping.

Note that the adjacent barrier-coping sections moved approximately 20 mm (0.79 in.) due to their connection to the same 9.14 m (30 ft) moment slab as the N.J. barrier section that was impacted. The permanent defection of the wall panels was measured as shown in Figure

5.51. The maximum permanent movement measured in the wall panels beneath the impact barrier section was approximately 6 mm (0.24 in.). Note that negative values indicate movement toward the traffic side of the barrier. Such movement may be the result of the panel being loaded eccentrically and experiencing some rotation.

4) Panel Analysis

The wall reinforcement was instrumented with a total of 5 strain gages to capture the strains in the panel during the bogie impacts as shown in Figure 5.52. The maximum compressive strain was 0.0018 occurred at 0.123 sec (see Figure 5.53) at the location of uppermost layer of strip. Note that positive values for the vertical direction strain gages indicate movement toward the traffic side of the barrier. The strains at the horizontal centerline of the panel and at the second layer of strips were less than 0.0002.

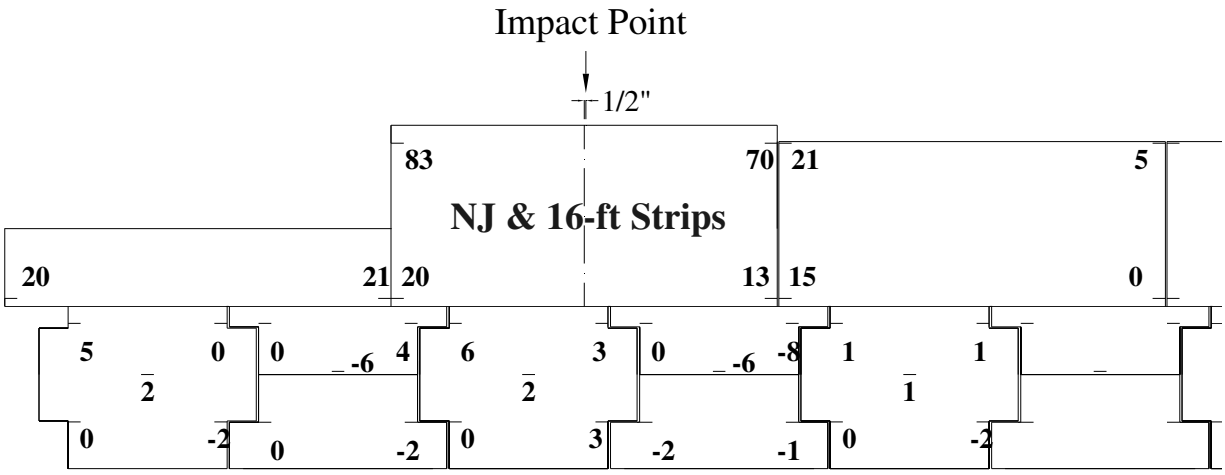

Figure 5.51 Permanent deflection of barrier and panels (Test 1, units: mm)

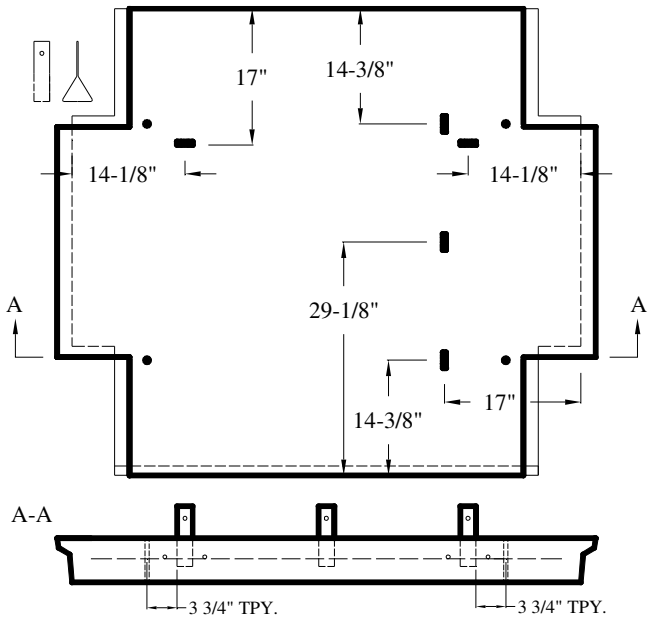

Figure 5.52 Location of concrete statin gages (Test 1)

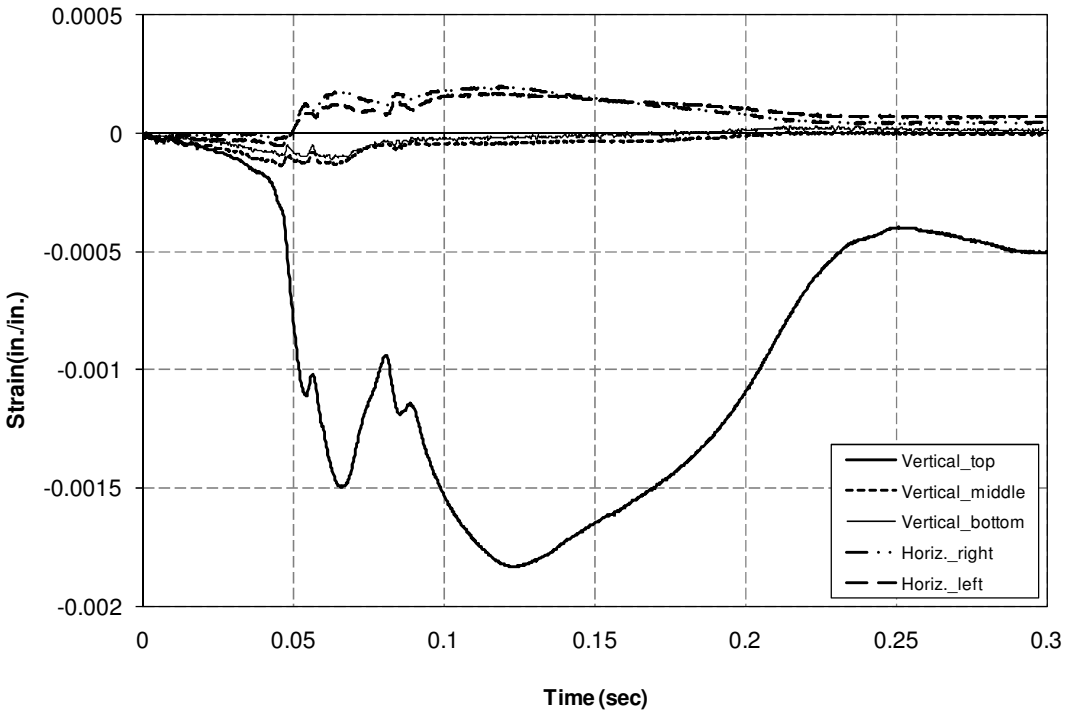

Figure 5.53 Strain on the panel (Test 1)

5) Component Damage

Damage to the barrier-coping section resulting from the bogie impact is shown in Figure 5.54. Cracks were observed across the entire length of the New Jersey barrier section at a height of approximately 38.1 cm (15 in.) above ground or above the "toe" of the barrier. The vertical reinforcing bars were exposed along some of these cracks due to fracture and spalling of the concrete. Although difficult to see in the pictures, the cracks radiated upward on either side of the barrier centerline in a U-shaped pattern observed in previous testing of safety shape barriers. This damage mechanism, which had a maximum length of 2.6 m (8.43 ft), was not as pronounced as in past testing because the short length of this precast barrier section caused other failure modes to occur at similar failure loads.

Cracking in the soil was observed approximately 1.22 m (48 in.) from the front face of the barrier, which corresponds with the location of the end of the moment slab. The crack, shown in Figure 5.54(c), was about 1.91 cm (¾ in.) wide and extended along the entire length of the 9.14 m (30 ft) long moment slab. Although numerous cracks were observed on the back side of the barrier (see Figure 5.54(d)), they were not as wide or pronounced as those on the front of the barrier. Damage to the panel beneath the point of impact on the barrier is shown in Figure 5.55. The leveling concrete on top of the wall panel was broken and shifted over the front edge of the panel due to contact with the inside face of the coping. The bonding of the leveling concrete to the top of the wall panel caused the top corner of the wall panel to spall as shown in Figure 5.55(b) and (c).

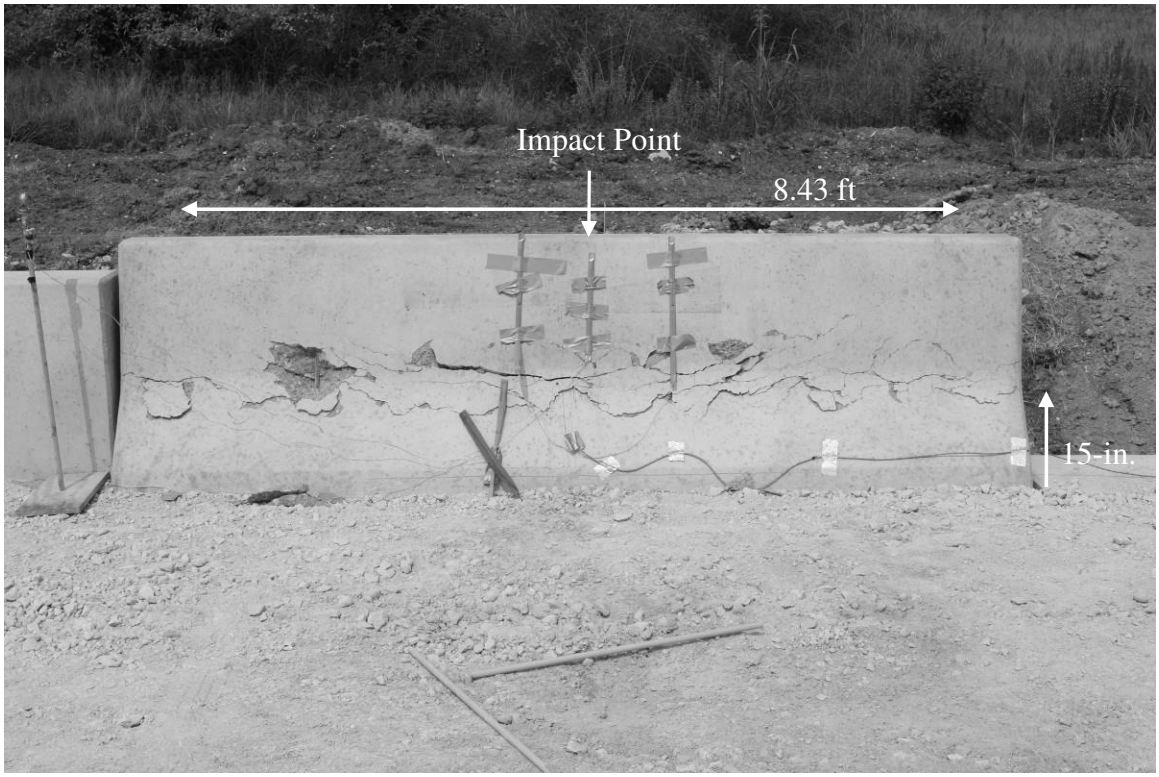

(a) Front side of the barrier

Figure 5.54 Damage to barrier after Test 1

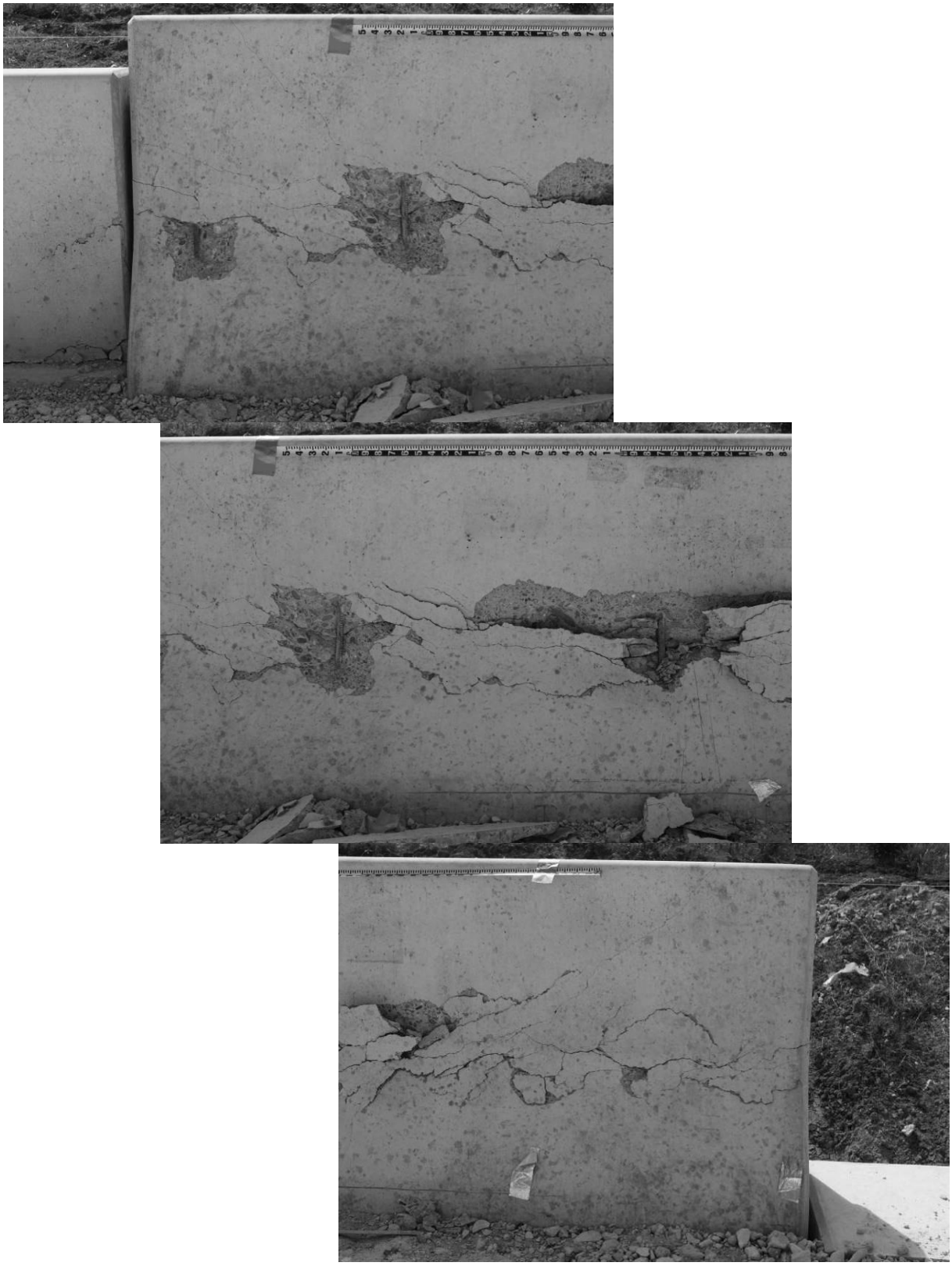

(b) Close-up front side of the barrier

Figure 5.54 Damage to barrier after Test 1 (Continued)

(c) Side view of the barrier

(d) Back view of the barrier

Figure 5.54 Damage to Barrier after Test 1 (Continued)

(a) Surface of panel

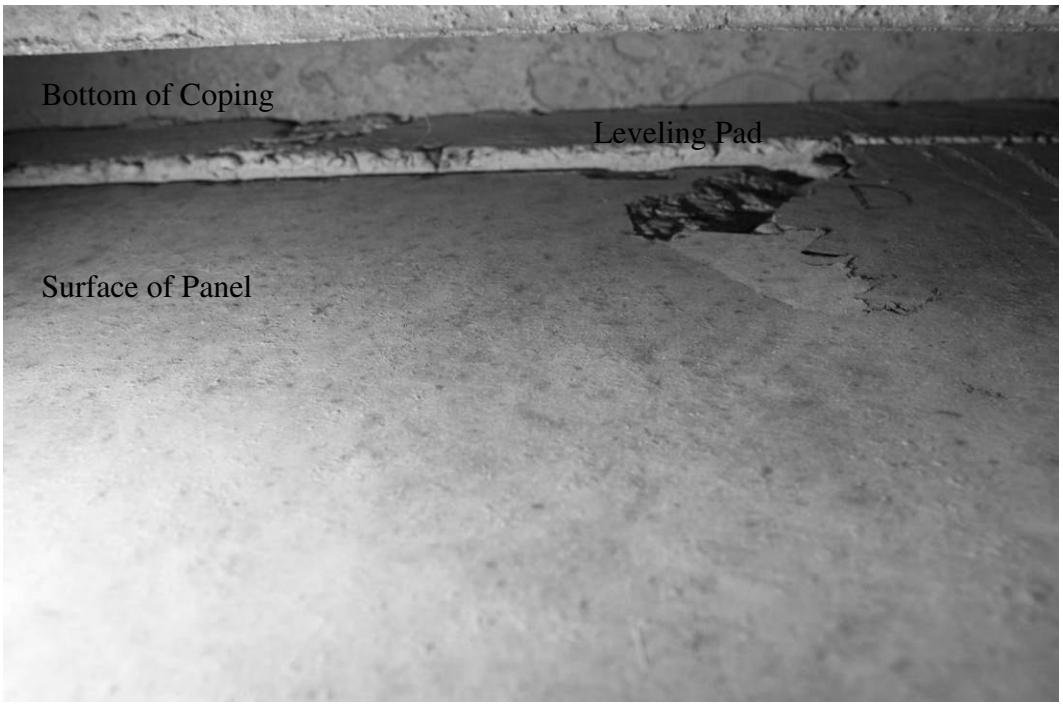

(b) Top of panel inside of recessed coping

Figure 5.55 Damage to panel and leveling pad after Test 1

(c) Close up of panel inside of recessed coping

Figure 5.55 Damage to panel and leveling pad after Test 1 (Continued)

5.3.3 Bogie Test 2: Vertical Concrete Barrier with 8 Ft Bar Mats

The second bogie test was conducted on a vertical concrete barrier connected to the mid-span of the undisturbed 9.14 m (30 ft) moment slab adjacent to the moment slab used in Test 1. This vertical barrier section was located above a wall segment that was reinforced with 2.43 m (8 ft) long bar mats. The 2,268 kg (5,000 lb) bogie vehicle, shown in Figure 5.56, impacted the reference point of the vertical barrier head-on at a speed of approximately 32.7 km/h (20.3 mph). The reference point was along the top edge of the barrier and approximately 37.15 cm (14 5/8 in.) from its centerline to coincide with the location of one of the two bar mats comprising each of the two layers of wall reinforcement below the barrier.

1) Data from Accelerometers

As previously discussed, the range of the accelerometers attached to the top of the barrier and end of the moment slab was increased after Test 1. However, as shown in Figure 5.57(b),

some of the accelerations still exceeded the revised range set for the barrier accelerometer. Consequently, analysis of this data must be done with appropriate caution. To prevent further occurrence of this problem, the range of the barrier accelerometer was increased substantially for subsequent tests.

Data obtained from the bogie-mounted accelerometer were analyzed and the results are presented in Figure 5.57. As shown in Figure 5.57(b), the maximum 50-msec average acceleration was -13.01 g. Based on this acceleration and the mass of the bogie, the maximum 50-msec average impact force was calculated to be 294.03 kN (66.1 kips) (see Figure 5.58(a)). The velocity-time and horizontal displacement-time histories of the bogie are shown in Figure 5.58(c) and (d), respectively. These time histories were calculated through integration of the acceleration data.

The maximum 50-msec average acceleration of the barrier, as measured by the accelerometer at the top of the barrier, was 10.71 g in the direction of impact (see Figure 5.59(a)). The velocity-time history of the barrier, as calculated by integration of the raw acceleration data, is shown in Figure 5.59(b). The displacement-time history obtained from integration of the velocity history is shown in Figure 5.59(c).

The raw acceleration-time history for the moment slab is shown in Figure 5.57(c). The increased range of the accelerometer was sufficient to obtain the peak acceleration of the moment slab. However, after impact, the accelerometer had a non-zero offset. The problem was traced to a connection issue that was resolved prior to the next test on this moment slab. The 50-msec average acceleration for the moment slab and the associated velocity and displacement time-histories are shown in Figure 5.60.

Figure 5.61 Targets affixed to the displacement bars attached to the top and bottom of the barrier-coping section (see Figure 5.61 and and Figure 5.62) were used as reference points to determine angular and translational displacement of the barrier from analysis of high-speed video. From the film analysis, the maximum dynamic displacement of the barrier was 15.34 cm (6.04 in.) at the top of the barrier and 2.4 cm (0.93 in.) at the bottom of the coping. The permanent displacement of the barrier was 10.16 cm (4 in.) at the top of the barrier and 1.27 cm (0.5 in.) at the bottom of the coping.

Two additional targets affixed to the displacement bars attached to the wall panel at locations corresponding to the upper and lower layers of wall reinforcement were used to

determine angular and translational displacement of the panel from analysis of high-speed video. From the film analysis, the maximum dynamic displacement of the panel was 9.4 cm (0.37 in.) at the upper reinforcement layer of the panel and 2.54 mm (0.1 in.) at the bottom reinforcement layer. The permanent displacement of the panel was 5.08 mm (0.2 in.) at the upper reinforcement layer and 0.51 mm (0.02 in.) at the bottom reinforcement layer.

The corresponding displacement-time histories for the barrier-coping section and wall panel are shown in Figure 5.63. Figure 5.64 shows the force-displacement curve for the top of the barrier.

Figure 5.56 Test 2: vertical concrete barrier with 8 ft bar mats

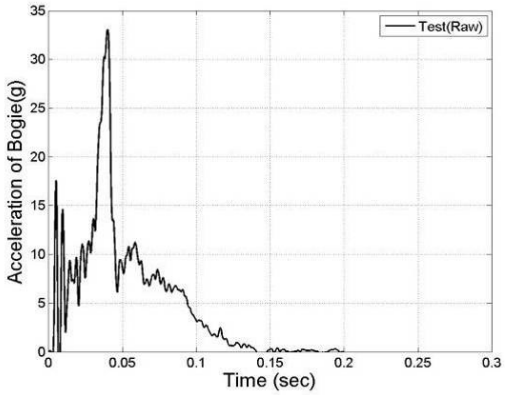

(a) Bogie

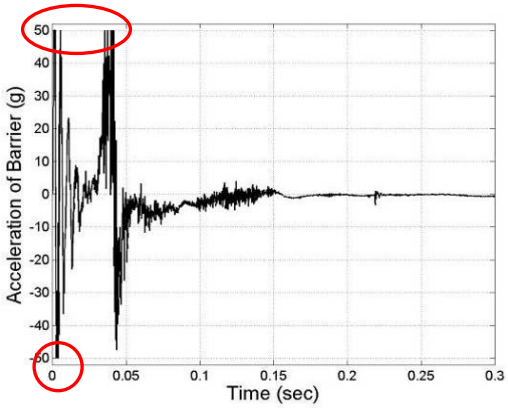

(b) Barrier

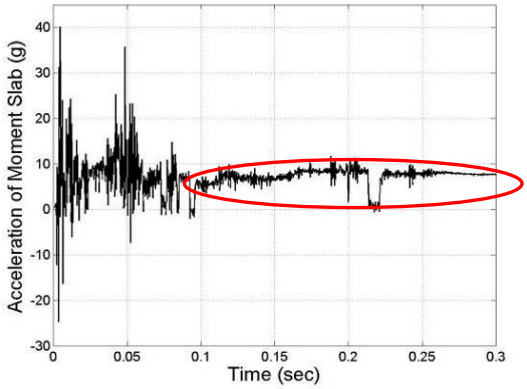

(c) Moment slab

Figure 5.57 Raw acceleration of bogie, barrier, and moment slab (Test 2)

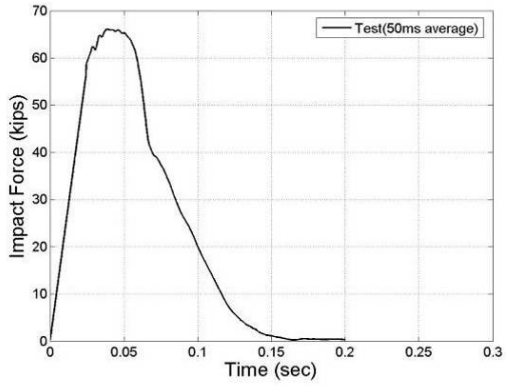

(a) Impact force

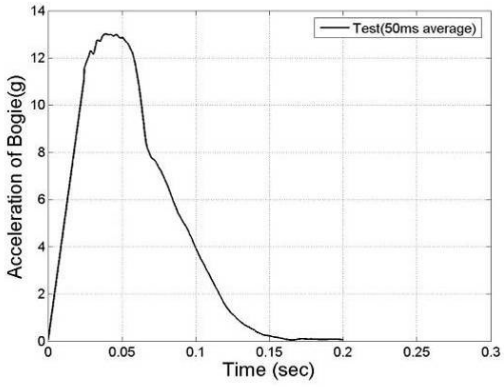

(b) Acceleration

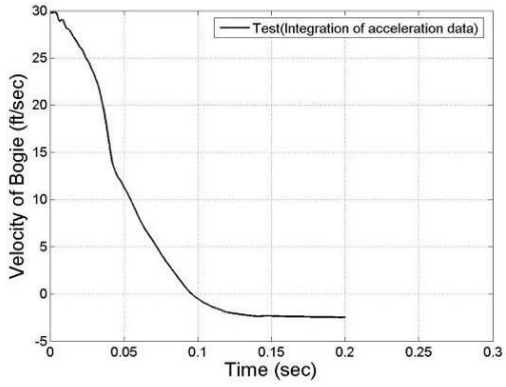

(c) Velocity

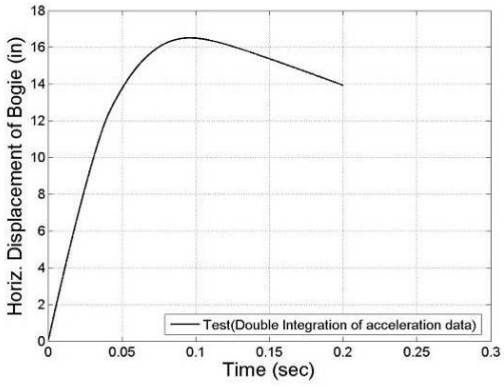

(d) Displacement

Figure 5.58 Force, acceleration, velocity, and displacement of bogie (Test 2)

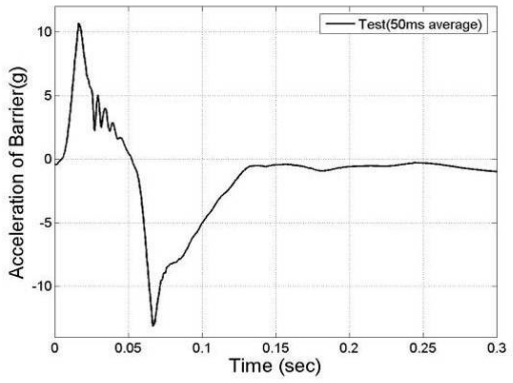

(a) Acceleration

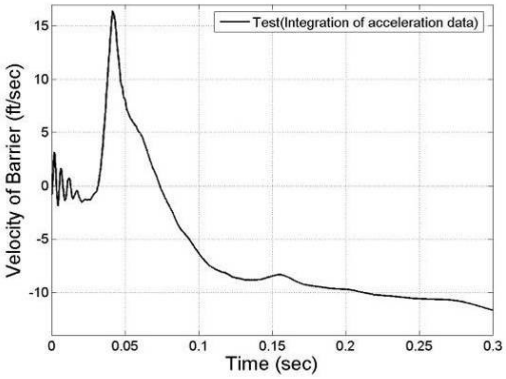

(b) Velocity

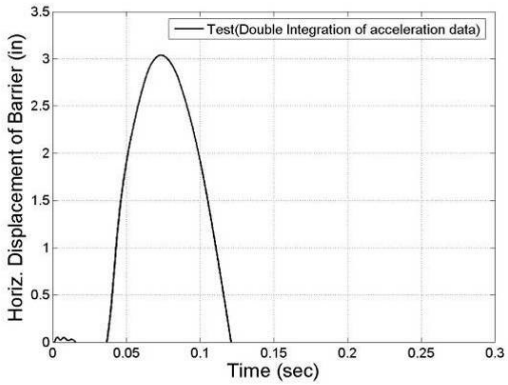

(d) Displacement

Figure 5.59 Acceleration, velocity, and displacement of barrier (Test 2)

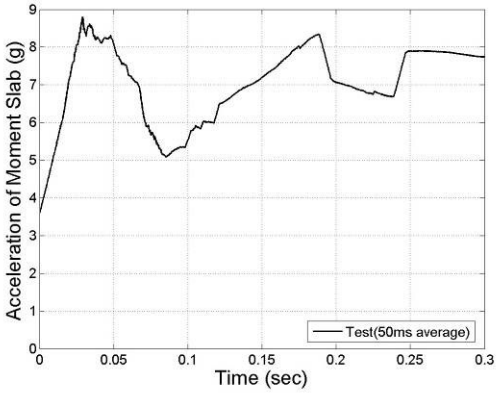

(a) Acceleration

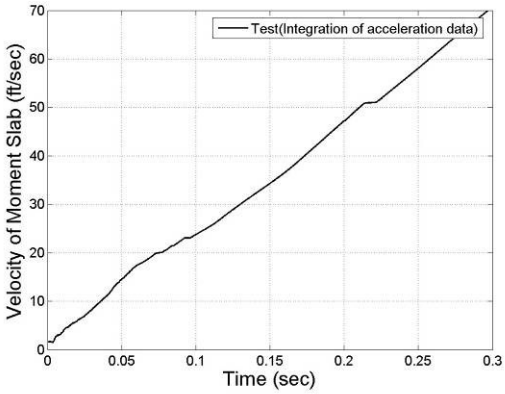

(b) Velocity

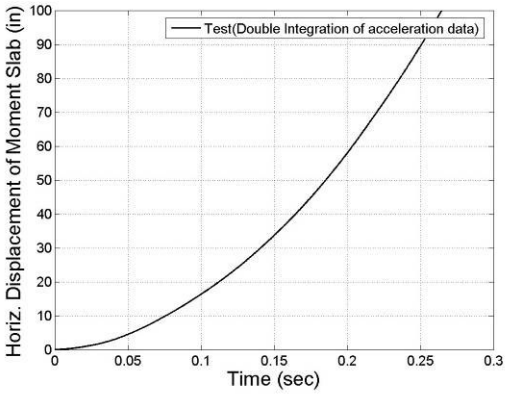

(d) Displacement

Figure 5.60 Acceleration, velocity, and displacement of moment slab (Test 2)

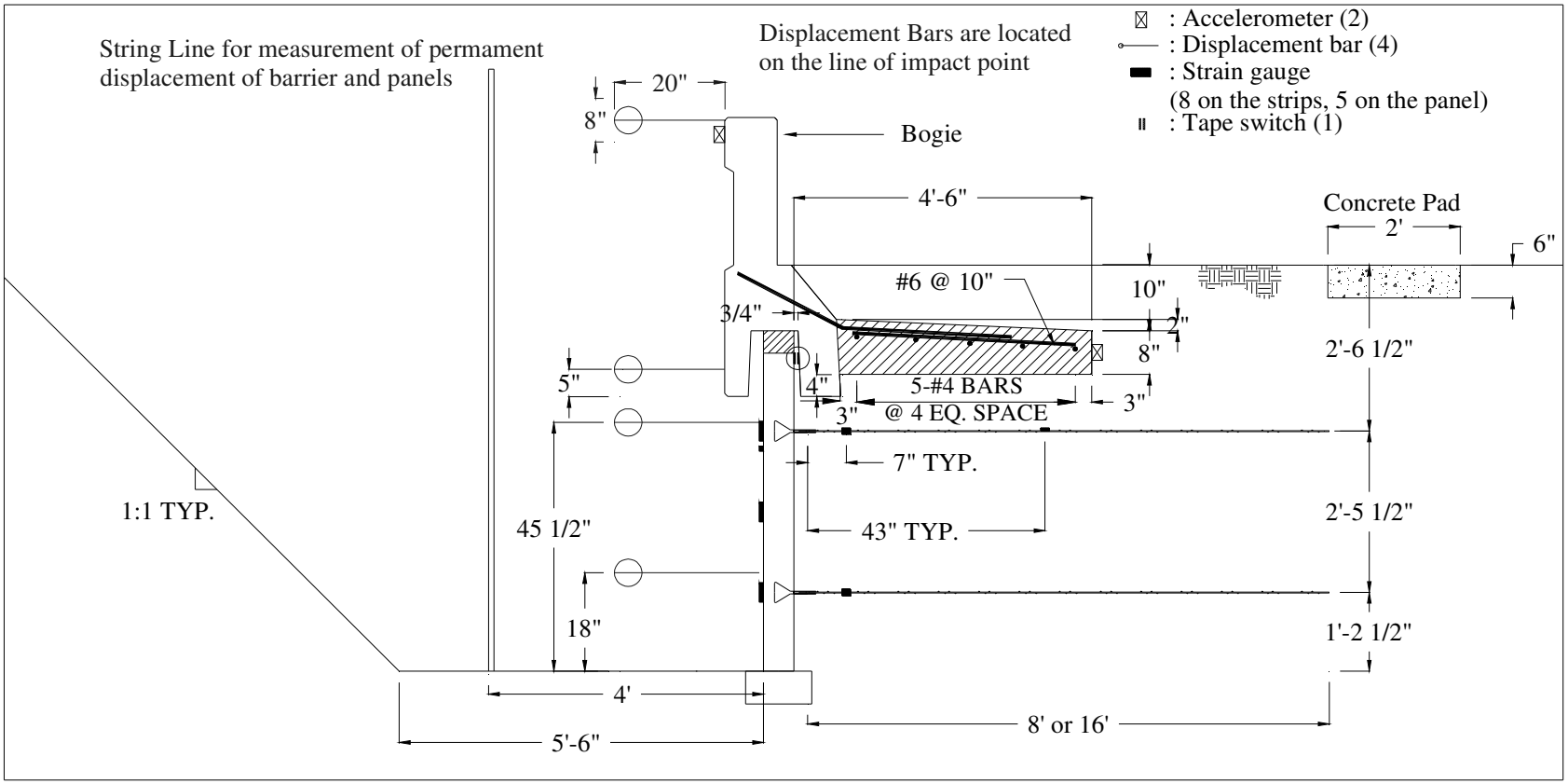

Figure 5.61 Side view of installation (Test 2, 3, and 4)

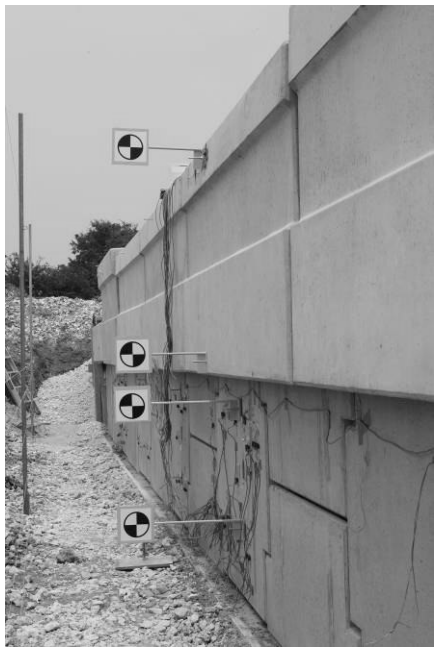

Figure 5.62 Location of displacement bBars affixed on the barrier and panels (Test 2)

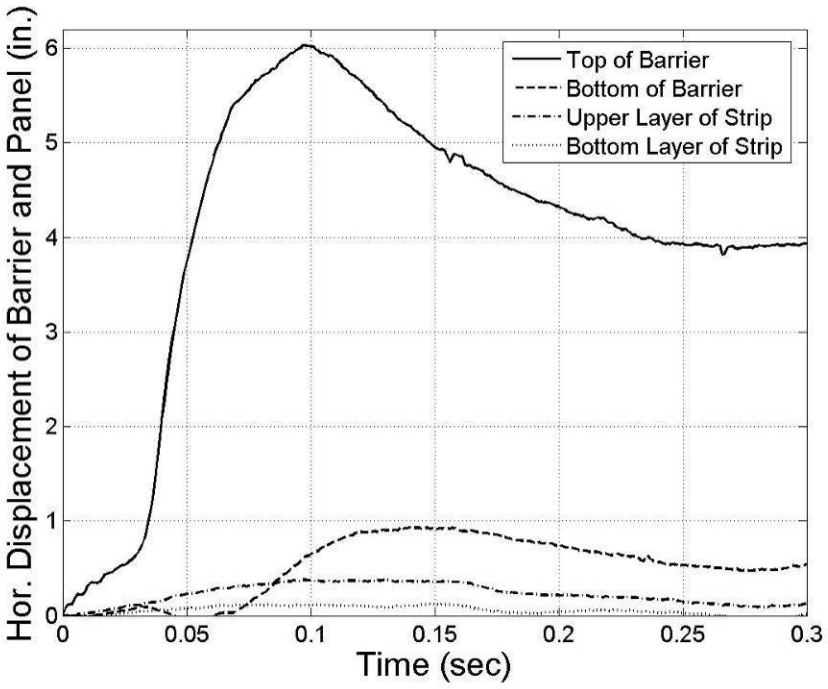

Figure 5.63 Horizontal displacement of barrier and panel measured from film (Test 2)

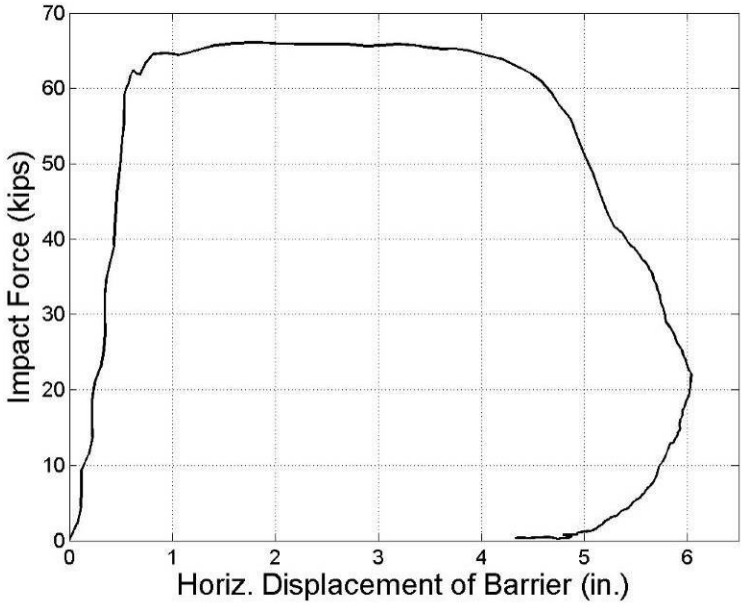

Figure 5.64 Force-displacement of the top of the barrier (Test 2)

2) Load in the Reinforcement Strips

A total of 8 strain gages were used to instrument the bar mats to capture the tensile forces transmitted into the reinforcement during the dynamic bogie vehicle impact. The locations of strain gages were assigned a numeric designator as shown in Figure 5.65. Note that two strain gages were used at locations 2-1 and 2-2 adjacent to the wall panel at the point of impact to provide some measurement redundancy at the location expected to experience maximum tensile loading. One gage was placed on top of the reinforcement and one gage was placed on the bottom of the reinforcement. Measurements obtained from the strain gages during testing indicated that the reinforcement experienced some bending in addition to tensile loading. The strain gages on the top and bottom of the reinforcement enabled the bending to be canceled out and the average tensile force in the reinforcement to be calculated.

Raw data obtained from the strain gages on the bar mats were analyzed and the results are presented in Figure 5.66. It can be seen in this figure that the contact switch placed on the top edge of the level-up concrete on top of the wall panels inside the recess of the coping indicated that the coping contacted the wall panel from 0.0806 sec to 0.1798 sec. The 50-msec

average of the raw data was analyzed to obtain design loads for the strips, and the results are presented in Figure 5.67. As with the strips in Test 1, there was some increase in force in the bar mats after the time of maximum barrier impact load. The maximum 50-msec average design strip loads corresponding to a design impact load of 240 kN (54 kips) were estimated as follows:

$$\text{Estimated Strip Load} = \frac{54}{66.1} \times \text{Maximum Strip Load} \qquad (5\text{-}10)$$

where 294.03 kN (66.1 kips) is the maximum 50-msec average impact load measured for the vertical wall barrier over 8 ft bar mats.

Table 5.11 presents a summary of the forces in the bar mat obtained from the second bogie impact test including the maximum force, maximum 50-msec average force, and an estimate of the maximum 50-msec average force for a 240 kN (54 kips) design impact.

3) Permanent Deflection of Barrier and Panels

The string lines located 1.22 m (4 ft) from the face of wall panels were used to measure the permanent deflection of barriers and panels after the bogie vehicle impact at different elevations. The permanent deflection was measured to be 99 mm (3.9 in.) and 45 mm (1.77 in.) at the top and 13 mm (0.51 in.) and 18 mm (0.71 in.) at the bottom corners of the coping as shown in Figure 5.68. Note that the reference impact point was 37.15 cm (14 5/8 in.) left of the centerline of the barrier-coping section as shown in Figure 5.68 to align with the instrumented bar mats. This corresponded to the side of the barrier with greater movement.

Note that the barrier-coping sections to the left and right of the section that was impacted had permanent movement at the top of the barrier of 25 mm (1 in.) and 32 mm (1.26 in.), respectively, due to their connection to the same 9.14 m (30 ft) moment slab as the vertical barrier section that was impacted. The permanent defection of the wall panels was measured as shown in Figure 5.68. The maximum permanent movement measured in the wall panels beneath the impact barrier section was approximately 5 mm (0.2 in.).

4) Panel Analysis

The wall reinforcement was instrumented with a total of 5 strain gages to capture the resistance of the panel during the bogie impacts as shown in Figure 5.69. The maximum compressive strain of 0.00016 occurred at 0.056 sec (see Figure 5.70) at the location of uppermost layer of strips. Note that positive values for the vertical direction strain gages indicate movement toward the traffic side of the barrier. The strains at the horizontal centerline of the panel and at the second layer of strips were 0.00012 and 0.00007, respectively.

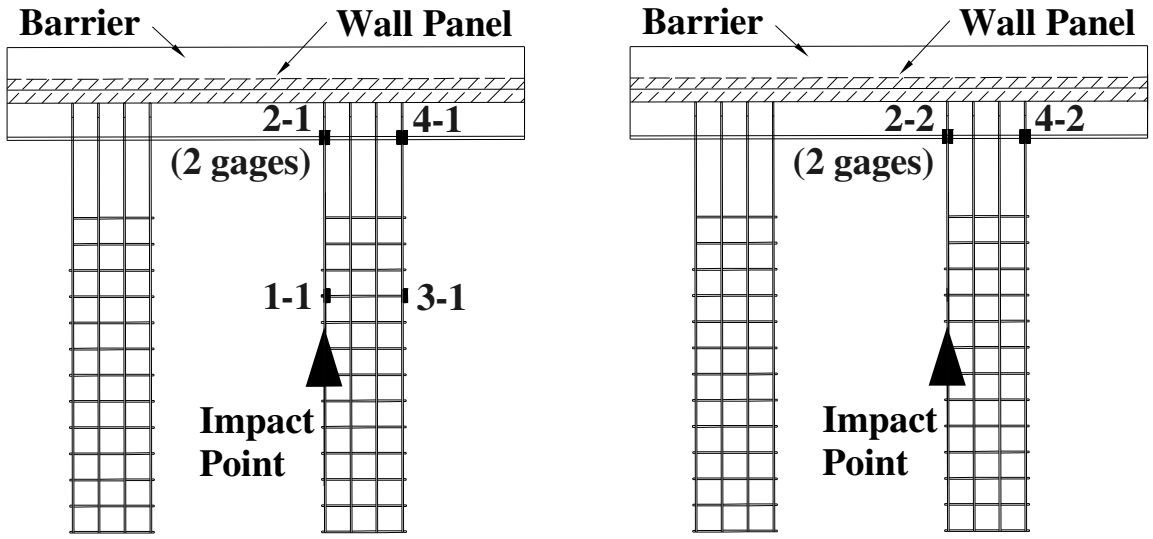

(a) Upper layer **(b) Bottom layer**

Figure 5.65 Location of strain gages and labeling (Test 2)

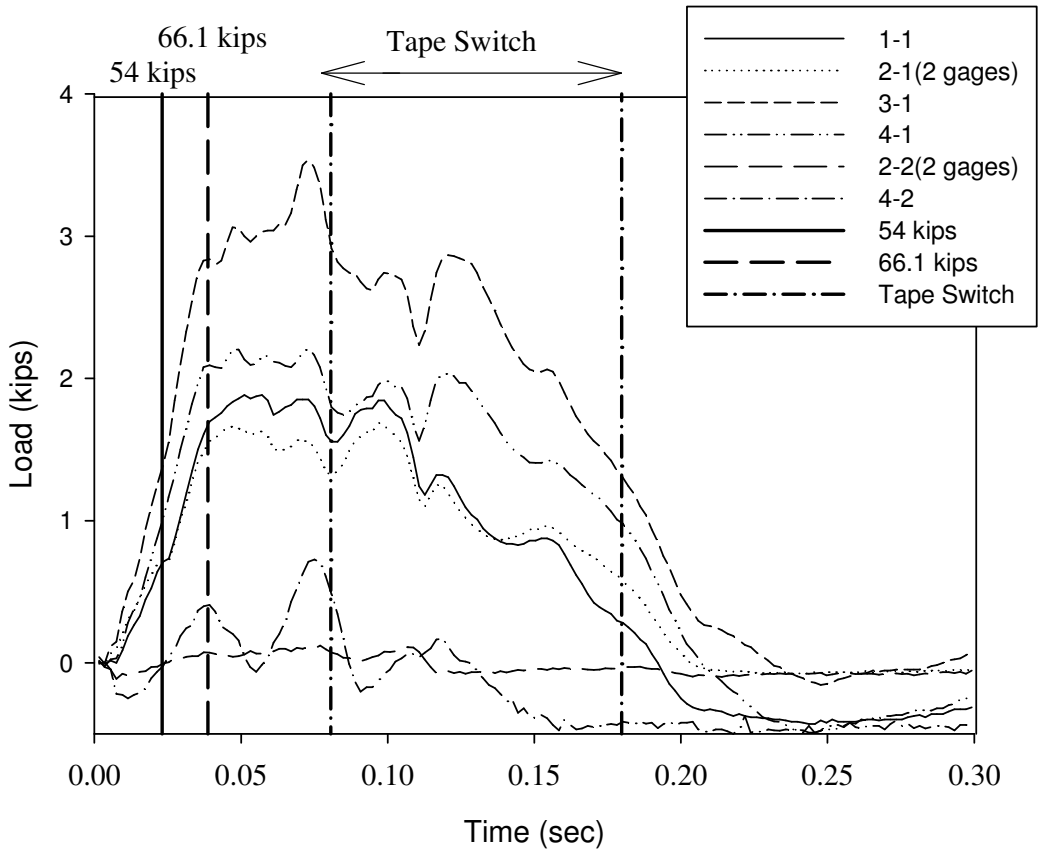

Figure 5.66 Strip load of raw data on the strips (Test 2)

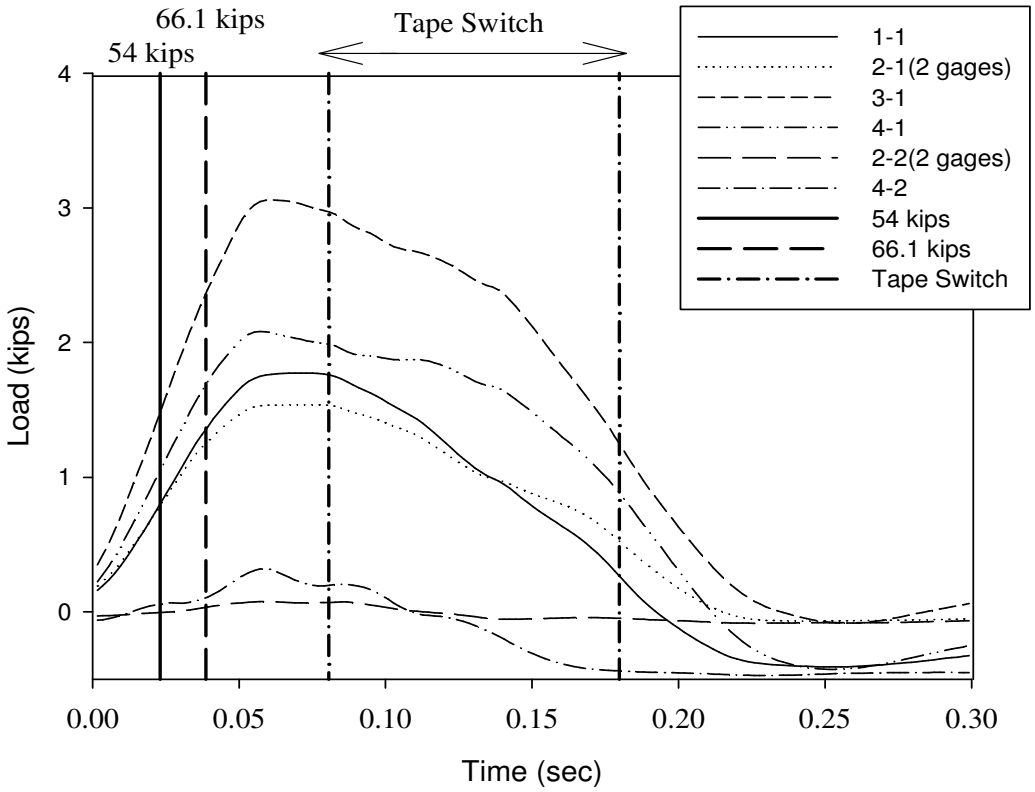

Figure 5.67 Strip load of 50 msec average on the strips (Test 2)

Table 5.11 Load on the Wall Reinforcement (Test 2)

	Upper layer (kips)				Bottom layer (kips)	
	Impact point, Behind (1-1)	Impact point, Front (2-1)	Next to impact point, Behind (3-1)	Next to impact point, Front (4-1)	Impact point, Front (2-2)	Next to impact point, Front (4-2)
Maximum Load from Raw Data (t = 0.0742 sec)	1.81	1.53	3.53	2.19	0.1	0.72
Maximum 50 msec avg. Load (t = 0.0607 sec)	1.76	1.54* (1.44-T 1.63-B)	3.06	2.07	0.08* (-0.16-T 0.31-B)	0.31
Estimated Design Load	1.29	1.13	2.25	1.52	0.06	0.23

* Average of top and bottom loads

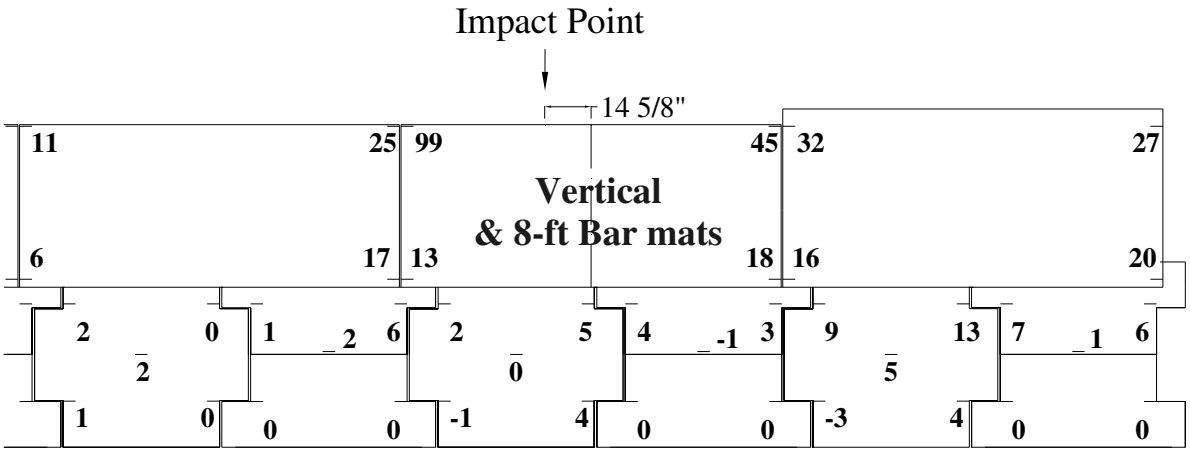

Figure 5.68 Permanent deflection of barrier and panels (Test 2, units: mm)

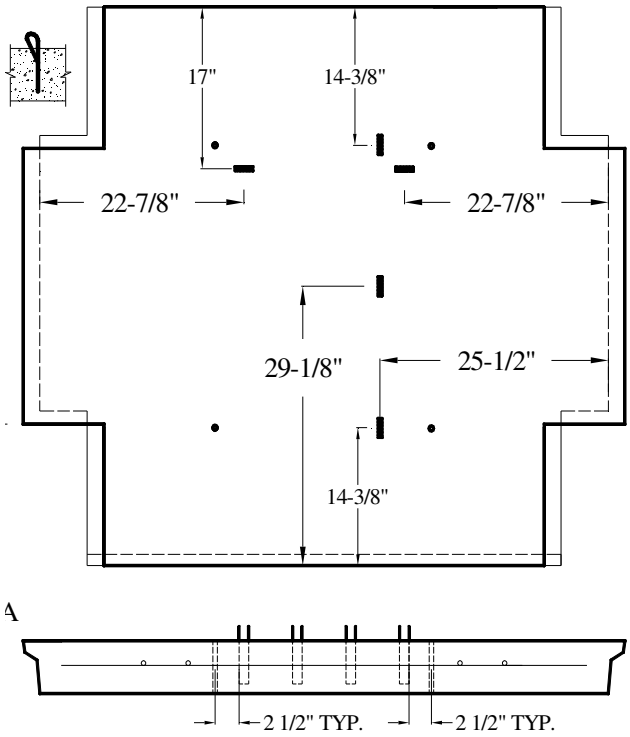

Figure 5.69 Location of concrete statin gages (Test 2)

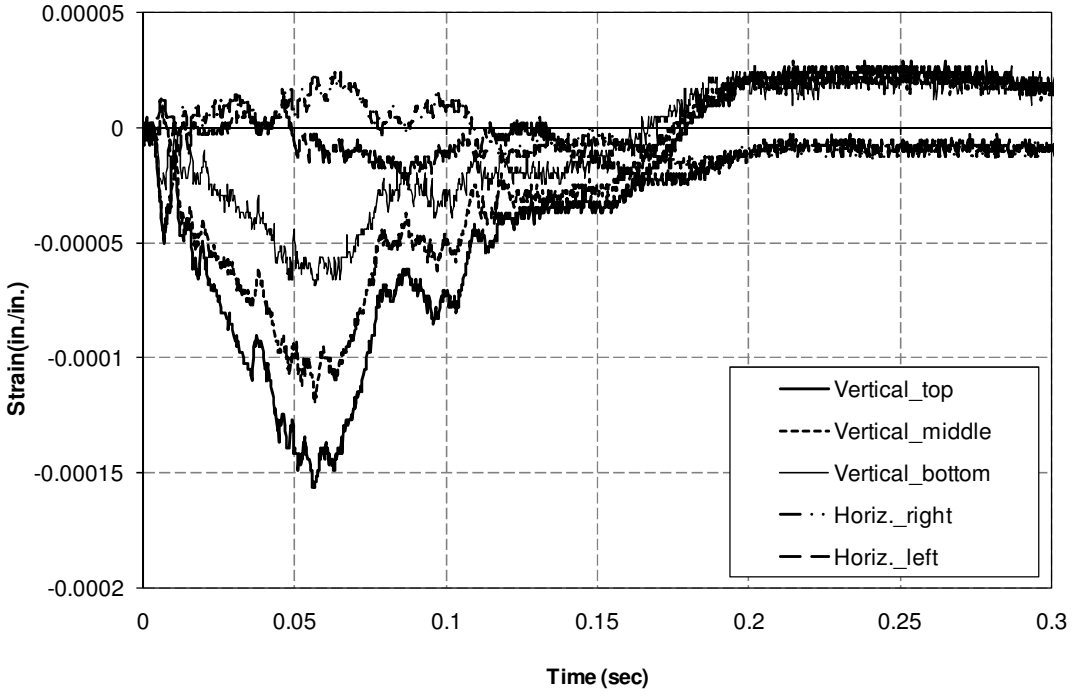

Figure 5.70 Strain on the panel (Test 2)

5) Component Damage

Damage to the vertical wall barrier-coping section resulting from the bogie impact is shown in Figure 5.71. Left of the point of impact, the vertical barrier failed in a classical yield line pattern by developing a vertical "hinge" line at the point of impact and a diagonal hinge line radiating from the bottom to the top of the barrier. However, because the bogie impact point was offset 37.15 cm (14 5/8 in.) from the centerline of the barrier to align with the bar mat, there was insufficient strength to develop a similar yield line failure on the right side of the barrier. Rather, a lower strength cantilever bending failure mode controlled on the right side of the barrier. Longitudinal cracks developing from this failure mode were observed at the groundline connection between the barrier and coping and approximately 15.2 cm (6 in.) above the groundline from the point of impact to the end of the vertical barrier (see Figure 5.71(b)).

Cracking in the soil was observed approximately 1.22 m (48 in.) from the front face of the barrier, which corresponds with the location of the end of the moment slab. The crack, shown in Figure 5.71(c), was about 1.3 cm (½ in.) wide and extended along the entire length of the 9.15 m (30 ft) long moment slab. Damage to the back of the vertical barrier, shown in Figure 5.71(e) and (f), mirrors that on the front face of the barrier. Most pronounced are the diagonal hinge line and the longitudinal crack at the interface between the vertical barrier and coping.

Damage to the panel beneath the point of impact on the barrier is shown in Figure 5.72. As shown in Figure 5.72(a), the surface of the panel showed little distress. The leveling concrete on top of the wall panel was broken and shifted over the front edge of the panel due to contact with the inside face of the coping. The bonding of the leveling concrete to the top of the wall panel caused the top edge of the wall panel to spall as shown in Figure 5.72(b).

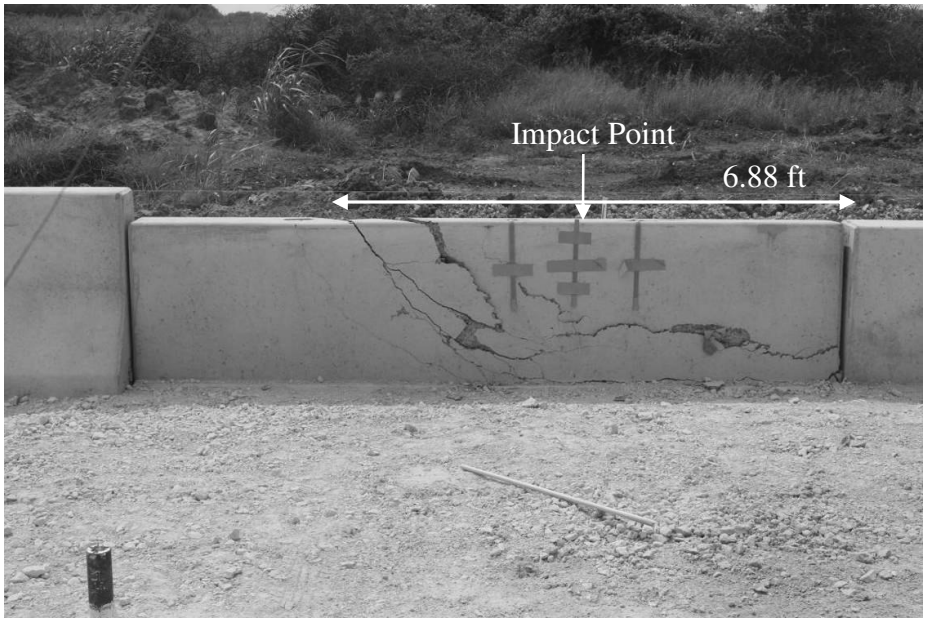

(a) Front view of the barrier

Figure 5.71 Cracks on the barrier after test (Test 2)

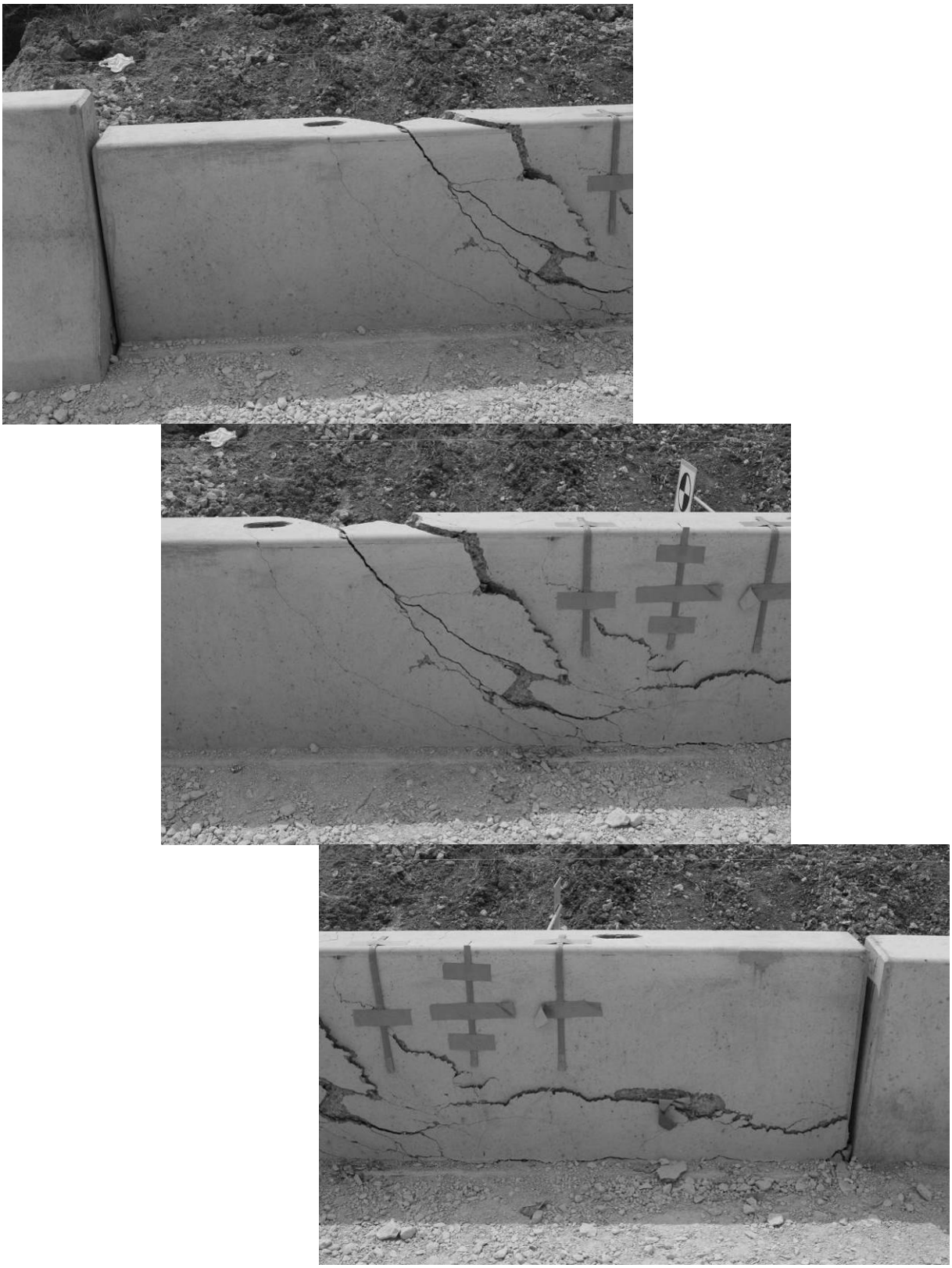

(b) Close-up front side of the barrier

Figure 5.71 Cracks on the barrier after test (Test 2) (Continued)

(c) Side view of the barrier

(d) Close-up side view of the barrier

Figure 5.71 Cracks on the barrier after test (Test 2) (Continued)

(e) Back view of the barrier

(f) Close-up back view of the barrier

Figure 5.71 Cracks on the barrier after test (Test 2) (Continued)

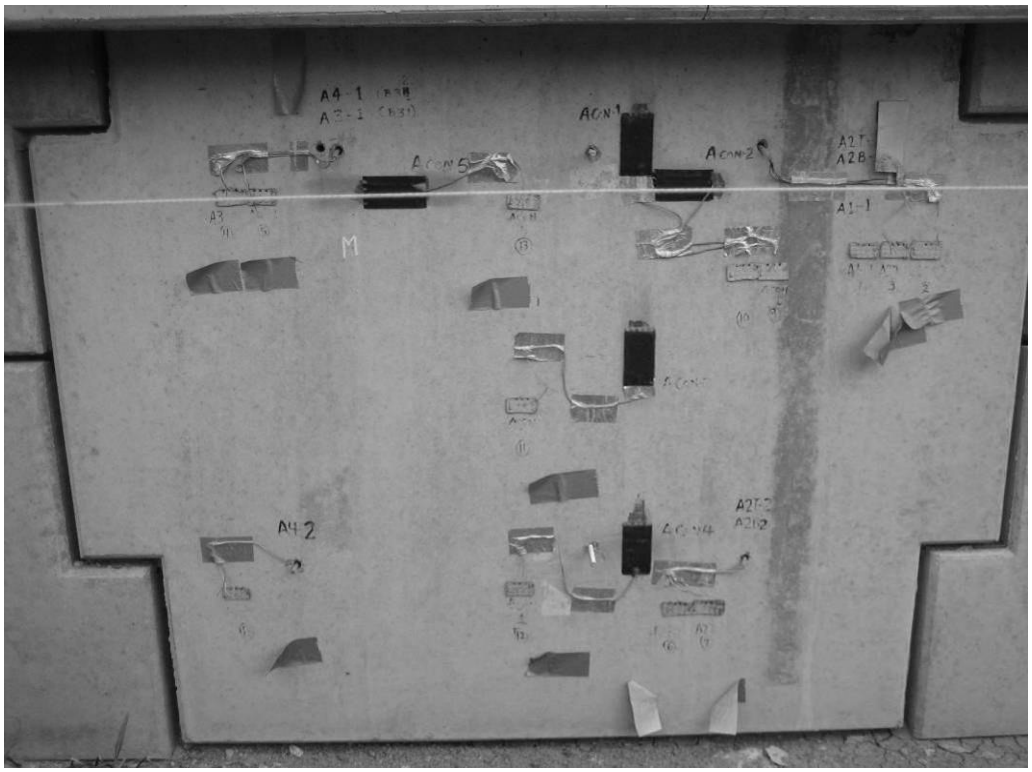

(a) Surface of panel

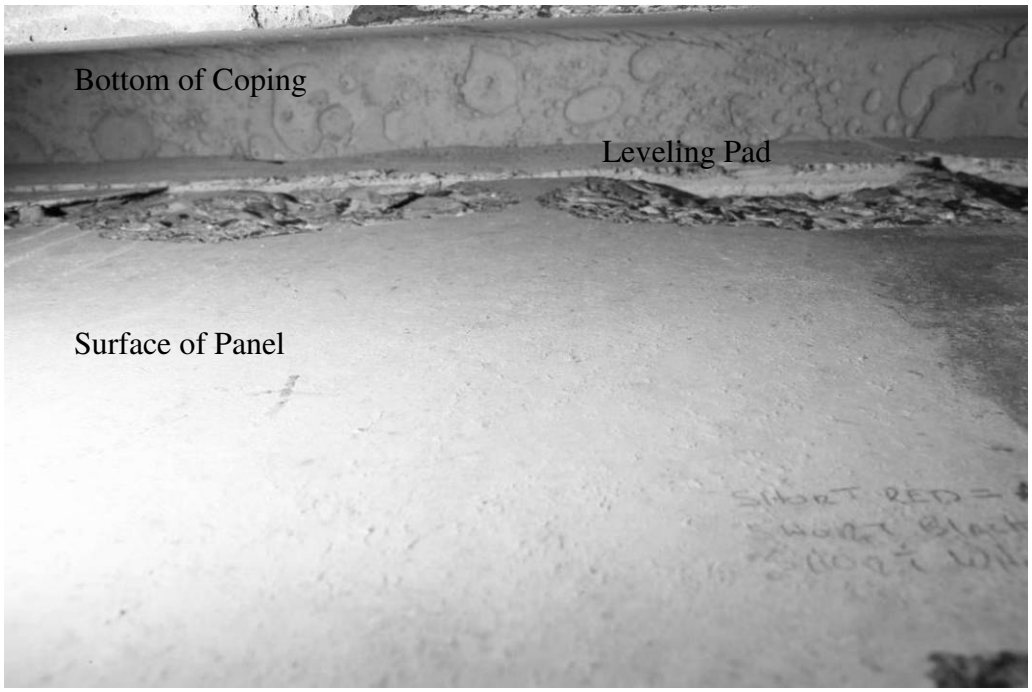

(b) Inside of panel

Figure 5.72 Cracks on the panel and leveling pad after test (Test 2)

5.3.4 Bogie Test 3: Vertical Concrete Barrier with 8 Ft Strips

Upon completion of the first two reference tests, the soil on and around the two moment slabs was recompacted for the following tests. The third bogie test was conducted on a vertical concrete barrier connected to the end of the 9.14 m (30 ft) moment slab above the wall section with 2.43 m (8 ft) long steel reinforcement strips. The 2,268 kg (5,000 lb) bogie vehicle, shown in Figure 5.73, impacted the reference point of the vertical barrier head-on at a speed of approximately 32.5 km/h (20.2 mph). The reference point was along the top edge of the barrier and approximately 12.1 cm (4 3/4 in.) from its centerline to coincide with the location of a steel strip in the wall reinforcement below the barrier.

1) Data from Accelerometers

The increased range used for the barrier and moment slab accelerometers was sufficient to capture the accelerations arising from the bogie impact. The raw acceleration data for the bogie, barrier, and moment slab are shown in Figure 5.74.

Data obtained from the bogie-mounted accelerometer were analyzed and the results are presented in Figure 5.75. As shown in Figure 5.75(b), the maximum 50-msec average acceleration was -13.82 g. Based on this acceleration and the mass of the bogie, the maximum 50-msec average impact force was calculated to be 312.13 kN (70.17 kips) (see Figure 5.75(a)). The velocity-time and horizontal displacement-time histories of the bogie are shown in Figure 5.75(c) and (d), respectively. These time histories were calculated through integration of the acceleration data.

The maximum 50-msec average acceleration of the barrier, as measured by the accelerometer at the top of the barrier, was 10.16 g in the direction of impact (see Figure 5.76(a)). The velocity-time history of the barrier, as calculated by integration of the raw acceleration data, is shown in Figure 5.76(b). The displacement-time history obtained from integration of the velocity history is shown in Figure 5.76(c).

The 50-msec average acceleration for the moment slab is shown in Figure 5.77(a). The velocity-time and vertical displacement-time histories of the moment slab are shown in Figure

5.77(b) and (c), respectively. The velocity-time history and displacement time histories were calculated by integration of the raw acceleration data.

Targets affixed to the displacement bars attached to the top and bottom of the barrier-coping section (see Figure 5.61 and Figure 5.78) were used as reference points to determine angular and translational displacement of the barrier from analysis of high-speed video. From the film analysis, the maximum dynamic displacement of the barrier was 13.1 cm (5.17 in.) at the top of the barrier and 3 cm (1.16 in.) at the bottom of the coping. The permanent displacement of the barrier was 6.35 cm (2.5 in.) at the top of the barrier and 1.5 cm (0.6 in.) at the bottom of the coping.

Two additional targets affixed to the displacement bars attached to the wall panel at locations corresponding to the upper and lower layers of wall reinforcement were used to determine angular and translational displacement of the wall panel from analysis of high-speed video. From the film analysis, the maximum dynamic displacement of the panel was 2.3 cm (0.92 in.) at the upper reinforcement layer and 0.5 cm (0.19 in.) at the bottom reinforcement layer. The permanent displacement of the panel was 1.4 cm (0.55 in.) at the upper reinforcement layer and 0.5 cm (0.18 in.) at the bottom reinforcement layer.

The corresponding displacement-time histories for the barrier-coping section and wall panel obtained from film analysis are shown in Figure 5.79. Figure 5.80 shows the impact force-displacement curve for the top of the barrier.

Figure 5.73 Test 3: Vertical wall barrier with 8 ft long strip

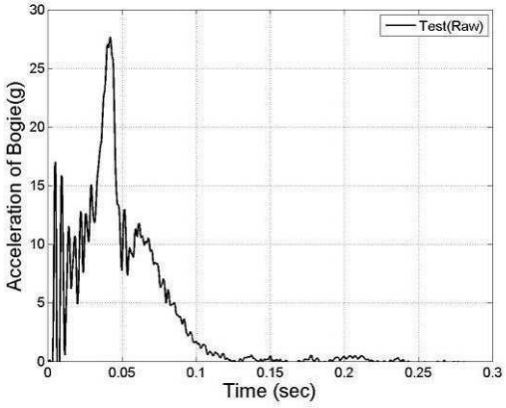

(a) Bogie

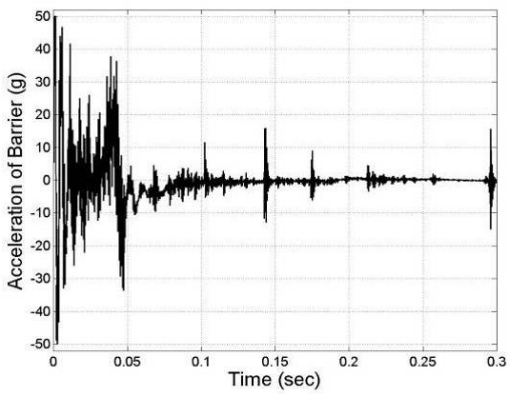

(b) Barrier

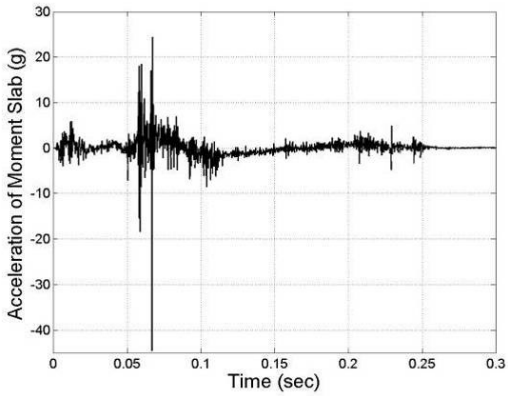

(c) Moment slab

Figure 5.74 Raw acceleration of bogie, barrier, and moment slab (Test 3)

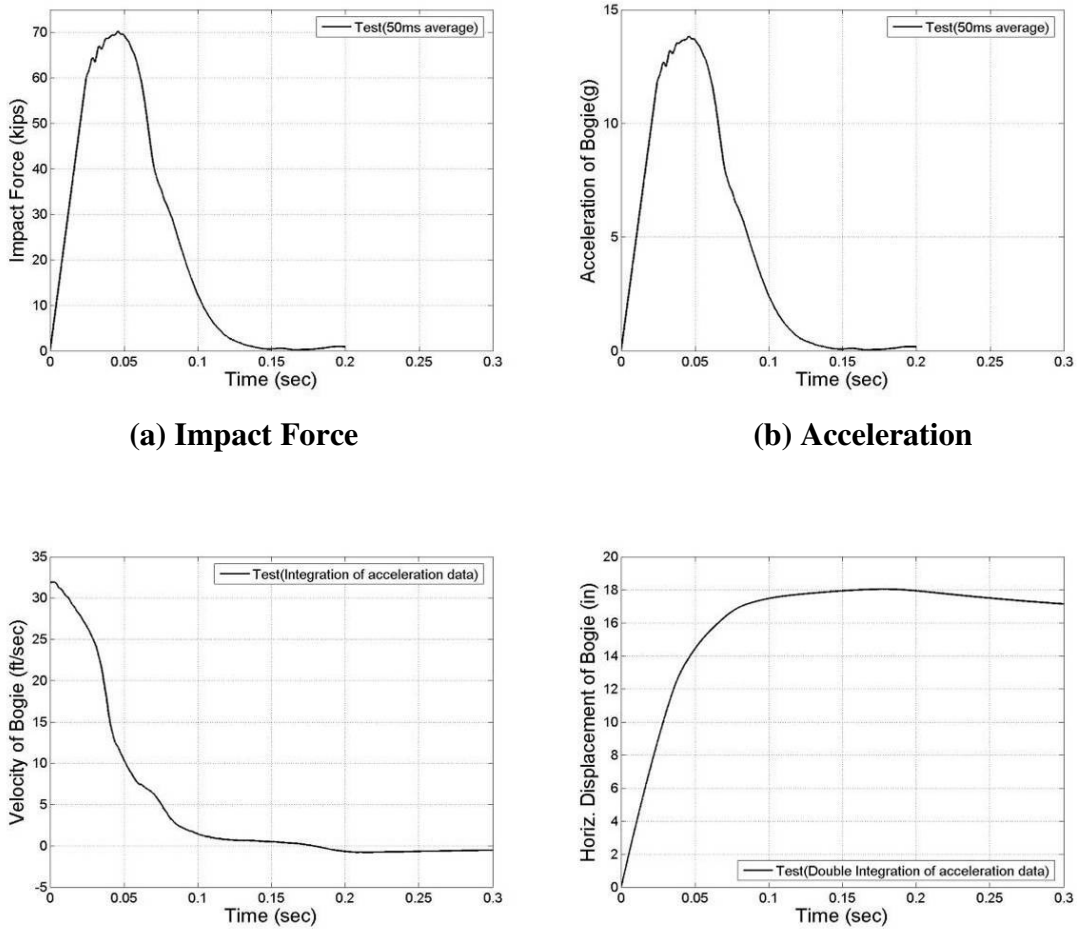

(a) Impact Force **(b) Acceleration**

(c) Velocity **(d) Displacement**

Figure 5.75 Force, acceleration, velocity, and displacement of bogie (Test 3)

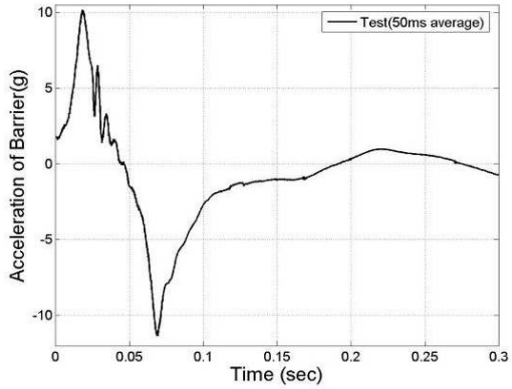

(a) Acceleration

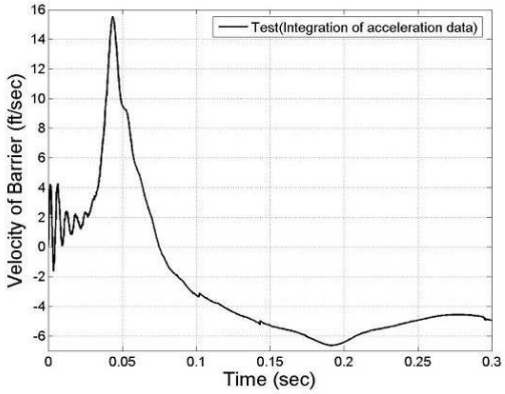

(b) Velocity

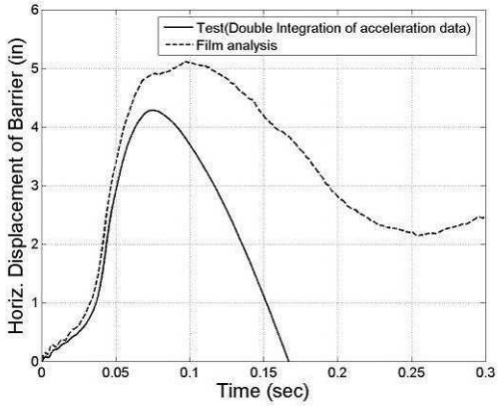

(d) Displacement

Figure 5.76 Acceleration, velocity, and displacement of barrier (Test 3)

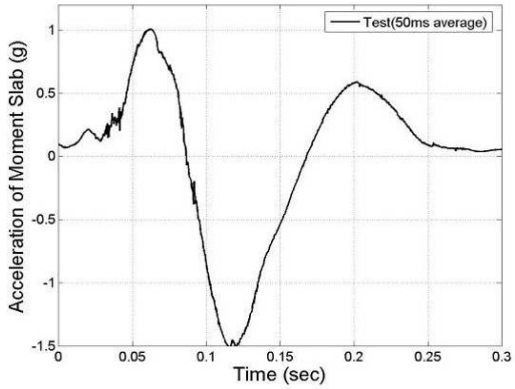

(a) Acceleration

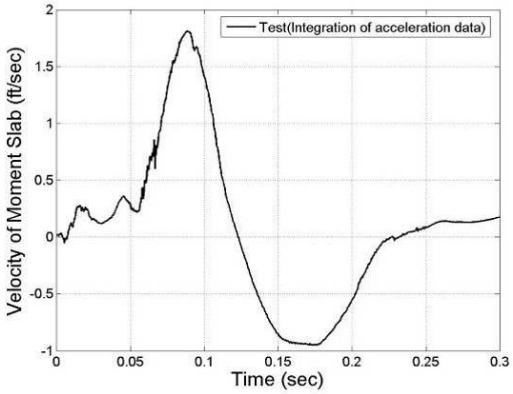

(b) Velocity

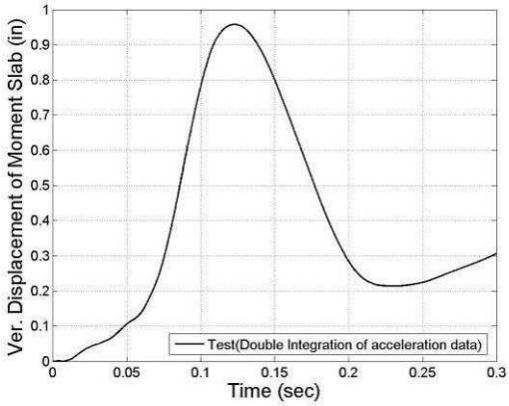

(d) Displacement

Figure 5.77 Acceleration, velocity, and displacement of moment slab (Test 3)

Figure 5.78 Location of displacement bars affixed on the barrier and panels (Test 3)

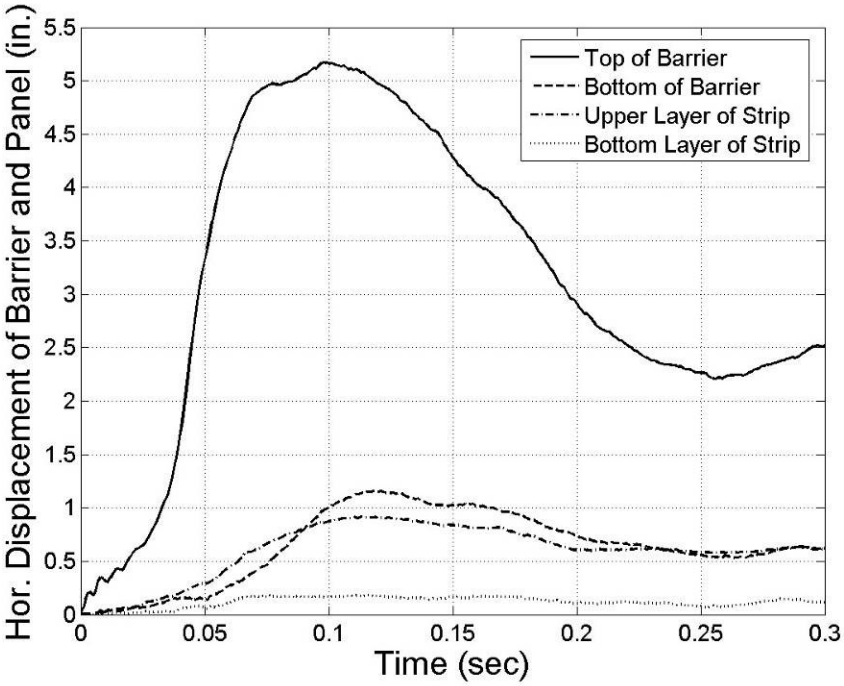

Figure 5.79 Horizontal displacement of barrier and panel measured from film (Test 3)

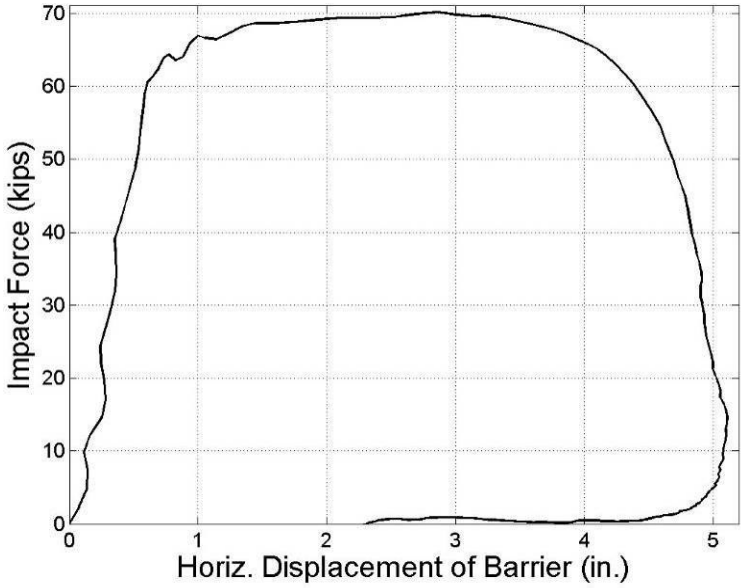

Figure 5.80 Force-displacement of the top of the barrier (Test 3)

2) Load in the Reinforcement Strips

A total of 8 strain gages were used to instrument the strips to capture the tensile forces transmitted into the reinforcement during the dynamic bogie vehicle impact. To enable comparison of loads on the strips, the locations of strain gages were assigned a numeric designator as shown in Figure 5.81. Note that two strain gages were used at locations 2-1 and 2-2 adjacent to the wall panel at the point of impact to provide some measurement redundancy at the location expected to experience maximum tensile loading. One gage was placed on top of the reinforcement and one gage was placed on the bottom of the reinforcement. Measurements obtained from the strain gages during testing indicated that the reinforcement experienced some bending in addition to tensile loading. The strain gages on the top and bottom of the reinforcement enabled the bending to be canceled out and the average tensile force in the reinforcement to be calculated.

Raw data obtained from the strain gages on the bar mats were analyzed and the results are presented in Figure 5.82. A contact switch placed on the top edge of the level-up concrete on top of the wall panels inside the recess of the coping activated twice from 0.0522 sec to

0.115 sec and from 0.1605 sec to 0.2385 sec, which indicates that the coping was in contact with the wall panel and/or leveling concrete during these times. The 50-msec average of the raw data was analyzed to obtain design loads for the strips, and the results are presented in Figure 5.83. As shown in this figure, there was some increase in force in the strips observed after the time of maximum barrier impact load, but the increase was not as significant as that seen in Test 1. The maximum 50-msec average design strip loads corresponding to a design impact load of 240 kN (54 kips) were estimated as follows:

$$\text{Estimated Strip Load} = \frac{54}{70.17} \times \text{Maximum Strip Load} \qquad (5\text{-}11)$$

where 312.13 kN (70.17 kips) is the maximum 50-msec average impact load measured for the vertical wall barrier over 2.43 m (8 ft) strips.

Table 5.12 presents a summary of the forces in the steel strips obtained from the third bogie impact test including the maximum force, maximum 50-msec average force, and an estimate of the maximum 50-msec average force for a 240 kN (54 kips) design impact.

3) Permanent Deflection of Barrier and Panels

The string lines located 1.22 m (4 ft) from the face of the wall panels were used to measure the permanent deflection of barriers and panels after bogie vehicle impact. After the bogie vehicle impact of the vertical barrier, the permanent deflection was measured to be 63 mm (2.48 in.) and 53 mm (2.09 in.) at the top corners of the barrier and 17 mm (0.7 in.) and 15 mm (0.59 in.) at the bottom corners of the coping as shown in Figure 5.84. Note that the reference impact point was offset 9.5 cm (3 3/4 in.) left from the centerline of the barrier-coping section as shown in Figure 5.84 to align with the steel strip reinforcement. The left side of the barrier on Figure 5.84 was therefore slightly closer to the reference impact point.

The barrier-coping sections to the left of the section that was impacted had permanent movement at the top of the barrier of 24 mm (0.95 in.). This indicates that the shear dowels are effective in transferring load to the adjacent moment slab. The permanent defection of the wall panels was measured as shown in Figure 5.84. The maximum permanent movement measured in the wall panels beneath the impact barrier section was approximately 16 mm 0.63 in.), which was about three times the movement observed in the previous tests with the 4.88 m

(16 ft) strips and 2.43 m (8 ft) bar mats. The magnitude of movement appears to indicate that the strips reached their pullout capacity. This is supported by the lower loads measured in the strips for this test compared to the previous tests.

4) Panel Analysis

The wall reinforcement was instrumented with a total of 5 strain gages to capture the resistance of the panel during the bogie impacts as shown in Figure 5.85. The maximum compressive strain of 0.00022 occurred at 0.056 sec (see Figure 5.86) at the location of uppermost layer of strips. Note that positive values for the vertical direction strain gages indicate movement toward the traffic side of the barrier. The strains at the horizontally centerline of the panel and at the second layer of strips were 0.00018 and 0.00014, respectively.

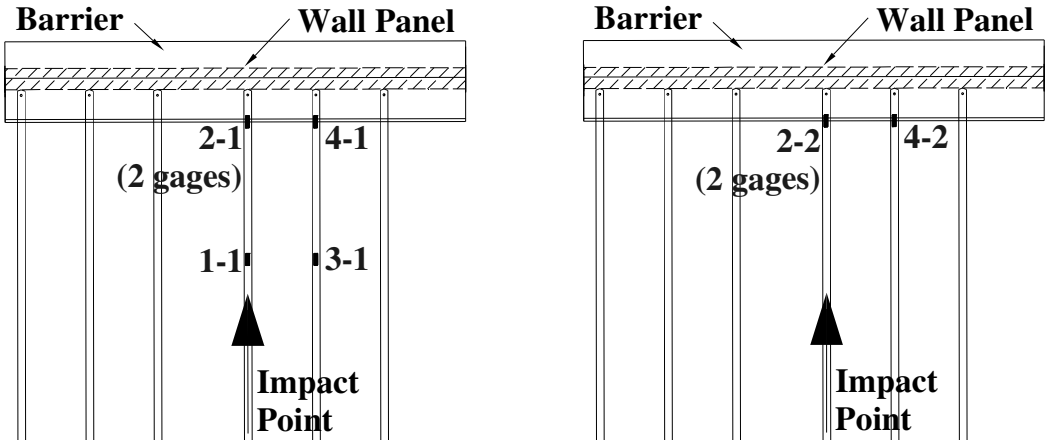

(a) Upper layer **(b) Bottom layer**

Figure 5.81 Location of strain gages and labeling (Test 3)

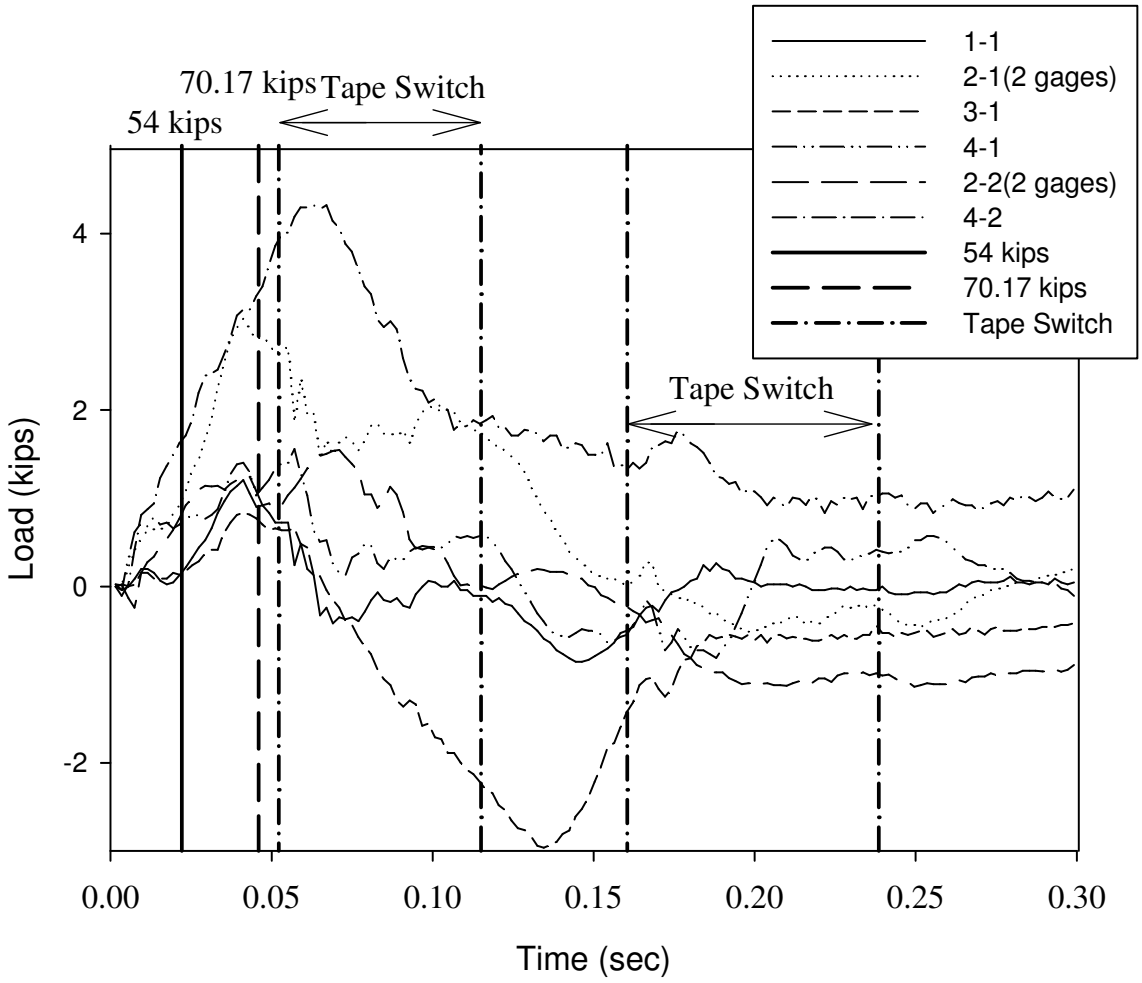

Figure 5.82 Strip load of raw data on the strips (Test 3)

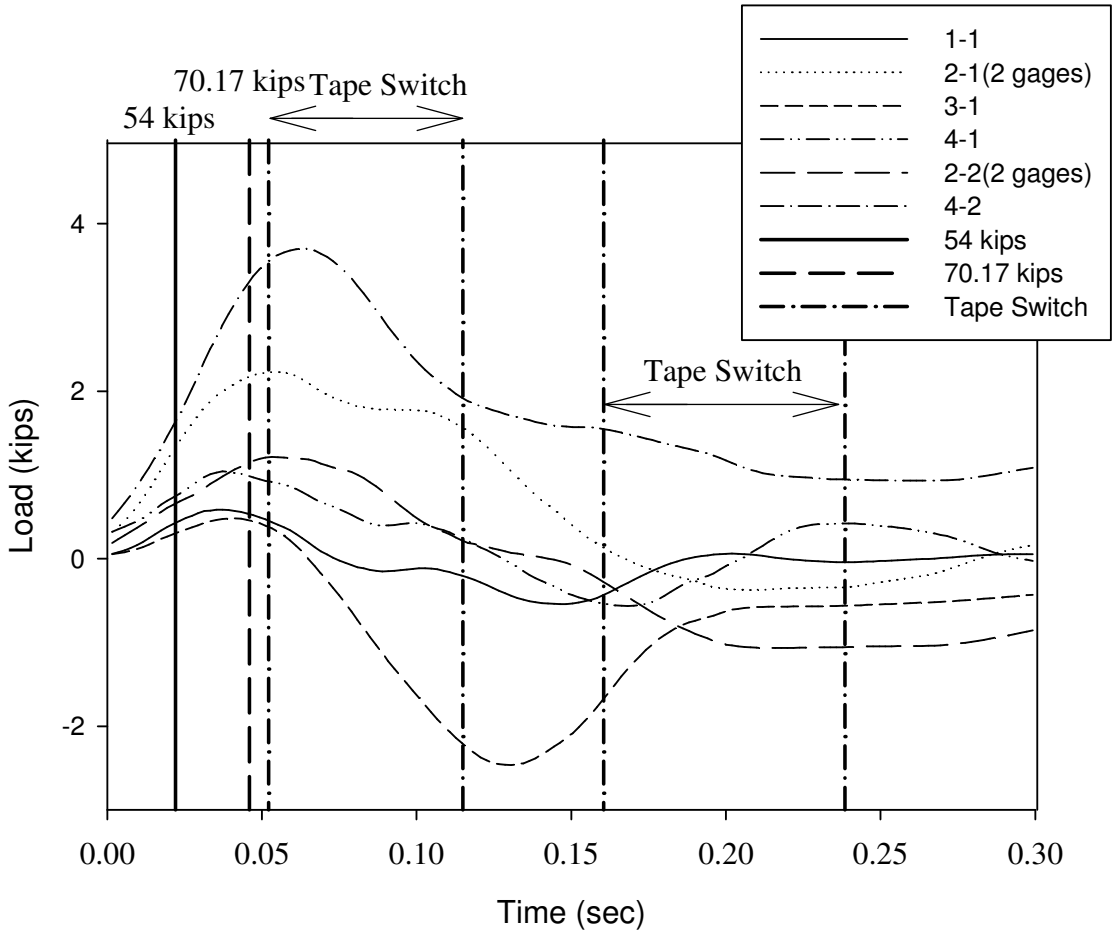

Figure 5.83 Strip load of 50 msec average on the strips (Test 3)

Table 5.12 Load on the Wall Reinforcement (Test 3)

	Upper layer (kips)				Bottom layer (kips)	
	Impact point, Behind (1-1)	Impact point, Front (2-1)	Next to impact point, Behind (3-1)	Next to impact point, Front (4-1)	Impact point, Front (2-2)	Next to impact point, Front (4-2)
Maximum Load from Raw Data (t = 0.0643 sec)	-0.11	1.76	0.37	0.53	1.38	4.46
Maximum 50 msec avg. Load (t = 0.0635 sec)	0.24	2.13* (-0.3-T 4.56-B)	0.06	0.79	1.19* (0.98-T 1.4-B)	3.71
Estimated Design Load	0.18	1.57	0.04	0.58	0.88	2.73

* Average of top and bottom loads

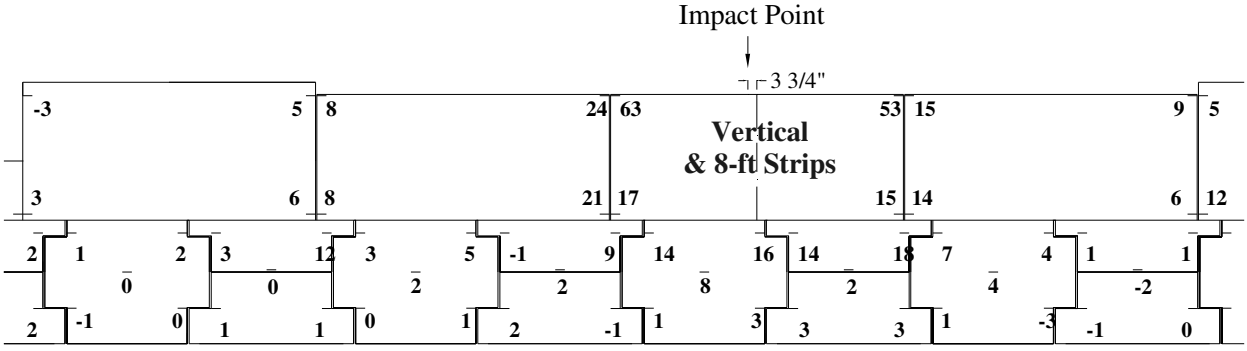

Figure 5.84 Permanent deflection of barrier and panels (Test 3, units: mm)

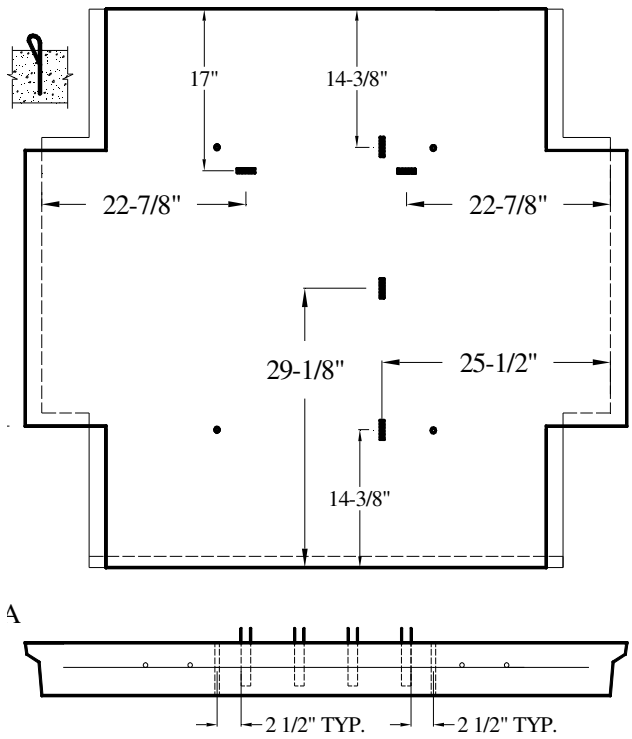

Figure 5.85 Location of concrete statin gages (Test 3)

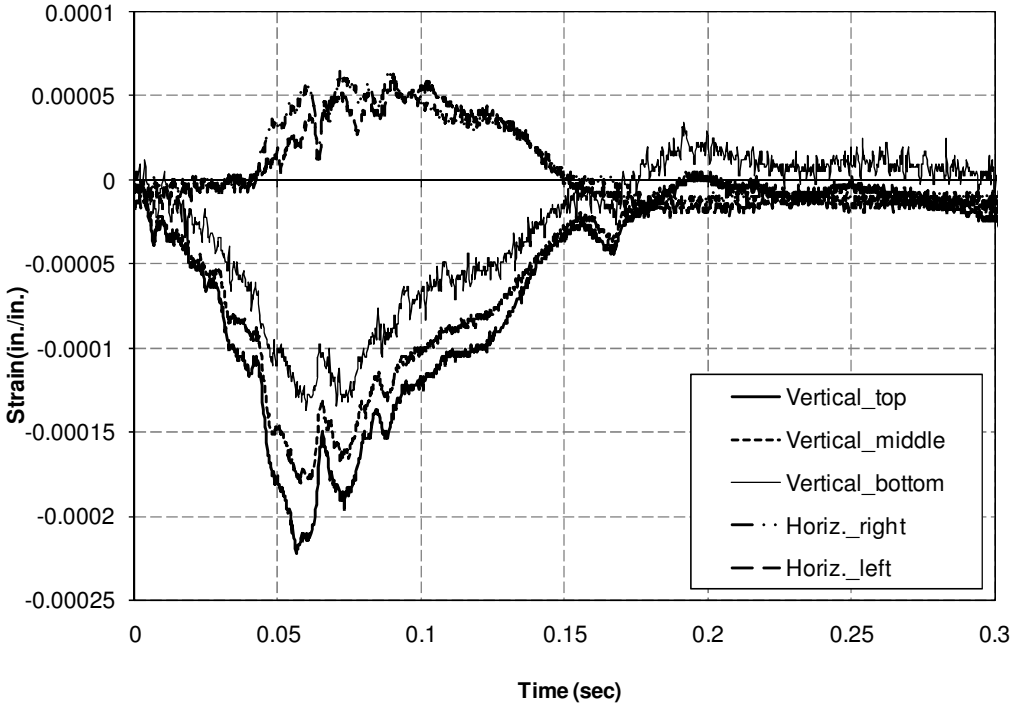

Figure 5.86 Strain on the panel (Test 3)

5) Component Damage

Damage to the vertical wall barrier-coping section resulting from the bogie impact is shown in Figure 5.87. Although difficult to discern from the photos because the crack withs are not large, the vertical barrier failed in a classical yield line pattern by developing a vertical "hinge" line at the point of impact and two diagonal hinge lines radiating from the bottom to the top of the barrier on either side of impact. As shown in Figure 5.87(b), three cracks were observed along the diagonal hinge lines. The length between the two inside most cracks on either side of the impact point was 1.98 m (6.51 ft). The lengths between the middle and outer sets of cracks were 2.19 m (7.17 ft) and 2.52 m (8.28 ft), respectively.

Cracking in the soil was observed approximately 1.22 m (48 in.) from the front face of the barrier, which corresponds with the location of the end of the moment slab. The cracking, shown in Figure 5.87(c), extended 18.29 m (60 ft) along the entire length of both moment slabs. This indicates that the two No.9 shear dowels placed between the moment slabs were able to transfer substantial load to the adjacent moment slab. Damage to the back of the vertical barrier is shown in Figure 5.87(e). Damage to the panel beneath the point of impact on the barrier is shown in Figure 5.88. As shown in this figure, the surface of the panel showed little distress.

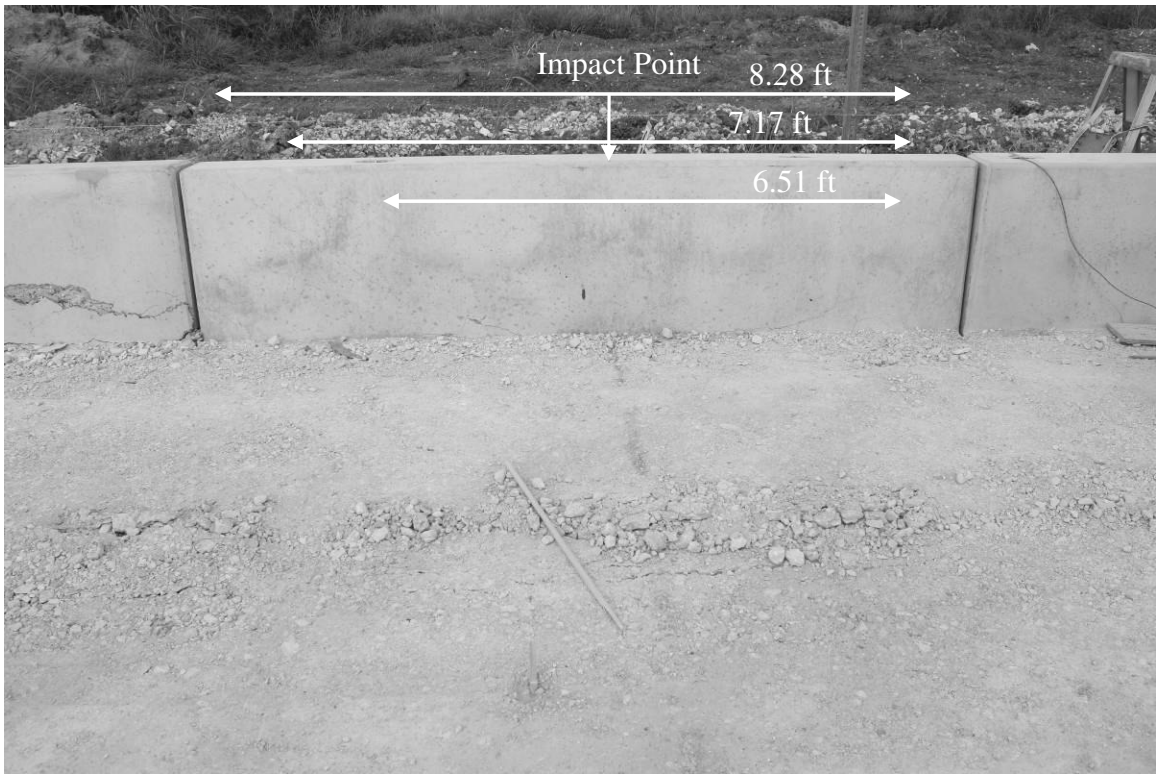

(a) Front view of the barrier

Figure 5.87 Cracks on the barrier after test (Test 3)

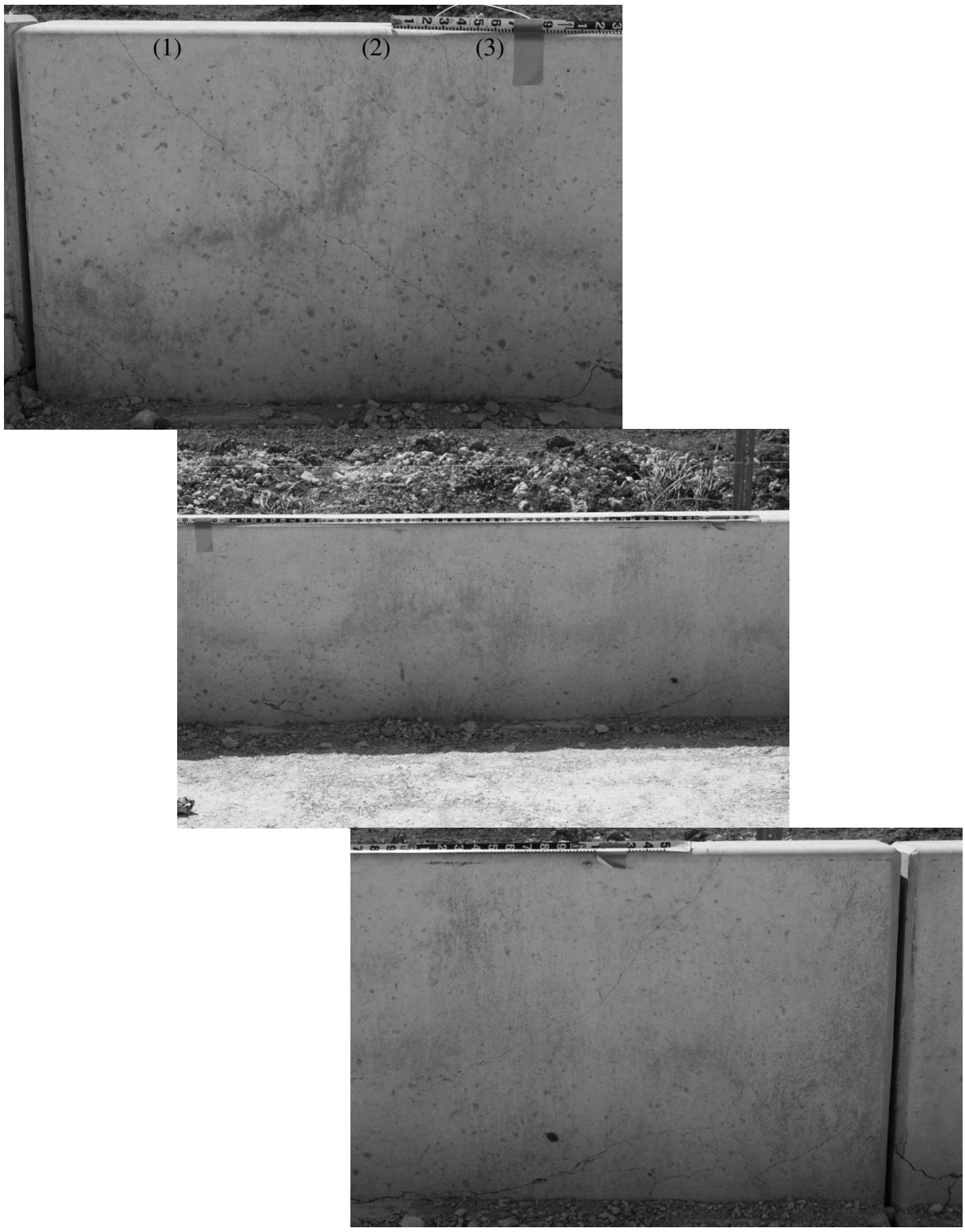

(b) Close-up front view of the barrier

Figure 5.87 Cracks on the barrier after test (Test 3) (Continued)

(c) Side view of the barrier

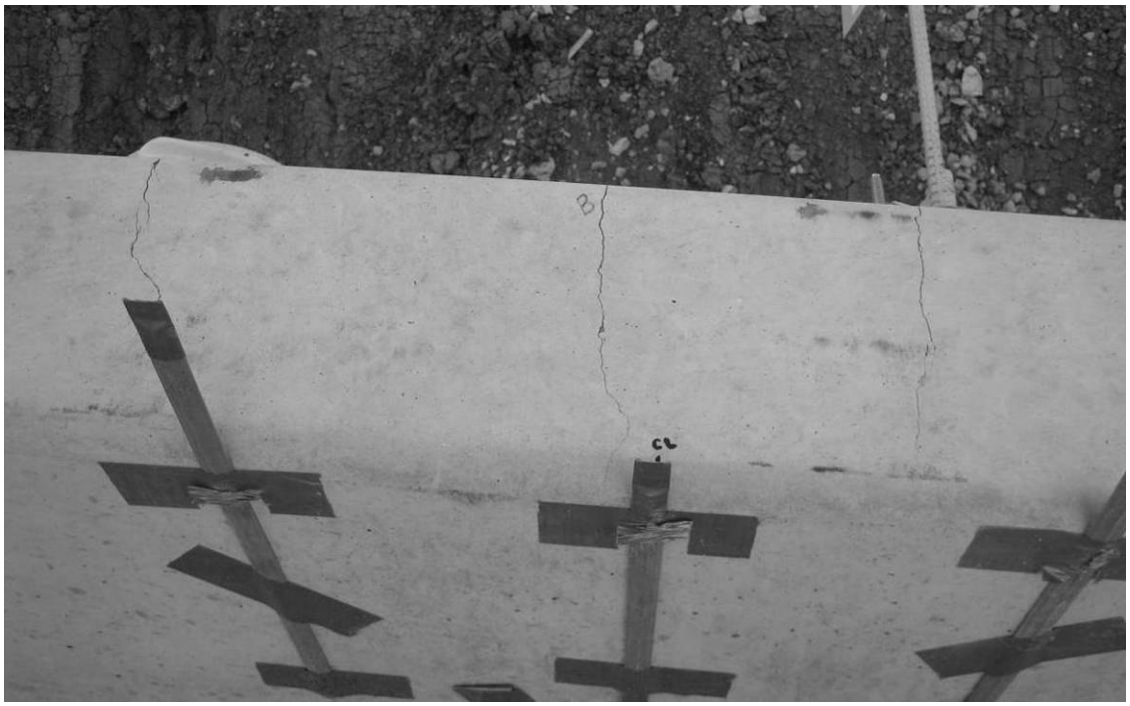

(d) Top view of the barrier

Figure 5.87 Cracks on the barrier after test (Test 3) (Continued)

(e) Back view of the barrier

Figure 5.87 Cracks on the barrier after test (Test 3) (Continued)

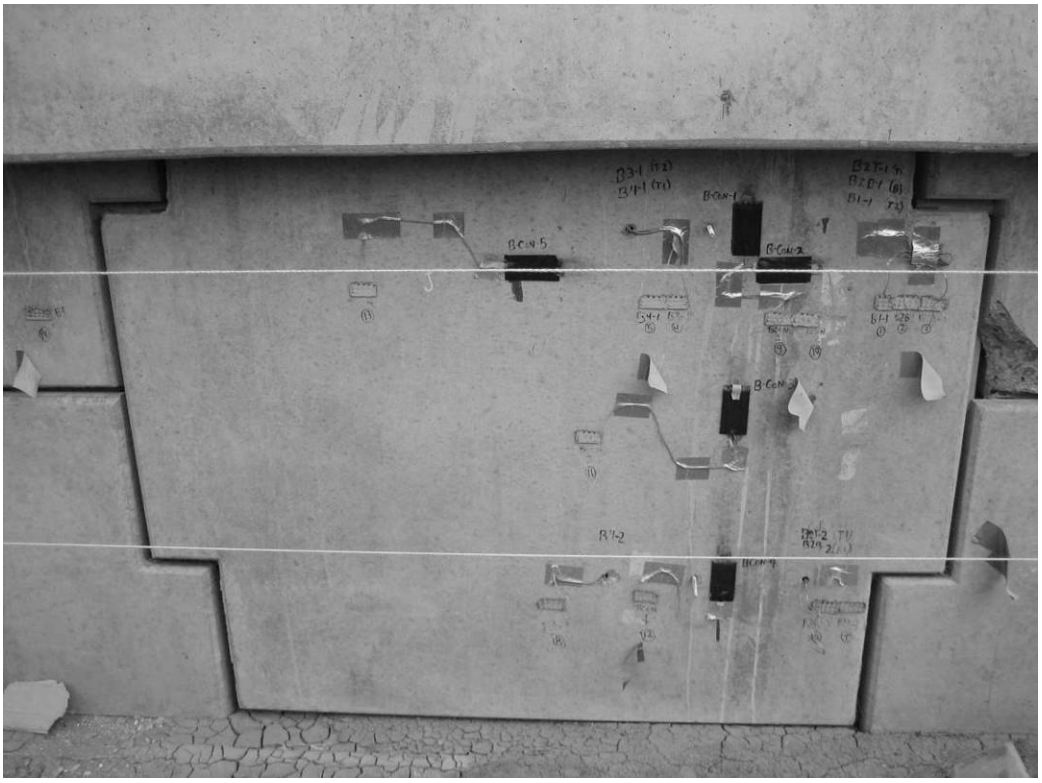

Figure 5.88 Panel surface after test (Test 3)

5.3.5 Bogie Test 4: Vertical Concrete Barrier with 16 Ft Strips

Test 4 was similar to Test 3 with the exception that the vertical barrier was installed over a segment of wall having 4.88 m (16 ft) long reinforcement strips. As in Test 3, the vertical barrier was connected to the end of a 9.14 m (30 ft) moment slab doweled to the adjacent moment slab using two No.9 bars. The 2,268 kg (5,000 lb) bogie vehicle as shown in Figure 5.89 impacted the center of the vertical barrier headon at a speed of approximately 32.5 km/h (20.2 mph), which was the same as reference Test 3. The reference point was along the top edge of the barrier and approximately 4.13 cm (1 5/8 in.) from its centerline to coincide with the location of a steel strip in the wall reinforcement below the barrier.

1) Data from Accelerometers

The raw acceleration data for the bogie, barrier, and moment slab are shown in Figure 5.90. Data obtained from the bogie-mounted accelerometer were analyzed and the results are presented in Figure 5.91. As shown in Figure 5.91(b), the maximum 50-msec average acceleration was -12.69 g. Based on this acceleration and the mass of the bogie, the maximum 50-msec average impact force was calculated to be 286.55 kN (64.42 kips) (see Figure 5.91(a)). The velocity-time and horizontal displacement-time histories of the bogie are shown in Figure 5.91(c) and Figure 5.91(d), respectively. These time histories were calculated through integration of the acceleration data.

The maximum 50-msec average acceleration of the barrier, as measured by the accelerometer at the top of the barrier, was 13.04g in the direction of impact (see Figure 5.92(a)). The velocity-time history of the barrier, as calculated by integration of the raw acceleration data, is shown in Figure 5.92(b). The displacement-time history obtained from integration of the velocity history is shown in Figure 5.92(c).

The 50-msec average acceleration for the moment slab is shown in Figure 5.93(a). The velocity-time history of the moment slab is shown in Figure 5.93(b). The velocity-time history was calculated by integration of the raw acceleration data.

Targets affixed to the displacement bars attached to the top and bottom of the barrier-coping section (see Figure 5.61 and Figure 5.94) were used as reference points to determine angular and translational displacement of the barrier from analysis of high-speed video. From the film analysis, the maximum dynamic displacement of the barrier was 15.3 cm (6.02 in.) at the top of the barrier and 1.75 cm (0.69 in.) at the bottom of the coping. The permanent displacement of the barrier was 7.62 cm (3 in.) at the top of the barrier and 0.56 cm (0.22 in.) at the bottom of the coping.

Two additional targets affixed to the displacement bars attached to the wall panel at locations corresponding to the upper and lower layers of wall reinforcement were used to determine angular and translational displacement of the wall panel from analysis of high-speed video. From the film analysis, the maximum dynamic displacement of the panel was 0.76 cm (0.3 in.) at the upper reinforcement layer of the panel and 0.18 cm (0.07 in.) at the bottom reinforcement layer. The permanent displacement of the panel was 0.18 cm (0.07 in.). There was little discernable movement of the panel at the bottom reinforcement layer.

The corresponding displacement-time histories for the barrier-coping section and wall panel obtained from film analysis are shown in Figure 5.95. Figure 5.96 shows the impact force-displacement curve for the top of the barrier.

Figure 5.89 Test 4: Vertical wall barrier with 16 ft long strips

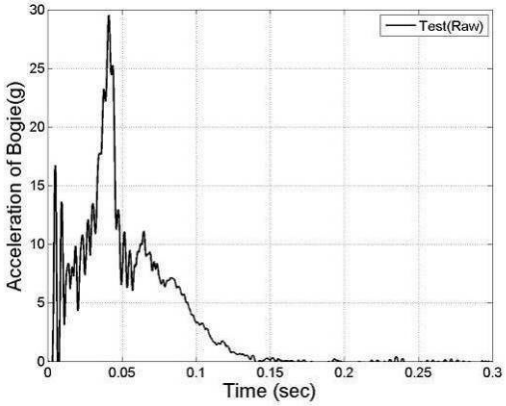

(a) Bogie

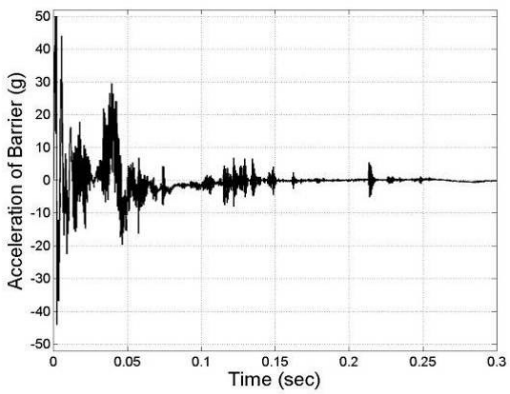

(b) Barrier

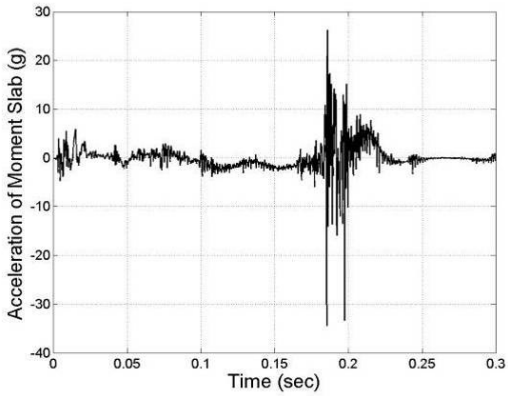

(c) Moment slab

Figure 5.90 Raw acceleration of bogie, barrier, and moment slab (Test 4)

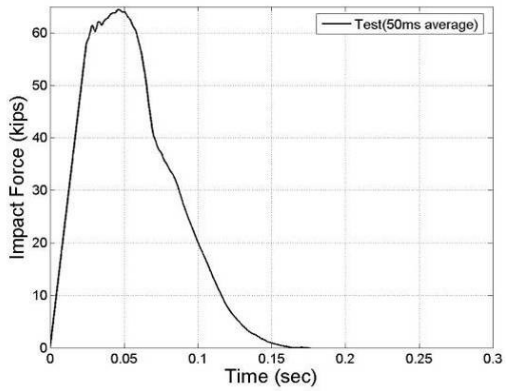

(a) Impact Force

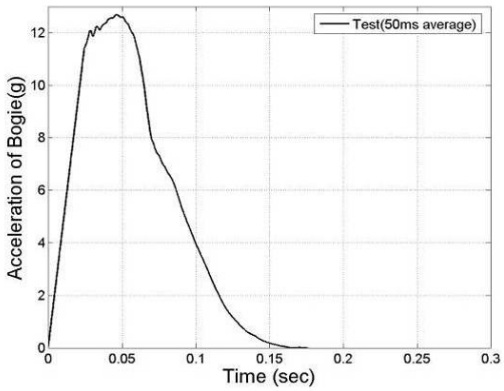

(b) Acceleration

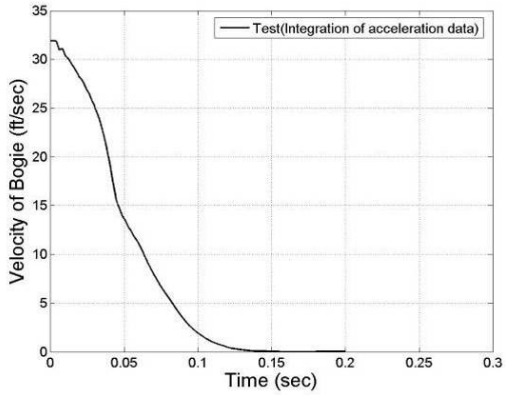

(c) Velocity

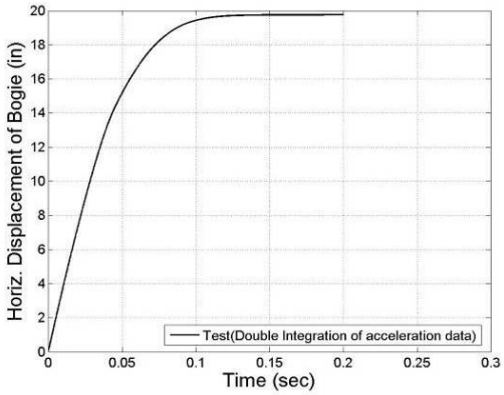

(d) Displacement

Figure 5.91 Force, acceleration, velocity, and displacement of bogie (Test 4)

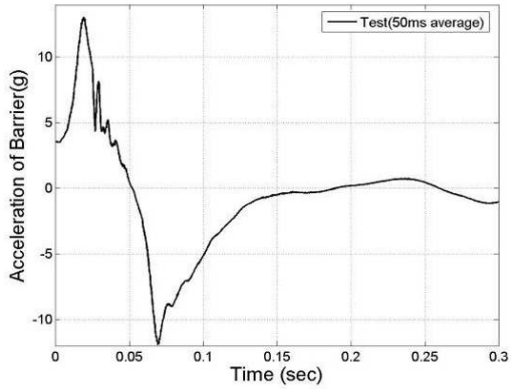

(a) Acceleration

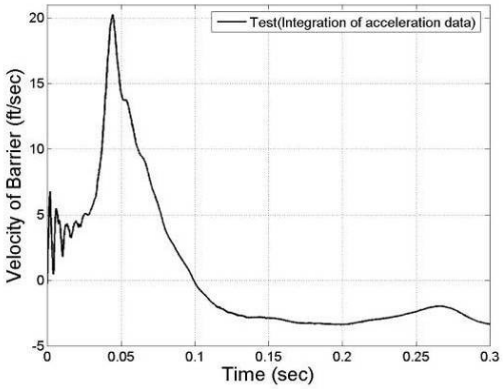

(b) Velocity

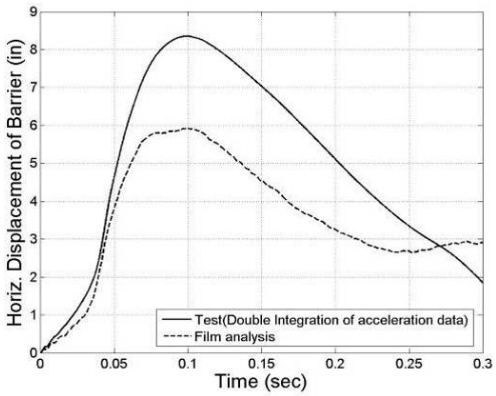

(d) Displacement

Figure 5.92 Acceleration, velocity, and displacement of barrier (Test 4)

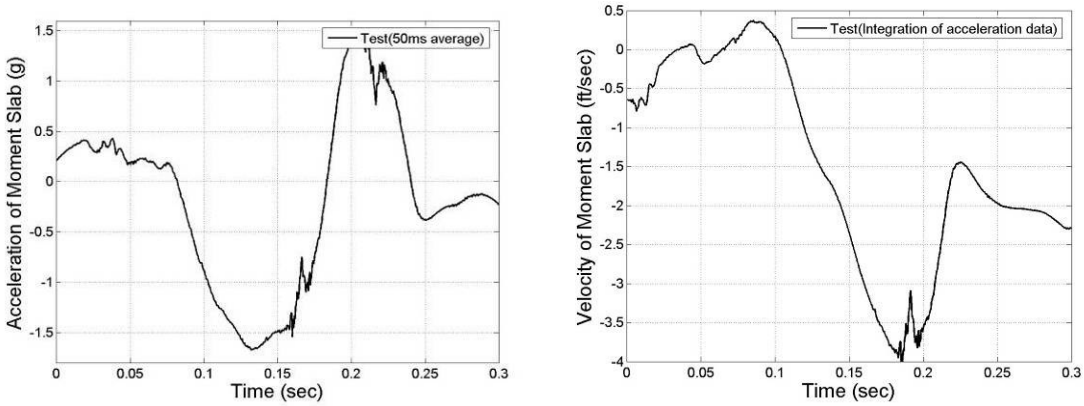

(a) Acceleration **(b) Velocity**

Figure 5.93 Acceleration and velocity of moment slab (Test 4)

Figure 5.94 Location of displacement bars affixed on the barrier and panels (Test 4)

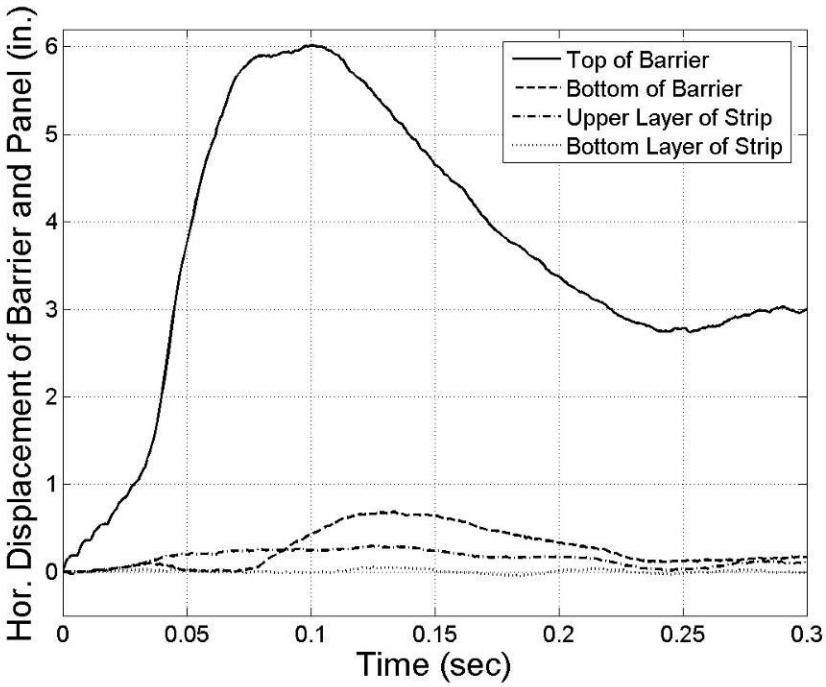

Figure 5.95 Horizontal displacement of barrier and panel measured from film (Test 4)

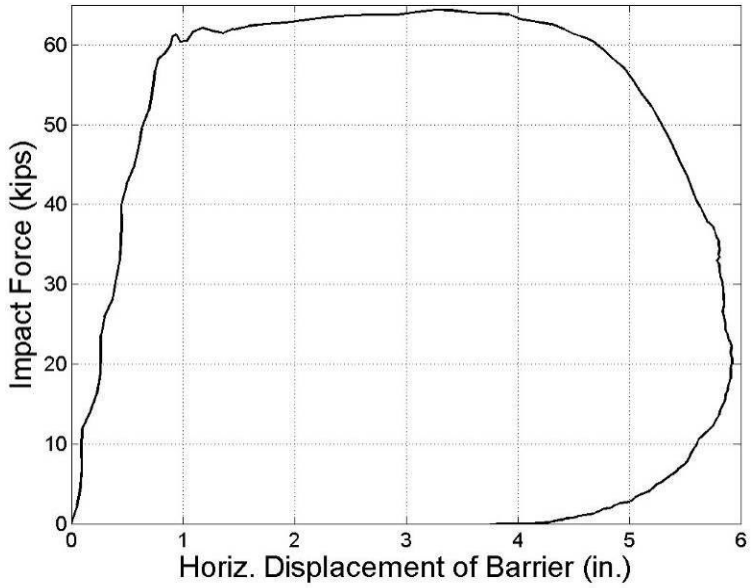

Figure 5.96 Force-displacement of the top of the barrier (Test 4)

2) Load in the Reinforcement Strips

A total of 8 strain gages were used to instrument the strips to capture the tensile forces transmitted into the reinforcement during the dynamic bogie vehicle impact. To enable comparison of loads on the strips, the locations of strain gages were assigned a numeric designator as shown in Figure 5.97. Note that two strain gages were used at locations 2-1 and 2-2 adjacent to the wall panel at the point of impact to provide some measurement redundancy at the location expected to experience maximum tensile loading. One gage was placed on top of the reinforcement and one gage was placed on the bottom of the reinforcement. Measurements obtained from the strain gages during testing indicated that the reinforcement experienced some bending in addition to tensile loading. The strain gages on the top and bottom of the reinforcement enabled the bending to be canceled out and the average tensile force in the reinforcement to be calculated.

Raw data obtained from the strain gages on the bar mats were analyzed and the results are presented in Figure 5.98. A contact switch placed on the top edge of the level-up concrete on top of the wall panels inside the recess of the coping activated twice from 0.0655 sec to 0.1183 sec and from 0.173 sec to 0.1802 sec, which indicates that the coping was in contact with the wall panel and/or leveling concrete during these times. The 50-msec average of the raw data was analyzed to obtain design loads for the strips, and the results are presented in Figure 5.99. As shown in this figure, there was some increase in force in the strips observed after the time of maximum barrier impact load, but the increase was not as significant as that seen in Test 1. The maximum 50-msec average design strip loads corresponding to a design impact load of 240 kN (54 kips) were estimated as follows:

$$\text{Estimated Strip Load} = \frac{54}{64.42} \times \text{Maximum Strip Load} \qquad (5\text{-}12)$$

where 286.55 kN (64.42 kips) is the maximum 50-msec average impact load measured for the vertical wall barrier over 4.88 m (16 ft) strips.

Table 5.13 presents a summary of the forces in the steel strips obtained from the fourth bogie impact test including the maximum force, maximum 50-msec average force, and an estimate of the maximum 50-msec average force for a 240 kN (54 kips) design impact.

3) Permanent Deflection of Barrier and Panels

The string lines located 1.22 m (4 ft) from the face of wall panels were used to measure the permanent deflection of barriers and panels after bogie vehicle impact at different elevations. After bogie vehicle impact of the vertical barrier, the permanent deflection was measured to be 67 mm (2.64 in.) and 68 mm (2.68 in.) at the top corners of the barrier and 2 mm (0.08 ins) and 8 mm (0.31 in.) at the bottom corners of the coping as shown in Figure 5.100. Note that the reference impact point was offset 4.13 cm (1 5/8 in.) left of the centerline of the barrier-coping section as shown in Figure 5.100 to align with the steel strip reinforcement.

The permanent defection of the wall panels was measured as shown in Figure 5.100. The maximum permanent movement measured in the wall panels beneath the impact barrier section was only about 4 mm (0.16 in.), which is considerably less than the movement observed in the previous test of the vertical barrier with the 8 ft strips.

4) Panel Analysis

The wall reinforcement was instrumented with a total of 5 strain gages to capture the resistance of the panel during the bogie impacts as shown in Figure 5.101. The maximum compressive strain of 0.0024 occurred at 0.11 sec (see Figure 5.102) at the location of uppermost layer of strips. Note that positive values for the vertical direction strain gages indicate movement toward the traffic side of the barrier. As shown in Figure 5.102, the strain dropped suddenly after 0.05 sec. The strains at the horizontal centerline of the panel and at the second layer of strips were 0.00014 and 0.00008, respectively.

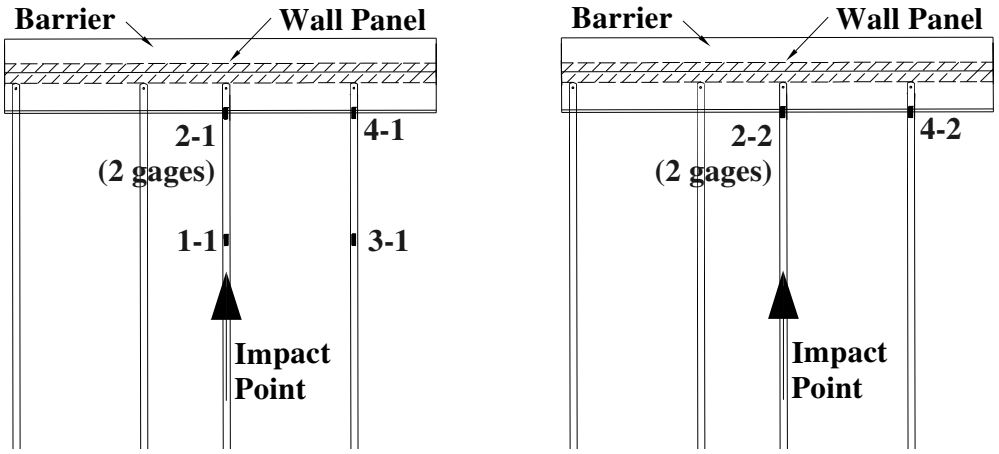

(a) Upper layer **(b) Bottom layer**

Figure 5.97 Location of strain gages and labeling (Test 4)

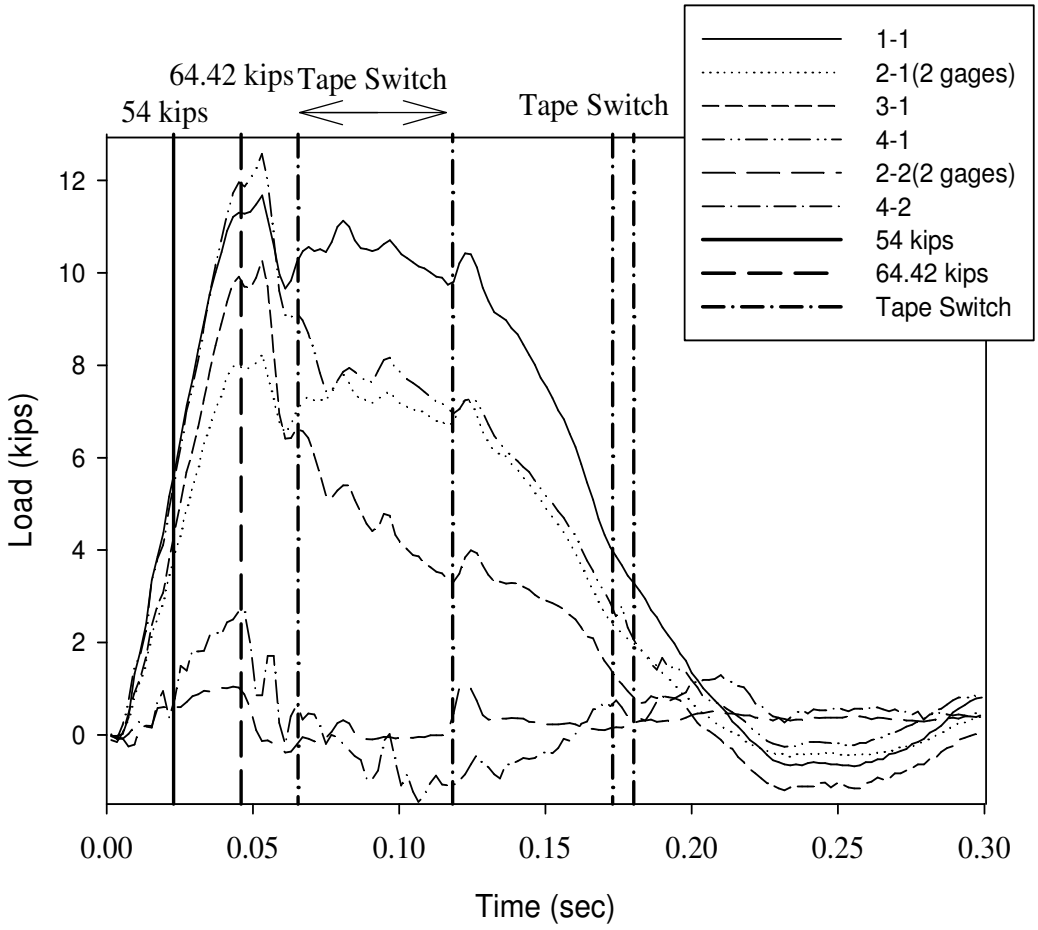

Figure 5.98 Strip load of raw data on the strips (Test 4)

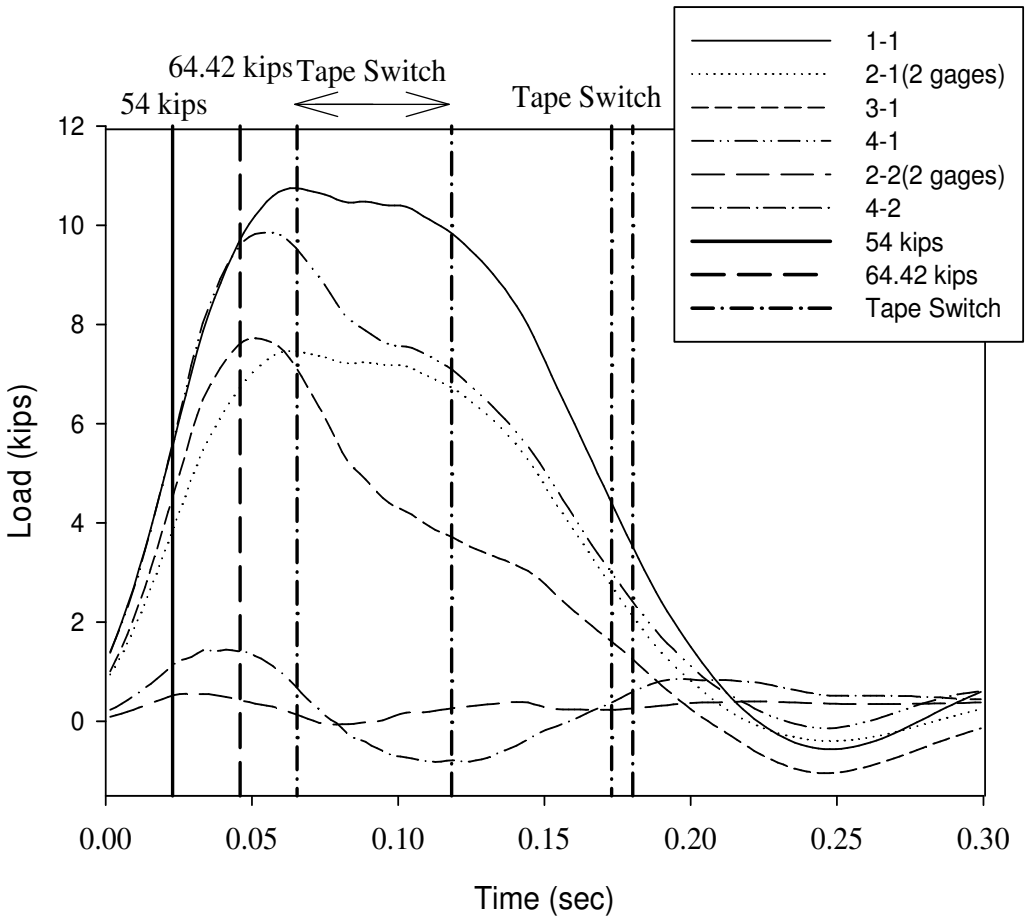

Figure 5.99 Strip load of 50 msec average on the strips (Test 4)

Table 5.13 Load on the Wall Reinforcement (Test 4)

	Upper layer (kips)				Bottom layer (kips)	
	Impact point, Behind (1-1)	Impact point, Front (2-1)	Next to impact point, Behind (3-1)	Next to impact point, Front (4-1)	Impact point, Front (2-2)	Next to impact point, Front (4-2)
Maximum Load from Raw data (t = 0.054 sec)	11.59	8.08	10.25	12.51	-0.16	1.25
Maximum 50 msec avg. Load (t = 0.0645 sec)	10.75	7.46* (7.53-T 7.4-B)	7.2	9.58	0.15* (-2.44-T 2.74_B)	0.73
Estimated Design Load	7.91	5.49	5.3	7.05	0.11	0.54

* Average of top and bottom loads

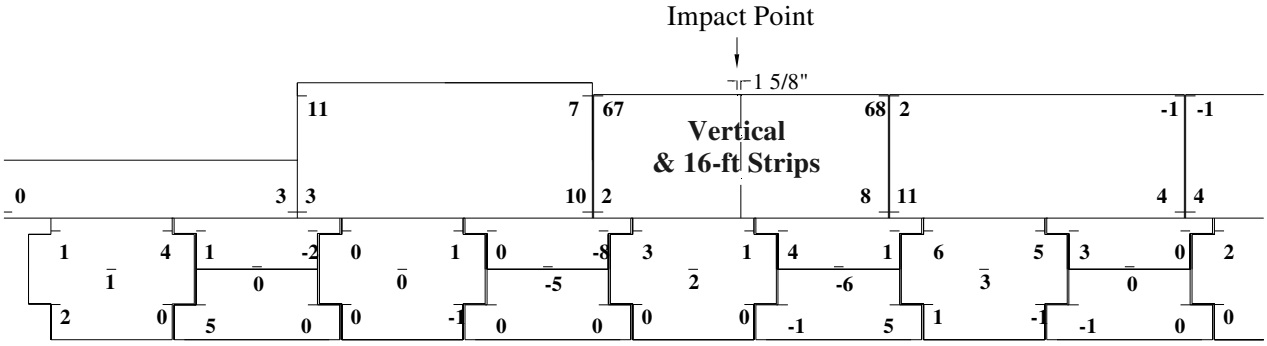

Figure 5.100 Permanent deflection of barrier and panels (Test 4, units: mm)

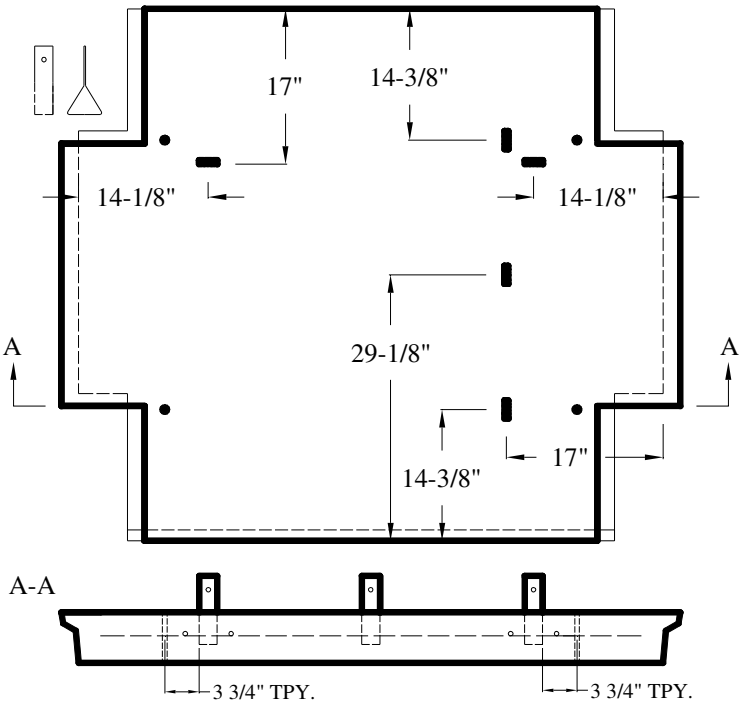

Figure 5.101 Location of concrete statin gages (Test 4)

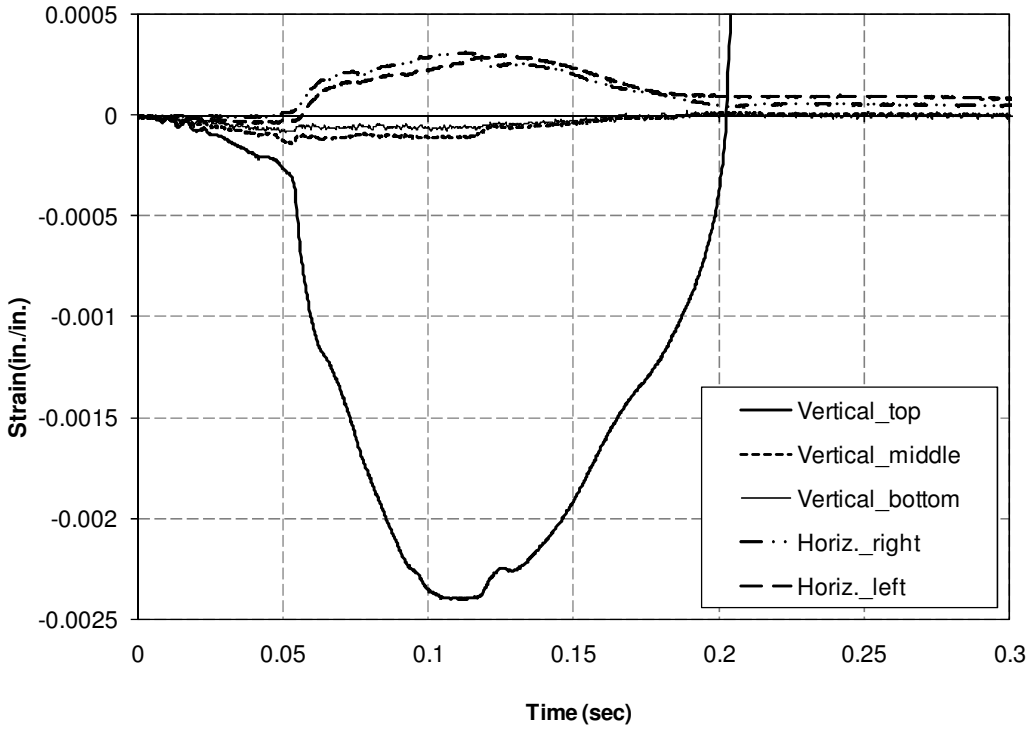

Figure 5.102 Strain on the panel (Test 4)

5) Component Damage

Damage to the vertical wall barrier-coping section resulting from the bogie impact is shown in Figure 5.103. Although difficult to discern from the photos because some of the crack widths are not large, the vertical barrier has characteristics of a classical yield line pattern by developing a vertical "hinge" line at the point of impact and two diagonal hinge lines radiating from the bottom to the top of the barrier on either side of impact. As shown in Figure 5.103(b), several cracks were observed along the diagonal hinge lines. The length between the two inside most cracks on either side of the impact point was 1.76 m (5.77 ft). There were also signs of a flexural type failure mode with the entire length of the barrier cracked near the groundline at the connection between the barrier and coping and also 50.8 cm (20 in.) above ground.

Cracking in the soil was observed approximately 1.22 m (48 in.) from the front face of the barrier, which corresponds with the location of the end of the moment slab. The cracking, shown in Figure 5.103(c), extended 18.29 m (60 ft) along the entire length of both moment slabs. This indicates that the two No.9 shear dowels placed between the moment slabs were able to transfer substantial load to the adjacent moment slab. Damage to the back of the vertical barrier is shown in Figure 5.103(e). Damage to the panel beneath the point of impact on the barrier is shown in Figure 5.104. Note that the panel is cracked along its length at an elevation corresponding to the upper layer of reinforcement. It appears the additional resistance provided by the 4.88 m (16 ft) strips enabled more load to be transferred to the wall panel.

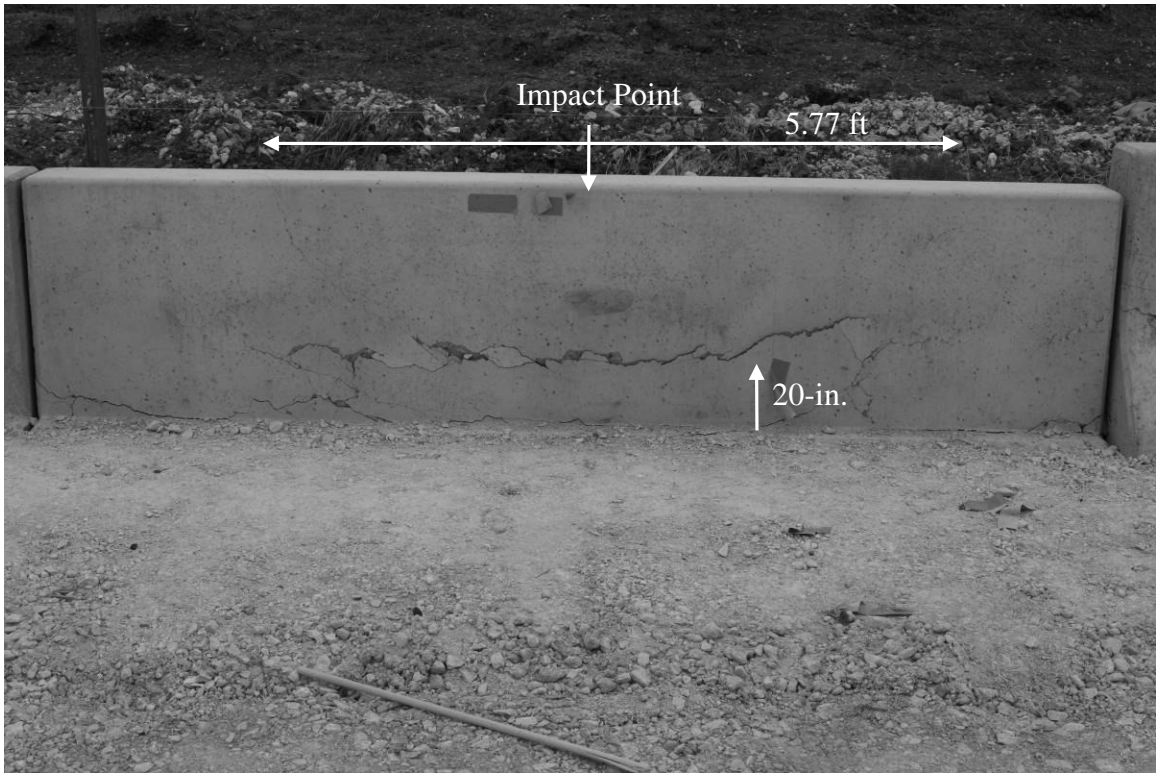

(a) Front view of the barrier

Figure 5.103 Cracks on the barrier after test (Test 4)

(b) Close-up front view of the barrier

Figure 5.103 Cracks on the barrier after test (Test 4) (Continued)

(c) Side view of the barrier

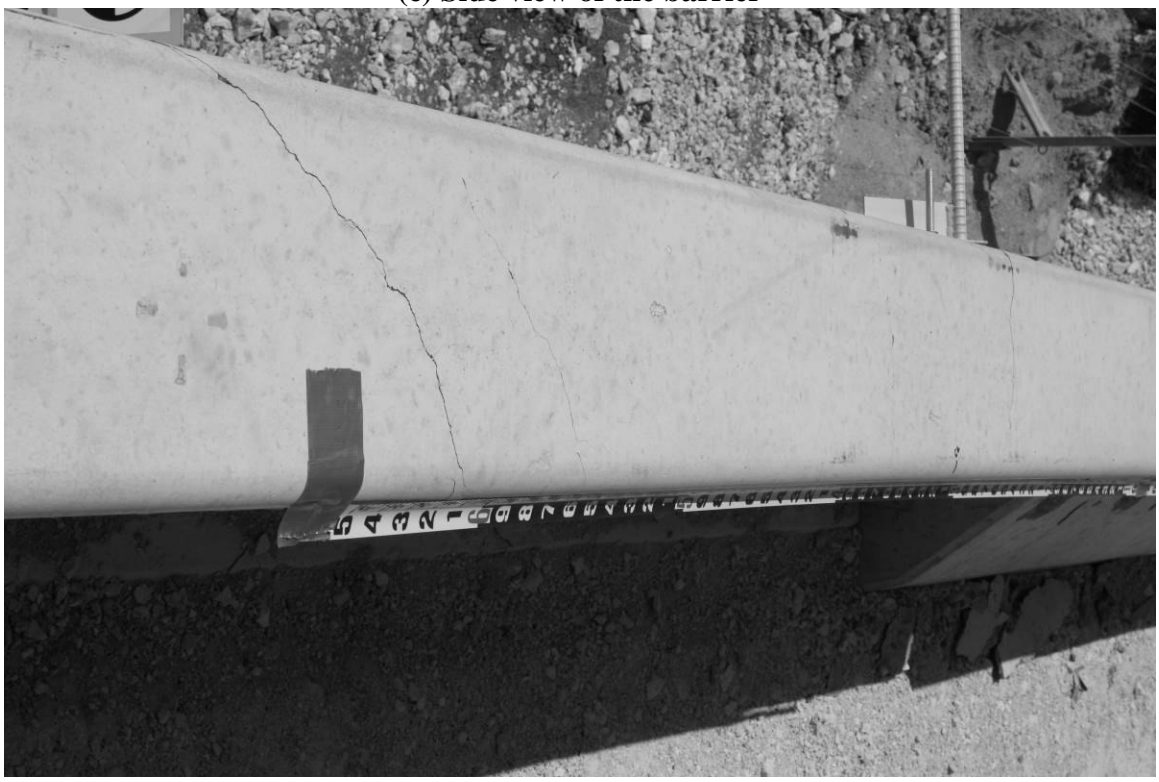

(d) Top view of the barrier

Figure 5.103 Cracks on the barrier after test (Test 4) (Continued)

(e) Back view of the barrier

Figure 5.103 Cracks on the barrier after test (Test 4) (Continued)

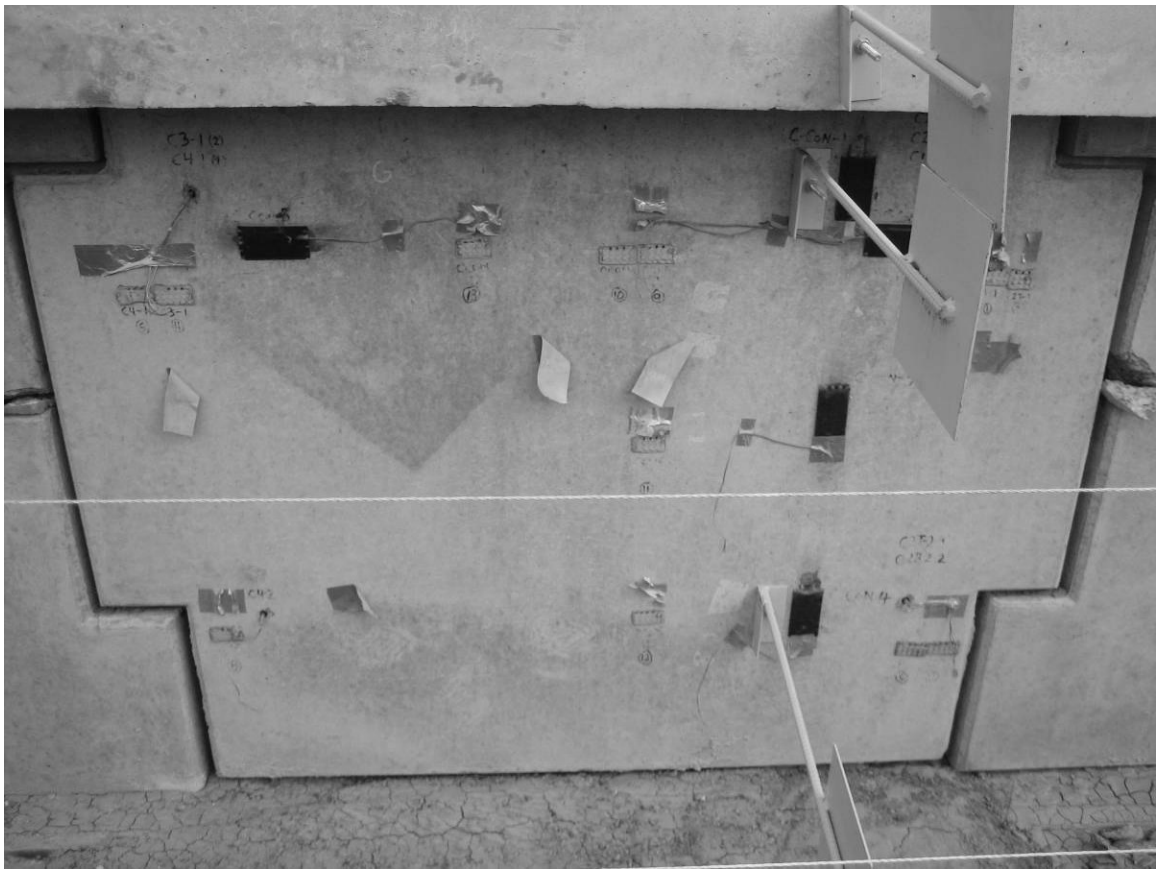

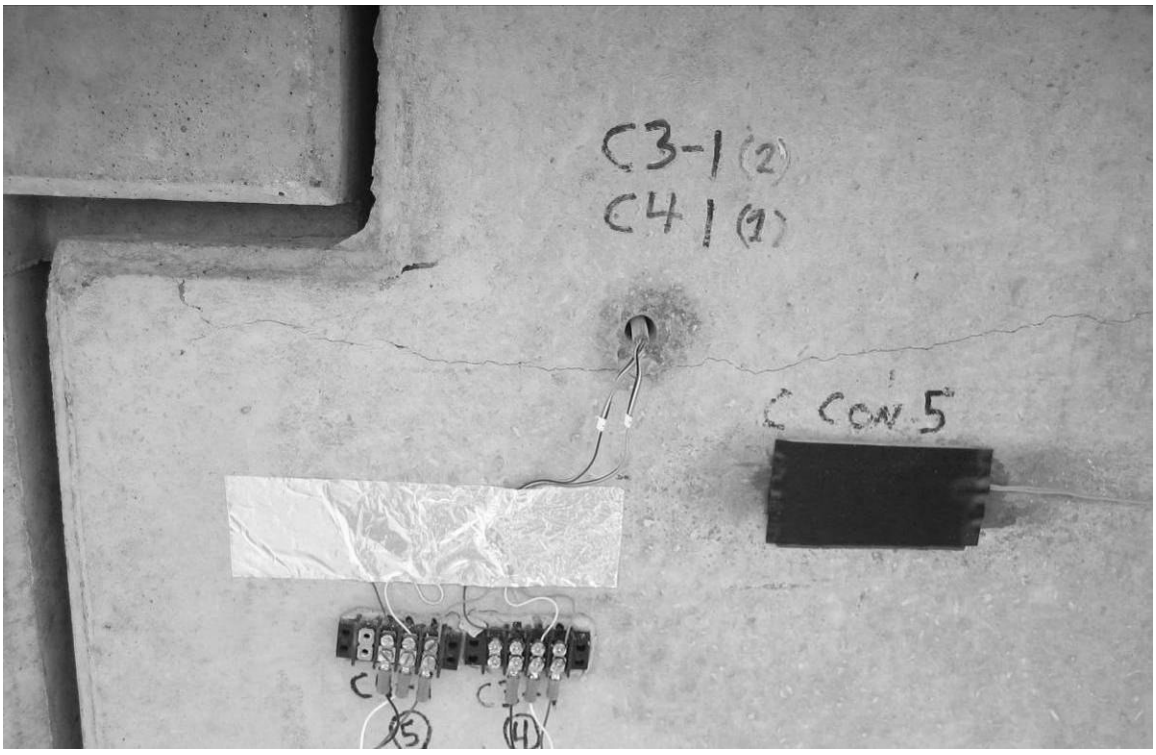

Figure 5.104 Cracks on the panel after test (Test 4)

5.4 Summary of Bogie Tests

Four reference tests were conducted as summarized in **Table 5.14**. The impact speeds of bogie vehicle varied from 32.5 km/h (20.2 mph) to 35.08 km/h (21.8 mph). The barrier types used were an 81.28 cm (32 in.) tall N.J. shape barrier (Test 1) and a 68.58 cm (27 in.) tall vertical wall barrier (Test 2 through Test 4). Wall reinforcement types included 4.88 m (16 ft) steel strips at a density of 4 per panel (Test 1 and 4), 2.43 m (8 ft) bar mat (Test 2), and 2.43 m (8 ft) steel strips at a density of 6 per panel (Test 3).

The maximum 50-msec average impact load on the barriers varied from 286.55 kN (64.42 kips) to 326.5 kN (73.4 kips) and are all higher than the 240 kN (54 kips) dynamic force associated with the design of barriers for AASHTO TL-3 and TL-4 levels.

Table 5.14 also presents the dynamic and permanent deflection at the top and bottom of the barrier and at the upper and lower layer of reinforcement. The maximum dynamic horizontal displacement at the top of the barrier varied from 131 mm (5.17 in.) to 156 mm (6.14 in.). The maximum dynamic horizontal displacement at the bottom of the barrier varied from 18 mm (0.69 in.) to 30 mm (1.16 in.). The maximum dynamic horizontal displacement of the panel at the top layer of reinforcement varied from 8 mm (0.3 in.) to 23 mm (0.92 in.). The maximum dynamic horizontal displacement of the panel at the bottom layer of reinforcement varied from 0 mm to 5 mm (0.19 in.).

The permanent movements of the target locations were obtained in two ways: high speed film analysis and distances from the reference string line stretched in front of the wall. The string line permanent measurements consisted of measuring the distance with a tape measure from the target to the string before and after each test. The permanent horizontal displacement at the top of the barrier varied from 6.3 mm (0.25 in.) to 99 mm (3.9 in.). The permanent horizontal displacement at the bottom of the barrier varied from 8 mm (0.31 in.) to 20 mm (0.79 in.). The permanent horizontal displacement of the panel at the level of the top row of reinforcement varied from 1 mm (0.04 in.) to 16 mm (0.63 in.). The permanent horizontal displacement of the panel at the level of the bottom row of reinforcement varied from 0 mm to 4.1 mm (0.16 in.).

Table 5.14 Bogie Test Results

	Test 1	Test 2	Test 3	Test 4
Barrier Type	New Jersey	Vertical Wall	Vertical Wall	Vertical Wall
Reinforcement	16 ft long Strip (4 per panel)	8 ft long Bar Mat	8 ft long Strip (6 per panel)	16 ft long Strip (4 per panel)
Speed of Bogie Vehicle	21.8 mph	20.3 mph	20.19 mph	20.19 mph
Peak Bogie Acceleration	14.45 g	13 g	13.82g	12.69 g
Impact Force	73.4 kips	66.1 kips	70.17 kips	64.42 kips
Peak Barrier Acceleration	7.36 g	10.71 g	10.16 g	13.04 g
Peak Moment Slab Acceleration	1.84 g	-	1 g	-
Displacement Top of Barrier (in.)	6.14(dynamic) 3.0(permanent)	6.04(dynamic) 4.0 (permanent)	5.17 (dynamic) 2.5 (permanent)	6.02 (dynamic) 3.0 (permanent)
Displacement Bottom of Coping (in.)	1.12 (dynamic) 0.55 (permanent)	0.93(dynamic) 0.5 (permanent)	1.16 (dynamic) 0.6 (permanent)	0.69 (dynamic) 0.22 (permanent)
Displacement of Panel (in.) (upper layer)	0.63 (dynamic) 0.24 (permanent)	0.37(dynamic) 0.2 (permanent)	0.92 (dynamic) 0.55 (permanent)	0.3 (dynamic) 0.07 (permanent)
Displacement of Panel (in.) (bottom layer)	No movement	0.1 (dynamic) 0.02 (permanent)	0.19 (dynamic) 0.18 (permanent)	0.07 (dynamic) 0.0 (permanent)
Max, 50 msec Avg. Loads In Strips At Top Layer	7.19 kips* (7.95 kips-T, 6.43 kips-B) **	1.54 kips* (1.44 kips-T, 1.63 kips-B) **	2.13 kips* (-0.3 kips-T, 4.56 kips-B) **	7.46 kips* (7.53 kips-T, 7.4 kips-B) **
Estimated Design Load At Top Layer	5.29 kips	1.13 kips	1.57 kips	5.49 kips
Max, 50 msec Avg. Loads In Strips At Bottom Layer	-1.2 kips* (-0.48 kips-T, -1.92 kips-B) **	0.08 kips* (-0.16 kips-T, 0.31 kips-B) **	1.19 kips* (0.98 kips-T, 1.4 kips-B) **	0.15 kips* (-2.44 kips-T, 2.74 kips-B) **
Estimated Design Load At Bottom Layer	-0.88 kips	0.06 kips	0.88 kips	0.11 kips

** average of top and bottom loads.*

*** T means top and B means bottom of the strip.*

Even though the wall systems were subjected to loads higher than design conditions, all movements were considered acceptable from a performance point of view. The wall system comprised of the 2.44 m (8 ft) strip reinforcement (Test 3) had the highest panel movements, while the lowest movements were recorded for the configuration that incorporated 4.88 m (16 ft) strips and the vertical wall barrier (Test 4). However, the Test 4 configuration also had the most extensive panel damage. In this test, the top panel exhibited a horizontal flexure crack along a line corresponding to the location of the top layer of reinforcement.

5.5 Comparison of Test and Simulation

A comparison between the results of bogie test 1 (N.J. barrier with 4.88 m (16 ft) long strip) and the numerical simulations was performed to determine if further calibration of the numerical model was needed. The calibrated model was used in the subseqent study of the 3.05 m (10 ft) high MSE wall and barrier described in Section 6. To enable comparison of forces and displacements, selected strip locations have been assigned an alphanumeric designator that describes their horizontal position relative to the bogie impact point and the corresponding vertical reinforcement layer (see Figure 5.105).

As shown in Figure 5.106 and Figure 5.107, the damage profile that develops in the simulated barrier is similar to that observed in the test in that it occurs above the toe of the barrier and has a parabolic shape. However, due to the short (3.05 m or 10 ft) length of the precast barrier section that was modeled, much of the damage eventually radiates out to the free ends of the section.

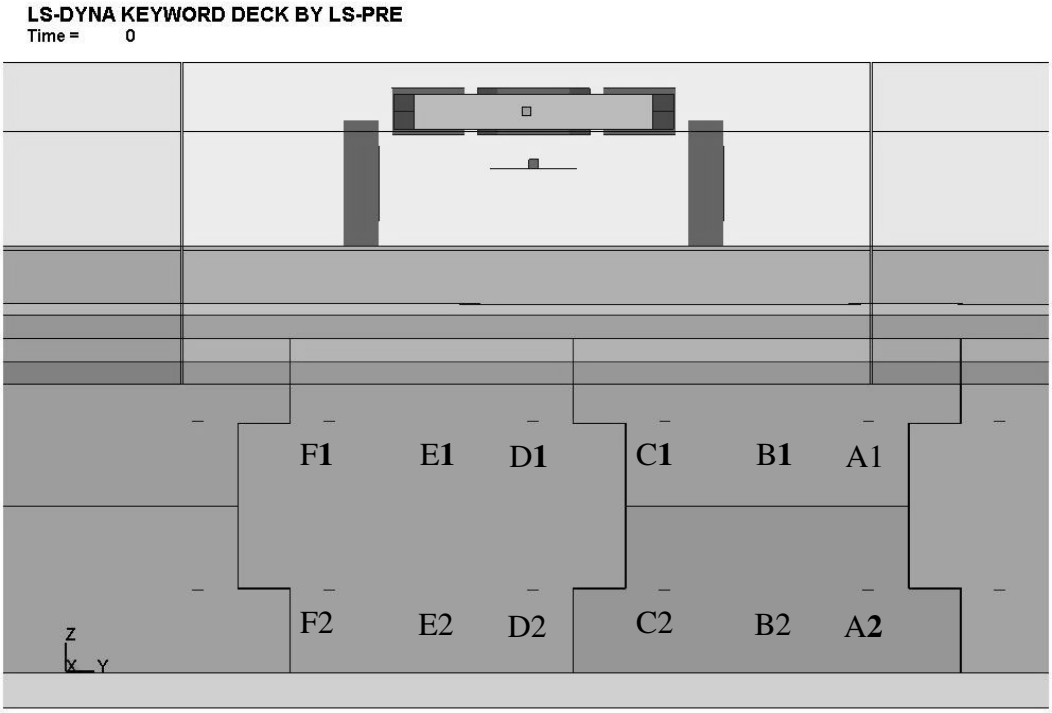

Figure 5.105 Strip location indicator

(a)

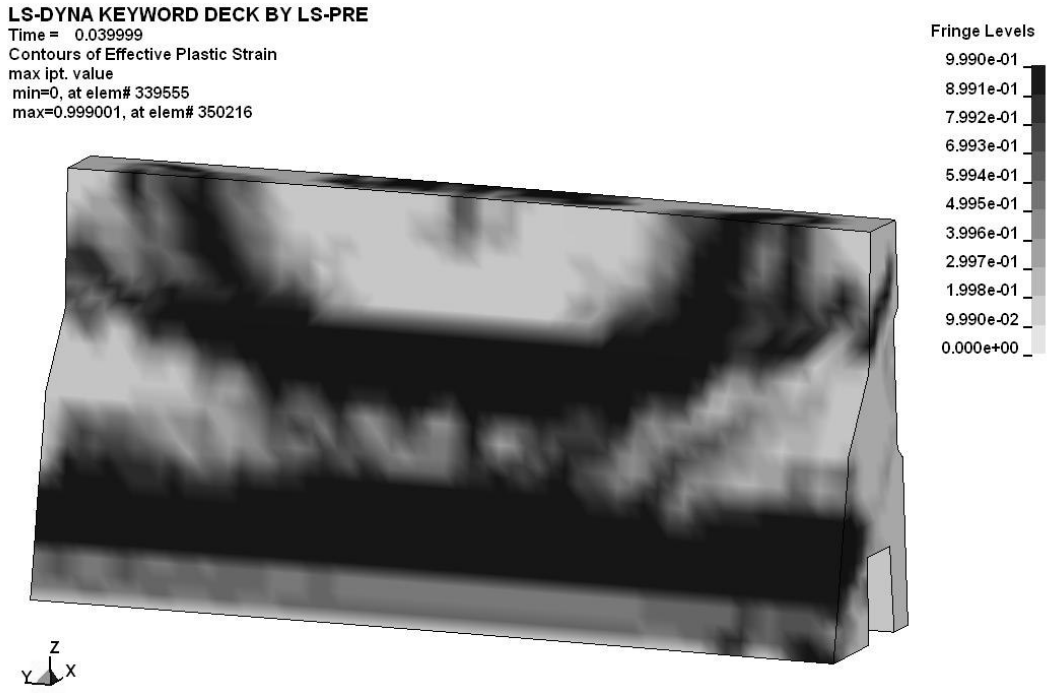

(b)

Figure 5.106 Concrete damage profile on frontside of (a) test 1 and (b) simulation

(a)

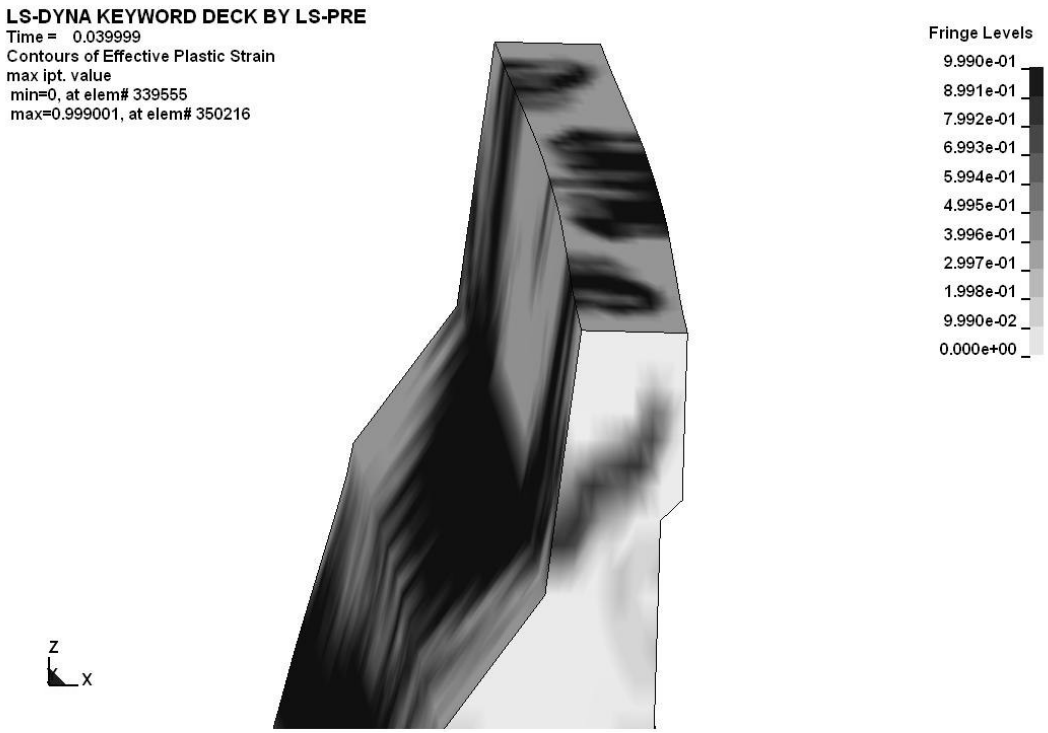

(b)

Figure 5.107 Concrete damage profile on side view of (a) test 1 and (b) simulation

The maximum 50-msec average impact loads on the barrier were 326.5 kN (73.4 kips) from bogie test 1 and 365.1 kN (81.85 kips) from the simulation as shown in Figure 5.108. The comparison of the horizontal displacement of the barrier and the wall panel is shown in Figure 5.109.

The strip loads in the simulation include the static load due to the earth pressure and the dynamic load due to the barrier impact. In order to compare the simulation results to the test, the static load in the strips was calculated based on AASHTO LRFD and subtracted from the simulation result as shown in Table 5.15. The static loads in the upper and lower layers of reinforcement were computed to be 3.69 kN (0.83 kips) and 7.07kN (1.59 kips), respectively. Figure 5.110 shows the comparison of the raw data of load on the strip. In the simulation, the maximum dynamic load in the strip was calculated to be 33.23 kN (7.47 kips) (36.92 kN (8.3 kips) (total load) – 3.69 kN (0.83 kips) (strip load)). The maximum dynamic load measured in the strip in test 1 was 34.7 kN (7.8 kips) at 0.0675 sec. The load was shown drop down at this time in both cases and then rebound. The 50-msec average of the forces in the strip with maximum load is shown in Figure 5.111. The maximum loads were shown to be 27.58 kN (6.2 kips) at 0.05 sec in the bogie test 1 and 25.22 kN (5.67 kips) (28.91 kN (6.5 kips (total load) – 3.69 kN (0.83 kips) (strip load)) at 0.045 sec in the simulation.

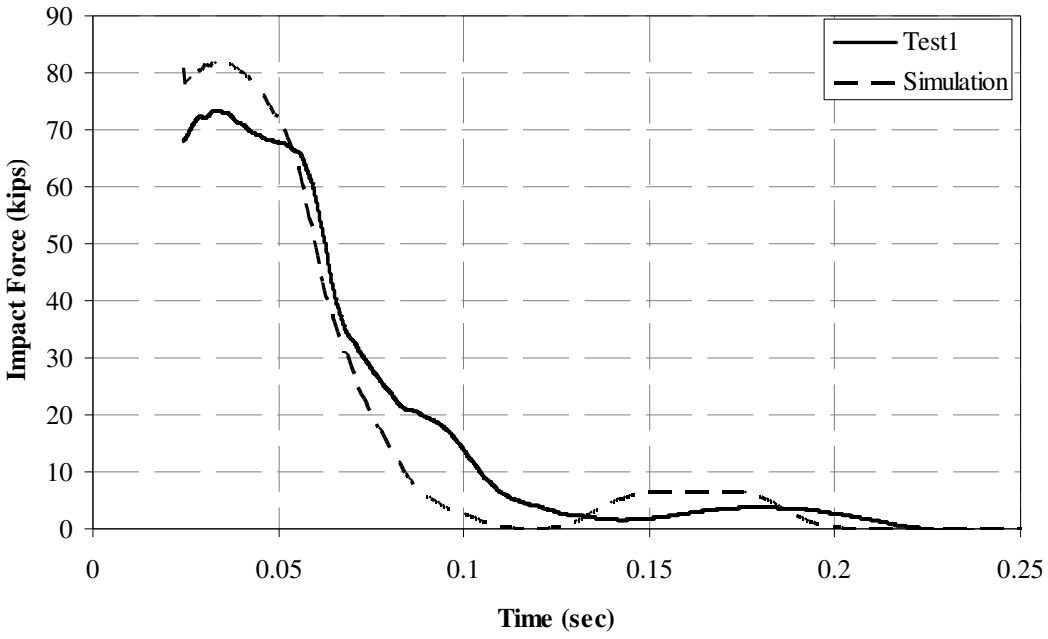

Figure 5.108 Impact load

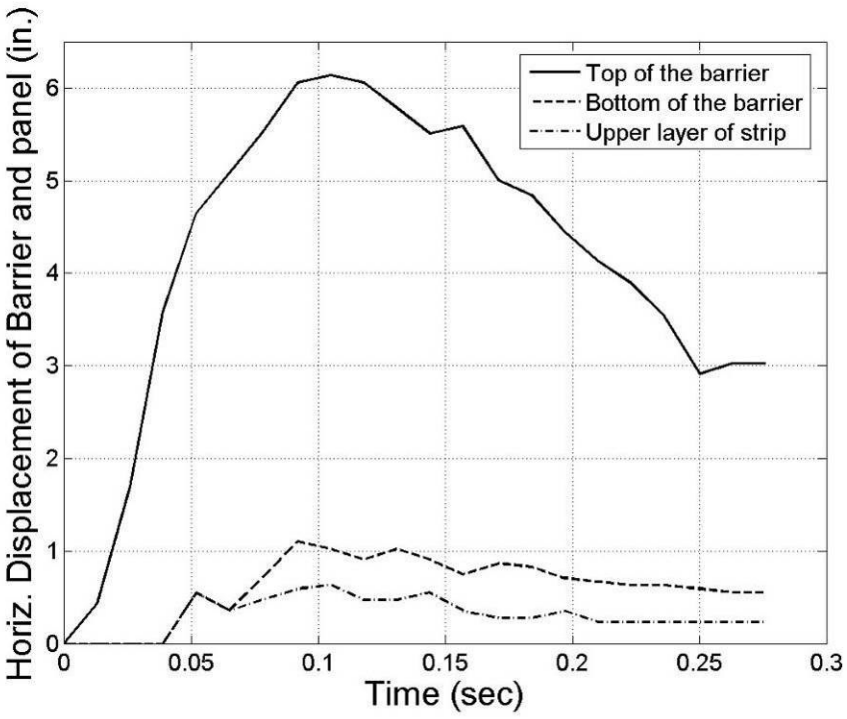

(a)

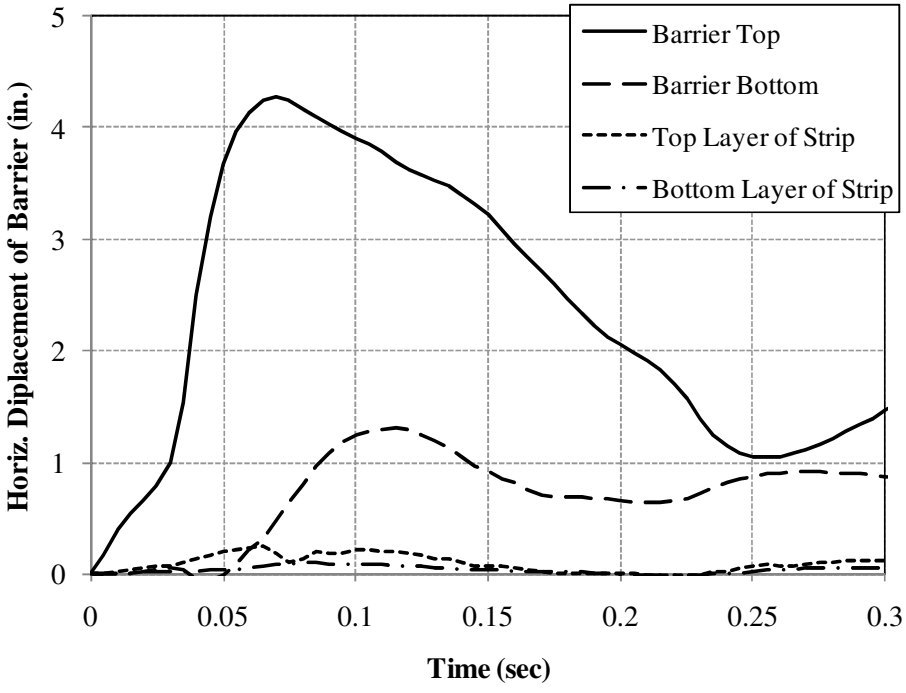

(b)

Figure 5.109 Displacement of barrier and panel of (a) Test 1 and (b) simulation

Table 5.15 Total Loads on the Wall Reinforcement

	Static Load By AASHTO LRFD (kips)	Dynamic Load By measured (kips)	Total Load By measured (kips)	Total Load by simulation (kips)
Top Layer	0.83	7.19 (raw) 5.29 (50 msec avg.)	8.02 (raw) 6.12 (50 msec avg.)	8.3 (raw) 5.22 (50 msec avg.)
Second Layer	1.59	-1.2 (raw) -0.88 (50 msec avg.)	-	8.3 (raw) 3.83 (50 msec avg.)

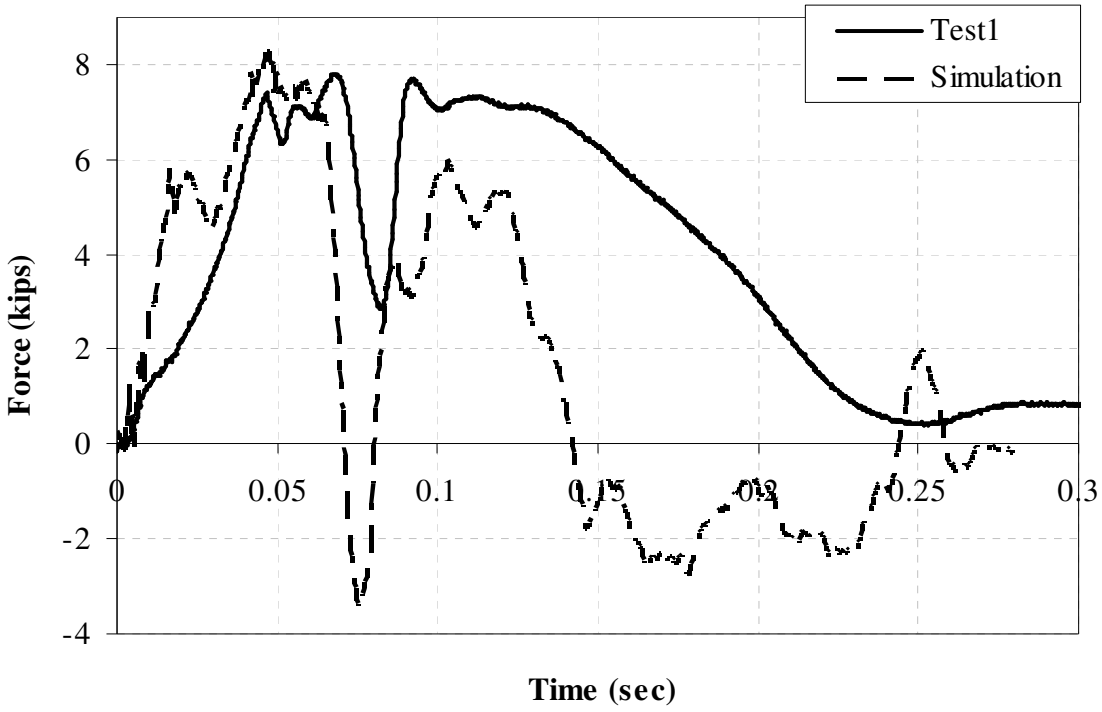

Figure 5.110 Comparison of raw data of load on the strip

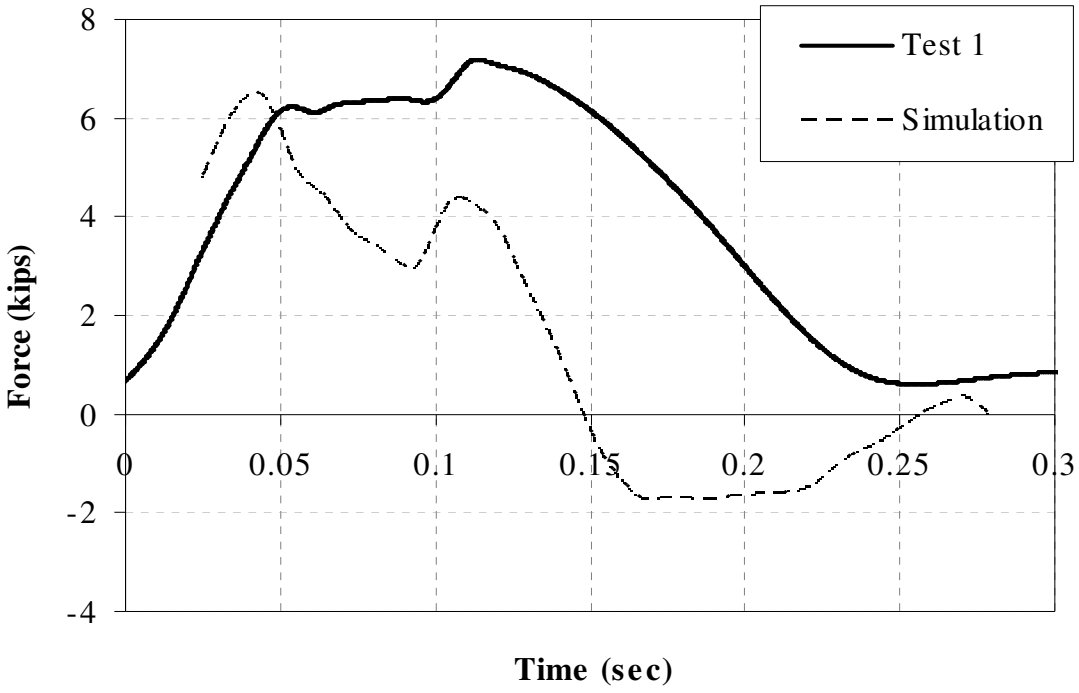

Figure 5.111 Comparison of 50-msec average data of load on the strip

The strain on the wall panel was evaluated as shown in Figure 5.112. The maximum compressive strain in the simulation wall panel was 0.0021 at 0.045 sec. The simulation reasonably captured the rate of strain increase and maximum strain in the panel, but did not capture a delay in the response of the panel that occurred during the first 0.05 sec of the tests with 4.88 m (16 ft) long reinforcement strips (test 1 and 4).

This bogie impact simulations and tests were used to support the development of design guidelines and predict the performance of the barrier-moment slab system and MSE wall in the full-scale crash test. These efforts are described in the following sections of the report.

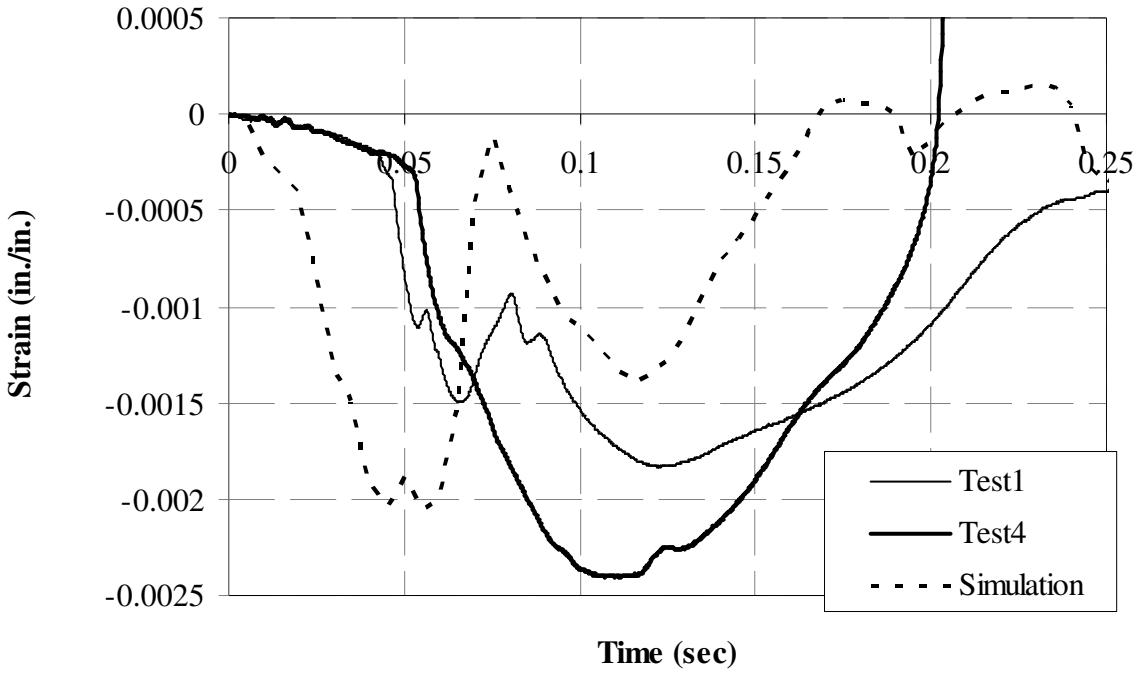

Figure 5.112 Panel strain at D1

6 10 FT HIGH MSE WALL AND BARRIER STUDY

A full-scale crash test was performed to validate the preliminary design guidelines and/or modify them as necessary. The finite element analysis using LS-DYNA was performed to help plan and predict the outcome of the TL-3 crash test.

6.1 10 Ft High MSE Wall and Barrier Study Description

The total length of the installation was about 27.43 m (90 ft). The MSE wall on which the nine 3.05 m (10 ft) long precast barrier-coping sections were placed is approximately 2.74 m (9 ft) tall and comprised of full and half-panel sections that are approximately 1.52 m (5 ft) wide. The bottom wall panels were placed on a 30.48 cm (1 ft) wide × 15.24 cm (6 in.) thick concrete leveling pedestal. The MSE wall had three layers of reinforcement. The steel reinforcement strips were 3.05 m (10 ft) long. The wall panels were recessed inside the coping of the precast barrier-coping sections a distance of 1.9 cm (¾ in.). The moment slabs connecting the 3.05 m (10 ft) long precast barrier-coping sections were cast-in-place in three 9.14 m (30 ft) lengths. The three 1.37 m (4.5 ft) wide × 9.14 m (30 ft) long moment slabs were connected to one another using two No.9 shear dowels across each joint.

The barrier portion of the precast barrier-coping sections consists of a vertical concrete barrier that conforms to the Texas Type T221 traffic barrier. The barrier portion is 0.81 m (2.67 ft) in height (measured from the roadway to the top of barrier), and 30.48 cm (12 in.) wide at the top.

At the direction of the project panel, the draft AASHTO Manual for Assessing Safety Hardware (MASH) was used for the full-scale crash test. MASH test designation 3-11 involves a 2,270 kg (5,000 lb), ½-ton, 4-door pickup truck (denoted 2270P) impacting the barrier at a spped of 100 km/h (62 mph) and an angle of 25 degrees. At the time the finite element analysis was performed, a model of the 2270P design vehicle was not available. Therefore, the impact simulation was performed with a model of a Chevrolet C2500 pickup that conforms to the design test vehicle of NCHRP Report 350.

6.1.1 Calculation of MSE Wall Capacity

AASHTO LFRD *(1)* was used to estimate the forces expected in the reinforcement strips due to both gravity and impact loads for the planned MSE wall with 3.05 m (10 ft) long strips. This information ultimately was compared to forces estimated through numerical simulation and measured in the TL-3 crash test.

The pullout resistance of the reinforcement was calculated to be 8.85 kN (1.99 kips) (F*=1.62) at the upper most layer, 14.23 kN (3.2 kips) (F*=1.43) at the second layer, and 17.97 kN (4.04 kips) (F*=1.25) at the third layer. The static load per strip due to gravity was calculated to be 2.94 kN (0.66 kips) at the upper most layer, 5.25 kN (1.18 kips) at the second layer, and 7.61 kN (1.71 kips) at the third layer. In this analysis, the traffic surcharge was not considered. The dynamic load per strip due to barrier impact was calculated to be 1.73 kN (0.39 kips) at the upper most layer, 1.16 kN (0.26 kips) at the second layer, and 0.67 kN (0.13 kips) at the third layer. Therefore, the total load per strip was calculated to be 4.63 kN (1.04 kips) at the upper most layer, 6.36 kN (1.43 kips) at the second layer, and 9.92 kN (2.23 kips) at the third layer. The ratios between the load and resistance are 1.91 at the uppermost layer, 2.23 at the second layer, and 1.81 at the third layer. A summary of resistance and load per strip is presented in Table 6.1.

Table 6.1 Resistance and Force in case of MSE Wall with 10 ft Long Strip.

	(1) $\mathbf{T_{Static}}$ Static Load (kips)	**(2)** $\mathbf{T_{Dynamic}}$ Dynamic Load (kips)	**(3)=(1)+(2)** $\mathbf{T_{Total}}$ Total Load (kips)	**R** Resistance (kips)	**Factor of Safety**
Top Layer	0.66	0.39	1.04	1.99 (F*=1.62)	1.91
Second Layer	1.18	0.26	1.43	3.2 (F*=1.43)	2.23
Third Layer	1.71	0.13	2.23	4.04 (F*=1.25)	1.81

6.1.2 Calculation of Barrier Capacity

The ultimate load capacity for the 81.28 cm (32 in.) tall vertical barrier was computed to be 440.95 kN (99.13 kips) using the yield line failure mechanism in AASHTO LRFD. The length of the failure mechanism calculated for the barrier section analyzed was 1.75 m (5.73 ft) for the 81.28 cm (32 in.) tall vertical wall barrier. This indicates that, provided the coping has sufficient capacity to develop the ultimate strength of the barrier, the 3.05 m (10 ft) section length selected for evaluation in the TL-3 crash test should be sufficient for developing the primary failure mechanism for the barrier.

6.2 Finite Element Analysis

The MSE wall model that used in the bogie impact simulation was modified to model the proposed full-scale test installation. The modifications to the model included:

1- extending the model length from 9.14 m (30 ft) to 18.28 m (60 ft) by incorporating two moment slab components each of which is 9.14 m (30 ft) long,
2- incorporating two 2.26 cm (9/8 in.) diameter, 91.4 cm (36 in.) long dowel connectors between the moment slabs,
3- modeling the 81.28 cm (32 in.) high vertical barrier with explicit reinforcement details as shown in Figure 6.1,
4- raising the wall height to reflect a MSE wall configuration compressed of two rows of 1.52 m (5 ft) tall panels,
5- incorporating 3.05 m (10 ft) long soil reinforcement strips,
6- using a density of three strips per panel for the top layer of reinforcement, and a density of two strips per panel for the other layer of reinforcement, and
7- incorporating the model of the Chevrolet C2500 pickup truck (reflective of the 2000P test vehicle in NCHRP Report 350).

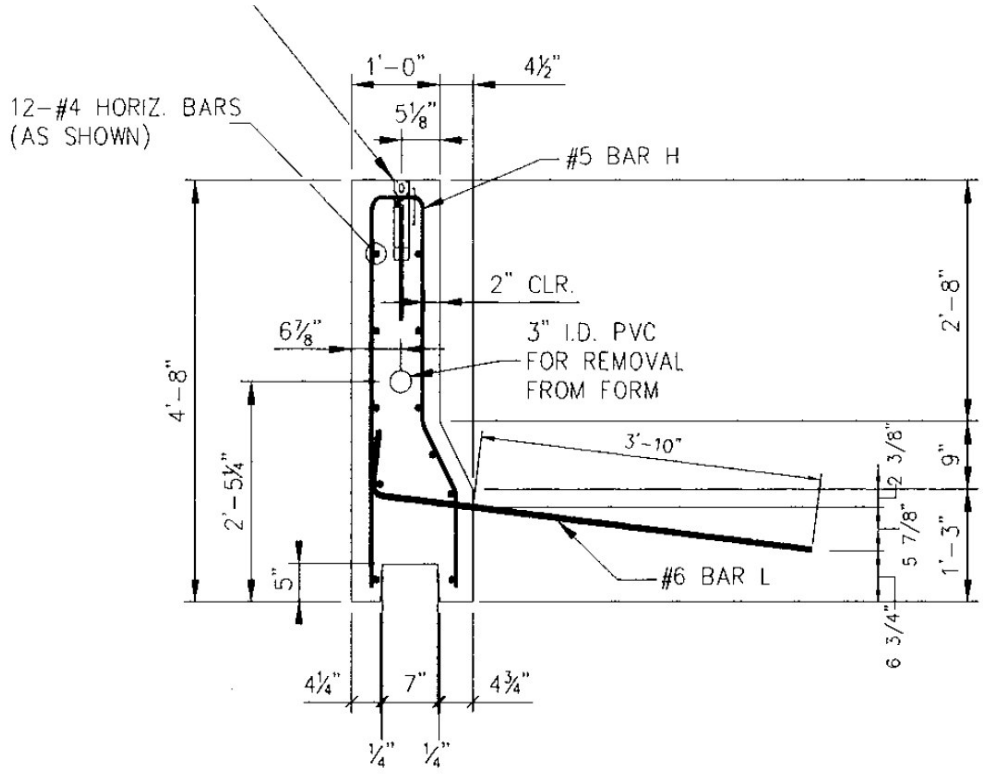

Figure 6.1 RECO vertical concrete barrier detail

Figure 6.2 and Figure 6.3 show the model setup of the 3.49 m (11.46 ft) high MSE wall with the Chevrolet C2500 vehicle model. The vehicle model was given an initial velocity of 100 km/hr (62 mph) and impacted the barrier at an angle of 25 degrees per Test Level 3-11 impact conditions. To enable comparison of forces and displacements, barriers and selected strip locations were assigned an alphanumeric designator that describes their horizontal position and vertical reinforcement layer. For example, strip "B3-A-1st" is positioned beneath the third barrier at vertical position A in the first (i.e., upper) layer of reinforcement. Figure 6.4 shows the rebar details of vertical concrete barrier and moment slab which was modeled based on the drawings provided by RECO. Figure 6.5 shows the relative position of the vehicle with respect to the middle barrier joint. This barrier joint is aligned with the joint between the two moment slab sections that were modeled.

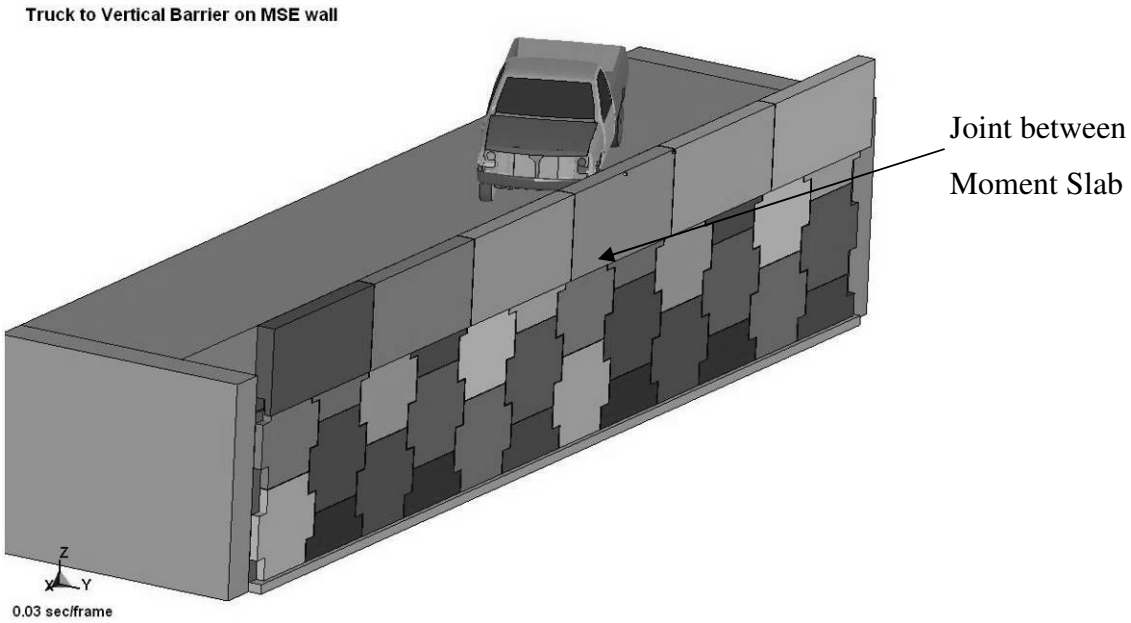

(a) 3D view

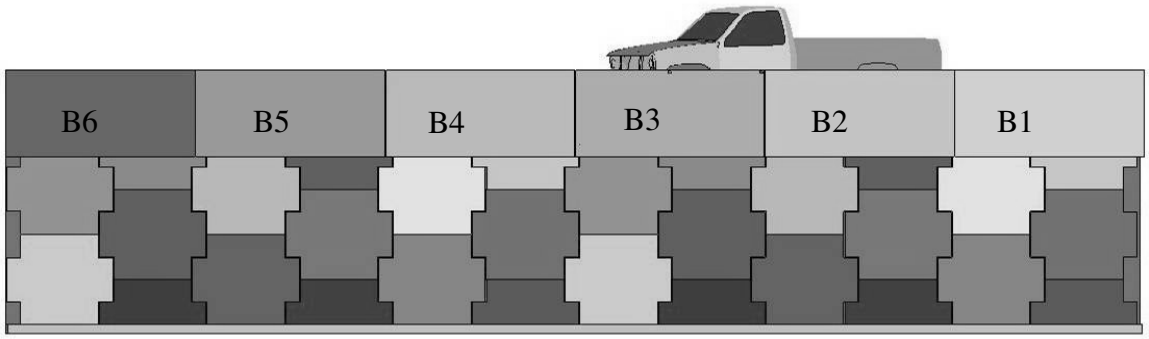

(b) Elevation view

Figure 6.2 MSE wall, barrier and C2500 model

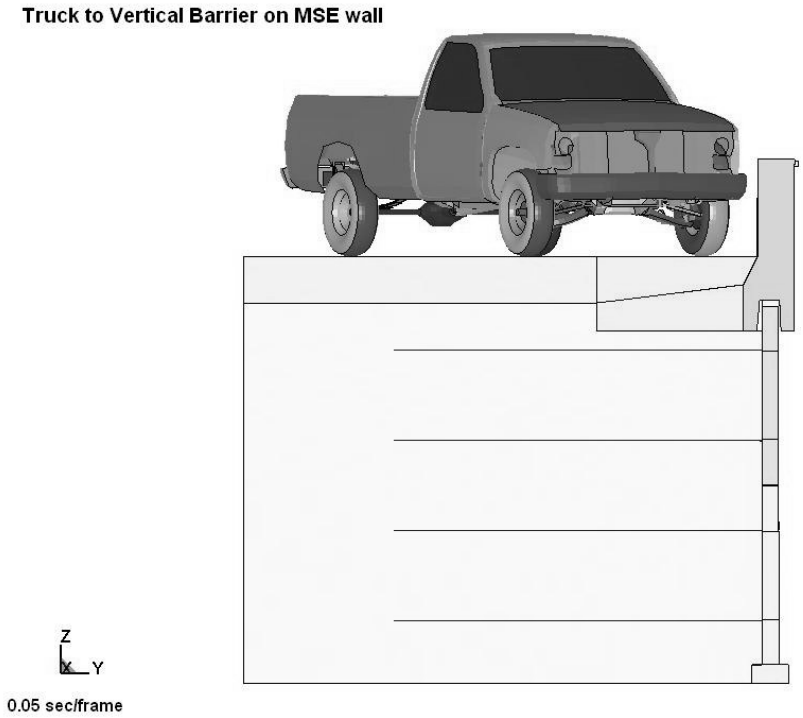

Figure 6.3 Down stream view of model showing profile of barrier and embedded soil strips

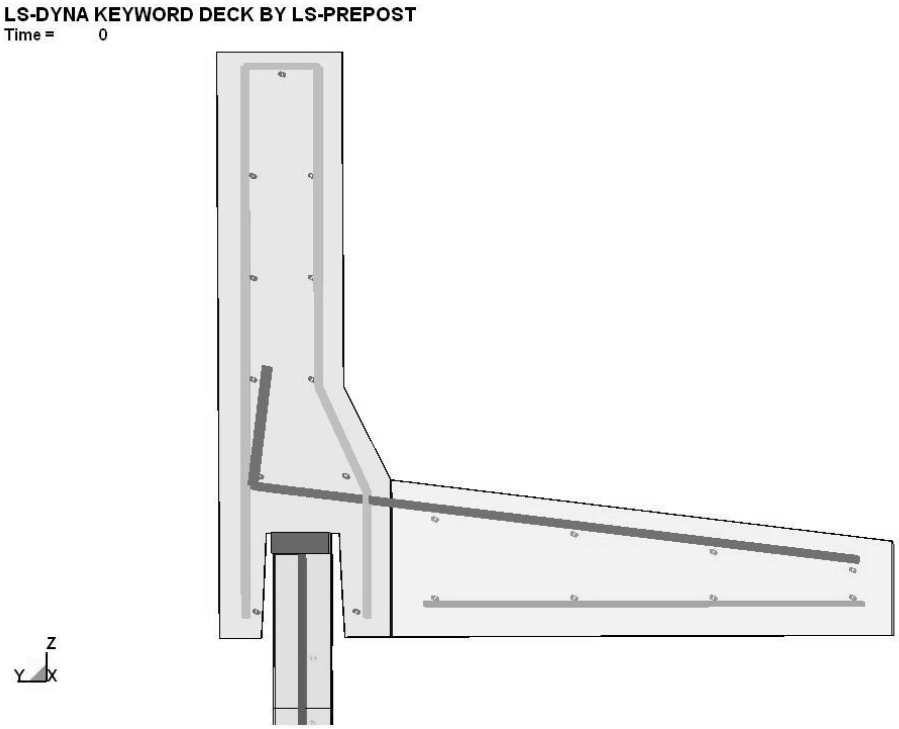

Figure 6.4 Rebar detail in the barriers and panels of model

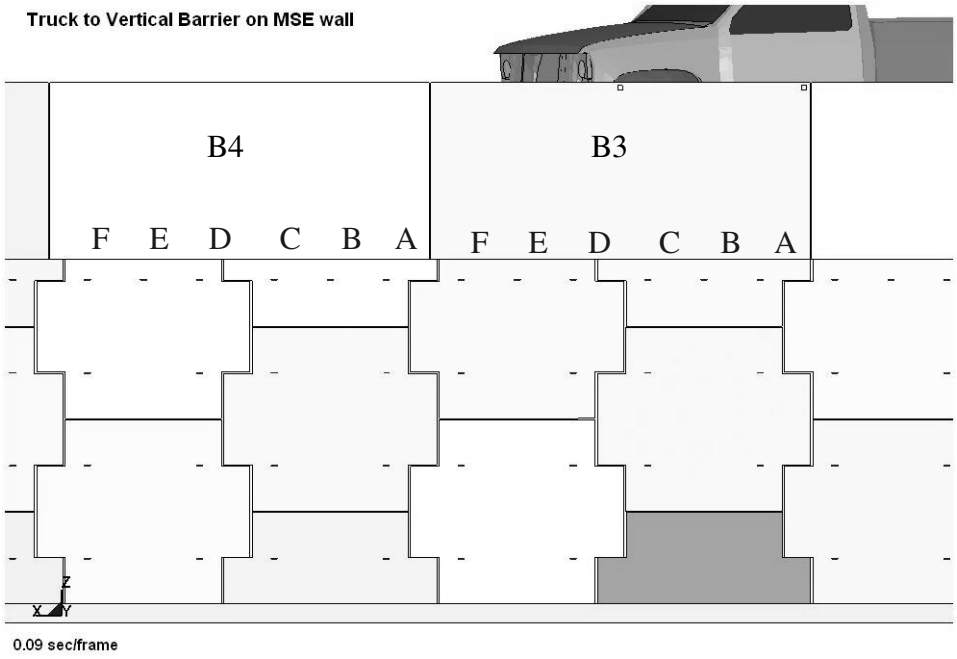

Figure 6.5 Side view of the model showing the distribution of the strips

The first phase of the simulation process was to account for the steady state conditions of the system due to the gravitational load. The weight of the system was measured and used as a convergence criterion for the steady state solution The total mass of the model for the vertical wall barrier on top of the MSE wall with 3.05 m (10 ft) long strips is 664,630 kg (45,542 slug or 1,465,258 lb mass). The weight of the system is calculated to be 6,517 kN (1,465 kips) using the mass of the finite element model and the acceleration of gravity. Therfore, after accounting for gravitationad load, the weight of model system should converge to the calculated system weight. The weight of the finite element model was 6,531 kN (1,468 kips) at the end of initialization step. A reasonable agreement shows that the weight of the finite element model approached the calculated weight of the model system as shown in Figure 6.6.

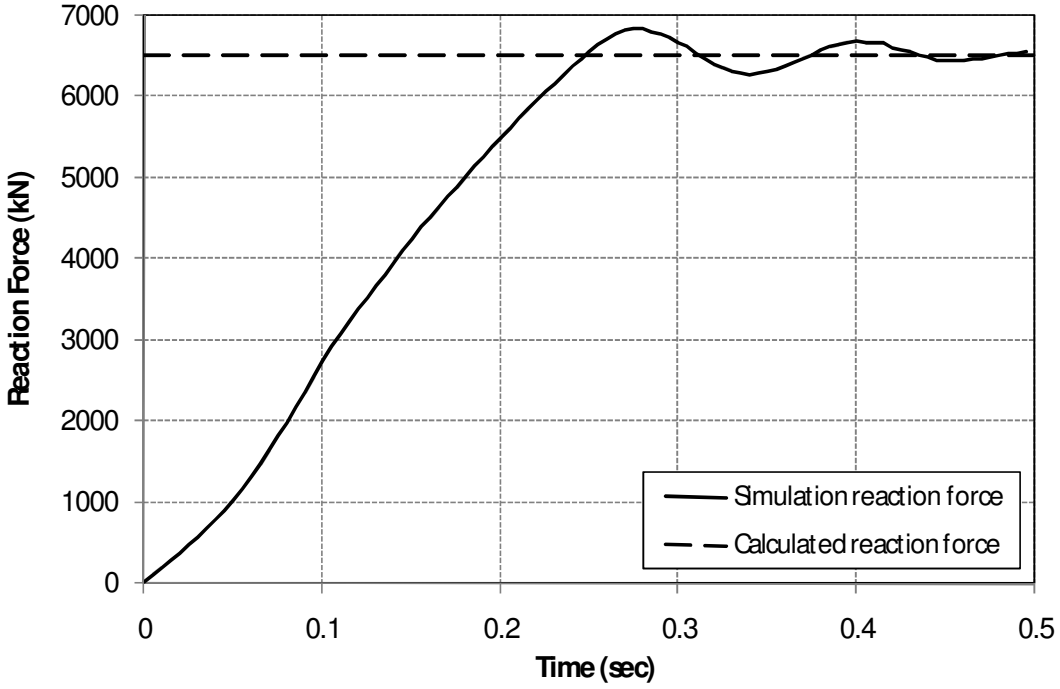

Figure 6.6 System reaction force of the MSE wall model

The initialized model was then set-up with the C2500 vehicle model and the impact simulation was conducted. The vehicle was successfully contained and redirected by the barrier. Figure 6.7 shows sequential images of the impact that correspond to the events described below.

0.06 sec: Maximum force on the barrier

0.1 sec: Maximum load in the strips

0.195 sec: Back slap impacts of the barrier

0.345 sec: Back bumper impacts the barrier

0.5 sec: Vehicle exits the barrier

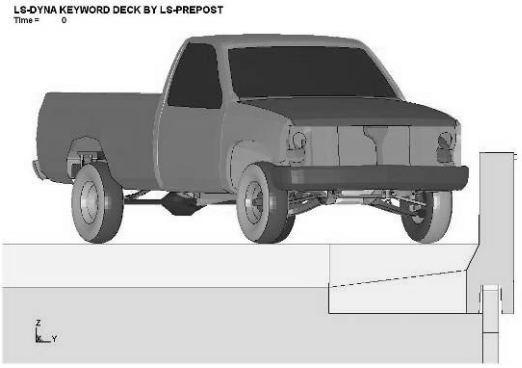

(a) 0 sec

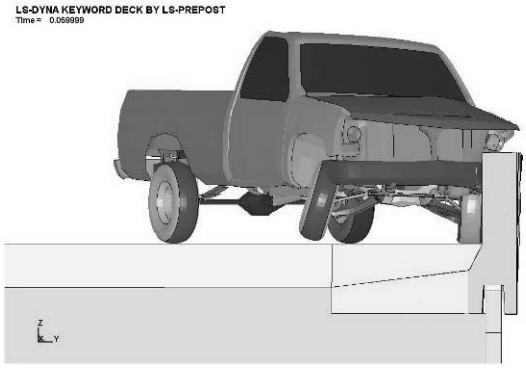

(b) 0.06 sec

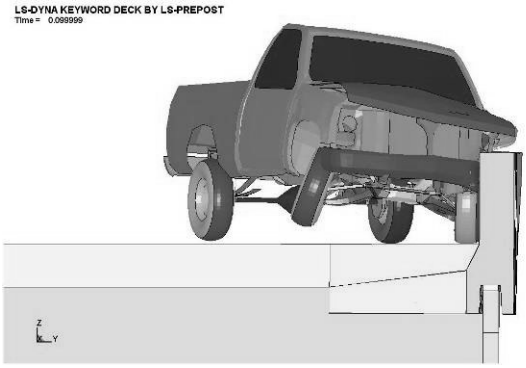

(c) 0.1 sec

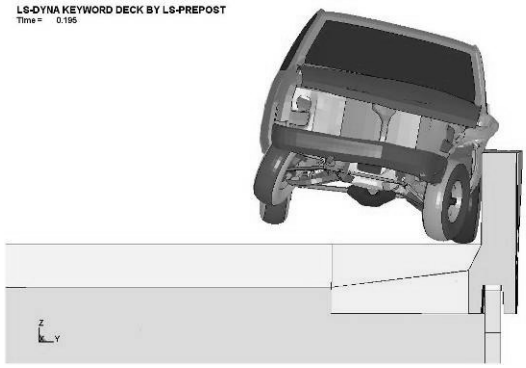

(d) 0.195 sec

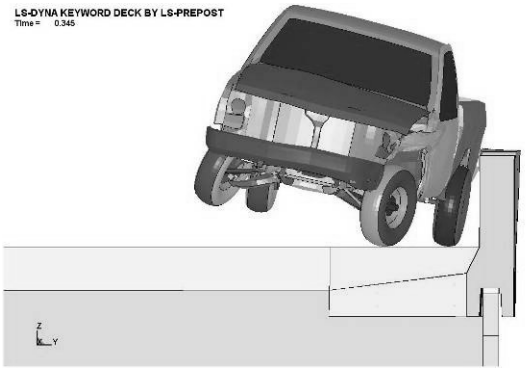

(e) 0.345 sec

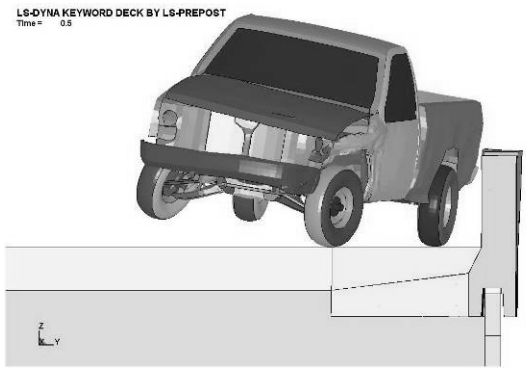

(f) 0.5 sec

Figure 6.7 Vehicle position at each significant moment

6.2.1 Data from Accelerometers

The calculated impact force on the barrier was 248.21 kN (55.8 kips) at 0.0575 sec as shown in Figure 6.8. At 0.198 sec, the second peak impact force occurred due to the back slap impact.

The damage to the concrete barrier is shown in Figure 6.9 and Figure 6.10. The concrete barrier exhibited a damage profile typically observed in impacts on barrier joints. The damage profiles shown in Figure 6.9 and Figure 6.10 are limited to the surface elements and did not indicate failure of the barrier.

The maximum displacement at the top of the barrier occurred in barrier section "B4". The displacement-time history for this barrier section is shown in Figure 6.11. The initial imipact induced a displacement of 4.14 cm (1.63 in.) at the top of the barrier. The barrier was rebounding back when the back slap impact occurred, which resulted in a maximum displacement of 4.85 cm (1.91 in.). As the barrier was rebounding from the back slap, the rear bumper of the pickup contacted the barrier and the barrier displacement momentarily increased to 3.73cm (1.47 in.).

Figure 6.12 shows the displacement distribution on barrier segments "B3" and "B4" at 0.1 sec.

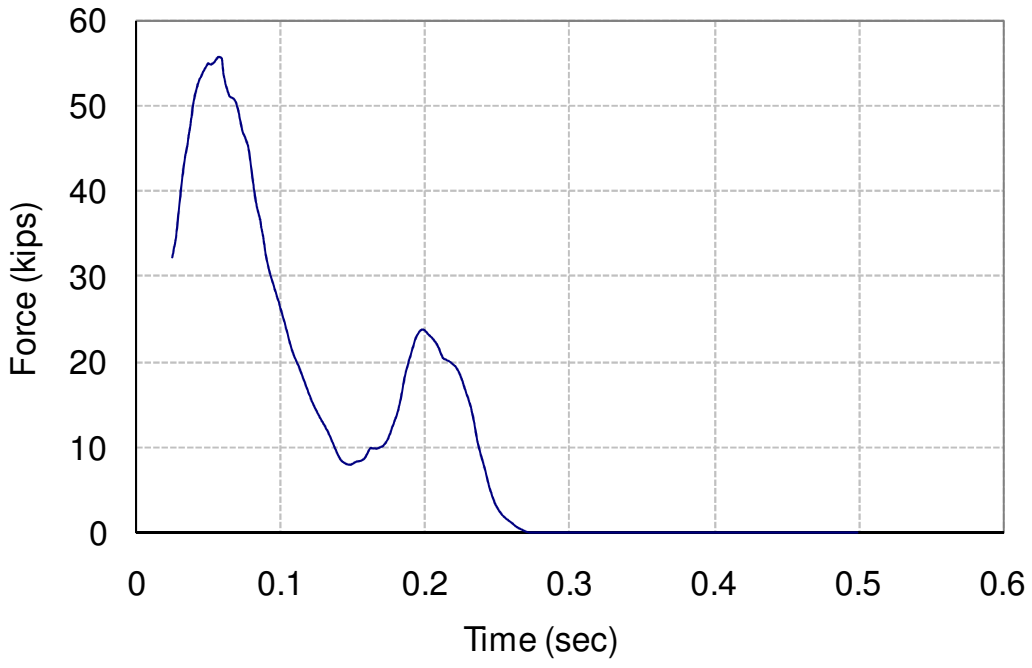

Figure 6.8 Time history of impact force on barrier (50-msec average)

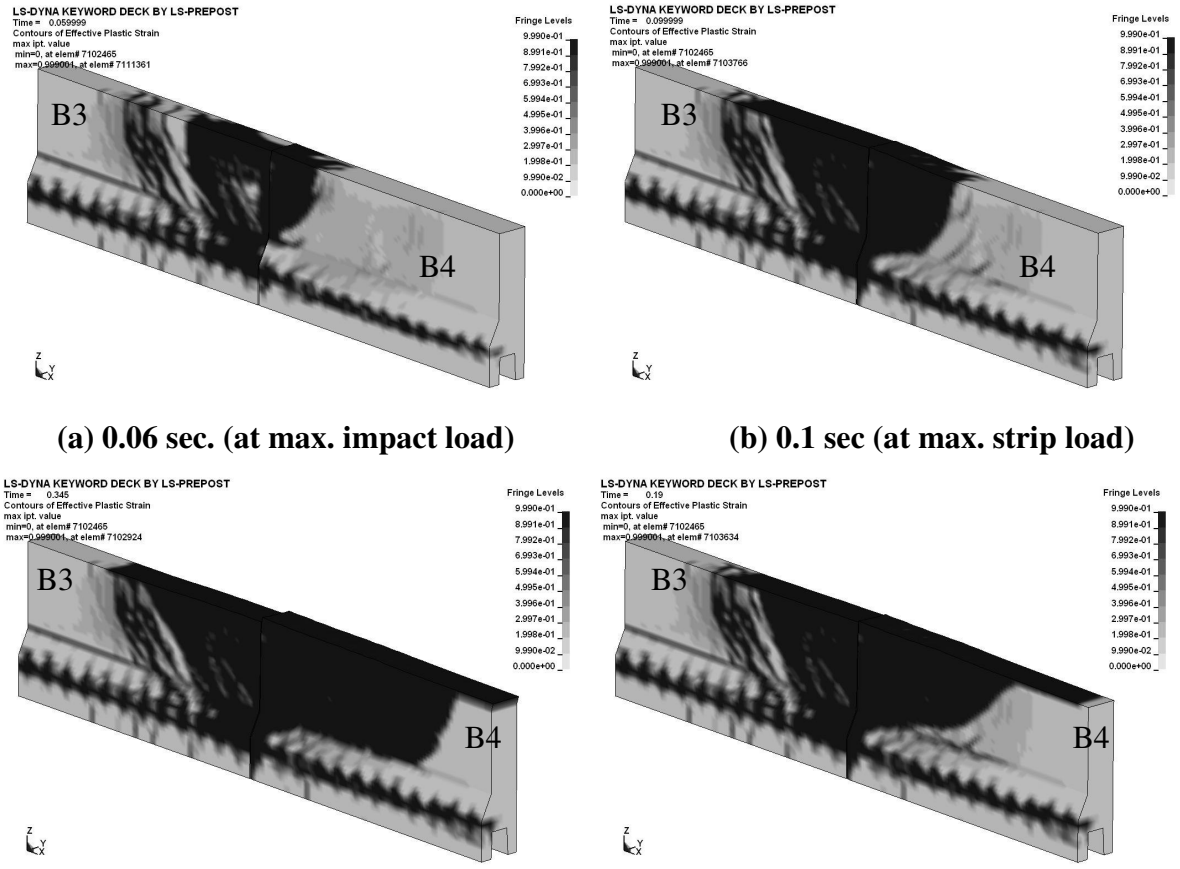

(a) 0.06 sec. (at max. impact load) **(b) 0.1 sec (at max. strip load)**

(c) 0.19 sec. (at rear tire hit) **(d) 0.345 sec. (at back bumper hit)**

Figure 6.9 Damage to the concrete barrier at the front of the joint

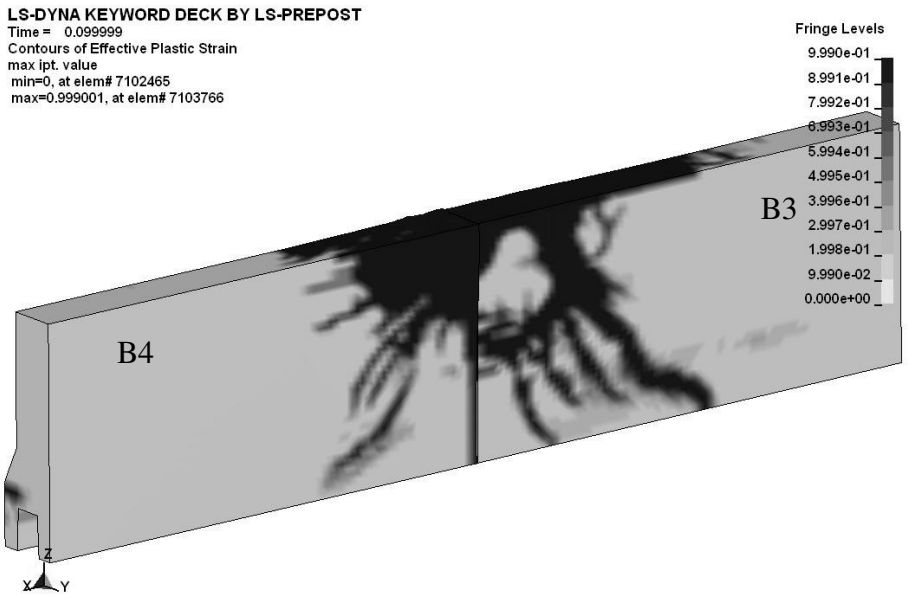

Figure 6.10 Damage of back of the concrete barrier (0.1 sec)

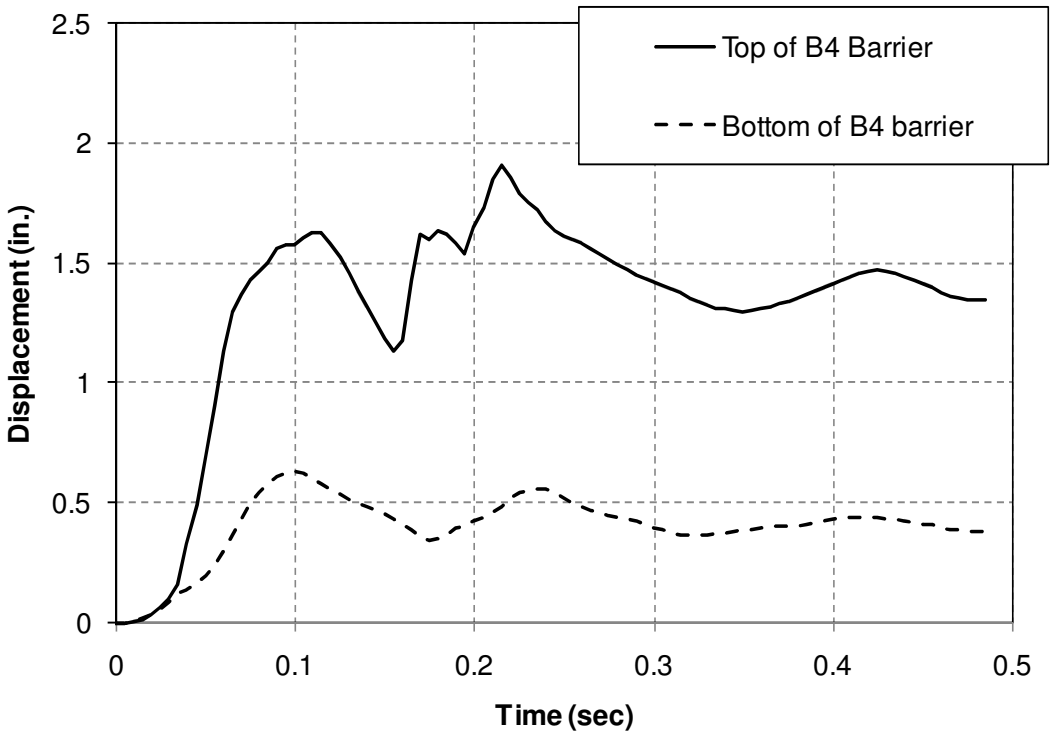

Figure 6.11 Barrier displacement time history (Barrier "B4")

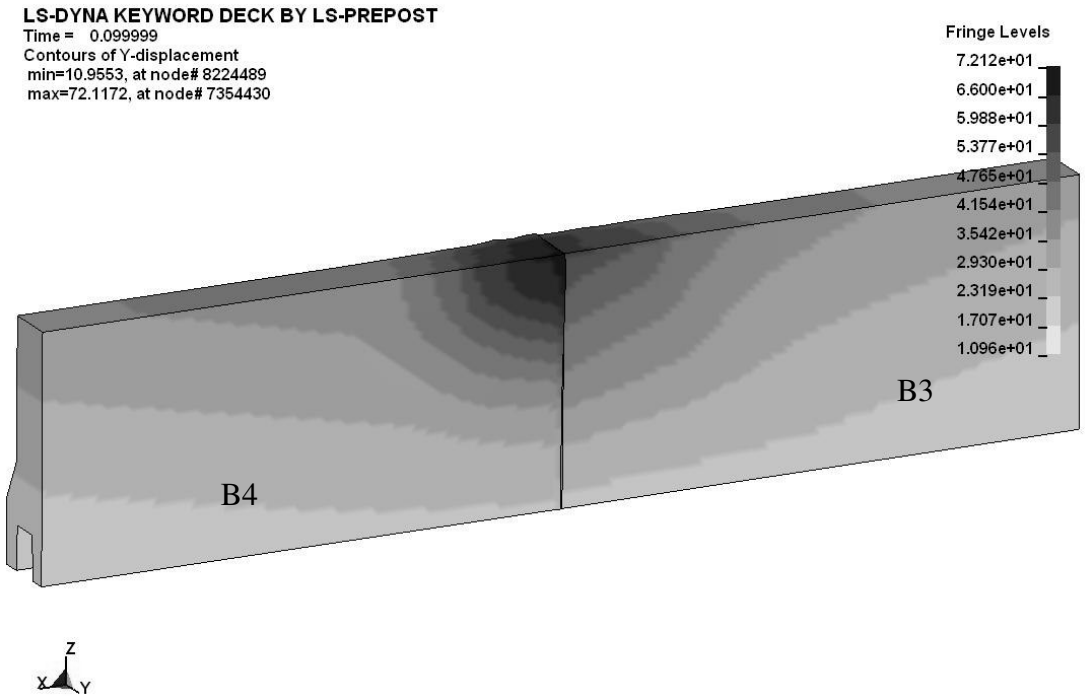

Figure 6.12 Distribution of barrier displacement (Barrier "B3" and "B4")

6.2.2 Data of the Strip

The load-time histories for selected strips in the upper layer of reinforcement are presented in Figure 6.13(a). The 50-msec moving average is shown in Figure 6.13(b). Figure 6.14 through Figure 6.16 show 50-msec average load-time histories for strips in the second through fourth layers of reinforcement, respectively. The maximum 50-msec average load in the strips is 18.7 kN (4.2 kips) in strip "B4-A-1st" (Figure 6.13(b)). The strip loads in each layer show similar load histories, therefore, one strip was chosen to represent the load at each layer in Figure 6.17.

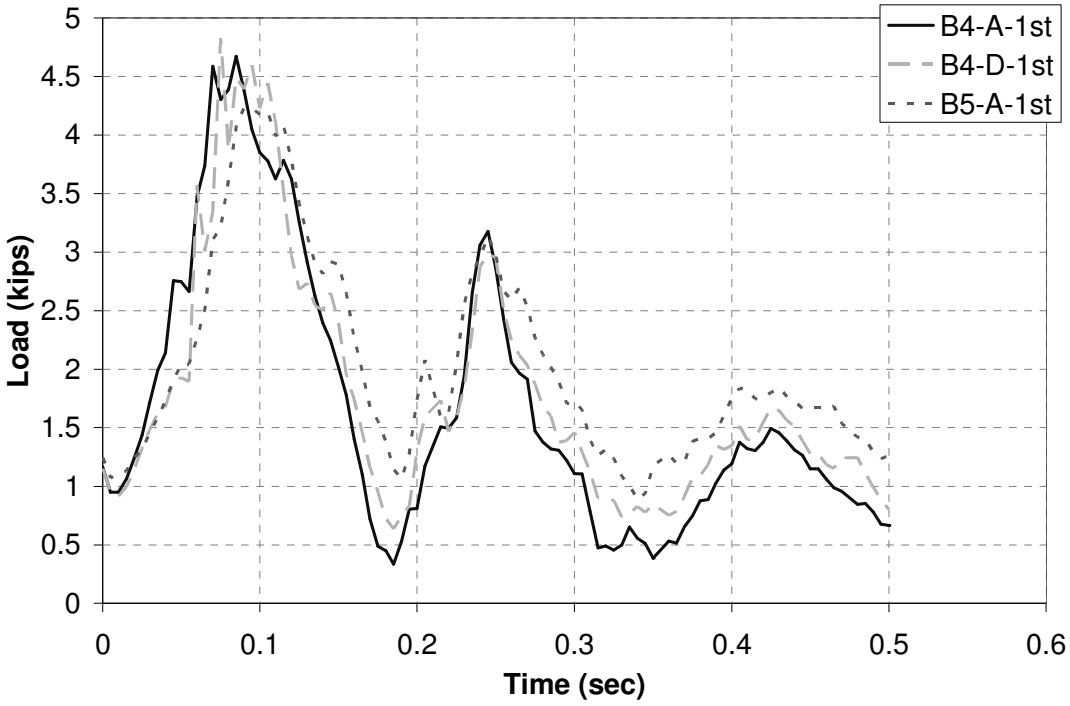

(a) Raw data

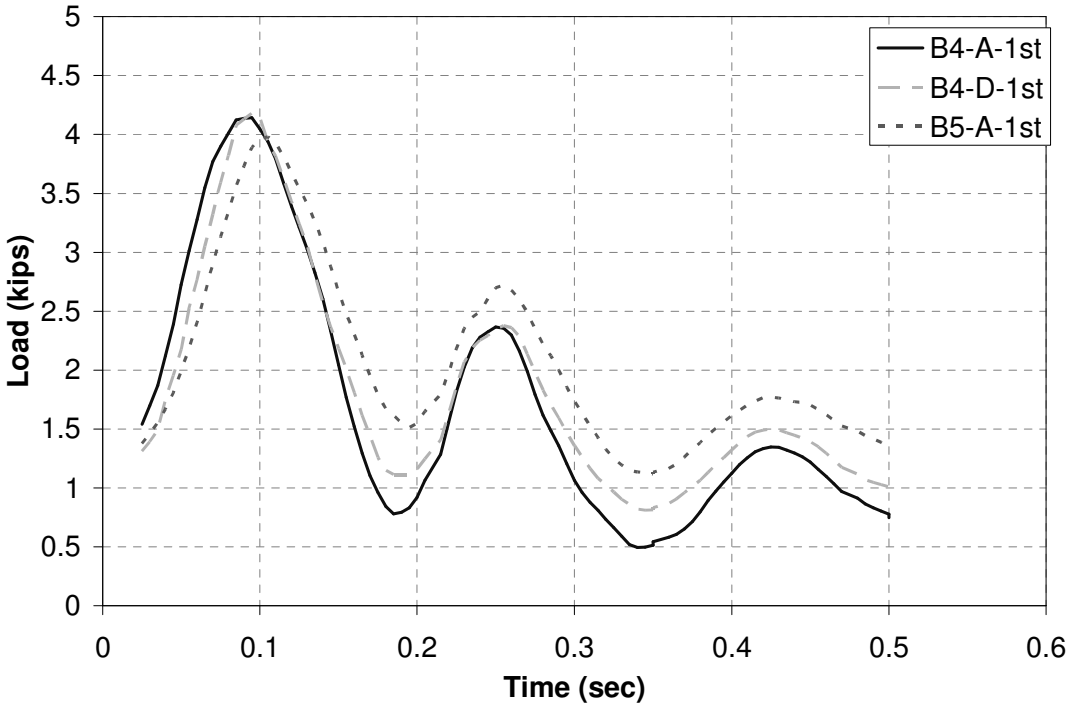

(b) 50 ms average

Figure 6.13 Total load in the strip at uppermost layer

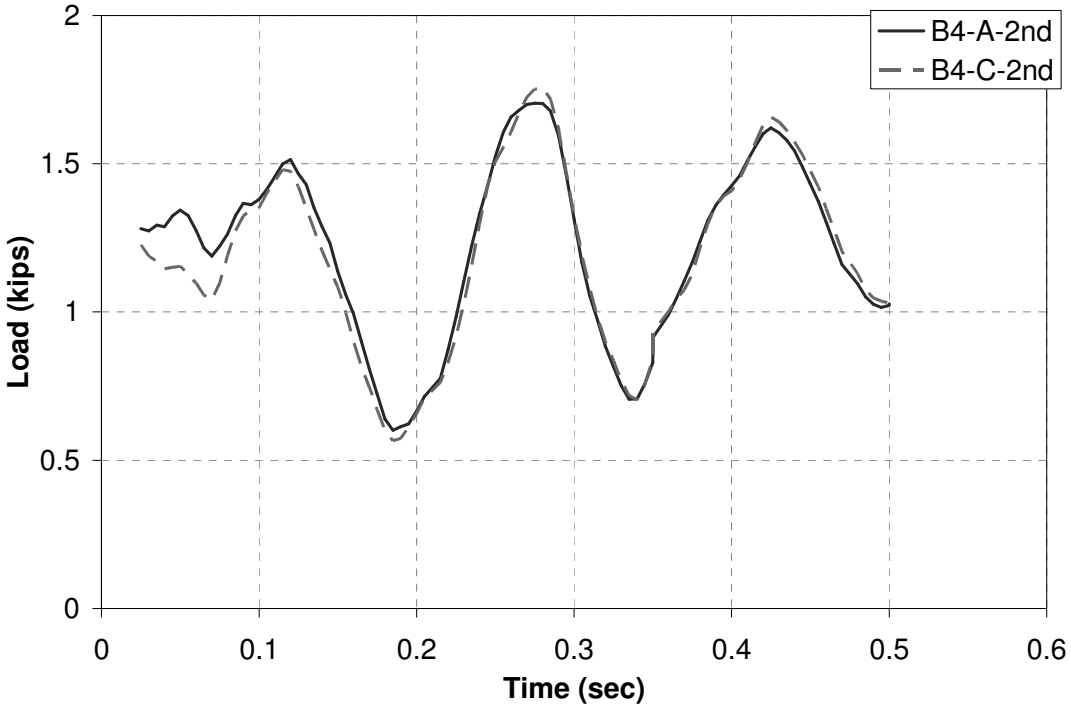

Figure 6.14 Total load in the strip at second layer

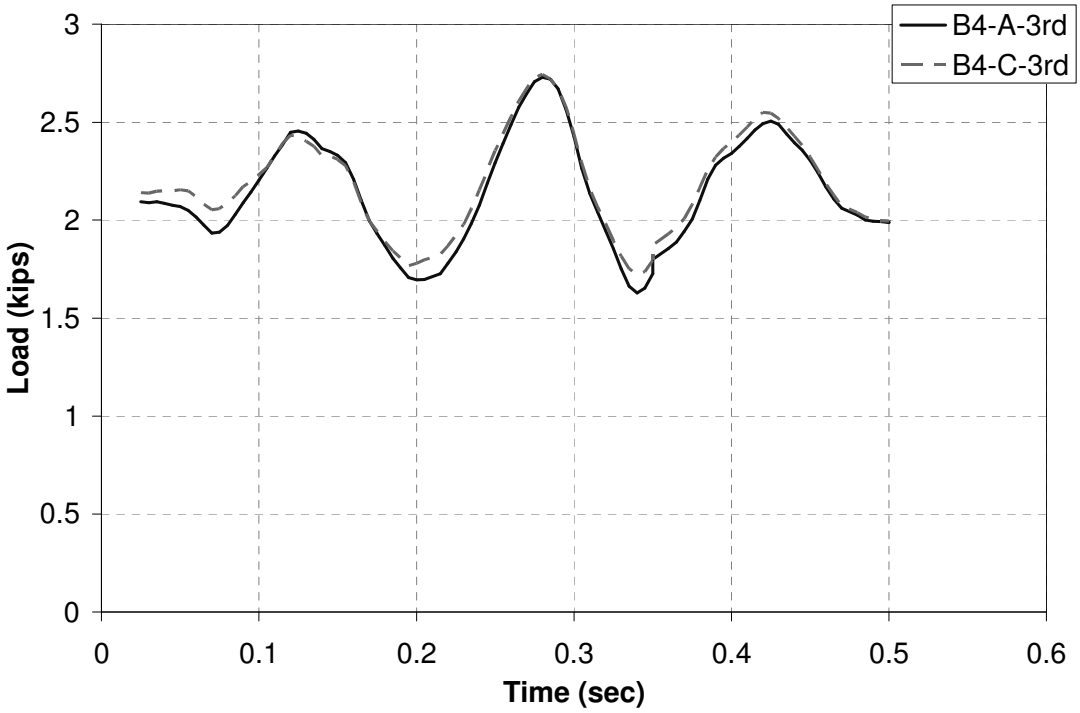

Figure 6.15 Total load in the strip at third layer

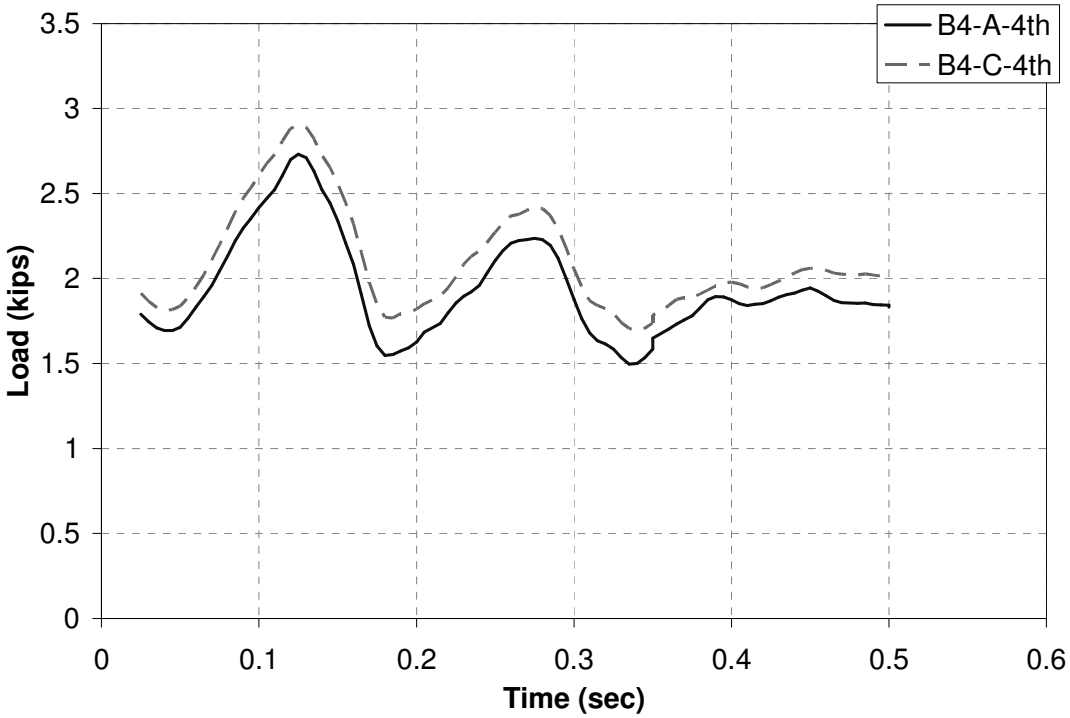

Figure 6.16 Total load in the strips at fourth layer.

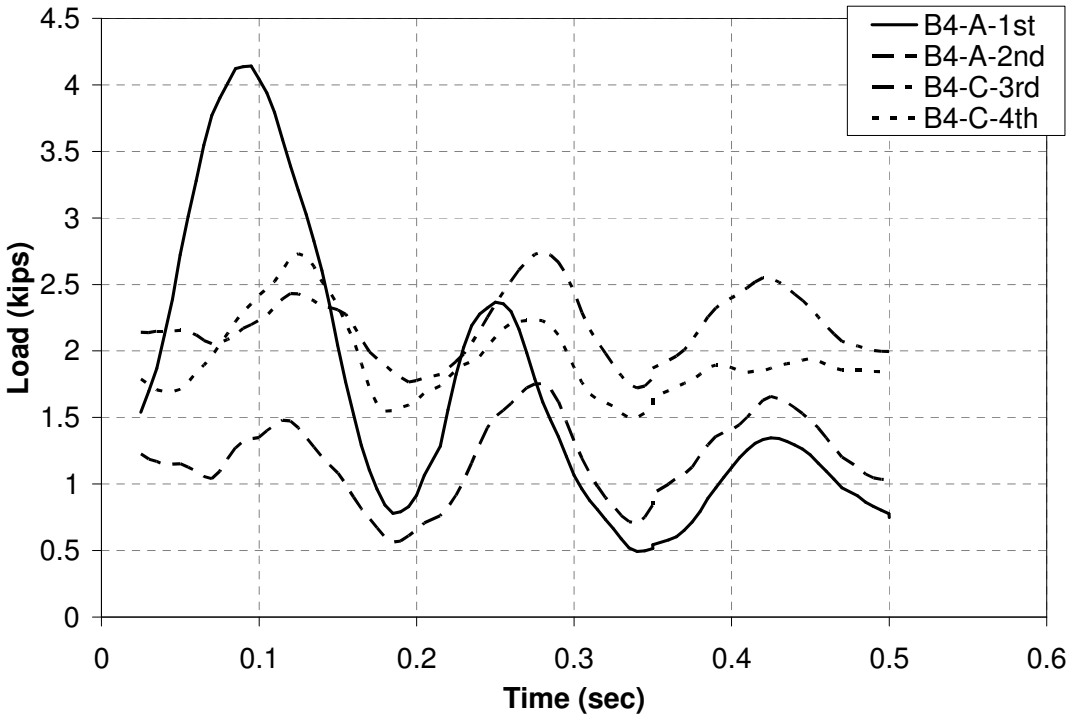

Figure 6.17 Load in the strips for all layers

Maximum displacement of the strips was 0.28 cm (0.11 in.) at 0.085sec at strip "B4-A-1st" as shown in Figure 6.18. Since the strips and panels were tied together, the maximum displacement of the panel also corresponds to this value. Figure 6.19 shows the displacement distribution of the strips at 0.085 sec.

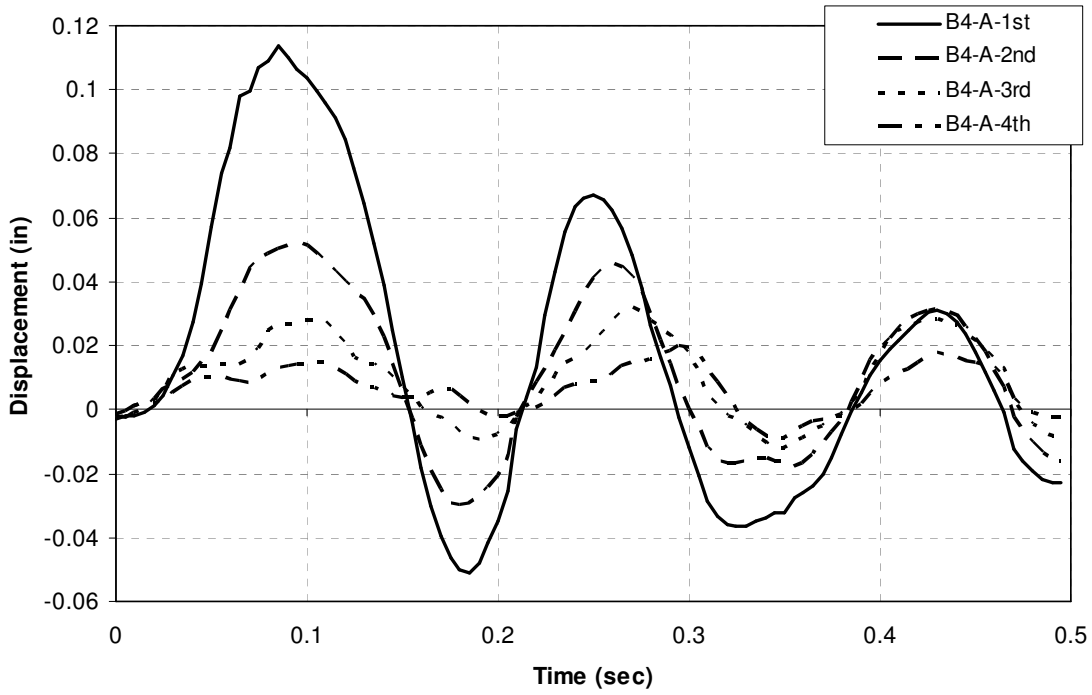

Figure 6.18 Displacement in the strips at B4-A

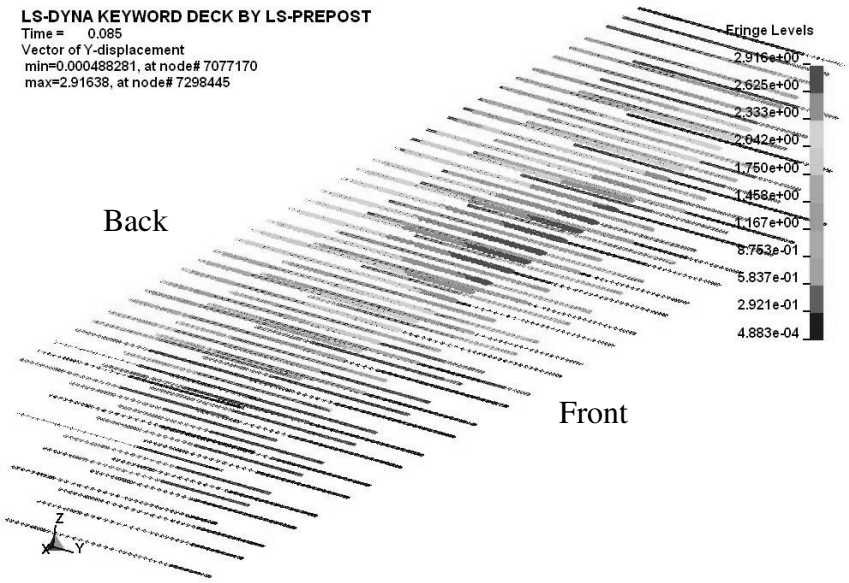

Figure 6.19 Distribution of displacement in the strips at 0.085 sec

6.2.3 Panel Analysis

The strain on the wall panel was evaluated as shown in Figure 6.20. The maximum compressive strain was 18 microstrains at 0.065 sec.

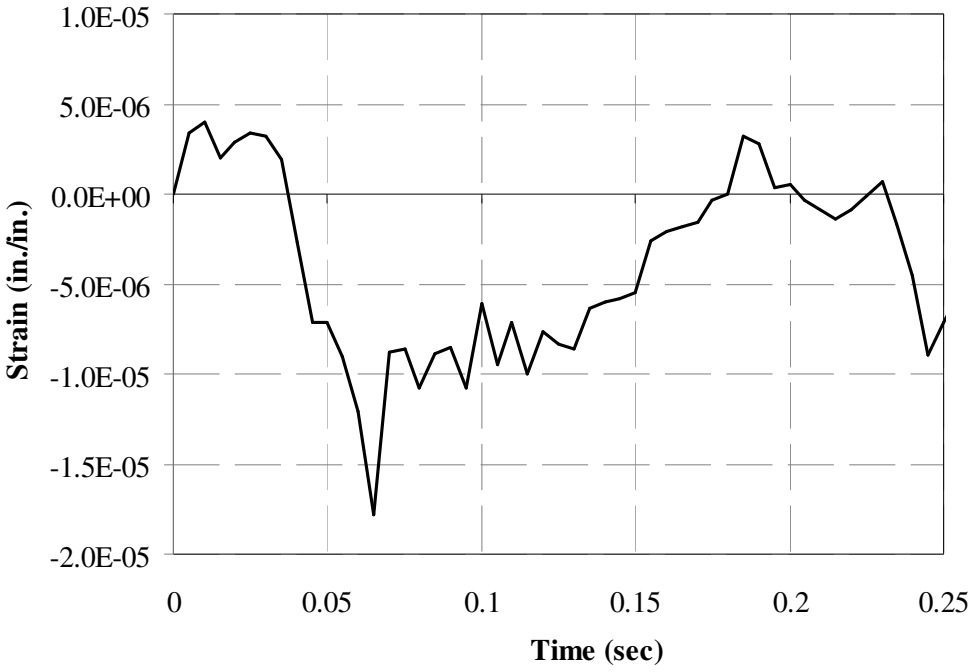

Figure 6.20 Panel strain at D1

6.3 TL-3 Crash Test

6.3.1 10 Ft High MSE Wall Construction and Test Installation

An overall layout of the 3.05 m (10 ft) high MSE wall test installation is shown in Figure 6.21. The instrumented MSE wall was about 27.43 m (90 ft) long and approximately 2.74 m (9 ft) tall and comprised of full and half-panel sections that are approximately 1.52 m (5 ft) wide. The bottom wall panels were placed on a 30.48 cm (1 ft) wide × 15.24 cm (6 in.) thick concrete leveling pedestal. The MSE wall had three layers of reinforcement. The uppermost layer is at a depth of 0.91 m (3 ft) below the ground surface. The vertical spacing of the successive reinforcement layers is approximately 0.76 m (2.5 ft). The steel reinforcement strips are 3.05 m (10 ft) long. The reinforcement had a density of three strips per layer per panel. The wall panels were recessed inside the coping of the precast barrier-coping sections. The barrier-coping sections rested on a 6.67 cm (2 5/8 in.) layer of a level-up concrete placed on top of the wall panels. The moment slabs connecting the 3.05 m (10 ft) long precast barrier-coping sections were cast-in-place in three 9.14 m (30 ft) lengths. The three 1.37 m (4.5 ft) wide × 9.14 m (30 ft) long moment slabs were connected to one another using two No.9 shear dowels across each joint.

Figure 6.22 shows a cross section of the barrier-coping section and MSE wall. Figure 6.23 shows photos of the instrumented MSE wall before the TL-3 crash test. The barriers and panels were assigned alphanumeric designators as described earlier. The precast barrier-coping sections, concrete wall panels, and steel strip wall reinforcement were provided by RECO at no cost to the project.

The well-graded sand backfill material used for the MSE wall construction followed the gradation limits of TxDOT Type B backfill material shown in Table 6.2 *(30)*. A grain size analysis was performed for the backfill material to determine the relative proportions of different grain sizes as shown in Figure 6.24. The particle diameters corresponding to 10% fines, D_{10}, and 60% fines, D_{60}, were 0.25 mm and 1.1 mm, respectively. The coefficient of uniformity, Cu (= D_{60} / D_{10}) was determined to be 4.4. The friction factor, F^*, was calculated to be 1.84 at the ground level.

Selected reinforcement strips in the MSE wall were instrumented with strain gages to capture the tensile forces transmitted into the reinforcement during the full-scale crash test. A total of 14 strain gages were used. The four strips in the upper layer and the three strips in the middle layer of reinforcement on the wall panel immediately downstream from the impact location were instrumented. The simulation results indicate that these strips develop the maximum tensile loads during impact. Two strain gages were used at each selected location (one on the top of the strip and one on the bottom of the strip) to compensate for any bending in the strip.

A contact switch was placed on the top edge of the traffic face (inside face) of the wall panels inside the coping recess. The switch indicates the time (referenced from impact) at which the barrier slides and/or rotates sufficiently for the coping to contact the wall panel.

The wall panel attached to the instrumented strips was instrumented with three concrete strain gages to capture normal strains in the panel induced from impact loads transmitted into the MSE wall through the soil and generated from direct contact of the barrier-coping section with the top of the wall panel. The strain gages were placed in a vertical position along the height of the panel. A strain gage was placed adjacent to the anchorage locations for the upper and lower layer of reinforcement, and one strain gage was placed in the center of the panel between the two layers of reinforcement.

An accelerometer was mounted behind and at the top of the barrier section immediately downstream of impact (which was shown in the simulation to experience the maximum load and displacement). An accelerometer also was placed on the end of the 9.14 m (30 ft) long moment slab to which this barrier section was attached at its midpoint to measure any acceleration or motion imparted to the moment slab during impact.

Figure 6.22. Detailed drawings of the test installation and photographs of the construction procedure are presented in Appendix E and F, respectively.

6.3.2 Impact Conditions

The MASH *(9)* test guidelines were applied for the TL-3 crash test. MASH test 3-11 *(9)* involves a 2270P vehicle weighing 2,270 kg ± 50 kg (5,000 lb ± 100 lb) and impacting the bridge rail at an impact speed of 100 km/h ± 4 km/h (62.2 mph ± 2 mph) and an angle of 25

degrees ± 1.5 degrees. The target impact point was 1.2 m (4 ft) upstream of the fourth barrier joint. The 2004 Dodge Ram 1500 quad-cab pickup truck used in the test weighed 2246 kg (4951 lb) and the actual impact speed and angle were 101.7 km/h (63.2 mph) and 25.6 degrees, respectively. The actual impact point was 1.3 m (4.3 ft) upstream of the fourth barrier joint.

6.3.3 Test Vehicle

A 2004 Dodge Ram 1500 quad-cab pickup truck, shown in Figure 6.25 and Figure 6.26, was used for the crash test. Test inertia weight of the vehicle was 2,246 kg (4,951 lb). The height to the lower edge of the vehicle front bumper was 349 mm (13.75 in.), and the height to the upper edge of the front bumper was 660 mm (26.0 in.) The vehicle was directed into the installation using the cable reverse tow and guidance system, and was released to be free-wheeling and unrestrained just prior to impact. Detailed test vehicle properties and information are presented in Appendix G.

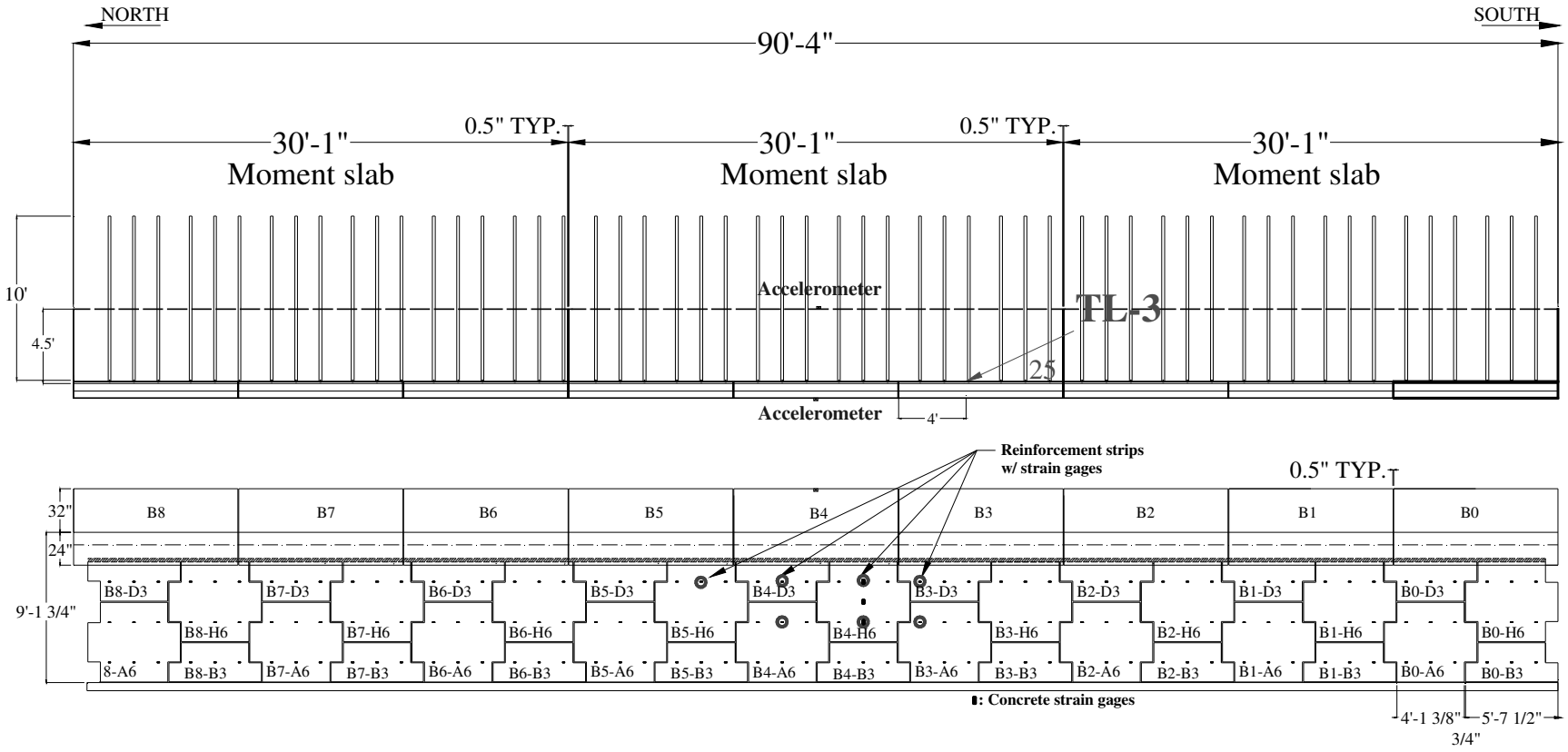

Figure 6.21 Layout of the barrier on MSE wall

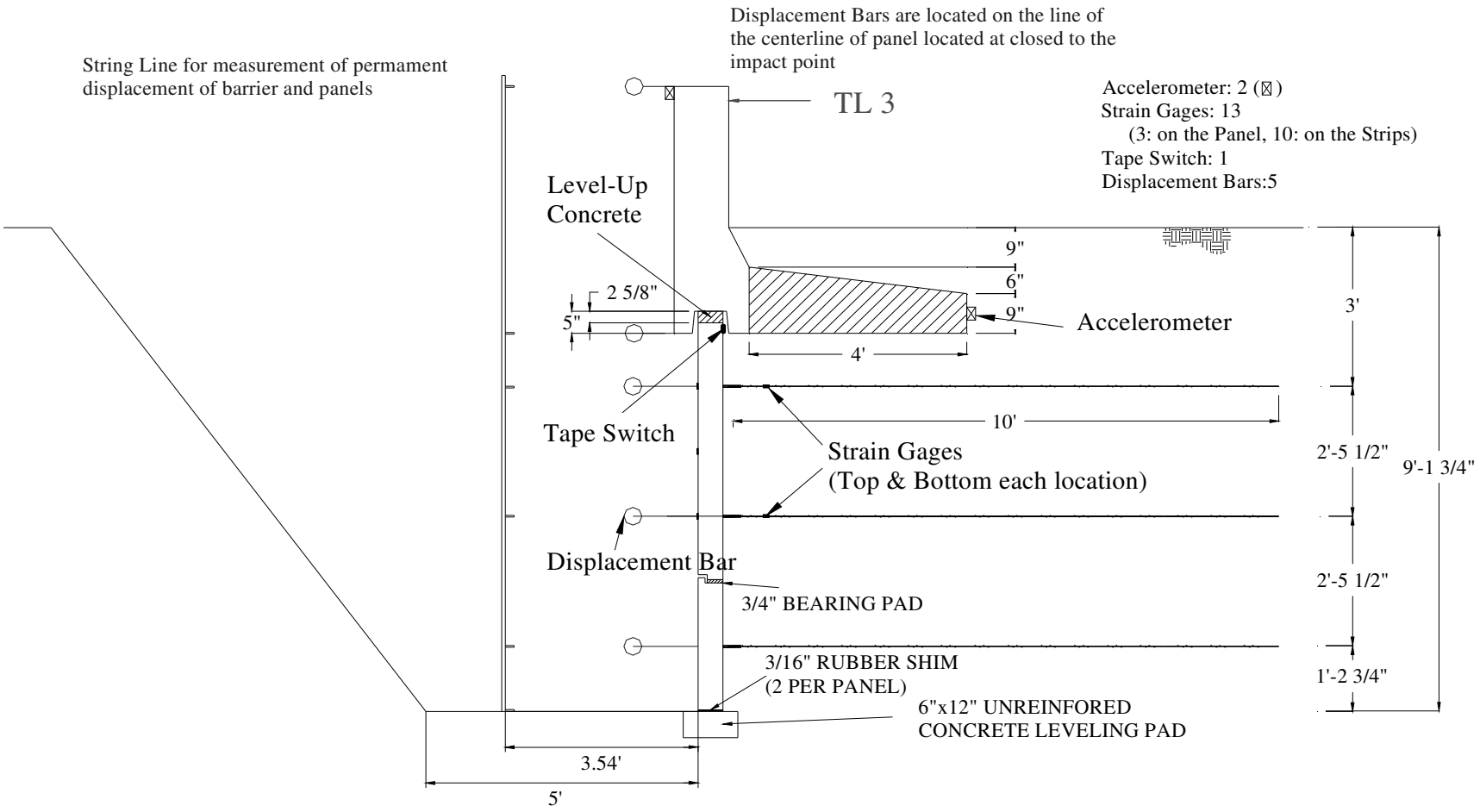

Figure 6.22 Side view of TL-3 crash test with 32 in. tall vertical wall barrier

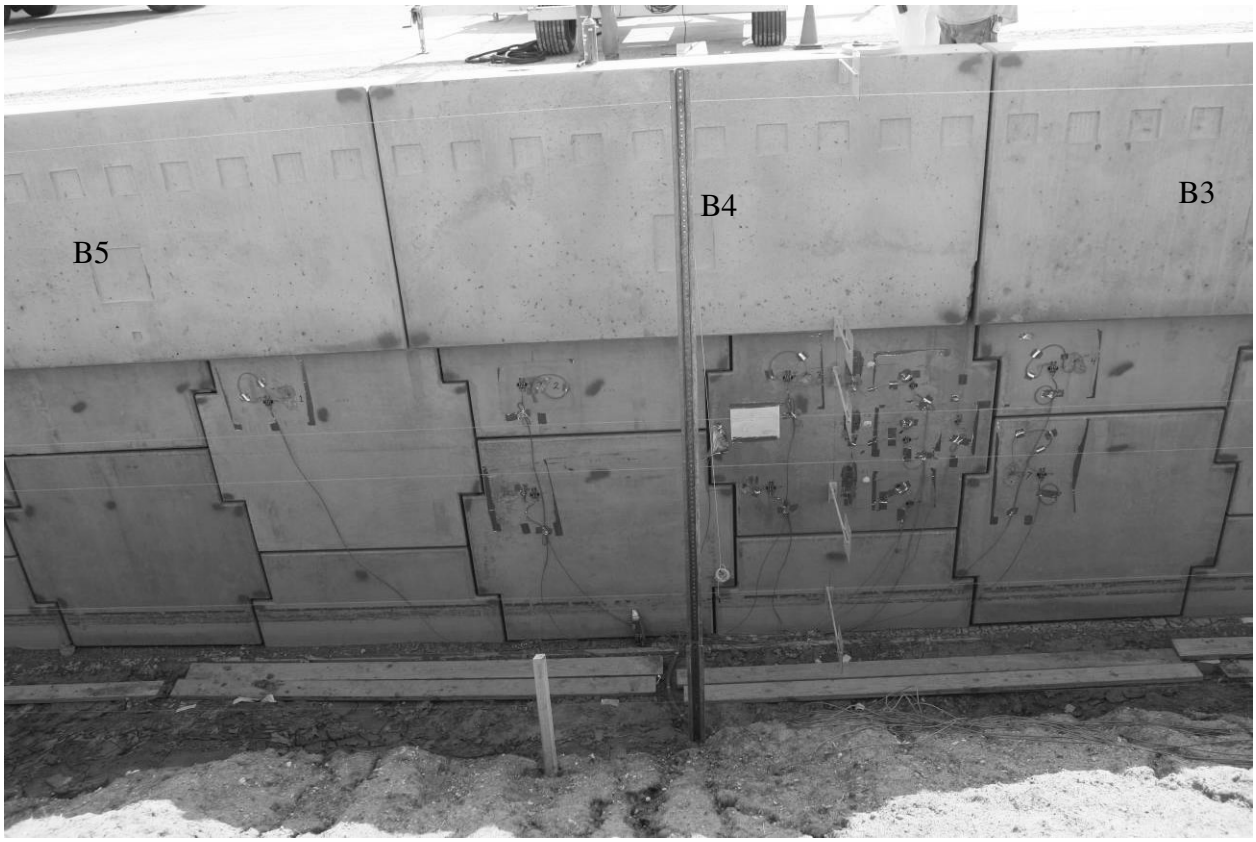

Figure 6.23 Barrier on MSE wall prior to testing

Table 6.2 Gradation Limits for TxDOT Type B Select Backfill *(30)*

Sieve Size	Percent Retained
3 in.	0
No. 4	See Note
No. 40	40-100
No. 200	85-100

Note: If 85% or more material is retained on the No. 4 sieve, the backfill will be considered rock backfill.

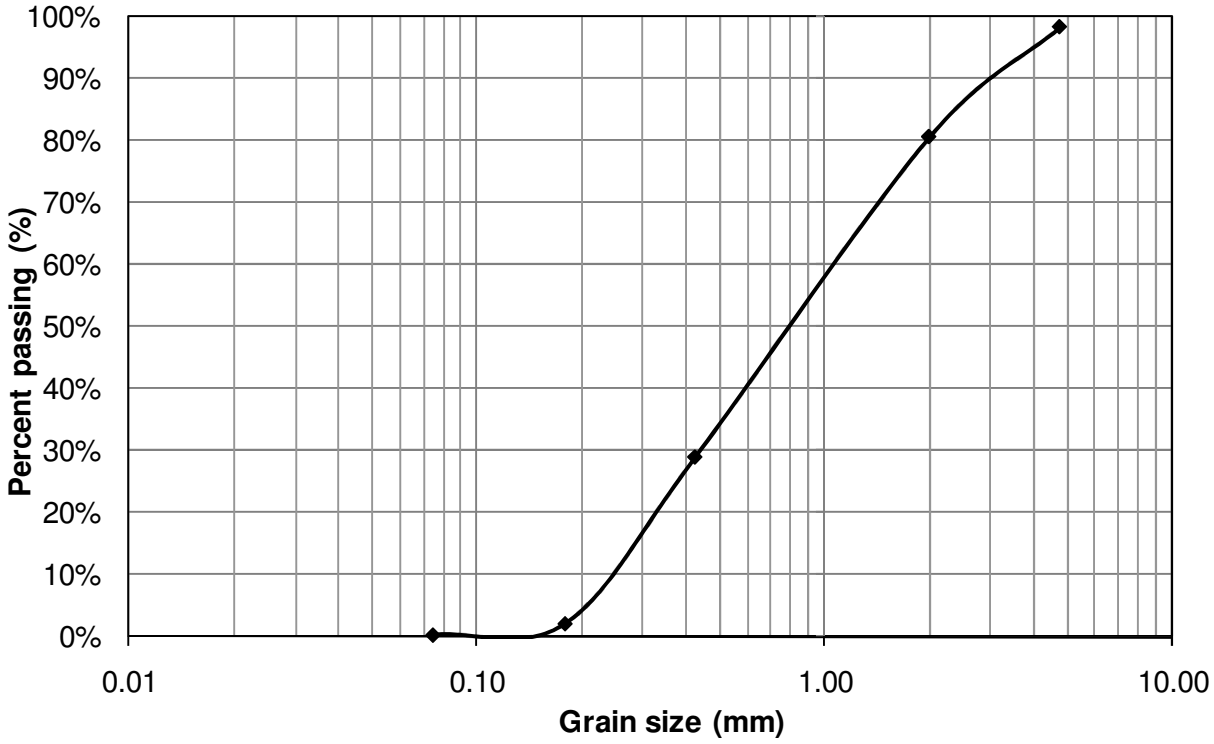

Figure 6.24 Particle size distribution curve of the backfill for TL-3 crash test

Figure 6.25 Vehicle/installation geometrics

Figure 6.26 Vehicle before test

6.3.4 Test Description

The 2270P vehicle, traveling at an impact speed of 101.7 km/h (63.2 mph), impacted the MSE Wall 1.31 m (4.3 ft) upstream of the fourth barrier joint at an impact angle of 25.6 degrees. At approximately 0.027 sec after impact, the vehicle began to redirect, and at 0.092 sec, the right front tire began to ride up the barrier face. The right rear tire lost contact with the ground surface at 0.129 sec, and the right rear of the vehicle began to rise at 0.147 sec. At 0.166 sec, the vehicle was traveling parallel with the barrier at a speed of 92.4 km/h (57.4 mph). The rear of the vehicle contacted the barrier at 0.186 sec, and the vehicle began to roll counterclockwise at 0.237 sec. At 0.338 sec, the vehicle lost contact with the barrier and was traveling at an exit speed and angle of 88.8 km/h (54.9 mph) and 7.9 degrees, respectively. As the vehicle continued forward, the vehicle yawed clockwise and came to rest 53.34 m (175 ft) downstream of impact and 1.83 m (6 ft) forward of the traffic face of the barrier. Sequential photographs of the test period are shown in Appendix H.

6.3.5 Test Article and Vehicle Damage

Damage to the barrier was mostly cosmetic, as shown in Figure 6.27 and Figure 6.28. In the soil forward of the face of the barrier, there were 2 cracks. The first was a 4 mm (0.16 in.) crack 1,321 mm (52 in.) forward of the traffic face of the barrier that started at the joint between barrier B2 and B3 and ended at the joint between barrier B5 and B6. The second was a 2 mm (0.08 in.) crack 1,372-1,727 mm (54-68 in.) forward of the traffic face of the barrier, starting 6 m (2 ft) upstream of the joint between barrier B0 and B1 and ending 0.6 m (2 ft) downstream of the joint between barrier B2 and B3. Length of contact of the vehicle with the barrier was 4.1 m (13.6 ft). No measurable deflection of the barrier occurred.

The 2270P vehicle sustained damage to the front left and left side, as shown in Figure 6.29. The left upper A-arm, left outer tie rod end, left frame rail and rear axle were deformed and the left upper ball joint broke. Also damaged were the front bumper, hood, grill, radiator and support, fan, left front fender, left front and rear doors, left and right exterior bed, rear bumper and tailgate. The windshield sustained stress cracks at the left lower corner which radiated upward toward the roof and center. Maximum exterior crush to the vehicle was 40 cm (15.75 in.) in the left side plane at the left front corner at bumper height. Maximum

occupant compartment deformation was 54 mm (2.1 in.) laterally across the cab at hip height in the instrument panel area. Photographs of the interior of the vehicle are shown in Figure 6.30.

6.3.6 Occupant Risk

Data from the accelerometer, located at the vehicle center of gravity, were digitized for evaluation of occupant risk and were computed as follows. In the longitudinal direction, the occupant impact velocity was 12.8 ft/s (3.9 m/s) at 0.088 s, the highest 10-msec occupant ridedown acceleration was -4.4 Gs from 0.088 to 0.098 sec, and the maximum 50-msec average acceleration was -6.5 Gs between 0.009 and 0.059 sec. In the lateral direction, the occupant impact velocity was 29.2 ft/s (8.9 m/s) at 0.088 sec, the highest 10-msec occupant ridedown acceleration was 9.2 Gs from 0.199 to 0.209 s, and the maximum 50-msec average was 15.7 × Gs between 0.037 and 0.087 sec. Theoretical Head Impact Velocity (THIV) was 34.6 km/h or 9.6 m/s at 0.087 sec; and Post-Impact Head Deceleration (PHD) was 9.3 Gs between 0.199 and 0.209 sec. These data and other pertinent information from the test are summarized in Figure 6.31.

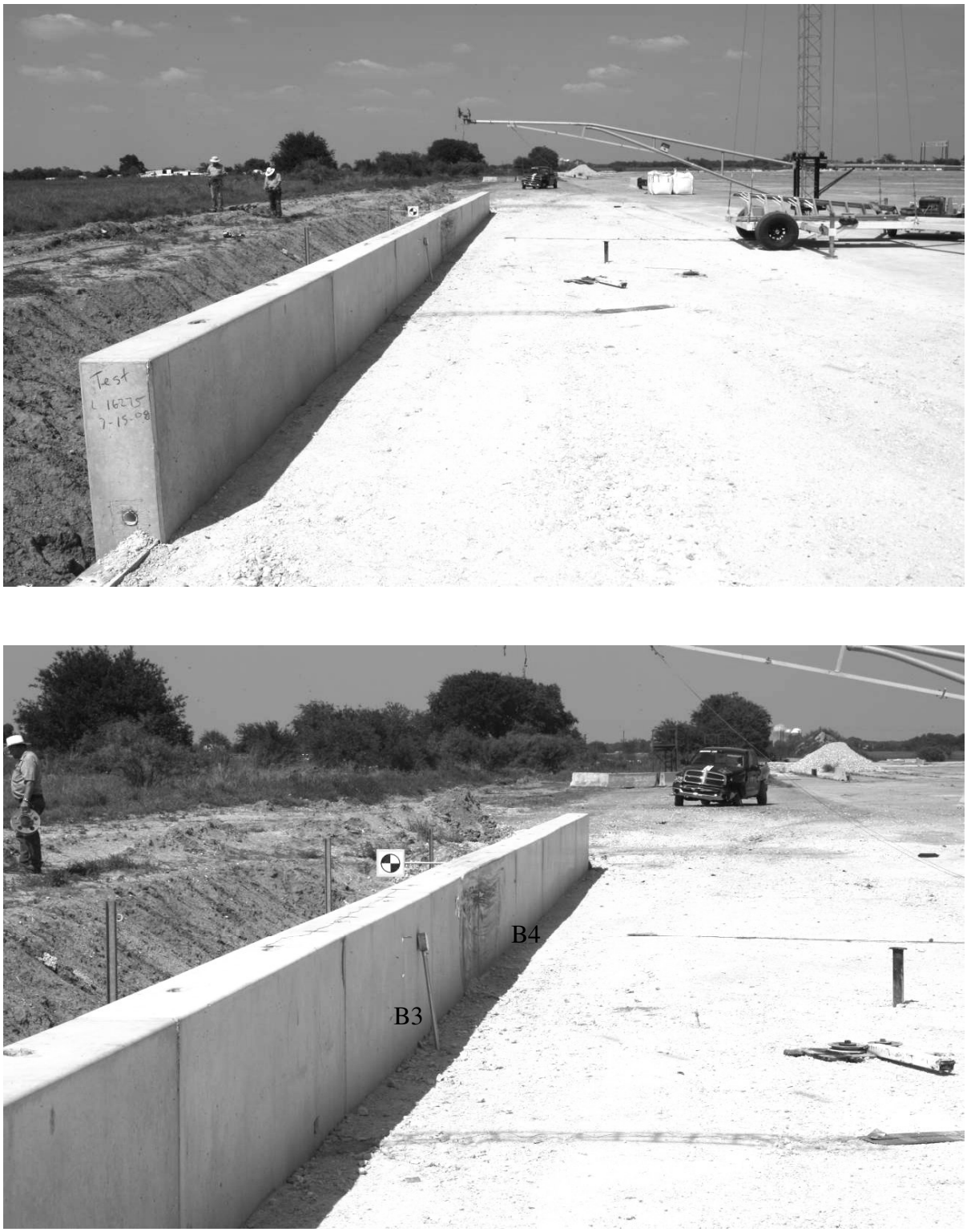

Figure 6.27 Vehicle trajectory path after test

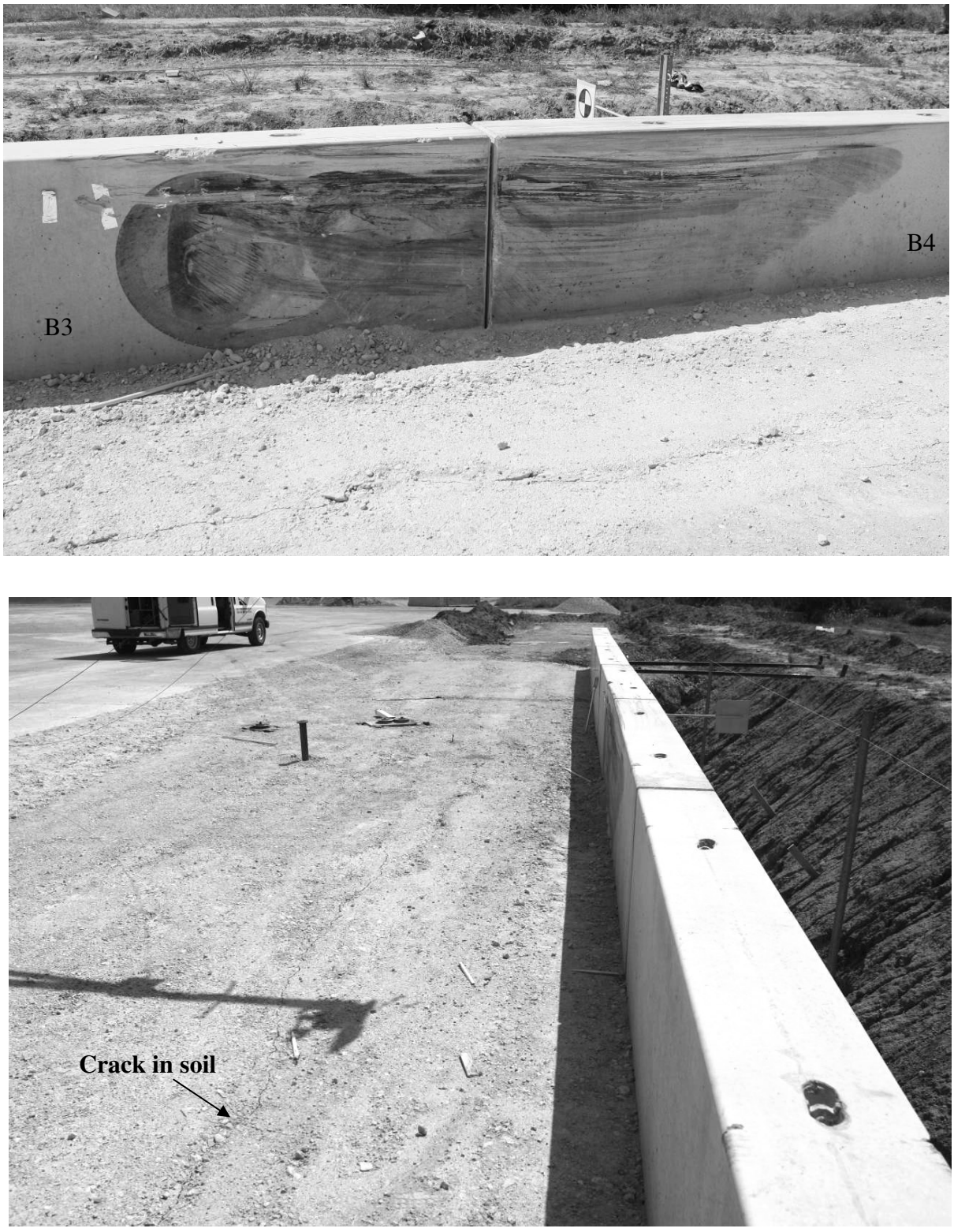

Figure 6.28 Installation after test

Figure 6.29 Vehicle after test

Before Test

After Test

Figure 6.30 Interior of vehicle for test

0.000 s

0.086 s

0.171 s

0.340 s

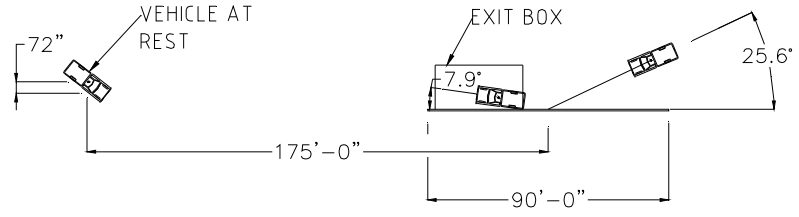

General Information
- Test Agency ..... Texas Transportation Institute
- Test No. 475350-1
- Date 2008-09-25

Test Article
- Type ..... 32 in. Vertical Barrier (T-221)
- Name ..... MSE Wall
- Installation Length ..... 90 ft
- Material or Key Elements .....

Soil Type and Condition ..... TxDOT Type B Backfill, Dry

Test Vehicle
- Type/Designation 2270P
- Make and Model ..... 2004 Dodge Ram 1500 Quad-Cab
- Curb ..... 4794 lb
- Test Inertial ..... 4951 lb
- Dummy ..... No. Dummy
- Gross Static ..... 4951 lb

Impact Conditions
- Speed ..... 63.2 mi/h
- Angle ..... 25.6 degrees
- Location/Orientation ..... 4.3 ft upstream of 4th joint

Exit Conditions
- Speed ..... 54.9 mi/h
- Angle ..... 7.9 degrees

Occupant Risk Values
- Impact Velocity
  - Longitudinal ..... 12.8 ft/s
  - Lateral ..... 29.2 ft/s
- Ridedown Accelerations
  - Longitudinal ..... -4.4 Gs
  - Lateral ..... 9.2 Gs
- THIV ..... 34.6 km/h
- PHD ..... 9.3 Gs
- Max. 0.050-s Average
  - Longitudinal ..... -6.5 Gs
  - Lateral ..... 15.7 Gs
  - Vertical ..... -3.7 Gs

Post-Impact Trajectory
- Stopping Distance ..... 175 ft downstream 6 ft toward traffic

Vehicle Stability
- Maximum Yaw Angle ..... 42 degrees @ 1.04 s
- Maximum Pitch Angle ..... -10 degrees @ 1.64 s
- Maximum Roll Angle ..... -39 degrees @ 0.58 s
- Vehicle Snagging ..... No
- Vehicle Pocketing ..... No

Test Article Deflections
- Dynamic 0
- Permanent 0
- Working Width 0

Vehicle Damage
- VDS 11LFQ5
- CDC 11FLEW4
- Max. Exterior Deformation ..... 15.75 inches
- Max. Occupant Compartment Deformation ..... 2.1 inches
- OCDI LF0000100

Figure 6.31 Summary of results for *MASH08* test 3-11 on the MSE wall

6.3.7 Data from Accelerometers

In order to estimate the impact force from the vehicle accelerometer data, Eq. (6-1) was used.

$$F_i = F_x \sin\phi - F_y \cos\phi = m(\overrightarrow{a_x} \sin\phi - \overrightarrow{a_y} \cos\phi) \quad (6\text{-}1)$$

where F_i is the impact force; ϕ is the impact angle (25 degrees); $F_x = m\overrightarrow{a_x}$ is the longitudinal component of truck impact force; $F_y = m\overrightarrow{a_y}$ is the horizontal component of truck impact force; and m is the mass of truck. The coordinate systems for the truck and barrier are schematically shown in Figure 6.32.

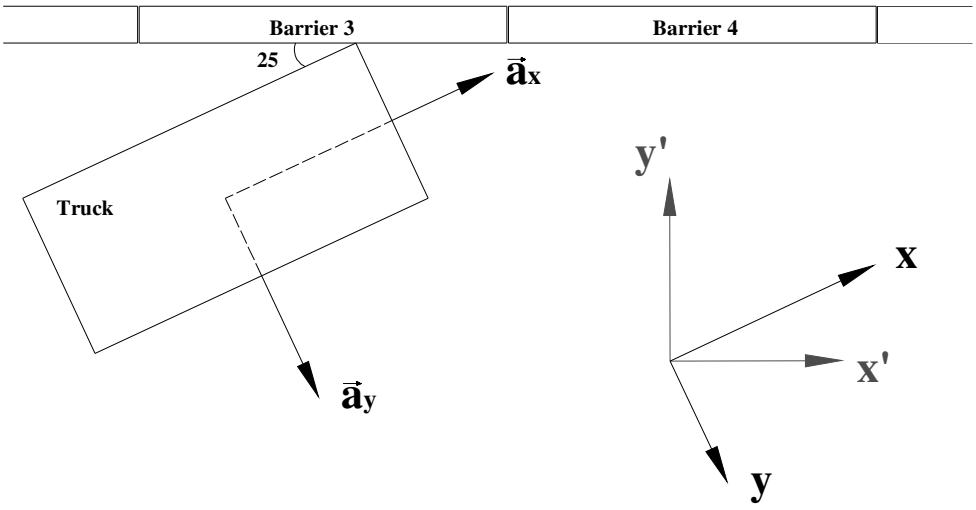

Figure 6.32 Coordinate to induce the impact force from accelerometer

Data obtained from the truck-mounted accelerometer were analyzed and the results are presented in Figure 6.33. As shown in Figure 6.33(a) and (b), the maximum 50-msec average longitudinal and lateral accelerations were -6.5 g and 15.67 g, respectively. Based on these accelerations and the mass of the truck, the maximum 50-msec average impact force was calculated to be 257.11 kN (57.8 kips). Comparison between the test results and simulation results shows reasonable agreement as shown in Figure 6.33(c). The impact force was 240 kN (54 kips) in simulation because the weight of truck used in simulation (2,000 kg or 4,409 lb) was less than the weight of the truck used in test (2,270 kg or 5,000 lb). The velocity-time history of the truck, which was calculated by integration of the acceleration data, is shown in Figure 6.33(d).

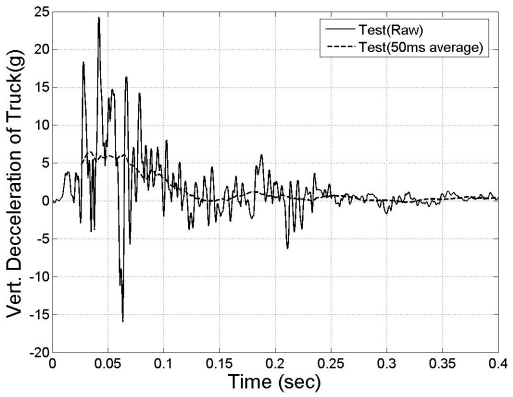

(a) Longitudinal deceleration

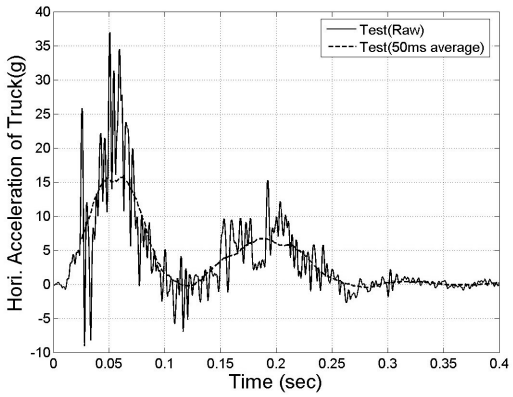

(b) Horizontal acceleration

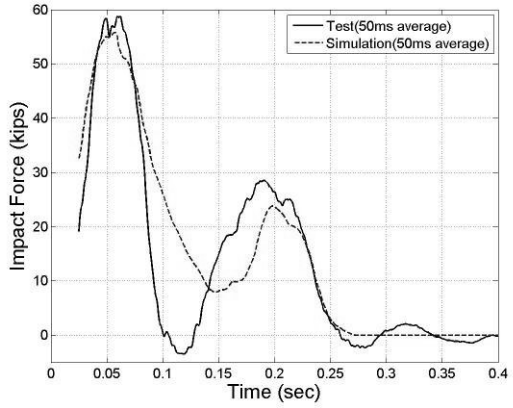

(c) Impact force

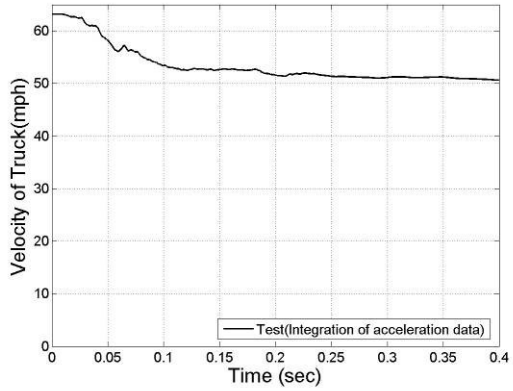

(d) Velocity

Figure 6.33 Acceleration, impact force and velocity of truck

The maximum 50-msec average acceleration of the barrier, as measured by the accelerometer at the top of the barrier, is shown Figure 6.34(a). The barrier acceleration oscillated in the range of 1.5g to -1.5g. Examination of the impact events helps explain the barrier acceleration-time history. The barrier initially accelerated toward the field side of the installation as a result of the initial impact. As the vehicle was redirecting, the barrier began to rebound and accelerate back toward the traffic side. The back slap impact of the rear of the vehicle once again resulted in an acceleration of the barrier toward the field side, followed by the barrier rebounding and accelerating back toward the traffic side.

The velocity-time history of the barrier, as calculated by integration of the raw acceleration data, is shown in Figure 6.34(b). Some error in this time history is evidently given that the velocity did not return to zero at the end of the test. This error is magnified in the displacement-time history obtained from integration of the velocity history. Figure 6.34(c) presents displacement-time history from both double integration of the acceleration data and from analysis of the high-speed film, which is considered to be more accurate.

The maximum 50-msec average acceleration of the moment slab is shown in Figure 6.35(a). The velocity-time and vertical displacement-time histories of the moment slab are shown in Figure 6.35(b) and Figure 6.35(c), respectively. The velocity-time history and displacement-time histories were calculated by integration of the acceleration data.

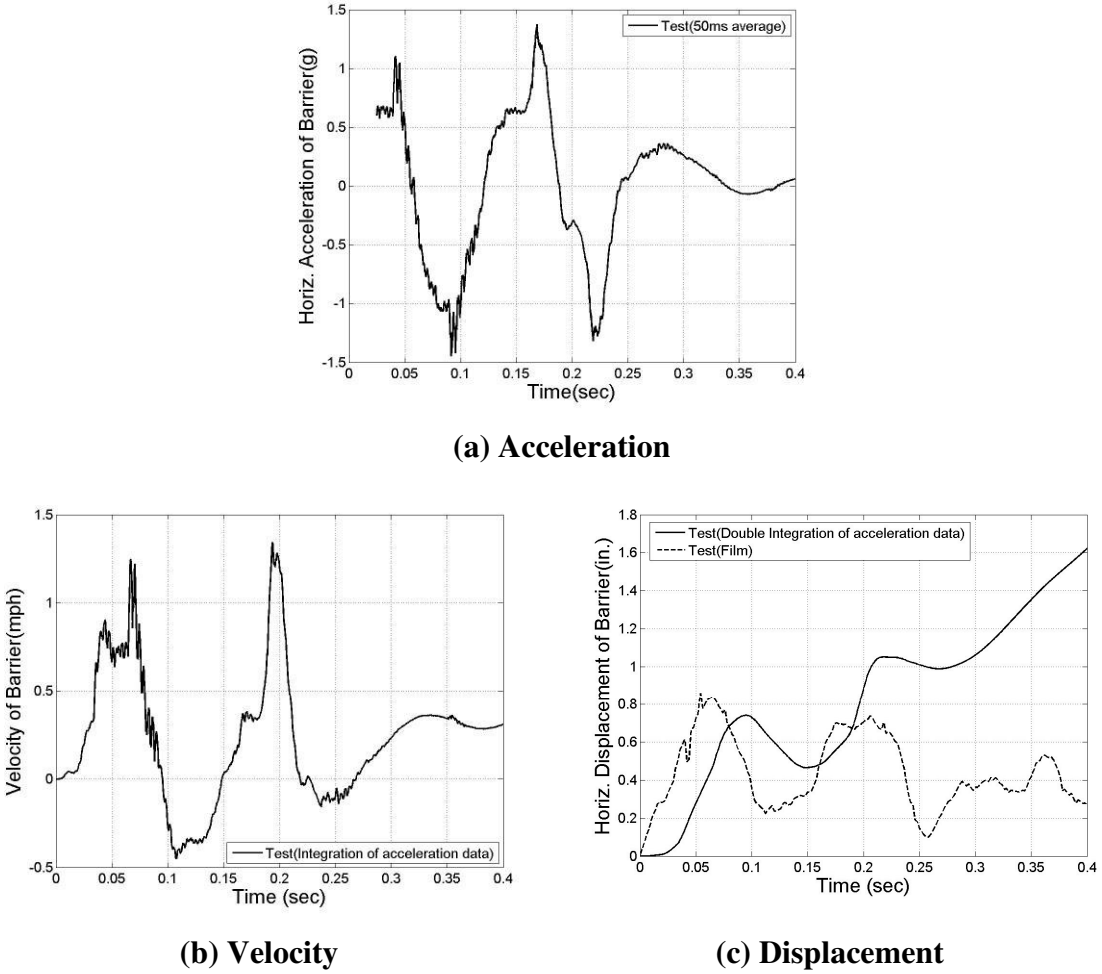

(a) Acceleration

(b) Velocity

(c) Displacement

Figure 6.34 Acceleration, velocity, and displacement of barrier

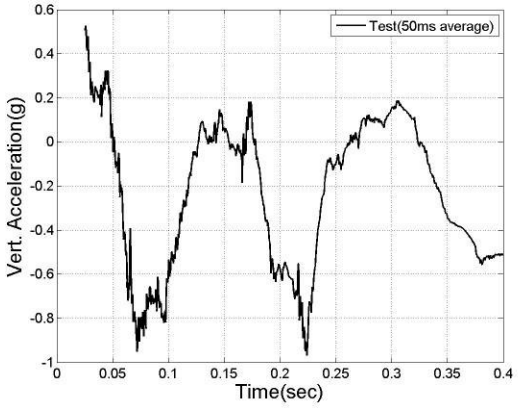

(a) Acceleration

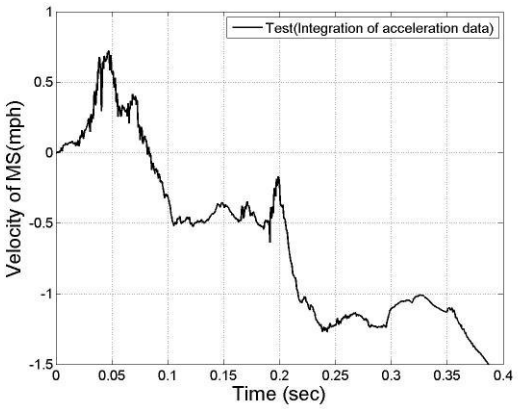

(b) Velocity

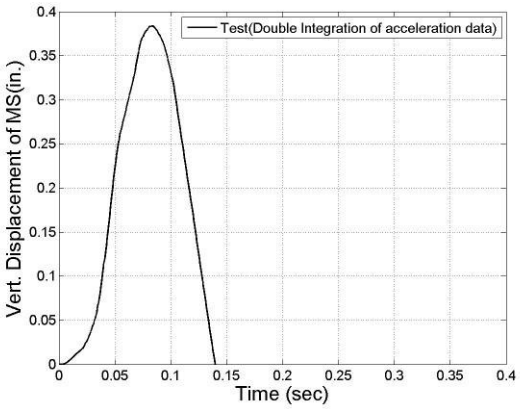

(c) Displacement

Figure 6.35 Acceleration, velocity, and displacement of moment slab

6.3.8 Photographic Instrumentation

Targets affixed to the displacement bars attached to the top and bottom of the barrier-coping section (see Figure 6.22 and Figure 6.36) were used as reference points to determine angular and translational displacement of the barrier from analysis of high-speed video. Two distinct impacts are evident in the displacement data corresponding to the front and rear vehicle-barrier contact. The dynamic displacement associated with the initial impact of the barrier was 2.13 cm (0.84 in.) at the top of the barrier and 1.3 cm (0.51 in.) at the bottom of the coping. After first impact, the barrier began to rebound. The subsequent rear impact (back slap) resulted in the dynamic displacements at the top of the barrier and bottom of the coping of 1.88 cm (0.74 in.) and 1.4 cm (0.55 in.), respectively. The permanent displacement of the barrier was 94 mm (0.37 in.) at the top of the barrier and 6.4 mm (0.25 in.) at the bottom of the coping.

Three additional targets affixed to the displacement bars attached to the wall panel at locations corresponding to these layers of wall reinforcement were used to determine angular and translational displacement of the panel from analysis of high-speed video. From the film analysis, the maximum dynamic displacement of the panel was 10.7 mm (0.42 in.) at the upper most layer of reinforcement. The permanent displacement of the panel was 6.1 mm (0.24 in.) at the upper reinforcement layer. No movement was measured at the second reinforcement layer.

Figure 6.36 Location of displacement bars affixed on the barrier and panels

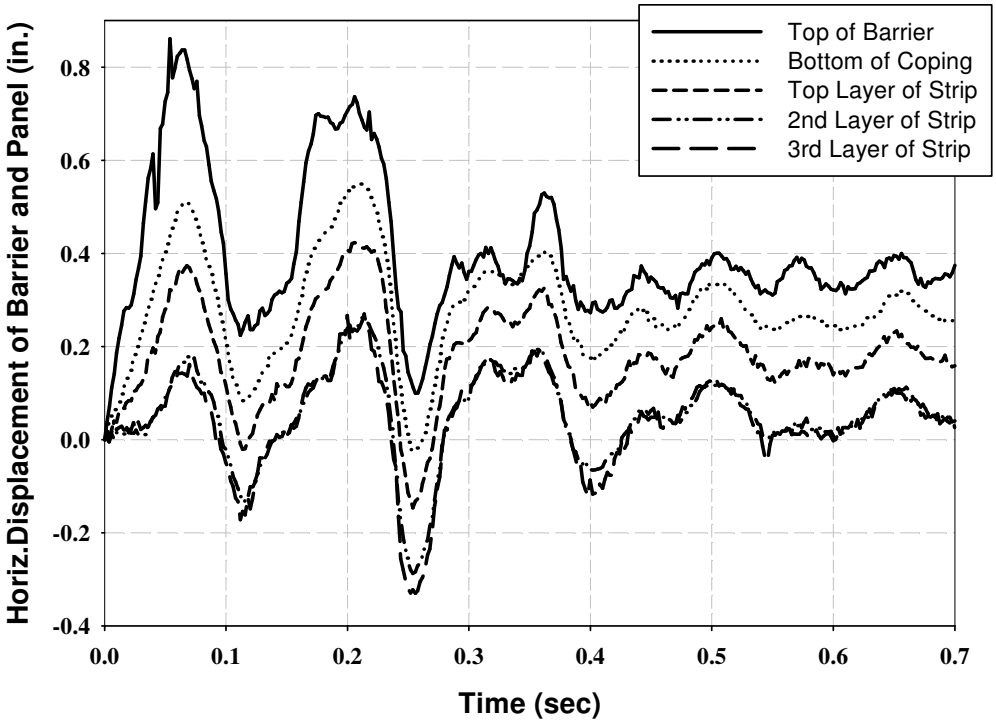

Figure 6.37 Horizontal displacement of barrier and panel (Film)

6.3.9 Load on the Strip from Strain Gages

A total of 7 wall reinforcement strips were instrumented with two strain gages (top and bottom) to capture the tensile forces transmitted into the reinforcement during the vehicle impact. To enable comparison of forces and displacements, barriers and selected strip locations have been assigned alphanumeric designators that describe their horizontal position and vertical reinforcement layer. For example, strip "B4-F-1st" is positioned beneath the downstream end of the fourth barrier in the first (i.e., upper) layer of reinforcement as shown in Figure 6.38.

Raw data obtained from the strain gages on the strips were analyzed and the results are presented in Figure 6.39. The 50-msec average of the raw data was analyzed to obtain design loads for the strips, and the results are presented in Figure 6.40. As previously noted, the impact load was 257.11 kN (57.8 kips) at 0.05 sec, which is close to the barrier design load of 240 kN (54 kips) prescribed by AASHTO. A summary of the maximum dynamic loads measured in the strips is shown in Table 6.3.

The static load in the strips was measured during the construction to allow computation of the total load in the strips during impact. The average static load in the uppermost layer of reinforcement was 3.34 kN (0.75 kips) and the average static load in the second layer of reinforcement was 8.23 kN (1.85 kips). A comparison of the measured static loads with those calculated by AASHTO LRFD is shown in Table 6.4.

Table 6.5 shows the total measured load (measured static load + measured dynamic load) in the reinforcement strips in comparison to the calculated resistance of the strips using the AASHTO LRFD 11.10.6.3.2-1. The pullout resistance of the strip was calculated to be 9.56 kN (2.15 kips) at uppermost layer of strips and 15.4 kN (3.46 kips) at the second layer.

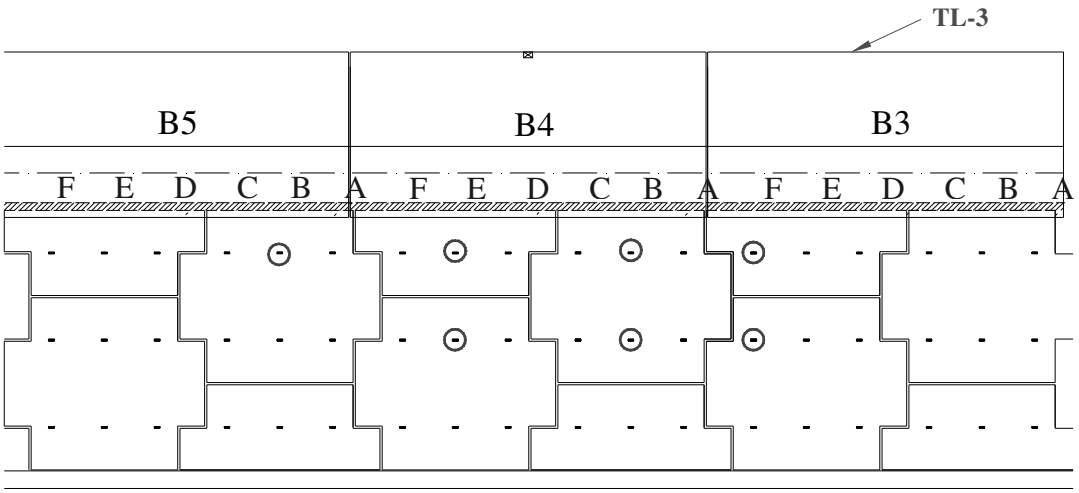

Figure 6.38 Location indicators for strain gages on the strips

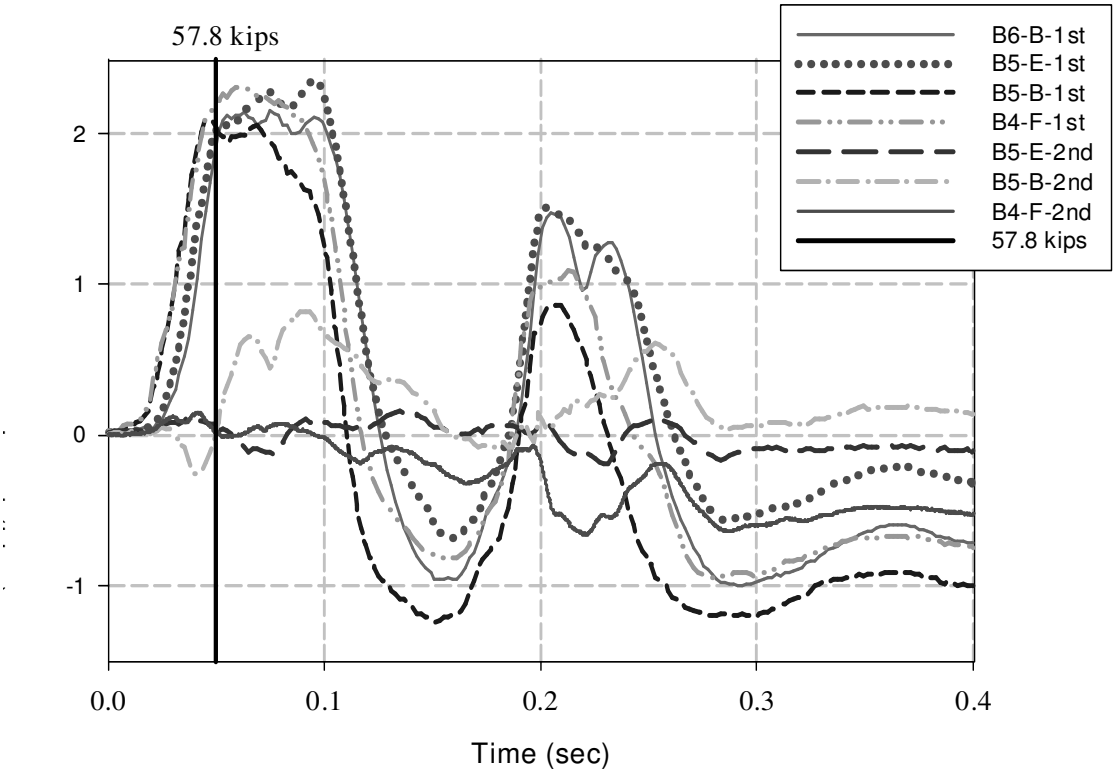

Figure 6.39 Dynamic strip load of raw data on the strips

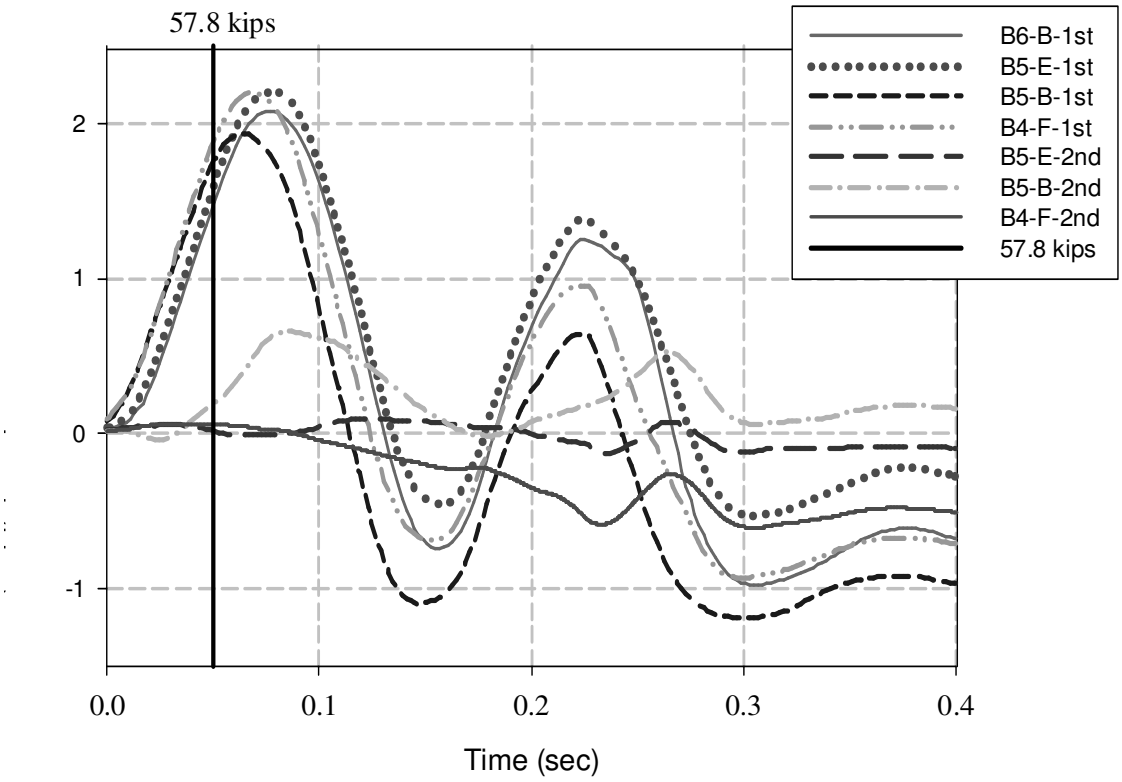

Figure 6.40 Dynamic strip load of 50 msec average on the strips

Table 6.3 Dynamic Loads on the Wall Reinforcement

	Top layer (kips)			
	B5-B-1st	B4-E-1st	B3-B-1st	B2-F-1st
Maximum Load from Raw Data	2.15	2.37	2.10	2.32
Maximum 50 msec avg. Load	2.08	2.21	1.94	2.20
	Second Layer (kips)			
		B4-E-2nd	B4-B-2nd	B3-F-2nd
Maximum Load from Raw Data		0.16	0.83	0.15
Maximum 50 msec avg. Load		0.09	0.66	0.06

Table 6.4 Static Loads on the Wall Reinforcement

	Static Load By measured (kips)	Static Load By AASHTO (kips)
Top Layer	0.75	0.66
Second Layer	1.85	1.18

Table 6.5 Total Loads on the Wall Reinforcement

	Static Load By measured (kips)	Dynamic Load * By measured (kips)	Total Loads (kips)	Resistance By AASHTO** (kips)
Top Layer	0.75	2.20	2.69	2.15
Second Layer	1.85	0.66	2.51	3.46

*: Dynamic load was used maximum one of the 4 max. 50 msec average load.

**: AASHTO LRFD 11.10.6.3.2-1

6.3.10 Panel Analysis

The wall panel was instrumented with three strain gages to capture the strains in the panel at points corresponding to the three layers of wall reinforcement. Figure 6.41 shows the 50-msec average strain time history of the panel at each reinforcement layer. The maximum strain in the panel occurred at a point corresponding to the upper layer of reinforcement and had a magnitude of 55.3 microstrains.

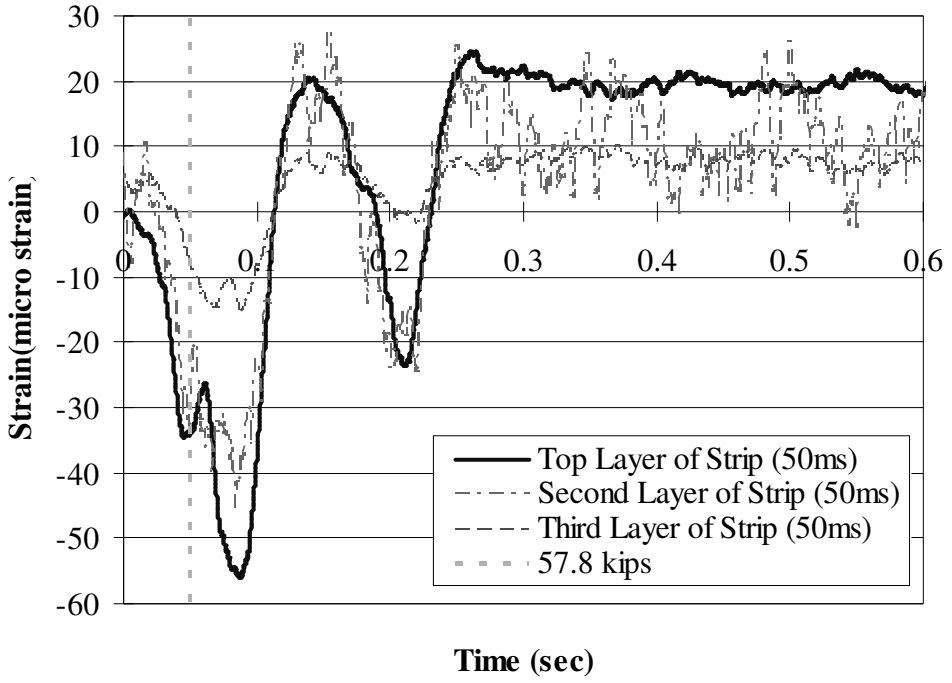

Figure 6.41 Strain on the panel

6.3.11 Other Instrumentations

String lines located 108 cm (3.54 ft) from the face of wall panels were used to measure the permanent deflection of the barriers and panels after vehicle impact at different elevations. After vehicle impact, the permanent deflection ranged from 13 mm (0.51 in.) at the top of barrier segment "B4" to 1 mm (0.04 in.) at the bottom of the coping on barrier segment "B5" as shown in Figure 6.42. The maximum residual displacement occurred at the joint of barrier segment "B3" and "B4". The permanent deflection obtained from the film analysis, which tracked targets affixed to the barrier-coping section, was 9.4 mm (0.37 in.) at top of the barrier and 6.4 mm (0.25 in.) at the bottom of the coping. Note that the location of the target is the centerline of the panel (B5-H6).

The permanent defection of the wall panels ranged from 5 mm (0.20in.) to 1 mm (0.04 in.) as shown in Figure 6.42. Note that negative values indicate movement toward the traffic side of the barrier. Such movement may be the result of the panel being loaded eccentrically and experiencing some rotation. The contact switch placed on the top edge of the level-up

concrete on top of the wall panels inside the coping recess indicated that the coping did not contact the wall panel.

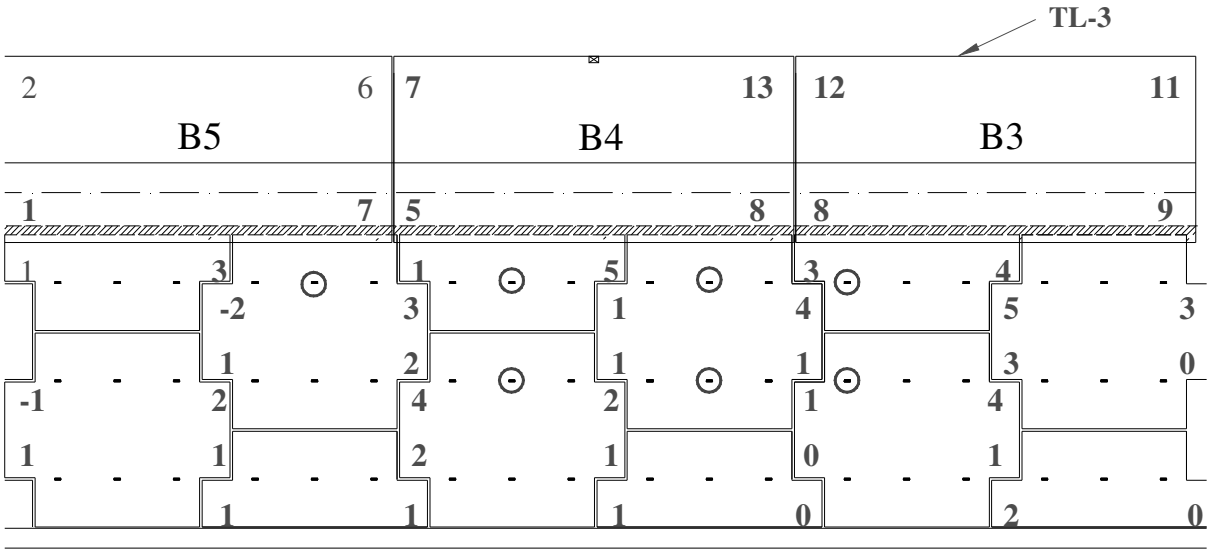

Figure 6.42 Permanent deflection of barrier and panels (units: mm).

6.4 Conclusions

The roadside barrier mounted on the edge of the MSE wall performed acceptably according to the evaluation criteria specified for *MASH* test designation 3-11, as shown in Table 6.6.

The roadside barrier on MSE wall contained and redirected the 2270P vehicle. The vehicle did not penetrate, underride, or override the installation. No lateral movement of the barrier was noted. No detached elements, fragments, or other debris was present to penetrate or show potential for penetrating the occupant compartment, or to present hazard to others in the area. Maximum occupant compartment deformation was 5.33 cm (2.1 in.) in the lateral area across the cab. The 2270P vehicle remained upright during and after the collision event. Maximum roll was 39 degrees. Occupant risk factors were within the limits specified in *MASH*.

Table 6.6 Performance Evaluation Summary for MASH08 Test 3-11 on the MSE Wall.

Test Agency: Texas Transportation Institute Test No.: 475350-1 Test Date: 2008-09-25

***MASH08* Evaluation Criteria**	Test Results	Assessment
Structural Adequacy		
A. Test article should contain and redirect the vehicle or bring the vehicle to a controlled stop; the vehicle should not penetrate, underride, or override the installation although controlled lateral deflection of the test article is acceptable	The roadside barrier on MSE wall contained and redirected the 2270P vehicle. The vehicle did not penetrate, underride, or override the installation. No lateral movement of the barrier was noted.	Pass
Occupant Risk		
D. Detached elements, fragments, or other debris from the test article should not penetrate or show potential for penetrating the occupant compartment, or present an undue hazard to other traffic, pedestrians, or personnel in a work zone.	No detached elements, fragments, or other debris was present to penetrate or show potential for penetrating the occupant compartment, or to present hazard to others in the area.	Pass
Deformations of, or intrusions into, the occupant compartment should not exceed limits set forth in Section 5.3 and Appendix E of MASH08.	Maximum occupant compartment deformation was 2.1 inches in the lateral area across the cab.	Pass
F. The vehicle should remain upright during and after collision. The maximum roll and pitch angles are not to exceed 75 degrees.	The 2270P vehicle remained upright during and after the collision event. Maximum roll was 39 degrees.	Pass
H. Longitudinal and lateral occupant impact velocities should fall below the preferred value of 9.1 m/s (30 ft/s), or at least below the maximum allowable value of 12.2 m/s (40 ft/s).	Longitudinal occupant impact velocity was 12.8 ft/s, and lateral occupant impact velocity was 29.2 ft/s.	Pass
I. Longitudinal and lateral occupant ridedown accelerations should fall below the preferred value of 15.0 Gs, or at least below the maximum allowable value of 20.49 Gs.	Longitudinal ridedown acceleration was -4.4 Gs, and lateral ridedown acceleration was 9.2 Gs.	Pass
Vehicle Trajectory		
For redirective devices, the vehicle shall exit the barrier within the exit box.	The 2270P vehicle did not cross the exit box.	

6.5 Comparison of Test and Simulation

A comparison between the results of the TL-3 test and the numerical simulations was conducted to establish confidence in the simulation for use in the guideline development process. Since the numerical simulation was modeled prior to perform the TL-3 test, the differences between the TL-3 test and simulation are shown

1- While a 27.43 m (90 ft) long MSE wall was constructed for the test, a18.28 m (60 ft) long MSE wall was modeled to reduce computational costs of the simulation.
2- While the wall was two full panels high (3.05 m or 10 ft) in the simulation, the test used a wall that was one and half panels high (2.29 m or 7.5 ft) as shown in Figure 6.43. However, the simulation results indicate that the load in the fourth layer of strips was negligible.
3- The simulation model had a density of 3 strips per layer per panel in the first layer and 2 strips per layer per panel in the other layers. In the test, all layers of reinforcement ahd a density of 3 strips per layer per panel.
4- The panel orientation at the location of impact (see circle in Figure 6.43) was different in simulation and test. However, this should not affect the loads in the strips.
5- The C2500 pick truck model (reflective of NCHRP Report 350) was used in the simulation has different characteristics than the 2270P truck (reflective of MASH) used in the TL-3 test as shown in Figure 6.44.
6- The coping detail of the barrier differed between model and test installation as shown in Figure 6.45. Although field practice varies, the 25.4 cm (10 in.) coping depth and 10.16 cm (4 in.) high leveling pad used in the simulation is considered to be a typical detail. However, because the test barrier sections were cast using forms developed for a concrete pavement application and the depth of the recess had to be adjusted for the asphalt concrete application to provide the necessary strength in the coping section.

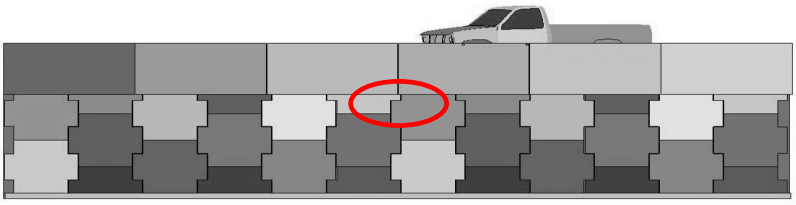

(a) Simulation

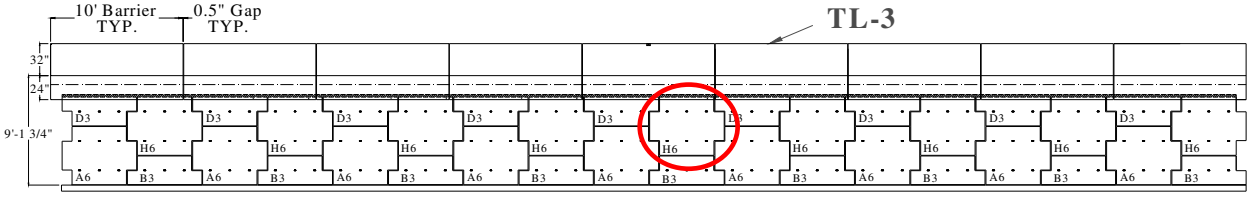

(b) TL-3 Test

Figure 6.43 Difference of wall panel details

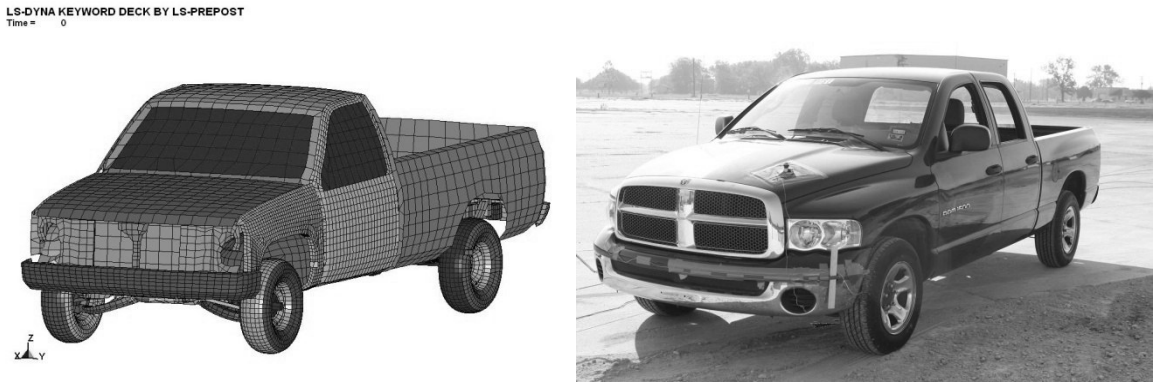

Figure 6.44 Comparison of truck of (a) simulation and (b) TL-3 test

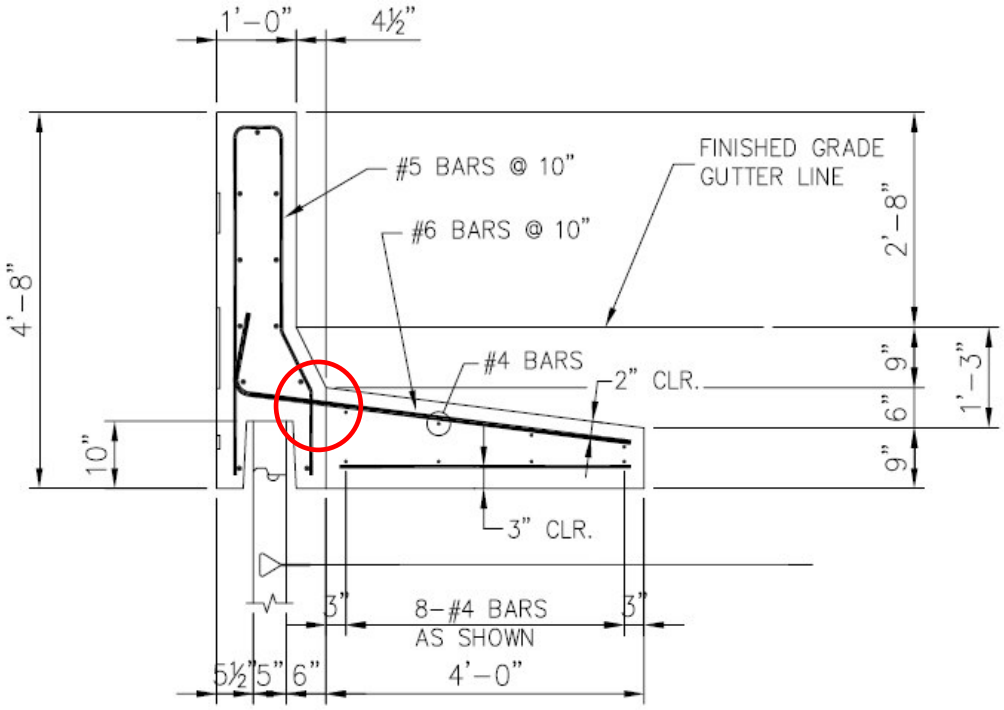

(a) Simulation

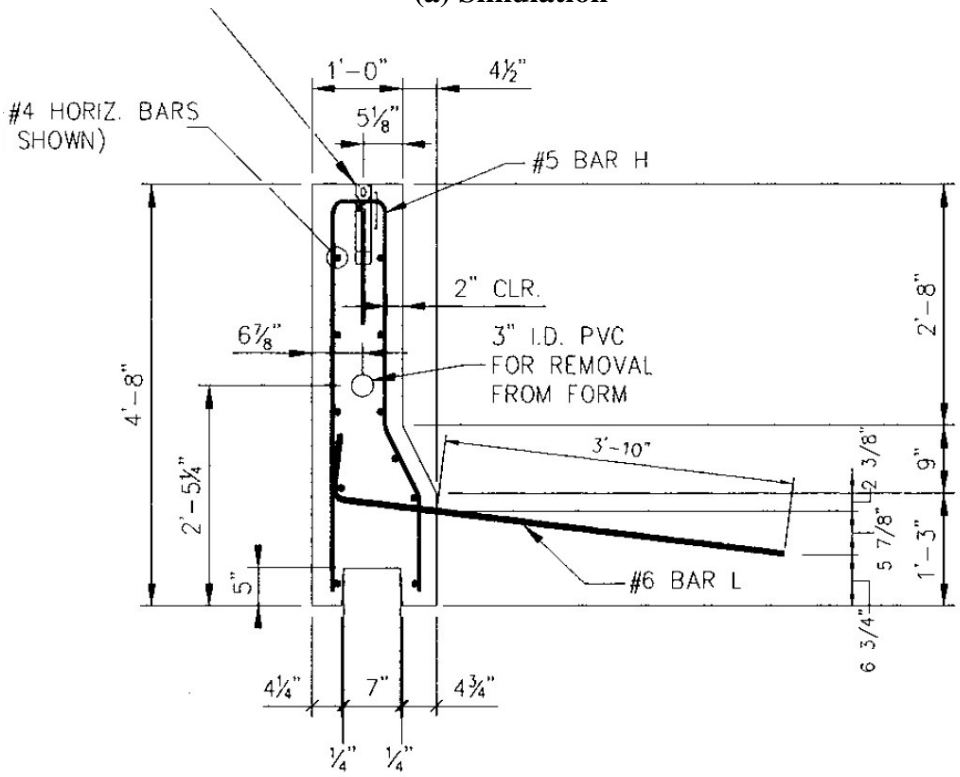

(b) TL-3 Test

Figure 6.45 Difference of barrier details

Sequential images from the simulation and TL-3 test are shown in Figure 6.46. The correlation is considered reasonable give the difference in pickup truck body styles. In addition, the maximum 50-msec average impact loads on the barrier were 248.21 kN (55.8 kips) in the simulation and 257.11 kN (57.8 kips) in the TL-3 test as shown in Figure 6.47. The displacement of barrier is shown in Figure 6.48. The simulation overpredicts the displacement at the top of the barrier.

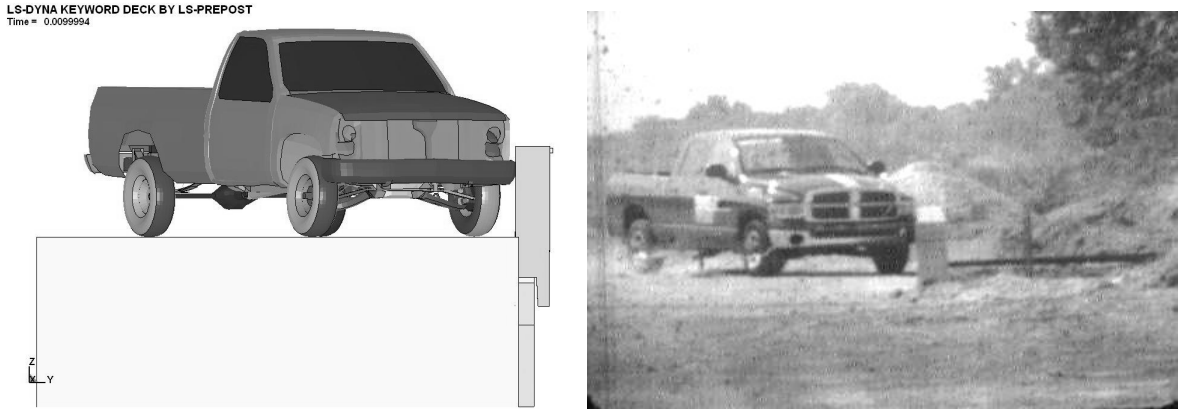

(a) 0 sec

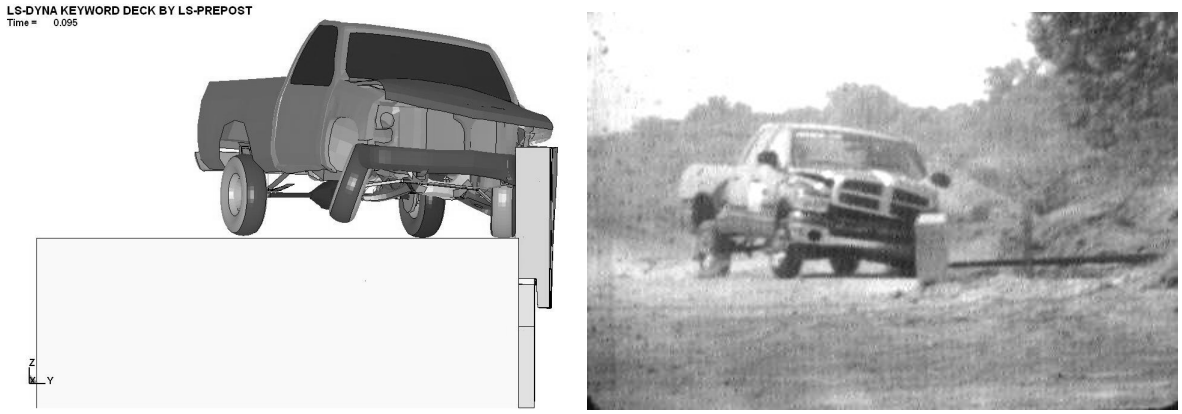

(b) 0.085 sec

Figure 6.46 Comparison of sequential photos

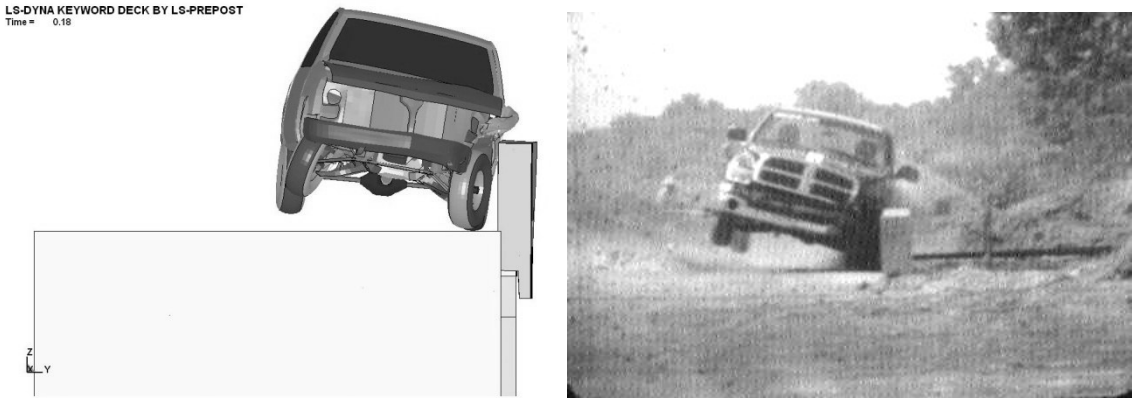

(c) 0.17 sec

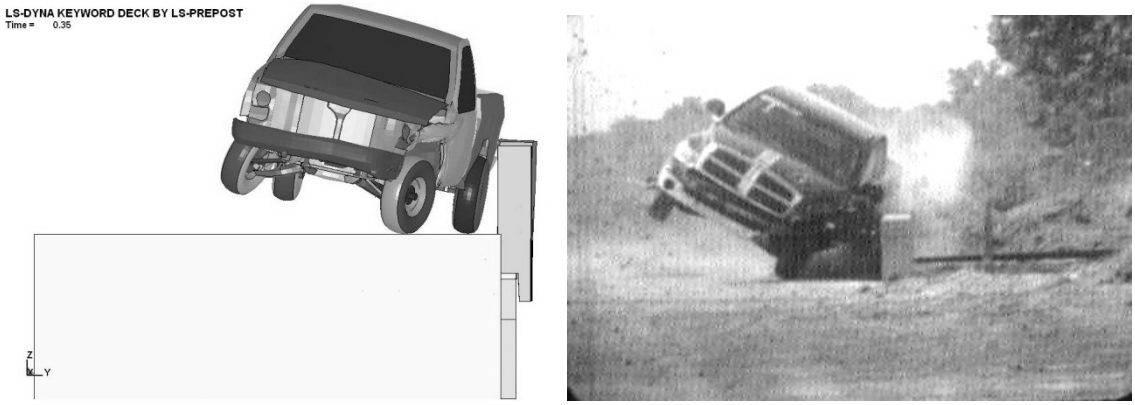

(d) 0.34 sec

Figure 6.46 Comparison of sequential photos (Continued)

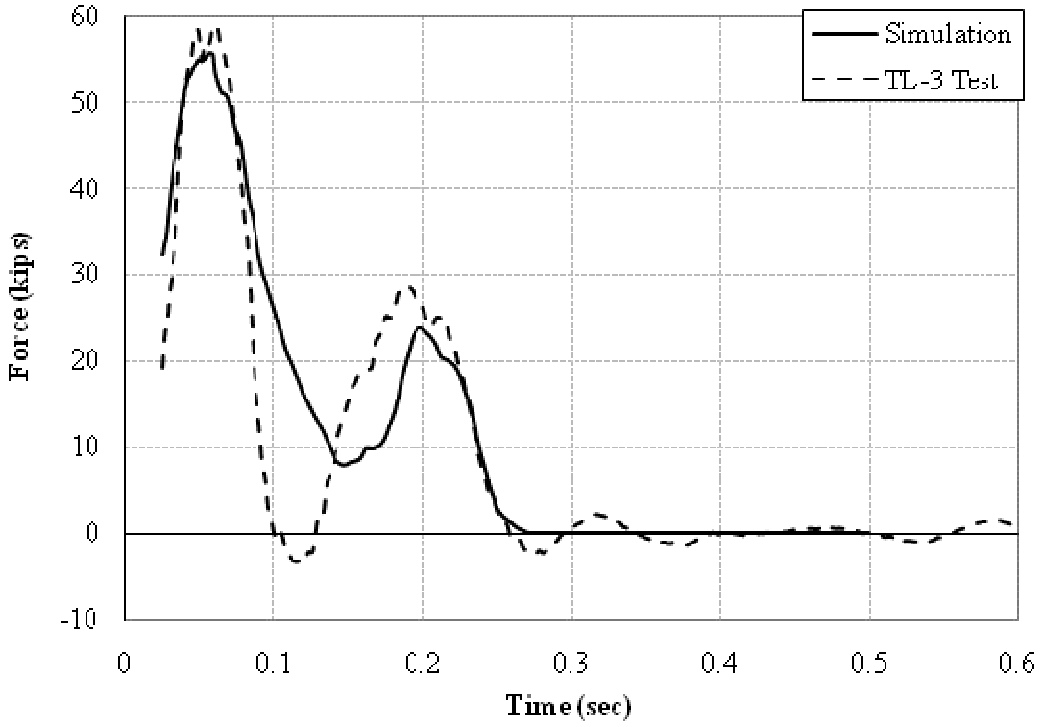

Figure 6.47 Impact load on the barrier

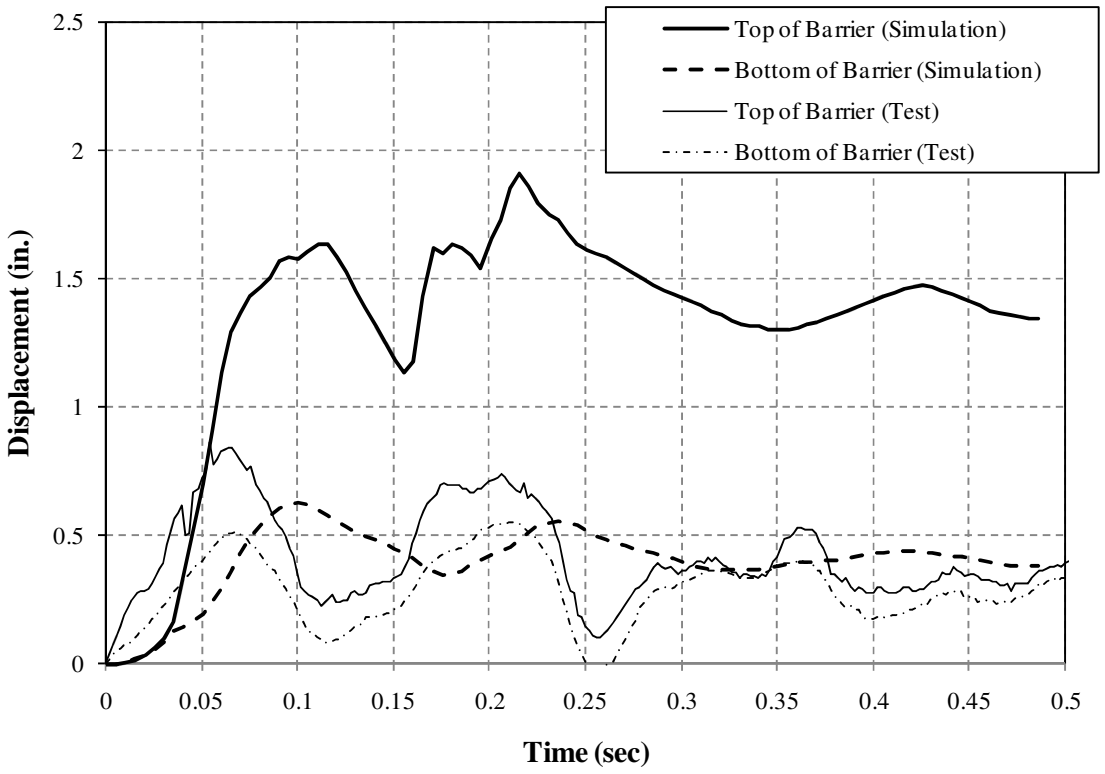

Figure 6.48 Displacement of barrier

The strip load in the simulation includes the static load due to earth pressure and the dynamic load due to the barrier impact. Therefore, the measured average static load in the reinforcement (Table 6.4) was substracted from the simulated strip load to provide a simulated dynamic impact load to the measured dynamic impact load (Table 6.7 and Figure 6.49). The simulation overpredicted the maximum strip load in the upper layer of reinforcement but captured the trands in the load-time history of the strip (Figure 6.49(a)). The simulation underpredicted the maximum strip load in the second layer of reinforcement but captured the trands in the load-time history of the strip (Figure 6.49(b)).

Table 6.7 Total Loads on the Wall Reinforcement

	Static Load By measured (kips)	Dynamic Load By measured (kips)	Dynamic Load by simulation (kips)
Top Layer	0.75	2.20	3.39
Second Layer	1.85	0.66	-

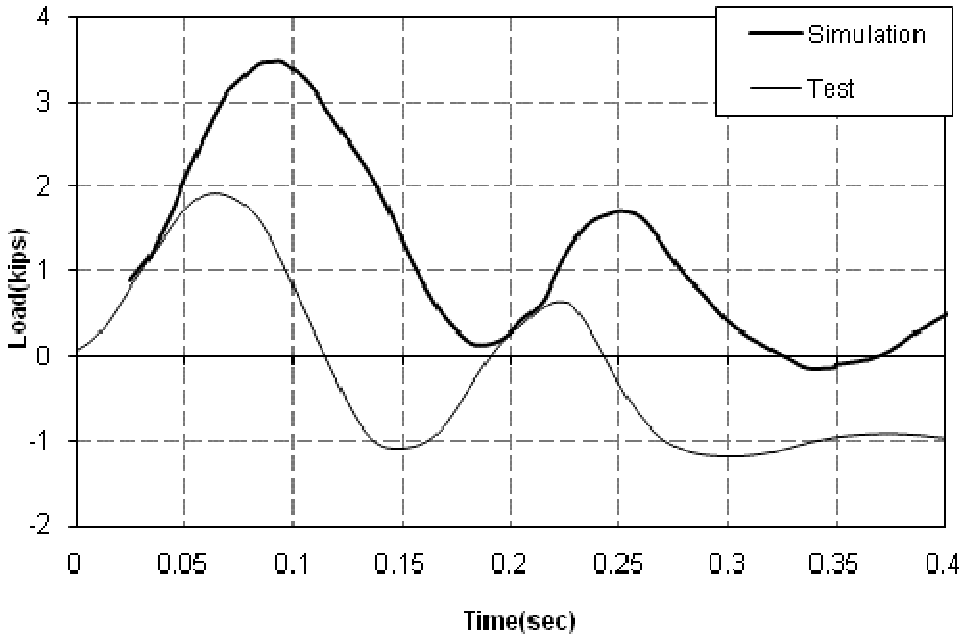

(a) First layer of strip

Figure 6.49 Comparison of 50 msec average data of load on the strip.

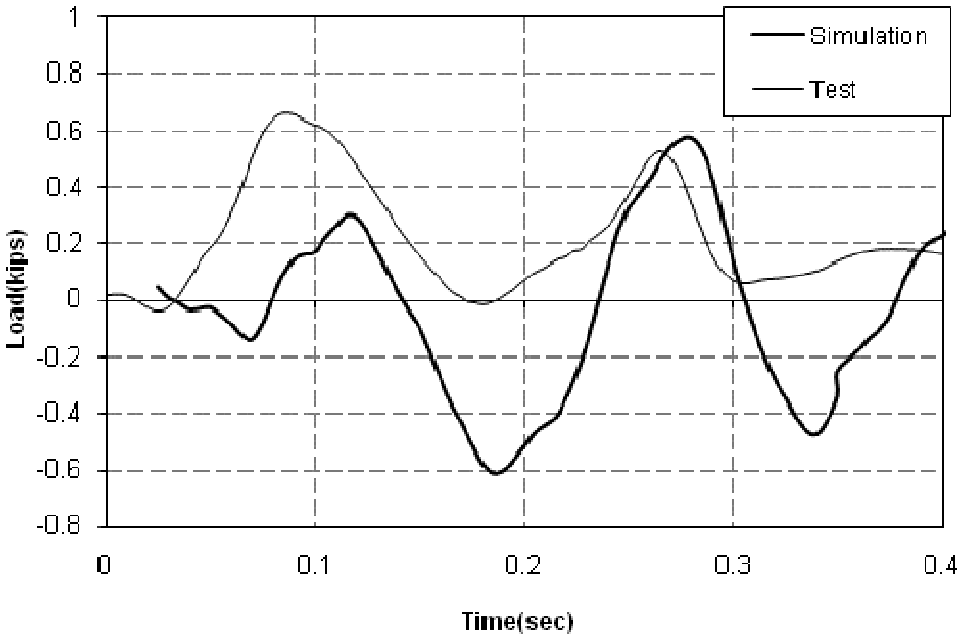

(a) Second layer of strip

Figure 6.49 Comparison of 50 msec average data of load on the strip (Continued).

The strain on the wall panel was evaluated as shown in Figure 6.50. The maximum compressive strain was about 60 microstrain at 0.08 sec in the test, and about 18 micro strain at 0.065 sec in the simulation. In the simulation, the impact occurred above a half panel rather than a full height panel so the estimated panel strain was smaller than in the test.

As can be seen the comparison, the simulation is closer to the results of TL-3 test. This simulation and test was evaluated to support the verification of design guidelines.

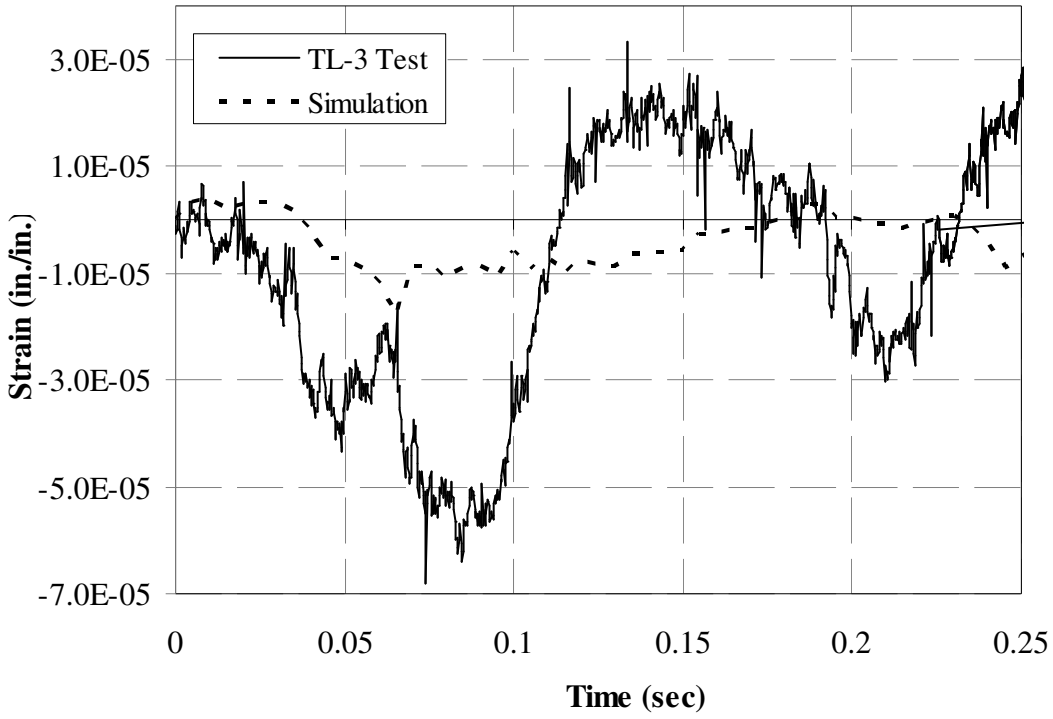

Figure 6.50 Comparison of panel strain at B4-A1.

7 DESIGN GUIDELINES

Design guidelines were developed as part of this project for three components:

- the barrier moment slab system,
- the MSE wall reinforcement and
- the wall panel.

The guidelines set in terms of AASHTO Load and Resistance Factor Design (LRFD). Depending on the design, two points of rotation are possible as shown in Figure 7.1. The point of rotation should be determined based on the interaction between the barrier coping and top wall panel. With reference to Figure 7.1, the point of rotation should be taken as Point A if the top of the wall panel is isolated from contact with the coping by presence of an air gap or sufficiently compressible material. The point of rotation should be taken as Point B if there is direct bearing between the bottom of the coping and the top of the wall panel or level up concrete.

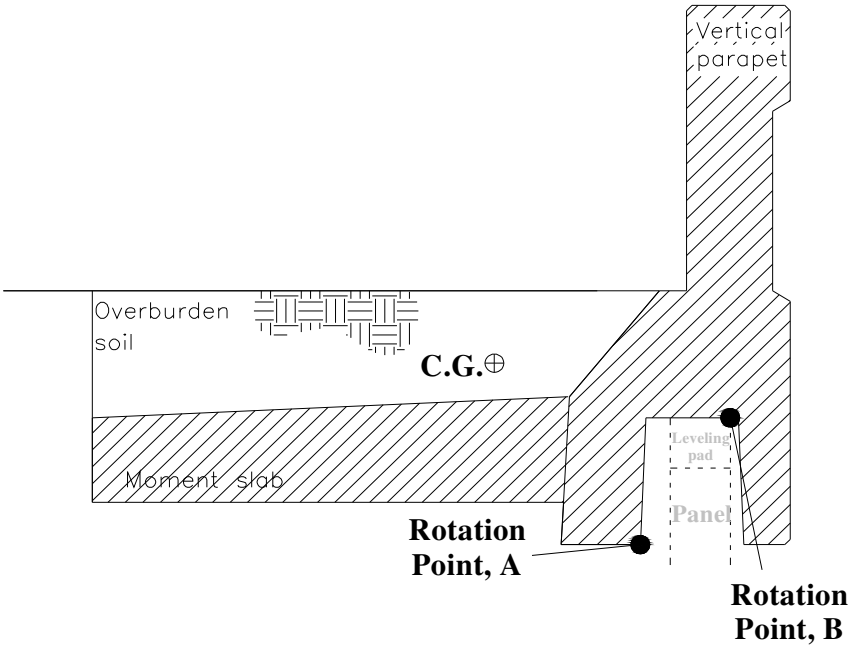

Figure 7.1 Barrier-moment slab system for design guideline

7.1 Guidelines for the Barrier

The barrier, the coping, and moment slab should be safe against structural failure. A barrier should be designed according to AASHTO LRFD Chapter 13 (*1*). Any section along the coping and moment slab should not fail in bending when the barrier is subjected a design impact load. Two modes of stability failure are possible in addition to structural failure of the barrier system. They are sliding and overturning of the barrier-moment slab system.

7.1.1 Sliding of the Barrier

The factored static resistance (ϕ P) to sliding of the barrier-moment slab system along its base should be greater than or equal to the factored equvalent static load (γ L_s) due to the dynamic impact force (Figure 7.2).

$$\phi P \geq \gamma L_s \tag{7-1}$$

(For the load level TL-3, Ls is 44.48 kN (10 kips), ϕ resistance factor is 0.8 (AASHTO Table 10.5.5-1), and γ load factor is 1.0 (extreme event)).

The static force P should be calculated as:

$$P = W \tan\varphi \tag{7-2}$$

where W is the weight of the monolithic section of barrier and moment slab plus any material laying on top of the moment slab and φ is the friction angle of the soil. The factored equivalent static load should be applied to the length of the moment slab between joints. Any coupling between adjacent moment slabs or friction that may exist between free edges of the moment slab and the surrounding soil should be neglected.

7.1.2 Overturning of the Barrier

The factored static moment resistance (ϕ M) to overturning of the barrier-moment slab system should be greater than or equal to the factored static load (γ L_s) due to the impact force times the moment arm h_a or h_b taken as the vertical distance from the point of impact due to the dynamic force to the point of rotation A or B (Figure 7.2).

$$\phi M \geq \gamma L_s (h_A \text{ or } h_B) \quad (7\text{-}3)$$

(For the load level TL-3, L_s is 44.48 kN (10 kips), ϕ resistance factor is 0.9, and γ load factor is 1.0 (extreme event)).

M should be calculated as:

$$M = W (l_A \text{ or } l_B) \quad (7\text{-}4)$$

where W is the weight of the monolithic section of barrier and moment slab plus any material laying on top of the moment slab, and l_A or l_B is the horizontal distance from the center of gravity of the weight W to the point of rotation A or B. The moment contribution due to any coupling between adjacent moment slabs, shear strength of the overburnden soil, or friction which may exist between the backside of the moment slab and the surrounding soil should be neglected.

7.1.3 Breaking of the Coping in Bending

The factored dynamic moment resistance (ϕM_d) to breaking of the coping in bending of the barrier-moment slab system should be greater than or equal to the factored dynamic load (γL_d) times the moment arm h_c taken as the vertical distance from the point of impact of the dynamic force to the middle of the weakest section of the coping (Figure 7.3).

$$\phi M_d \geq \gamma L_d (h_c) \quad (7\text{-}5)$$

(For the load level TL-3, L_d is 240.2 kN (54 kips), ϕ resistance factor is 0.9, and γ load factor is 1.0 (extreme event)).

M_d is the ultimate moment of the weakest section of the coping.

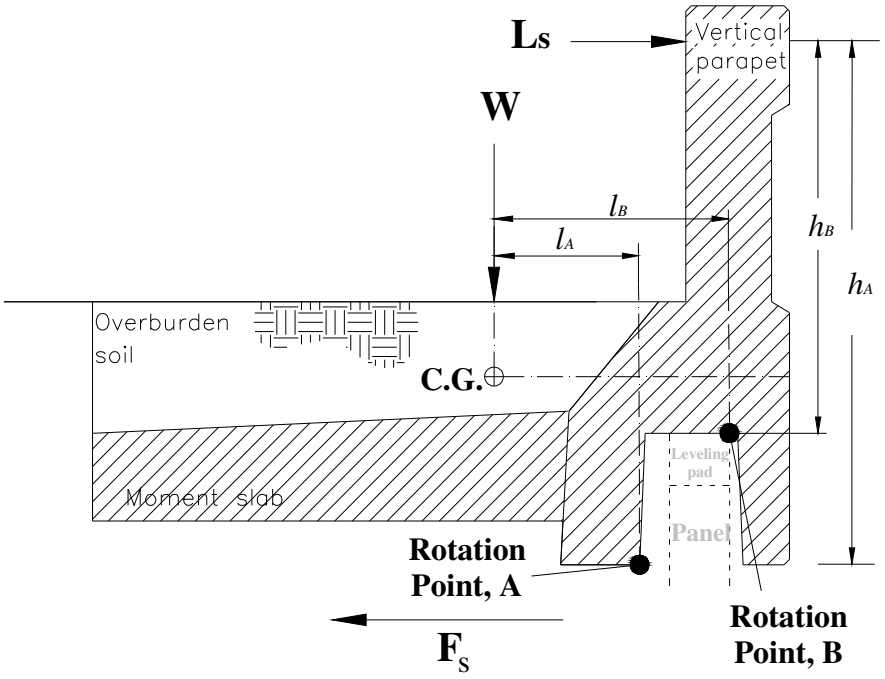

Figure 7.2 Barrier-moment slab system for barrier design guideline (sliding and overturning)

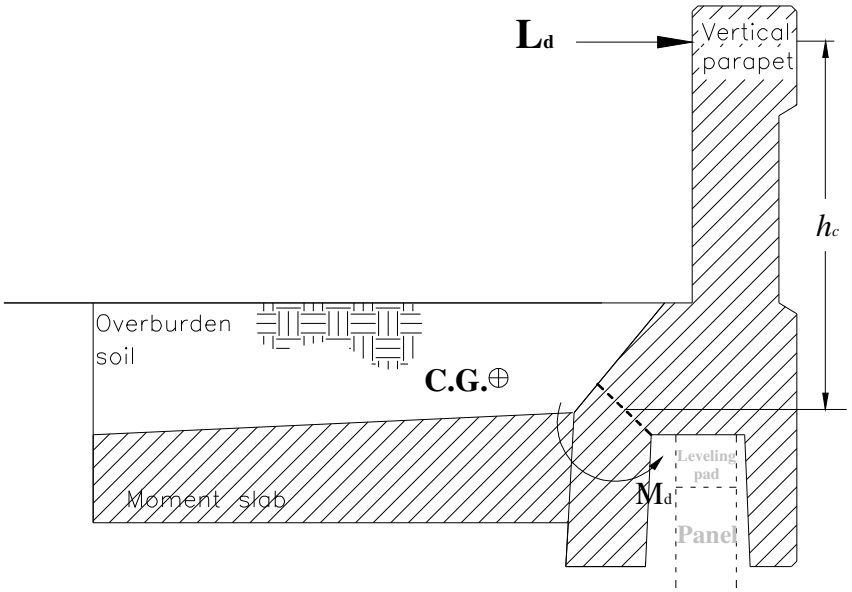

Figure 7.3 Barrier-moment slab system for barrier design guideline (breaking of coping in bending)

7.2 Guidelines for the Reinforcement

The reinforcement guidelines should ensure that the reinforcement does not pullout or break during a barrier impact with the chosen design vehicle.

7.2.1 Pullout of the Reinforcement

1) Pressure Diagram Approach

The capacity of the reinforcement calculated by common static methods should be compared to the dynamic impact loads because no significant difference was found between the static capacity and the dynamic capacity of the reinforcement.

The factored static resistance (ϕ P) to pullout of the reinforcement should be greater than or equal to the sum of the factored static load (γ_s F_s) due to the earth pressure and the factored dynamic load (γ_d F_d) due to the impact. The static impact load F_s should be obtained from the static earth pressure p_s times the tributary area A_t of the reinforcement unit. The dynamic load F_d should be obtained from the pressure p_d of the pressure diagram (Figure 7.4) times the tributary area A_t of the reinforcement unit. The pressure p_{LL} due to the traffic live load should be considered based on the load combination of EXTREME EVENT II in AASHTO LRFD.

$$\phi P \geq \gamma_s F_s + \gamma_d F_d + \gamma_{LL} p_{LL} \quad (7\text{-}6)$$

$$\phi P \geq \gamma_s p_s A_t + \gamma_d p_d A_t + \gamma_{LL} p_{LL} \quad (7\text{-}7)$$

(For the load level TL-3, p_d is given by the pressure diagram shown in Figure 7.4, ϕ resistance factor is 1.0, γ_d load factor is 1.0, γ_s load factor is 1.0, and γ_{LL} load factor is 0.5)

The reinforcement resistance P for strips should be calculated as (AASHTO 11.10.6.3.2-1):

$$P = F^* \sigma_v 2b L \quad (7\text{-}8)$$

where F* is the resistance factor (sliding plus bearing), σ_v is the vertical effective stress on the reinforcement, b is the width of the strip, and L is the full length of the reinforcement. The value of F* should be obtained from the current AASHTO guidelines (Figure 7.5).

The reinforcement resistance P for bar mats should be calculated as:

$$P = F^* \sigma_v \pi D n L \quad (7\text{-}9)$$

where D is the diameter of the bar mats and n is the number of longitudinal bars.

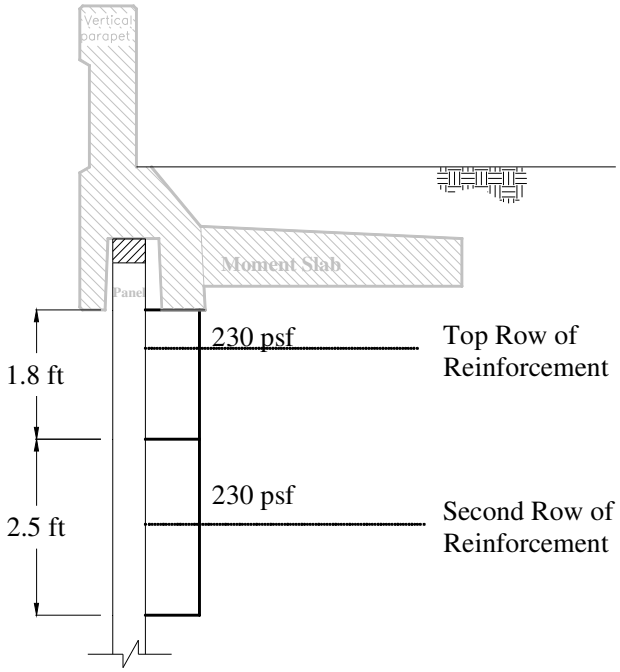

Figure 7.4 Pressure diagram p_d for reinforcement pullout

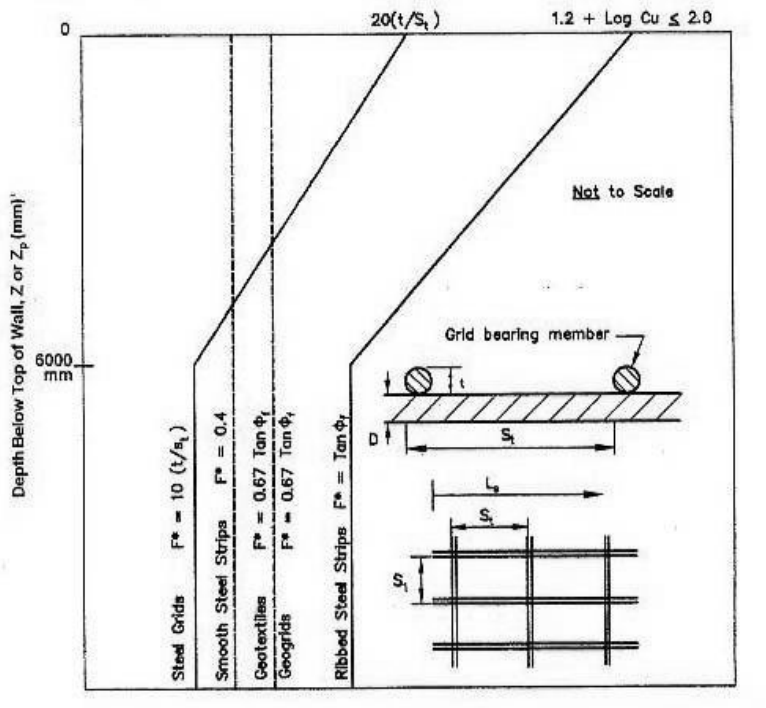

Figure 7.5 Default values for the pullout friction factor, F^* (AASHTO LRFD Figure 11.10.6.3.2-1)

2) Line Load Approach

The factored static resistance (ϕ P) to pullout of the reinforcement should be greater than or equal to the sum of the factored static load (γ_s F_s) due to the earth pressure and the factored dynamic load (γ_d F_d) due to the impact. The static impact load F_s should be obtained from the static earth pressure p_s times the tributary area A_t of the reinforcement unit. The dynamic impact load F_d should be obtained from the line load Q_d of the line load diagram (Figure 7.6) times the longitudinal spacing (S_L) of the reinforcement. The pressure p_{LL} due to the traffic live load should be considered based on the load combination of EXTREME EVENT II in AASHTO LRFD.

$$\phi P \geq \gamma_s F_s + \gamma_d F_d + \gamma_{LL} p_{LL} \quad (7\text{-}10)$$

$$\phi P \geq \gamma_s p_s A_t + \gamma_d Q_d S_L + \gamma_{LL} p_{LL} \quad (7\text{-}11)$$

(For the load level TL-3, Q_d is given by the line load diagram shown in Figure 7.6, ϕ resistance factor is 1.0, γ_d load factor is 1.0, γ_s load factor is 1.0, and γ_{LL} load factor is 0.5)

The reinforcement resistance P for strips should be calculated as (AASHTO 11.10.6.3.2-1):

$$P = F^* \sigma_v 2b L \quad (7\text{-}12)$$

where F* is the resistance factor (sliding plus bearing), σ_v is the vertical effective stress on the reinforcement, b is the width of the strip, and L is the full length of the reinforcement. The value of F* should be obtained from the current AASHTO guidelines (Figure 7.5).

The reinforcement resistance P for bar mats should be calculated as:

$$P = F^* \sigma_v \pi D n L \quad (7\text{-}13)$$

where D is the diameter of the bar mats and n is the number of longitudinal bars.

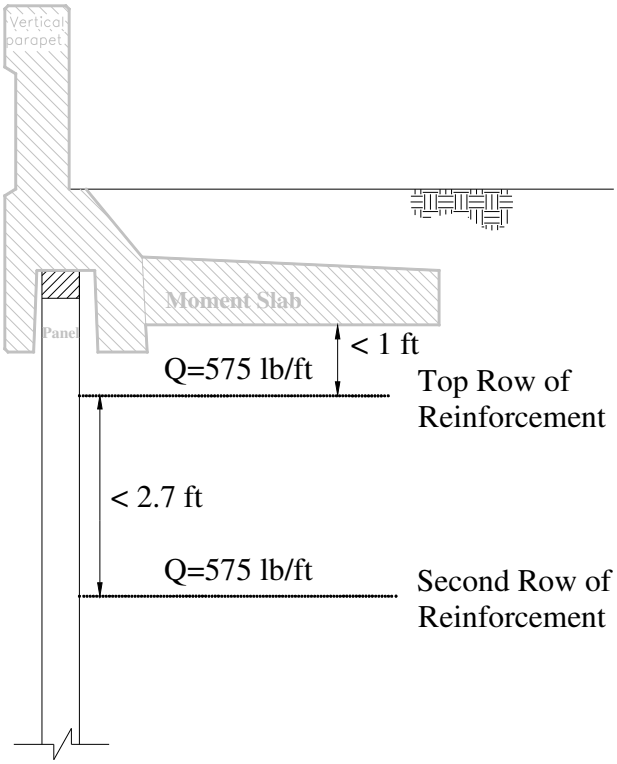

Figure 7.6 Line load Q_d for reinforcement pullout

7.2.2 Rupture of the Reinforcement

1) Pressure Diagram Approach

The factored resistance (ϕ R) to rupture of the reinforcement should be greater than or equal to the sum of factored static load (γ_s F_s) due to the earth pressure and the factored dynamic load (γ_d F_d) due to the impact. The static load F_s should be obtained from the static earth pressure p_s times the tributary area A_t of the reinforcement unit. The dynamic load F_d should be obtained from the dynamic pressure p_d of the pressure diagram (Figure 7.7) times the tributary area A_t of the reinforcement unit.

$$\phi R \geq \gamma_s F_s + \gamma_d F_d \tag{7-14}$$

$$\phi R \geq \gamma_s p_s A_t + \gamma_d p_d A_t \tag{7-15}$$

(For the load level TL-3, p_d is given by the pressure diagram shown in Figure 7.7, ϕ resistance factor is 1.0, and γ_d load factor is 1.0, and γ_s load factor is 1.0)

The reinforcement resistance R for strips or bar mats should be calculated as:

$$R = \sigma_t A_s \tag{7-16}$$

where σ_t is the tensile strength of the reinforcement, and A_s is the cross section area of the reinforcement.

$$A_s = b \times E_c \text{ for Strip} \tag{7-17}$$

where E_c is the strip thickness corrected for corrosion loss. (AASHTO Figure 11.10.6.4.1-1)

$$A_s = \frac{\pi D^{*2}}{4} \text{ for Bar mats} \tag{7-18}$$

where D^* is the diameter of bar or wire corrected for corrosion loss. (AASHTO Figure 11.10.6.4.1-1)

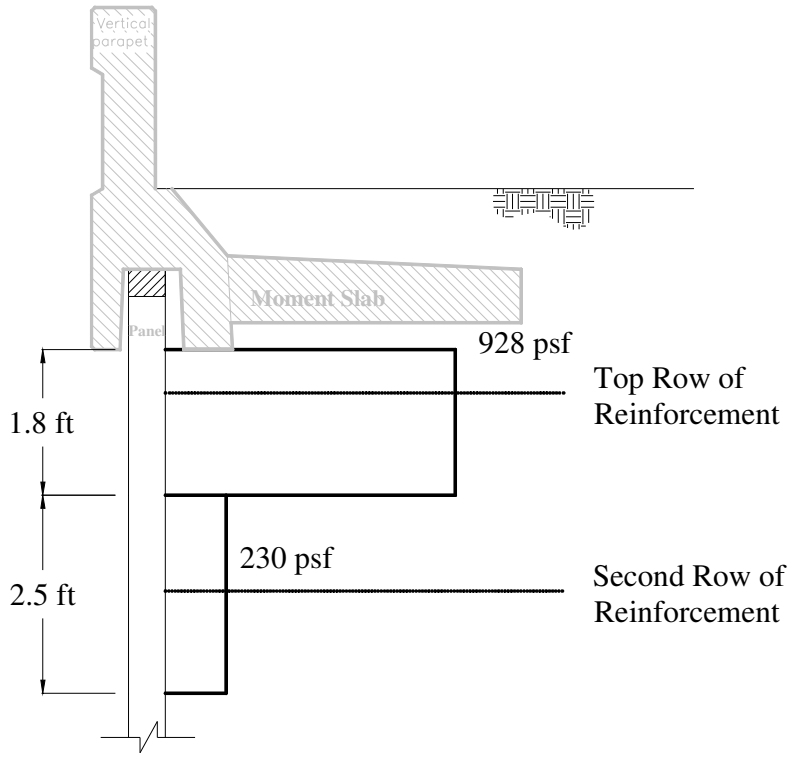

Figure 7.7 Pressure diagram p_d for reinforcement rupture

2) Line Load Approach

The factored resistance (ϕ R) to rupture of the reinforcement should be greater than or equal to the sum of factored static load (γ_s F_s) due to the earth pressure and the factored dynamic load (γ_d F_d) due to the impact. The static load F_s should be obtained from the static earth pressure p_s times the tributary area A_t of the reinforcement unit. The dynamic load F_d should be obtained from the line load Q_d of the line load diagram (Figure 7.8) times the longitudinal spacing (S_L) of the reinforcement.

$$\phi R \geq \gamma_s F_s + \gamma_d F_d \quad (7\text{-}19)$$

$$\phi R \geq \gamma_s p_s A_t + \gamma_d Q_d S_L \quad (7\text{-}20)$$

(For the load level TL-3, Q_d is given by the line load diagram shown in Figure 7.8, ϕ resistance factor is 1.0, and γ_d load factor is 1.0, and γ_s load factor is 1.0)

The reinforcement resistance R for strips or bar mats should be calculated as:

$$R = \sigma_t A_s \quad (7\text{-}21)$$

where σ_t is the tensile strength of the reinforcement, and A_s is the cross section area of the reinforcement.

$$A_s = b \times E_c \text{ for Strip} \tag{7-22}$$

where E_c is the strip thickness corrected for corrosion loss. (AASHTO Figure 11.10.6.4.1-1)

$$A_s = \frac{\pi D^{*2}}{4} \text{ for Bar mats} \tag{7-23}$$

where D^* is the diameter of bar or wire corrected for corrosion loss. (AASHTO Figure 11.10.6.4.1-1)

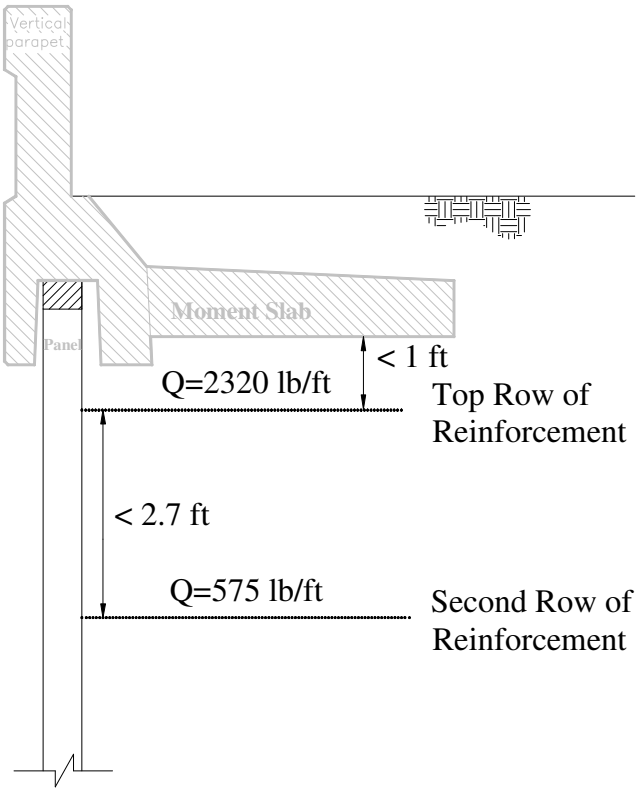

Figure 7.8 Line load Q_d for reinforcement rupture

7.3 Guidelines for the Wall Panel

The wall panel design guidelines should ensure that the panel does not break during a barrier impact with the chosen design vehicle. The factored ultimate moment resistance (ϕM_u) should be greater than or equal to the factored moment (γM_i) on the panel during the impact at the location of the upper layer of reinforcement as shown in Eq. (7-24).

$$\phi M_u \geq \gamma M_i \tag{7-24}$$

(ϕ resistance factor is 0.9 (AASHTO 5.5.4.2), and γ load factor is 1.0)

1) Rotation Point A

The panel should resist a moment of no less 1.78 kN m/m (0.4 kips ft/ft).

2) Rotation Point B

The moment M_i, is generated from the horizontal shear load H on top of the panel times the moment arm *l* and the vertical load V which is transferred from the barrier to the panel during the impact times the moment arm (*t/2*) where *t* is the thickness of the panel as shown in Figure 7.9.

$$M_i = H \times l + V \times t/2 \tag{7-25}$$

The panel should be design for a shear load and vertical load equal to 4.89 kN/m (1.1 kips/ft) and 53.33 kN/m (12.0 kips/ft), respectively.

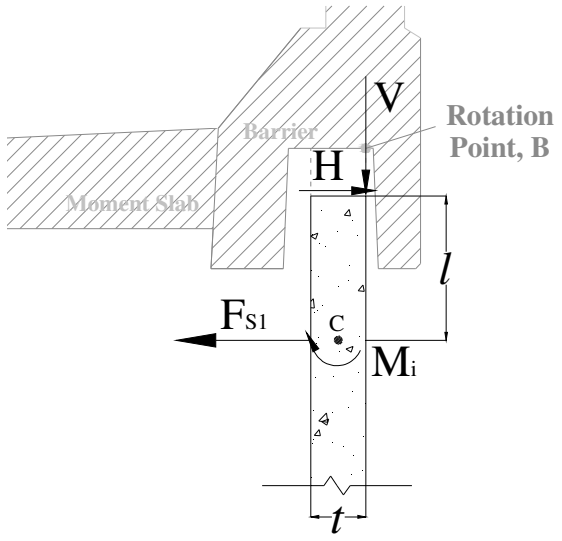

Figure 7.9 Resistance of wall panel for rotation point B

7.4 Data to Back-Up Guidelines

7.4.1 Barrier

The guidelines were developed based on analysis and testing of N.J. profile and vertical wall concrete barrier. However, the results should be applicable to other common barrier types.

Note that our calculations indicate that a 1.37 m (4.5 ft) wide, 9.14 m (30 ft) long moment slab without the shear strength of soil on top of it is the minimum required to satisfy the above requirements. We have also found that the overturning mode occurs before the sliding mode and is, therefore, the controlling mechanism.

The above proposed design guidelines are based on the evidence presented below. Note that a decision was made to aim for a barrier-moment slab design which would generate 2.54 cm (1 in.) movement during impact. This 2.54 cm (1 in.) movement was considered acceptable as it would likely require little or no repair of the underlying MSE wall, and should not affect the impact performance of the barrier system.

The static analysis for sliding and overturning is conducted using equilibrium equations as described in section 3.2.1. Two points of rotation were considered for sliding and overturning as shown in Figure 7.10 and Figure 7.11. These figures show the barrier force that a 1.37 m (4.5 ft) wide moment slab of varying length can resist when discounting the shear strength of the soil on top of it. As can be seen, the overturning mode develops less resistance than the sliding mode for both points of rotation. Thus, the overturning mode controls design. This is not to say that the barrier does not slide during impact. It did slide slightly during both the static and the dynamic test, but the majority of the movement was due to rotation.

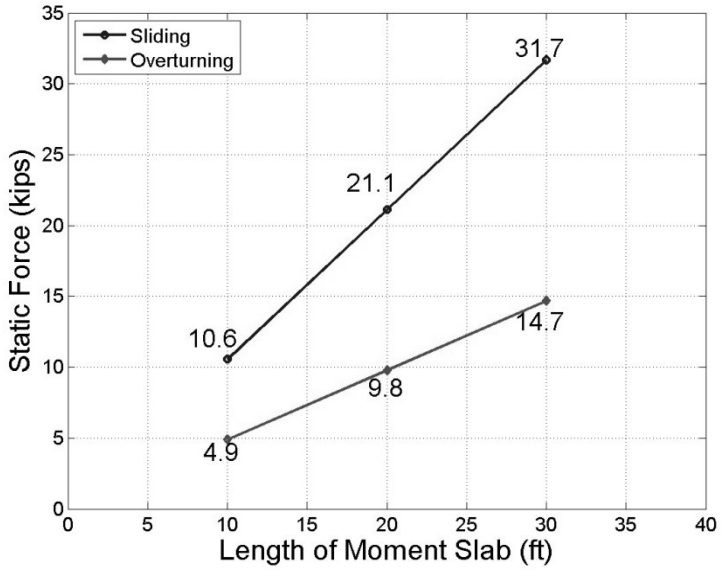

Figure 7.10 Static load by analytical solution (Point of Rotation A)

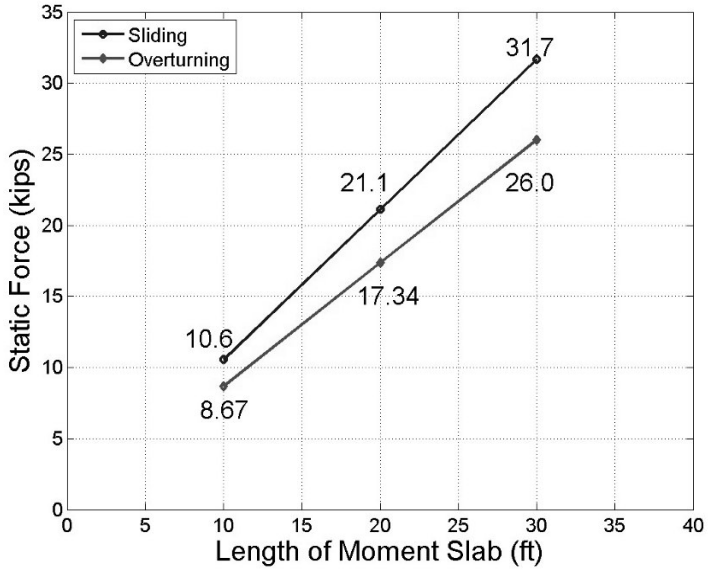

Figure 7.11 Static load by analytical solution (Point of Rotation B)

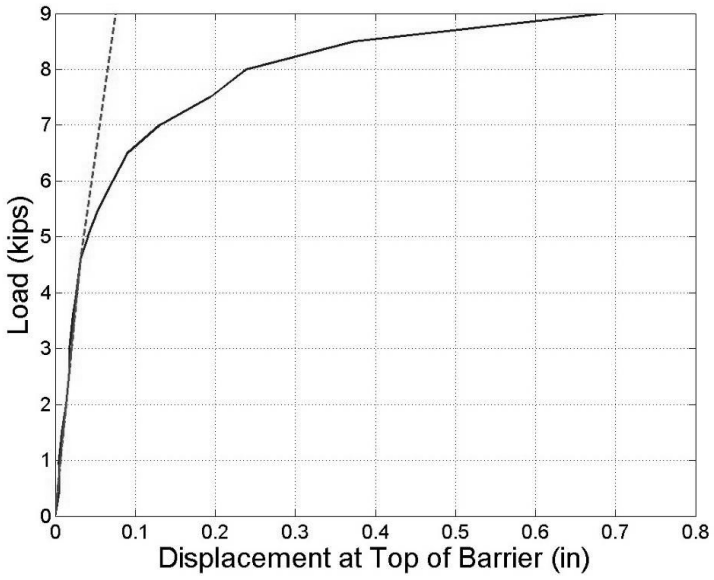

Figure 7.12 Static test data at the top of barrier

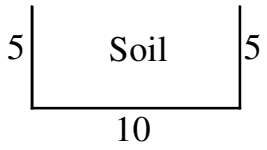

Figure 7.13 Soil resistance areas with respect to the length of the moment slab

By extrapolation, a 1.37 m (4.5 ft) wide and 6.1 m (20 ft) long moment slab barrier assembly would resist 44.48 kN (10 kips) without soil on its periphery and 71.17 kN (16 kips) with peripheral soil. As the length of moment slab increases, the friction associated with the side soil would be neglected. Therefore, by further extrapolation, a 1.37 m (4.5 ft) wide and n × 3.05 m (10 ft) long moment slab barrier assembly would resist n×22.24 kN (5 kips) without soil on its periphery and n × 31.14 kN (7 kips) with peripheral soil. Table 7.1 shows the values of the static resistance developed by a barrier with a 1.37 m (4.5 ft) wide moment slab of varying length. The resistance is split in two parts: the load due to dead weight and the load due to soil friction along the perimeter of the moment slab.

Table 7.1 Total Static Load with Respect to the Length of Barrier

Length of Moment Slab (ft)	(1) Resistance from Moment slab and overburden (kips)	(2) Soil resistant (kips)	(3) = (1)+(2) Total static load (kips)	(3) / (1) Ratio
10	5	4	9	1.8
:	:	:	:	:
10 × n	5 × n	2 × n	7 × n	1.4

A dynamic impact test was performed with a bogie on the same 1.37 m (4.5 ft) wide and 3.05 m (10 ft) long barrier-moment slab system. At 20.9 km/h (13 mph), the bogie generated a maximum 50-msec average impact force of 193.05 kN (43.4 kips), and moved the top of the barrier 8.9 cm (3.5 in.). The numerical simulation was used to predict and compare the dynamic test as shown in Figure 7.14. The numerical simulation gave 204.62 kN (46 kips) and 8.9 cm (3.5 in.). Table 7.2 shows the maximum 50-msec average impact load and the corresponding displacement at the top of the barrier according to the numerical simulations of bogie vehicle impacts into a 3.05 m (10 ft) long barrier-moment slab system at different speeds. Figure 7.15 is a comparison between the static load test results (load-deflection curve), the numerical simulations (peak impact force and corresponding displacement), and the result of the two dynamic bogie tests (20.9 km/h (13 mph) and 28.97 km/h (18 mph)). This comparison shows the amplification due to the inertia force with the increase in velocity at impact. This gave credibility to the numerical simulations. Numerical simulation was then used to find what peak dynamic load which would generate a peak displacement of the top of the barrier of 2.54 cm (1 in.) for different lengths of the 1.37 m (4.5 ft) wide moment slab.
Figure 7.16. Another numerical simulation indicated that a bogie impact at 28.97 km/h (18 mph) on a 9.14 m (30 ft) long moment slab would generate a dynamic force of 384.74 kN (78.4 kips) at 2.4 cm (0.96 in.) of movement, and that the same 9.14 m (30 ft) long moment slab would resist 65.39 kN (14.7 kips) statically without counting on the shear strength of the soil on top of it.

These data indicate that a 240 kN (54 kips) dynamic load associated with 2.54 cm (1 in.) movement is approximately equivalent to a 44.48 kN (10 kips) static load when the shear

strength of the soil above the moment slab is discounted. These data further indicate that a 9.14 m (30 ft) moment slab gives a factor of safety of 1.5 against the 240 kN (54 kips) dynamic design load for a 2.54 cm (1 in.) movement and a 1.5 factor of safety against a 44.48 kN (10 kips) static design load.

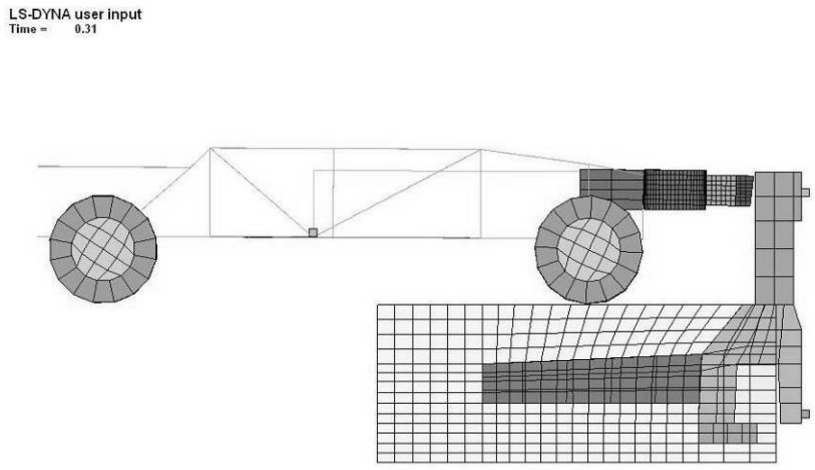

Figure 7.14 Finite element model for dynamic analysis

Table 7.2 Impact Loads with Various Velocities of Bogie on 10 ft Barrier System.

Velocity of bogie (mph)	Maximum displacement of barrier (in.)	Impact force (kips)
2	0.14	6.79
5	0.97	23.33
8	1.73	34.35
10	2.35	39.95
13	3.56	46.00

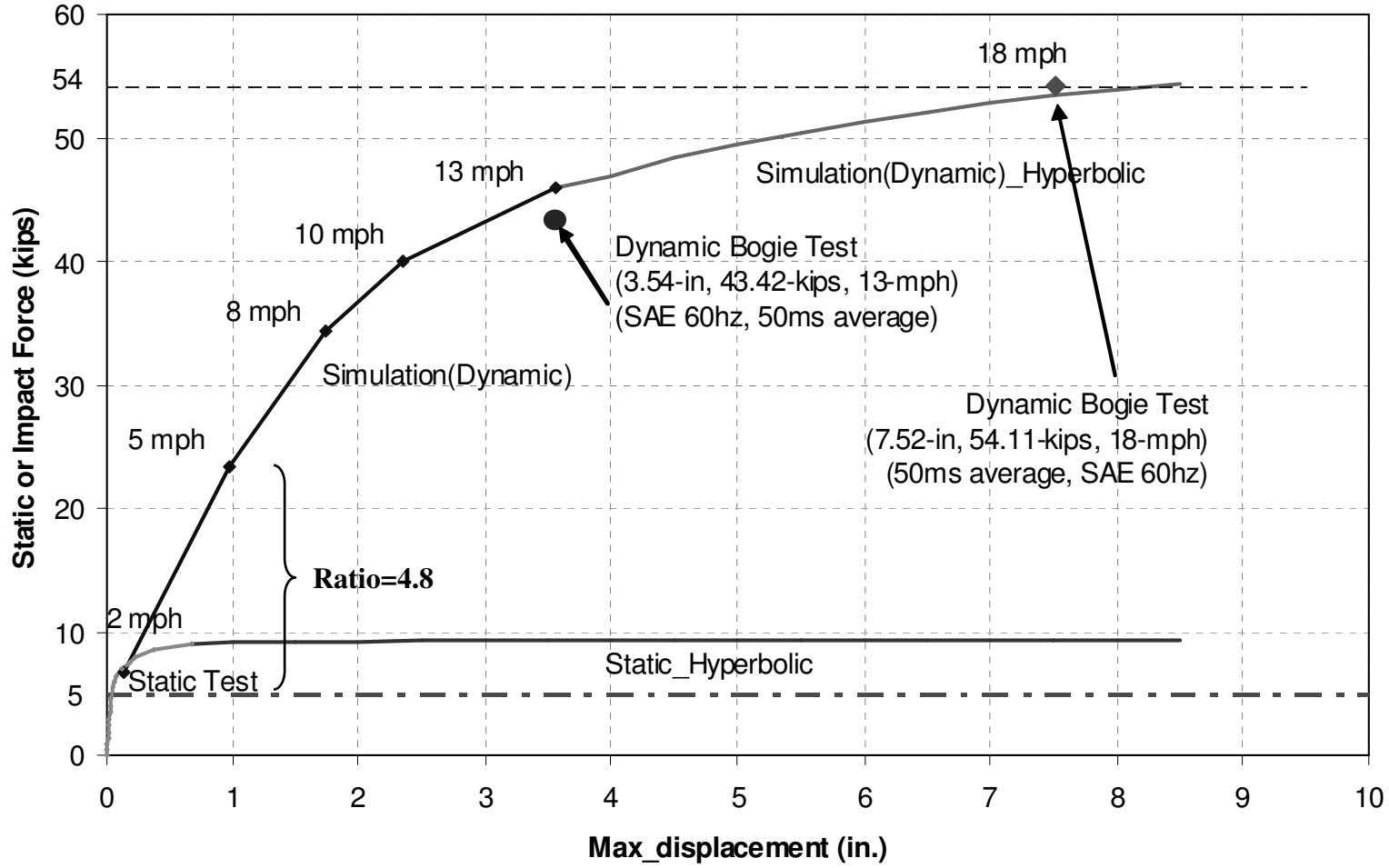

Figure 7.15 Comparison of static test and dynamic test and finite element model of 10 ft barrier-moment slab system

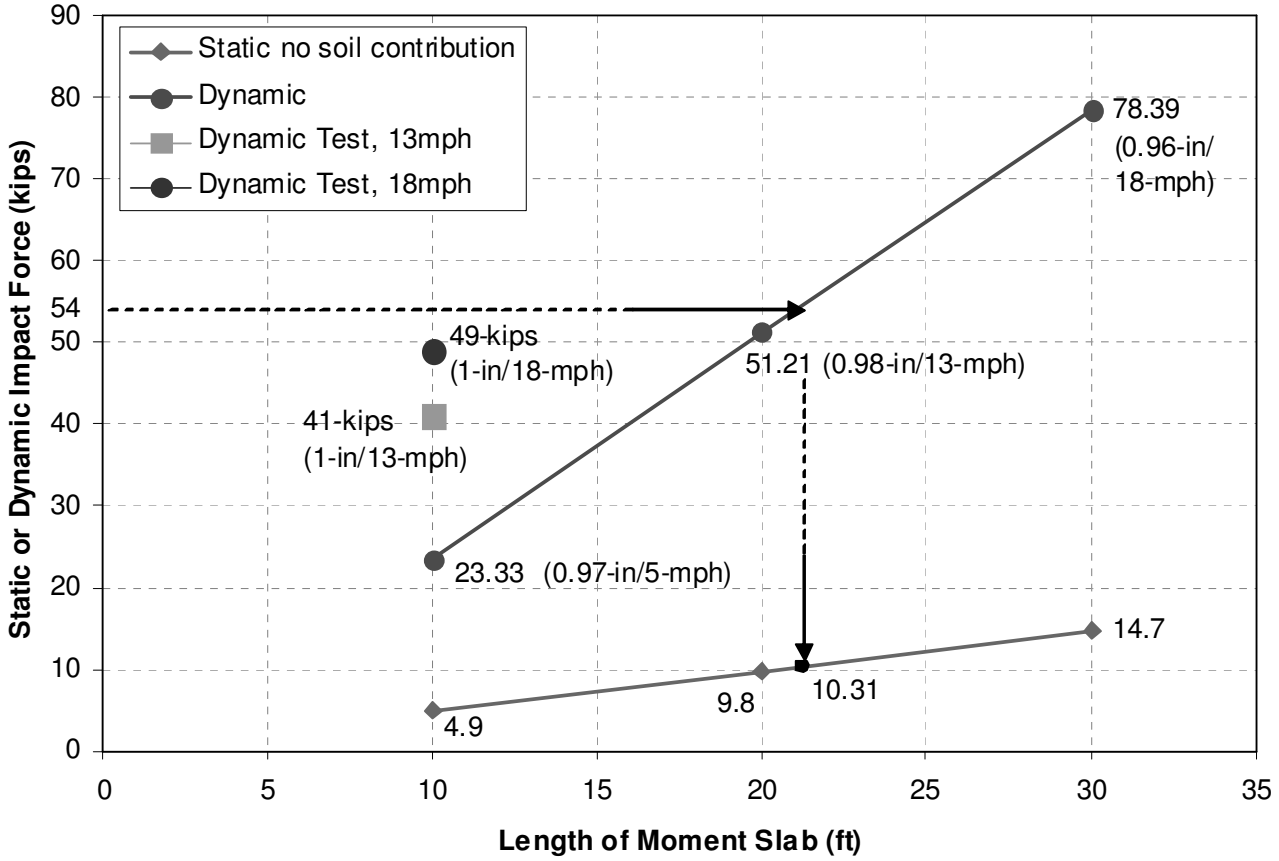

Figure 7.16 Comparison of static and dynamic impact force in 1 in. maximum displacement

Figure 7.17 shows the ratio of the dynamic force over the static force (with and without shear resistance) as a function of the 4.5 ft wide moment slab length. Note that for the 9.14 m (30 ft) barrier the ratio is very close to 5.4 which is equal to 240.2 kN / 44.48 kN (54 kips / 10 kips).

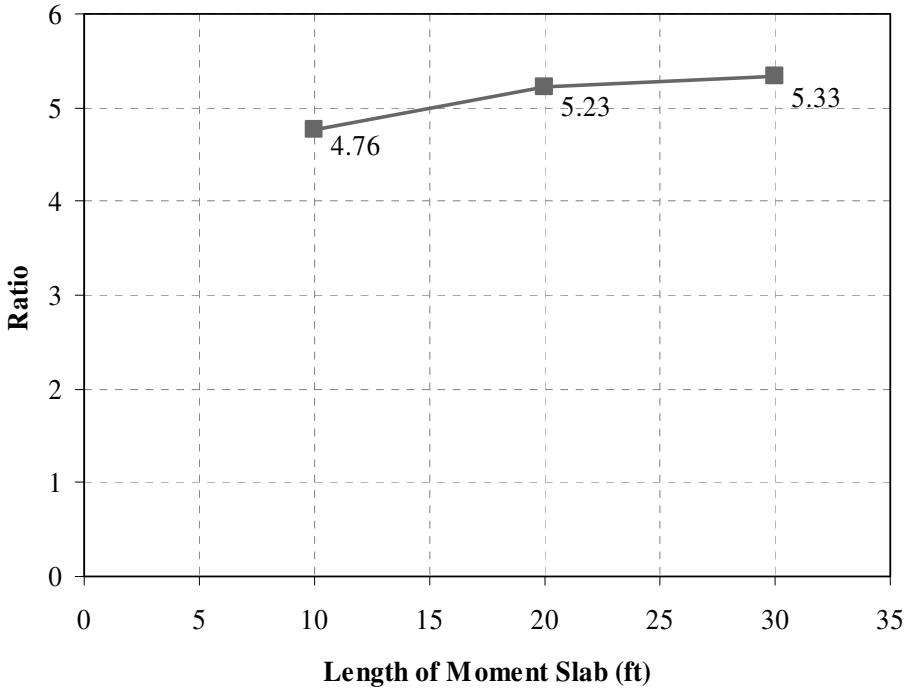

Figure 7.17 Ratio of static load and dynamic impact load

7.4.2 Reinforcement

Four bogie tests were conducted to develop the design guidelines for a barrier system on top of an MSE wall. The impact speeds varied from 32.5 km/h (20.19 mph) to 35.1 km/h (21.8 mph). The maximum load on the barrier (50-msec average) varied from 286.47 kN (64.4 kips) to 326.5 kN (73.4 kips). In order to capture the tensile forces transmitted into the reinforcement during the dynamic impact, strain gages were installed. The placement of these strain gages was selected to measure the maximum tensile load in each layer of reinforcement as well as give an indication of the distribution of forces in the lateral, longitudinal, and vertical directions.

The maximum dynamic loads in the reinforcement in excess of the static load measured during the impact varied from 9.47 kN (2.13 kips) to 33.18 kN (7.46 kips) in the upper most layer. The load used is the one corresponding to the location where two strain gages (top and bottom of the strip) were available to get an average value. Higher loads were registered at locations where only one gage was available. However, it appears that significant bending occurred which made the single strain gage readings doubtful and unreliable.

The maximum load in the strip closest to the impact (upper most layer) in excess of the static load was 33.18 kN (7.46 kips) for the 4.88 m (16 ft) long strips under the vertical wall (Test 4) and 31.98 kN (7.19 kips) for the 4.88 m (16 ft) long strips under the N.J. barrier (Test 1). Assuming the increase in strip load is proportional to the barrier impact load, the design strip loads corresponding to a design impact load of 240 kN (54 kips) can be estimated to be 24.42 kN (5.49 kips)and 23.53 kN (5.29 kips), respectively.

For the 2.44 m (8 ft) long strips case, the maximum load in the strip closest to the impact (top layer) in excess of the static load was 9.47 kN (2.13 kips) under the vertical wall (Test 3). The design strip load in excess of static corresponding to a design impact load of 240 kN (54 kips) can be estimated to be 6.98 kN (1.57 kips).

The maximum load in excess of static in the single bar closest to the impact load (upper most layer) in the bar mat which was 2.44 m (8 ft) long was 6.85 kN (1.54 kips) (Test 2). The design strip load in excess of static corresponding to a design impact load of 240 kN (54 kips) can be estimated to be 5.03 kN (1.13 kips).

Even though the reinforcement appears to have reached its maximum pull out resistance during impact, the overall performance of the wall was very satisfactory in all 4 tests. Therefore it was decided that having the reinforcement working at maximum pull out resistance would be acceptable. The design recommendations were based on a pressure diagram approach to be resisted by the reinforcement while using the design loads in excess of static recorded in the tests.

1) Pullout of the Reinforcement

The pullout tests in the laboratory were performed at rates varying from quasi-static rates all the way to rates approaching impact loading rates. Because no consistent rate effect was

found, the recommended design guidelines require that the pullout resistance of the reinforcement be calculated according to common static methods and sized to resist the full dynamic loads.

The design strip load in excess of static in Test 3, which is for a 2.44 m (8 ft) long strip, was used to develop the design guideline for pullout of the reinforcement. This test was selected because the wall performed well during that impact. During Test 4 with strips that were 4.88 m (16 ft) long, the strips developed a higher load because the system was stiffer. As a result the wall panel developed a crack during impact. Therefore the stiffer 16 ft long strips are not a good thing in this case.

The resistance (*P*) for the 8ft long strips was calculated to be 6.58 kN (1.48 kips) for the upper most layer and 11.52 kN (2.59 kips) for the second layer using Eq. (2-1) in Section 2 (AASHTO 11.10.6.2). The pullout friction factor F* was 1.789 for the upper most layer and 1.584 for the second layer.

The dynamic maximum design load (50-msec average) in excess of static in the strip at the upper most layer was measured and then interpolated back to the 54 kips impact load to be 6.98 kN (1.57 kips). The static load at the upper most layer was calculated to be 2.5 kN (0.56 kips) by AASHTO LRFD. The total design load was thus calculated to be 9.47 kN (2.13 kips) at the upper most layer. Since this measured total design load (9.47 kN or 2.13 kips) in the strip was higher than the resistance (6.58 kN or 1.48 kips), the resistance was used to obtain the dynamic design load in excess of static at the upper most layer. The controlling design load in excess of the static due to static earth pressures was calculated to be 4.09 kN (0.92 kips). This represents a static load, equivalent to a dynamic load, which would indicate that an 8 ft long strip would perform well in the case of a TL-3 impact. The value of 4.09 kN (0.92 kips) was found by calculating the total resistance of the 8 ft strip at the depth of the first layer (6.58 kN or 1.48 kips) minus the calculated load due to static earth pressures from AASHTO LRFD (2.5 kN (0.56 kips)).

At the second layer, the same process was followed. The measured dynamic load in excess of static was 3.91 kN (0.88 kips). The static earth pressure load for the second layer was calculated to be 4.89 kN (1.1 kips) by AASHTO LRFD. The total load was therefore calculated to be 8.81 kN (1.98 kips) which is less than the calculated pull out load at that depth (11.52 kN or 2.59 kips). Therefore, the measured dynamic load in excess of static was

used as the controlling dynamic load in excess of static for pullout design. Table 7.3 shows the measured dynamic load, calculated static load, total load, resistance, and the controlling load for pullout design.

The dynamic pressure per strip was calculated as shown in Table 7.4. For the 2.44 m (8 ft) long strip with a density of 3 strips per panel per layer, the tributary area was 0.37 m^2 (3.94 ft^2). The dynamic design pressure was calculated as shown in Table 7.4. The dynamic design pressure in excess of the static earth pressure for pullout is recommended to be 11.01 kPa (230 psf) for the upper most layer and 11.01 kPa (230 psf) for the second layer as shown in Figure 7.4.

Table 7.3 Test Results and Calculation of Design Strip Load for Pullout Design

	8 ft	8 ft	$p \times A_t$	P_c
	(1) Measured Dynamic Load * (kips)	(2) Static ** (kips)	(3) = (1) + (2) Total (kips)	(4) Calculated Resistance ** (kips)
Top Layer	1.57 ((4)-(2) = 0.92†)	0.56	2.13	1.48
Second Layer	0.88†	1.1	1.98	2.59

*: adjusted for 54 kips design impact load
**: calculated from AASHTO 11.10.6.2 – 11.10.6.3
†: controlling loads for reinforcement breaking

Table 7.4 Dynamic Design Load for Pullout Design

	Total Design Pressure, *p* (psf)
Top Layer	0.92 kips / 3.94 ft^2 * **= 234 psf**
Second Layer	0.88 kips / 3.94 ft^2 * **= 223 psf**

2) Rupture of the Reinforcement

The reinforcement resistance to rupture, R, for a strip was calculated as:

$$R = \sigma_t A_s \quad (7\text{-}26)$$

where σ_t is the tensile strength of the reinforcement (ASTM Grade 60, therefore, 414 MPa (60 ksi)), and A_s is the cross sectional area of the reinforcement.

$$A_s = b \times E_c \quad (7\text{-}27)$$

where E_c is the strip thickness corrected for corrosion loss. (AASHTO Figure 11.10.6.4.1-1) (E_c = 1.984 mm = 0.078 in.)

$$A_s = 50.8 \text{ mm} \times 1.984 \text{ mm} = 100.787 \text{ mm}^2 = 0.156 \text{ in}^2 \quad (7\text{-}28)$$

The reinforcement resistance to rupture R was calculated to be 41.64 kN (9.36 kips). In order to develop the design guideline against rupture of the reinforcement, the highest design load on the strip measured in the test was used. The maximum dynamic 50-msec average load on the strip located in the upper most layer was 24.42 kN (5.49 kips) (Test 4). In the second layer, the measured maximum dynamic load was 3.91 kN (0.88 kips). Therefore, the controlling design strip load for rupture of the reinforcement were 24.42 kN (5.49 kips) for the upper most layer and 3.91 kN (0.88 kips) for the second layer.

The dynamic pressure per strip for rupture of the reinforcement was calculated as shown in Table 7.5. For 2.44 m (8 ft) long strip with a density of 3 strips per panel per layer, the tributary area was 0.37 m^2 (3.94 ft^2). For 4.88 m (16 ft) long strip with a density of 2 strip per panel per layer, the tributary area was 0.55 m^2 (5.91 ft^2). The dynamic design pressure in excess of static earth pressure to consider in the design against rupture of the reinforcement was calculated as shown in Table 7.6. The dynamic design pressure for rupture of the reinforcement is recommended to be 44.53 kPa (930 psf) for the upper most layer and 11.01 kPa (230 psf) for the second layer as show in Figure 7.7.

Table 7.5 Test Results and Calculation of Design Strip Load for Breaking Design

					$p \times A_t$		B	
	(1) Measured Dynamic Load* (kips)		(2) Static** (kips)		(1)+(2)=(3) Total (kips)		(4) Calculated Resistance** (kips)	
	8 ft	16 ft	8 ft	16 ft	8 ft	16 ft	8 ft	16 ft
Top Layer	1.57	5.49†	0.56	0.83	2.13	6.32	9.36††	9.36
Second Layer	0.88†	0.11	1.1	1.59	1.98	1.7	9.36	9.36

*: adjusted for 54 kips design impact load
**: calculated from AASHTO 11.10.6.4.3
†: controlling loads for reinforcement breaking
††: Reinforcing steel is ASTM Grade 60.

Table 7.6 Design Load on the Strip for Breaking Design

	Total Design Pressure, *p* (psf)
Top Layer	5.49 kips / 5.91 ft^2 * **= 928 psf**
Second Layer	0.88 kips / 3.94 ft^2 * **= 223 psf**

7.4.3 Wall Panel

1) Bending Strength of the Wall Panel.

During the all full scale impact tests, none of the panel had any damage except one. This was the top panel in the case of the bogie test which reached 286.55 kN (64.42 kips) and where the strips were 4.88 m (16 ft) long reinforcement (Test 4). The panel had a horizontal

crack as shown in Figure 7.18. It is necessary to calculate the maximum resisting moment of a typical wall panel.

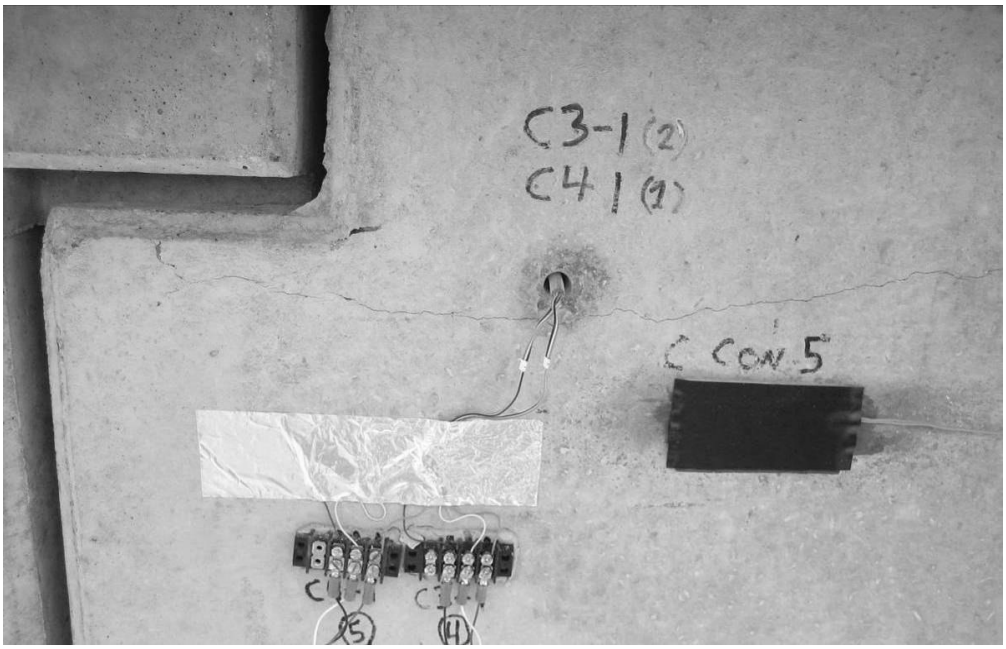

Figure 7.18 Cracks on the panel (Test 4)

The panel is assumed be a simple rectangular beam as shown in Figure 7.19. The width of the beam *b* is the thickness of the wall panel and the height of the beam *h* is a unit width (30.48 cm or 1 ft) of wall panel. The following three steps are followed to calculate the resistance of the wall panel:

1. cracking of the panel on the tension side,
2. yielding of the reinforcement, and
3. rupture of the reinforcement.

1) Cracking stage (Figure 7.19)

In this step, the beam is uncracked. The strain is very small and the stress distribution is essentially linear. The resistance of the wall panel in this step is calculated to be 10.63 kN m/m (2.39 kips ft/ft) using Eq. (7-29).

$$M_{cr} = \frac{I_g f_r}{c_b} \tag{7-29}$$

where $f_r = 7.5\sqrt{f_c^{'}}$ is the tensile stress of the concrete, the compressive strength of the concrete $f_c^{'}$ is 27 MPa (4000 psi), $I_g = \frac{bh^3}{12}$ is the gross second moment of area, *b* is the width of the panel, (30.48 cm or 1 ft), *h* the thickness of the panel (13.97 cm or 5.5 in), and c_b the distance from the center of the beam to the tension reinforcements (7 cm or 2.75 in.).

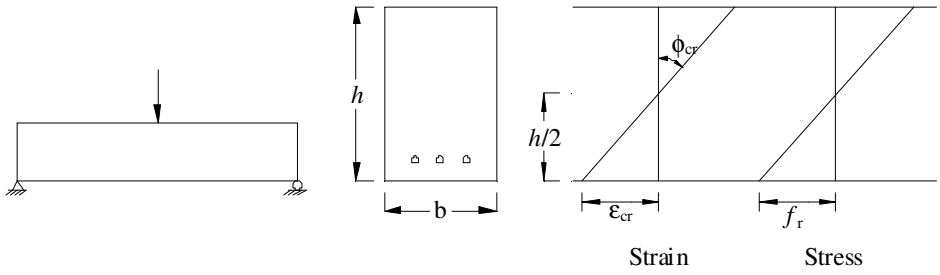

Figure 7.19 Uncracked status on wall panel

2) yielding of the reinforcement (Figure 7.20)

When the stresses at the bottom of the beam reach the tensile strength of the concrete, the concrete cracks. After cracking, the tensile force in the concrete is transferred to the reinforcement. When the reinforcement reaches its yield point, the beam curvature increases. The panel resistance was calculated to be 12.54 kN m/m (2.82 kips ft/ft) using Eq. (7-30).

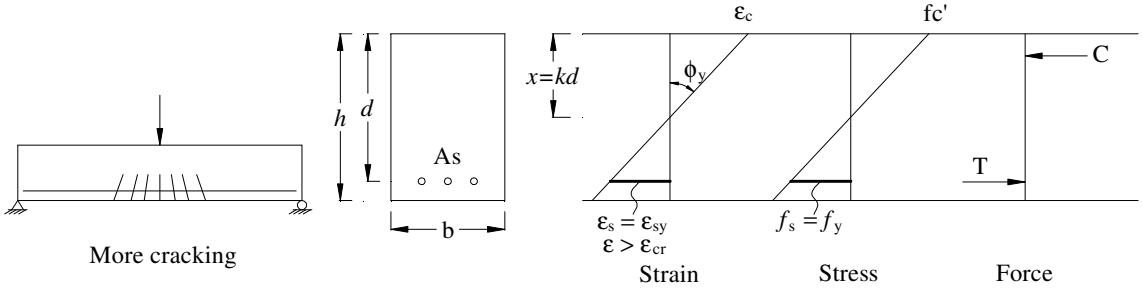

Figure 7.20 Yielding status on wall panel

$$M_n = A_s f_y d\left(1-\frac{k}{3}\right) \tag{7-30}$$

where A_s is the reinforcement area (2×0.71 cm^2 or 2×0.11 in^2), f_y the reinforcement yield strength (414 MPa (60 ksi)), d the effective depth of the tension reinforcement (14 cm (5.5in.) / 2 = 7 cm (2.75 in.)), $k = \sqrt{(\rho n)^2 + 2\rho n} - \rho n$ the factor to obtain the distance from the top of the beam to the neutral axis (0.21), ρ the reinforcement ratio (0.33), and n the modular ratio (8.04).

3) Rupture of the reinforcement (Figure 7.21)

After yielding of the reinforcement, the stresses in the beam are as shown in Figure 7.21. The concrete reaches its full compressive strength just as the steel reinforcement reaches its yield-point tensile strength. The wall panel resistance in this step was calculated to be 12.68 kN m/m (2.85 kips ft/ft) using Eq. (7-31 and 7-32).

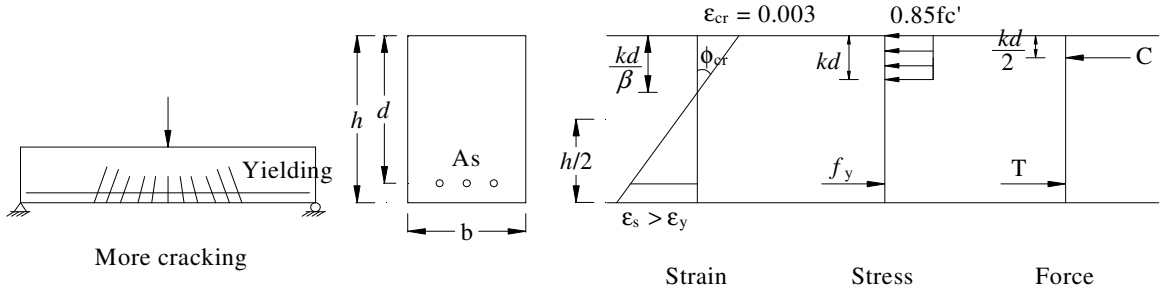

Figure 7.21 Ultimate status on wall panel

$$M_n = A_s f_y d\left(1-\frac{k}{2}\right) \tag{7-31}$$

$$C = T \rightarrow 0.85 f_c^{'} kdb = A_s f_y \tag{7-32}$$

From Eq. (7-32), the factor to obtain the distance from the top of the beam to the neutral axis *k* was calculated to be 0.1176. Then the moment was calculated to be 12.68 kN m/m (2.85 kips ft/ft).

All in all, the panel can resist up to 10.63 kN m/m (2.39 kips ft/ft) before cracking of the concrete develops, then it can resist 12.54 kN m/m (2.82 kips ft/ft) before the reinforcement start yielding, and then it can resist 12.68 kN m/m (2.85 kips ft/ft) before the reinforcement reaches its ultimate strength. Figure 7.22 shows the moment vs. curvature relationship for the wall panel.

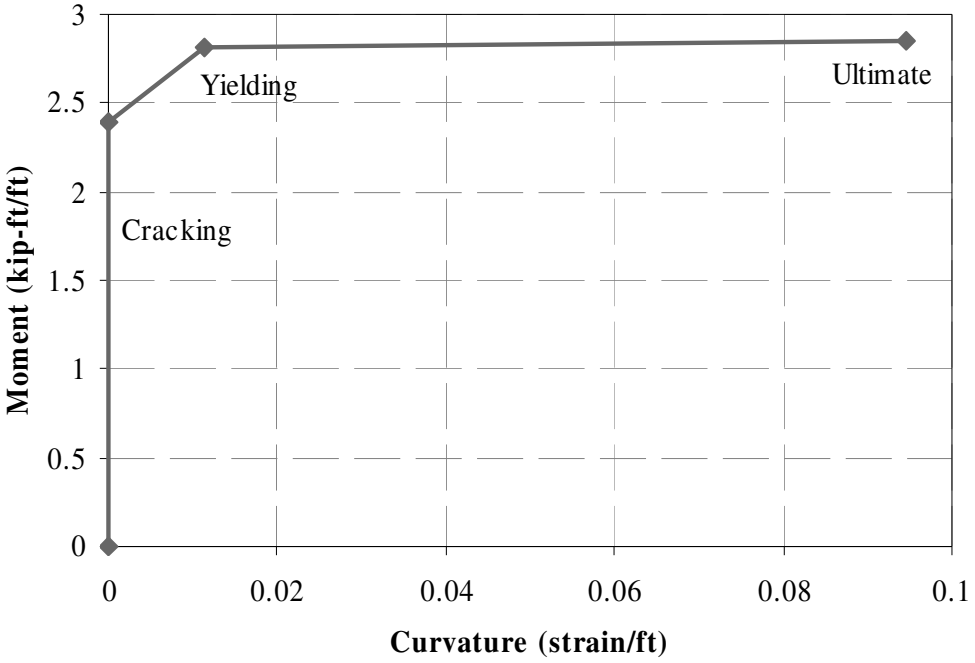

Figure 7.22 Moment curvature curve of wall panel

2) Numerical Simulation of the Wall Panel Behavior.

Since the numerical simulation results showed reasonable agreement with the test results, the simulation was used to help analyze the panel behavior during impact (Table 7.7). Figure 7.23 shows a comparison of the strains measured on the panel surface during Test 1 and 4 and the strains predicted in the numerical simulation. While there is some difference between the time scales, the maximum strain and slope of strain increase on the panel show reasonable agreement.

Table 7.7 Comparison of Test Results and Simulation

	Test 1 (NJ barrier, 16 ft strip, 21.8 mph)	Test 4 (Vertical Barrier, 16 ft long strip, 20.19 mph)	Simulation (NJ Barrier, 16 ft long strip, 21.8 mph)
Impact force Max. 50 msec avg. (kips)	73.4	64.42	81.5
Total Strip Load (kips)	6.12 (5.29* + 0.83**)	6.32 (5.49*+0.83**)	6.5
Maximum Strain on the Panel	-0.0018	-0.0024	0.002

*: Measured dynamic load on the strip

**: AASHTO Calculated static load on the strip

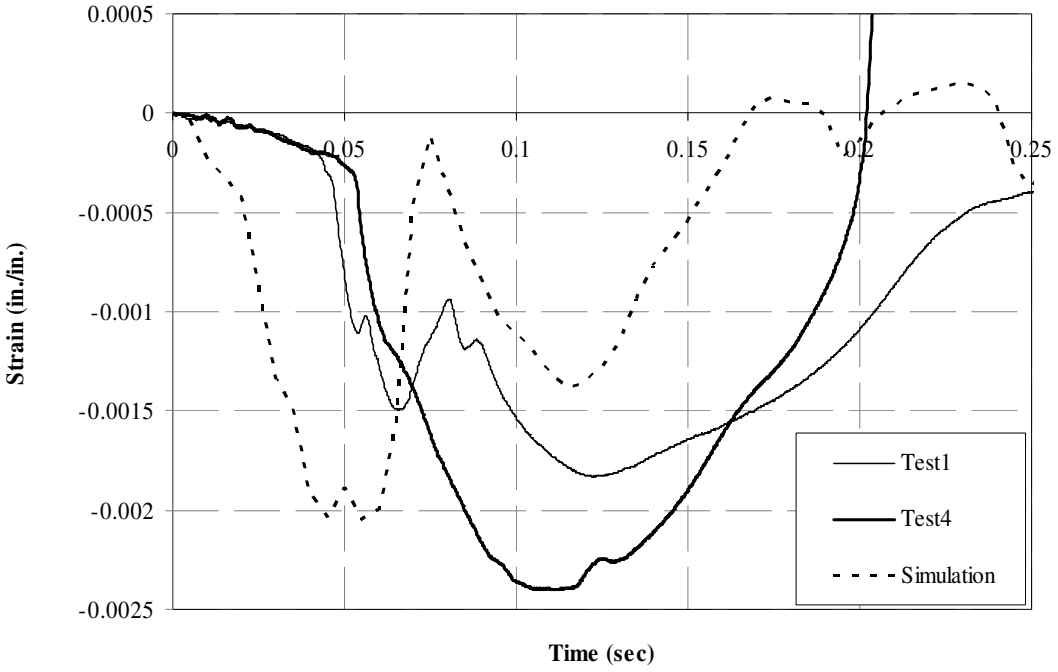

Figure 7.23 Strain on the panel

Two simulations were conducted to consider the two points of rotation.

Rotation Point A

In this case, the recessed portion of the wall panel is artificially truncated to represent rotation around point A as shown in Figure 7.24. The detailed model description is presented in Section 5.1. Because the simulation corresponded to a peak dynamic force of 359.06 kN (80.72 kips) when the design calls for 240 kN (54 kips), the results of the numerical simulation were decreased accordingly. The ratio of 240 kN / 359.06 kN (54 kips / 80.72 kip) was used as a reduction factor.

The distribution of bending moment along the panel at the time of peak force during the impact is shown in Figure 7.4.19. The bending moment at the location of the top layer of reinforcement is 0.8 kN m/m (0.18 kips ft/ft) and the maximum bending moment is 1.78 kN m/m (0.4 kips ft/ft). Therefore, the panel has sufficient capacity to resist the moment generated during the impact.

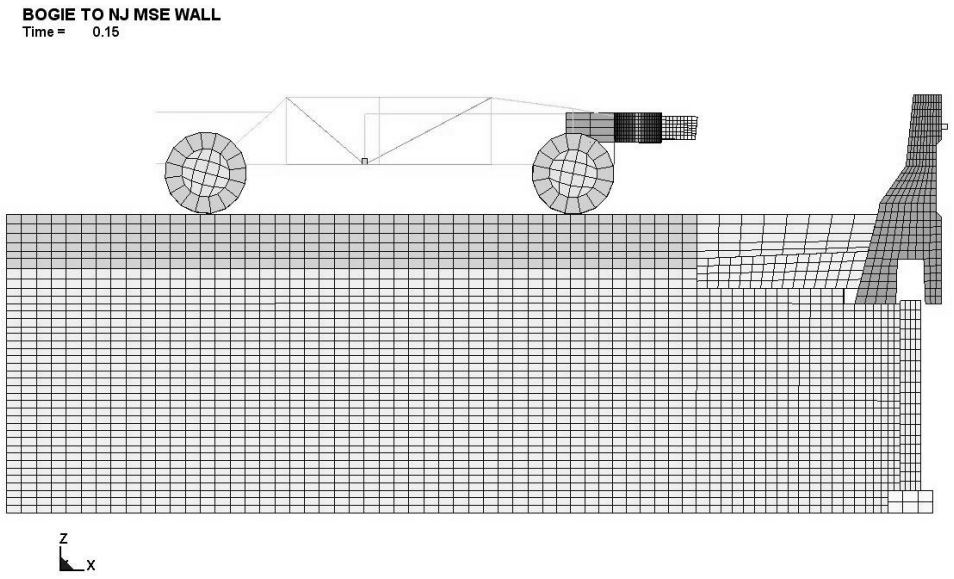

Figure 7.24 Simulation for panel analysis (Rotation Point A)

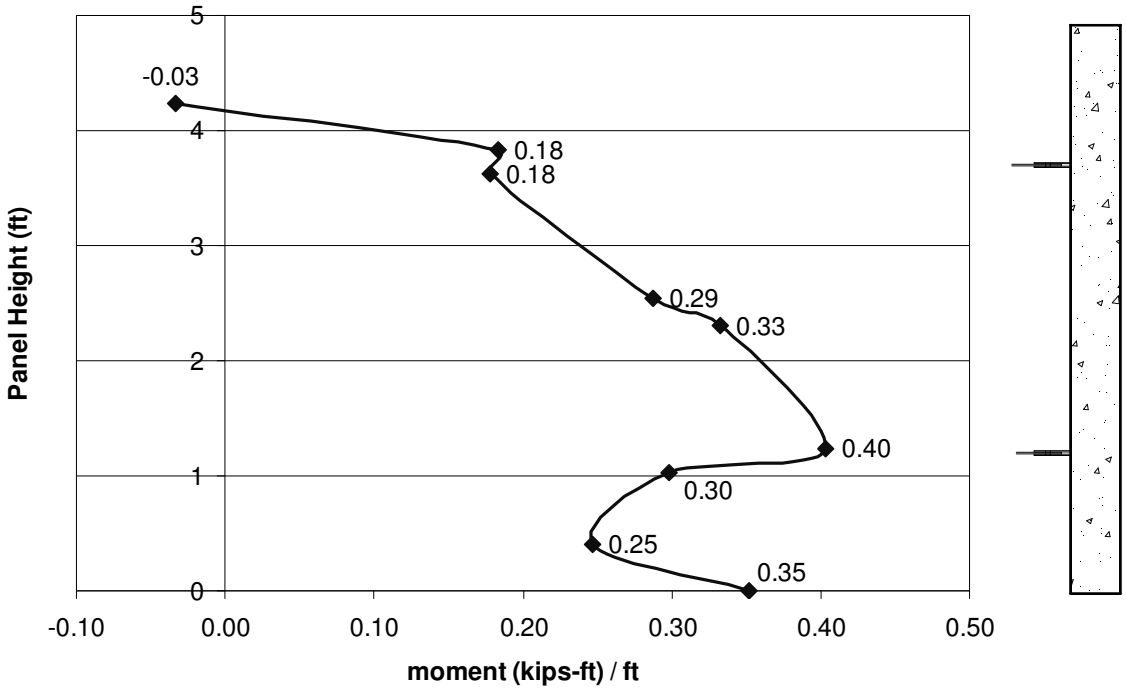

Figure 7.25 Bending moment on the panel (Rotation Point A)

Rotation Point B

In this case, the panel is penetrating into the recessed portion of the coping as shown in Figure 7.26. The detailed model description is presented in Section 5.1. In this case, the maximum bending moment per unit length of wall at the location of the top level of reinforcement can be calculated by a simple model as shown in Figure 7.27: sum of the shear load *H* at the top of the panel section times the distance *l* between the top of the panel and the level of the first reinforcement plus the vertical load *V* on top of the panel which is transferred from the barrier during the impact times the moment arm (*t/2*) where *t* is the thickness of the panel. Because the simulation corresponded to a peak dynamic force of 360.31 kN (81 kips) when the design calls for 240 kN (54 kips), the results of the numerical simulation were decreased accordingly. The ratio of 360.31 kN / 240 kN (54 kips / 81 kips) was used as a reduction factor.

The distribution of shear load, vertical load, and bending moment along the panel at the time of peak force during the impact is shown in Figure 7.4.28, Figure 7.4.29, and Figure 7.4.30, respectively. The predicted shear load was 6.98 kN (1.57 kips) at the top of the panel

during the impact due to the friction between the leveling pad and the panel. The vertical load transferred by the barrier was 76.2 kN (17.13 kips). Using both shear and vertical loads, the bending moment was calculated to be 18.15 kN-m/m (4.15 kips-ft/ft) which is higher than the capacity (12.9 kN-m/m or 2.9 kips-ft/ft) of the panel. Therefore, the panel does not have sufficient capacity to resist the moment due to the impact in Test 4. The recommended design shear and vertical loads of the panel were decreased using the ratio of 12.9 kN-m/m / 18.15 kN-m/m (2.9 kips-ft/ft / 4.15 kip-ft/ft). The panel should be design for a shear load and vertical load equal to 4.89 kN/m (1.1 kips/ft) and 53.33 kN/m (12.0 kips/ft), respectively.

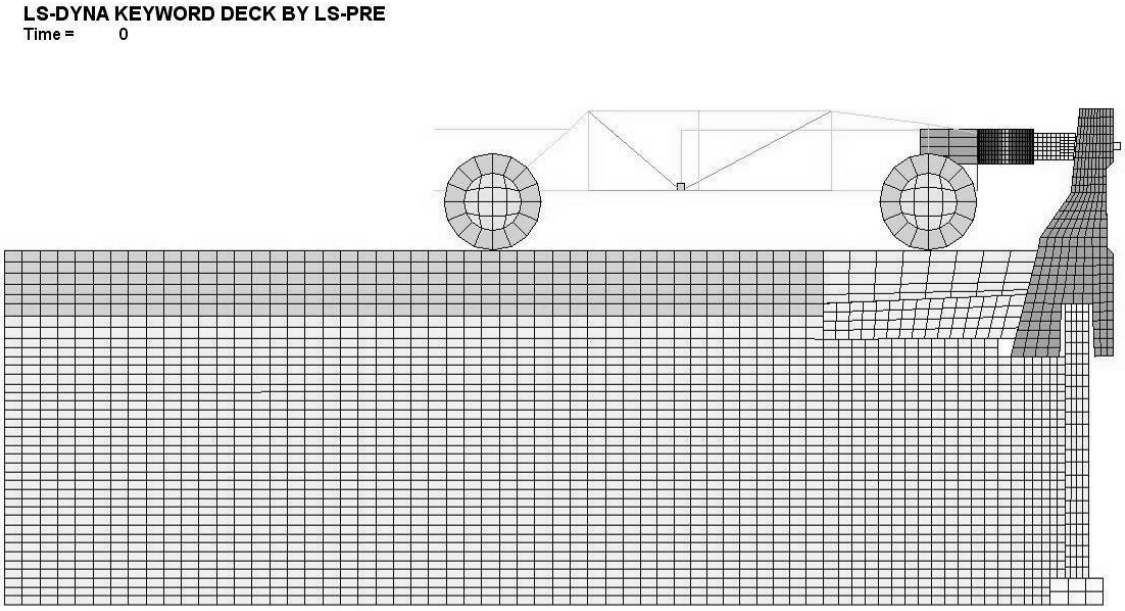

Figure 7.26 Simulation of N.J. barrier with 16 ft long strips

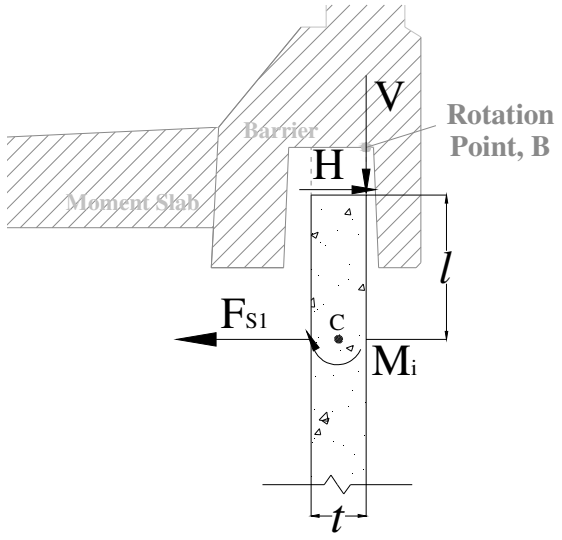

Figure 7.27 Free body diagram on the panel (Rotation Point B)

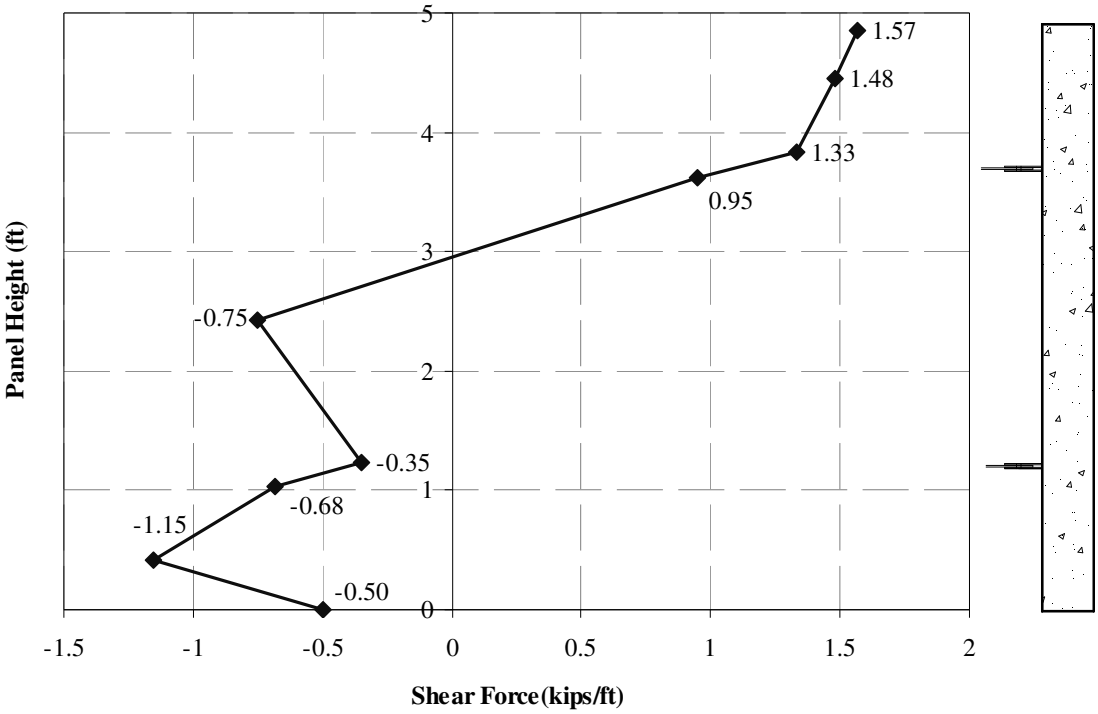

Figure 7.28 Shear load on the panel

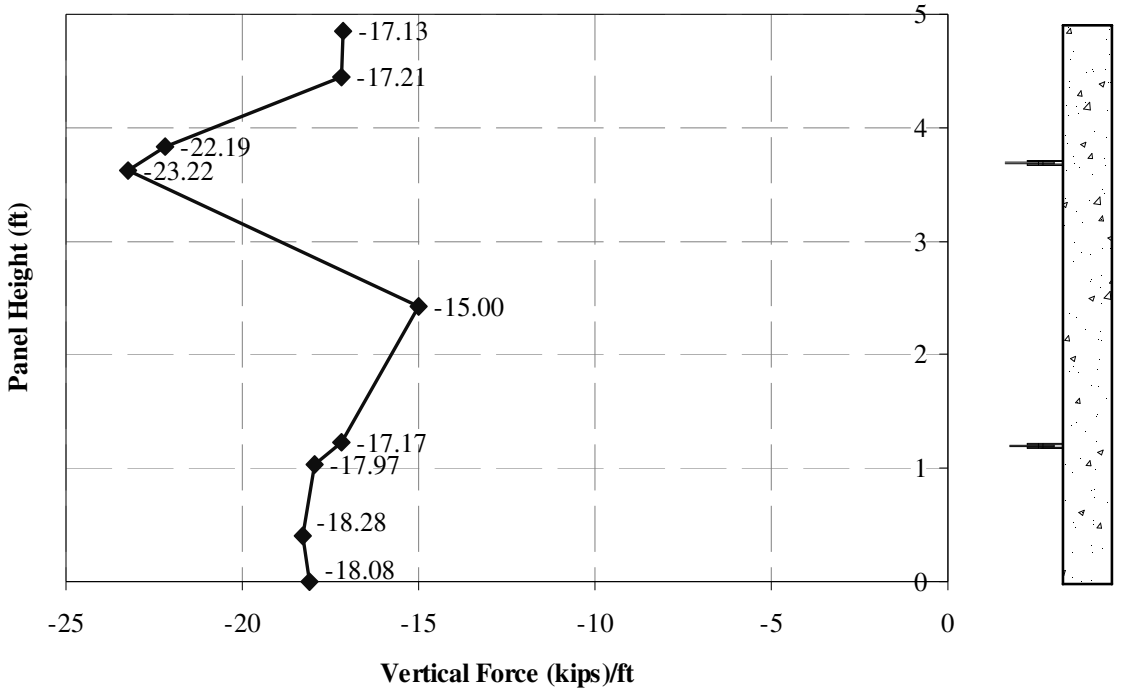

Figure 7.29 Vertical load on the panel

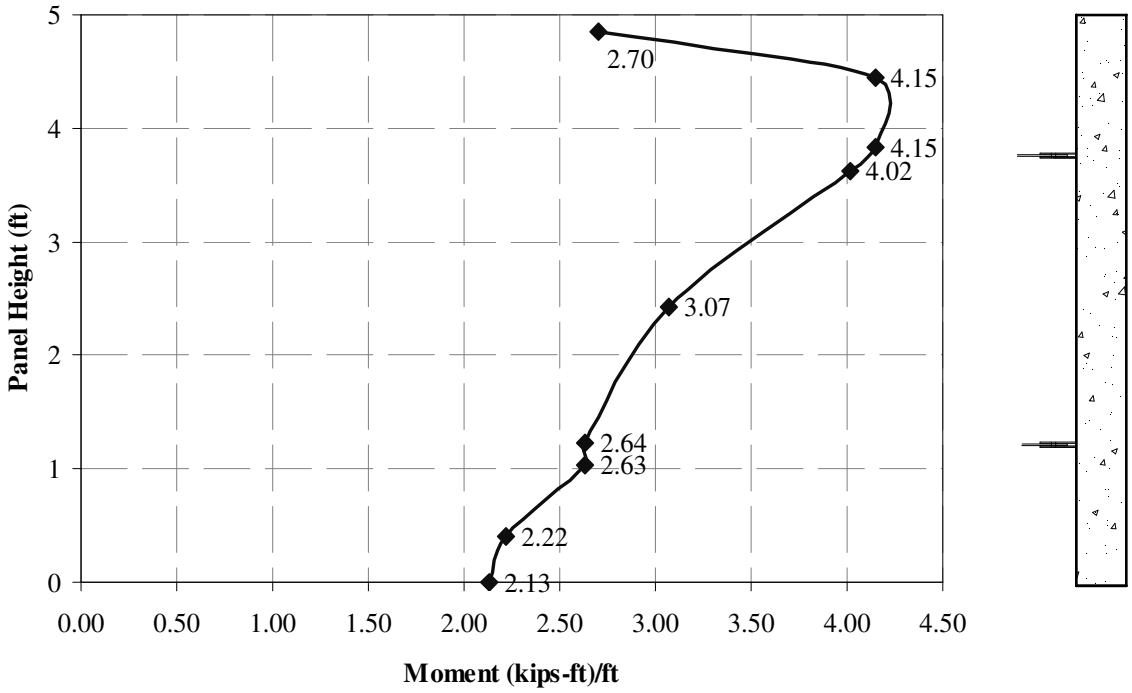

Figure 7.30 Bending moment on the panel

8 CONCLUSION

Traffic barriers which can resist vehicle impact without being tied to a structure are needed at the top of MSE walls. These barriers are usually constructed in an L shape so that the impact load on the vertical part of the L can be resisted by the inertia force required to uplift the horizontal part of the L. The design load for such barriers has changed from 44.5 kN (10 kips) to 240 kN (54 kips) over the last decade. This jump has created concern about which load should be used.

A design procedure was developed for roadside barrier systems mounted on the edge of a MSE wall. Three components of the structural system are addressed in the design procedure: the barrier-coping-moment slab system, the wall reinforcement, and the wall panel. The stability of the barrier system was investigated using static and dynamic analytical solutions, full-scale static and dynamic impact load tests, and numerical modeling. It was determined that barrier stability can be satisfied using static equilibrium analyses with an equivalent static load of 44.5 kN (10 kips). Using the dynamic barrier load of 240 kN (54 kips) is appropriate for the strength design of the barrier, but will result in an overly conservative design of the moment slab.

Guidelines for MSE wall reinforcement subject to a barrier impact were desired from reinforcement pullout tests, full-scale impacts of barrier systems mounted on an MSE test wall, and numerical modeling. No influence of rate effects was found in the reinforcment pullout tests. Therefore, conventional reinforcement design procedures are appropriate for determining the dynamic pullout resistance of the wall reinforcement. In the dynamic bogie vehicle impact tests, the barrier systems were loaded to failure. While the barriers sustained significant damage, the overall behavior of the wall was satisfactory. The displacements of the wall panels were acceptable, and there was no panel damage observed except for a longitudinal failure crack in one panel at the upper layer of reinforcement in one of the test configurations with 4.88 m (16 ft) long strips. The loads measured in the reinforcement indicate that the reinforcement was brought to its ultimate pullout capacity. However, since the impact duration was so short and the the displacements were within tolerable limits, this is considered acceptable. The measured maximum dynamic loads in the strips were found to be 3 to 5 times higher than the calculated maximum static loads by AASHTO LRFD guidelines.

The measured loads were therefore factored to coincide with current design practice. Pressure diagrams and line loads were developed for the dynamic loads that should be considered in the reinforcement.

The full-scale dynamic bogie impact tests and dynamic impact simulations were used to develop design guidelines for the wall panels to resist the moment applied during a barrier impact. The guidelines define recommended design loads due to the increased load in the reinforcement and the contact forces transmitted into the wall panel from direct bearing of the barrier-coping system as appropriate.

A full-scale vehicle crash test into a vertical wall barrier mounted on the edge of a 2.74 m (9 ft) tall MSE wall was performed to verify the guidelines. The barrier system performed acceptably and met the evaluation criteria of the AASHTO Manual for Assessing Safety Hardware (MASH). Damage and displacement of the barrier system and underlying MSE wall were minimal.

The resulting guidelines are presented in Section 7 of this report. They were developed following AASHTO LRFD design practices and consider two different points of bearing and rotation of the barrier system. One point of rotation is applicable if the wall panels are isolated from contact with the coping by presence of a suitable air gap or sufficiently compressible material. The other point of rotation addresses the scenario of direct bearing of the barrier-coping system on top of the wall panels.

The design procedures for the barrier system address sliding, overturning, and structural adequency of the coping. The reinforcement design procedure considers pullout and rupture of the reinforcement. The dynamic design loads are specified using both a pressure diagram and line load approach. The guidelines also present design loads for the wall panels for both points of rotation of the barrier system.

REFERENCES

1. *AASHTO LRFD Bridge Design Specifications Third Edition*. American Association of State Highway and Transportation Officials. Washington, D.C., 2004.
2. Elias, V., B.R. Christopher, and R.R. Berg, *Mechanically Stabilized Earth Walls and Reinforced Soil Slopes Design and Construction Guidelines*, Ryan R. Berg & Associates, Inc.; National Highway Institute, Federal Highway Administration, U.S. Department of Transportation, Washington, D.C., 2001.
3. *Proposed Full-scale testing procedures for guardrails and guide posts.* Highway Research Circular No. 482, Highway Research Board Committee on Guardrails and Guide Posts, Washington, D.C., 1962.
4. Bronstad, M.E. and J.D. Michie, *Recommended Procedures for Vehicle Crash Testing of Highway Appurtenances,* NCHRP Report 153, Transportation Research Board, National Research Council, Washington, D.C., 1974.
5. *Recommended Procedures for Vehicle Crash Testing of Highway Appurtenances,* Transportation Research Board Circular No. 191, Transportation Research Board, National Academy of Sciences, Washington, D.C., 1978.
6. Michie, J.D., *Recommended Procedures for the Safety Performance Evaluation of Highway Appurtenances*, NCHRP Report 230, Transpotation Research Board, National Research Council, Washington, D.C., 1981.
7. Ross, H.E., D.L. Sicking, R.A. Zimmer, and J.D. Michie, *Recommended Procedures for the Safety Performance Evaluation of Highway Features*, National Cooperative Research Program (NCHRP) Report No. 350, Transportation Research Board, Washington, D.C., 1993.
8. Polivka, K.A., R.K. Faller, D.L. Sicking, J.R. Rohde, B.W. Bielenberg, and J.D. Reid, *Performance Evaluation of the Midwest Guardrail system – Update to NCHRP 350 Test No. 3-11 with 28" C.G. Height (2214MG-2)*, NCHRP 22-14(2), National Research Council, Washington, D.C., 2006.
9. *Manual for Assessing Safety Hardware*, American Association of State Highway and Transportation Officials. Washington, D.C., 2008.

10. *Standard Specifications for Highway Bridges Ninth Edition*. American Association of State Highway and Transportation Officials. Washington, D.C., 1965.
11. *Standard Specifications for Highway Bridges* 17th Edition. American Association of State Highway and Transportation Officials. Washington, D.C., 2002.
12. Noel, J.S., T.J. Hirsch, C.E. Buth, and A. Arnold, Loads on Bridge Railings, *Transportation Research Record 796*, TRB, National Research Council, Washington, D.C., 1981, pp 31-35.
13. Beason, W.L. and T.J. Hirsch, *Measurement of Heavy Vehicle Impact Forces and Inertia Properties*, Report No. FHWA-RD-89-120, Texas Transportation Institute, College Station, TX, 1989.
14. *AASHTO Guide Specifications for Bridge Railings*, American Association of State Highway and Transportation Officials. Washington, D.C., 1989.
15. Buth, C.E., et al., *Safer Bridge Railings, Volume 1: Summary Report*, Report No. FHWA/RD-82/072, Federal Highway Administration, U.S. Department of Transportation, Washington, D. C., 1984.
16. *AASHTO LRFD Bridge Design Specifications* First Edition. American Association of State Highway and Transportation Officials. Washington, D.C., 1996.
17. Alberson, D.C., W.F. Williams, W.L. Menges, and R.R. Haug, *Testing and Evaluation of the Florida Jersey Safety Shaped Bridge Rail*. Research Report. 9-8132-1. Texas Transportation Institute, College Station, TX, 2004.
18. *Crash Testing of a Precast Traffic Barrier Atop a Reinforced Earth Wall: Technical Bulletin: MSE -8*, The Reinforced Earth Company, Virginia, 1995.
19. *Standard Specifications for Highway Bridges* 15th Edition. American Association of State Highway and Transportation Officials. Washington, D.C., 1992.
20. Hallquist, J.O., *LS-DYNA: Keyword User's Manual, Version 971*, Livermore Software Technology Corporation (LSTC), Livermore, California, 2007.
21. Beer, F. P. and E. R. Johnston, *Vector Mechanics for Engineers: Dynamics*, 7th Ed., McGraw-Hill, New York, 2004.
22. Lee, H.S. and A. Bobet, *Design of MSE Walls for Fully Saturated Conditions*. Report No. FHWA-IN-JTRP-2002/13 for the Joint Transportation Research Program, Washington, D.C., 2002.

23. *Apparent Coefficient of Friction, f^* to be Used in the Design of Reinforced Earth Structures: Technical Bulletin: MSE -6*, The Reinforced Earth Company, Virginia, 1995.
24. Murray, Y.D., *Users Manual for LS-DYNA Concrete Material Model 159*, Publication FHWA-HRT-05-063. Federal Highway Administration, U.S. Department of Transportation, Virginia, 2007.
25. Desai, D.S., H.J. Siriwardane, Constitutive Laws for Engineering Materials with Empahsis on Geologic Materials, Prentice-Hall, Inc. N.J. 1984.
26. Chen, W.F. and E. Mizuno, Nonlinear Analysis in Soil Mechanics, Theory and Implementation, Elsevier, Amsterdam-Oxford-New York-Tokyo, 1990.
27. Hofstetter, G., J.C. Simo, and R.L. Taylor, A Modified Cap Model: Closest Point Solution Algorithms, *Computers & Sturctures,* Vol. 46, No.2, 1993, pp. 203-214.
28. Wu, J.T.H., K.Z.Z. Lee, S.B. Helwany, and K. Ketchart, *Design and Construction Guidelines for Geosynthetic-Reinforced Soil Bridge Abutments with a Flexible Facing*, NCHRP Report 556, NCHRP, Transportation Research Board, Washington, D.C., 2006.
29. ACI 318-08: Building Code Requirements for Structural Concrete and Commentary, American Concrete Institue, Michigan, 2008
30. *Standard Specifications for Construction and Maintenance of Highways, Streets, and Bridges*, Texas Department of Transportation, Texas, 2004.

APPENDIX A
DESIGN OF MSE WALL

1. 5-ft high MSE wall with 8-ft long strips design

INPUT

Wall								
Wall height,	H =	6.19	ft					
Reinforcing fill leng	L =	8	ft					
	B =	8.46	ft					
Soil unit weight,	γ_f =	0.125	kcf					
Traffic surcharge,	q =	0	ksf					
Reinforcement fill, ϕ	35	degrees	->	0.61	radians			
			->	tanϕ =	0.70	->	Ka =	0.27
Retained fill, ϕ =	30	degrees	->	0.52	radians			
			->	$\tan\phi_f$ =	0.58	->	Kaf =	0.33
Panel								
Vertical spacing of strips, S_v=		2.46	ft	density of strip per panel =			6	
Panel width =		4.92	ft					
Panel thickness =		0.46	ft					
max. tension per strip =		7.2	kips					

1. External Stability

1.1 Static Mass Stability

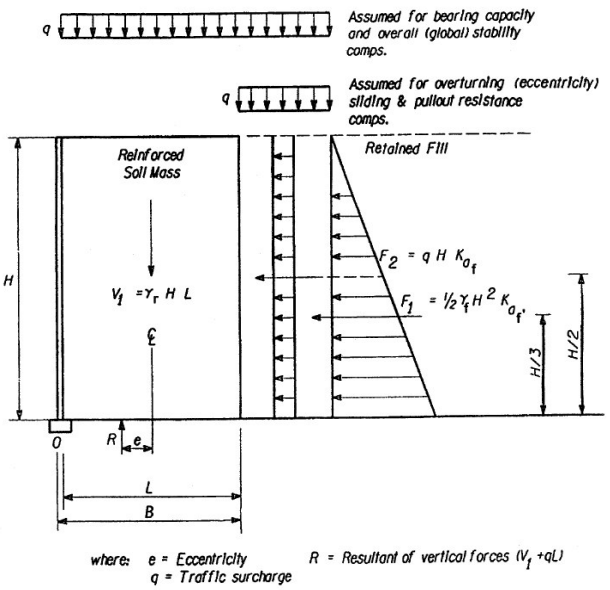

1.1.1 Vertical loads

R.E. Soil	V1=	0.125	(kcf) ×	6.19	(ft) ×	8	(ft) =	6.19 kips/ft
	Moment arm of V1 =	4	ft					
	M_{v1}=	6.19	(kips/ft) ×	4	(ft) =	24.76	ft-kips/ft	
Traffic	V2=	0	(ksf) ×	8	(ft) =	0	kips/ft	
surcharge	Moment arm of V2 =	4	ft					

M_{v2}= 0 (kips/ft) × 4 (ft) = 0 ft-kips/ft

$\sum V$ = 6.19 kips/ft $\sum M_v$ = 24.76 ft-kips/ft

1.1.2 Horizontal loads

R.E. Soil F1= 1/2 × 0.125 (kcf) × 38.3161 (ft^2) × 0.33 = 0.80 kips/ft

Moment arm of F1 = 6.19 /3 = 2.06 ft

M_{F1}= 0.80 (kips/ft) × 2.06 (ft) = 1.65 ft-kips/ft

Traffic F2= 0 (ksf) × 6.19 (ft) × 0.33 = 0.00 kips/ft

surcharge Moment arm of F2 = 6.19 /2 = 3.10 ft

M_{F2}= 0.00 (kips/ft) × 3.10 (ft) = 0.00 ft-kips/ft

$\sum F$ = 0.80 kips/ft $\sum M_F$ = 1.64706 ft-kips/ft

1.1.3 Sliding

Sliding Safety Factor = 1.5

Sliding = $\frac{V1^* \tan\phi}{\sum F_h}$ = 4.48 ≥ 1.5 OK

1.1.4 Overturning

Sliding Safety Factor = 2

Sliding = $\frac{\sum M_{v1}}{\sum M_F}$ = 15.03 ≥ 2 OK

1.2 Bearing Capacity at Base

eccentricity = $\frac{L}{2} - \frac{\sum M_v - \sum M_h}{\sum V}$ = 0.27 ft

≤ $\frac{B}{6}$ = 1.41 ft OK

σ_v= $\frac{\sum V}{(L-2e)}$ = 0.83 ksf

2. Internal Stability

2.1 Without Impact Load

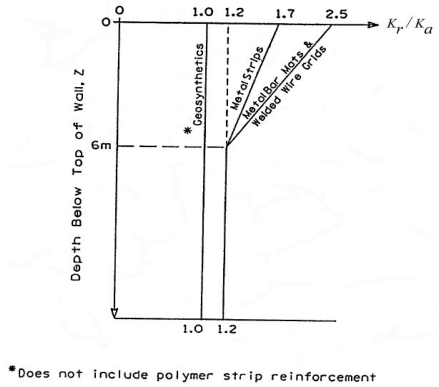

2.1.1 Compute Kr

Kr = 1.7 × Ka = 0.46 at 0 ft

Kr = 1.2 × Ka = 0.33 under 20 ft

Use interpolation at other depth

2.1.2 Fisrt strip at h1=2.53 ft

h1 = 2.53 ft

Kr = 0.444

a) Vertical loads

R.E. Soil V1= 0.125 (kcf) × 2.53 (ft) × 8 (ft) = 2.53 kips/ft

Moment arm of V1 = 4 ft

M_{v1}= 2.53 (kips/ft) × 4 (ft) = 10.12 ft-kips/ft

Traffic V2= 0.25 (ksf) × 8 (ft) = 2.00 kips/ft

surcharge Moment arm of V2 = 4 ft

M_{v2}= 2.00 (kips/ft) × 4 (ft) = 8.00 ft-kips/ft

$\sum V$ = 4.53 kips/ft $\sum M_v$ = 18.12 ft-kips/ft

b) Horizontal loads

R.E. Soil F1= 1/2 × 0.125 (kcf) × 6.40 (ft^2) × 0.33 = 0.13 kips/ft

Moment arm of F1 = 2.53 /3 = 0.84 ft

M_{F1}= 0.13 (kips/ft) × 0.84 (ft) = 0.11 ft-kips/ft

Traffic surcharge F2= 0 (ksf) × 2.53 (ft) × 0.33 = 0.00 kips/ft

Moment arm of F2 = 2.53 /2 = 1.27 ft

M_{F2}= 0.00 (kips/ft) × 1.27 (ft) = 0.00 ft-kips/ft

$\sum F$ = 0.13 kips/ft $\sum M_F$ = 0.11246 ft-kips/ft

2.1.2.1 Reinforcing strip tension (considering the traffic surcharge)

$$\text{eccentricity} = \frac{L}{2} - \frac{\sum M_v - \sum M_h}{\sum V} = 0.02 \text{ ft}$$

$$\leq \frac{B}{6} = 1.41 \text{ ft} \quad \text{OK}$$

$$\sigma_v = \frac{\sum V}{(L-2e)} = 0.57 \text{ ksf}$$

σ_h= K σ_v= 0.44 × 0.57 ksf = 0.25 ksf

A_t per strip = 4.87 (ft) × 2.43 (ft) / 3 = 3.94 ft^2

I assumed the panel shape is rectangular shape, but same area and the area is devided by 6 for strips.

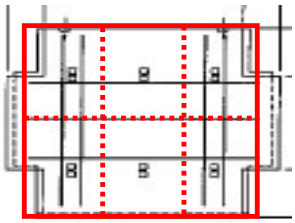

Total tension = 3.94 ft^2 × 0.25 ksf = **1.00** kips per strip

2.1.2.2 Effective length safety factor (no traffic surcharge)

$$\text{eccentricity} = \frac{L}{2} - \frac{\sum M_{v1} - \sum M_h}{\sum V1} = 0.04 \text{ ft}$$

$$\leq \frac{B}{6} = 1.41 \text{ ft} \quad \text{OK}$$

$$\sigma_v = \frac{\sum V1}{(L-2e)} = 0.32 \text{ ksf}$$

σ_h= K σ_v= 0.44 × 0.32 ksf = 0.14 ksf

A_t per strip = 4.87 (ft) × 2.43 (ft) / 3 = 3.94 ft^2 0.16125

Total tension = 3.94 ft^2 × 0.14 ksf = **0.56** kips per strip 0.07901

2.1.2.3 Resistance in friction of one strip against soil

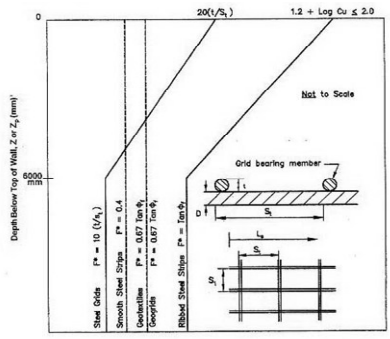

Figure 11.10.6.3.2-1 Default Values for the Pullout Friction Factor, *F.**

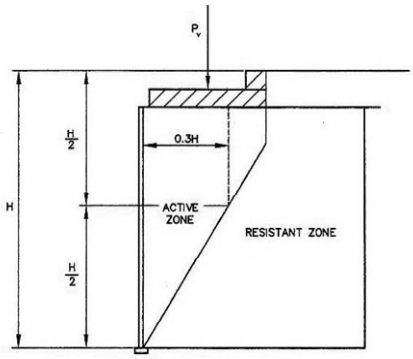

Figure 11.10.10.1-2 Location of Maximum Tensile Force Line in Case of Large Surcharge Slabs (Inextensible Reinforcements).

a) F^*

Kr = 2.00 at 0 ft

Kr = $\tan \phi_f$ = 0.33 under 20 ft

Use interpolation at other depth

F^* = 1.789

b) L = 8 ft

c) 2b = 0.328 ft (from RECo example for high Adherence Strips)

R = $2b \times L \times \sigma_v \times F^*$ = **1.48** kips

2.1.2.4 Location of Maximum Tensile Force

If the height of reinforcement layer is above the H/2, the location of max. tensile force is located in 0.3H.

0.3H = 1.857 ft H/2 = 3.095 ft

$L_{max.}$ = 1.857 ft

2.1.3 Second strip at h2=4.99 ft

h1 = 4.99 ft

Kr = 0.427

a) Vertical loads

R.E. Soil	V1=		0.125 (kcf) ×	4.99 (ft) ×	8 (ft) =	4.99	kips/ft
	Moment arm of V1 =		4 ft				
	M_{v1}=		4.99 (kips/ft) ×	4 (ft) =	19.96	ft-kips/ft	
Traffic	V2=		0.25 (ksf) ×	8 (ft) =	2.00	kips/ft	
surcharge	Moment arm of V2 =		4 ft				
	M_{v2}=		2.00 (kips/ft) ×	4 (ft) =	8.00	ft-kips/ft	
	$\sum V$ =	6.99 kips/ft		$\sum M_v$ =	27.96	ft-kips/ft	

b) Horizontal loads

R.E. Soil	F1=	1/2 ×	0.125 (kcf) ×	24.90 (ft^2) ×	0.33 =	0.52	kips/ft
	Moment arm of F1 =		4.99 /3 =	1.66 ft			
	M_{F1}=		0.52 (kips/ft) ×	1.66 (ft) =	0.86	ft-kips/ft	
Traffic	F2=		0 (ksf) ×	4.99 (ft) ×	0.33 =	0.00	kips/ft

surcharge Moment arm of F2 = 4.99 /2 = 2.50 ft

M_{F2}= 0.00 (kips/ft) × 2.50 (ft) = 0.00 ft-kips/ft

$\sum F$ = 0.52 kips/ft $\sum M_F$ = 0.86 ft-kips/ft

2.1.3.1 Reinforcing strip tension (considering the traffic surcharge)

$$\text{eccentricity} = \frac{L}{2} - \frac{\sum M_v - \sum M_h}{\sum V} = 0.12 \text{ ft}$$

$$\leq \frac{B}{6} = 1.41 \text{ ft} \quad \text{OK}$$

$$\sigma_v = \frac{\sum V}{(L-2e)} = 0.90 \text{ ksf}$$

σ_h= K σ_v= 0.43 × 0.90 ksf = 0.38 ksf

A_t per strip = 4.87 (ft) × 2.43 (ft) / 3 = 3.94 ft^2

Total tension = 3.94 ft^2 × 0.38 ksf = **1.52** kips per strip

2.1.3.2 Effective length safety factor (no traffic surcharge)

$$\text{eccentricity} = \frac{L}{2} - \frac{\sum M_{v1} - \sum M_h}{\sum V1} = 0.17 \text{ ft}$$

$$\leq \frac{B}{6} = 1.41 \text{ ft} \quad \text{OK}$$

$$\sigma_v = \frac{\sum V1}{(L-2e)} = 0.65 \text{ ksf}$$

σ_h= K σ_v= 0.43 × 0.65 ksf = 0.28 ksf

A_t per strip = 4.87 (ft) × 2.43 (ft) / 3 = 3.94 ft^2

Total tension = 3.94 ft^2 × 0.28 ksf = **1.10** kips per strip

2.1.3.3 Resistance in friction of one strip against soil

a) F^* = 1.584

b) L = 8 ft

c) 2b = 0.328 ft (from RECo example for high Adherence Strips)

R = $2b \times L \times \sigma_v \times F^*$ = **2.59** kips

2.1.3.4 Location of Maximum Tensile Force

0.3H = 1.857 ft H/2 = 3.095 ft

$L_{max.}$ = 0.72 ft

* Summary

Rein. Laye NO.	Z (ft)	e (ft)	$_v$ (ksf)	Kr	$_h$ (ksf)	**T (kips)**	$L_{max.}$ (ft)	**R (kips)**	FS
1	2.53	0.04	0.32	0.444	0.14	**0.56**	1.857	**1.48**	2.66
2	4.99	0.17	0.65	0.427	0.28	**1.10**	0.72	**2.59**	2.36

T: the horizontal force supported by a single reinforcement due to the tributary area of reinforcement, with no traffic surcharge

2.2 Including Impact Load

load (kips)	length of slab (ft)	f (degrees)	45+(ϕ/2) (degrees)	45+(ϕ/2) radian	tan(45+(ϕ/2))	l (ft)	l+2
10	4.5	35	62.5	1.09	1.92	8.64	10.64

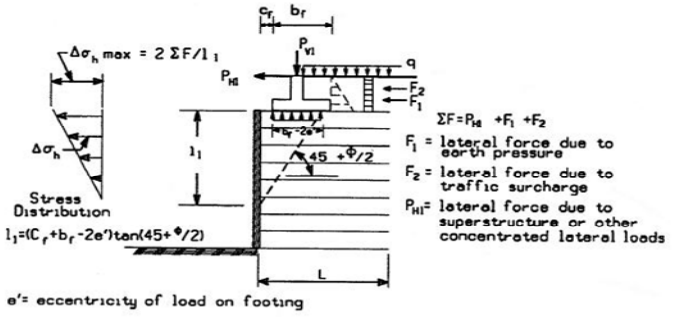

a. Distribution of Stress for Internal Stability Calculations.

2.2.1 Tensile stress

5 ft.-> ∑F = 2 kpf

Rein. Laye NO.	Layer (ft)	l_1 (ft)	$\Delta\sigma_{h\ max}$ (ksf)
	1.67		0.46
1	2.53	7.78	0.42
2	4.99	5.32	0.29

* Summary of only impact load

Rein. Laye NO.	Z (ft)	σ_v (ksf)	$\Delta\sigma_{h\ max}$ (ksf)	A_t (ft^2)	T_{impact} (kips)
1	2.53	0.32	0.42	3.94	1.64
2	4.99	0.65	0.29	3.94	1.12

T: the horizontal force supported by a single reinforcement due to the tributary area of reinforcement

* Summary of Total

Rein. Laye NO.	Z (ft)	σ_v (ksf)	σ_h (ksf)	$\Delta\sigma_{h\ max}$ (ksf)	Total σ_h (ksf)	A_t (ft^2)	**T (kips)**
1	2.53	0.32	0.14	0.42	0.56	3.94	**2.20**
2	4.99	0.65	0.28	0.29	0.56	3.94	**2.22**

T: the horizontal force supported by a single reinforcement due to the tributary area of reinforcement with no traffic surcharge

2.2.2 Pullout stress

20 ft.-> $\sum F$ = 0.5 kpf

Rein. Laye NO.	Layer (ft)	l 1 (ft)	$\Delta\sigma_{h\ max}$ (ksf)
	1.67		0.12
1	2.53	7.78	0.10
2	4.99	5.32	0.07

* Summary of only impact load

Rein. Laye NO.	Z (ft)	σ_v (ksf)	$\Delta\sigma_{h\ max}$ (ksf)	A_t (ft^2)	T_{impact} (kips)
1	2.53	0.32	0.10	3.94	0.41
2	4.99	0.65	0.07	3.94	0.28

T: the horizontal force supported by a single reinforcement due to the tributary area of reinforcement

* Summary of Total

Rein. Laye NO.	Z (ft)	σ_v (ksf)	σ_h (ksf)	$\Delta\sigma_{h\ max}$ (ksf)	Total σ_h (ksf)	A_t (ft^2)	**T (kips)**
1	2.53	0.32	0.14	0.10	0.25	3.94	**0.97**
2	4.99	0.65	0.28	0.07	0.35	3.94	**1.38**

T: the horizontal force supported by a single reinforcement due to the tributary area of reinforcement

APPENDIX B

STATE-OF-PRACTICE SURVEY

Name: _____ **Title: _____**

Agency Name & Address: _____

_____

_____

_____

Instructions (for electronic completion of survey):

For fill-in responses: You may enter your response by either tabbing through the form or by clicking on the shaded area. Please use as much space as needed to explain a selection of "Other."

For check boxes: To check or uncheck a box, either type an "X" in the box or click on the box with your mouse. Unless noted otherwise, you can check more than one box for each item.

MSE Walls

1) Estimate percentage of each type of reinforcement used in MSE walls in your state:

Steel strips _____% Wire mesh/bar mats _____%

Geosynthetic grids _____% Other (explain) _____% _____

2) Estimate percentage of each type of facing panel used in your state:

Concrete panel _____% Modular block _____%

Other (explain) _____% _____

3) Estimate percentage of each type of facing panel connection used in your state:

Dowels _____% Tongue & Groove _____%

Ship Lap _____% Other (explain) _____% _____

Please provide standards and specifications for MSE walls used in your state (including soil backfill, panels, and reinforcement)

Barriers

4) Estimate percentage of each category of barrier used atop MSE walls in your state:

Guardrail (post mounted) _____% Bridge Rail (slab/pavement attached) _____%

5) Estimate percentage of each type of guardrail used atop MSE walls in your state:

Strong post W-beam _____% Weak post W-beam _____%

Thrie beam _____% Box beam _____%

Cable _____% Other (explain) _____% _____

6) Estimate percentage of each type of bridge rail used atop MSE walls in your state:

Concrete safety shape (N.J., F-shape, single slope) _____%

Vertical concrete wall _____% Concrete beam & post _____%

Concrete parapet w/ steel rail _____% Steel _____%

Other (explain) _____% _____

7) Estimate percentage of precast barrier versus cast-in-place barrier used atop MSE walls in your state:

Precast coping & barrier unit _____% Precast coping with cast-in-place barrier _____%

Cast-in-place coping & barrier _____% Other (explain) _____% _____

8) If precast barrier used, please specify minimum segment length allowed _____

Please provide standard detail sheets for each type of barrier used atop MSE walls in your state.

Barrier Connection to Wall/Pavement

9) Estimate percentage of each type of pavement used in your state in conjunction with MSE wall applications:

RCP _____% ACP _____%

Please answer the following in regard to post-mounted guardrail placed atop MSE walls:

10) Lateral offset of guardrail from edge of wall _____

Please answer the following in regard to slab-attached bridge rails placed atop MSE walls:

For ACP pavement applications:

11) Thickness of barrier/slab footing _____ 12) Width of slab/footing _____

13) Is barrier/slab footing continuous ☐ or jointed ☐?

14) If jointed, what is joint spacing? _____

15) Is barrier flush with wall ☐ Offset from face of wall ☐

16) If offset, by what distance? _____

17) Is wall panel coped/recessed into bottom of coping? No ☐ Yes ☐

18) If yes, by how much? _____

19) Is lateral and vertical barrier movement connected ☐ or disconnected/isolated ☐ from wall panel?

For RCP pavement applications:

20) Thickness of barrier/slab footing _____ 21) Width of slab/footing _____

22) Is barrier/slab footing continuous ☐ or jointed ☐?

23) If jointed, what is joint spacing? _____

24) Is barrier flush with wall ☐ Offset from face of wall ☐

25) If offset, by what distance? _____

26) Is wall panel coped/recessed into bottom of coping? No ☐ Yes ☐

27) If yes, by how much? _____

28) Is lateral and vertical barrier movement connected ☐ or disconnected/isolated ☐ from wall panel?

29) How is barrier slab connected to pavement? Integrally poured ☐ Doweled ☐

Please provide standard connection/construction details used in your state.

Design

MSE Walls

30) How much horizontal load do you consider to be transferred to the top of the MSE wall due to barrier impact? _____

Barrier

31) NCHRP Report 350 Test Level TL-3 ☐ TL-4 ☐ TL-5 ☐

32) Do you follow AASHTO LRFD Bridge Specification, Chapter 13 "Railings," for bridge railing design: No ☐ Yes ☐

If answer to previous question is "No":

33) What is magnitude of barrier design load? _____

34) What is the height of the applied design load? _____

Please cite source _____

Connections

Barrier to Wall

35) How is maximum bending moment in the barrier and barrier slab/footing determined? _____

36) How is maximum shear in the barrier and barrier slab/footing determined? _____

For ACP pavement applications:

37) How do you calculate the required width and thickness of the barrier slab/footing? _____

For RCP pavement applications:

38) Do you calculate the bending moment in the pavement slab due to impact load on barrier? No ☐ Yes ☐

If yes, explain how _____

Please provide procedures for design of barriers on MSE walls (cite applicable manuals/references/guidelines (e.g., AASHTO LRFD or ASD Bridge Specification)).

Performance

39) Are you aware of any failures of MSE walls or barriers atop MSE walls due to vehicular impact? No ☐ Yes ☐

If yes, which components failed (check all that apply):

Barrier ☐ Coping ☐ Slab/Pavement ☐ Wall Panel ☐

Please provide any documentation (e.g., photographs, accident report, site details) that may exist for any known failures.

40) Are you aware of any other performance issues associated with MSE walls or barriers atop MSE walls? No ☐ Yes ☐

If yes, please describe _____

APPENDIX C

DETAILED DRAWING OF MSE WALL FOR BOGIE TEST

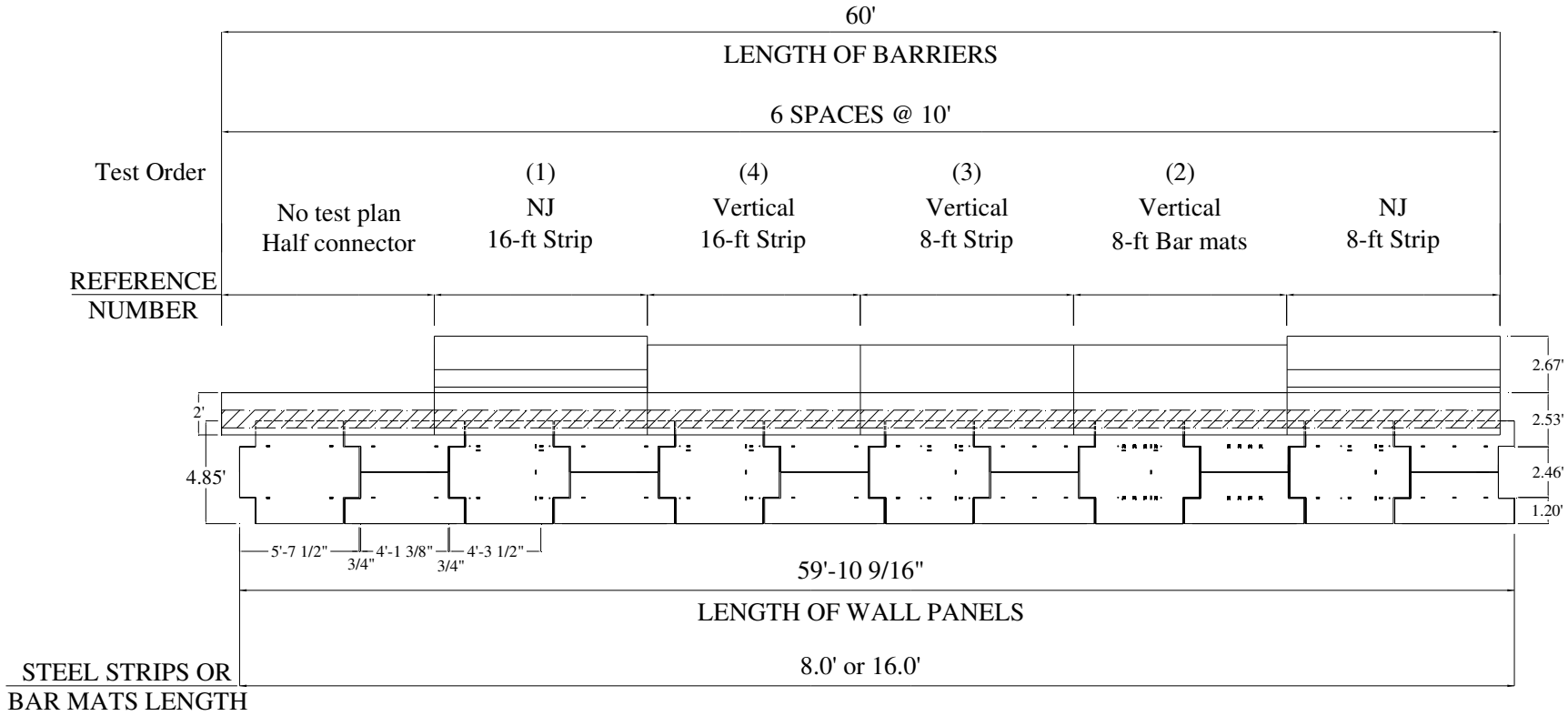

Figure C 1 Updated Overall Elevation of Installation for Bogie Reference Tests

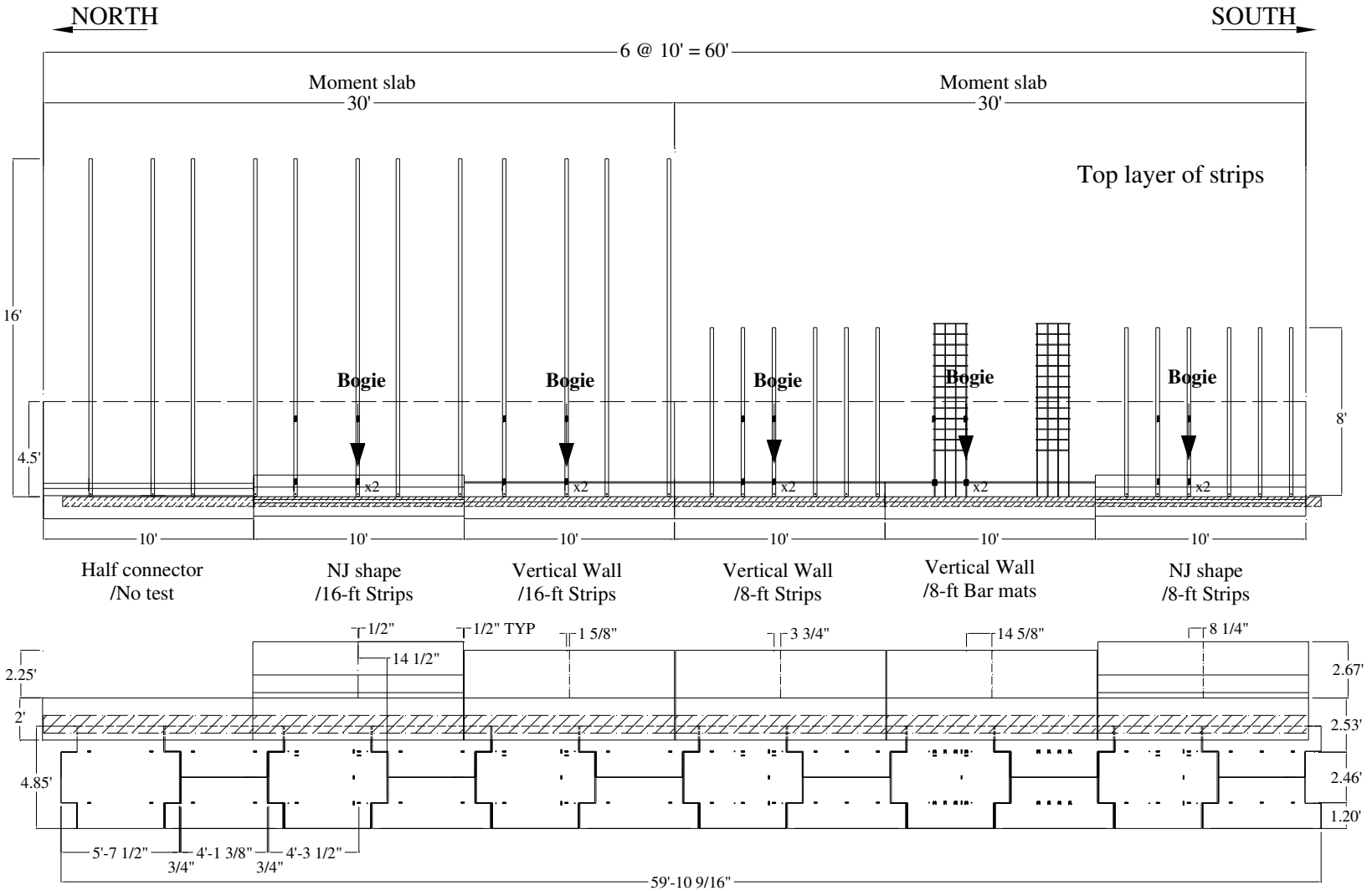

Figure C 2 First Reinforcement Layer

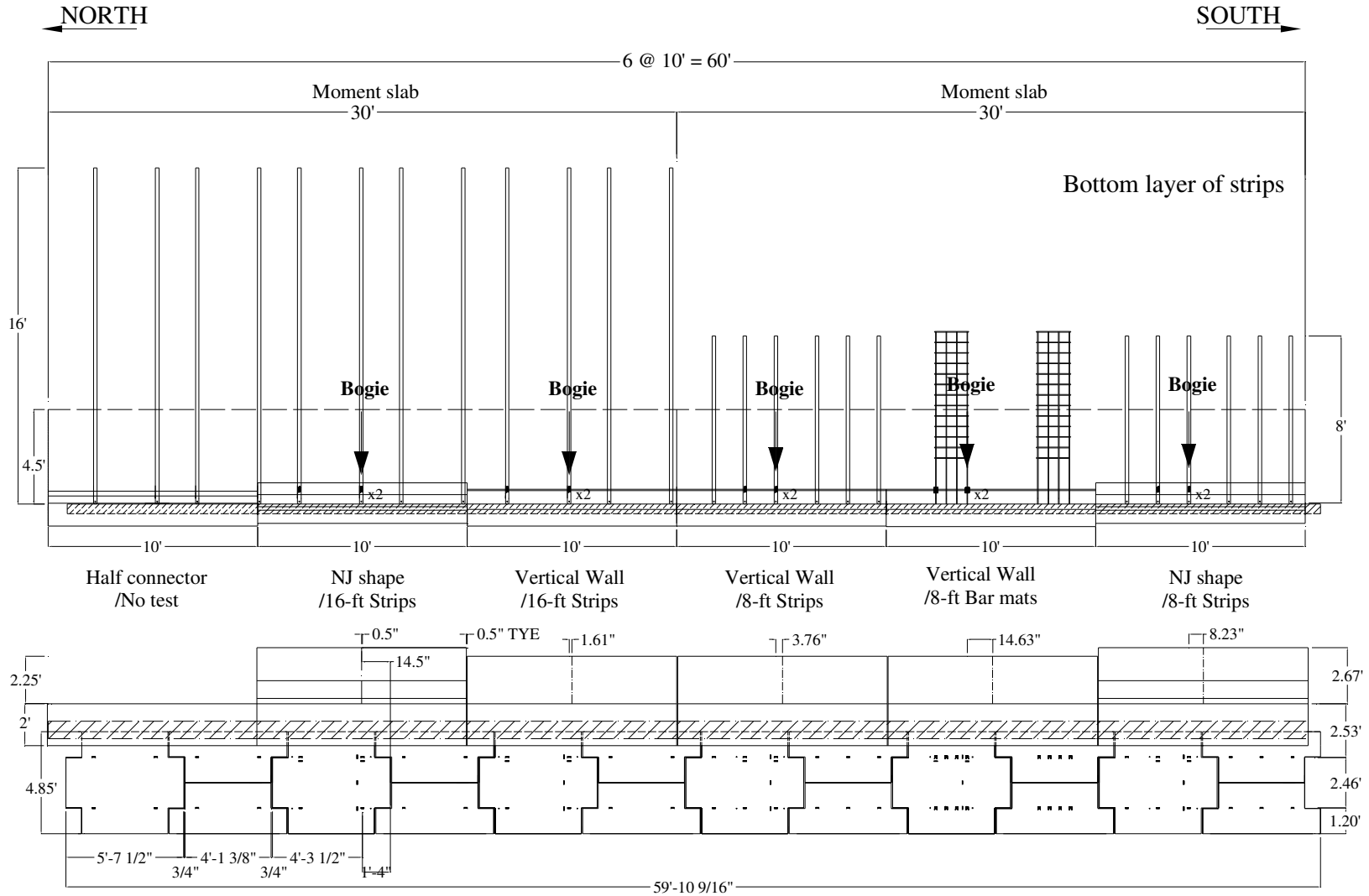

Figure C 3 Second Reinforcement Layer

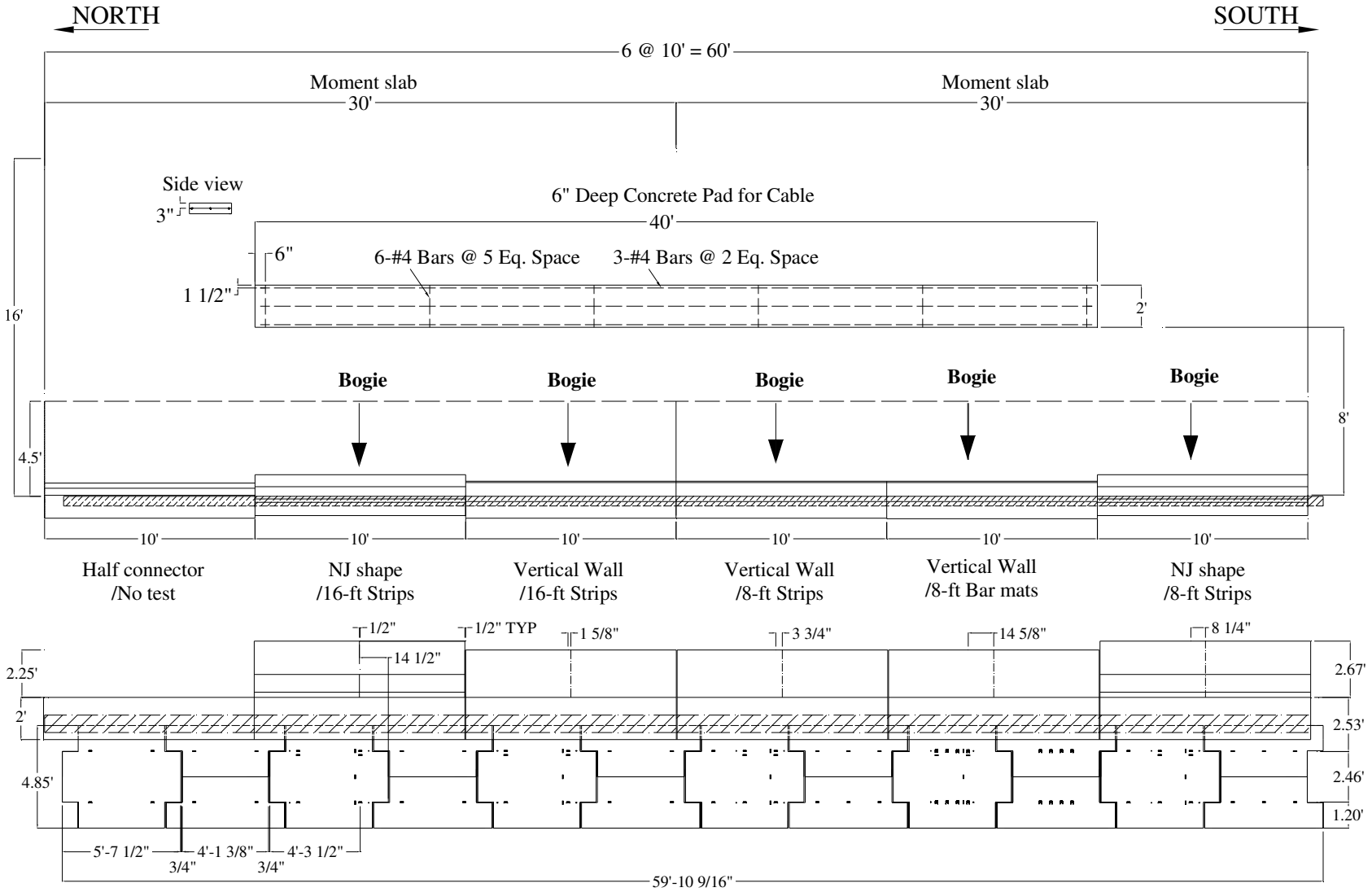

Figure C 4 Concrete Pad of Toe-System for Bogie Vehicle

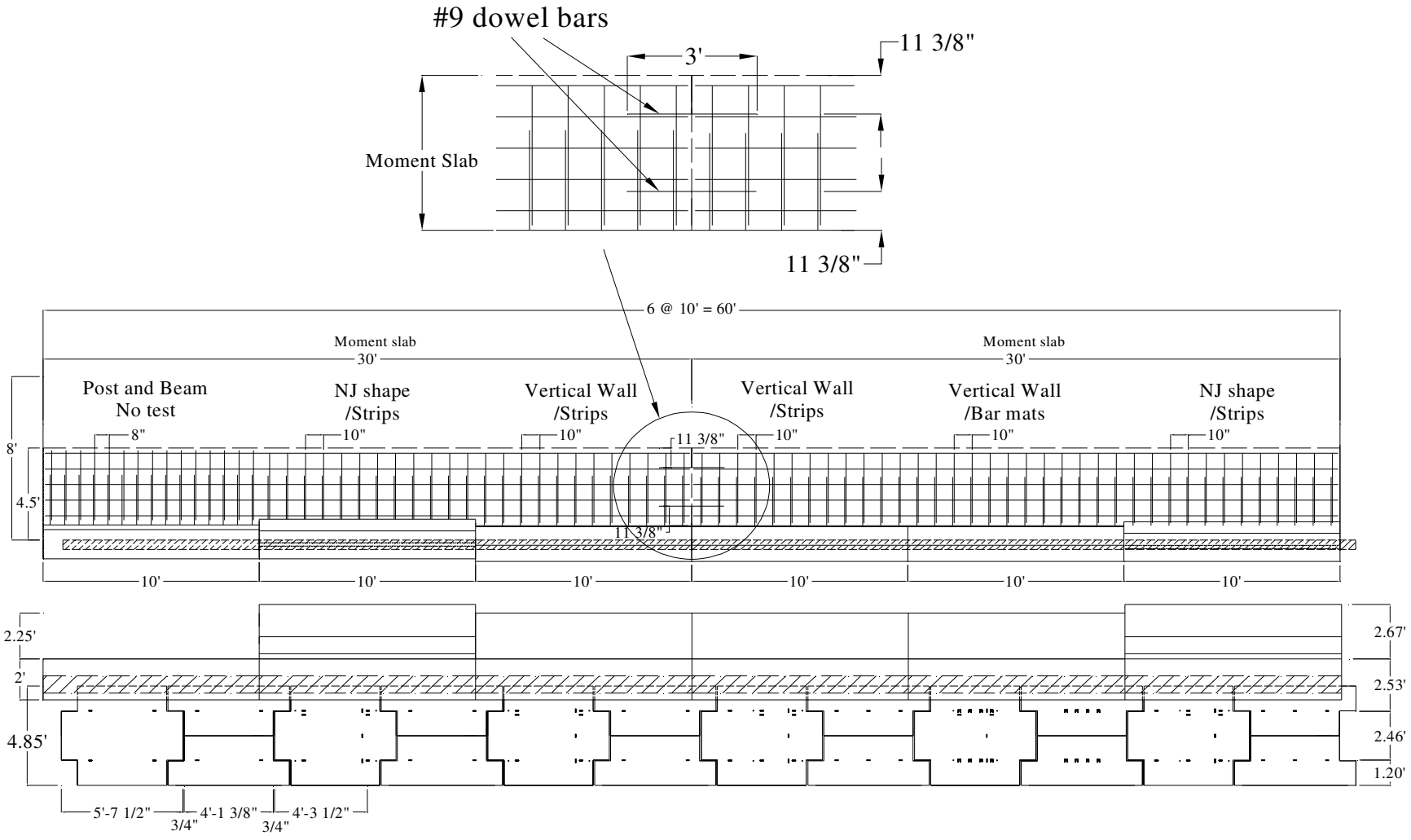

Figure C 5 Detailed Connection of Two 30-ft Moment Slab

APPENDIX D
BOGIE TEST MSE WALL CONSTRUCTION PROCEDURE

Figure D.1 Delivery of Backfill Material

Figure D.2 Excavation for MSE Wall

Figure D.3 Completed Excavation and Temporary Shoring

Figure D.4 Form and Pour Concrete Pedestal

Figure D.5 Place Initial Course of Wall Panels

Figure D.6 Spread and Compact Backfill to Bottom Layer of Reinforcement

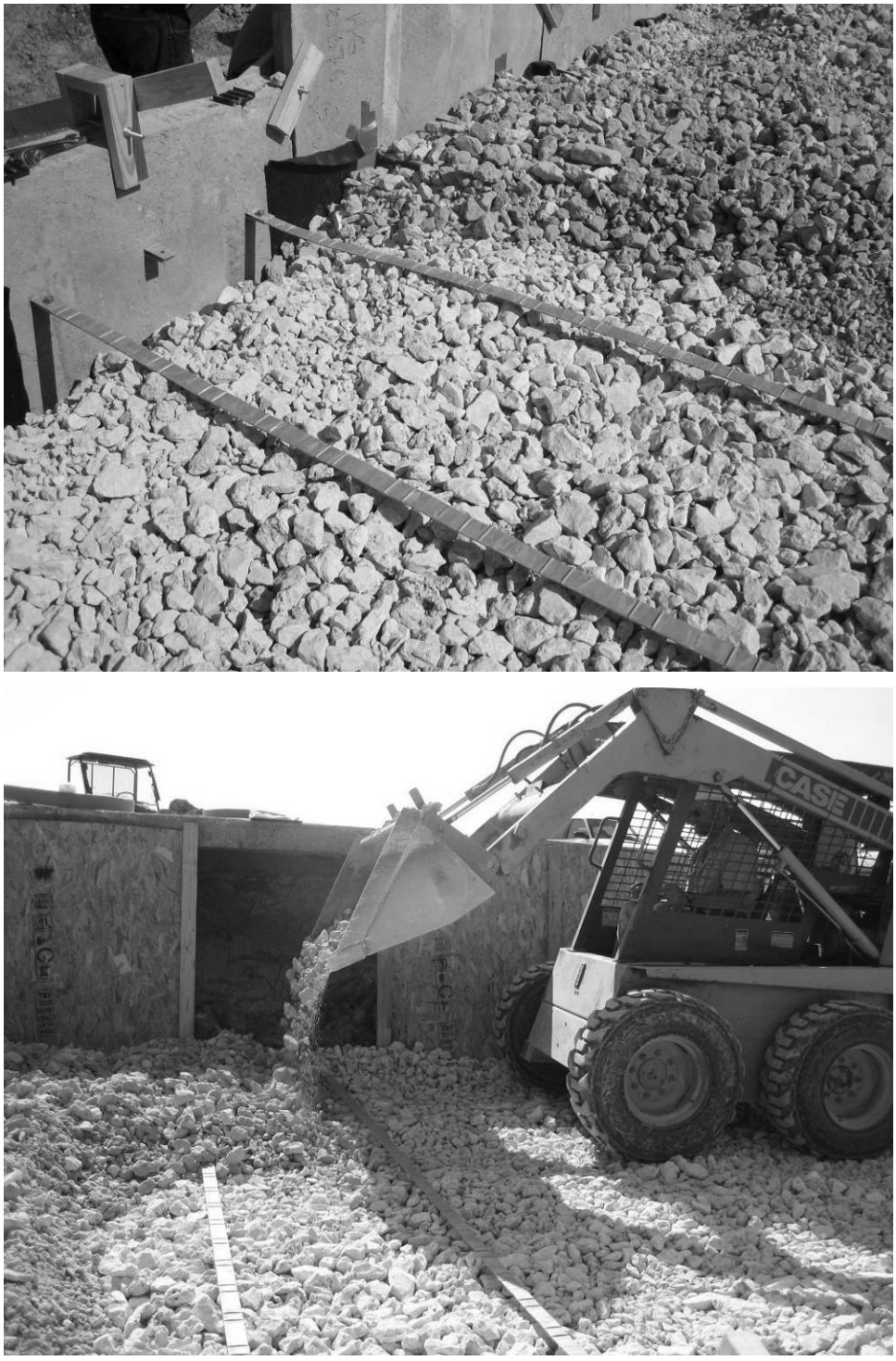

Figure D.7 Install Bottom Layer of Reinforcement

256

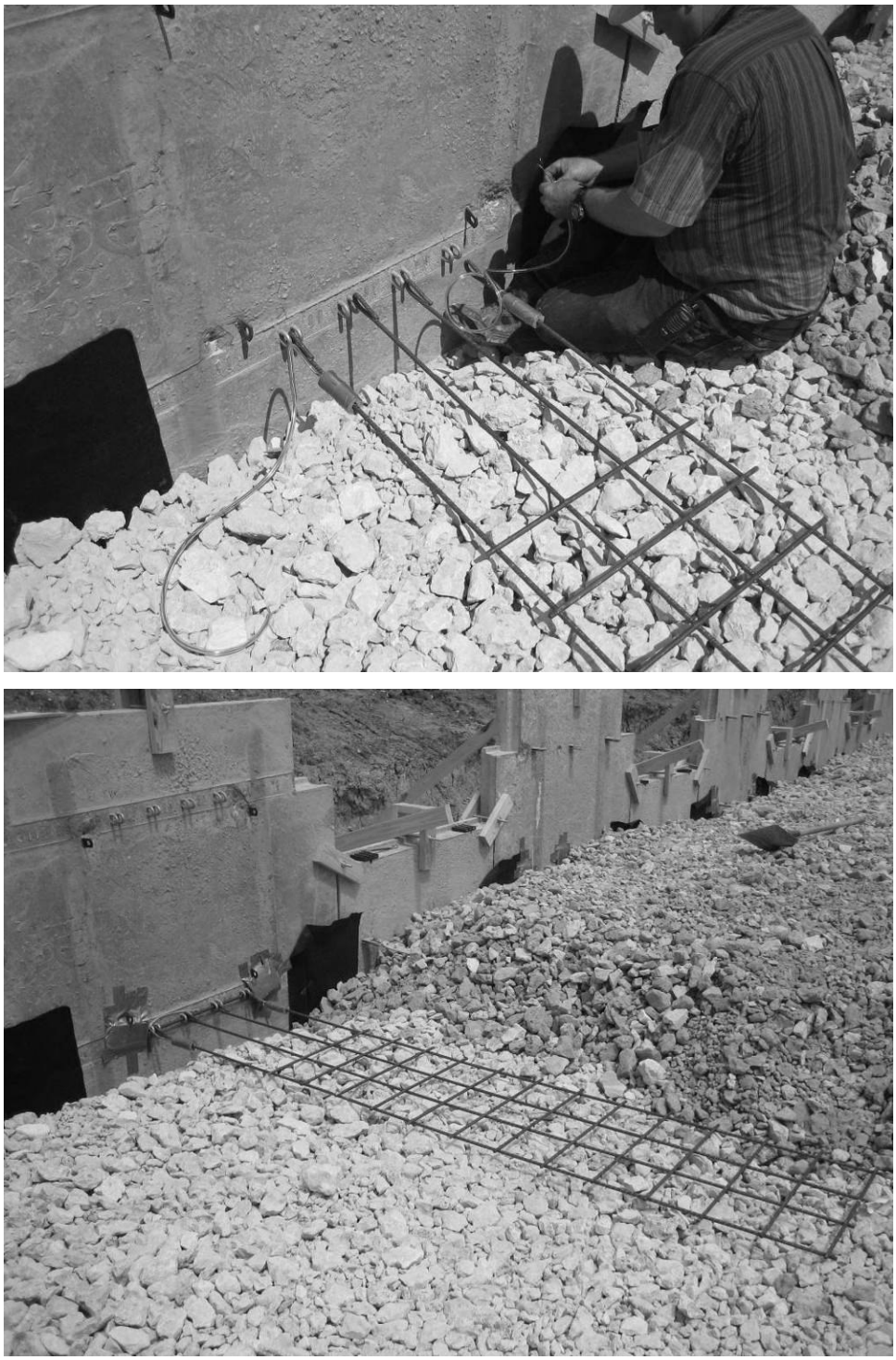

Figure D.8 Install Bar Mat Reinforcement

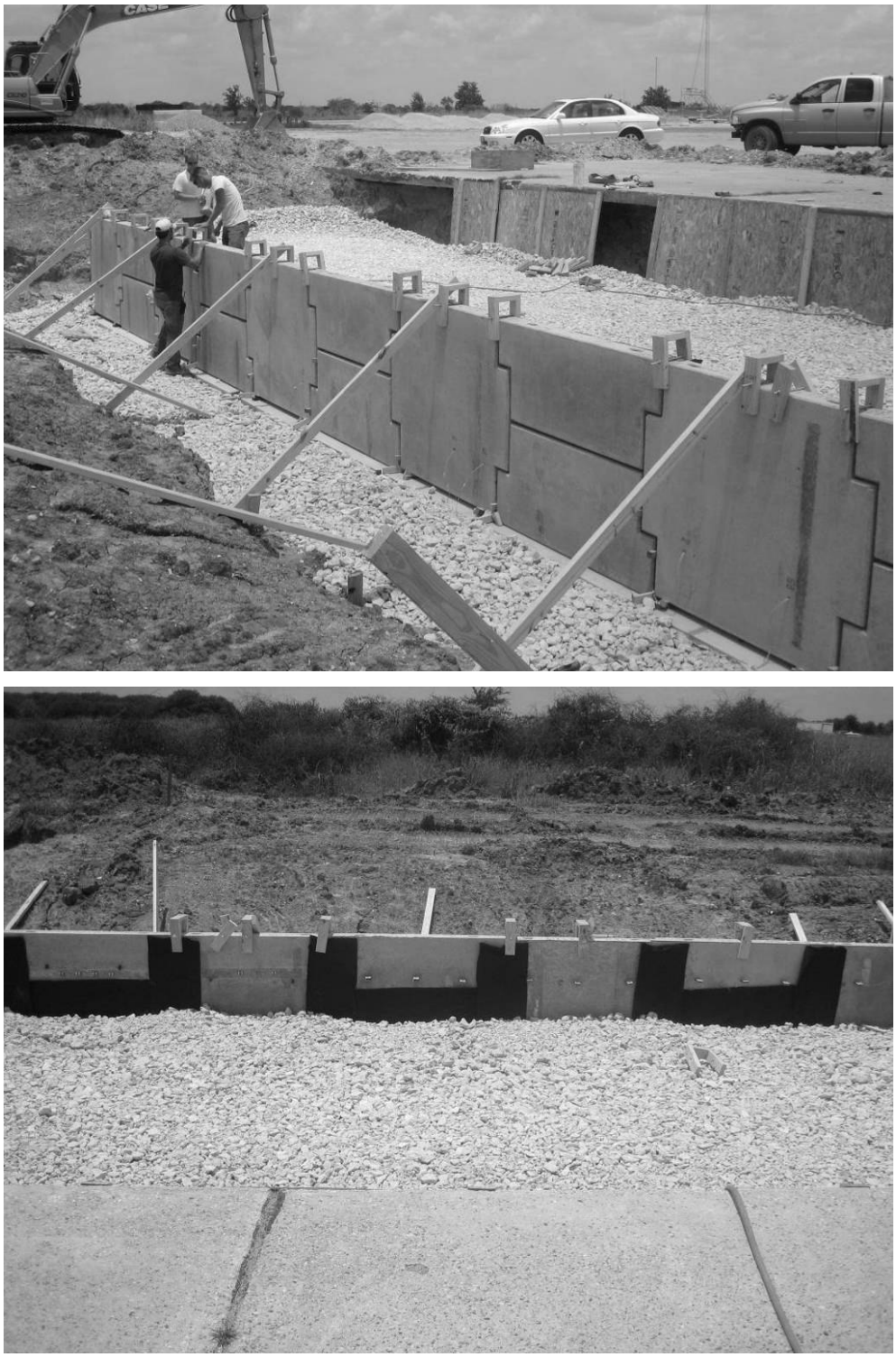

Figure D.9 Place Second Course of Panels and Backfill to Top Layer of Reinforcement

Figure D.10 Completed MSE Wall Construction

Figure D.11 Form and Pour Concrete Leveling Pad atop Wall Panels

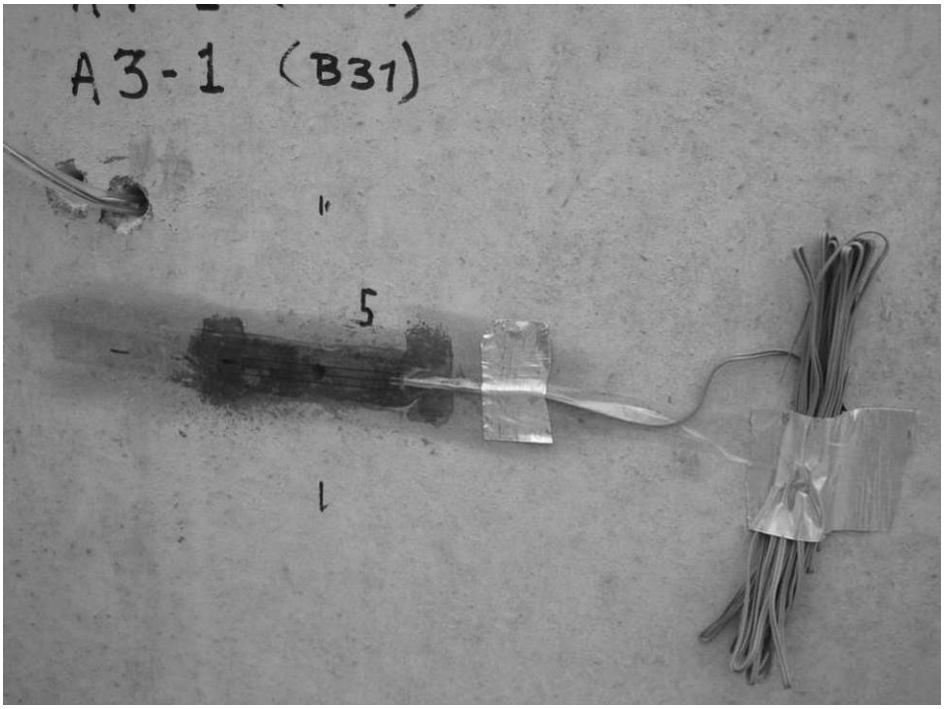

Figure D.12 Install Concrete Strain Gages on Exterior Face of Wall Panels

Figure D.13 Install Tape Switches on Inside Face of Wall Panels/Level Up Concrete

Figure D.14 Place Barriers atop Wall Panels

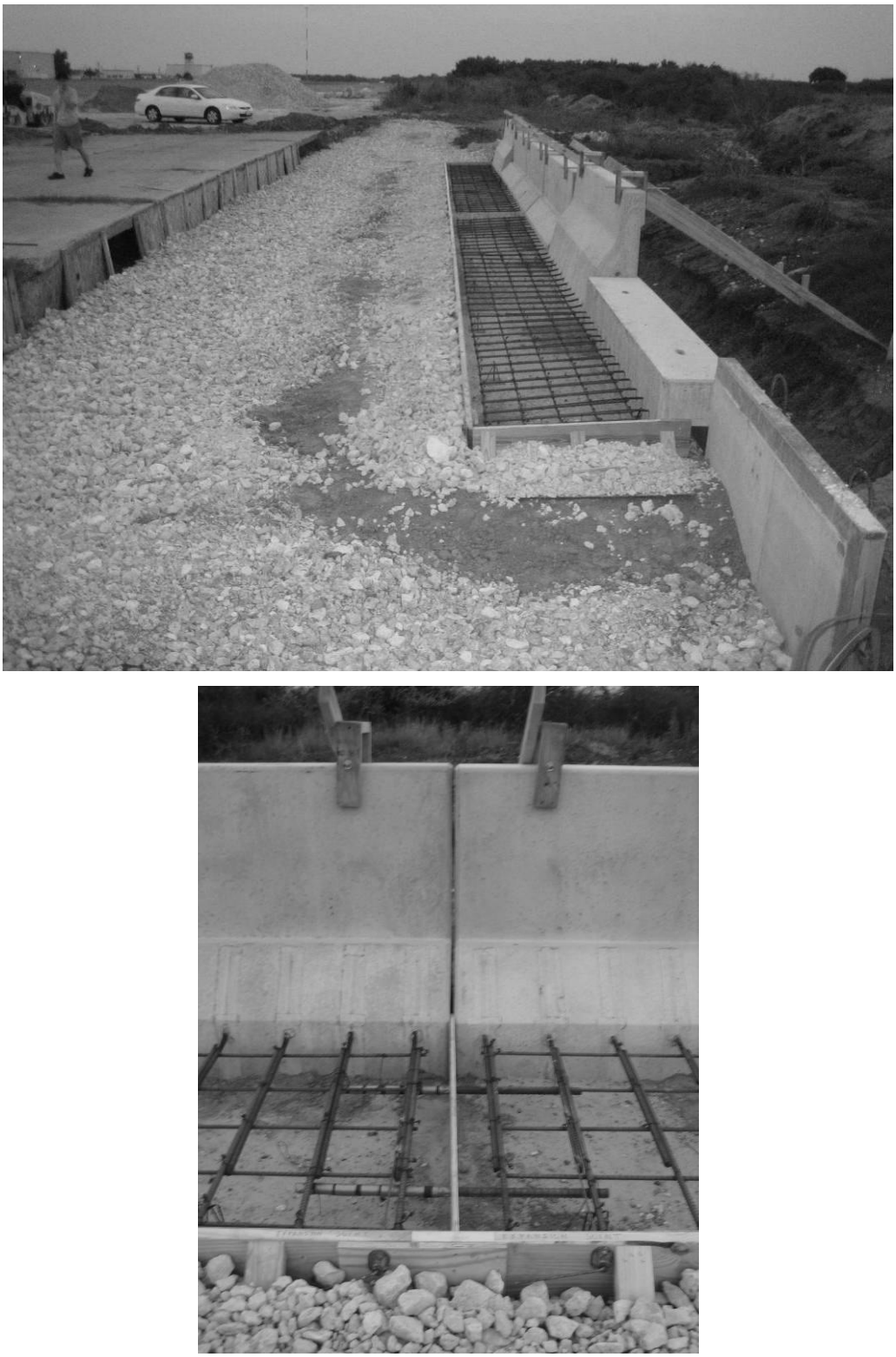

Figure D.15 Form Moment Slab and Install Reinforcing Bars

Figure D.16 Pour Concrete for Moment Slab

Figure D.17 Completed Moment Slab

Figure D.18 Installation of Accelerometers on the Moment Slabs

Figure D.19 Form of Pad for Tow-System for Bogie Vehicle

Figure D.19 Pour Concrete for Tow-System Pad

Figure D.20 Completed Concrete Pad for Tow-System

Figure D.21 Fill the Soil above the Moment Slab and Backfill

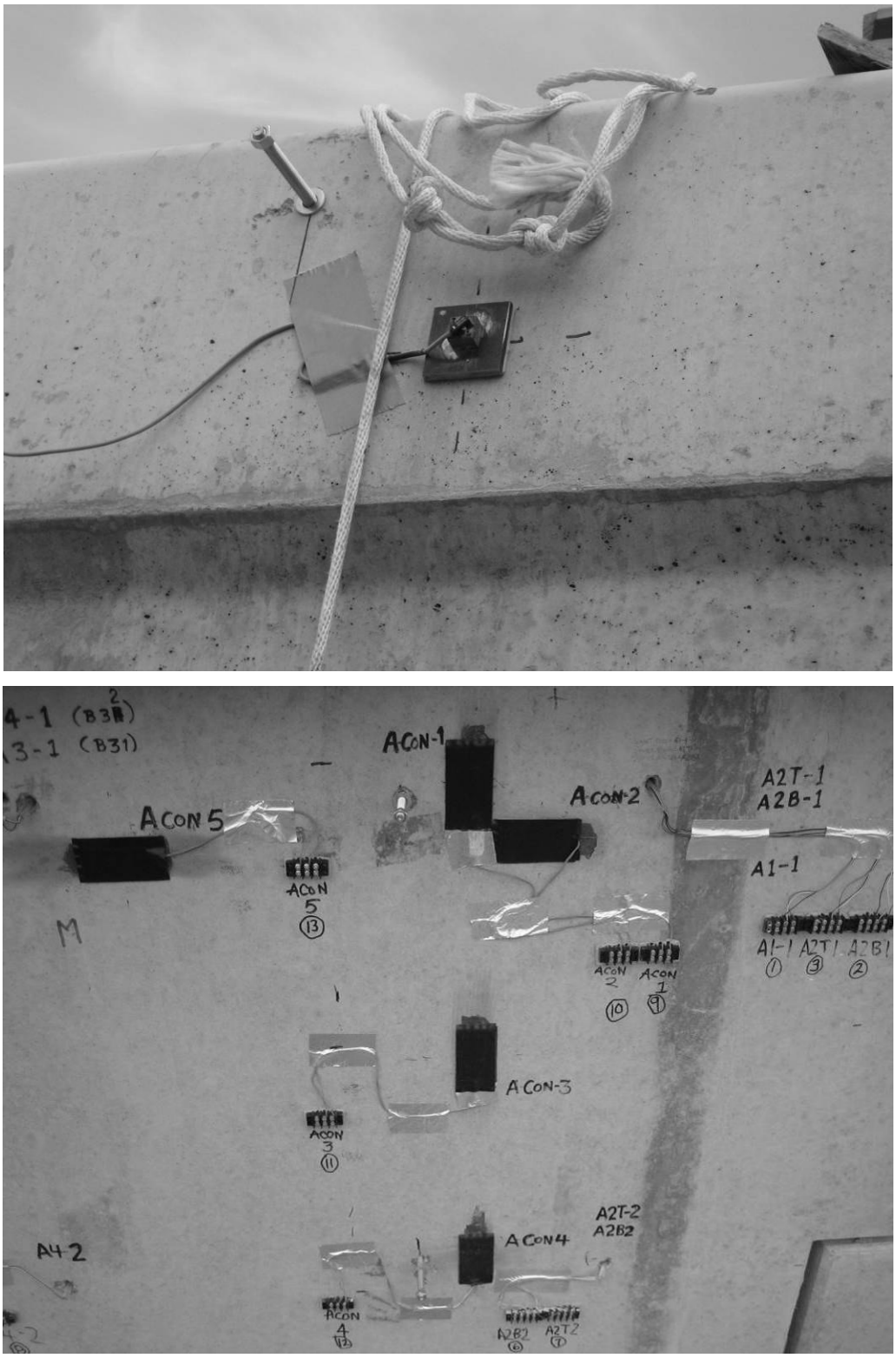

Figure D.22 Installation of Accelerometers on top of the Barrier and Connection Bolts for Displacement Bars

Figure D.23 Installation of String Line

(a) Measure the Distance before Test

(b) Installation of Tow-System for Bogie Vehicle

(c) Installation of Displacement Bars with Target for High-Speed Film

Figure D.24 Preparation on Test Day

APPENDIX E

DETAILED DRAWING OF MSE WALL FOR TL-3 TEST

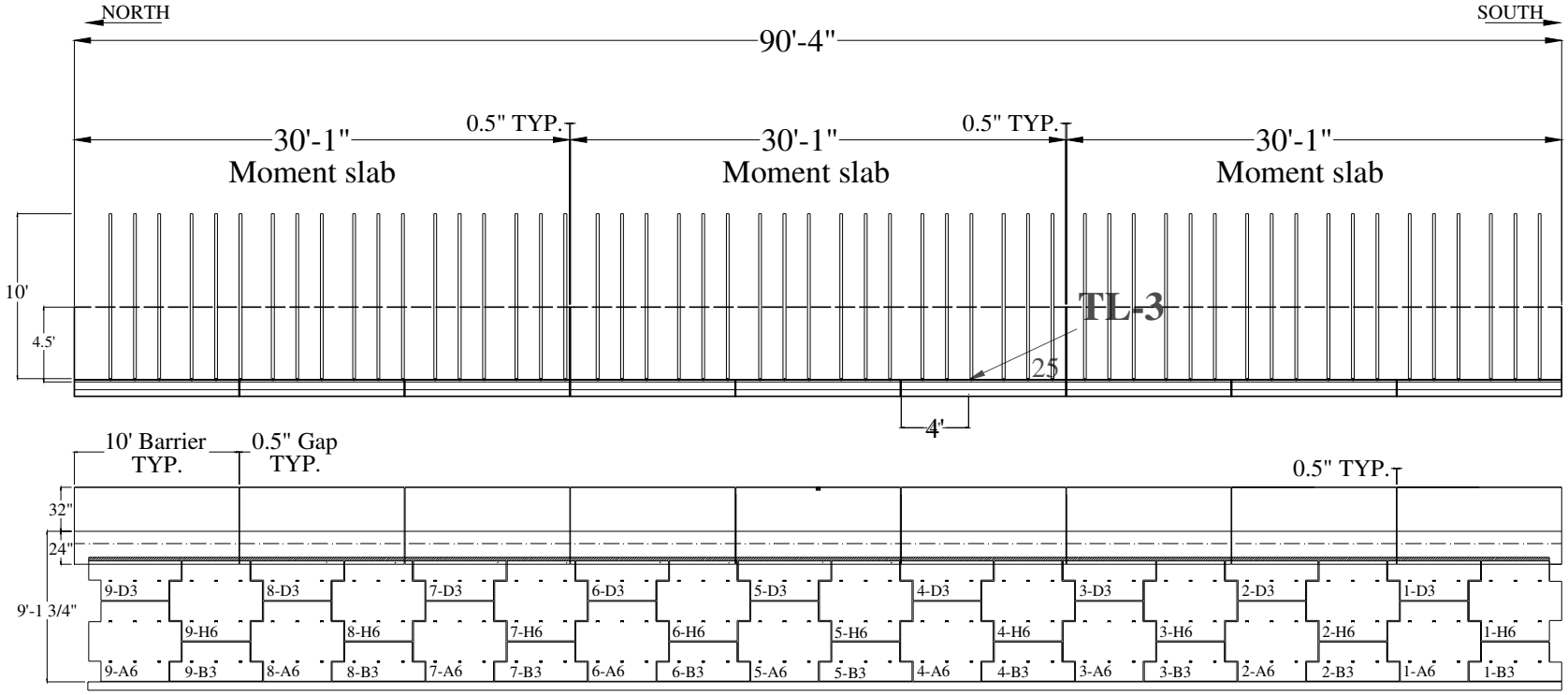

Figure E 1 Overall Layout for TL-3 Crash Test

1) Moment Slab

The precate parapet rail shall be braced until the moment slab can structurally support the rail. Workers shall not stand or work down in front of the wall until the rail has been structurally supported by the moment slab.

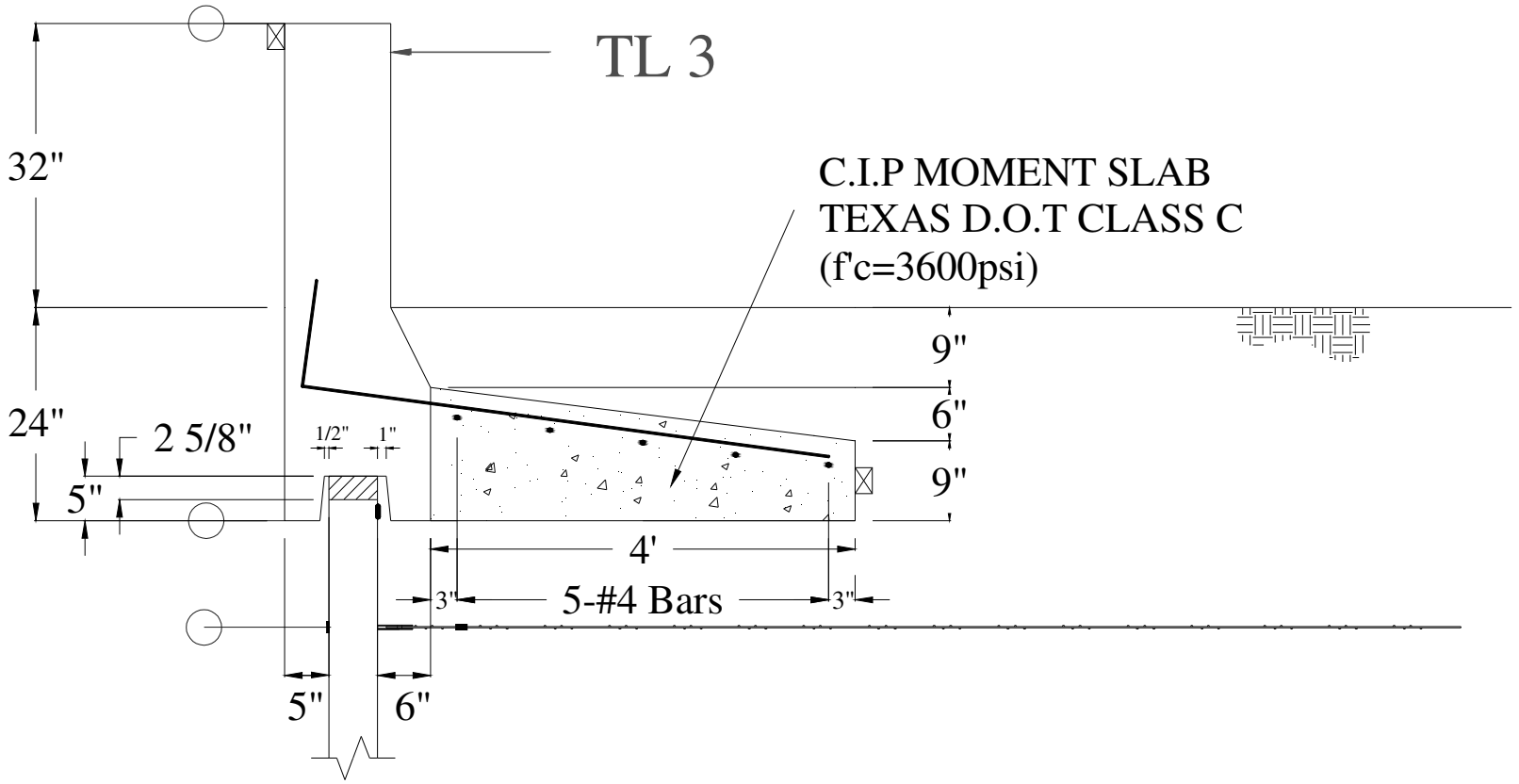

Figure E 2 C.I.P Moment Slab Detail

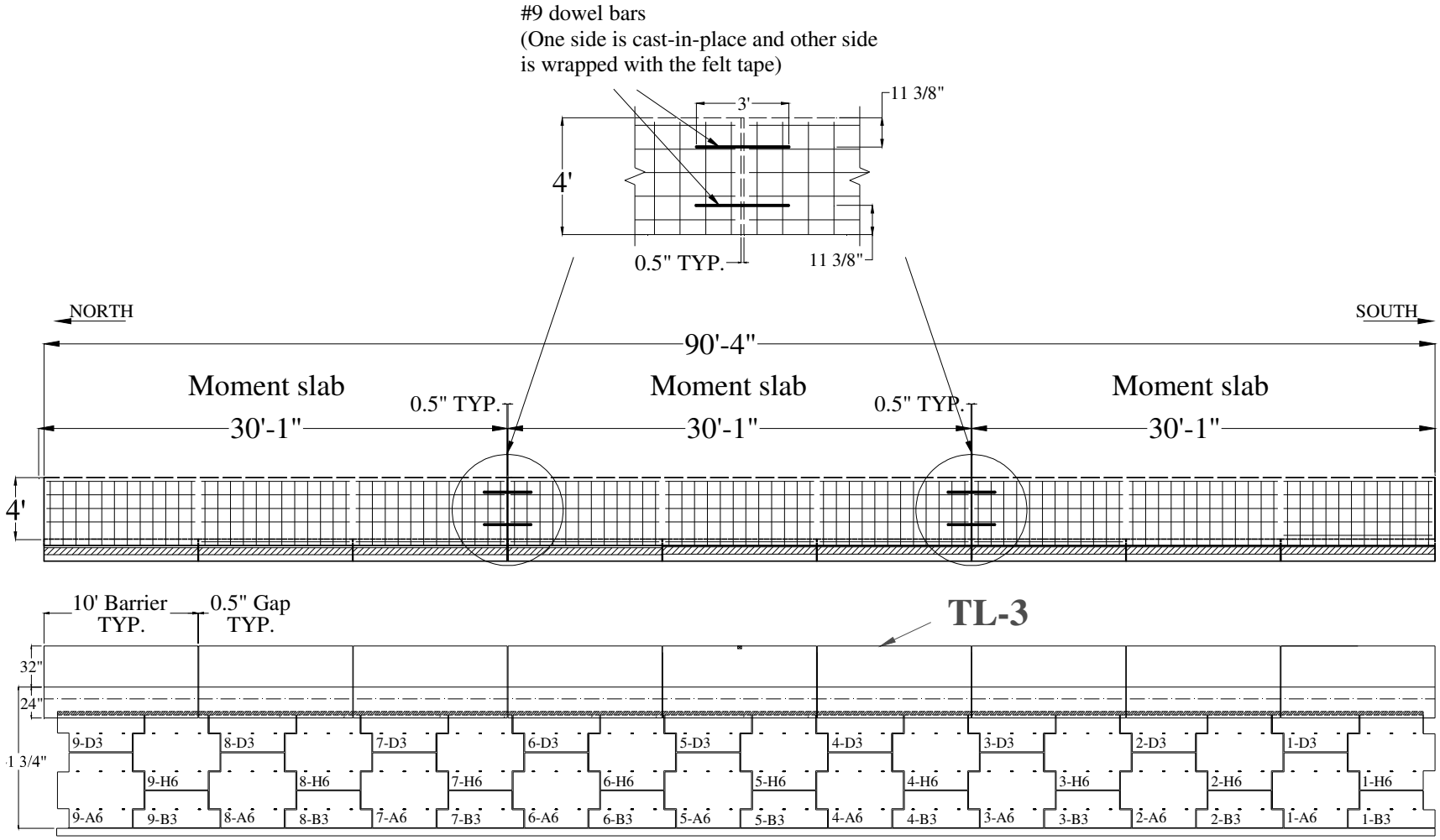

Figure E 3 Dowels in Moment Slab

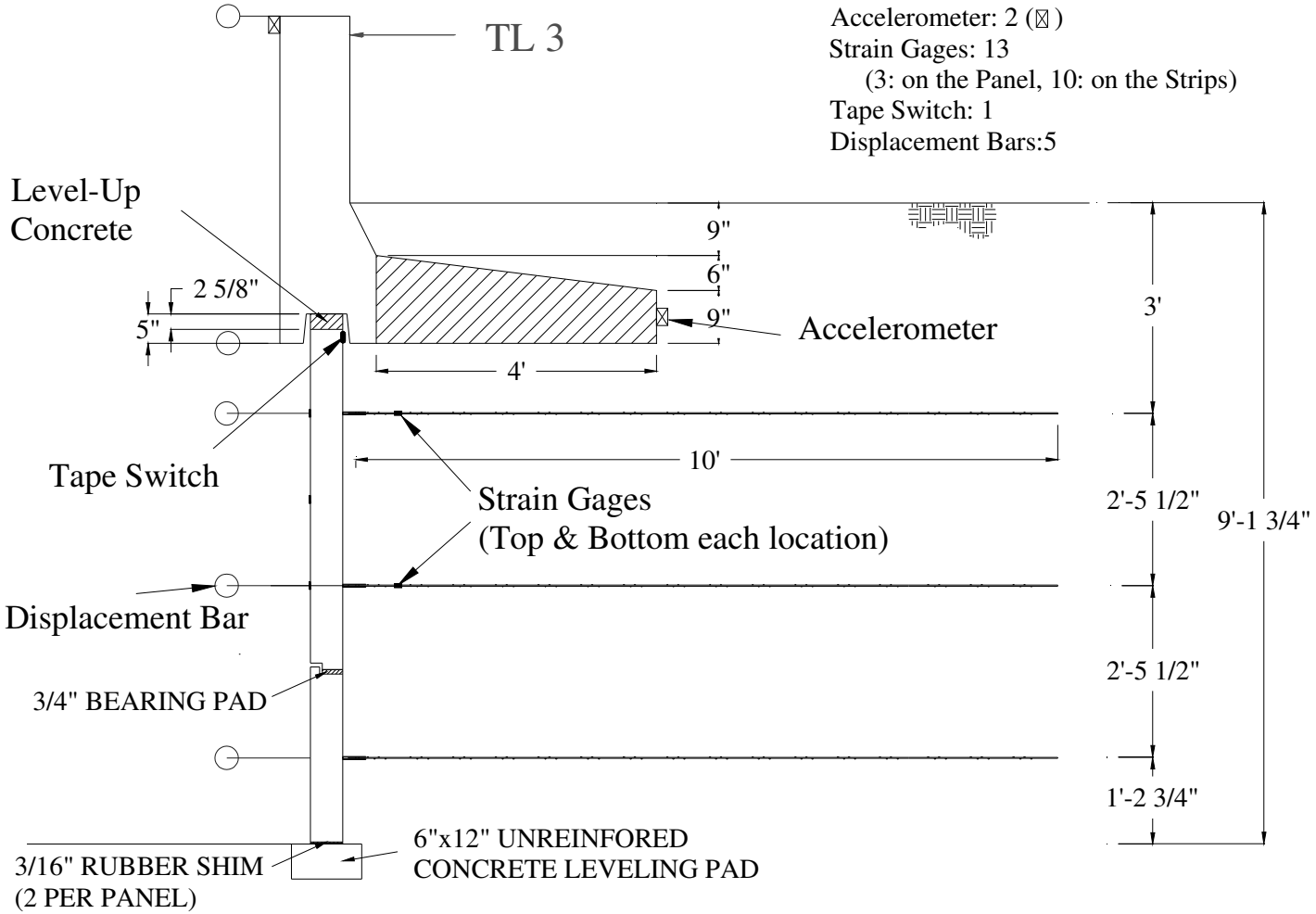

Figure E 4 Side View of TL-3 Crash Test with 32-in. Tall Vertical Wall Barrier Parapet

1) Steel Strain Gages on Reinforcement Strips

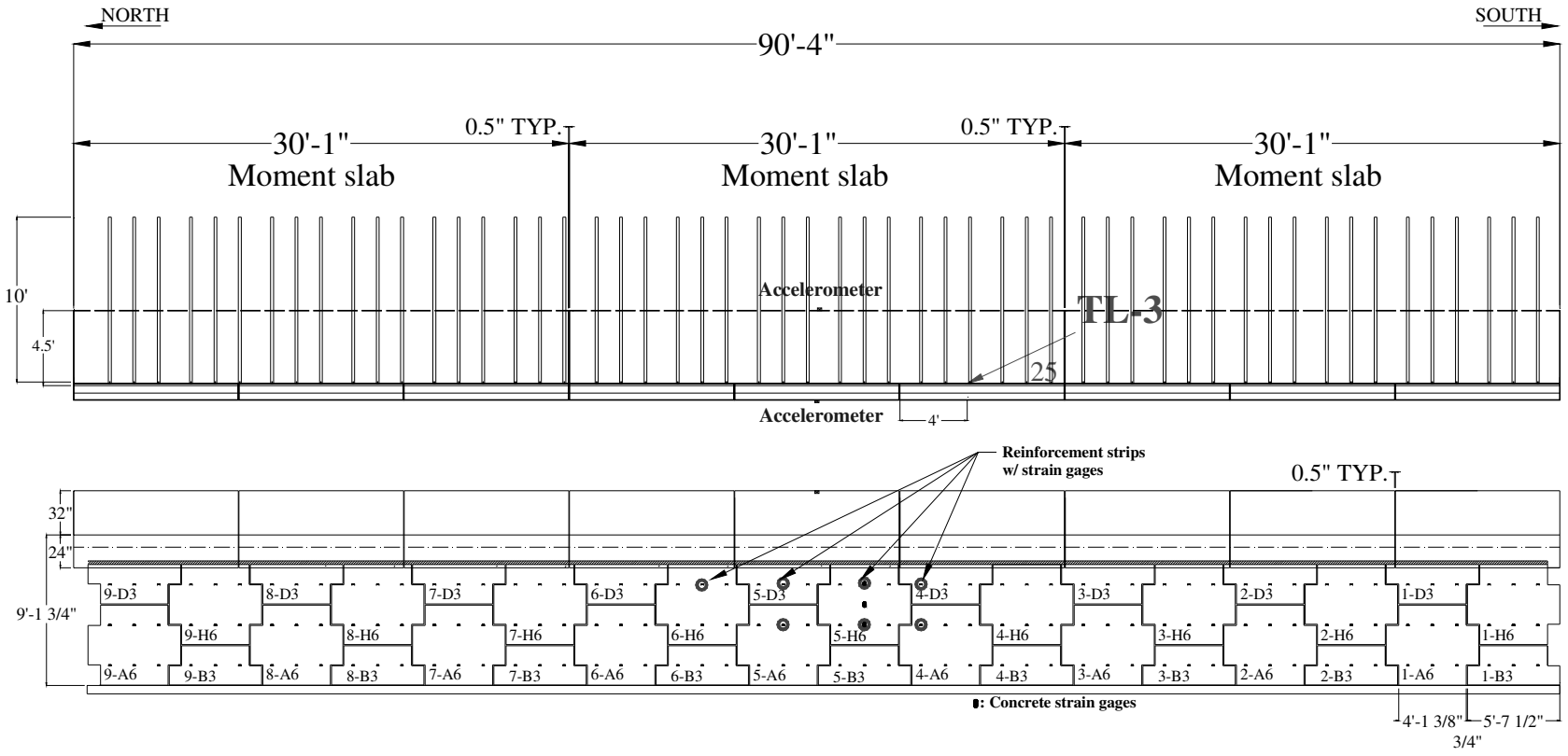

Figure E 5 Details of Strain Gages on Reinforcement Strips

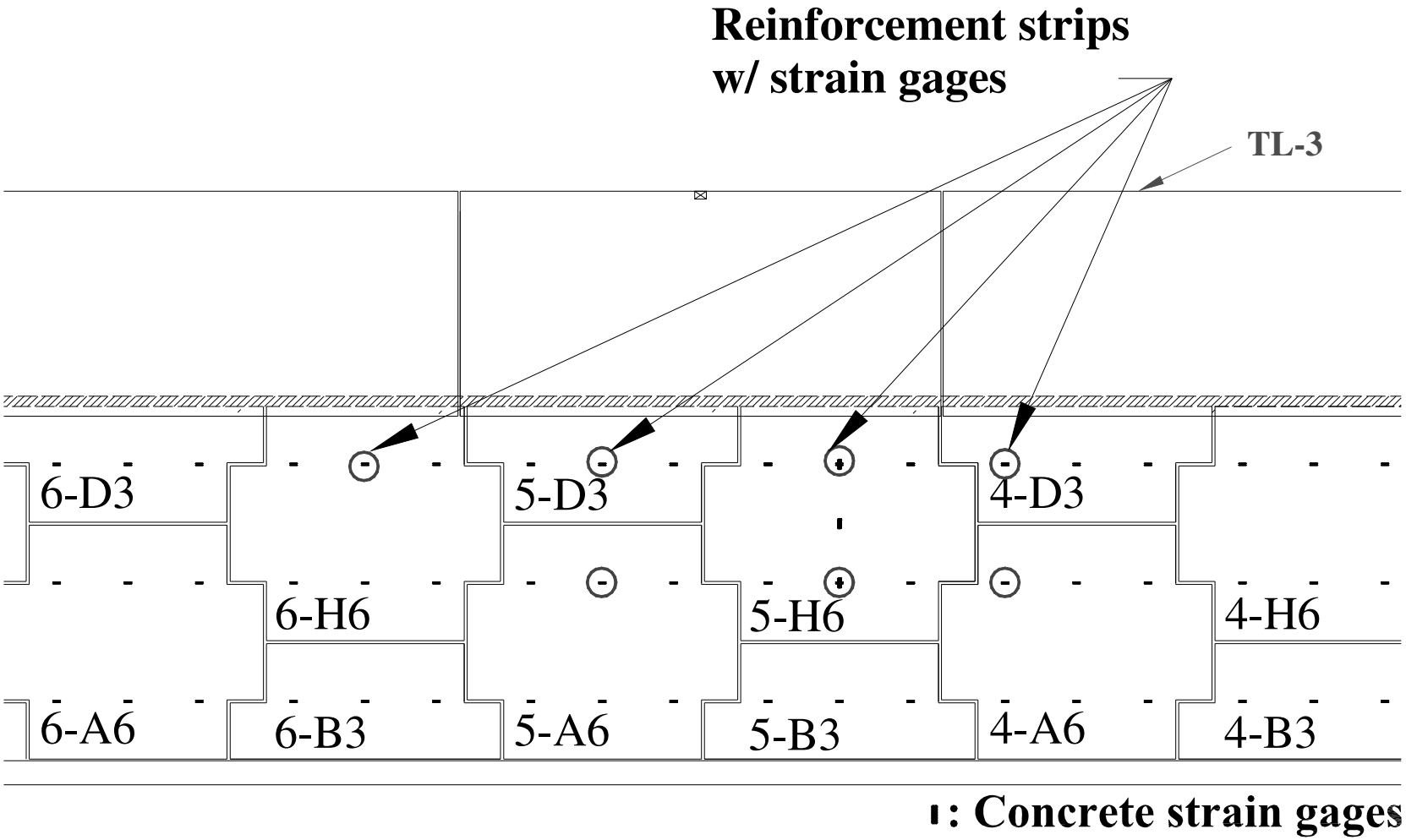

Figure E 6 Details of Strain Gages on Reinforcement Strips

Strain Gauge Instrumentation of Steel Reinforcement Strips (7 strips × 2 gages = 10 gages total)

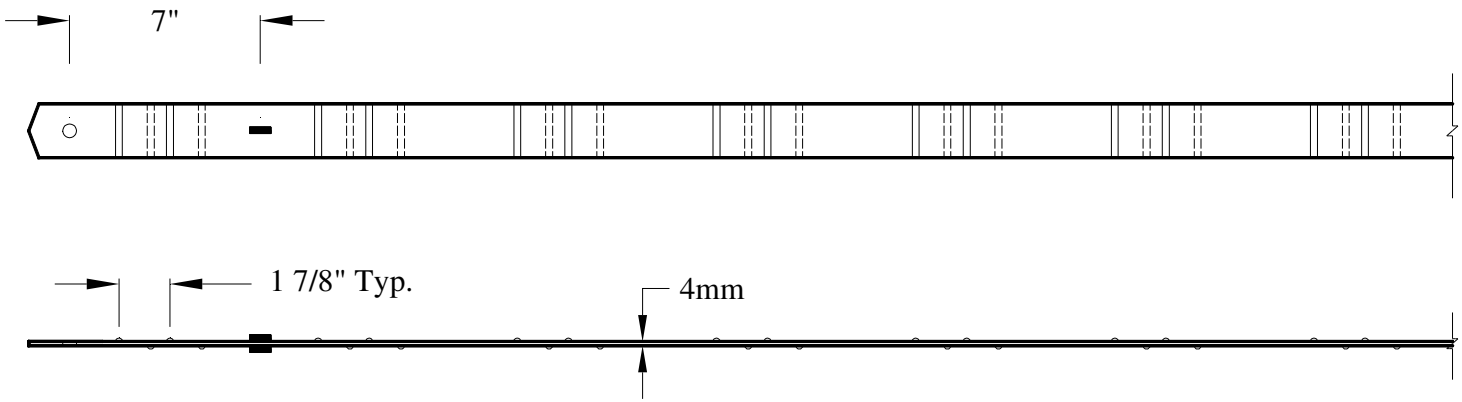

Figure E 7 Location of Steel Strain Gages on Steel Reinforcement Strips

Note: The strain gages installed on top and bottom of each strip.

2) Concrete Strain Gages on Wall Panel

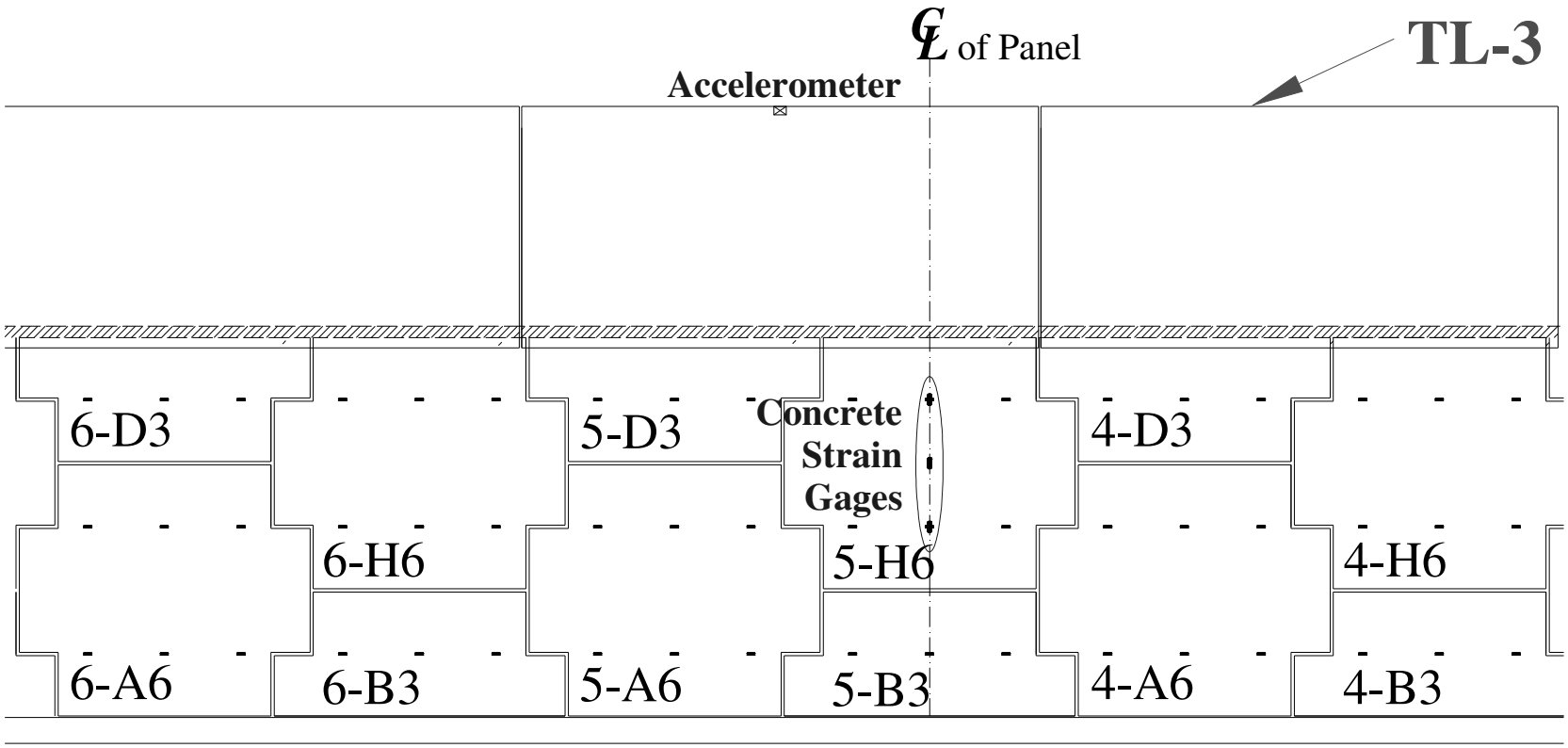

Figure E 8 Location of Concrete Strain Gages on Wall Panel

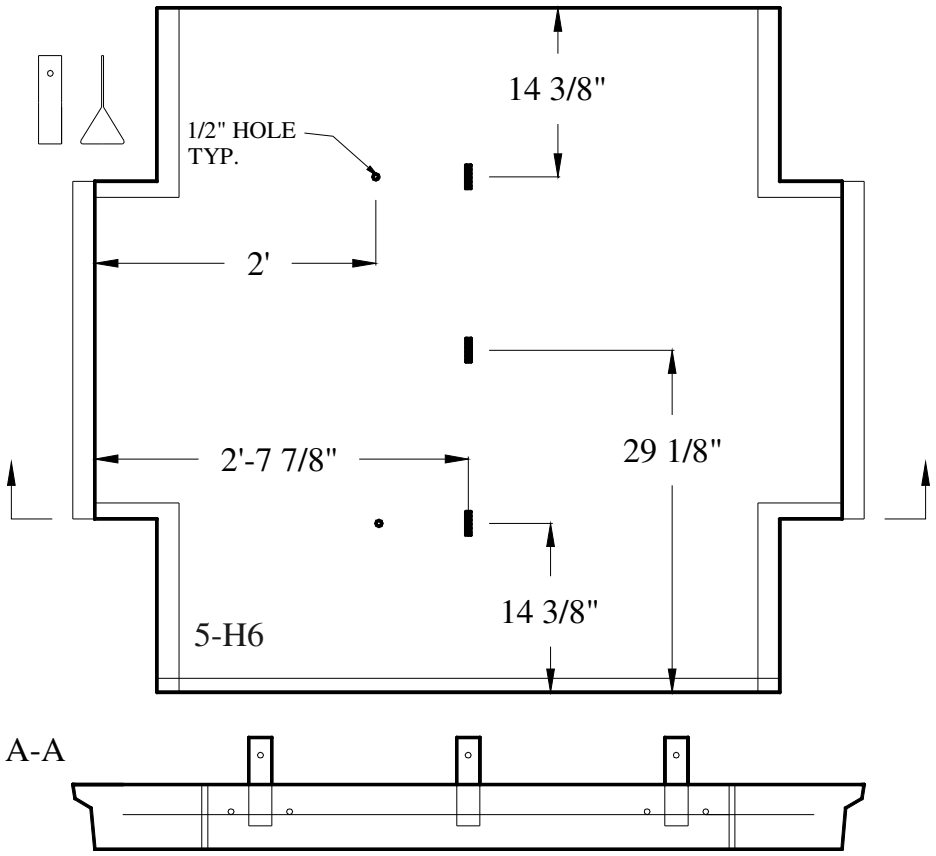

Figure E 9 Location of Concrete Strain Gages on Wall Panel

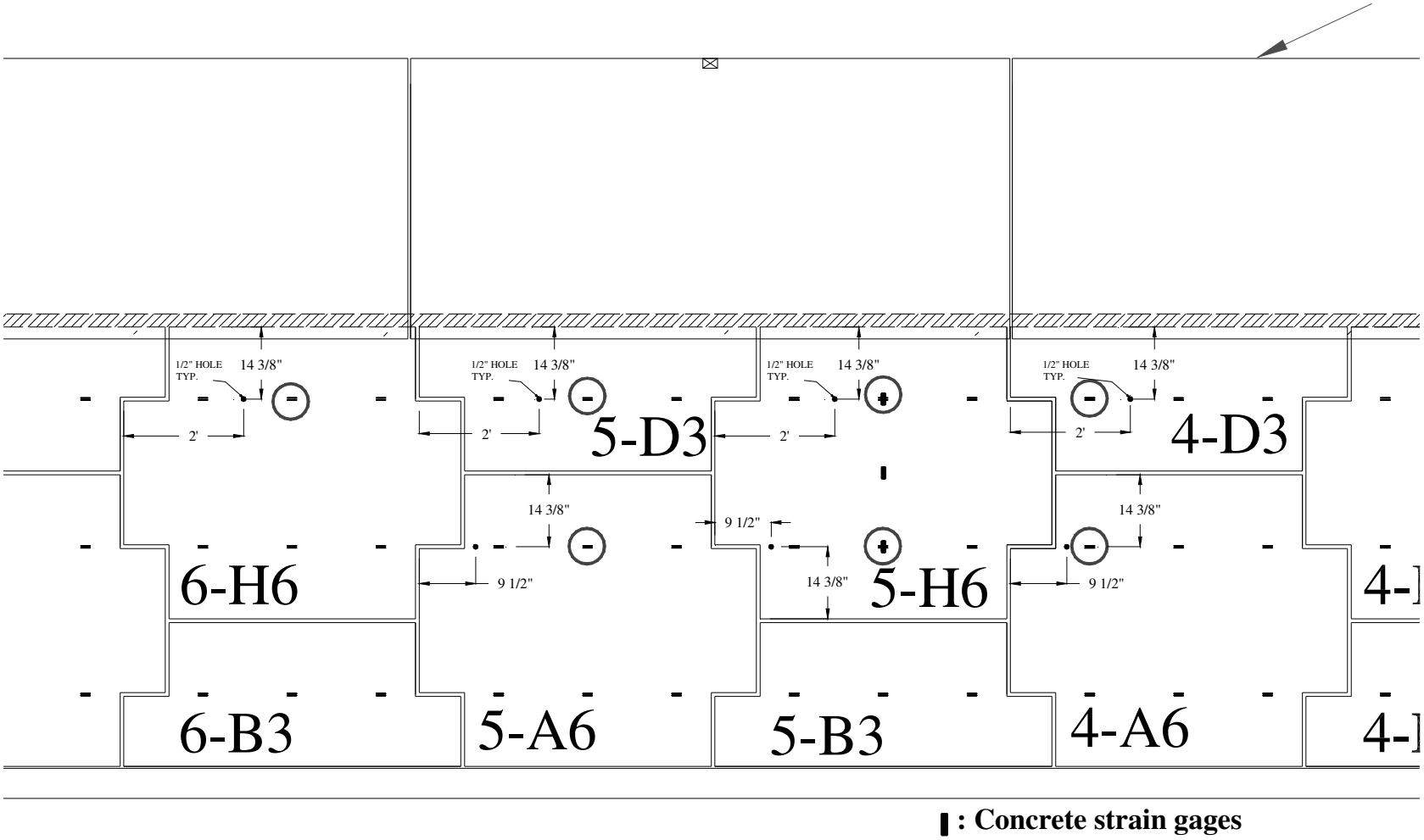

Figure E 10 Location of Hole for Stain Gage Wire

3) Tape Switch

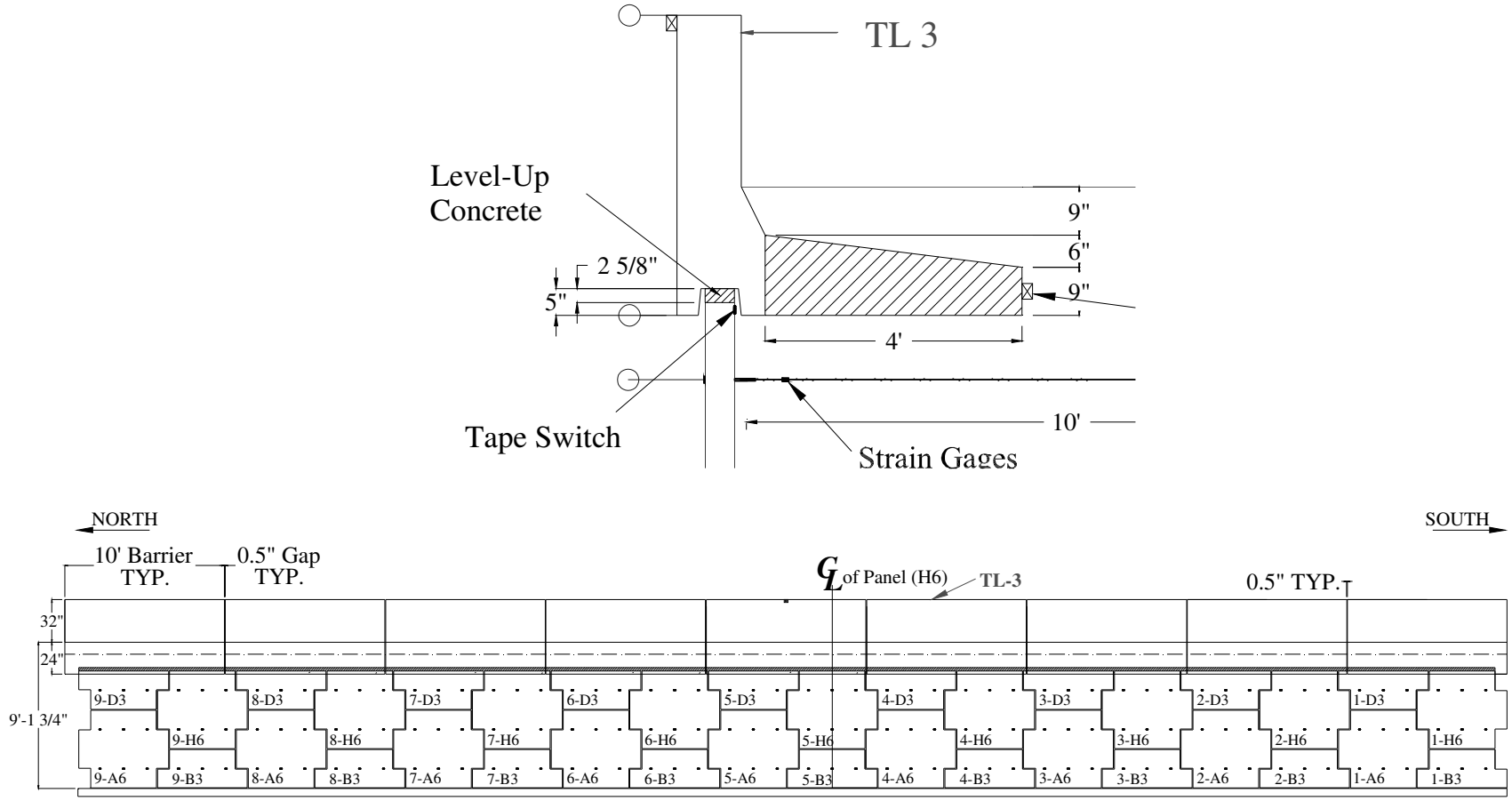

Figure E 11 Location of Tape Switch

4) Displacement Bar

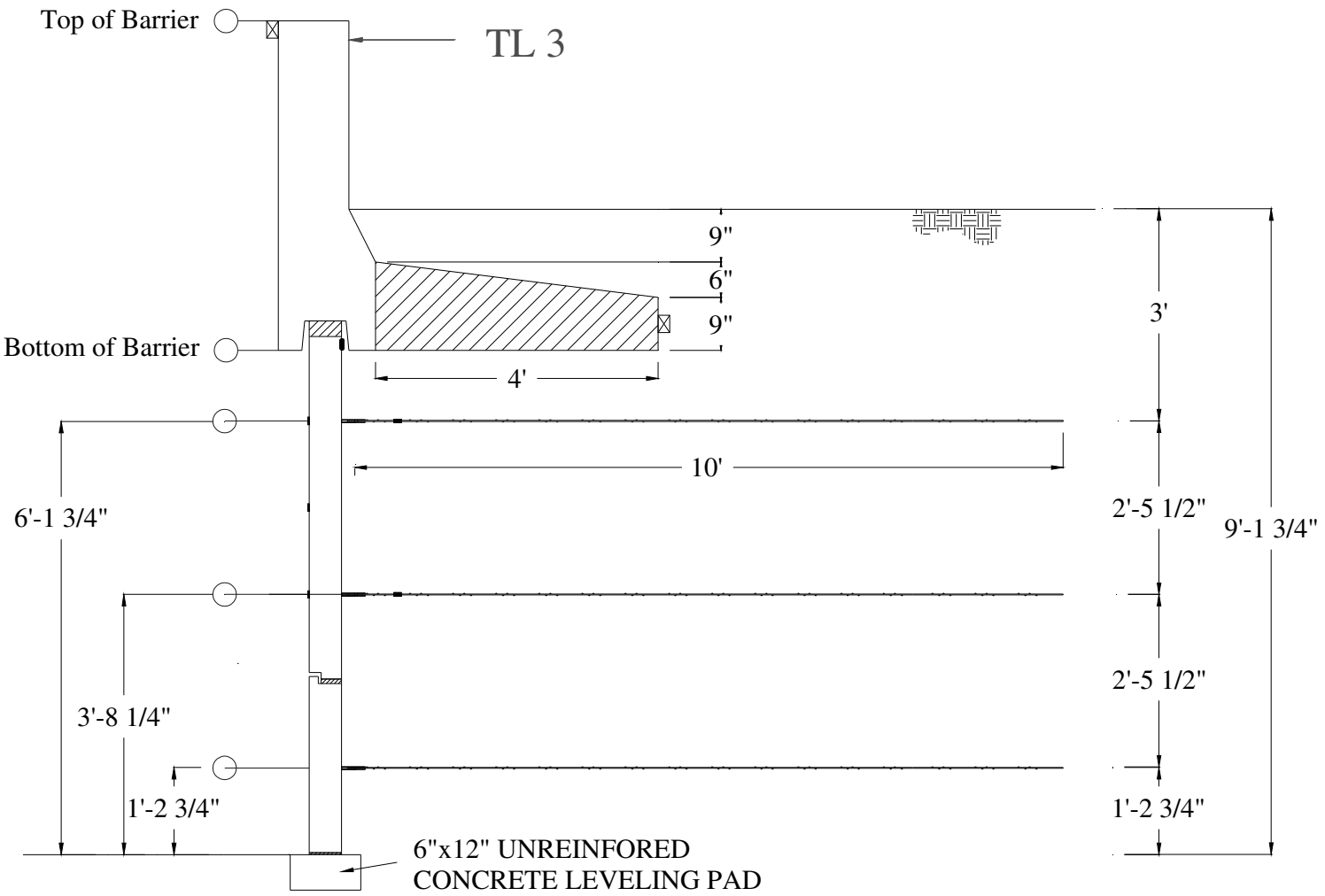

Figure E 12 Location of Displacement Bars on Wall Panels

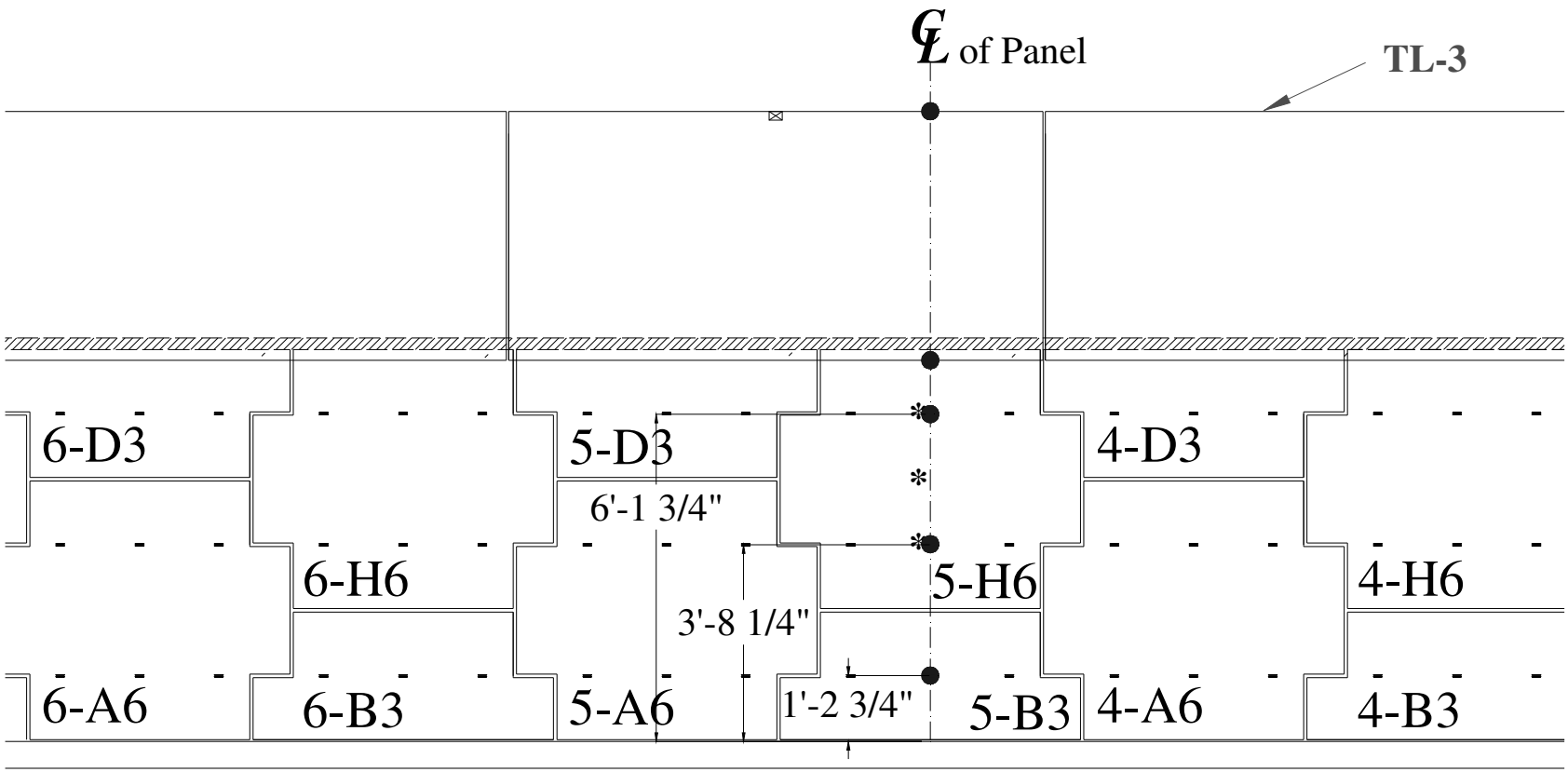

Figure E 13 Location of Displacement Bars on Wall Panels (Cont.)

5) Accelerometers on the Barrier and Moment slab

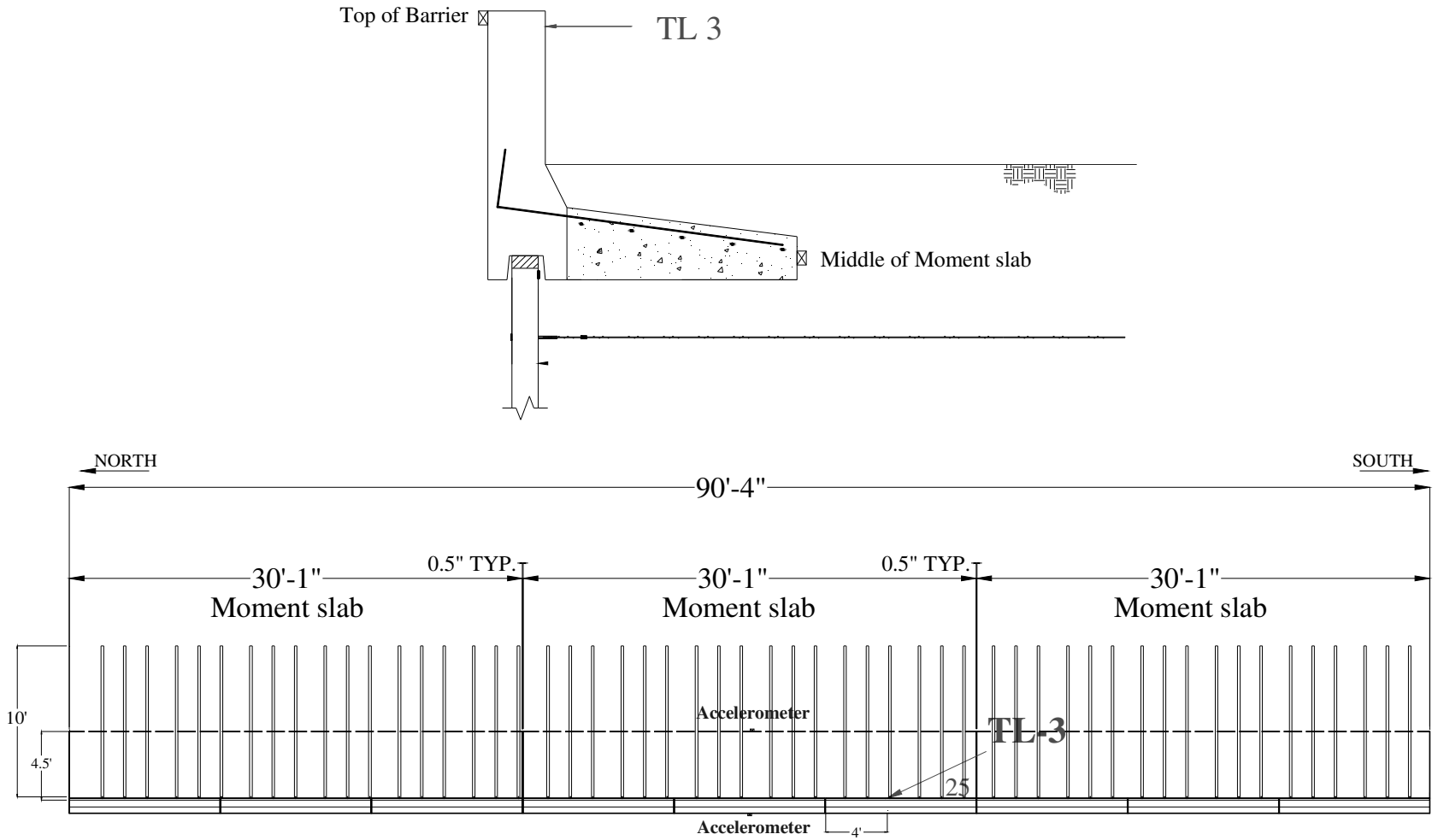

Figure E 14 Location of Accelerometers.

APPENDIX F

TL-3 TEST VEHICLE PROPERTIES AND INFORMATION

Date: 2008-09-25 Test No.: 475350-1 VIN No.: 1D7HA18N74S569024

Year: 2004 Make: Dodge Model: Ram 1500 Quad-Cab

Tire Size: 245/70R17 Tire Inflation Pressure: 35 psi

Tread Type: Highway Odometer: 162279

Note any damage to the vehicle prior to test:

• Denotes accelerometer location.

NOTES:

Engine Type: V-8
Engine CID: 4.7 liter

Transmission Type:
x Auto or ___ Manual
___ FWD x RWD ___ 4WD

Optional Equipment:

Dummy Data:
Type: No dummy
Mass:
Seat Position:

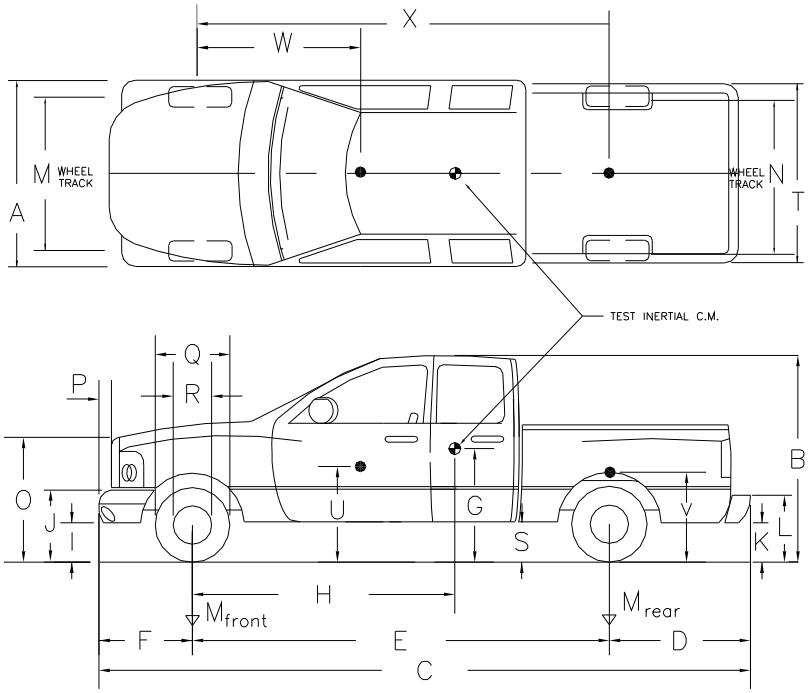

Geometry: inches

A	77.0	F	37.0	K	18.0	P	3.5	U	27.5
B	74.0	G	28.2	L	27.5	Q	30.0	V	33.0
C	224.5	H	62.4	M	68.2	R	18.2	W	59.5
D	47.0	I	13.8	N	67.2	S	15.4	X	140.5
E	140.5	J	26.0	O	44.5	T	75.5		

Wheel Center Ht Front ___ Wheel Well Clearance (FR) ___ Frame Ht (FR) ___

Wheel Center Ht Rear ___ Wheel Well Clearance (RR) ___ Frame Ht (RR) ___

GVWR Ratings:		**Mass:** lb	Curb	Test Inertial	Gross Static
Front	3650	M_{front}	2730	2751	
Back	3900	M_{rear}	2064	2200	
Total	6650	M_{Total}	4794	4951	

Mass Distribution:
lb LF: 1357 RF: 1394 LR: 1096 RR: 1104

Figure B1. Vehicle properties for test 475350-1.

Table B1. Exterior crush measurements for test 475350-1.

Date: 2008-09-25 Test No.: 475350-1 VIN No.: 1D7HA18N74S569024

Year: 2004 Make: Dodge Model: Ram 1500 Quad-Cab

VEHICLE CRUSH MEASUREMENT SHEET[1]

Complete When Applicable	
End Damage	Side Damage
Undeformed end width _____ Corner shift: A1 _____ A2 _____ End shift at frame (CDC) (check one) < 4 inches _____ ≥ 4 inches _____	Bowing: B1 _____ X1 _____ B2 _____ X2 _____ Bowing constant $\frac{X1+X2}{2}$ = _____

Note: Measure C_1 to C_6 from Driver to Passenger side in Front or Rear impacts – Rear to Front in Side Impacts.

Specific Impact Number	Plane* of C-Measurements	Direct Damage		Field L**	C_1	C_2	C_3	C_4	C_5	C_6	±D
		Width** (CDC)	Max*** Crush								
1	Front plane at bumper ht	19.7	13.8	23.6	13.8	9.1	6.3	3.1	0.8	0	-14.2
2	Side plane at bumper ht	19.7	15.8	63.0	2.8	---	---	---	14.6	15.8	+77.2
	MEASUREMENTS IN										
	INCHES										

[1]Table taken from National Accident Sampling System (NASS).

*Identify the plane at which the C-measurements are taken (e.g., at bumper, above bumper, at sill, above sill, at beltline, etc.) or label adjustments (e.g., free space).

Free space value is defined as the distance between the baseline and the original body contour taken at the individual C locations. This may include the following: bumper lead, bumper taper, side protrusion, side taper, etc.
Record the value for each C-measurement and maximum crush.

**Measure and document on the vehicle diagram the beginning or end of the direct damage width and field L (e.g., side damage with respect to undamaged axle).

***Measure and document on the vehicle diagram the location of the maximum crush.

Note: Use as many lines/columns as necessary to describe each damage profile.

Table B2. Occupant compartment measurements for test 475350-1.

Date: 2008-09-25 Test No.: 475350-1 VIN No.: 1D7HA18N74S569024

Year: 2004 Make: Dodge Model: Ram 1500 Quad-Cab

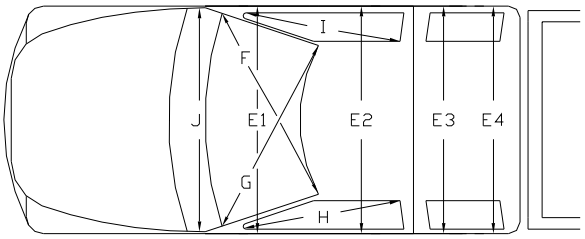

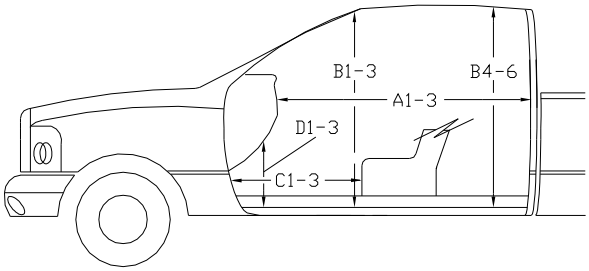

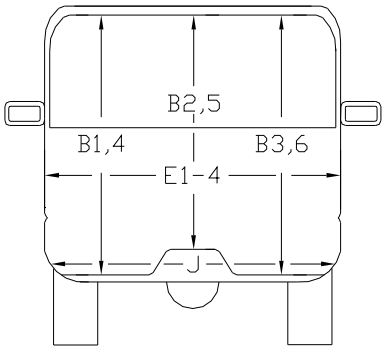

*Lateral area across the cab from driver's side kickpanel to passenger's side kickpanel.

OCCUPANT COMPARTMENT DEFORMATION MEASUREMENT	Before (mm)	After (mm)
A1	64.6	64.6
A2	64.9	64.9
A3	65.4	65.4
B1	44.7	44.7
B2	39.2	39.2
B3	45.3	45.3
B4	48.8	48.8
B5	45.2	45.2
B6	48.8	48.8
C1	29.5	29.5
C2	-----	-----
C3	27.4	27.4
D1	12.6	12.6
D2	2.4	2.4
D3	11.6	11.6
E1	63.3	61.2
E2	64.3	63.8
E3	64.2	63.5
E4	64.2	63.0
F	59.6	------
G	59.6	-----
H	39.6	-----
I	39.6	-----
J*	22.9	21.6

APPENDIX G

TL-3 TEST SEQUENTIAL PHOTOGRAPHS

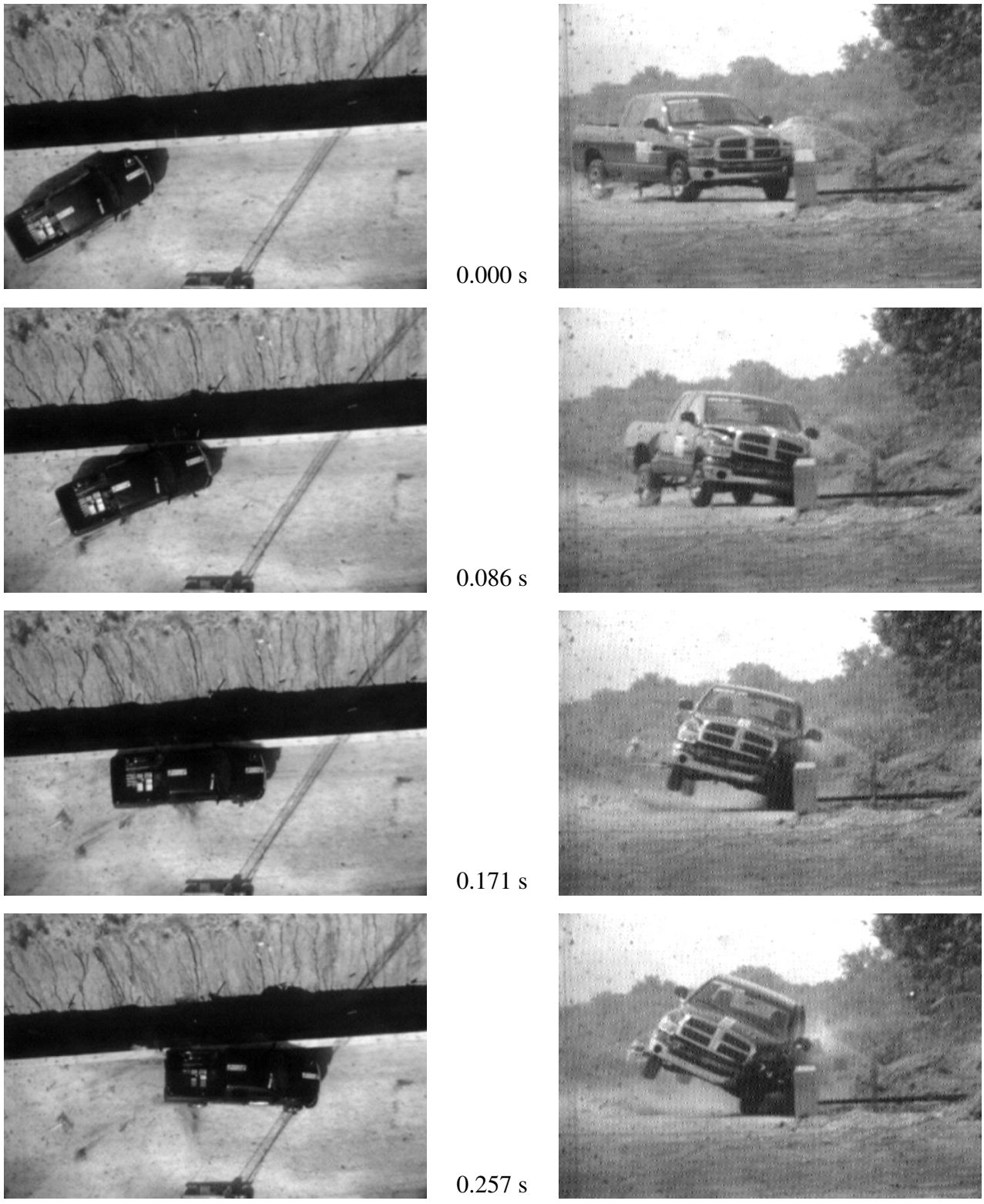

Figure B2. Sequential photographs for test 475350-1(overhead and frontal views).

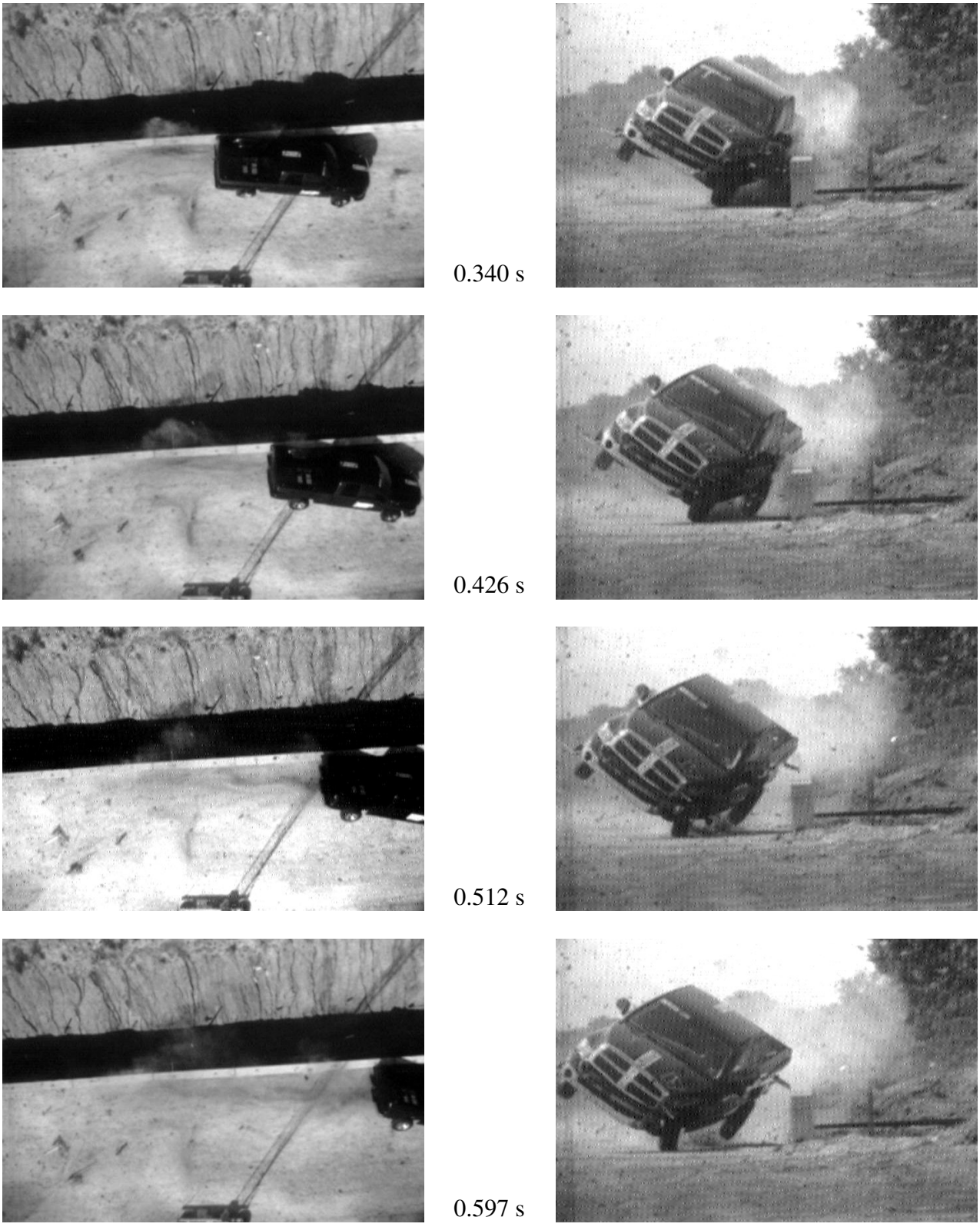

Figure B2. Sequential photographs for test 475350-1 (overhead and frontal views) (continued).

VITA

Kang Mi Kim received a Bachelor of Science degree in the Department of Civil Engineering from Chonnam National University, Korea in February 2001. She obtained a Master of Science degree in the Department of Civil Engineering with emphasis in structural engineering from Yonsei University, Korea in February 2003. After that, she joined the Zachry Department of Civil Engineering at Texas A&M University in August 2004 and received her Doctor of Philocophy degree in May 2009. Her research interests are structural mechanics, finite element analysis of structural systems, roadside structure, and MSE wall design.

She can be reached at

Roadside Safety Program - Riverside 7091
Texas Transportation Institute
The Texas A&M University System
3135 TAMU
College Station, TX 77843-3135